IAEA-208 VOL. 2

NEUTRON CROSS SECTIONS FOR REACTOR DOSIMETRY

VOL.II
CONTRIBUTED PAPERS

PROCEEDINGS OF A CONSULTANTS' MEETING
ON INTEGRAL CROSS-SECTION MEASUREMENTS
IN STANDARD NEUTRON FIELDS FOR REACTOR DOSIMETRY
ORGANIZED BY THE
INTERNATIONAL ATOMIC ENERGY AGENCY
AND HELD IN VIENNA, 15–19 NOVEMBER 1976

A TECHNICAL DOCUMENT ISSUED BY THE
INTERNATIONAL ATOMIC ENERGY AGENCY, VIENNA, 1978

NEUTRON CROSS SECTIONS FOR REACTOR DOSIMETRY
IAEA, VIENNA, 1978
Printed by the IAEA in Austria

PLEASE BE AWARE THAT
ALL OF THE MISSING PAGES IN THIS DOCUMENT
WERE ORIGINALLY BLANK

FOREWORD

The Consultants' Meeting on Integral Cross Section Measurements in Standard Neutron Fields for Reactor Dosimetry was convened by the IAEA Nuclear Data Section in Vienna, 15 - 19 November 1976, as part of the IAEA Programme on Benchmark Neutron Fields Applications for Reactor Dosimetry, described in INDC(SEC)-54/L+Dos, July 1976.

The need for the application of benchmark neutron fields, particularly for the validation and improvement of neutron data required for reactor dosimetry, was recognized by the IAEA Consultants' Meeting on Nuclear Data for Reactor Neutron Dosimetry, held in September 1973 [INDC(NDS)-56/U], and supported by the Agency's Working Group on Reactor Radiation Measurements and International Nuclear Data Committee.

The importance and usefulness of this approach was well demonstrated by the US Interlaboratory LMFBR Reaction Rate (ILRR) programme [Nuclear Technology 25, no.2, Feb. 1975] and was extensively discussed at the First ASTM-EURATOM Symposium for Reactor Dosimetry, Petten, Sept. 1975 [EUR-5667 e/f].

The present Consultants' Meeting is the first international meeting devoted to this subject; it summarizes progress in this field in laboratories of the IAEA member states.

The main results of the meeting are as follows:

- a comprehensive survey of benchmark neutron fields available at present for reactor dosimetry applications and their classification in three categories;
- review of the methods used at present for spectral characterization of neutron fields: direct spectrometry, activation, analytical calculations, and of results obtained with these methods;
- review of the present status of integral and differential neutron cross-section data for reactor dosimetry and new classification of the reactions in two categories;
- discussion of methodology for validation and adjustment of differential neutron data on the basis of integral data;
- better understanding has been reached between scientists working in the fields of integral and differential data measurements.

The proceedings of the meeting are published in two volumes. Volume I contains the review papers and Volume II the contributed papers presented at the meeting. The summary report, published as INDC(NDS)-81/L+M, is included in Volume I because of its importance for a better understanding of the results of the meeting.

M.F. Vlasov

Scientific Secretary

TABLE OF CONTENTS OF VOLUMES I AND II

C O N T E N T S , V o l u m e I : REVIEW PAPERS

I. OVERVIEW

II. SPECTRAL CHARACTERIZATION OF BENCHMARK NEUTRON FIELDS

III. INTEGRAL DATA IN BENCHMARK NEUTRON FIELDS

IV. DIFFERENTIAL CROSS-SECTION DATA FOR REACTOR DOSIMETRY

V. VALIDATION AND ADJUSTMENT OF DIFFERENTIAL CROSS SECTIONS ON THE BASIS OF INTEGRAL DATA

C O N T E N T S , V o l u m e II : CONTRIBUTED PAPERS

I. SPECTRAL CHARACTERIZATION OF BENCHMARK NEUTRON FIELDS

II. INTEGRAL DATA IN BENCHMARK NEUTRON FIELDS

I. SPECTRAL CHARACTERIZATION OF BENCHMARK NEUTRON FIELDS

I.1. Standards for Thermal Neutrons at the PTB

S. R. Wagner
Physikalisch-Technische Bundesanstalt (PTB), Braunschweig
Federal Republic of Germany

Abstract:

The characteristics of standard neutron fields in the thermal energy region are described. This type of fields is realized as (1) source-driven flux density standards consisting of fairly large moderating blocks and providing a homogeneous field within a cavity. (2) A thermal neutron reference beam is extracted from the FMRB reactor of the PTB. In both cases the thermal spectrum is obtained using the cadmium difference method.

1. Thermal neutron flux density standards

Thermal flux density standards are stable devices which allow well defined irradiations of probes and detectors for calibration purposes. Two such devices have been installed at the PTB having differently sized irradiation volumes at different flux density levels, but both in the low flux density range.

1.1 Neutron flux density standard I

The basic concept originates from G. von Droste and was realized by M. Matzke and H.J. Bortfeldt/1/. Fig. 1 shows the essential features. A cube (50 cm side length) composed of bricks of reactor grade graphite is immediately surrounded by 2 cm thick graphite plates and, at a distance of 7.5 cm, by 25 cm thick paraffin walls, which act as moderator and reflector. One Am-Be(α,n) neutron source (source strength about $2.7 \cdot 10^6$ s^{-1}) is centered at each of the six side walls. Paraffin discs, the size of which was optimized experimentally, are mounted in front of the sources within the interstice between graphite and paraffin wall in order to achieve a homogeneous thermal neutron field within the graphite cube. Additional paraffin blocks at the corners serve the same end.
The graphite cube, together with parts of the front and bottom walls, moves on rails in order to allow access to the irradiation position. This is an air volume of 10 cm x 10 cm x 10 cm, which may be enlarged, in the center of the graphite cube.

The neutron field within the graphite cube was investigated by means of gold foil activation. Details of the procedure, the evaluation and the necessary corrections may be found in ref. /1/. The conventional flux density of neutrons with energies below cadmium cut-off $\varphi_{th} = n_{th} v_o$ (n_{th} number density of neutrons with energies below cadmium cut-off, $v_o = 2200$ m s^{-1}) is given for June 1, 1974

$$\varphi_{th} = (3.69 \pm 0.08) \cdot 10^3 \text{ cm}^{-2} \text{ s}^{-1}$$

(overall uncertainty, relative value 2.1 %, corresponding to a confidence level of about 68 %). The flux density was observed to be constant within the irradiation volume to better than 0.3 %. The Cd-ratio of 20 µm thick gold foils was 7.64, which has led to the ratio

$$\frac{\varphi_{th}}{\varphi_e} = 39.1$$

(φ_e mean spectral energy flux density of intermediate energy neutrons).

1.2 Neutron flux density standard II

This standard (see fig. 2) was constructed by J. Bortfeldt and M. Matzke /2/. Here the graphite cube (reactor grade) has a side length of only 20 cm with a smaller cylindrical irradiation volume (5 cm dia., 5 cm high). The graphite cube is encased by a 1 cm thick Plexiglas (lucite) sheet, this again surrounded by 25 cm thick paraffin. The paraffin jacket is divided by 1 cm thick Plexiglas sheets in such a manner that the graphite cube can easily be removed or exchanged. The outer faces of the paraffin are shielded by boron wood. 8 Am-Be(α,n) sources are mounted at the ends of the spatial diagonals of the graphite cube, the edges of which are cut away.

Details of the measurements carried out for the calibration of the standard are given in ref. /2/. Fig. 3 shows the spatial distribution of the flux density as observed with a small boron counter. Therefrom the flux density buckling is derived as $/B^2/ = 0.014$ cm^{-2}, which means that the neutron field is sufficiently homogeneous over an area of 1 cm^2, the size of the activation foils being as commonly used. As the buckling is negligeable, the thermal flux density will be almost independent of the moderator temperature. This was checked by means of gold

foil activation at moderator temperatures of 286 K, 294 K and 301 K resulting in a relative flux density variation

$$\left|\frac{\delta\varphi_{th}}{\varphi_{th}}\right| < 3 \cdot 10^{-4} \left|T - T_o\right|$$

(T, T_o in Kelvins)

Assuming a Maxwell distribution for the spectral flux density of thermal neutrons, the corresponding temperature parameter T_n at room temperature (293 K) was determined by means of dysprosium discs of varying thickness as

$$T_n = (303 \pm 12)\ K$$

The conventional flux density of thermal neutrons with energies below cadmium cut-off at the irradiation position was determined by means of 1 cm dia. gold foils of varying thickness irradiated without or with a 1 mm thick cadmium shield. The measurements were evaluated to

$$\varphi_{th} = (1.746 \pm 0.014) \cdot 10^4\ cm^{-2}\ s^{-1}$$

as of January 1, 1976. The uncertainty corresponds to a confidence level of 68 % and includes correspondingly estimated systematic uncertainties.

The cadmium-ratio of 20 µm thick gold foils was determined as

$$R_{cd} = 9.05 \pm 0.05$$

leading to

$$\frac{\varphi_{th}}{\varphi_e} = 47 \pm 3$$

(φ_e mean spectral energy flux density of intermediate energy neutrons).

1.3 Calibration procedures (cf. /2/)

1.3.1 Reference neutron fields

Other thermal neutron flux density reference devices may be calibrated in units of the well defined flux density of a standard as described before by simple activity ratio measurements, with gold foils, provided the moderating characteristics in the region of the irradiation positions are similar in both devices, i.e. the gold probes must cause equal flux density perturbations (brought about by flux density depression and self-shielding).

The expression for the conventional flux density below cadmium cut-off is

$$\varphi_{th} = \frac{a - F_{cd}\, a_{cd}}{g\, \mu_a\, F\, (1+K)}$$

a specific saturation activity of gold foil,

a_{cd} specific saturation activity of cadmium covered foil,

F_{cd} cadmium correction factor /3/,

μ_a mass activation coefficient $\mu_a = n_{Au}\sigma_a/\varrho$;
n_{Au} number density of gold atoms, ϱ density of gold,
σ_a activation cross section of gold at a neutron velocity $v_o = 2200$ mm s^{-1}

g Westcott-factor /3/,

F correction for self-shielding and flux density depression,

$1+K$ correction for perturbations in the activity measurements,

(a, a_{cd}, F, K all depend on the thickness of the probe).

From the above equation we get the unknown flux density $\varphi_{th,u}$
(u denotes the quantities in the reference device to be calibrated)

in terms of the standard flux density φ_{th} as

$$\varphi_{th,u} = k \cdot \frac{1 - \frac{k_{cd}}{k}\frac{F_{cd}}{R_{cd}}}{1 - \frac{F_{cd}}{R_{cd}}} \varphi_{th}$$

with $$k = \frac{a_u}{a}, \; k_{cd} = \frac{a_{cd,u}}{a_{cd}}$$

As the uncertainties of k and k_{cd} are only statistical ones, $\varphi_{th,u}$ is obtained to almost the same uncertainty as φ_{th}.

1.3.1 Activation probes

For measuring the thermal neutron flux density in a different neutron environment with characteristics differing from those of the standard e.g. in a reactor, the flux density depression and the temperature dependence of the factors F and g have to be taken into account. Often it is necessary or desirable to use an activation probe other than gold. Then, the flux density depression and the temperature dependences of the factors F and g have to be taken into account. When using dysprosium, $R_{cd} >> 1$ holds, hence no measurement under cadmium cover is necessary. After calibrating the probe in the standard, the thermal flux density at the point of interest is obtained as (d thickness of the probe)

$$\varphi_{th,u} = (1+\kappa)_u \; k \frac{g}{g_u} \frac{F(d)}{F'_u(d)} \varphi_{th}$$

The correction factor F(d) takes into account self-shielding and flux density depression of the activation probe in the standard. The corresponding factor $F_u(d)$ at the point of interest is split into $(1+\kappa)_u$ for flux density depression and F'_u for self-shielding. The flux density depression in the standard may be neglected for most activation probes. Omitting the temperature dependence of the self-shielding, too, $F(d) = F'_u$ results. Generally the uncertainty of the factor $(1+\kappa)_u$

is larger than that of φ_{th}. In the neighborhood of fuel elements it amounts to from 1 % to 3 %. This also applies for the factor F. In view of these facts it does not seem necessary to reduce the uncertainty in the flux density determination of the standard.

1.4 International intercomparison of thermal flux density standards

From 1966 to 1968, an international intercomparison was undertaken, which was initiated by the International Bureau of Weights and Measures (BIPM) and in which 11 laboratories participated. The results were evaluated by E.J. Axton /3/. Though not all the results of the measurements performed in this intercomparison were consistent it may be stated nevertheless that at that time the values of the unit of thermal flux density as established by the national standard laboratories differed only by about 2 percent.

2. Thermal neutron reference beam

2.1 Characteristics of the beam

This device was described by Kluge and Knauf /4/. A collimated beam of thermal neutrons for which the neutron current density is well known over its cross sections, can be a useful device for the calibration of neutron detectors and dosimeters, especially, if its current density is considerably higher than the flux densities of customary thermal neutron flux density standards, which generally do not exceed 10^4 $cm^{-2}s^{-1}$ To this end a, well collimated beam of thermal neutrons was extracted from the Research and Measuring Reactor FMRB of the PTB. Fig. 4 shows a cross section of the reactor. This is an open tank light water reactor with some special features. Its core consists of two fuel zones, each of which is controlled separately. They are coupled to one other by a 60 cm wide, 80 cm high heavy water tank extending over the entire core width. This heavy water region is penetrated by a through-going beam tube. From this tube, well moderated neutrons may be extracted by means of a scatterer with relatively low fast neutron and gamma ray contamination. The scatterer (beryllium 50 mm dia., 15 mm thick) and

collimator (graphite and lead) arrangement is shown in fig. 5. Final collimation of the beam is achieved by 2 boron wood orifices.

The current density distribution over the beam cross section was determined by means of a lattice consisting of gold wires activated in the beam and cut into pieces of 2 mm length thereafter, the activity of which was measured. In fig. 6 the resulting current density contours are mapped. Within a circle of 20 mm diameter around the beam axis, the current density does not vary by more than $\pm$ 2 %. The degree of collimation can be judged from fig. 7 which shows the course of the current density over the horizontal central cross section of the beam.

At a reactor power of 1 MW, the thermal neutron current density at the target amounts to $1.2 \cdot 10^7$ cm^{-2} s^{-1}, the cadmium ratio as observed with 20 µm thick gold foils of 10 mm diameter is 10.7. The resulting mean spectral energy flux density of intermediate energy neutrons is $\varphi_e = 1.4 \cdot 10^5$ cm^{-2} s^{-1} /5/. Assuming a fission spectrum for the spectral current density of fast neutrons, their current density at the target position is $4.7 \cdot 10^4$ cm^{-2} s^{-1} (see /6/).

2.2 Calibration of detectors of dimensions than the beam

Large volume detectors may be calibrated in the standard beam as described Matzke /5/, by moving the detector stepwise over the beam cross section, measuring its response at each position and determining the overall calibration factor by succeeding integration. The procedure is quite simple for detectors of cylindrical symmetry (see /5/ for details).

References

/1/ M. Matzke und H.J. Bortfeldt: Der Neutronenflußdichtestandard I der Physikalisch-Technischen Bundesanstalt. Metrologia 7, 153 (1971)

/2/ J. Bortfeldt und M. Matzke: Der Flußdichte-Standard II für thermische Neutronen der Physikalisch-Technischen Bundesanstalt. To be published in PTB-Mitteilungen.

/3/ E.J. Axton: Results of Intercomparison of the Thermal Flux Density Unit (1966 - 1968). Metrologia 6, 25 (1970)

/4/ H. Kluge und K. Knauf: Das Kalibrierbündel thermischer Neutronen am Forschungs- und Meßreaktor Braunschweig. To be published in PTB-Mitteilungen.

/5/ M. Matzke: Kalibrierung großvolumiger Neutronendetektoren mit isotrop und einheitlich gerichtet einfallenden thermischen Neutronen. Proceedings Second Symposium on Neutron Dosimetry in Biology and Medicine. Neuherberg/München 1974. EUR 5273 d-e-f.

/6/ W.G. Alberts: Neutronenflußdichten am Forschungs- und Meßreaktor Braunschweig (FMRB). PTB-Mitt. 83, 161 (1973).

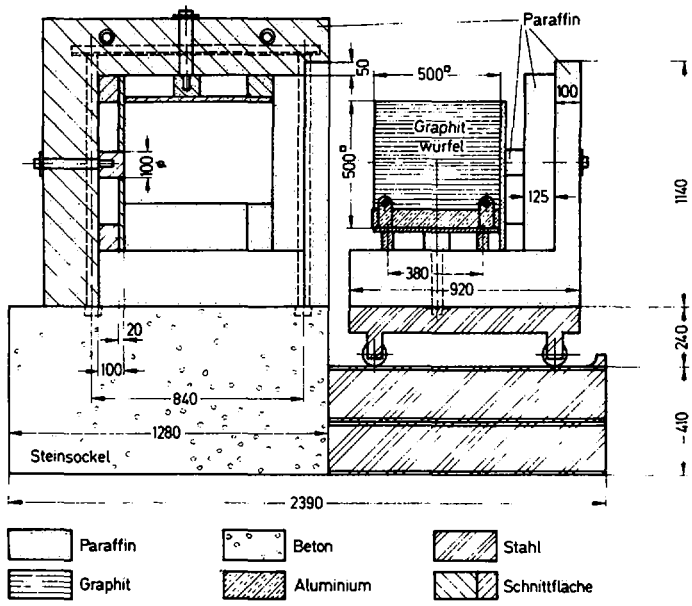

Fig. 1 Cross section of Thermal Flux Density Standard I of PTB

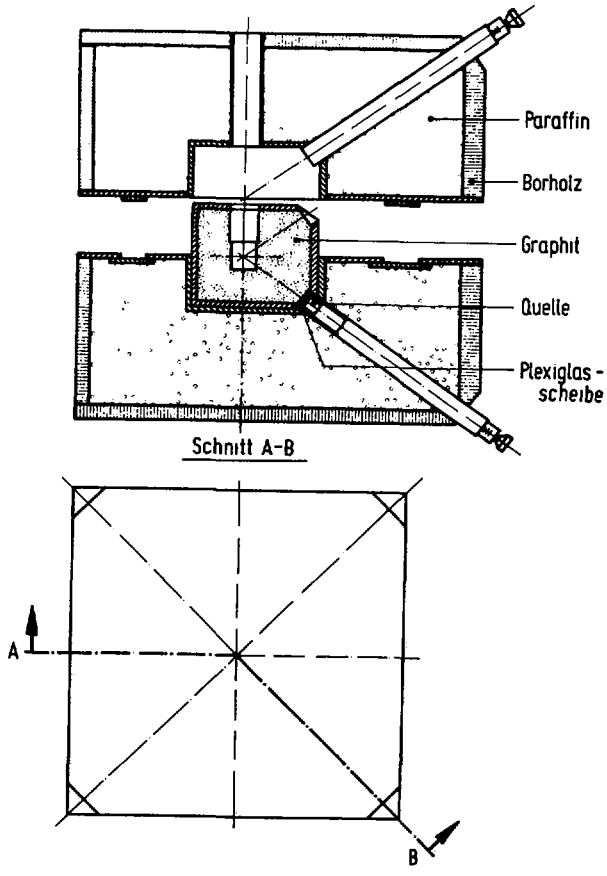

Fig. 2 Thermal Flux Density Standard II of PTB. Cross section A-B in two planes of symmetry.

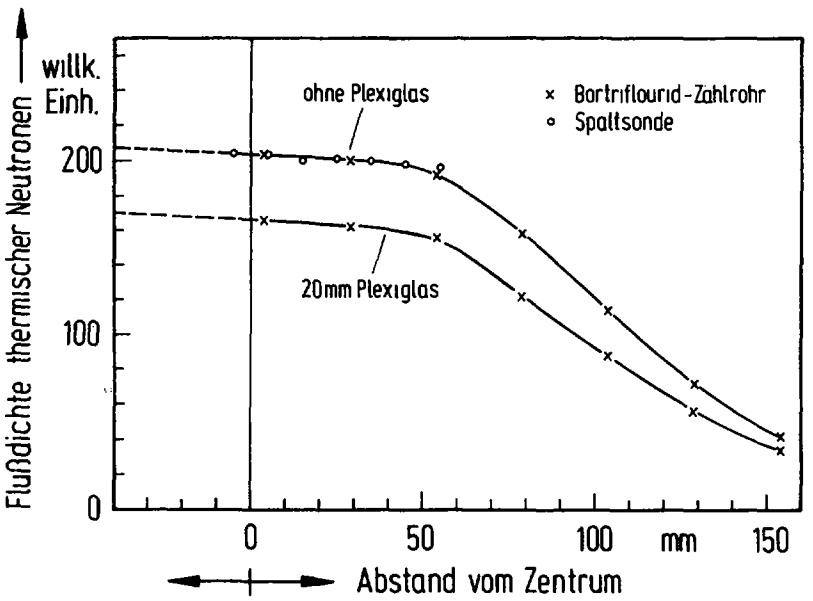

Fig. 3 Flux density of thermal neutrons in the irradiation channel

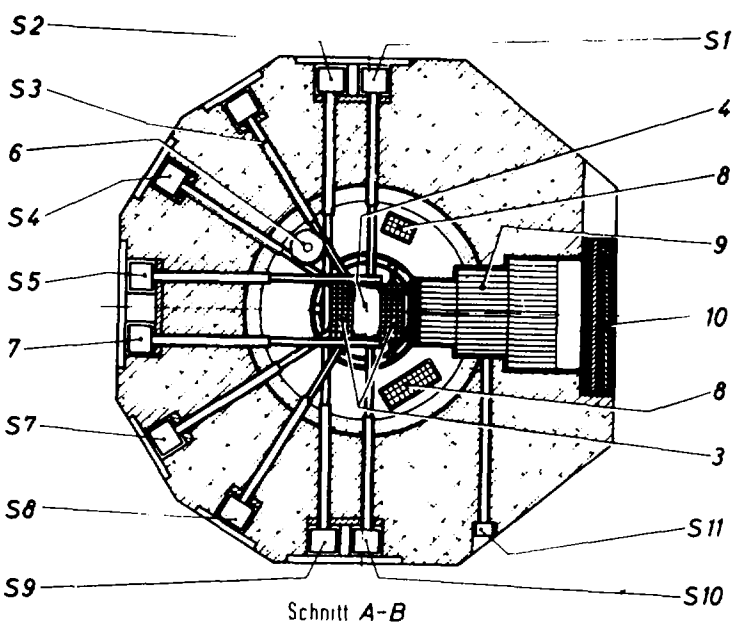

Fig. 4 Cross section of reactor FMRB of PTB

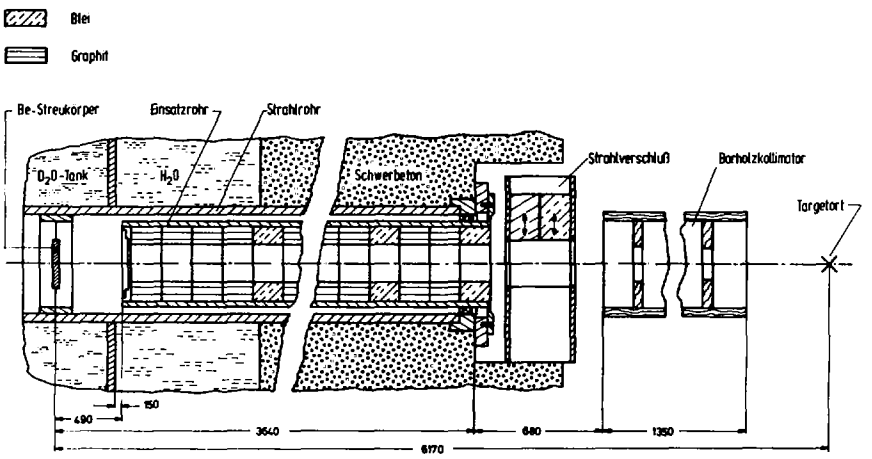

Fig. 5 Collimator arrangement in central beam tube of FMRB

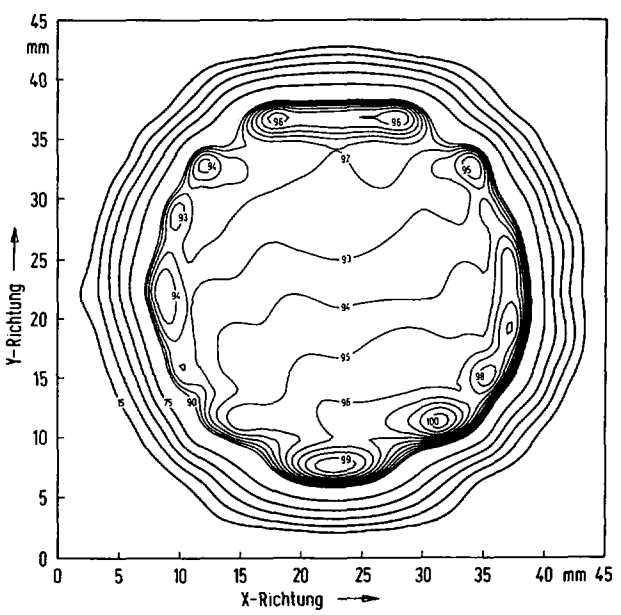

Fig. 6 Thermal neutron flux density contours of standard beam at target position.

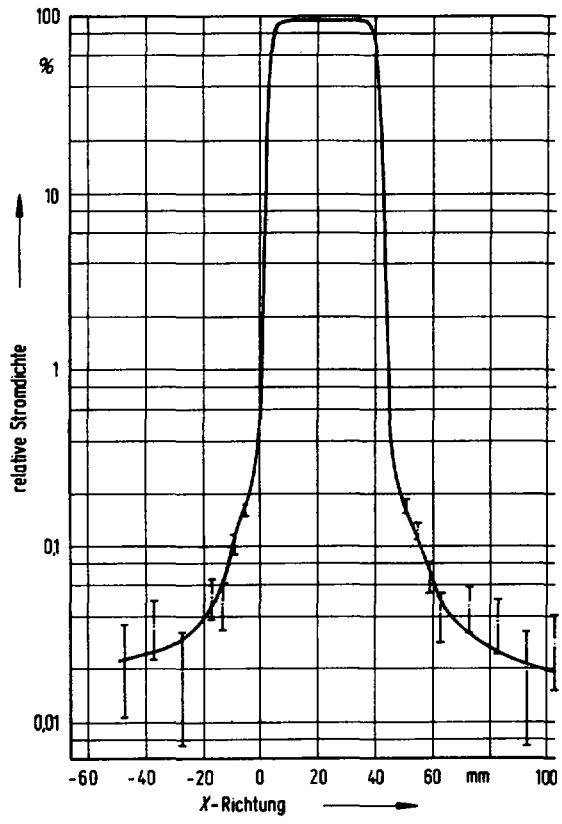

Fig. 7 Horizontal cross section of contour map through the center of the beam.

I.2. Fast Neutron Standards at the PTB

by S. R. Wagner

Physikalisch-Technische Bundesanstalt (PTB), Braunschweig
Federal Republic of Germany

Abstract:

Fast neutron standards realized at the PTB are described. (1) A Ra-Be(α,n) source serves as primary neutron source strength standard. (2) A standard fission neutron spectrum is represented by a ^{252}Cf spontaneous-fission neutron source. (3) Fast neutron standard fields are produced by a 3.75 MV Van-de-Graaff accelerator and an isochronous cyclotron. For the intermediate energy region filtered neutron beams (24.5 keV and 2 keV) are installed at the FMRB reactor.

1. Standards of source strength

Standard neutron sources of well defined and stable source strength are mostly used to calibrate other neutron sources, e.g. for reactor physics applications, or to calibrate neutron detectors with respect to their neutron sensitivity with neutrons of an energy distribution characteristic for the source type. They are mostly of the type Ra-Be(γ,n) and Ra-Be(α,n). ^{241}Am-Be(α,n)-sources are used as secondary standards.

The source strength standard of the PTB is a Ra-Be(α,n) source containing 136 mg Radium. Its source strength B was determined in 1959 by von Droste and Kolb, and in 1960, 1966, 1968 and 1972 by Bortfeldt and Matzke /1/, by the water bath method using gold foil activation. The latest result as per 1. 1. 1972 is

$$B = (2.02_7 \pm 0.02_7) \cdot 10^6 \ s^{-1}$$

at a confidence level of 68 % (taking systematic uncertainties into account). The corresponding relative uncertainty is 1.3 %.

This source participated in an early international intercomparison /5/ which showed that already in 1960 the maximum spread in the realization of the unit of neutron source strength as established by the standard laboratories was only 3.8 %. In later intercomparisons this spread was reduced to 3.0 % /6/. Especially the $MnSO_4$-bath method of source strength determination was further developed and under favor-

able conditions; a relative uncertainty of only 0.7 % is claimed for the results obtained in this way (cf /4/).

Other neutron sources are routinely calibrated as to their source strength by means of a precision long counter relative to the primary standard or a secondary standard, depending on their type. As the sensitivity of the long counter is not perfectly flat as a function of incident neutron energy, and as the energy dependence is not precisely known, only sources of the same type, the spectral distribution of which can be assumed to be sufficiently similar, should be compared by this method. In order to average the anisotropic emission of cylindrical sources, these are rotated around an axis through their center of symmetry perpendicular to the cylinder axis with an angular velocity proportional to $1/\sin\vartheta$ (ϑ being the angle between the cylinder axis of the source and the detector).

Calibrations of neutron sources with spectra differing from that of the standard source are normally performed in a water bath or in a paraffin cube with detectors placed at different distances from the source.

The spectral distribution of the neutrons emitted by the Ra-Be-standard source was determined at the PTB by Kluge /2/ and Zill /3/ in the energy range from 0.25 to 11 MeV (fig. 1). This was the first time that the low energy range of a Ra-Be(α,n) source was investigated experimentally. The observed spectrum showed a large fraction of low energy neutrons as conjectured earlier by De Pangher /15/, Romain et al /16/, and Geiger /4/. Due to these investigations the mean energy of the emitted neutrons was derived to be 2.8 MeV compared to the 3.6 MeV generally adopted until then. The spectral distribution of neutrons from a ^{241}Am-Be(α,n) source was also investigated by Kluge and Zill (l.c.) in the range from 0.2 to 11 MeV (fig. 2). Although the low energy fraction of neutrons was found to be not as large as with the Ra-Be(α,n) source, it nevertheless was large enough to change the mean energy from the 4.3 MeV commonly assumed in the past to 3.9 MeV (and from 4.5 MeV to 3.4 MeV in the case of the ^{239}Pu-Be(α,n) sources, cf. fig. 3; cf. also ref. /14/ for all spectra mentioned and for the mean energies).

2. Californium-252 fission neutron sources as neutron spectrum standard

Although Californium-252 spontaneous fission sources are not suited as source strength standards because of their short half-life, they have earned great merits as fission neutron spectrum standards (see e.g. /7,8/). In most applications, however, the flux density at the place of irradiation and hence the source strength have to be known also to a considerable degree of accuracy. The source strength was determined for the ^{252}Cf-sources of the PTB, each emitting about 10^9 s^{-1}, by the water bath method and gold foil activation with a relative uncertainty of $\pm$ 1.6 % (overall uncertainty at a confidence level of 68 %) /9/. A comparison of ^{252}Cf-source strength determinations at the NBS and the PTB via precision fission chamber measurements (V. Spiegel of NBS) resulted in the following preliminary values*):

method	B_{PTB}/B_{NBS}
PTB: water bath NBS: $MnSO_4$ bath	1.792 $\pm$ 1.5 % (possible correlations not taken into account)
^{238}U-fission chamber	1.802 $\pm$ 0.005
^{235}U-fission chamber	1.799 $\pm$ 0.006

The fission neutron spectrum of ^{252}Cf-sources has been investigated experimentally several times (e.g. /17, 18, 19, 20/) and the agreement reached is quite close. Recent measurements at the PTB, done by proton recoil spectrometry (telescope with gaseous radiator /3/, with solid radiator /2/ and by spectrum unfolding of activation detector measurements, M. Matzke) seem to indicate significant deviations from a pure Maxwellian shape to lower amplitudes, especially in the region between the most probable neutron energy and, say, 2 MeV.

---

*) not yet confirmed by the NBS.

At the PTB, a measurement of amplitude ratios for the fission spectra of ^{235}U, ^{239}Pu (both for thermal neutron fission) and ^{252}Cf still is under way, using the two neutron spectrometers mentioned above for all three spectra in as nearly identical geometry as possible. Preliminary results for ^{235}U and ^{239}Pu are shown in fig. 4 /21/.

3. Fast neutron flux density standards at the PTB

The new laboratory for neutron dosimetry of the PTB was especially designed to provide precisely known fast neutron flux densities over a wide range of well defined energies for calibration purposes in neutron metrology and dosimetry (see ref. /10/ for details of the installation).

Two machines, a 3.75 MV Van-de-Graaff accelerator and an isochronous cyclotron (2 to 24 MeV protons, 3 to 14 MeV deuterons, 5 to 36 MeV $^{3}He^{++}$, 6 to 28 MeV He^{++}), both with special pulse features, feed their beams alternatively into the same system of beam guides. In this way, neutrons over a very wide energy range up to about 30 MeV are available at the same irradiation place. In particular, the familiar "energy gap" between 8 and 12 MeV can be bridged. The Van-de-Graaff accelerator went into operation in 1975, the cyclotron has just been commissioned.

A ground plan of the experimental area is hown in fig. 5. Its heart is a large thick-walled experimental hall 24 m wide, 30 m long, 14 m high with a low-mass floor (aluminium grid) at 4.5 m height. The Van-de-Graaff accelerator is installed in a well shielded room on the same level, whereas the cyclotron is downstairs on the ground of the building, but feeding its accelerated particles into the switching magnet of the beam tube fan (6.25 m above ground) via two 90^{o} bending magnets.

Extensive Monte-Carlo-calculations have been performed to estimate neutron background in the experimental hall. In refs. /11, 12/ details are given for background flux densities, their spectral distribution

and their time dependences being a function of the distance between the target and the detector. The results show that the main contribution of fast neutron background originates in the target for target-detector distances up to about 2 m (for a low mass target construction, up to larger distances for a heavier construction), the influence of the concrete walls being not so serious.

Neutron flux density measurements are performed in the low energy range by means of a proportional counter (filled with H_2, CH_4 or a mixture of both gazes) with pulse-shape discrimination of γ-radiation and correcting for end and wall effects according to the results of Monte-Carlo-calculations. For higher energies, a proton recoil telescope is used. The associated particle method for the neutron source strength determination at the target is in preparation. The first two methods mentioned were applied at the PTB in measurements at 0.900 MeV and resulted in an agreement within 1 %, the estimated overall uncertainties of each method being 3 to 4 %.

Shortly after having been commissioned in 1975, the Van-de-Graaff accelerator took part in an international intercomparison of the unit of fast neutron flux density as realized in the 8 participating laboratories. This action was initiated by the International Bureau of Weights and Measures (BIPM). The intercomparison was performed at neutron energies of 0.25 and 0.565 by means of a ^3He proportional counter als transfer instrument (target distance 50 cm, background negligeable at PTB), and at 2.2, 2.5 and 14.5 MeV (the latter was not used in the PTB) with a BF_3-proportional counter in a 20 cm dia. polyethylen sphere (target distance 150 cm, background determination by distance variation and by measurement with shadow cone), which was also used for the lower energies.

The PTB stated the overall uncertainty of the flux density determinations at 0.25 and 0.565, where the proportional counter was used, as amounting to 3.1 % (for a confidence level of 68 % including statisti-

cal and correspondingly estimated systematic contributions), and as being 2.4 % at 2.2 and 2.5 MeV, where the telescope was used.

The results of the intercomparison have not yet been evaluated by the BIPM. Nevertheless, considerable discrepancies seem to show up from the untreated raw data. The spreads in the values reported are according to my rough estimation:

neutron energy in MeV	transfer instrument	maximum spread
0.250	^{3}He-counter	8 %
	BF_3-counter in moderator	13 %
0.565	^{3}He-counter	6 %
	BF_3-counter in moderator	6.5 %
2.2	BF_3-counter in moderator	10 %
2.5	do.	9 %

It seems as if some more work will be required to render the situation more satisfactory.

4. Intermediate energy neutrons reference beams

In order to bridge the energy gap between thermal neutrons and those which can be satisfavtorily produced by accelerators, say about 50 keV, two filtered beam facilities are being installed at the FMRB-reactor of the PTB, a scandium filter for 2 keV-neutrons and an iron filter for 24.5 keV (neutron current density in the order of several 10^3 cm^{-2} s^{-1}) which will be available for calibration purposes in the mid of 1977 (W.G. Alberts and K. Knauf).

References

/1/ J. Bortfeldt and M. Matzke: Die Quellstärke der Standard-Neutronenquelle der Physikalisch-Technischen Bundesanstalt. PTB-Mitt. 84, 254 (1974)

/2/ H. Kluge: Das Neutronenspektrum radioaktiver Be(α,n)-Quellen im Energiebereich oberhalb 1 MeV. Z.Naturf. 24a, 1289 (1969)

/3/ H.-W. Zill: Das Neutronenspektrum radioaktiver Be(α,n)-Quellen im Energiebereich unterhalb 1 MeV. Z.Naturf. 24a, 1287 (1969)

/4/ K.W. Geiger, R. Hum, and C.J.D. Jarvis: Neutron Spectrum of a Ra-Be(,n) Source. Can.J.Phys. 42, 1097 (1964)

/5/ E.J. Axton: Neutron-Source Calibrations: A Review. Nucl. 19 No. 3, 90 (1971)

/6/ K.W. Geiger: Recent improvements in the Absolute Calibration of Neutron Sources. Metrologia 4, 8 (1968)

/7/ W.G. Alberts, J. Bortfeld, E. Günther, K. Knauf, M. Matzke, G. Rassl, V. Siegel, and K.F. Walz: Measurement of Cross Sections for Threshold Reactions induced by Californium-252 Spontaneous Fission Neutrons. Proceedings of a Conference "Nuclear Cross Sections and Technology". National Bureau of Standards Special Publication 425, Washington 1975, p. 273

/8/ J.A. Grundl, V. Spiegel, C.M. Eisenhauer, H.T. Heaton, II, D.M. Gilliam, J. Bigelow: A Californium-252 Fission Spectrum Irradiation Facility for Neutron Reaction Rate Measurements. To be published in Nucl. Techn.

/9/ M. Matzke: Source Strength Determination of Californium-252 Sources. Symposium International sur l'Utilisation du Californium 252, Paris 26 - 28 Avril 1976.

/10/ M. Cosack, R. Jahr, H. Schölermann, R. Taubert und E. Waibel: Das Projekt "Neutronendosimetrie" der Physikalisch-Technischen Bundesanstalt. PTB-Mitt. 81, 343 (1971).
H. Schölermann, M. Kutscha: Eigenschaften des gepulsten 3.75 MV-Van-de-Graaff Beschleunigers. PTB Jahresbericht für 1974, Ber.Nr. 6.16, S. 226
H.J. Brede, R. Jahr: Eigenschaften des gepulsten CV-28-Kompaktzyklotrons. PTB Jahresbericht für 1974, Ber.Nr. 6.17, S. 226

/11/ H. Schölermann: Berechnung des Anteils von Streuneutronen an verschiedenen Meßplätzen in der geplanten Experimentierhalle des Bauvorhabens Neutronendosimetrie der Physikalisch-Technischen Bundesanstalt. PTB-Bericht Neutr.-Dos. 1/70, Braunschweig, März 1970

/12/ G. Dietze, R. Jahr and H. Schölermann: Effect of Neutron Background on the Standardization of Neutron Fields. Proceedings of the First Symposium on Neutron Dosimetry in Biology and Medicine, Neuherberg/München, May 1972, EUR 4896 d-f-e, p. 912

/13/ M. Cosack, M. Kutscha and A. Paulsen: The Proton Recoil Proportional Counter as a Device to Measure Neutron Fluxes at Energies below 100 keV. l.c. /12/, p. 267

/14/ H. Kluge, K. Weise, H.W. Zill: Measurement of Spectral Distribution from Radioactive sources and Uranium-235 Fission, and the Resulting Fluence-Dose Convosious Factors. Neutron Monitoring for Radiation Protection Purposes, IAEA, Wien 1973, Vol. I, p. 13

/15/ J. De Pangher: Double moderator neutron dosimeter. Nucl.Instr.Meth. 5, 61 (1959)

/16/ F.A. St. Romain, T.W. Bonner, R.L. Bramblett, and J. Hanna: Low-energy neutrons from the reaction $^{9}Be(\alpha,n)^{12}C$. Phys.Rev. 126, 1794 (1962)

/17/ L. Green, J.A. Mitchel, and N.M. Steen: The Californium-252 Fission Neutron Spectrum from 0.5 to 13 MeV. Nucl.Sci.Eng. 50, 257 (1973)

/18/ H. Werle and H. Bluhm: Fission-Neutron Spectra Measurements of ^{235}U, ^{239}Pu and ^{252}Cf. J.Nucl.En. 26, 165 (1972)

/19/ H.H. Knitter, A. Paulsen, H. Liskien, and M.M. Islam: Measurements of the neutron energy spectrum of the spontaneous fission of ^{252}Cf. Atomkernenergie 22, 84 (1973)

/20/ J.A. Grundl and C.M. Eisenhauer: Fission Spectrum Neutrons for Cross section Validation and Neutron Flux Transfer. Proceedings of a Conference "Nuclear Cross Sections and Technology". National Bureau of Standards Special Publication 425, Washington 1975, Vol. I, p. 250

/21/ H. Kluge, K. Weise, H.W. Zill: Verhältnis der spektralen Stromdichten für Neutronen aus der Spaltung von ^{239}Pu und ^{235}U durch thermische Neutronen. PTB Jahresbericht für 1975, Ber.Nr. 3.7.2, S. 253.

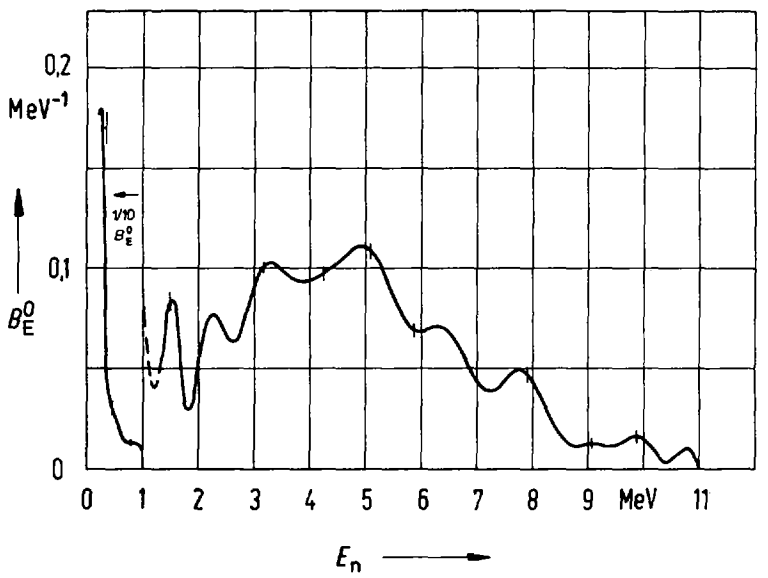

Fig. 1 Observed neutron spectrum of a Ra-Be(α,n) source

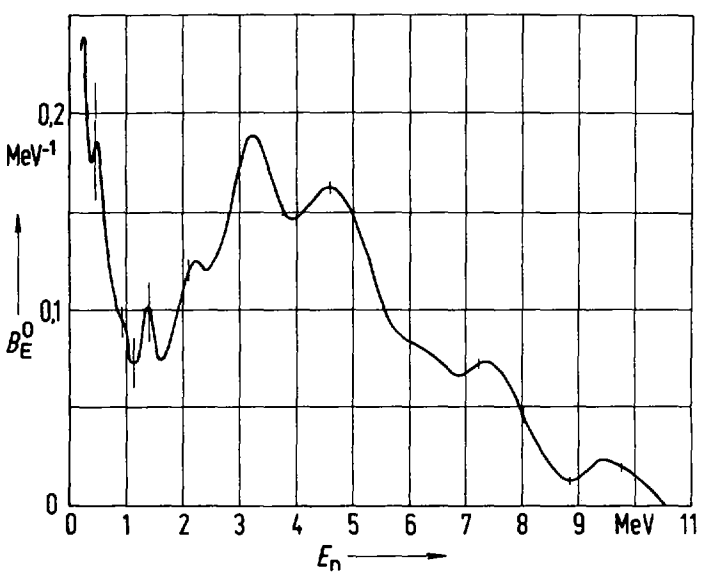

Fig. 2 Observed neutron spectrum of a ^{241}Am-Be(α,n) source

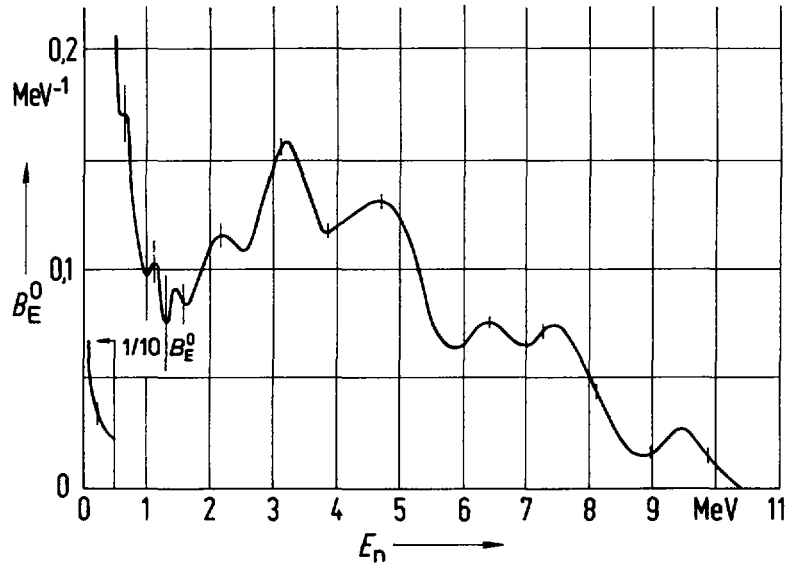

Fig. 3 Observed neutron spectrum of a ^{239}Pu-Be(α,n) source.

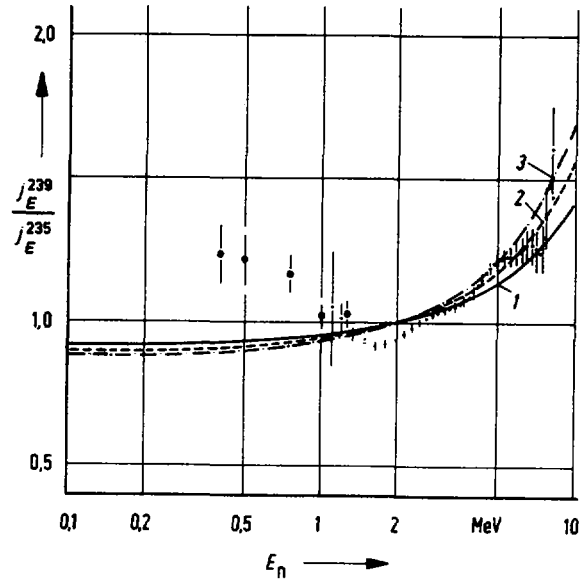

Fig. 4 Spectral neutron current density ratios j_E^{239} (^{239}Pu thermal fission) to j_E^{235} (^{235}U thermal fission) as function of neutron energy E_n /21/.
⊙ ⊙ ⊙ proton recoil telescope with gaseous radiator /3/,
..... proton recoil telescope with solid radiator /4/.
Calculated ratios assuming as Maxwell distribution

$$j_E/j = \frac{2}{\sqrt{\pi}\, T^{3/2}} \; E \exp(-E/T)$$

curve 1: T = 1.39 MeV for ^{239}Pu
T = 1.31 MeV for ^{235}U

curve 2: T = 1.39 MeV for ^{239}Pu
T = 1.29 MeV for ^{235}U

curve 3: T = 1.40 MeV for ^{239}Pu
T = 1.28 MeV for ^{235}U

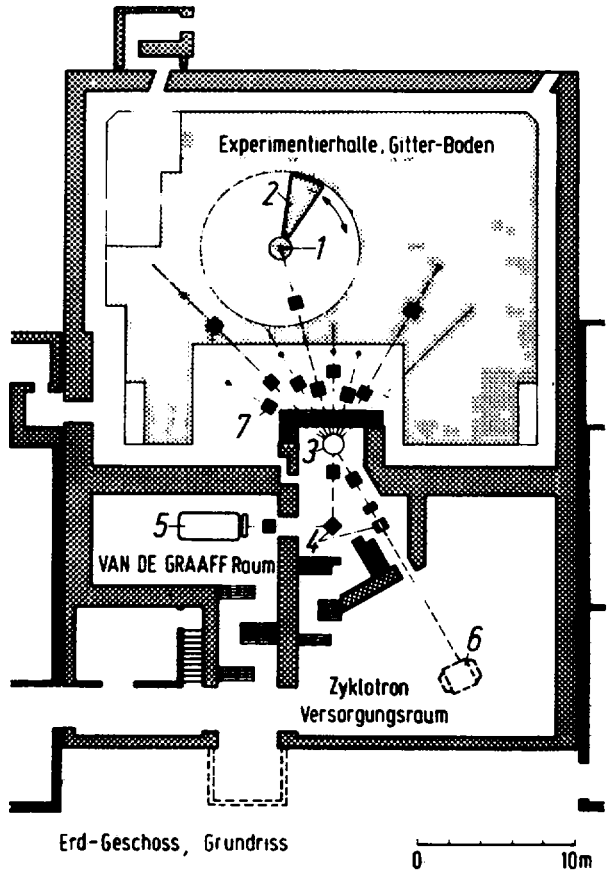

Fig. 5 Neutron Dosimetry Laboratory of PTB. Ground Plan of experimental hall an adjoining accelerator housings

I.3. A CALIFORNIUM-252 FISSION SPECTRUM IRRADIATION FACILITY FOR NEUTRON REACTION RATE MEASUREMENTS

J.A. Grundl, V. Spiegel, C.M. Eisenhauer,
H.T. Heaton, II, D.M. Gilliam
National Bureau of Standards
Washington, D.C. 20234

J. Bigelow, Oak Ridge National Laboratory
Oak Ridge, TN 37830

This report was presented by J.A. Grundl and is published in Nuclear Technology, 32, 315 (March 1977). Here only the abstract is given.

ABSTRACT

Spontaneous fission sources of ^{252}Cf, lightly encapsulated and with neutron source strengths approaching 10^{10}n/sec, have been developed especially for integral cross section measurements and neutron reaction rate calibrations. An irradiation facility at the National Bureau of Standards makes use of these sources in two well-investigated geometries. A free-field neutron flux in the range of 10^{7}n/cm^{2} sec and fluences of up 10^{13}n/cm^{2} are established at the facility based only upon a distance measurement and the absolute source strength of the national standard Ra-Be photoneutron source. The error in the ^{252}Cf source strength ($\pm$ 1.1%) dominates the total free-field flux uncertainty of $\pm$ 1.4% (1σ). Neutron scattering effects in the source capsule and support structures, and neutron return from concrete and earth boundaries have been calculated and investigated experimentally. In the worst case they contribute $\pm$ 0.7% to the total flux response uncertainty for all observed neutron reaction rates, including those with sensitivity to low-energy neutrons.

I.4. The IAEA Programme on Intercomparison of the Computer Codes for Neutron Spectra Unfolding by Activation Technique

Progress report by B. Cross, IAEA

Since this is a progress report I will make it informal; if you have questions, please ask them. One of the reasons of presenting such a progress report is to sollicit suggestions and ideas from the assembled experts.

At the Workshop in Petten last year it was recommended that the IAEA undertake an effort in determining the usefulness of the spectral unfolding codes to determine the neutron spectra from activation of foils. This project was undertaken initially by Dr. Czock at the Agency - unfortunately, Dr. Czock just had a chance to start this activity before his contract expired. Since then we have not had a chance to do much except get some ideas as to how we should proceed. What I would like to do is to tell you what we are hoping to do in the future, the plans that we have, the techniques we hope to use to evaluate these codes and tell you what Dr. Czock's replacement will be doing in the next two years.

The basic problem is: given a set of activities which can be calculated by the realtionship $A_i = \int_0^\infty \sigma_i (E) \varphi(E) dE$, calculate the flux spectrum in which these foils were irradiated. This is a standard problem which has been addressed by several codes. Various intercomparisons of these codes have been performed. There is one which was based on a recommendation of the IAEA Working Group on Reactor Radiation Measurements, in April 1971, which was reported by Fischer in 1974. There was a Consultants Meeting on Nuclear Data for Reactor Neutron Dosimetry held at the Agency in which Dr. Dierckx gave a paper on some work that he did. The International Working Group

on Reactor Radiation Measurements in Petten, September 1975, recommended that the IAEA continue to promote the use of multiple foil technique for neutron flux spectrum determination and made several recommendations as to what the Agency could do.

The previous intercomparisons have suffered from various faults either in techniques employed or their basic design. In summing up his report in 1974 Fischer stated that "the goal of the project has only partially been reached". Some of the problems that he mentioned were:

1) The participants used very different energy point systems; the influence of the energy point number on the results has up to now not satisfactorily been investigated.

2) Participants use their own cross section libraries.

3) The actual spectrum in which the activities were determined was not exactly characterized because it was an experimental situation.

We have an approach which I believe has been tried before but which we would like to try again and it hopefully will be acceptable. It is on this that I would like to have your comments and criticisms so that we can undertake an effort which will be of use in the field.

The problem is that the activities which are obtained have in the past frequently been obtained in an experimental manner; in obtaining these activities, you have counting error statistics. These you were trying to match up with an experimentally determined spectrum; you do not know exactly what it is, since it is experimentally determined. What we would like to do is to perform a mathematical checking of the codes by:

1. provide a series of artificial spectra (so that we know exactly what the correct solutions to the unfolding will be),
2. use a single cross-section library (it does not really make any difference what it is, ENDF/B, SAND-II or any others, just so we use a single cross section library),
3. perform the convolution to calculate exact activities (this would correspond to a SAND-II ACTIVITY run), and
4. using these exact activities we perform the deconvolution using various initial guess spectra (this would correspond to a series of SAND-II ITERATION runs).

(The reason why I speak of SAND-II is that this is the code that we currently have operational here.) From these SAND-II iteration runs we get out a resultant spectrum. If the code is infinitely precise, and we have computers with infinite precision, and the world would be nice, we should get the result $\Psi' = \Psi$, that the flux spectrum that we get out is equal to the spectrum that we put into the ACTIVITY run. Experience has shown that this is rarely the situation and that the output spectrum differs quite a bit from the true solution. What we want to investigate is how the "quality" of the solution spectrum is effected by the various input factors, specifically the input guess, the coverage of the foils, the number of foils, and errors in the foil activities. It is very rare in the real world that an exact determination of the flux spectrum is necessary; the quality of the spectrum required will be determined by what use you are going to be putting it to; you are going to hope that the degree of closeness in the region of interest will be adequate for what you are interested in. As far as we could tell with our research through the literature, there have been several attempts to quantify this, Fischer's alpha parameters among others and the technique of absolute and relative differences. However, as far as we can tell there is no accepted technique which would permit a quantitative intercomparison of the codes. If somebody develops a new code, which he claims is better than all the others, how can he be checked? What we would like to do is to develop a technique which will permit people to check the quality of one code against another using various parameters.

Unfortunately we have not yet been able to decide on any parameters that are adequate for this situation. This was the plight which Dr. Czock left and in which, unfortunately, the program has been in a holding pattern until his successor, Dr. Ertek, arrived.

At this point I guess I will appeal to the audience for their ideas, suggestions and comments. Perhaps you have performed inter-comparisons at your laboratories which you think are along the same line, or perhaps you know of additional intercomparisons which have appeared in the literature. Perhaps you have ideas which have not appeared in either place that you would like to give here.

Discussion:

Q.: How to chose the guess spectra?

A.: We will chose the "standard" spectra for various types of reaction, modify them to various degrees, and use these to calculate the activities . Input to the deconvolution runs would then be the unmodified "standard" spectra.

Q.: In these codes you have to input a guess spectrum, which requires a calculation or judgement about the type of spectrum. If the judgement of the person running the code is not sound, the guess spectrum could be significantly different from the correct solution.

A.: This is one of the tests which would have to be made and also the effect of the input guess upon the resultant spectrum - the sensitivity of the code to cross-section coverage with respect to the range of interest.

Q.: One useful parameter to check would be the activity of a detector which was not in the set you used to perform your deconvolution, especially detectors with "rather unpleasant" cross-section profiles.

A.: A good idea.

Q.: One weakness in the evaluation procedure you propose is that your activities are consistent which is not the case in actual life.

A.: After the initial evaluation step, we were planning to address this problem by adding random errors to the activities to investigate this effect on the codes.

Q.: Why don't you take a spectrum which has been measured by other techniques?

A.: It has no advantages over a synthetic spectrum.

Q.: But then you have measured activities, estimates of errors, etc.

A.: We want to start playing with an exact game. Obviously, we have to get back to the real world once we have developed our techniques for evaluation. To evaluate the codes, the exact game is necessary; to evaluate the codes' usefulness, we must get back to the real world.

I.5. Comparison of Neutron Spectrum Unfolding Codes

Willem L. Zijp
Jan H. Baard
Henk J. Nolthenius

Summary:

This report is the second progress report* on the comparison of three neutron spectrum unfolding codes: CRYSTAL BALL, RFSP-JÜL and SAND-II.
In this report the response of the codes for an input with only a few activity values was considered.
Also attention has been given to the influence of the convergence criterium for runs with CRYSTAL BALL and RFSP-JÜL.
The calculations have been performed for the STEK-4000 neutron spectrum using an old version of a SAND-II library, which was modified to take into account the self-shielding effect.
The results which are presented comprise the solution spectra, the improvement ratio and the ratios of output and input spectra.

*) The first progress report is published as RCN-76-059,(see Reference 2).

1. INTRODUCTION

This report describes the results obtained with three unfolding codes for an input deck which comprise only a few activity values. The calculations have been performed with three unfolding codes: CRYSTAL BALL, RFSP-JÜL and SAND-II.
The calculations had the aim to provide information on the behaviour of the codes in those energy regions where there is only poor detector response. In some calculations the input values for the measured activities were modified in order to study the behaviour of the codes under these circumstances.
Furthermore attention has been given to the influence of the convergence criterium for runs with CRYSTAL BALL and RFSP-JÜL
Comparison of the results of a series of runs gave information on the properties of the different solutions obtained for the various criteria and programs.
In all calculations use is made of the input data and the activity values (see table 1 and fig. 1) obtained for the STEK-4000 core (see ref. |1|).
The cross section data applied in the calculations were obtained from an old SAND-II library with cross sections, modified to take into account the effect of neutron selfshielding in the activation detectors.
The treatment and presentation of results is the same as in the previous progress report on the intercomparison of unfolding procedures |2|.
All calculations have been performed with the soft-ware described in |2| using a CDC-6600 computer.

2. CONVERGENCE CRITERIA FOR THE UNFOLDING CODES

The three unfolding codes have different methods to check whether the spectrum results after an iteration step fulfil the required agreement with the input data.

In the program CRYSTAL BALL the iteration procedure is ended if the "average relative deviation" is smaller than a specified number. This average relative deviation (ARD) is defined by the relation:

$$ARD = \left(\sum_{i=1}^{n} \left(\frac{A_i^m - A_i^c}{s_i^m} \right)^2 / n \right)^{\frac{1}{2}}$$

with:

- n number of input activity values;
- A_i^m measured activity (input value);
- A_i^c calculated activity at the last iteration step;
- s_i^m estimated uncertainty of the input activity.

A value of 1 for the ARD seems to be reasonable. In this case the average deviation of measured and calculated activity will be equal to the uncertainty in the input activity value.

In the program RFSP-JÜL the iteration procedure is ended, if the "mean activity error limit" (ERRE) is smaller than a given number.
This ERRE value is defined by the relation:

$$ERRE = \frac{1}{n} \sum_{i=1}^{n} \left| \frac{A_i^c - A_i^m}{A_i^m} \right|$$

It will be clear that in this case the choice of ERRE is somewhat difficult, but a value equal to the average of the estimated uncertainties of the input activities seems reasonable.

In the program SAND-II the iteration procedure is ended if the "deviation" parameter is smaller than a given number. This deviation (DEV) is defined by the relation:

$$DEV = S = \left[\sum_{i=1}^{n} \left\{ \left(\frac{A_i^m}{A_i^c} \right) - \overline{\left(\frac{A_i^m}{A_i^c} \right)} \right\}^2 / (n-1) \right]^{\frac{1}{2}}$$

A suitable choice for the value of DEV can be obtained for instance as the average of the estimated uncertainties of the input activities.

The three convergence criteria of the programs have no simple relationships.
To facilitate a comparison the DEV values (as used in the SAND-II program) were also calculated for the CRYSTAL BALL and the RFSP-JÜL solutions.

3. THE SPEED OF CONVERGENCE

The speed of convergence of CRYSTAL BALL and RFSP-JÜL can be influenced by the experimenter, while the speed of convergence of the SAND-II is always fixed.

An advantage of the adjustment of the speed of convergence is that the convergence criterium can be reached in a reasonable number of iterations. The CRYSTAL BALL and RFSP-JÜL code however can both yield rather easily "too good" output spectra.

The qualification "too good" refers to those spectra for which the S value is appreciably smaller than the value of the deviation parameter specified in the input.

If in that case the speed of convergence is decreased a more realistic S value can be obtained.

In practice often more iteration steps are required to reach the solution with the decreased speed of convergence.

The number of iterations is of interest since it is directly related to the computer time required to finish a job. This holds especially for CRYSTAL BALL.

For these reasons one should try to make an appropriate choice of the speed of convergence. The speed of convergence is adjusted with the parameter γ_0 in CRYSTAL BALL, and with the parameter ω in RFSP-JÜL.

When the parameters ω and γ_0 are decreasing, the convergence speed will in general increase.

The actual value of γ_0 in CRYSTAL BALL is also determined by the "DECREMENT" and "INCREMENT" factors to be specified in the input information.

The first factor prescribes the maximum change of the γ_0 value in each iteration step (after the first step, which is a spectrum normalization step).

The second factor corrects the γ_0, if a negative flux density value in the output spectrum is detected; a new output spectrum without negative values is then calculated for the γ_0 value multiplied with the increment factor.

4. INFLUENCE OF THE CONVERGENCE CRITERIUM FOR CRYSTAL BALL

Several runs have been performed with CRYSTAL BALL to calculate the neutron spectrum of the STEK-4000 facility. The input activities (for 15 reactions) and the best available information for the input spectrum were the same as described earlier |1|.
In these calculations a SAND-II cross section library modified for neutron selfshielding was applied (CCG-112B). The errors in the activities which had to be specified, were chosen equal to 4% for all activities.
The γ_0 and decrement and increment factors were chosen in such a way that the number of iterations (k) became >1; the maximum number of iteration in this series was 6.
The S and ARD values and the number of iterations obtained and the ratios of output and input spectra are shown in figures 2a...2g. From these figures the influence of the choice of the convergence criterium can be seen.
A high value for ARD gives small modifications while a low value gives appreciable corrections and often structure in the solution spectrum.
If the uncertainties in the activity values are given correctly and not arbitrarily as in these calculations, then the value 1 for the ARD will give a good solution, from the point of view of counting errors.
In figure 2h the normalized ratio of the output spectra which are obtained with ARD=1.08 and 0.926 is presented. The normalization is based on 10 values at the low energy side of the spectrum. This plot shows that the ARD=1 value has to be reached rather accurately to obtain a well defined solution. The deviation of the output spectra which are obtained for these two ARD values has a maximum of roughly 10% in these runs.

5. SOME CALCULATIONS WITH RFSP-JÜL

Several runs have been performed with the RFSP-JÜL program. These runs give information on:

- the influence of the speed of convergence on the improvement ratio and on the ratio of calculated and input spectrum;
- the improvement ratios calculated for input sets with various number of activity values;
- the influence of the standard deviation of the input activity values on the improvement ratios;
- the influence of the magnitude of the sine spectrum modifying function on the improvement ratios.

The input data applied in these calculations are the same as those mentioned previously. The uncertainties in the activities were 1% during these calculations.
The spectrum data were converted to a 50 energy group structure. In this conversion two successive $\phi(E)$ input values were interpolated with a linear function on $\phi(u)$ scale.
The results of the calculations are presented in figures 3 and 4. In these figures the improvement ratio and the ratio of output and input spectrum are plotted next to each other.
Due to a small mistake the improvement ratios were calculated with an amplitude of the sine function of 10% instead of 1% as intended [3].
The influence of this value was considered by performing two runs one with an amplitude of the sine function of 10% and one with an amplitude of 1% (see further 5.4).

5.1. Influence of the speed of convergence

In the figures 3a...3d the improvement ratios and the ratios of output and input spectrum are presented for a set of 15 detection reactions.
The speed of convergence is varied by using various values of ω (0, 5...30).
The number of iterations required to fulfil the convergence criterium varied from 1 to 21. These results showed that the improvement ratios and the flux density ratios are rather independent of the ω value.
For the smallest ω value, however, we observed a lower improvement ratio, while the general shape of the flux density ratio curve remains unchanged.
The reason of the change of the improvement ratio for low values of ω is not yet known.
In two plots (figure 4a and 4b) the improvement ratio and flux density ratio are calculated for only two input activity values (Co and Ni).
The improvement ratio for the small value of ω is also appreciably lower than the other improvement ratio while the flux density ratio curve remains also nearly unchanged.

5.2. Improvement ratio for various numbers of activity values

The plots of figure 3a, 3c, 4a and 4d give the improvement ratio for different number (n) of input activities. The plots (fig. 3a and 3c) give the improvement ratio for the set of 15 input activity values.
Figure 4c and 4d show three improvement ratios and flux density ratios. The improvement ratios were calculated with activity values of the reactions U(n,f) + Ni(n,p), U(n,f) + Co(n,γ) + Ni(n,p), and Co(n,γ) + Ni(n,p).
Figure 4a and 4b give the improvement ratio and flux density ratio for an input activity set with two values (for Co(n,γ) and Ni(n,p)).
It was expected that the improvement ratio for input activity sets with only a few reactions would be rather high especially at those positions with a rather large response of the reactions of interest.
The reason of this expectation was that no large influence on the corrections of the spectrum could be expected from other detectors having responses in clearly other energy regions.
From these series of plots it follows that rather low values of the improvement ratio are obtained for an input with only a few reactions. For this input set the improvement ratio is only larger than 1 for a few small energy regions. The reason of the small values of the improvement ratio for input activity sets with only a few values is not yet clear.

5.3. Influence of the standard deviation of the activities

Some calculations were done to study the influence of the magnitude and the sign of activity deviations on the calculated improvement ratio. For this reason the available activity values were modified in a few runs.
The results for the original activity values for the Ni(n,p) and the Co(n,γ) reactions are presented as the plots in figure 4a and 4b.
The S_o value gives the S-value for the input spectrum.
The two pairs of plots presented in figure 5 show the influence of a slight increase of the activity of the Ni(n,p) reaction and a decrease of Co(n,γ) value (figure 5a and 5b) and the opposite in figure 5c and 5d.
From these two pairs of plots no clear change in the improvement ratio can be seen.

The set of plots presented as figure 6c and 6d re obtained with the two activity values changed with about 40% in opposite directions. The change in the improvement ratio seems to be unimportant.

5.4. Influence of the amplitude of the sine function

Due to a small mistake the improvement ratio for the program RFSP-JÜL was calculated with an amplitude (A) of the sine variation of 0.1, while in the other programs a value of 0.01 was applied.
Two runs were performed to see the influence of the amplitude A of this variation. The results are the two sets of plots presented as figure 5c, 5d, 6a and 6b. From these results can be seen that this magnitude does not have a strong effect on the calculated improvement ratio.

6. NEUTRON SPECTRA CALCULATED WITH TWO OR THREE ACTIVITY VALUES

Several calculations have been performed with a rather small set of input activities. The neutron spectrum for the STEK-4000 facility is calculated with the three programs of interest.
The activity errors needed in CRYSTAL BALL and RFSP-JÜL were chosen as 4% and 1% respectively. Runs with two and three input activities were done. These series of runs were aimed to obtain some characteristics of the programs for simple input activity sets.
The results of the calculations are presented in figures 7...10 and in table 2 and 3.

6.1. Two activity values

The results for two activity values originating from $^{235}U(n,f)$ and $^{58}Ni(n,p)$ are presented in figure 7 and in the left part of table 2.

6.1.1. Improvement ratios

The improvement ratios obtained with the different programs show different shapes. The programs CRYSTAL BALL and SAND-II have both improvement ratios which in some energy regions become smaller than 1.

These values < 1 are obtained for energies smaller than 10^{-7} MeV and in the region from 10^{-2} - 1 MeV.
In figure 8 and table 2 results are presented obtained with the activity values from the reactions $^{57}Co(n,\gamma)$ and $^{58}Ni(n,p)$.
The improvement ratios of the programs CRYSTAL BALL and SAND-II show here also the same behaviour.
The improvement ratio for RFSP-JÜL is relatively small and in most energy regions equal to 1.
A value somewhat larger than one is obtained at the resonance energy of $^{59}Co(n,\gamma)$ at 0.132×10^{-3} MeV and in the response region of the $^{58}Co(n,p)$ reaction (e.g. above 0.920 MeV).
The reason of the high improvement ratio for this program in figure 7 is probably the rather broad resonance energy region for $^{235}U(n,f)$ (e.g. from about 10^{-6} to 10^{-4} MeV) where many peaks with roughly the same height occur.
The influence of the sharp resonances of $^{59}Co(n,\gamma)$ can also be seen in the improvement ratios calculated with the programs CRYSTAL BALL and SAND-II.

6.1.2. Flux density ratios

A comparison of the flux density ratios obtained in figure 7 and 8 shows the difference in modifying properties of the three programs. In figure 8 the most important response is obtained at the resonance of $^{59}Co(n,\gamma)$ and above about 1 MeV. Between these energy values the response is rather small.
In the flux density ratios these points are clearly visible in the CRYSTAL BALL and RFSP-JÜL flux density ratio plots.
The type of modification of the input is different for the three programs.

CRYSTAL BALL:

The modification between the points with clear detector reponse is a smooth function and in this case more or less linear. The $Co(n,\gamma)$ resonances at higher energies seem to have no influence (10^{-3} - 10^{-2} MeV).
Below and above these energy values the modification remains constant.

RFSP-JÜL:

The modifications are only present at the energy values where detector response is available.

Furthermore the modification seems to be proportional with the detector response; e.g. in the energy regions where only information from one detector is present energy dependent modifications are performed.
In the energy regions with rather small detector response no modifications are found (neglecting the normalization).

SAND-II:
The modifications in the spectrum are for this case a step function. The step is found at the threshold energy of the fast reaction.
The magnitude of the overall modification difference between the points with important detector response is the highest for RFSP-JÜL and the smallest for CRYSTAL BALL.
This effect is probably due to the influence of the spectrum modifications which may be performed in the energy regions with small response.

The results presented in figure 7 show the same effects as mentioned above. In this case the resonance region of $^{235}U(n,f)$ is broader and relatively lower. These effects can be seen in the improvement and flux density ratios.
The sharp change in the flux density ratio of CRYSTAL BALL is not present in figure 8. The modification by RFSP-JÜL in the resonance region is also extended over a broader energy region.

6.2. Three activity values

The results obtained for three activity values in the input of the programs are presented in figure 9 and 10 and table 3.
The activity values were selected in such a way that the response in the lower energy region was determined either by two important resonance response peaks or by a sharp resonance peak and rather broad resonance response; e.g. the combination of $Mn(n,\gamma)$ and $^{59}Co(n,\gamma)$ and the combination $^{59}Co(n,\gamma)$ and $^{235}U(n,f)$.
The response in the fast energy region was obtained from the reaction $^{58}Ni(n,p)$.
The main resonances of $^{55}Mn(n,\gamma)$ and $^{59}Co(n,\gamma)$ have energies of 1.32×10^{-4} and 3.37×10^{-4}MeV. The highest resonances of $^{235}U(n,f)$ are found between 10^{-5} and 10^{-4} MeV.

6.2.1. The improvement ratios

The improvement ratios presented in figure 9 and 10 have the same general shape as the ratios presented in figure 7 and 8. Remarkable are the low values obtained with RFSP-JÜL.
The influence of the selection of the two reactions in the resonance region can be seen clearly in the results obtained with the SAND-II program.

6.2.2. The flux density ratios

The ratios presented in figure 9 and 10 have also the characteristics described before. The correction in the region between the points with sharp responses is in this case not strictly linear (fig. 9) in the results of CRYSTAL BALL. This figure shows also that the resonances of $^{59}Co(n,\gamma)$ at 1.32×10^{-4} MeV determines the sharp change in modification, while the resonance region of ^{235}U seems less important.
The solution of SAND-II shows a rather strange effect; some valleys are present in the flux density ratio.
The energy values corresponding with these valleys are the same as the resonance energies of $^{59}Co(n,\gamma)$.
The valleys are nearly equally deep, while the cross section value accompanying the higher resonances are about a factor 100 and 1000 lower than those of the main resonance.

7. DISCUSSION

From the flux density ratios and the improvement ratios which are obtained for a few activity values some characteristics of the codes can be seen.
CRYSTAL BALL modifies the neutron spectrum in such a way that no steep gradients occur in the curve of the modifying factor.
A smooth line is found between two energy values with appreciable detector response.
RFSP-JÜL modifies the input neutron flux density spectrum depending on the response contribution at a particular energy. This effect introduces changes in the shape of the neutron spectrum also in those energy regions, where there is reponse from one reaction only.

SAND-II modifies the input neutron flux density spectrum in such a way that a step is found between the resonance and the fast energy region. The different shape which is found for the improvement ratio found for CRYSTAL BALL and SAND-II compared with the shape found for the improvement ratio obtained with RFSP-JÜL can be understood from the information obtained for the flux density ratios.
The modifying factors calculated with RFSP-JÜL are close or equal to 1 in the energy regions without proper detector response. This property of the program gives an improvement ratio equal to 1 in these energy regions.
The programs CRYSTAL BALL and SAND-II are both able to modify the neutron spectrum in energy regions with negligible detector response.
The curve of the modifying factor is different for both programs.
The jump (which is introduced by SAND-II) in the modifying factor can not be expected when looking at the actual neutron spectrum. For this reason the smooth modifying factor which is obtained with CRYSTAL BALL seems to have the best features under these circumstances.
But the improvement ratio found for the interpolation range shows that in this energy range the improvement is small and in a rather small energy region around 10^{-1} MeV a detoration of input spectrum information is found in these calculations.
Under particular circumstances the program SAND-II (as used here without smoothing) performs modifications depending only on the response. This gives the sharp peaks in the modification ratios. This occurs especially if more resonance detectors are present which have to give different modifications (see fig. 4 and fig. 7).
The solution criteria which are applied in these calculations were not in all cases the same for the three programs.
For a good comparison more attention has to be given to this point in future work.

8. REFERENCES

|1| Zijp, W.L.; Baard, J.H.; Nolthenius, H.J.: "Neutron spectra in the STEK facility, determined with the SAND-II activation technique" RCN-232 (Reactor Centrum Nederland, Petten, September 1975).

|2| Zijp, W.L.; Nolthenius, H.J.: "Progress report, Intercomparison of unfolding procedures (programs and libraries)" RCN-76-059 (Reactor Centrum Nederland, Petten, April 1976).

|3| Fischer, A.; Nolthenius, H.J.; Zijp, W.L.: "Comparison of SAND-II and RFSP-JÜL spectrum unfolding codes for several neutron spectra in the STEK facility" RCN-75-115 (Reactor Centrum Nederland, Petten, September 1975).

Table 1: Input data and convergence criteria

reaction	input activities for:											
	fig. 2 fig. 3	fig. 4a	fig. 4c fig. 4a xxx	fig. 4c	fig. 4c ...	fig. 5a	fig. 6a fig. 5c	fig. 6c	fig. 7	fig. 8	fig. 9	fig. 10
Fe58G01	1.657-17											
Ni58P	1.086-17	1.086-17	1.086-17	1.086-17	1.086-17	1.086-18	8.05-18	1.303-17	1.086-17	1.086-17	1.086-17	1.086-17
Na23G02	2.819-18											
U238G01	6.752-16											
Au197G02	2.073-15											
Co59G02	3.921-16	3.921-16	3.921-16	3.921-16		4.96-16	5.31-16	3.267-16		3.921-16	3.921-16	3.921-16
Mn55G02	1.529-16											1.529-16
Fe54P	8.144-18											
Ti46P	1.092-18											
Ti47P	1.968-18											
Ti48P	2.265-20											
Fe56P	8.682-20											
U238F	3.886-17											
U235F02	2.106-15			2.106-15	2.106-15				2.106-15		2.106-15	
In115N	2.629-17											
CRYSTAL BALL												
interations (k)									2	2	2	2
initial value γ_0	1000								1000	400	700	900
increment factor	10								3	3	3	3
decrement factor	0.1								0.1	0.1	0.1	0.1
act. error	0.04								0.04	0.04	0.04	0.04
ARD	1.08								1.0	0.99	1.0	0.98
S									5.8	5.5	4.8	4.9
RFSP-JÜL												
iterations (k)	6	2	9	8	9	1	1	21	9	9	8	8
ω	2	30	2	2	2	2	2	2	2	2	2	2
S	4.5	1.2	3.7	3.0	4.0	1.7	4.0	4.1	4.0	3.7	3.0	4.7
SAND-II												
iterations (k)	2								1	1	2	1
S	3.5								1.7	0.05	0.98	0.41

Table 2: Neutron flux densities.

group	energy region		2 foils U and Ni (fig. 7)			2 foils Ni and Co (fig. 8)		
			X-BALL	RFSP-JUL	SAND-II	X-BALL	RFSP-JUL	SAND-II
1	.105E+02...	.650E+01	.1269E+11	.12116E+11	**.1306E+11**	.1269E+11	.10515E+11	**.1311E+11**
2	.650E+01...	.400E+01	.8337E+11	.85676E+11	**.8637E+11**	.8336E+11	.82121E+11	**.8667E+11**
3	.400E+01...	.250E+01	.1931E+12	.21219E+12	**.2017E+12**	.1924E+12	.21130E+12	**.2034E+12**
4	.250E+01...	.140E+01	.4886E+12	.43597E+12	**.4950E+12**	.4862E+12	.41606E+12	**.5239E+12**
5	.140E+01...	.800E+00	.5258E+12	.45824E+12	**.4476E+12**	.5217E+12	.41290E+12	**.4642E+12**
6	.800E+00...	.400E+00	.6147E+12	.53867E+12	**.4996E+12**	.6076E+12	.47075E+12	**.3974E+12**
7	.400E+00...	.200E+00	.5351E+12	.48137E+12	**.4445E+12**	.5252E+12	.41948E+12	**.3536E+12**
8	.200E+00...	.100E+00	.4595E+12	.42359E+12	**.3908E+12**	.4482E+12	.36899E+12	**.3109E+12**
9	.100E+00...	.465E-01	.4406E+12	.41783E+12	**.3845E+12**	.4254E+12	.36467E+12	**.3059E+12**
10	.465E-01...	.215E-01	.3949E+12	.38078E+12	**.3538E+12**	.3781E+12	.33464E+12	**.2814E+12**
11	.215E-01...	.100E-01	.3509E+12	.34427E+12	**.3219E+12**	.3315E+12	.30423E+12	**.2561E+12**
12	.100E-01...	.465E-02	.3083E+12	.30781E+12	**.2903E+12**	.2870E+12	.27294E+12	**.2309E+12**
13	.465E-02...	.215E-02	.2663E+12	.26702E+12	**.2568E+12**	.2439E+12	.23981E+12	**.2043E+12**
14	.215E-02...	.100E-02	.2201E+12	.22273E+12	**.2164E+12**	.1979E+12	.20379E+12	**.1722E+12**
15	.100E-02...	.465E-03	.1750E+12	.17620E+12	**.1757E+12**	.1540E+12	.16504E+12	**.1398E+12**
16	.465E-03...	.215E-03	.1265E+12	.12707E+12	**.1291E+12**	.1085E+12	.11962E+12	**.1027E+12**
17	.215E-03...	.100E-03	.8788E+11	.88915E+11	**.9081E+11**	.7340E+11	.71839E+11	**.7224E+11**
18	.100E-03...	.465E-04	.5522E+11	.58328E+11	**.5763E+11**	.4606E+11	.52174E+11	**.4585E+11**
19	.465E-04...	.215E-04	.3201E+11	.34633E+11	**.3359E+11**	.2683E+11	.31813E+11	**.2672E+11**
20	.215E-04...	.100E-04	.1640E+11	.18133E+11	**.1728E+11**	.1378E+11	.16037E+11	**.1374E+11**
21	.100E-04...	.465E-05	.7586E+10	.93314E+10	**.8000E+10**	.6364E+10	.80068E+10	**.6364E+10**
22	.465E-05...	.215E-05	.6369E+10	.72655E+10	**.6721E+10**	.5354E+10	.61572E+10	**.5347E+10**
23	.215E-05...	.100E-05	.4267E+10	.49691E+10	**.4509E+10**	.3587E+10	.42092E+10	**.3587E+10**
24	.100E-05...	.465E-06	.2235E+10	.25902E+10	**.2362E+10**	.1878E+10	.21947E+10	**.1879E+10**
25	.465E-06...	.215E-06	.6716E+09	.86151E+09	**.7098E+09**	.5643E+09	.72838E+09	**.5647E+09**
TOTAL FOR 25 ABBN GROUPS			.5408E+13	.51166E+13	**.4929E+13**	.5182E+13	.45900E+13	**.4223E+13**
THE GROUPS ABOVE AND BELOW THE ABBN GROUPS								
0	.180E+02...	.105E+02	.7395E+09	.68620E+09	**.7596E+09**	.7399E+09	.57823E+09	**.7634E+09**
26	.215E-06...	.100E-09	.1900E+09	.26098E+09	**.2009E+09**	.1598E+09	.21994E+09	**.1598E+09**
TOTAL	.180E+02...	.100E-09	.5409E+13	.51175E+13	**.4930E+13**	.5182E+13	.45908E+13	**.4224E+13**

Table 3: Neutron flux densities

group	energy region		3 foils U+Co+Ni (fig. 9)			3 foils Mn+Co+Ni (fig. 10)		
			X-BALL	RFSP-JUL	SAND-II	X-BALL	RFSP-JUL	SAND-II
1	.105E+02...	.650E+01	.1285E+11	.10656E+11	.1323E+11	.1251E+11	.10088E+11	.1311E+11
2	.650E+01...	.400E+01	.8448E+11	.81655E+11	.8749E+11	.8215E+11	.79805E+11	.8666E+11
3	.400E+01...	.250E+01	.1958E+12	.20953E+12	.2041E+12	.1898E+12	.20610E+12	.2033E+12
4	.250E+01...	.140E+01	.4974E+12	.42047E+12	.4976E+12	.4790E+12	.40273E+12	.5225E+12
5	.140E+01...	.800E+00	.5357E+12	.42446E+12	.4384E+12	.5144E+12	.39615E+12	.4525E+12
6	.800E+00...	.400E+00	.6269E+12	.48727E+12	.4838E+12	.5985E+12	.44968E+12	.4103E+12
7	.400E+00...	.200E+00	.5450E+12	.43414E+12	.4280E+12	.5178E+12	.40060E+12	.3630E+12
8	.200E+00...	.100E+00	.4675E+12	.38183E+12	.3750E+12	.4418E+12	.35233E+12	.3208E+12
9	.100E+00...	.465E-01	.4461E+12	.37765E+12	.3682E+12	.4197E+12	.34813E+12	.3163E+12
10	.465E-01...	.215E-01	.3973E+12	.34751E+12	.3391E+12	.3724E+12	.31937E+12	.2918E+12
11	.215E-01...	.100E-01	.3495E+12	.31663E+12	.3082E+12	.3268E+12	.29029E+12	.2660E+12
12	.100E-01...	.465E-02	.3026E+12	.28450E+12	.2715E+12	.2830E+12	.26092E+12	.2341E+12
13	.465E-02...	.215E-02	.2571E+12	.25123E+12	.2345E+12	.2408E+12	.22885E+12	.2081E+12
14	.215E-02...	.100E-02	.2082E+12	.21499E+12	.2039E+12	.1952E+12	.19335E+12	.1774E+12
15	.100E-02...	.465E-03	.1609E+12	.17564E+12	.1662E+12	.1520E+12	.15366E+12	.1434E+12
16	.465E-03...	.215E-03	.1121E+12	.12759E+12	.1223E+12	.1074E+12	.10628E+12	.1076E+12
17	.215E-03...	.100E-03	.7476E+11	.72398E+11	.7661E+11	.7326E+11	.70712E+11	.7308E+11
18	.100E-03...	.465E-04	.4713E+11	.54644E+11	.5254E+11	.4608E+11	.50476E+11	.4645E+11
19	.465E-04...	.215E-04	.2770E+11	.33613E+11	.3170E+11	.2683E+11	.30382E+11	.2731E+11
20	.215E-04...	.100E-04	.1428E+11	.16697E+11	.1630E+11	.1379E+11	.15313E+11	.1410E+11
21	.100E-04...	.465E-05	.6618E+10	.82342E+10	.7332E+10	.6382E+10	.76457E+10	.6528E+10
22	.465E-05...	.215E-05	.5556E+10	.62993E+10	.5908E+10	.5355E+10	.58793E+10	.5484E+10
23	.215E-05...	.100E-05	.3727E+10	.43056E+10	.3990E+10	.3589E+10	.40193E+10	.3679E+10
24	.100E-05...	.465E-06	.1954E+10	.22452E+10	.2120E+10	.1880E+10	.20958E+10	.1927E+10
25	.465E-06...	.215E-06	.5872E+09	.74444E+09	.6506E+09	.5647E+09	.69562E+09	.5791E+09
TOTAL FOR 25 ABBN GROUPS			.5382E+13	.47449E+13	.4739E+13	.5111E+13	.43856E+13	.4296E+13
THE GROUPS ABOVE AND BELOW THE ABBN GROUPS								
0	.180E+02...	.105E+02	.7484E+09	.58950E+09	.7692E+09	.7293E+09	.55242E+09	.7633E+09
26	.215E-06...	.100E-09	.1661E+09	.22448E+09	.1832E+09	.1599E+09	.21007E+09	.1639E+09
TOTAL	.180E+02...	.100E-09	.5383E+13	.47458E+13	.4740E+13	.5112E+13	.43863E+13	.4297E+13

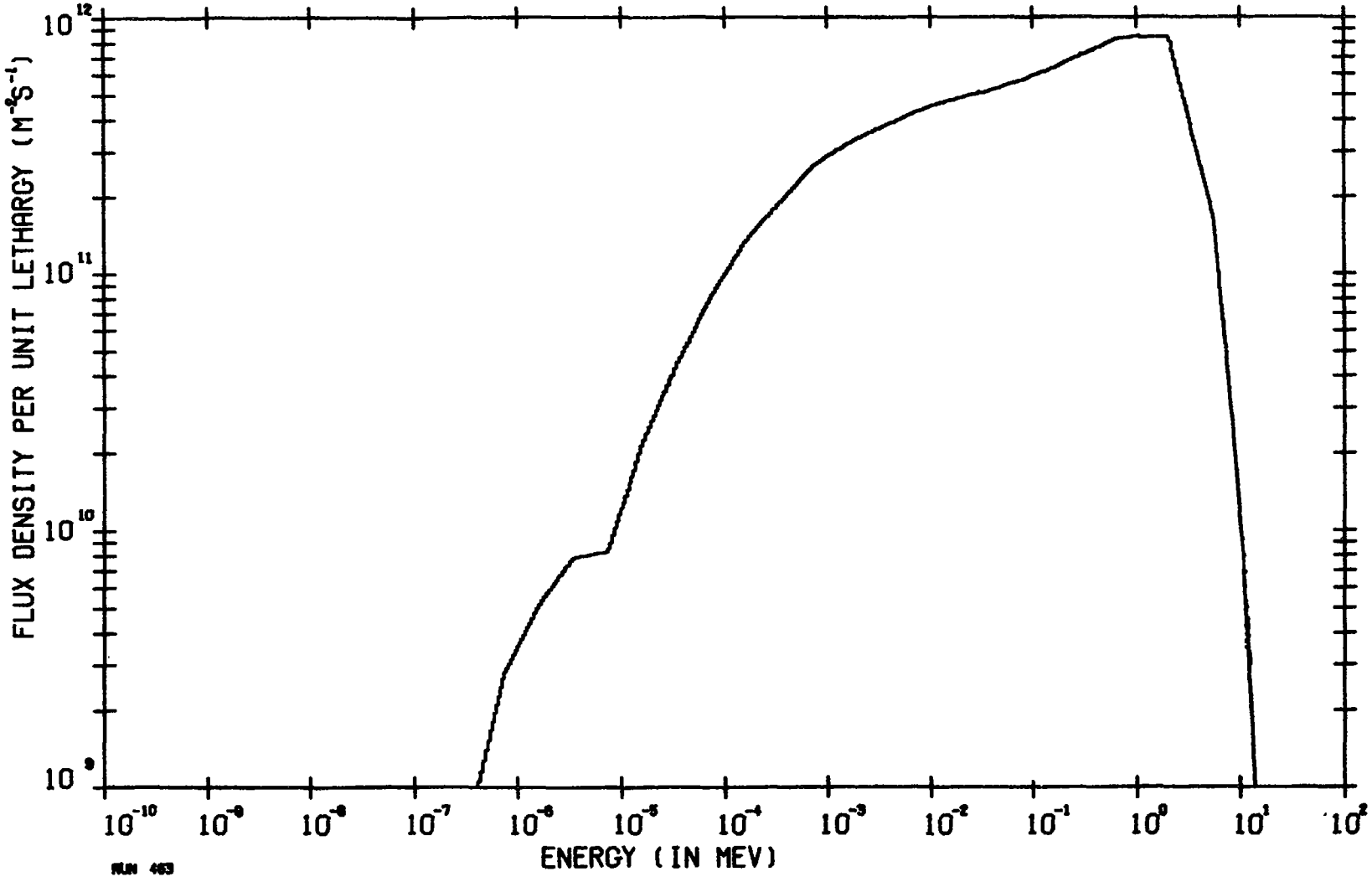

Fig. 1: INPUT SPECTRUM STEK-4000 IN 620 ENERGY GROUPS

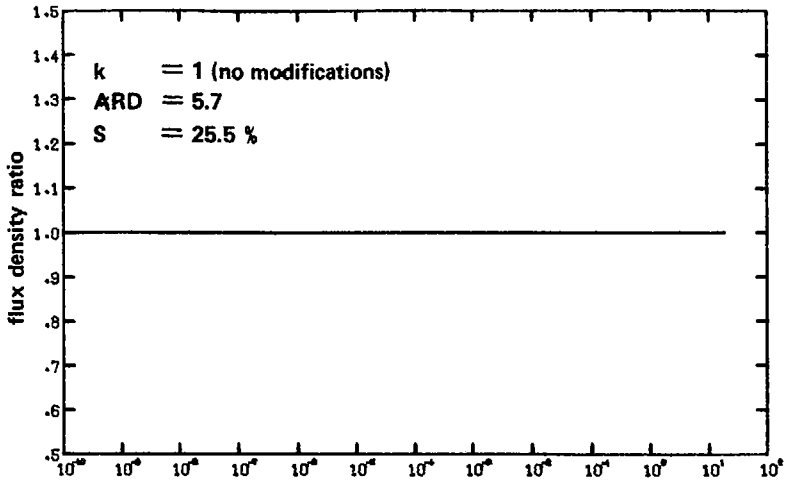

Fig. 2a.

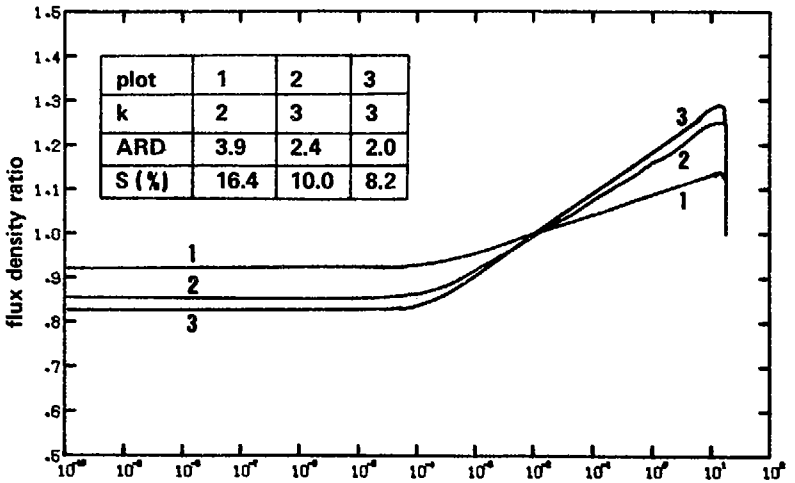

Fig. 2b.

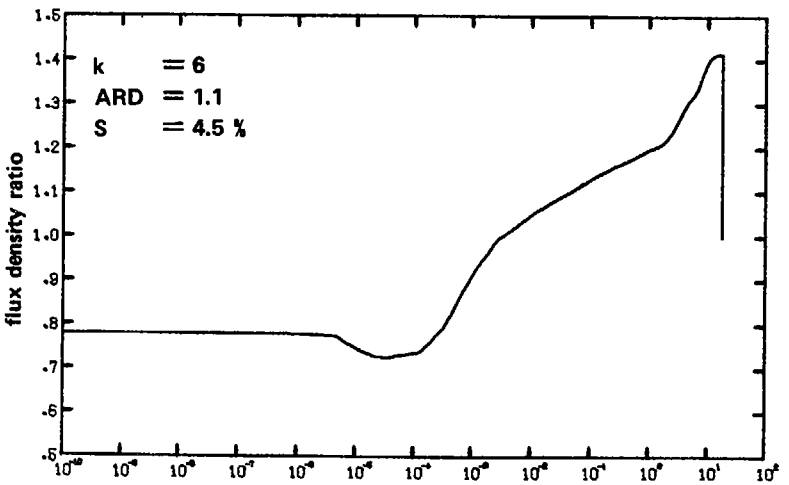

Fig. 2c.

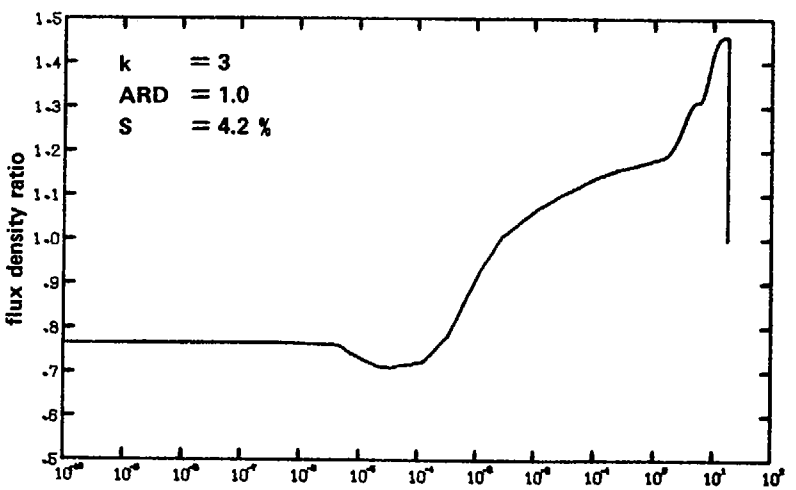

Fig. 2d.

SPECTRUM RATIOS FOR CRYSTAL BALL WITH DIFFERENT FITS.

Fig. 2a-2d presents ϕ_{out} (E)/ϕ_{in} (E) for decreasing ARD and S values.

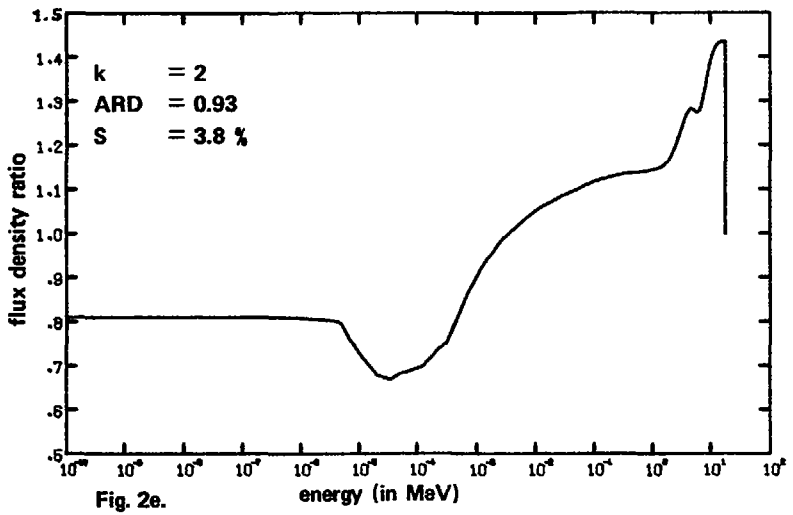

Fig. 2e.

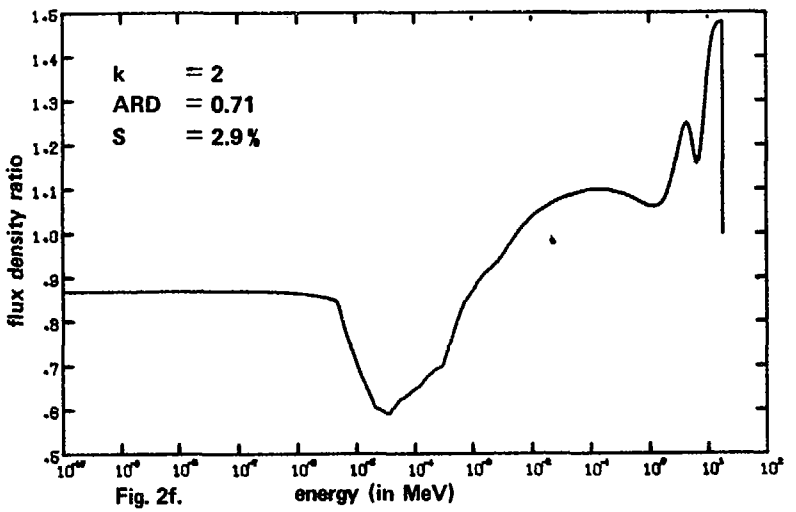

Fig. 2f.

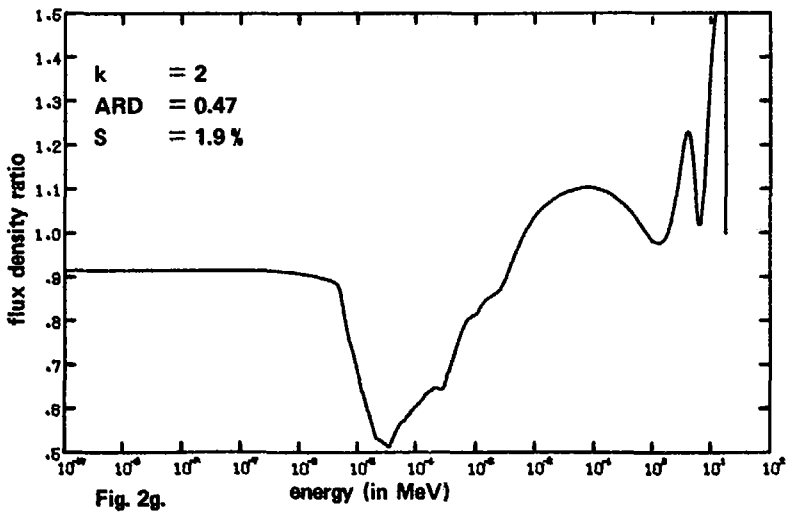

Fig. 2g.

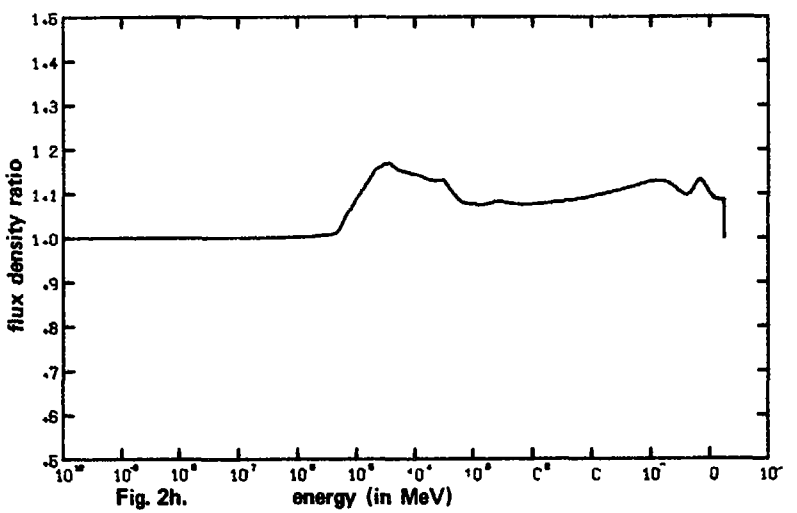

Fig. 2h.

SPECTRUM RATIOS FOR CRYSTAL BALL WITH DIFFERENT FITS.

Fig. 2e-2g present $\phi_{out}(E)/\phi_{in}(E)$ for decreasing ARD and S values. Fig. 2h presents the ratio of output spectra referred to in fig. 2c and 2e.

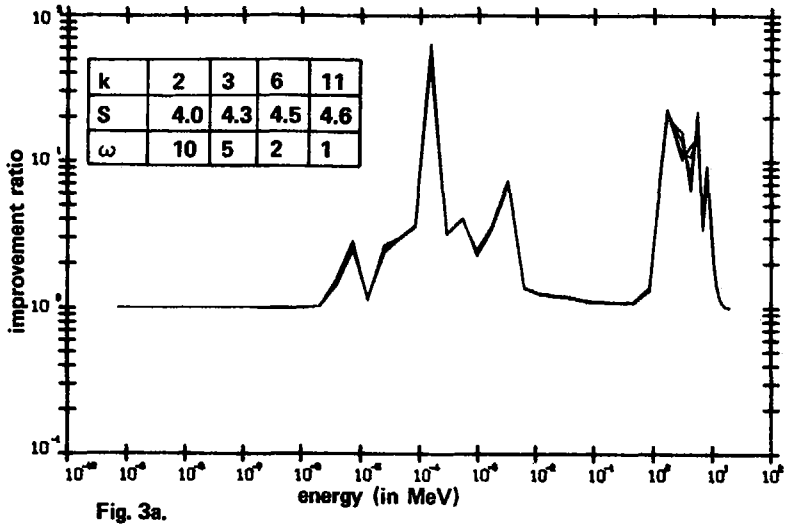

k	2	3	6	11
S	4.0	4.3	4.5	4.6
ω	10	5	2	1

Fig. 3a.

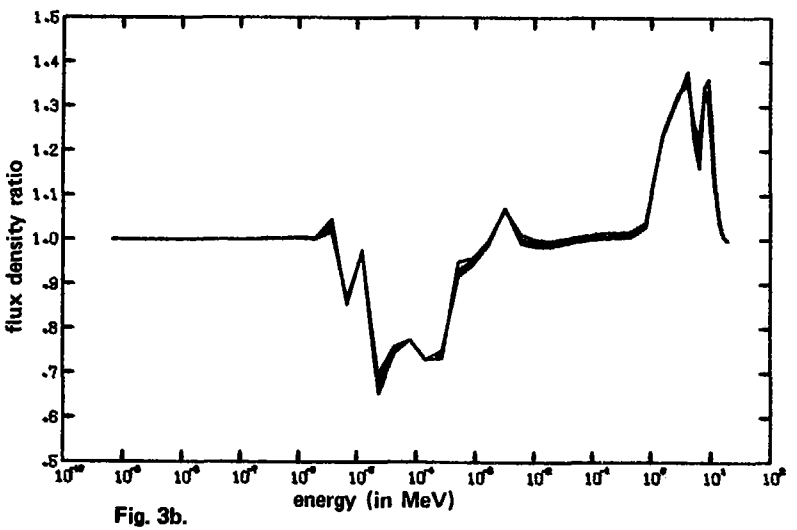

Fig. 3b.

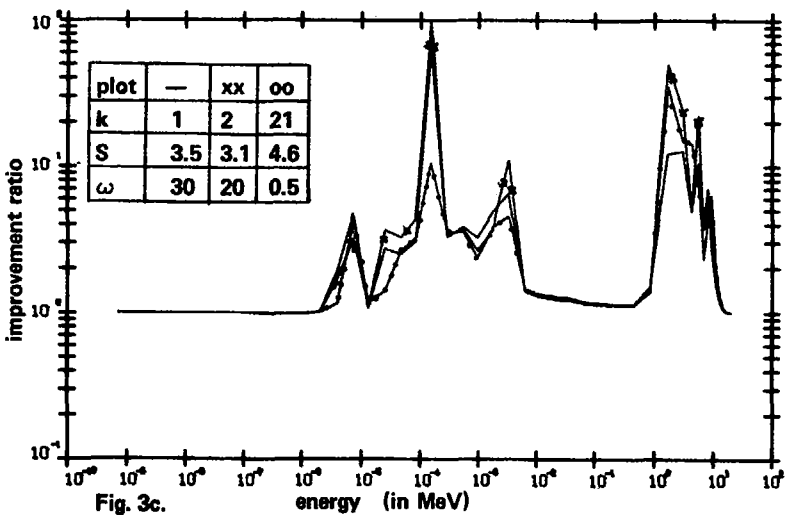

plot	—	xx	oo
k	1	2	21
S	3.5	3.1	4.6
ω	30	20	0.5

Fig. 3c.

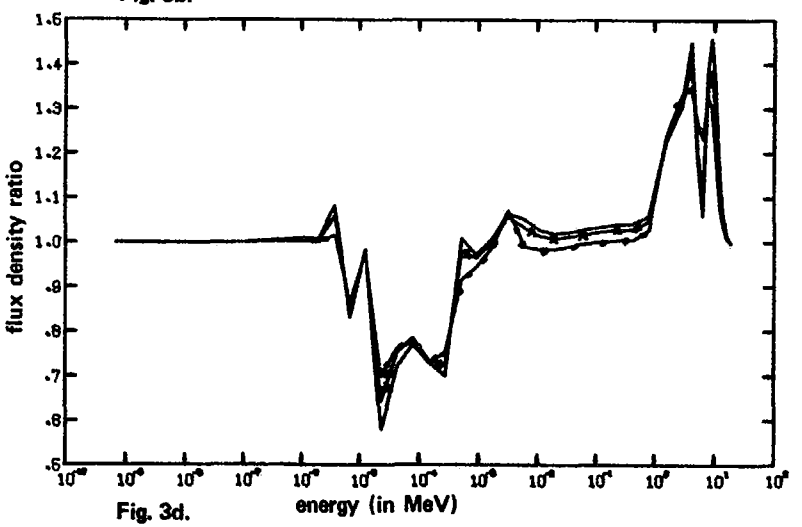

Fig. 3d.

IMPROVEMENT RATIOS AND SPECTRUM RATIOS FOR RFSP (15 detectors)

Fig. 3a and 3c present the improvement ratios for different values of ω. Fig. 3b and 3d present the $\phi^{out}(E)/\phi^{in}(E)$ for the different values of ω.

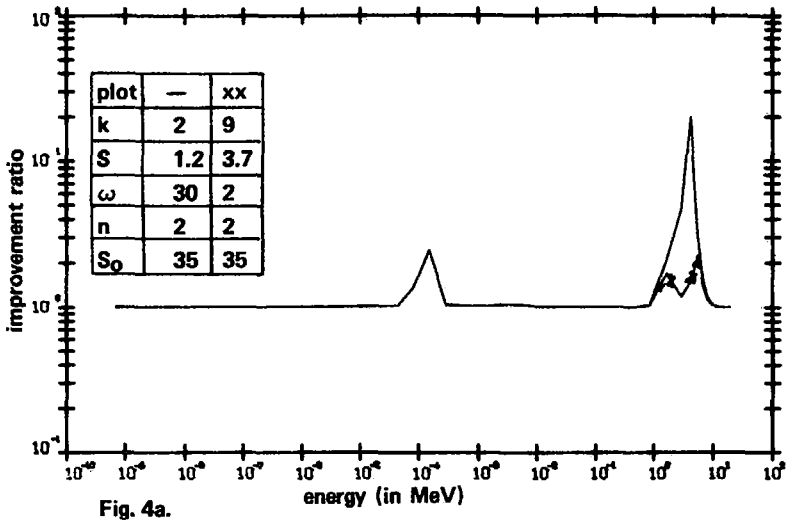

Fig. 4a.

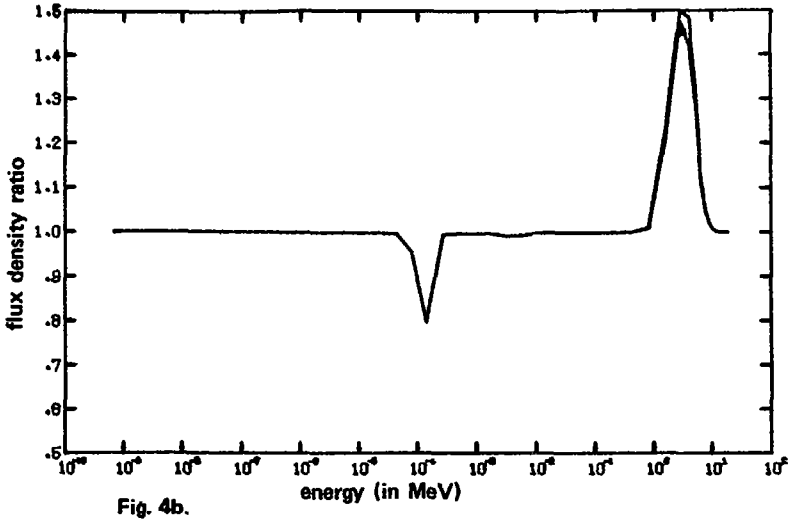

Fig. 4b.

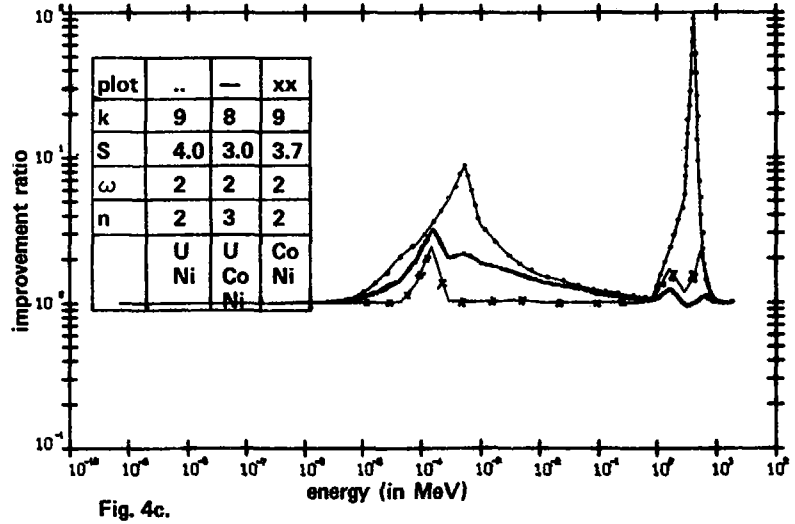

Fig. 4c.

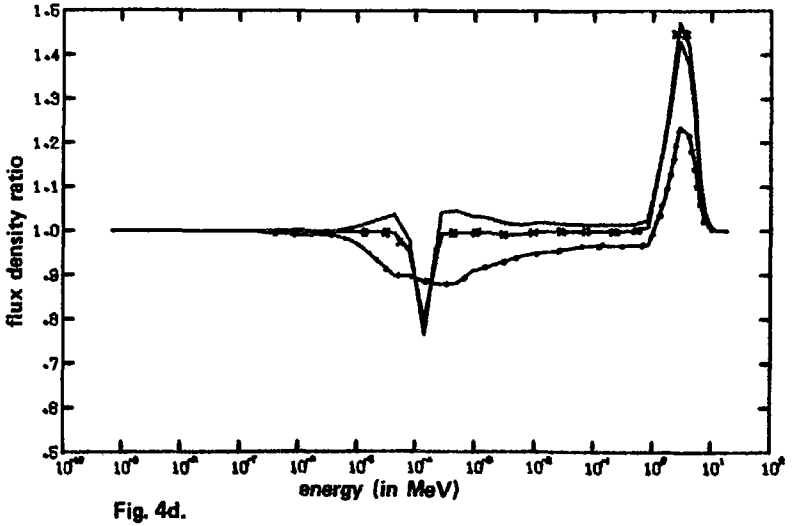

Fig. 4d.

IMPROVEMENT RATIOS AND SPECTRUM RATIOS FOR RFSP.

Fig. 4a and 4b present the ratios for 2 detectors (Co and Ni) and different ω values. Fig. 4c and 4d present the ratios for 2 and 3 detectors.

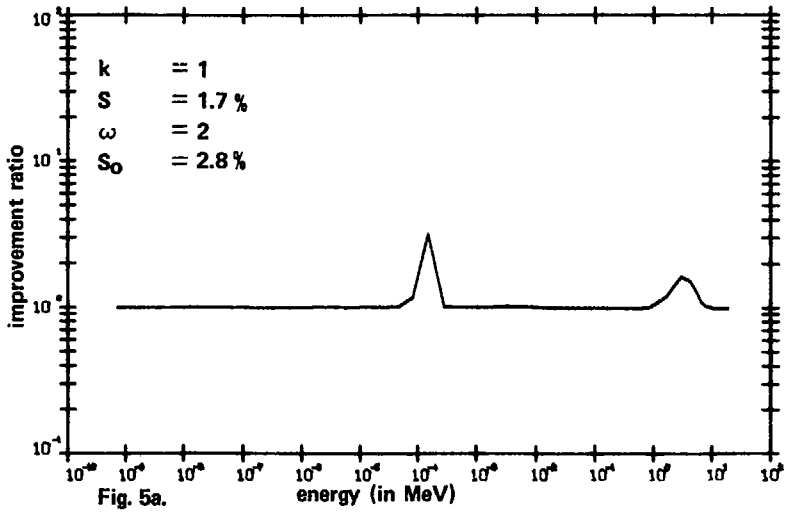

Fig. 5a.

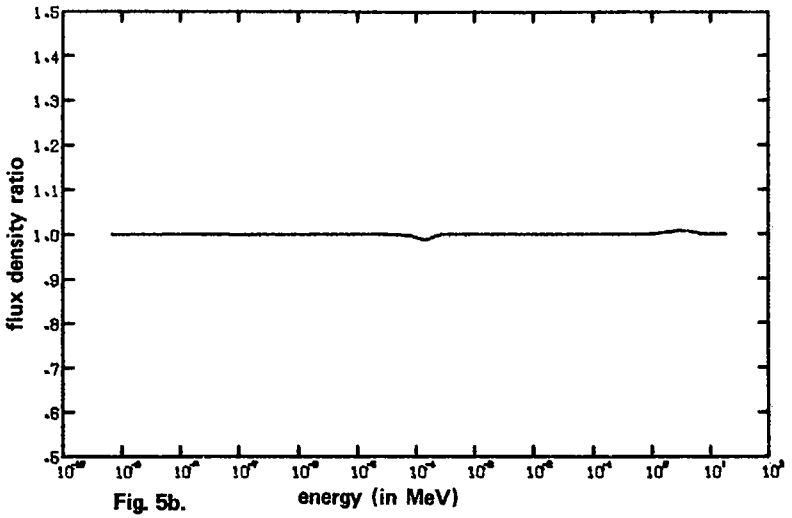

Fig. 5b.

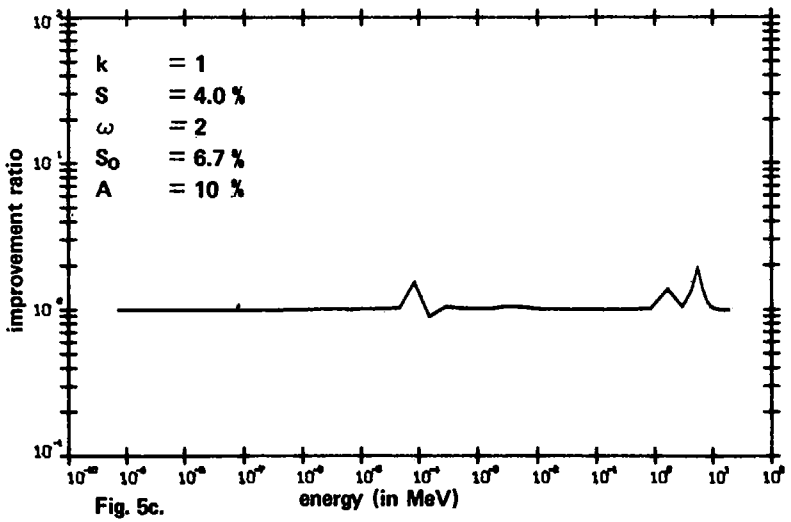

Fig. 5c.

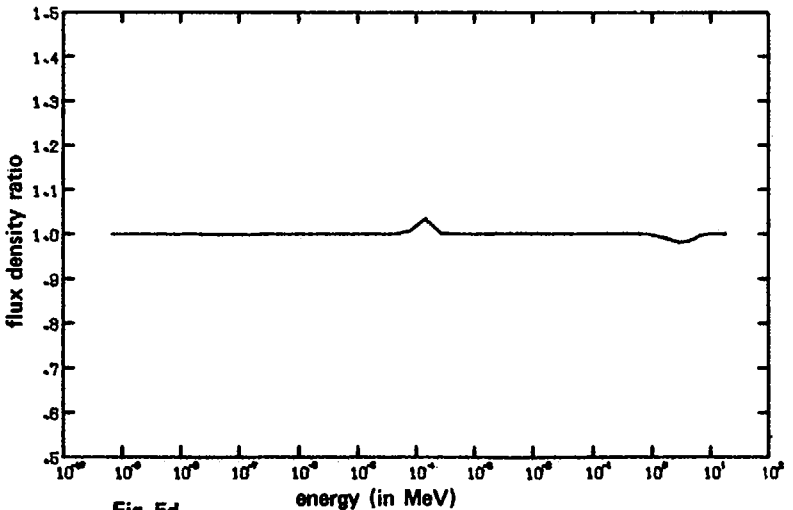

Fig. 5d.

IMPROVEMENT RATIO AND SPECTRUM RATIO FOR RFSP (2 detectors)

Fig. 5a and 5b present the results for a slight increase of the Ni activity. Fig. 5c and 5d present the results for a slight decrease of the Ni activity.

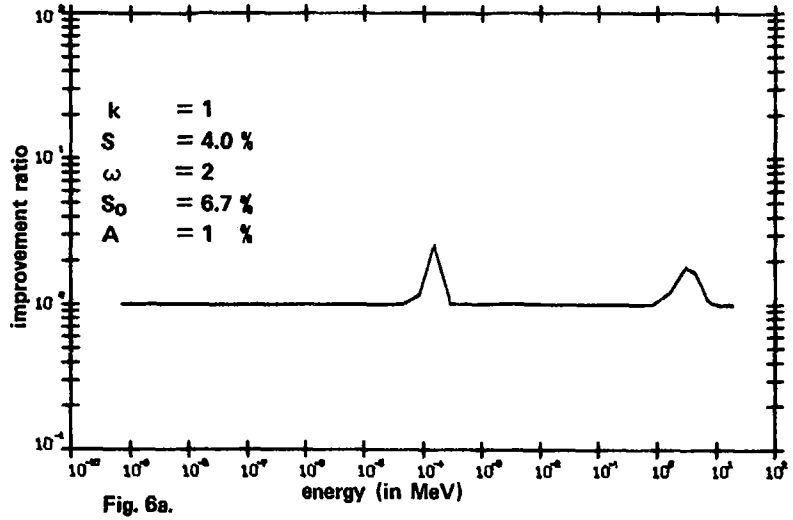

Fig. 6a.

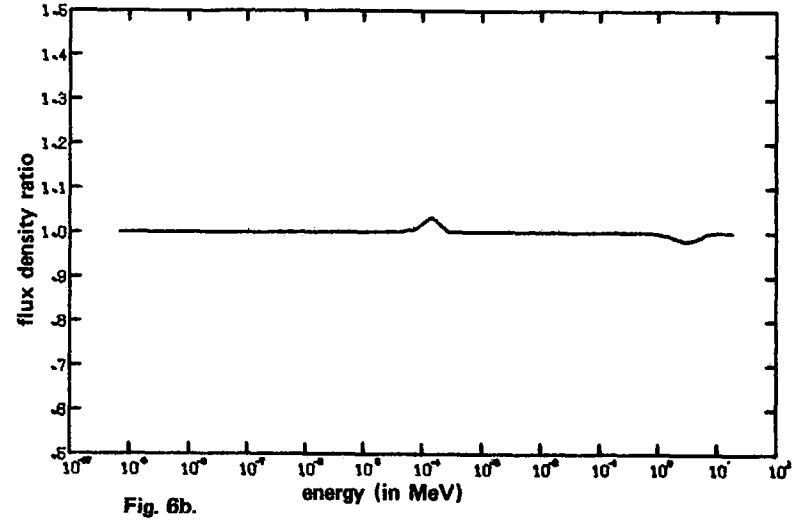

Fig. 6b.

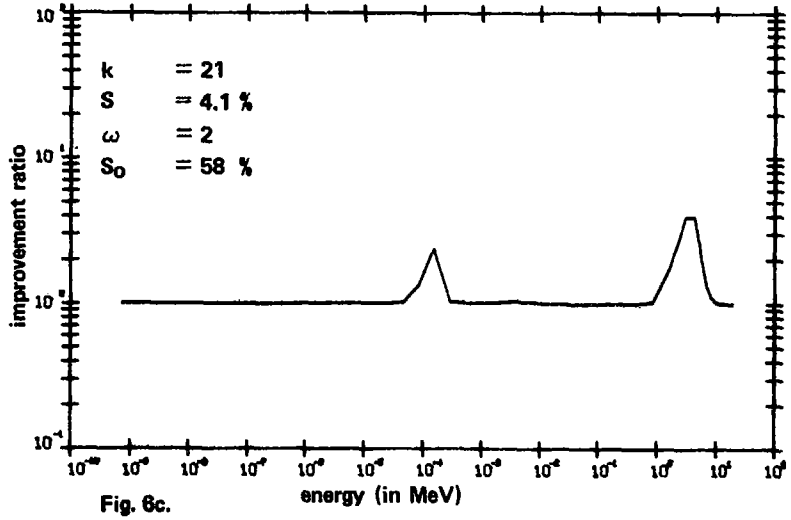

Fig. 6c.

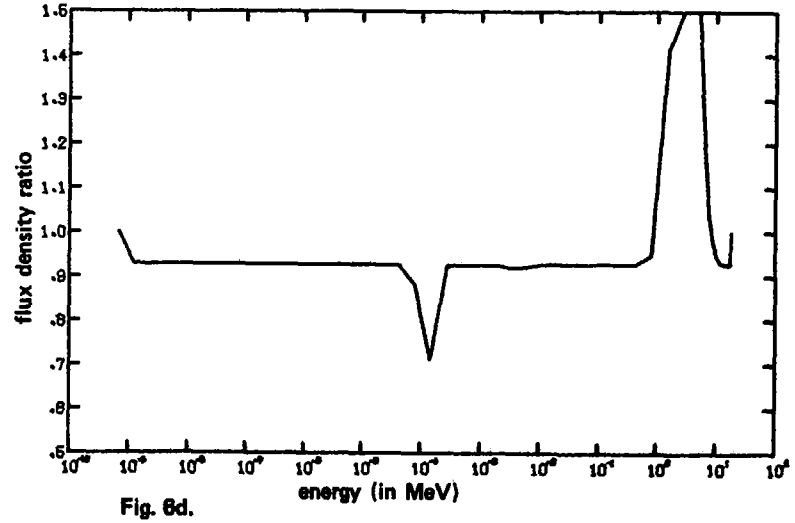

Fig. 6d.

IMPROVEMENT RATIOS AND SPECTRUM RATIOS FOR RFSP (2 detectors)

Fig. 6a and 6b present the results for the amplitude of the sine function of 0.01. Fig. 6c and 6d present the results for strongly changed activity values.

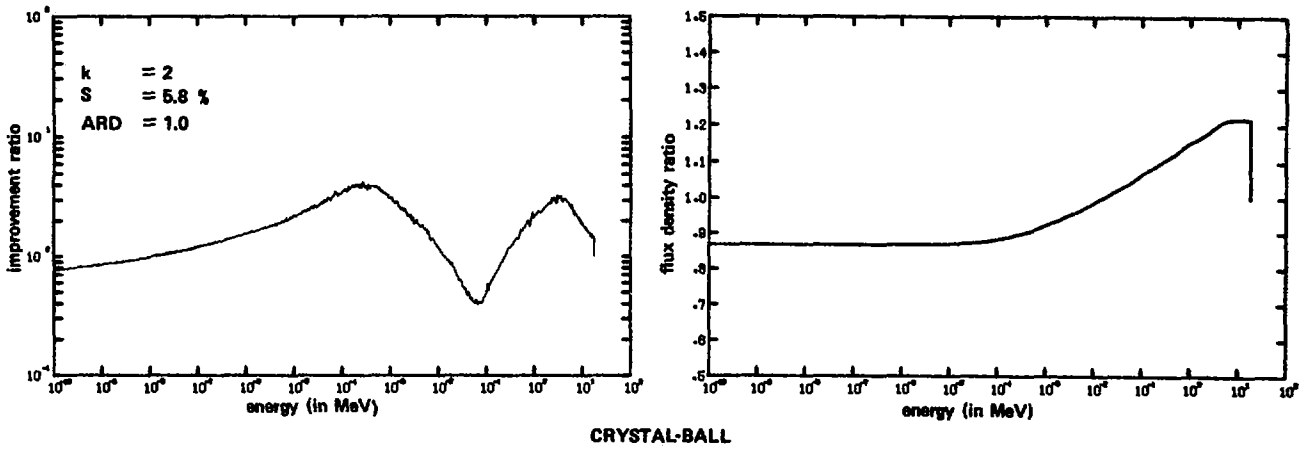

CRYSTAL-BALL

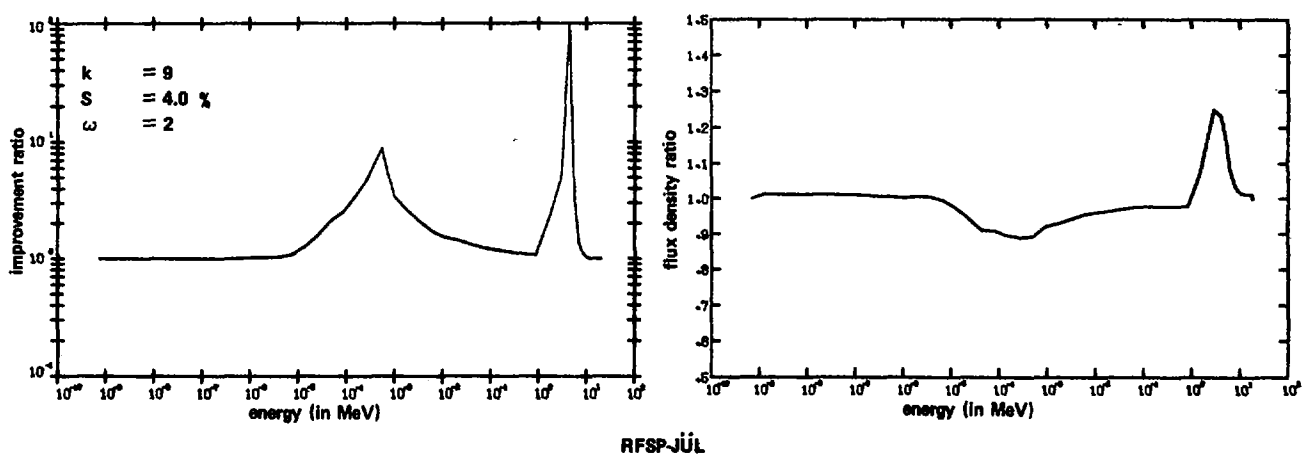

RFSP-JÜL

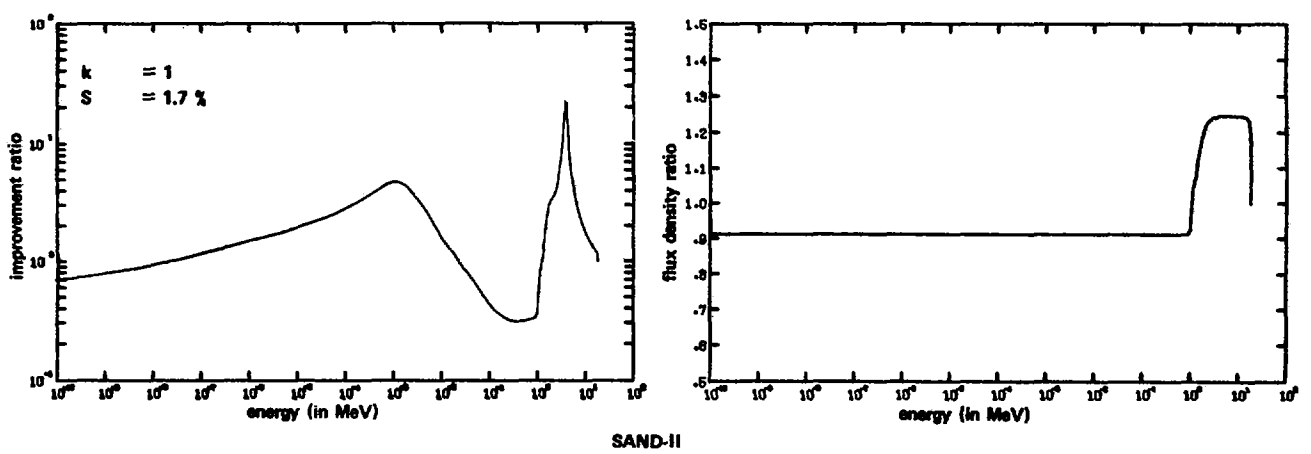

SAND-II

Fig. 7: RESULTS FOR THE U AND Ni SET

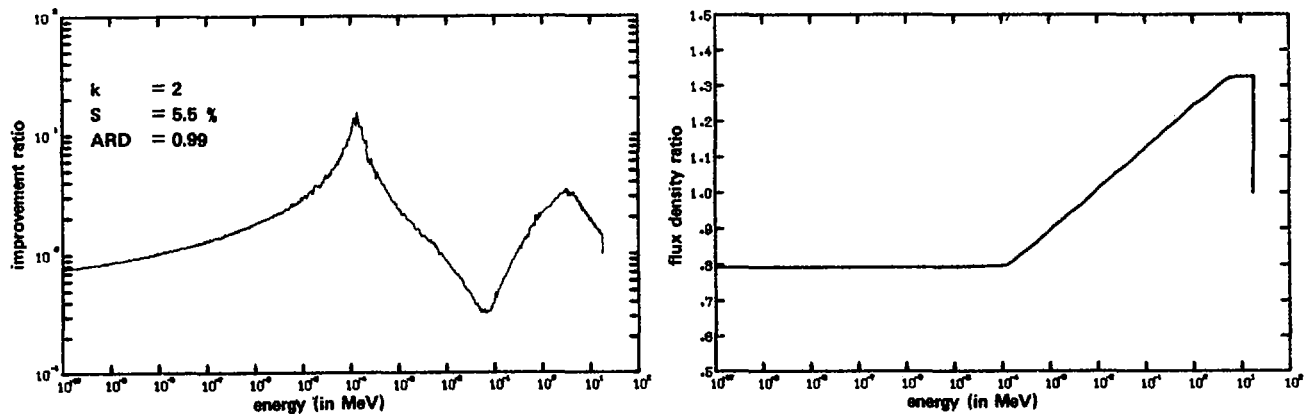

CRYSTAL-BALL

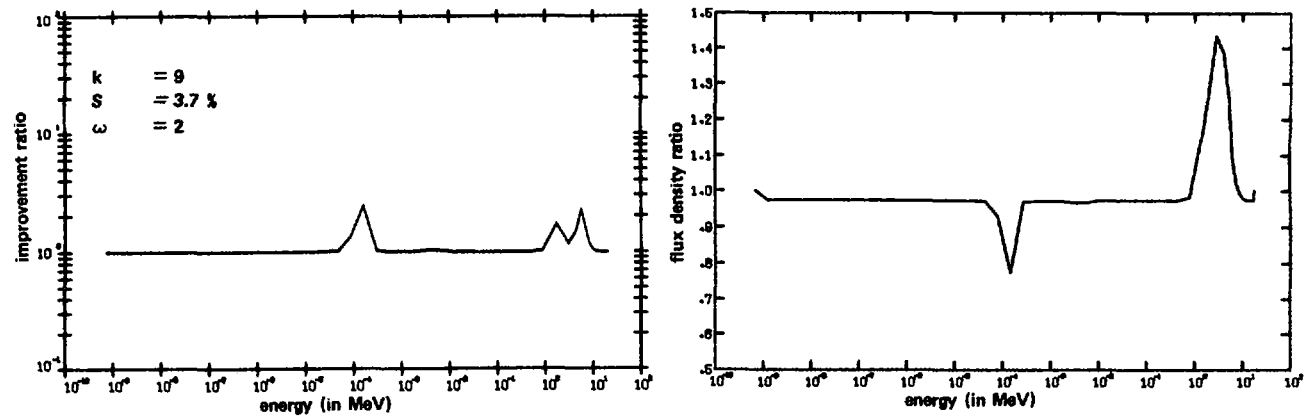

RFSP-JÜL

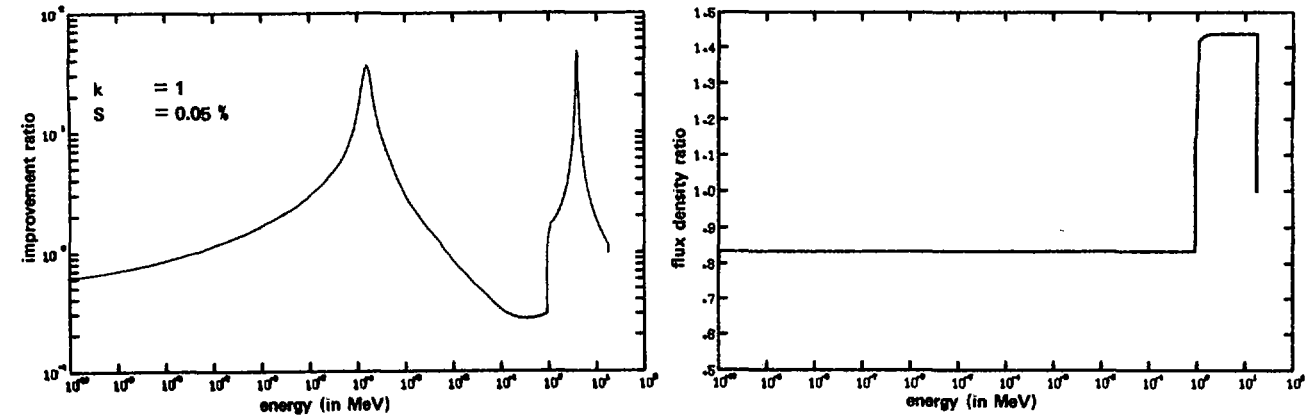

SAND-II

Fig. 8. RESULTS FOR THE Co AND NI SET.

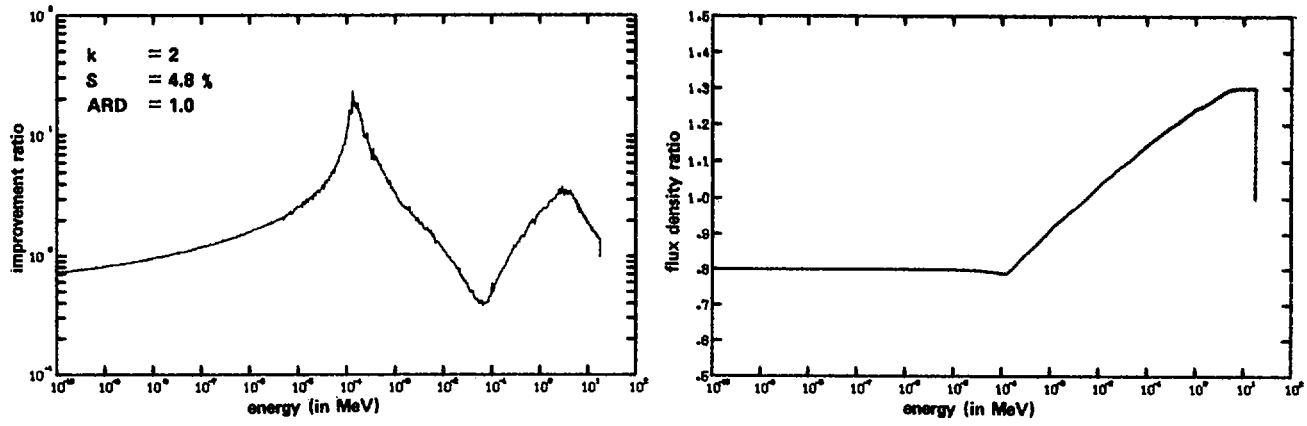

CRYSTAL BALL

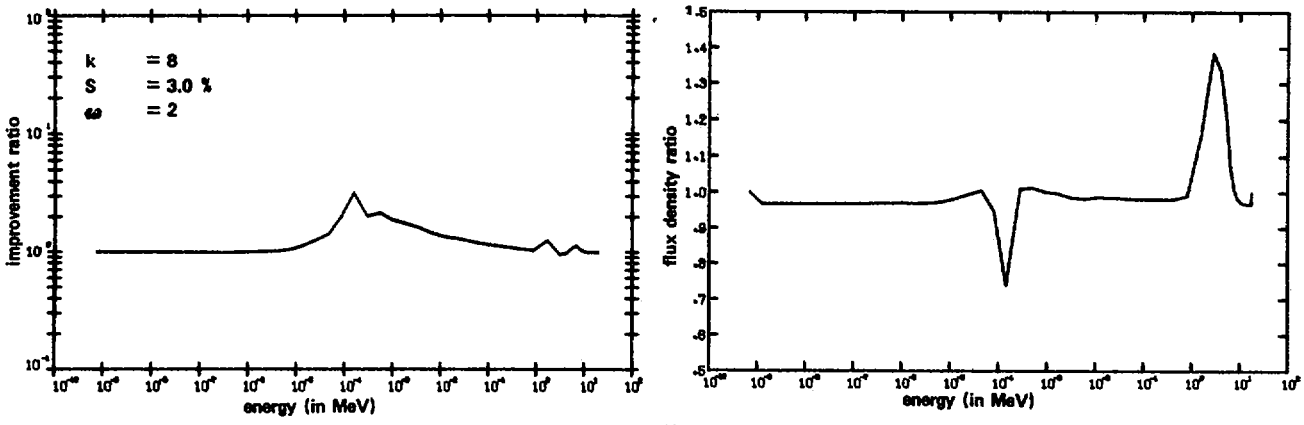

RFSP-JÜL

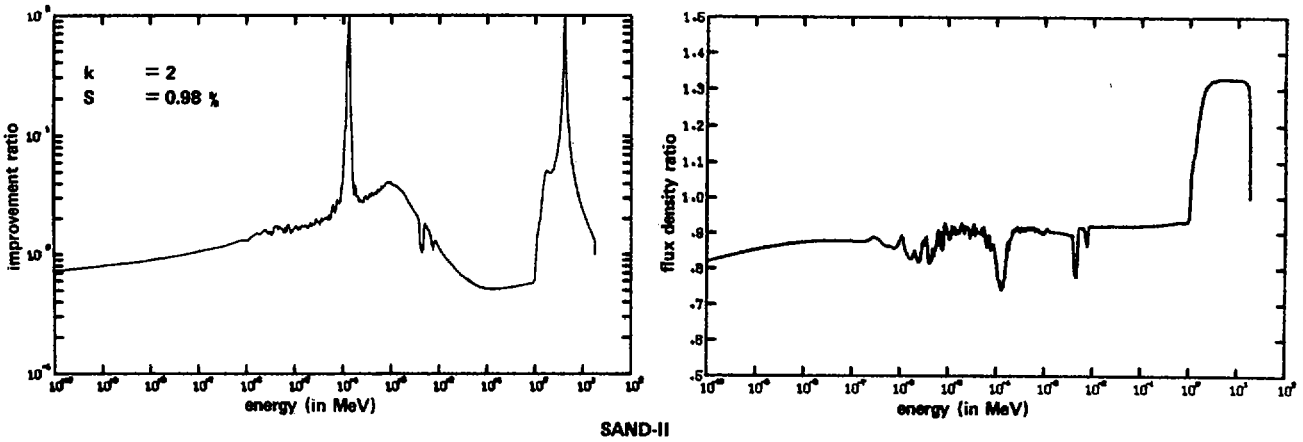

SAND-II

Fig. 9. RESULTS FOR THE U, Ni AND Co SET.

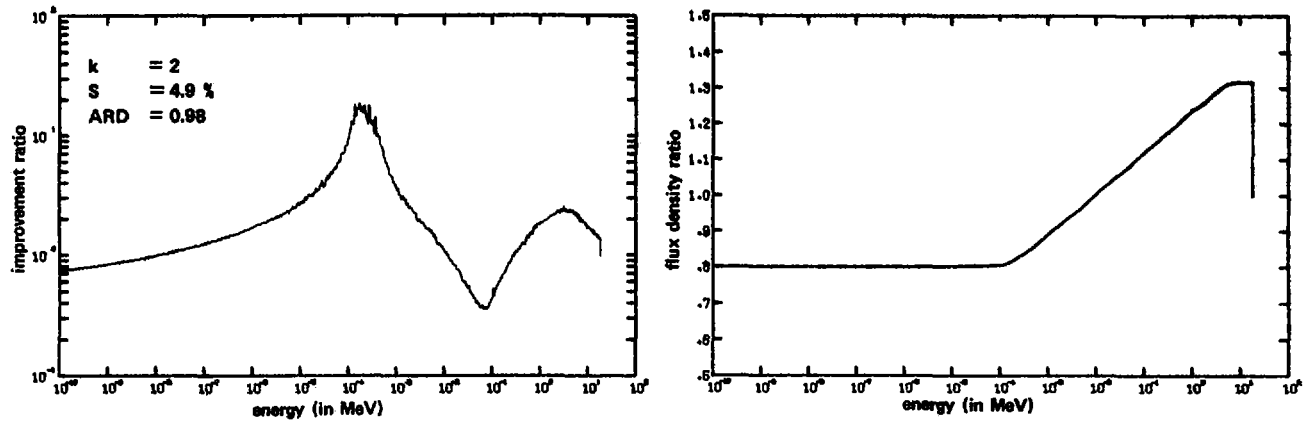

CRYSTAL-BALL

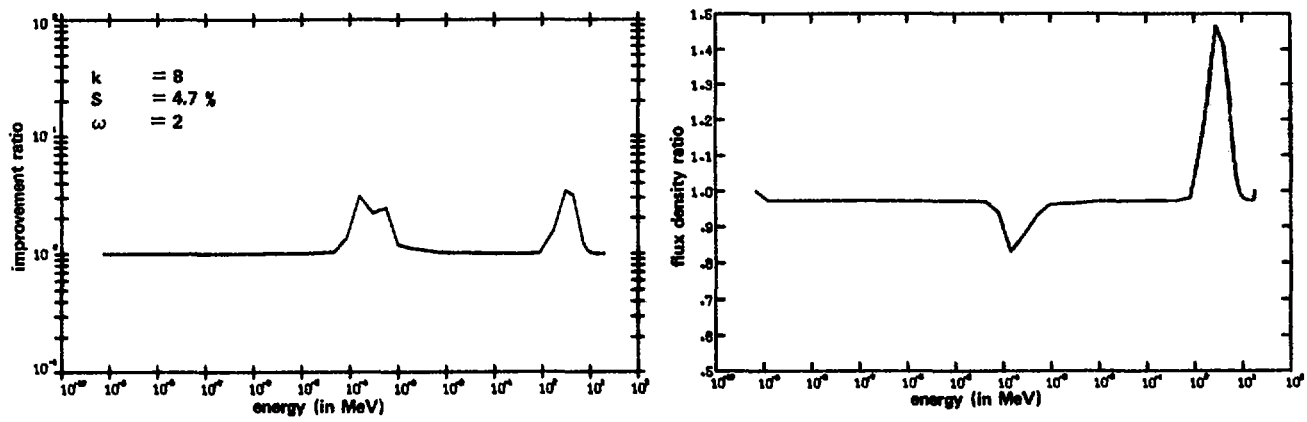

RFSP-JÜL

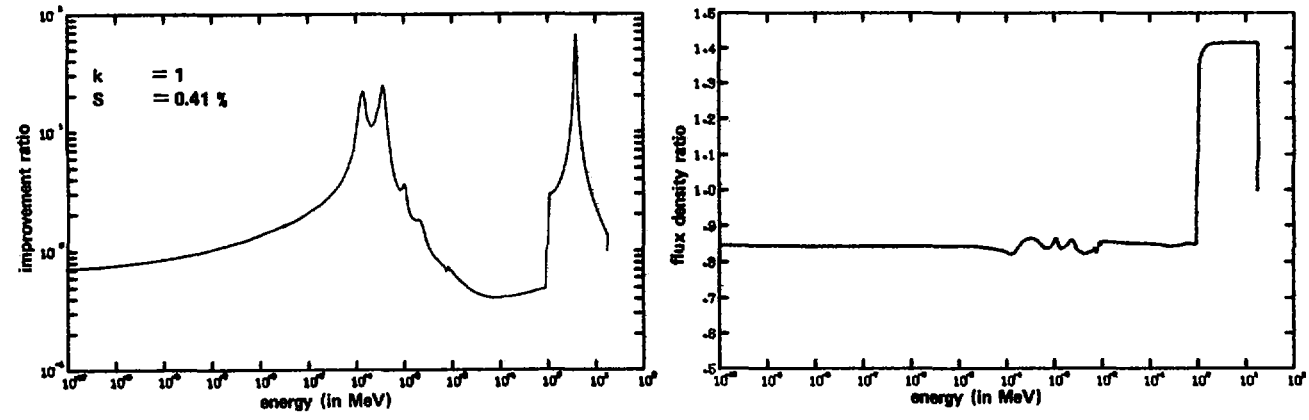

SAND-II

Fig. 10. RESULTS FOR THE Mn, Ni, AND Co SET

I.6. Spectral Characterization of the NISUS Neutron Field

J.G. Williams and A.H.M.A. Hannan

University of London Reactor Centre
Imperial College of Science and Technology, Silwood Park, Sunninghill,
Ascot, Berks. SL5 7PY. U.K.

ABSTRACT

Information on the central neutron spectrum of the standard neutron field NISUS consists of proton recoil proportional counter data, ^{6}Li solid state sandwich spectrometry data, fission rate ratios obtained using NBS-type fission chambers and activation foil data. In addition it is known that the NISUS spectrum closely resembles that of Mol-ΣΣ.

In this paper these data are briefly reviewed and a recommended evaluated spectrum is presented. The evaluation was performed by means of the code SIMMM which simultaneously evaluates spectra, reaction rates and dosimetry cross-sections. The fit between the spectrometry data, reaction rates and ENDF/BIV dosimetry data was very good. The SIMMM code does not produce any evaluations of errors, but these are subjectively estimated as ± 5% for the recommended spectrum in the energy range 67.4 keV - 7.41 MeV, and ± 20% outside this range.

Spectral characterization of the NISUS neutron field

1. INTRODUCTION

Information on the central neutron spectrum of the standard neutron field NISUS[1] consists of proton recoil proportional counter data obtained by J. Petr[2], ^{6}Li solid state sandwich spectrometry data of G. Koutzoukos[3], fission rate ratios obtained using N.B.S. type fission chambers[4] and activation foil data[5]. In addition we know from the fission rate[4] and activation foil data[5] that the NISUS spectrum closely resembles that of Mol-ΣΣ[6].

In this paper these data are briefly reviewed and a recommended evaluated spectrum is presented. The steps in the evaluation are as follows:

(1) The data from differential spectrometry techniques have been used to define the spectrum from ∿ 25 keV to 8 MeV. Outside this energy range the ΣΣ evaluated spectrum[6], based on ENDF/BIII data and transport theory, has been used. The spectrum obtained is referred to as the NISUS evaluated spectrometry data.

(2) The NISUS evaluated spectrometry data, the fission chamber and activation foil reaction rates, and the ENDF/BIV dosimetry cross section data, together with the respective error files have been input to a new code SIMMM which performs a simultaneous evaluation using a least squares minimization technique. The spectrum obtained as a result of this procedure is the NISUS recommended spectrum.

2. PROTON RECOIL PROPORTIONAL COUNTERS

The proton recoil spectrum measurements made by J. Petr are described in detail in his Ph.D. Thesis[2]. Five 4 cm diameter spherical counters of the type developed by Benjamin et al[7] were used. These counters were on loan from the UKAEA where they had been used by M.D. Carter of AEE, Winfrith.

The counters were supplied with sealed fillings of hydrogen at 0.488, 0.94, 3.528, 9.57 and 5.22 atmospheres. The 3.528 atm. counter also contained ∿ 5% methane and the 5.22 atm. counter contained argon at a partial pressure of 4.4 atmospheres. Energy calibrations were by means of ^{3}He gas included in the filling of the three higher pressure counters and for the other two by a ^{239}Pu alpha source, painted on the centre of the anode. Data for the ^{239}Pu energy calibrations, and the volumes and pressures of the counters were supplied by Carter.

The counters were loaded into NISUS by means of a 45 mm access hole in the natural uranium and boron carbide shells. The hole in the boron carbide was closed by means of a boron carbide plug having a residual hole of 10 mm diameter. The hole in the natural uranium was not closed.

Run to run normalization was by means of miniature BF_3 and fission counters installed in the graphite thermal column. Data from the spectrometers were unfolded using the SPEC4 code[8]. Proton range data used for the wall effect corrections were based on the data of Whaling[9] but modified by a factor of 1.10 as recommended by Kemshall[10]. This modification was found to greatly improve the agreement between the spectra obtained from counters filled to different pressures. The agreement between the various counters

was extremely good, especially since no arbitrary adjustment of the normalization of one counter to another was made.

The data from each counter have been reanalysed and condensed into the 99 group structure of the DLC library using the code RATIF, written by Petr[2] and subsequently modified by J.A. Mason and A.H.M.A. Hannan. The results from this condensation are given in Table 1 together with the values obtained by averaging the data from different counters. Each counter was given equal weight in this averaging despite the different statistical errors. The normalization of the data in this Table is arbitrary, but common to the five spectra. Errors given in the table are statistical only. Petr claims an overall systematic error of ± 3% for the composite spectrum in the energy range 40 keV - 2 MeV. This figure is lower than is usually claimed for this technique, but the quality of the data is undoubtedly unusually high. No correction for the counter body materials has been included, and so the errors have been relaxed to ± 5% (1σ) in the present evaluation of the unperturbed NISUS spectrum for this reason only.

3. ^{6}Li SOLID STATE SANDWICH SPECTROMETERS

The ^{6}Li spectrometry data of Koutzoukos are extensively documented in his Ph.D. thesis[3]. Many measurements of the NISUS spectrum were made using different reactor powers, ^{6}Li deposit thicknesses, diode depletion layer thicknesses and two different types of spectrometer body. All of the spectra obtained are in fairly good agreement, but one particular set of data has been chosen in the present evaluation as providing the best compromise between statistical accuracy, pile up and distortions due to penetration of the depletion layer. The spectrum which has been used is designated as Run 3 - 30 in reference[3]. Parameters of this

measurement were : LiF coating of 120 $\mu g.cm^{-2}$, radius 0.7 cm, separation of diodes 1 mm, radius of diodes 0.8 cm, gold layer 80 $\mu g.cm^{-2}$, depletion depth 300 μm

Data were collected simultaneously for both the sum and triton techniques, the former being used to obtain the neutron spectrum above $\sim$ 400 keV and the latter for the spectrum below $\sim$ 400 keV. Normalization of the two parts was obtained by taking account of the different dead times of the two data collection systems. The unfolding was done by the Gold[11] technique.

Cross-section data used for the $^6Li(n,\alpha)t$ reaction were based on the measurements of Clements and Rickard[12]. These data cover the energy range 150 keV to 3.9 MeV. At lower energies the data of Schwarz[13] and at higher energies renormalized data of Ribe[14] were used. This somewhat controversial choice of cross-section data is interesting in that although the data are very different from all other evaluations the spectrum produced provide very good consistency with the reaction rate measurements (see below). The Clements and Rickard cross-section measurement was in fact made using similar spectrometers to the ones used by Koutzoukos and can therefore be regarded as a response function measurement. For the analysis of the triton distribution, the angular distribution obtained by Rickard[15] by adjusting the data of Bluet[16] to force agreement between ^6Li spectrometry and time-of-flight data was used.

In the present work the data of Run 2 - 30 were collapsed into the 99 group DLC group structure and normalized to equal flux with the proton recoil data over the energy range 67.4 keV to 2.02 MeV. The results are shown in Table 2 together with the proton recoil spectrum. The errors are not shown but are dominated for the spectrum above 0.5 MeV by the uncertainty in the cross-

section, for which ± 5 - 10% is claimed[12]. In view of some differences of nearly a factor of 2 between this cross section and the ENDF/BIII file this seems hard to accept. The proton recoil data has been preferred throughout its energy range and the ^{6}Li data are only used outside this region. An error of ± 20% has been used in the present work for the ^{6}Li data in the energy range 2.02 MeV to 7.41 MeV. The ^{6}Li spectrum below 2.02 MeV has thus only been used for normalization purposes. It is worth noting, however that the agreement with the proton recoil data is good, generally well within ± 10%.

The NISUS evaluated spectrometry data thus consists of the data collected in the final column of Table 2. The extension at the high and low energy tails is not shown but consists of the ΣΣ evaluated spectrum[6], normalized to equal flux in the range 25 keV - 8 MeV and with an assigned error of ± 50%.

4. THE SIMMM CODE

The SIMMM code, developed by the present authors and Mrs. W. Carder, performs a simultaneous evaluation of spectra, reaction rates and dosimetry cross-sections. A set of evaluated quantitites $R^*_{i,j}$, $\sigma^*_{i,k}$ and $\phi^*_{j,k}$ are defined as those which minimise the function

$$F = \sum_{i,j} \left| \frac{(XK)R^*_{i,j} - R_{i,j}}{\Delta R_{i,j}} \right|^2 + \sum_{i,k} \left| \frac{\sigma^*_{i,k} - \sigma_{i,k}}{\Delta\sigma_{i,k}} \right|^2 + \sum_{j,k} \left| \frac{\phi^*_{j,k} - \phi_{j,k}}{\Delta\phi_{j,k}} \right|^2 ,$$

subject to the constraint $R^*_{i,j} = \sum_k (\sigma^*_{i,k} \cdot \phi^*_{j,k})$

Where

$R^*_{i,j}$ is the evaluated reaction rate for reaction i in field j,

$\sigma^*_{i.k}$ is the evaluated cross-section for reaction i in energy group k,

$\phi^*_{j,k}$ is the evaluated neutron flux for field j in energy group k.

R_{ij}, $\sigma_{i,k}$ and $\phi_{j,k}$ are the corresponding measured quantities and $\Delta R_{i,j}$, $\Delta\sigma_{i,k}$ and $\Delta\phi_{j,k}$ are the errors (1σ) on these.

XK is a normalization constant, which is evaluated by the program. Input guesses have to be supplied for XK and the other quantities to be evaluated. No dependence on input guesses has ever been found for the evaluated quantities, but the running time is very sensitive to these. In order to obtain an adequate guess for XK the program is usually run first with a modified minimisation function in which σ^* and ϕ^* are set equal to the measured quantities. The minimisation program used in the code MINROS[17] which uses the method of Rosenbrock[18].

The University of London CDC 7600 has been used in this work. On this machine the size of core memory available (100K words) limits the size of problem which can be run to, for example, 8 reactions in 1 spectrum and 20 energy groups, i.e. 181 unknown parameters to be evaluated. Such a problem has taken typically $\sim$ 380 central processor seconds, which is a large amount of computing resource on such a fast machine as the CDC 7600 ($\sim$ 80 allocation units at the University of London Computer Centre). It is possible that a faster minimisation could be achieved by evaluating the covariance matrix less frequently than is done by MINROS.

The evaluated NISUS spectrometry data, collapsed into a 20 group subset of the DLC 99 group structure, was input to the code, together with ENDF/BIV dosimetry cross sections collapsed from the SAND II 620 group structure library supplied by G. Minsart[19], and reaction rate data for NISUS[4),5)]. Collapsing of the 620 group ENDF/BIV data was done in two stages:

(1) The data were collapsed into the 99 group DLC structure using the code RATIF[2)] as modified by J.A. Mason and A.H.M.A. Hannan, with a fission spectrum weighting.

(2) The data were collapsed from 99 groups to 20 with the NISUS spectrum as weighting function.

The error matrix of McElroy[20)] was used with ENDF/BIV data. The reactions used were $^{197}Au(n,\gamma)$, $^{239}Pu(n,F)$, $^{237}Np(n,F)$, $^{238}U(n,F)$, $^{58}Ni(n,p)$, $^{27}Al(n,p)$, $^{56}Fe(n,p)$ and $^{27}Al(n,\alpha)$.

The fit obtained using these data in SIMMM was excellent. The final value of F was 2.33, which is a very low value for 7 degrees of freedom. The calculated reaction rates (R^*) agreed with the input values within 1% except for $^{27}Al(n,p)$ and $^{56}Fe(n,p)$ which were found to be 2.1% higher and 1.2% lower than the input values respectively. Cross-section changes were also all less than 1% except for the same two reactions. For $^{27}Al(n,p)$ the cross-section was reduced by 1.2%, 1.8% and 2.8% for energy groups 10.0 MeV - 7.41 MeV, 7.41 MeV - 6.07 MeV and 6.07 MeV - 4.49 MeV respectively. For $^{56}Fe(n,p)$ the cross-section was increased by 1.4%, 1.5% and 1.3% in the same groups. As far as the spectrum is concerned the largest change made was an increase of 4.7% in the energy group 7.41 MeV - 6.07 MeV except for some very large increases (up to 36%) in the low energy tail.

Final spectrum obtained normalized to unit total flux is shown in Table 3 together with the input spectrum. The absolute normalization obtained from SIMMM was a flux of 1.352×10^{8} n.cm^{-2}.sec^{-1}, corresponding to maximum reactor power of 100 kW and gold monitor reaction rate for position A[5] of 1.067×10^{-15} reactions nucleus^{-1}. sec^{-1}.

5. CONCLUSIONS

The main conclusions which can be drawn from the SIMMM run described above and other runs made previously are as follows:

(1) The NISUS evaluated spectrometry data describe the NISUS spectrum much better than does the ΣΣ evaluated spectrum[6]. The latter produces a much worse fit (F = 10.0) and changes of up to + 20% are obtained for the energy range 4.49 MeV - 6.07 MeV, as well as larger changes in the cross-section and reaction rate data.

(2) The above conclusion reinforces that obtained when the SAND-II data[20] were used.

(3) The ENDF/BIV data provides a better fit to the NISUS evaluated spectrometry data than does the SAND-II data. The fit to ΣΣ evaluated spectrometry data is not improved.

(4) The currently recommended NISUS spectrum is that obtained from SIMMM and shown in Table 3, with the reservation that the value for the energy group 5.5 keV - 7.4 keV is probably too high and the NISUS evaluated spectrometry data should be preferred for the energy range 24.8 keV - 67.4 keV. A compensating further

increase in the low energy tail below 24.8 keV is also implied.

(5) SIMMM does not at present produce any evaluation of errors in the final parameters. Subjective estimation of these leads to suggested errors for the recommended spectrum of ± 5% for the energy range 67.4 keV - 7.41 MeV, ± 20% outside this range.

(6) The implication that the Clement and Rickard[12] cross-section is the correct one to use for ^{6}Li spectrometry is somewhat intriguing and further work is needed to investigate this.

(7) The ENDF/BIV data provide such excellent consistency with the reaction rate data and NISUS spectrometry data that it may be inferred that the error matrix used is too conservative.

Finally it may be concluded that the SIMMM code is a very useful evaluation tool and the method should be applied to other neutron fields, preferably simultaneously.

REFERENCES

1) BESANT,C.B., EMMETT,J., CAMPBELL,C.G., KERRIDGE,M., and JONES,T.C., Nucl. Eng. Int., 18 , May (1973).

2) PETR,J., Ph.D. Thesis, University of London, I.C. (1973).

3) KOUTZOUKOS,G., Ph.D. Thesis, University of London, I.C. (1975).

4) FABRY,A., WILLIAMS,J.G., HANNAN,A.H.M.A., AZIMI-GARAKANI,D., 'This meeting, Vienna 15th-19th November (1976).

5) HANNAN,A.H.M.A., and WILLIAMS,J.G. ,This meeting, Vienna 15th-19th November (1976).

6) FABRY,A., DeLEEUW,G., and DeLEEUW,S., Nucl. Tech., 25 , 349 (1975).

7) BENJAMIN,P.W., KEMSHALL,C.D., and REDFEARN,J., Report AWRE-NR 1/64 (1964).

8) BENJAMIN,P.W., KEMSHALL,C.D., and BRICKSTOCK,A., Report AWRE-09/68 (1968).

9) WHALING,W., Handbuch der Physik, 34 , 193 (1958).

10) KEMSHALL,C.D., Private Communication (1974).

11) GOLD,R., ANL-6984 (1964).

12) CLEMENTS,R.T., and RICKARD,I.C., AERE-R7075, July (1975).

13) SCHWARZ,S., STROMBERG,L.G., BERGSTROM,A., Nucl. Phys. , 63 , 543 (1965).

14) RIBE,F.L., Physics Rev. , 103 , 741 (1956).

15) RICKARD,I.C., Nucl. Instr. and Meth., 113 , 169 (1973).

16) BLUET,J.C., et al., Proc. Int. Conf. Study of Nuclear Structure with Neutrons, Antwerp (1965).

17) SHEPPEY,G.C., D504 CERN 6600 Computer Program Library.

18) ROSENBROCK,H.H, Computer J., 31 ,75-82 (1960).

19) MINSART,G., Private Communication (1975).

20) McELROY,W.N., and KELLOGG,L.S., Nucl. Tech. , 25 ,180 (1975).

TABLE 1 PROTON RECOIL SPECTROMETRY DATA (from J. PETR).

Note: statistical errors are shown in brackets as the error on the last two digits.

GROUP NO.	UPPER ENERGY (MeV)	FLUX PER UNIT LETHARGY (ARBITRARY NORMALISATION)					
		0.488atm counter	0.94atm-counter	3.528atm counter	9.57atm counter	5.22atm counter	Average
21	2.019					0.759(36)	0.759(36)
22	1.827					0.760(32)	0.759(32)
23	1.653					0.861(32)	0.861(32)
24	1.496					0.875(32)	0.875(32)
25	1.353					0.942(31)	0.942(31)
26	1.225				1.096(26)	1.115(30)	1.106(24)
27	1.108				1.215(26)	1.218(28)	1.217(21)
28	1.003				1.375(25)	1.403(27)	1.389(22)
29	0.9072				1.538(25)	1.488(28)	1.513(25)
30	0.8209				1.644(25)		1.644(25)
31	0.7427				1.626(23)		1.626(23)
32	0.6721				1.731(23)		1.731(23)
33	0.6081			1.780(28)	1.756(23)		1.768(21)
34	0.5502			1.764(32)	1.728(22)		1.746(20)
35	0.4979			1.717(31)	1.655(22)		1.686(20)
36	0.4505			1.603(29)	1.587(19)		1.595(18)
37	0.4076			1.653(26)	1.621(19)		1.637(18)
38	0.3688			1.672(27)	1.621(19)		1.647(19)
39	0.3337			1.540(26)	1.581(19)		1.561(19)
40	0.3020		1.521(38)	1.591(24)	1.541(17)		1.551(16)
41	0.2732		1.479(37)	1.539(23)	1.516(17)		1.511(16)
42	0.2472		1.450(33)	1.451(22)	1.461(16)		1.454(14)
43	0.2237		1.402(32)	1.352(20)	1.360(15)		1.371(15)
44	0.2024		1.355(31)	1.291(19)	1.284(14)		1.310(14)
45	0.1832	1.247(45)	1.273(29)	1.234(19)	1.259(15)		1.253(13)
46	0.1657	1.131(42)	1.065(27)	1.098(16)			1.098(16)
47	0.1500	1.023(39)	1.143(26)	1.068(17)			1.078(17)
48	0.1357	0.978(37)	1.089(24)	1 052(14)			1.039(14)
49	0.1228	0.945(37)	0.972(22)	0.963(13)			0.960(13)
50	0.1111	0.856(20)	0.814(11)				0.835(11)
51	0.0865	0.733(17)	0.722(11)				0.727(10)
52	0.0674	0.593(16)	0.562(09)				0.578(09)
53	0.0525	0.448(13)	0.435(07)				0.442(07)
54	0.0409	0.321(10)					0.321(10)
55	0.0318	0.268(08)					0.268(08)
56	0.0248						

TABLE 2 EVALUATED SPECTROMETRY DATA.

GROUP NO.	UPPER ENERGY (MeV)	FLUX PER UNIT LETHARGY (ARBITRARY NORMALISATION)		
		PROTON RECOIL	LI6 SPECTROMETER	EVALUATED SPECTROMETRY
8	7.408		0.0807	0.0807 ± 20%
9	6.703		0.133	0.133 ± 20%
10	6.065		0.187	0.187 ± 20%
11	5.488		0.267	0.267 ± 20%
12	4.966		0.303	0.303 ± 20%
13	4.493		0.374	0.374 ± 20%
14	4.066		0.401	0.401 ± 20%
15	3.679		0.469	0.469 ± 20%
16	3.329		0.575	0.575 ± 20%
17	3.012		0.681	0.681 ± 20%
18	2.725		0.779	0.779 ± 20%
19	2.466		0.841	0.841 ± 20%
20	2.231		0.812	0.812 ± 20%
21	2.019	0.759	0.836	0.759 ± 5%
22	1 827	0.760	0.799	0.760 ± 5%
23	1.653	0.861	0.850	0.861 ± 5%
24	1.496	0.875	0.901	0.875 ± 5%
25	1.353	0.942	1.000	0.942 ± 5%
26	1.225	1.106	1.100	1.106 ± 5%
27	1.108	1.217	1.232	1.217 ± 5%
28	1.003	1.389	1.409	1.389 ± 5%
29	0.9072	1.513	1.581	1.513 ± 5%
30	0.8209	1.644	1.655	1.644 ± 5%
31	0.7427	1.626	1.668	1.626 ± 5%
32	0.6721	1.731	1.665	1.731 ± 5%
33	0.6081	1.768	1.727	1.768 ± 5%
34	0.5502	1.746	1.769	1.746 ± 5%
35	0.4979	1.686	1.721	1.686 ± 5%
36	0.4505	1.595	1.750	1.595 ± 5%
37	0.4076	1.637	1.827	1.637 ± 5%
38	0.3688	1.647	1.569	1.647 ± 5%
39	0.3337	1.561	1.526	1.561 ± 5%
40	0.3020	1.551	1.368	1.551 ± 5%
41	0.2732	1.511	1.340	1.511 ± 5%
42	0.2472	1.454	1.317	1.454 ± 5%
43	0.2237	1.371	1.317	1.371 ± 5%
44	0.2024	1.310	1.335	1.310 ± 5%
45	0.1832	1.253	1.139	1.253 ± 5%
46	0.1657	1.098	1.072	1.098 ± 5%
47	0.1500	1.078	1.026	1.078 ± 5%
48	0.1357	1.039	0.981	1.039 ± 5%
49	0.1228	0.960	0.972	0.960 ± 5%
50	0.1111	0.835	0.902	0.835 ± 5%
51	0.0865	0.727	0.792	0.727 ± 5%
52	0.0674	0.578	0.587	0.578 ± 5%
53	0.0525	0.442	0.444	0.442 ± 5%
54	0.0409	0.321	0.405	0.321 ± 5%
55	0.0318	0.268	0.378	0.268 ± 5%
56	0.0248		0.243	
57	0.0193		0.194	
58	0.0150		0.161	
59	0.0117			

TABLE 3 NISUS SPECTRUM EVALUATED BY SIMMM , compared with evaluated spectrometry data and Mol-ΣΣ evaluation[6].

GROUP NO.	UPPER ENERGY (MeV)	LETHARGY WIDTH	GROUP FLUX (NORM. TO UNITY)		RATIO TO ΣΣ EVALUATION	
			NISUS EVAL. SPECT.	SIMMM NISUS EVAL.	NISUS EVAL. SPECT.	SIMMM NISUS EVAL.
1	14.918	0.4	2.690E-04	2.701E-04	0.985	0.990
2	10.000	0. 3	1.716E-03	1.726E-03	0.985	0.991
3	7.4082	0.2	3.835E-03	3.887E-03	1.077	1.092
4	6.0653	0.3	1.356E-02	1.280E-02	1.333	1.258
5	4.4933	0.2	1.388E-02	1.318E-02	1.194	1.134
6	3.6788	0.3	3.090E-02	2.979E-02	1.090	1.051
7	2.7253	0.2	2.901E-02	2.834E-02	1.160	1.133
8	2.2313	0.3	4.384E-02	4.209E-02	0.958	0.920
9	1.6530	0.2	3.110E-02	3.008E-02	0.945	0.914
10	1.3534	0.5	1.105E-01	1.065E-01	0.991	0.955
11	0.82085	0.5	1.525E-01	1.472E-01	0.966	0.932
12	0.49787	0.5	1.456E-01	1.406E-01	0.937	0.905
13	0.30197	0.5	1.289E-01	1.248E-01	0.986	0.955
14	0.18316	0.5	9.724E-02	9.414E-02	1.060	1.026
15	0.11109	0.5	6.996E-02	6.774E-02	1.085	1.051
16	67.379E-03	2.5	1.097E-01	1.344E-01	0.985	1.207
17	5.531E-03	2.5	1.475E-02	1.892E-02	0.985	1.264
18	0.454E-03	2.5	2.643E-03	3.478E-02	0.985	1.297
19	37.267E-06	2.5	8.238E-05	8.216E-05	0.985	0.983
20	3.059E-06	2.0	0.0	0.0		
	0.414E-06					

I.7. Spectrum Characterization and Threshold Reaction Rate Measurements in the Neutron Field of VIPER

Edited by M H McTaggart

This work is the combined effort of the VIPER operating Staff and others including the following:-
W J Paterson, K L Shutler, M L Mullender, C D Kemshall, R Tremble, A F Thomas.

Assistance with some of the measurements by Staff of the Environmental and Medical Sciences Division at AERE is also acknowledged.

This work has been carried out with the support of the Procurement Executive, Ministry of Defence.

SNA
MOD (PE)
AWRE
Aldermaston
Berks.

1. INTRODUCTION

The transient neutron field in the VIPER facility is supplied by a short (400 μsec FWHM) burst of fissions in the reactor core. The transient is controlled by the inherent temperature coefficient of the fuel and though it can be used as a steady state reactor up to a power of a few kilowatts VIPER is not cooled and is not the type of fully characterized field designated "Standard Neutron Field". Nor is it a "Reference Neutron Field", though it is reasonably well characterized, because it is not necessarily available to a community of users. However, in the opinion of its operators it can be regarded as a "Controlled Neutron Environment" and as such could play a role in validating dosimetry data. Its unique feature of a short duration transient field is particularly useful when short lived activities are being studied. For its role as a test facility for weapon effects, the need for accurate definition of dose has meant that the radiation fields which it produces have been characterized with reasonable accuracy and this feature may be of value in the general area of cross-section checking which has applications in reactor design, CTR blanket design etc. as well as the particular dosimetry applications.

It has been used recently to provide delayed neutron data for the three main isotopes of interest to reactor designers, ^{235}U, ^{238}U and ^{239}Pu (to be published in J.BNES).

2. DETAILS OF IRRADIATION FACILITY

The VIPER reactor (Figure 1) consists of a core of 37% enriched uranium fuel pins in a matrix of aluminium loaded epoxy resin and copper surrounded by a 20 cm thick copper reflector. (Weale et al, 1968, McTaggart et al, 1968). The reactor can either produce a single fission burst or be operated at steady power for calibration measurements on ion chambers etc. In a normal full size pulse of 3.46×10^{17} fissions (2.9 kW-h) the power reaches a maximum of about 20,000 MW and has a full width at half maximum of 400 μs. For experimental purposes the pulse field is defined in terms of the temperature rise in the fuel at a standard position known as the "Reactor Temperature Rise" (RTR). A normal full-size pulse produces a RTR of 200°C.

3. CHARACTERIZATION OF VIPER NEUTRON FIELDS

Extensive measurements of flux, spectrum and selected reaction rates in and around VIPER have employed the wide range of neutron spectrometers available at AWRE (Kemshall et al) to derive spectra within the reflector irradiation cavity, outside the copper reflector and at a position 3m from the reactor. These three positions 1 , 2 and 3 in figure 1 give respectively high, medium and low neutron dose environments and allow a range of transient (and permanent) effects on materials, circuits etc. to be studied.

The Tables and graphs attached summarize the main features of these three positions. The threshold reaction rates of Np^{237} fission, $Ni^{58}(n,p)\,Co^{58}$ and $S^{32}(n,p)$ provide a check on the accuracy of the spectrum, within the measurement accuracies, and the normal procedure for a VIPER irradiation is to use one of the threshold detectors to determine the dose delivered to the item.

3.1 Large Irradiation Cavity

Figure 2 shows spectra at three positions within the cavity. They were measured by a combination of proton recoil techniques, spherical proportional counters and photo-plates. Using this spectrum and the cross-sections for S(n,p) from DFN 229 (AWRE data file number) and for Ni (n,p) from DFN 236 the predicted and measured reaction rates at the three locations are given in Table 1 . The differences are attributed to (i) absolute flux uncertainities (ii) cross-section errors (iii) measurement errors in the reaction rate determinations. The first is eliminated to some extent by comparing the ratios of reaction rates rather than their absolute values. The thresholds of both these reactions are above 1 MeV and though 15% of the activation arises from neutrons of energy greater than 5.7 MeV (the upper limit of the measured spectra) extrapolation errors are not expected to contribute more than 3% errors.

3.2 Outside Copper Reflector on North Face

Figure 3 shows the spectrum measured at this location covering the range 40 KeV to 2.5 MeV. The S (n,p) and Ni (n,p) reaction rates are included given in Table 1. Similar errors apply as to the large cavity measurements except that the upper limit of the spectrum of 2.5 MeV is below the corresponding limit of 5.7 MeV in the cavity measurement and extrapolation errors are clearly larger and more serious. An attempt to measure the U238 fission rate was made using a fission deposit with 0.03% U235. Because of the large component of scattered low energy neutrons the total fission rate in this deposit was due 60% to U235 fissions and 40% to U238 fission. The U235 correction therefore dominated the analysis and the measured value of 4×10^7 was less than the value predicted from the spectrum of 6.8×10^7 fissions g^{-1} in a full size pulse.

3.3 In Reactor Cell 3m from VIPER

The spectrum at this position was more extensively determined and the energy range was from 1 KeV to 10 MeV. As well as proportional counters and photo-plates, an organic scintillator with pulse shape discrimination (NE 213) was used to extend the upper limit to 10 MeV and a supporting measurement with a ^{3}He counter confirmed the other results. Table 2 - and Figure 4 give the spectrum in a full size VIPER pulse.

Gamma-ray dose measurements at the same position are given in Table 3 Corrections to the film dosimeter results for fast and thermal neutron contributions and for the indicated gamma ray energy were applied.

S (n,p) measurements were made at this position and comparison with the spectrum prediction is also included in Table 2.

4. ORIGIN OF CROSS-SECTION DATA

The S (n,p) and Ni (n,p) cross-sections were obtained from the DFN's quoted above ie Nos. 229 and 236 respectively. The origin of this data is:

AFWL-TR-65-34 (August 1965) by R C Barrall and W N McElroy (a full print-out of the data can be supplied on demand).

To calculate the reaction rates from the quoted spectra a flux weighting routine was used to obtain group cross-sections to suit the groups into which the measured spectra were arranged.

5. CONCLUSIONS

A neutron flux environment of transient duration is available in VIPER. In a full size VIPER pulse characterized by a 200°C temperature rise it gives a fluence above 1 MeV ranging from

$\emptyset$ n cm^{-2} in the large irradiation cavity

7.6×10^{-4} $\emptyset$ n cm^{-2} outside the north face and

7.2×10^{-5} $\emptyset$ n cm^{-2} 3 m from the reactor.

$\emptyset$ is defined in terms of the displacement damage fluence in silicon, for which the effective threshold is about 100 KeV and the "cross-section" is relatively flat from 200 KeV to 4 MeV. At the reference position in the irradiation cavity $\emptyset = 1.6 \times 10^{14}$ 1 MeV neutrons cm^{-2}, ie. the damage effects produced in silicon by the VIPER fluence are the same as would be produced by the quoted fluence of 1 MeV neutrons. The total fluence is not reliably determined by the measurements described because the low energy component has not been measured directly.

REFERENCES

McTaggart, M H Goodfellow, H McCormick, WB. and Weale JW.
The Fast Pulsed Reactor VIPER, Part 2:
Reactor physics measurements and analysis.
Journal of British Nuclear Energy Society 7, 328 (1968).

Weale JW, Goodfellow H. McTaggart MH and Warnke EG.
The fast pulsed reactor VIPER, Part 1: General description.
Journal of British Nuclear Energy Society 7, 313 (1968).

Kemshall C D.
Use of spherical proportional counters for neutron spectrum measurements, AERE R No. 0-31/73 (1973).

Delafield H J, Mullender M L, Gibson J A B, Kemshall C D,
Reading A H, Holt P D, and Boot S J
Measurements of the Uniformity of the Radiation Field
and the Neutron Leakage Spectrum of the VIPER Reactor
(To be published as an AEhE-R series report)

Table 1

Comparison of Predicted and Measured Sulphur and Nickel Activations

Location		Sulphur DPS/Gram		Nickel DPS/Gram	
		Predicted	Measured	Predicted	Measured
Large Cavity (1)	Front	3.03×10^4	3.6×10^4	6.5×10^3	7.4×10^3
	Centre	8.84×10^3	1.1×10^4	1.89×10^3	2.1×10^3
	West Wall	7.05×10^3	7.4×10^3	1.52×10^3	1.5×10^3
North Face (2)		23.16	22.0 ± 4.4	5.42	5.3 ± 0.4
3m position (3)		2.18	1.87 ± 0.20		

Table 2 - Neutron fluence spectrum for full size VIPER pulse (1 keV to 14 MeV)

Neutron energy eV	Fluence per lethargy n cm^{-2}	Neutron energy eV	Fluence per lethargy n cm^{-2}	Neutron energy eV	Fluence per lethargy n cm^{-2}	Neutron energy eV	Fluence per lethargy n cm^{-2}
0.1413E+8	0.5000E+1						
0.1259E+8	0.1000E+4 (1)						
0.1122E+8	0.8000E+5						
0.1000E+8	0.5139E+7						
0.8913E+7	0.6450E+8	0.8913E+6	0.2265E+11	0.8913E+5	0.4536E+11	0.8913E+4	0.3057E+11
0.7943E+7	0.2281E+9	0.7943E+6	0.2848E+11	0.7943E+5	0.5926E+11	0.7943E+4	0.3141E+11
0.7080E+7	0.2653E+9	0.7080E+6	0.3645E+11 (3)	0.7080E+5	0.5978E+11	0.7080E+4	0.2528E+11
0.6310E+7	0.4164E+9 (2)	0.6310E+6	0.4274E+11	0.6310E+5	0.5281E+11	0.6310E+4	0.2463E+11
0.5623E+7	0.4882E+9	0.5623E+6	0.4468E+11	0.5623E+5	0.4982E+11	0.5623E+4	0.2502E+11
0.5012E+7	0.5978E+9	0.5012E+6	0.4536E+11	0.5012E+5	0.4143E+11	0.5012E+4	0.2517E+11
0.4467E+7	0.6503E+9	0.4467E+6	0.5008E+11	0.4467E+5	0.3356E+11	0.4467E+4	0.2278E+11
0.3981E+7	0.8967E+9	0.3981E+6	0.6083E+11	0.3981E+5	0.2727E+11	0.3981E+4	0.1888E+11
0.3548E+7	0.1321E+10	0.3548E+6	0.6592E+11	0.3548E+5	0.2727E+11	0.3548E+4	0.1334E+11
0.3162E+7	0.1594E+10	0.3162E+6	0.6975E+11	0.3162E+5	0.3881E+11	0.3162E+4	0.1196E+11
0.2818E+7	0.1731E+10	0.2818E+6	0.7027E+11 (4)	0.2818E+5	0.5228E+11 (4)	0.2818E+4	0.1246E+11 (4)
0.2512E+7	0.2255E+10	0.2512E+6	0.6613E+11	0.2512E+5	0.4599E+11	0.2512E+4	0.1352E+11
0.2239E+7	0.2989E+10	0.2239E+6	0.5873E+11	0.2239E+5	0.3723E+11	0.2239E+4	0.1523E+11
0.1995E+7	0.3985E+10	0.1995E+6	0.6004E+11	0.1995E+5	0.3288E+11	0.1995E+4	0.1699E+11
0.1778E+7	0.5244E+10 (3)	0.1778E+6	0.6933E+11	0.1778E+5	0.3487E+11	0.1778E+4	0.1888E+11
0.1585E+7	0.6712E+10	0.1585E+6	0.5858E+11	0.1585E+5	0.3356E+11	0.1585E+4	0.2014E+11
0.1413E+7	0.8495E+10	0.1413E+6	0.6843E+11	0.1413E+5	0.3461E+11	0.1413E+4	0.2045E+11
0.1259E+7	0.1049E+11	0.1259E+6	0.7116E+11	0.1259E+5	0.3021E+11	0.1259E+4	0.1963E+11
0.1122E+7	0.1363E+11	0.1122E+6	0.5978E+11	0.1122E+5	0.2622E+11	0.1122E+4	0.1775E+11
0.1000E+7	0.1804E+11	0.1000E+6	0.4772E+11	0.1000E+5	0.2543E+11	0.1000E+4	0.1604E+11

Neutron spectrum given by:
(1) Extrapolation
(2) Organic scintillator, shape normalized to gas proportional counter
(3) Nuclear track plates
(4) Hydrogen recoil gas proportional counter

Table 3 - Gamma-ray measurements in free air at Position C 3 m from centre of VIPER reactor

Dosimeter	Measurement	γ-ray dose (rad)	γ-ray dose normalized to full size pulse (rad)	
TLD	Low power	44.4 ± 1.4	71.1 ± 2.2	73 ± 2
	Pulse	74.9 ± 2.7	74.9 ± 2.7	
Film	Low power	47.6 ± 0.5	76.2 ± 0.8	73 ± 3
	Pulse	70.0 ± 1.3	70.0 ± 1.3	
Paired ion chambers	Low power	~38	~60	

Notes (1) A derived factor of 0.96 has been used to correct the observed TLD results for their expected response to fast neutrons.

(2) A derived factor of 0.89 has been used to correct the observed film results for their expected response to fast and thermal neutrons. An additional correction of 0.65 was applied to allow for the films over-response to high energy γ-rays

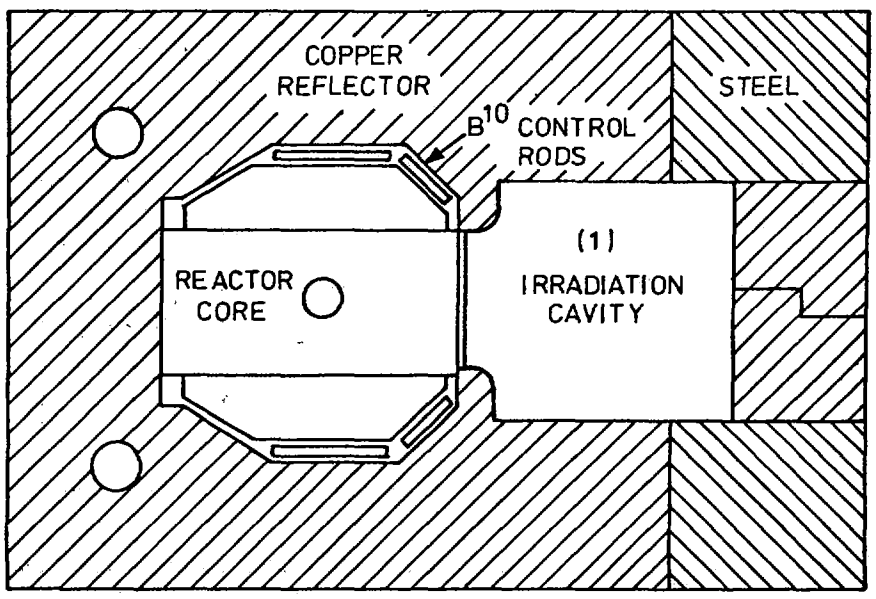

FIGURE 1. SECTION THROUGH VIPER REACTOR

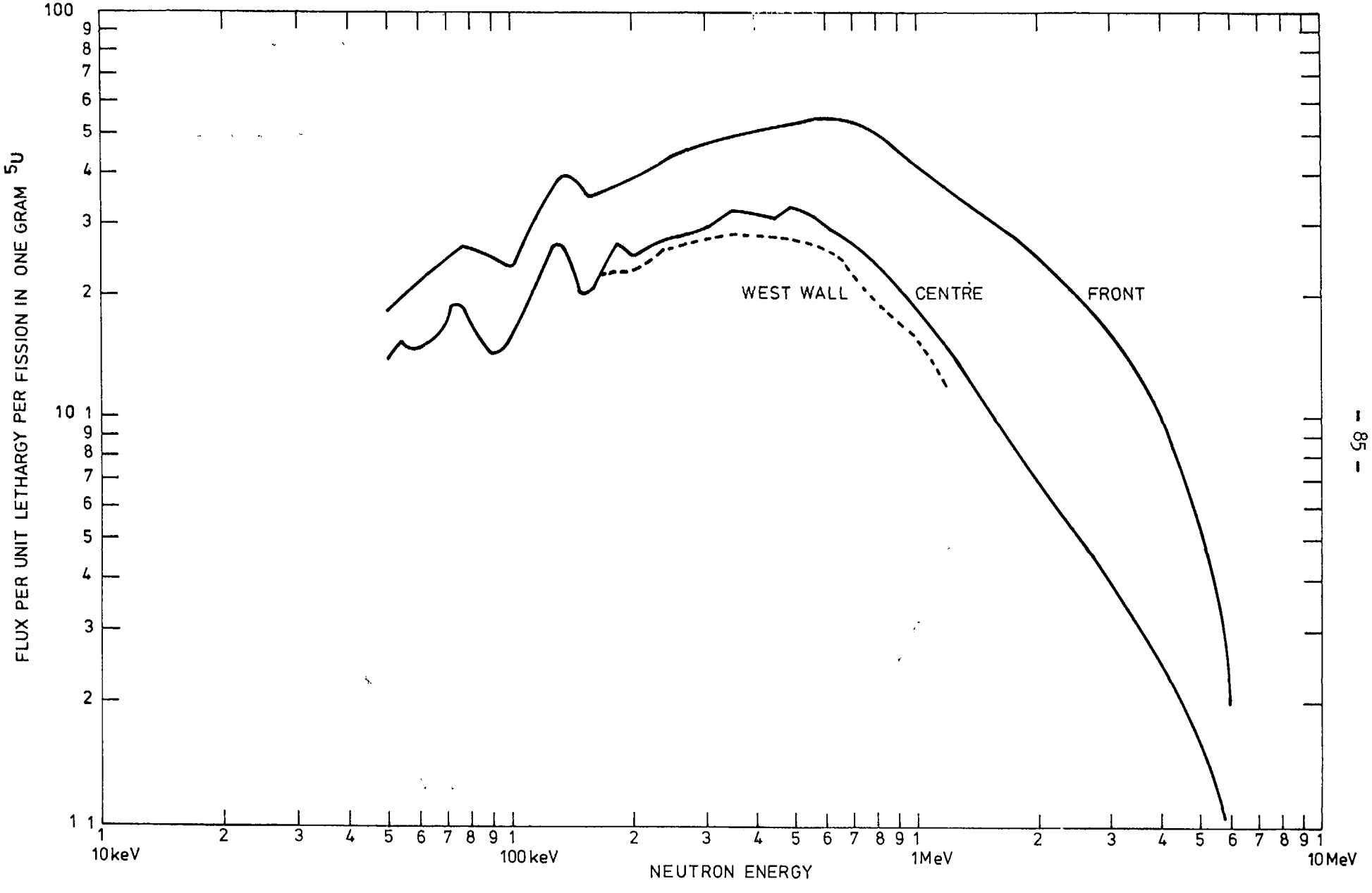

FIGURE 2. MEASURED NEUTRON SPECTA IN VIPER LARGE CAVITY

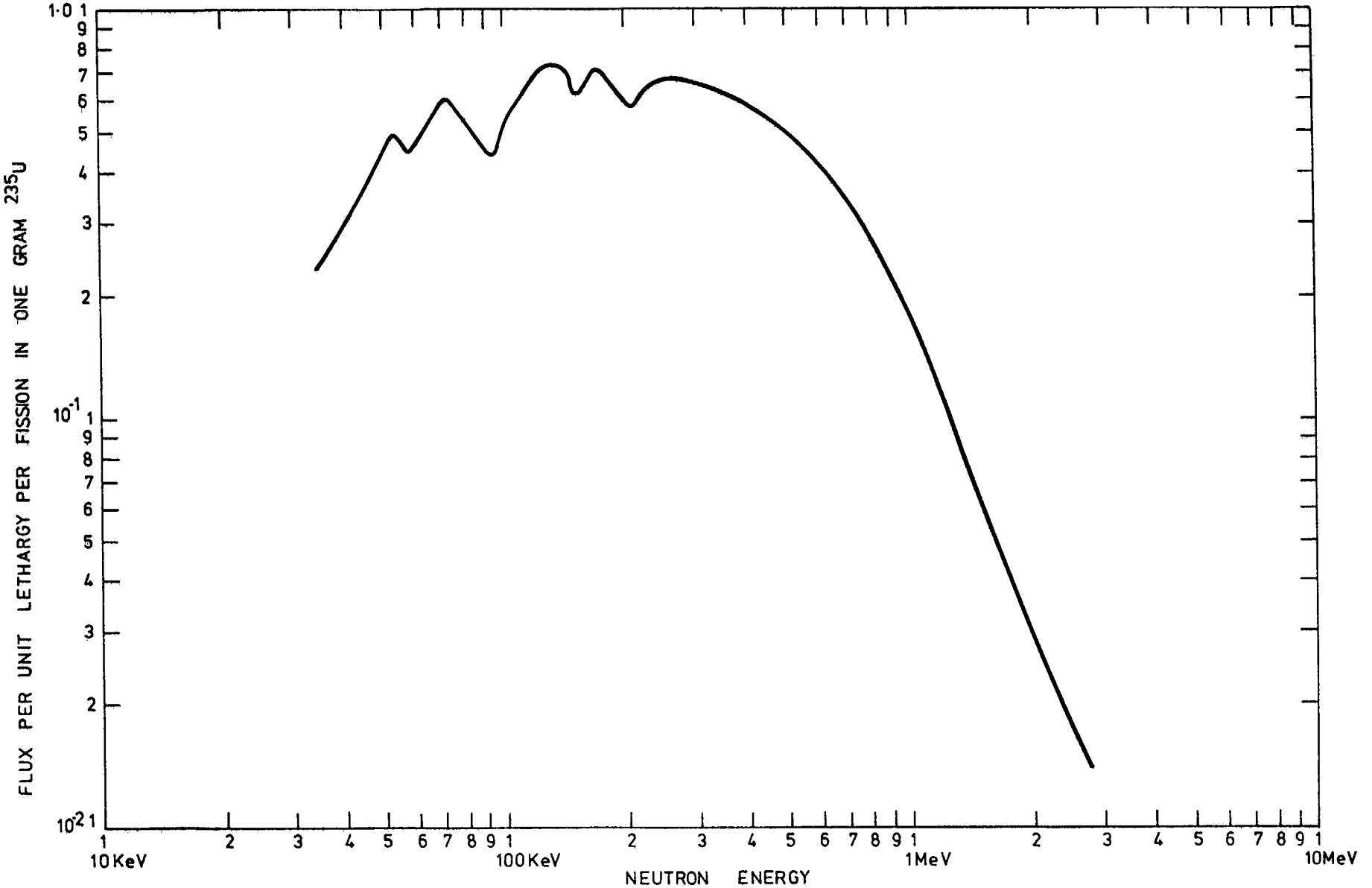

FIGURE 3. VIPER MEASURED SPECTRUM AT 87 cm FROM CORE CENTRE

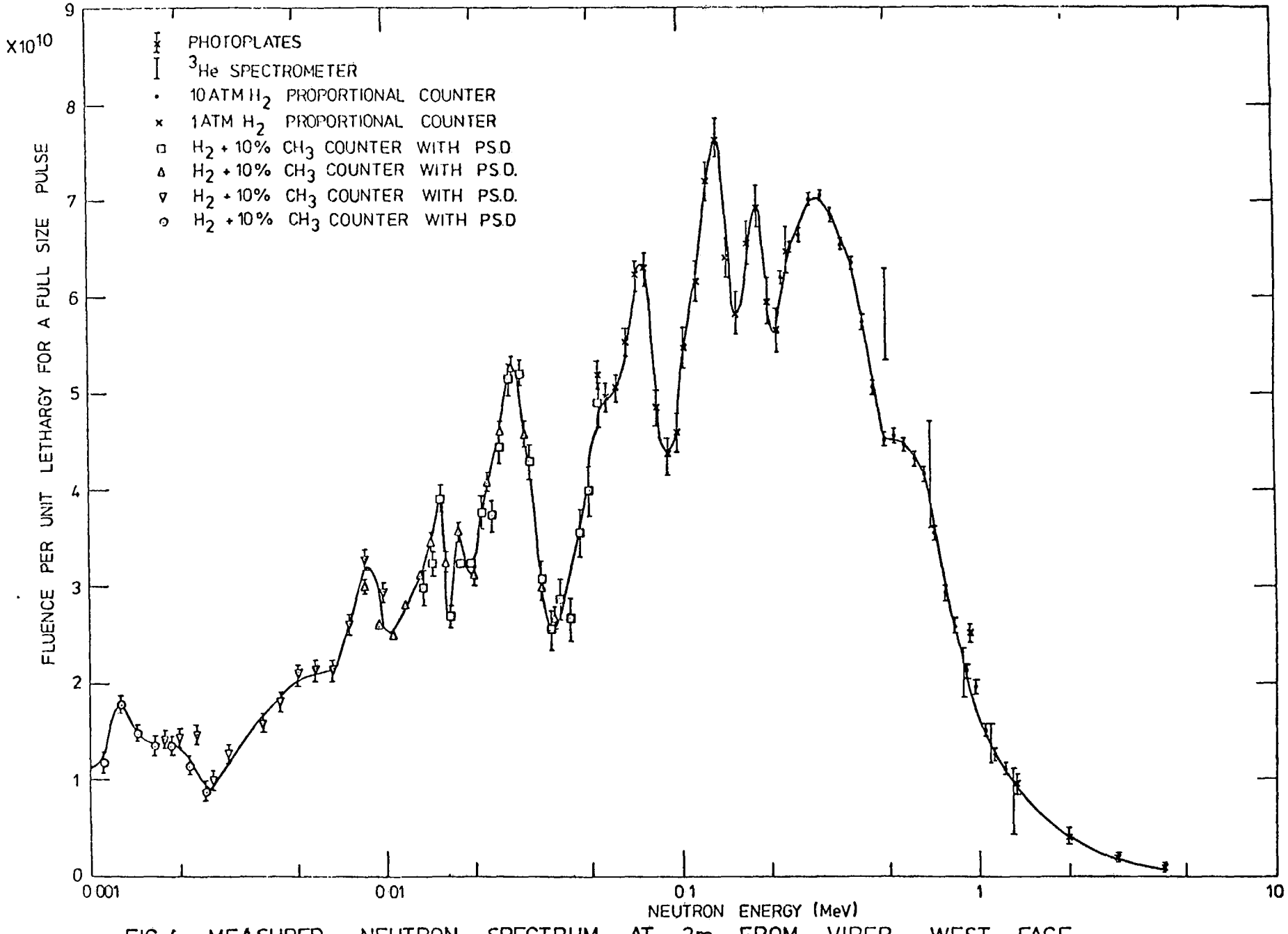

FIG. 4. MEASURED NEUTRON SPECTRUM AT 3m FROM VIPER WEST FACE

I.8. SEVERAL STUDIES OF NEUTRON STANDARD FIELDS IN THE FAST SOURCE REACTOR 'YAYOI'

A. Sekiguchi*, M. Nakazawa*, T. Kosako*

H. Wakabayashi+ and M. Akiyama+

Abstract: Based on the results of intercomparison of spectrometers, the neutron spectra in the reactor core or through the beam hole of reactor 'YAYOI' were evaluated experimentally. The absorbed dose value of hydrogen and carbon in the reactor core center were compared for three kinds of dose measurement techniques, and the good agreement was found between calorimeter data and foil + TLD data.

The central neutron field of the octagonal lead pile combined with a reactor core as a neutron source was also determined experimentally, and its usefulness as standard field is discussed.

1. Introduction

The fast neutron source reactor 'YAYOI' is a 2kW air cooled reactor fueled with 28kg of 93% enriched metal uranium, and the details are described in the appendix (1). It has been operated since 1971, and recently a pulsed operation of the reactor has also been developed using the pile oscillator systems. Moreover, it is promised to intensify the pulsed operation with the LINAC booster systems that are now under construction.

The 'YAYOI' has the capability to provide a variety of standard neutron fields by moving the core assembly in the different surroundings as are shown in Fig. 2 of appendix (1). At the present stage, however, three kind of neutron fields have been characterized based on the intercomparison studies of spectrometers and dosimeters. The fields are (1) the central neutron field of the reactor core, (2) the beam neutrons extracted from the blanket surface through the fast column beam hole, and (3) the central neutron field of the lead intermediate column.

*) Dept. of Nuclear Engineering, University of Tokyo, Japan
+) Nuclear Engineering Research Laboratory, Univ. of Tokyo, Japan

2. Intercomparison on Fast Neutron Spectrometry

To evaluate the results of a reactor fast neutron spectrometry, the intercomparison of spectrometers has been performed in the central neutron field of the reactor core and with the beam neutrons extracted from the fast column beam hole. The spectrometers used for intercomparison are Li-6 sandwich counter, activation foils and micro fission chambers in the case of core-center field, and NE-213 liquid scintillation counter, He-3 proportional counter, proton recoil proportional counter and double crystal type time of flight spectrometer in the case of beam neutron measurement. Unfortunately, the diameter of the glory hole which is penetrating the core-center is too small of 2cm to insert usual counter type spectrometers, except the specially prepaired Li-6 sandwich counter.

Among these works, NE-213 scintillation counter technique has been investigated independently by three groups of the different universities. This kind of comparison is one of the main objects of intercomparison.

Fig. 1 shows the result in the core-center field. When we use micro fission chambers, the data analysis has based on the assumption that the spectrum is composed of the following two semi-empirical spectrum modes.

$$\phi(u) = a \cdot \phi i(u) + b \cdot x(u)$$

where

$$\phi i(u) = \text{inelastically scattered mode}$$

$$= 11.73\, E^{1.8188} \exp(-3,7378E)$$

$$X(u) = \text{fission -spectrum mode}$$

$$= 0.77\, E^{1.5} \exp(-0.776E) \quad : E(MeV)$$

Coefficients of a and b have been determined from the reaction rates of four kind of chambers (enriched uranium, natural uranium, Thorium-232 and Neptunium chambers)by using the least square method. The result was $a/(a+b) = 0.432$.

The reaction-rate measurements of activation foils were carried out by independent two groups, and one set of the data has been simply analyzed by using the improved constants of Hughes' method explained in Appendix (2) which has been developed by one of the authors.

The result of spectrometry using a Li-6 sandwich counter has made remarkable differences from the others in the energy ranges of near 256keV and several MeV. The cause is not yet clear at present.

Fig. 2 shows the result of intercomparison of counter type spectrometers with the fast-column beam neutrons. As a whole, it will be said that th data are consistent each other within ±5% discrepancy, and detail descriptions of this study are now preparing. In this figure, however, it will be found that some appreciable discrepancy has been recognized for the results of NE-213 scintillation counter spectrometry obtained by the different two groups. At the present stage, it has been confirmed that the main reason of discrepancy is attributed to the difference of estimation of luminous output of the scintillator for recoil proton.

3. Dose Measurements in the Central Field of the Reactor Core

Several independent dosimetry works have been carried out in the core center of fast source reactor 'YAYOI', where neutron spectrum has been well established through both experiments and calculations as is shown in Fig. 1.

In-core neutron dosimeters like threshold and resonance foils, absolute fission chambers and sometimes solid-state fission track detectors have been used together with a thermo-luminescent gamma-ray detector (Mg_2Sio_4: Tb) with little neutron sensitivity. The absolute value of a total neutron flux and gamma-ray dose in the reactor core center has been determined from the data of the above dosimeters; $(7.5 \pm 0.5) \times 10^{11}$nv and 1.2 MR/hr respectively at the reactor operation of 2kW full power.

The value of parameters of parameter reprensentation of spectra have also been determined from the data of the above dosimeters. By using the reported value of the energy dependent KERMA values for the elements, the absorbed dose of several typical materials can be calculated easily corresponding to parameters. And some results have been tabulated.

The absorbed dose has been measured also by a calorimetric technique in the specimen of polyethylene, graphite, lead, aluminium and LiF deposited aluminium. And special purpose two Fricke dosimeters with two kinds of solvents of usual and heavy water have been applied for dose determination.

The results of three kinds of absorbed dose measurement have been compared about an absorbed dose value of hydrogen and carbon, whose result is shown in Table 1. It is confirmed that the best agreement is between calorimeter and foil, but a little deviation is found for Fricke dosimeter.

4. Studies on the Lead Column with a Combined Reactor Core

The lead column as an intense steady standard neutron field of intermediate energy region has been developed as a successive study of lead slowing-down time spectrometer[1]. The experimental configurations are shown in Fig. 3.

As a course of study for characterization, the slowing-down time spectrometry has been first applied by placing the portable pulsed neutron source using D-T reactions in the center of lead column, D-1.

A typical result is shown in Fig. 4, and agreed well with the parameter representation of spectrum based on the continuous slowing-down model. Some interesting observations have been made in relation to the effect of many structural iron materials being contained in the column. The slowing-down time spectrometry has been remarkably influenced by this iron content to be shortened the slowing-down time and to be broadened the energy resolution. Corresponding to this effect, the slowing-down time was modified by introducing a new concept of "effective Fe ratio" defined as the assumed value of space depended iron abundance in a homogeneously mixed field of iron and lead. When we use this modified value, the usual relation between slowing-down time and energy is retained. The results are shown in Table 2.

However, the neutron spectrum itself is not very much affected by the iron, fortunately. Because the shape of spectra depends only on the moderating ratio of medium, $\Sigma a/\xi\Sigma_s$, which is weakly influenced by iron content on account of both $\xi\Sigma_s$ and Σa of an iron have a similar energy dependency. On the other hand, the slowing-downtime depends on the value of $\xi\Sigma_s$ which is strongly influenced by the content of iron.

As a next stage of experiment, the central neutron field of the lead column have been measured by different techniques when the reactor was operated stationary at the off-center position named 'C-2' in Fig. 3. The preliminary result of spectrum determination by sandwich-foils, proton recoil

proportional counter(4 atm H_2gas) and He-3 proportional counter is shown in Fig. 5, and agreed well with the calculated one. It should be pointed out that all results are normalized to the absolute reactor power-level. And it is almost the same spectrum shape as the case of application of slowing down time technique.

In this configuration of the assembly, wide space of the central position of the lead pile have almost the same neutron spectrum, and this space could be utilized as a standard neutron field of intermediate energies. By placing the block of a heavy resonance material in this position, an intense characteristic neutron field in the typical reactor materials, such as uranium, sodium or their mixtures would be produced.

5. Conclusion

Three neutron fields in YAYOI that were named as core-cencer field, fast-column beam neutrons and lead intermediate pile have been characterized based on the successful results of intercomparison studies of spectrometers and/or several integral dosimeters. Each field presents a typical neutron spectral characteristics to be required for the standard field in a fast and intermediate energy region.

For the purpose of practical dosimetry use, simple and accurate parameter representations of the neutron spectra have been applied to both the core-center field and the lead intermediate pile. The computational results of transport-code have also been compared with the experimental results.

The pulsed operation of YAYOI with a Linac which are now preparing shall be led to an additional useful technique in the application of those standard neutron fields to the neutron spectrometry and dosimetry works.

Reference

(1) H. WAKABAYASHI, A. SEKIGUCHI, M. NAKAZAWA and O. NISHINO;
"Some New Applications of Neutron Slowing Down Time Spectrometry",
Journal of Nucl. Sci. & Technol. 7, 487, (1970)

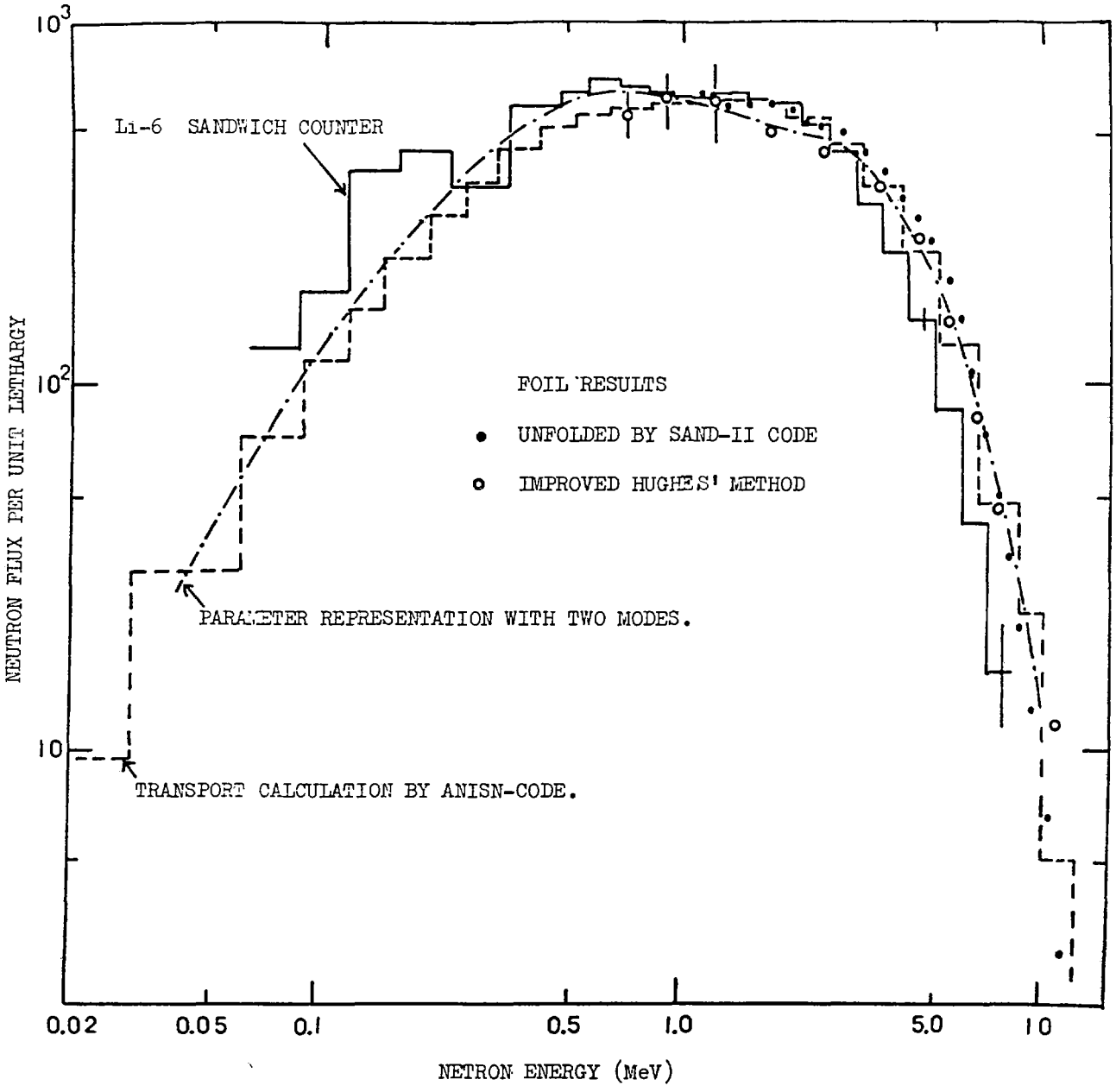

Fig.1 . Neutron Spectrum in the Central Field of 'YAYOI' core.

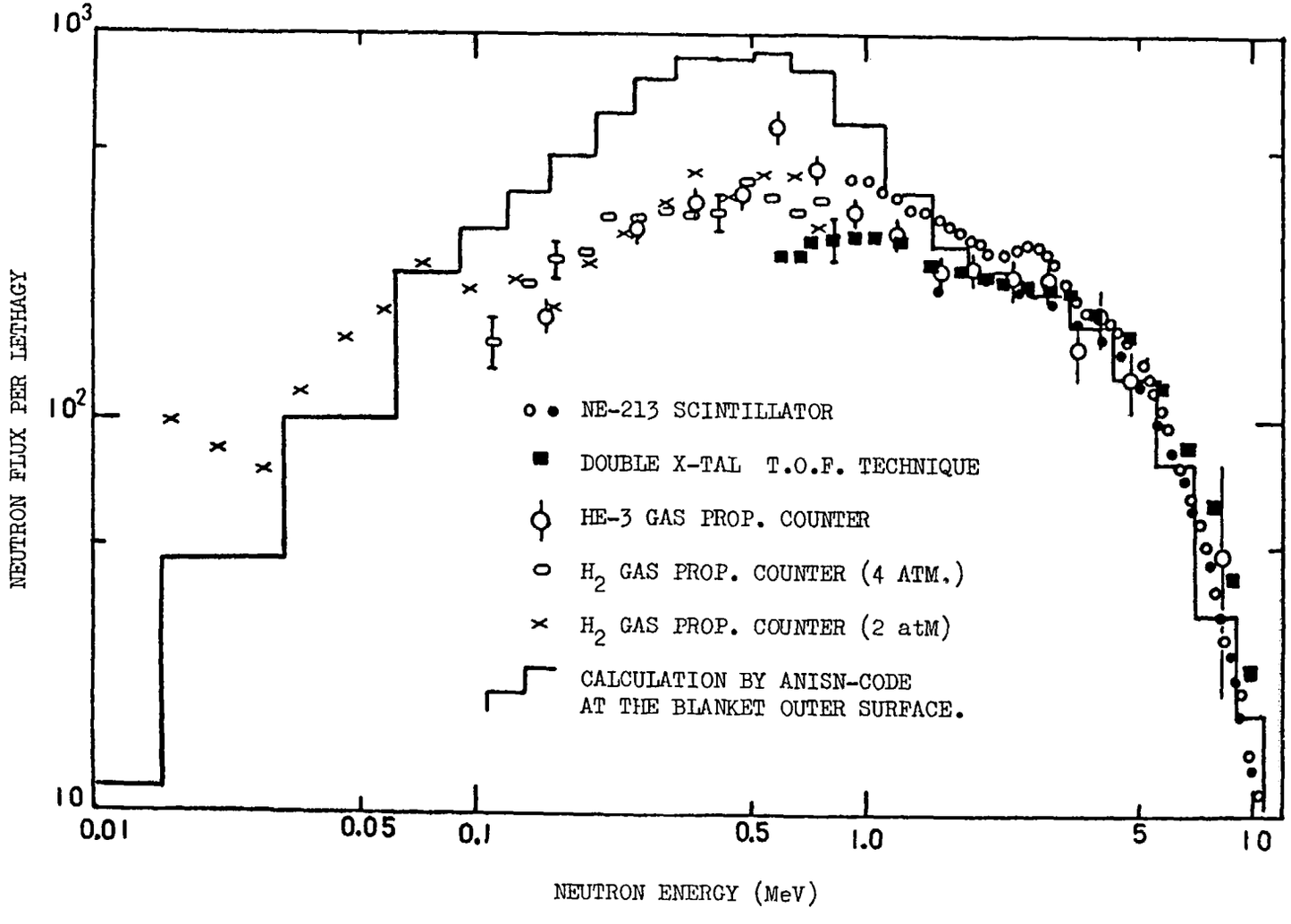

Fig. 2. The Fast-Column Beam Neutron Spectrum in YAYOI on the 1 WATT OPERATION

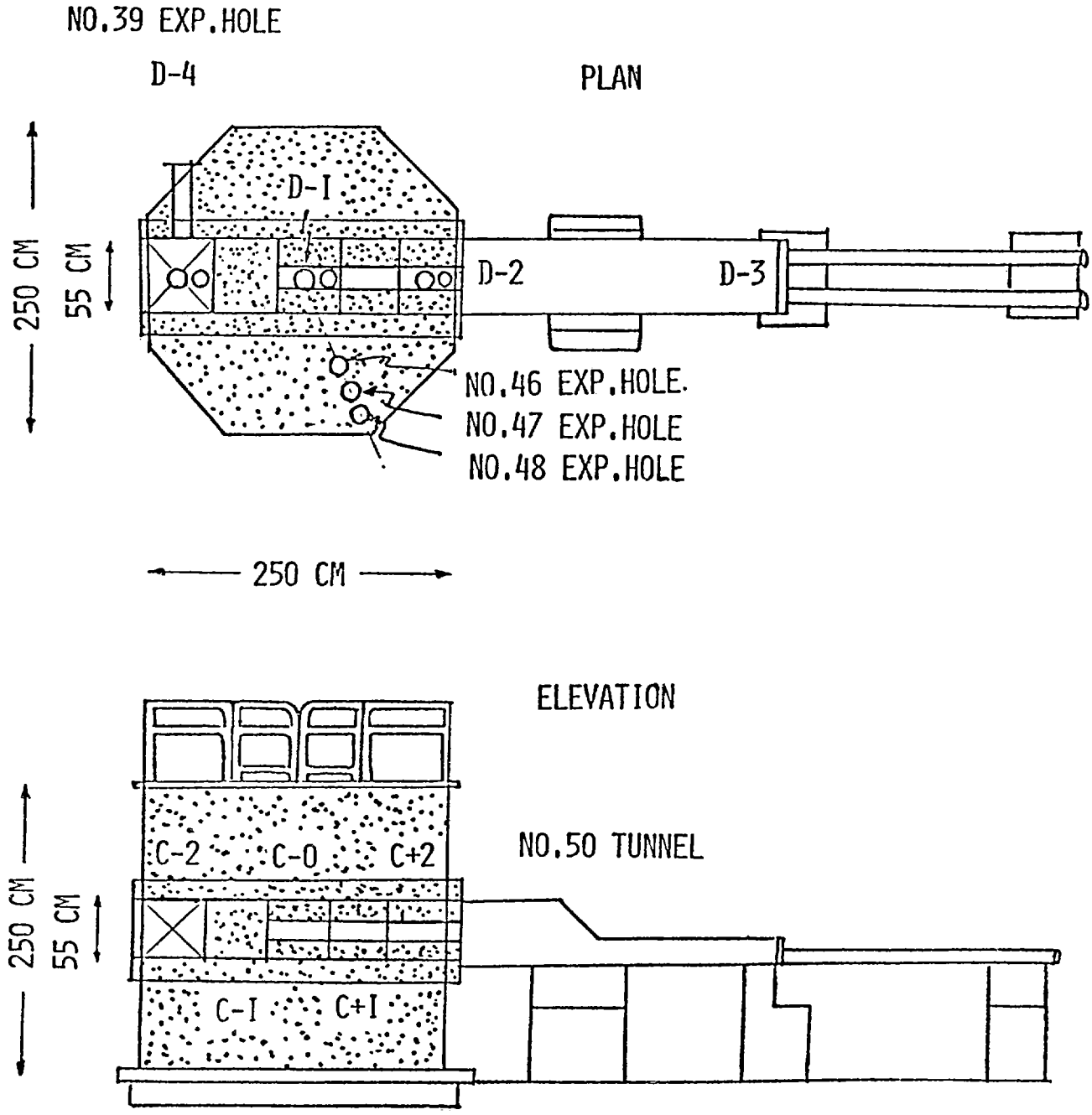

FIG.3 YAYOI OCTAGONAL PB-PILE
STANDARD MEASURING POINTS

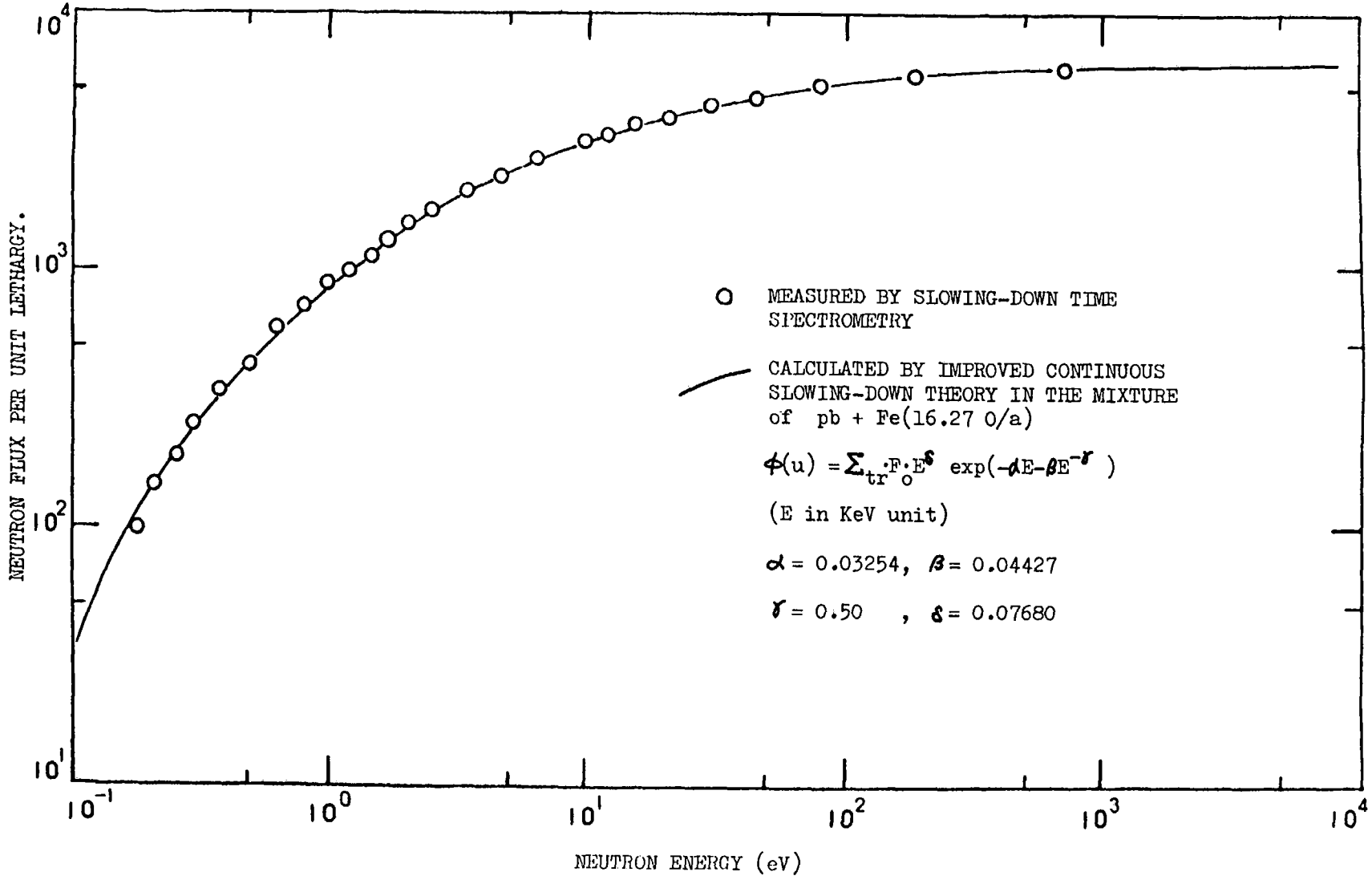

Fig.4. Neutron Spectrum of Lead Pile in YAYOI
(No. 47 Exp. Hole)

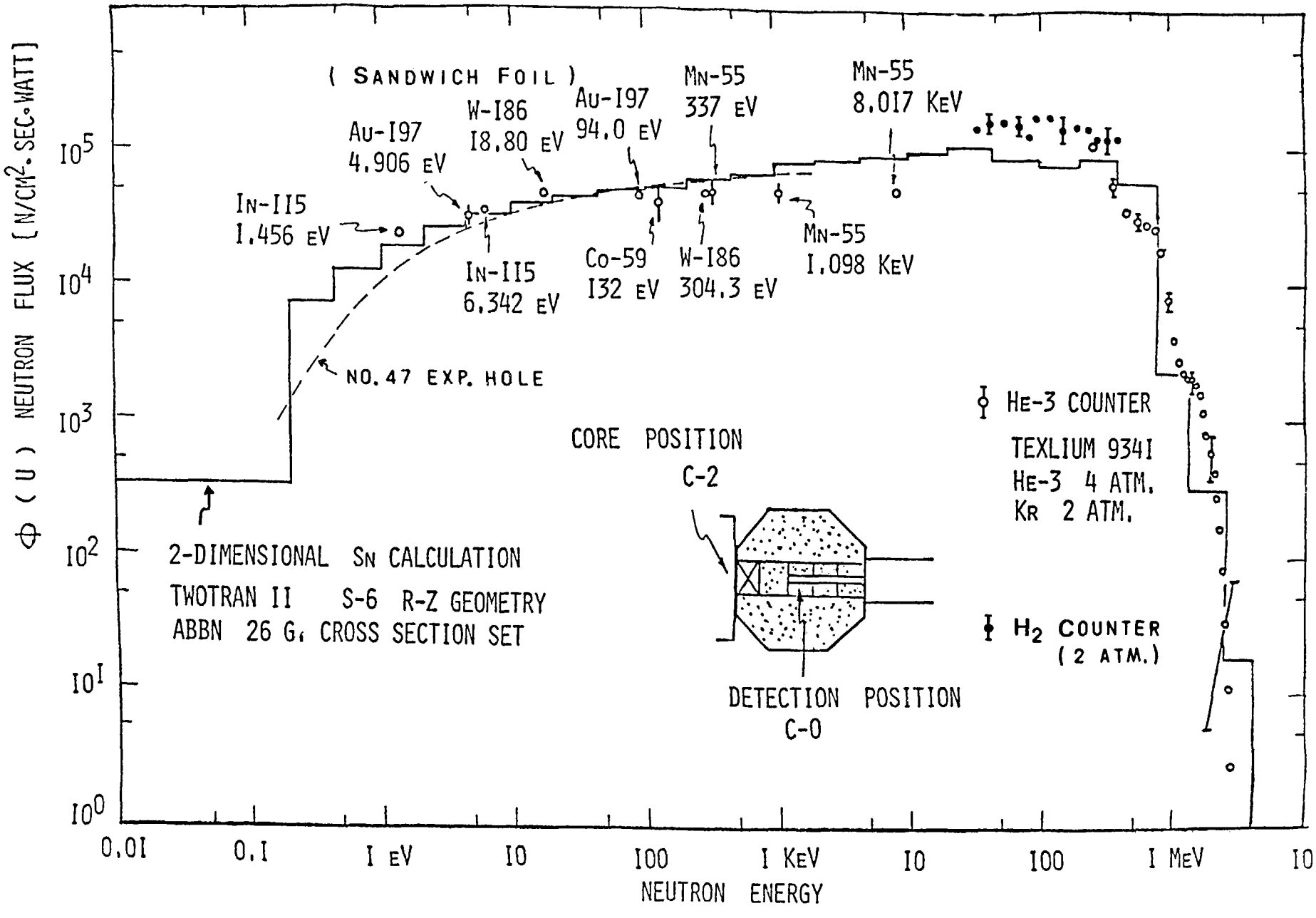

FIG. 5. CENTRAL NEUTRON STANDARD FIELD OF YAYOI OCTAGONAL PB-PILE

Comparison of the Measured Absorbed Dose Value

Table.1

Element		Foil + TLD	Calorimeter	Fricke-dosimeter
C	neutron	1.12	---	0.805
	γ-ray	1.05	---	0.846
	Total	2.17	2.104	1.651
H	neutron	44.5	---	54.10
	γ-ray	2.11	---	1.69
	Total	46.61	48.70	55.79

Unit: Mrad/hr at 2kW reactor power

Table.2 The results of slowing down time spectrometry in the lead column.

Exp. hole	position	Ag Resonance 5.19eV		C	Eff. Fe ratio
		Slowing-Down time	Resolution		
No. 46	65cm	101.6±4μs	180.39%	53.57	25.76a% 8.55w%
No. 47	90cm	123.5±4μs	60.30%	79.16	16.27a% 4.98w%

Appendix (1)

General Description of Reactor

The reactor has a core assembly that includes core, blanket, reflector, control rods with relevant drive mechanism, as well as a neutron source. This assembly is movable horizontally along a track that extends from the subpile room to the lead intermediate neutron pile. The assembly can be stopped and mechanically locked at pre-determined positions.

Changes brought to reactivity caused from moving the core position, are adjusted by shim rodl. The core is cylindrical, and made up of approx. 93 w% enriched metal uranium discs, surrounded by an annular blanket of depleted uranium. The core and blanket are contained inside the lead reflector-A of hollow cubic form. The reactor is shielded by heavy concrete and lined inside by lead reflector-B, 150 mm thick.

Within the concrete shield are installed a thermal column and a fast neutron column, on opposite sides of the reactor, next to the reflector-B. Many experimental holes are provided, both horizontal and vertical, in the concrete shield.

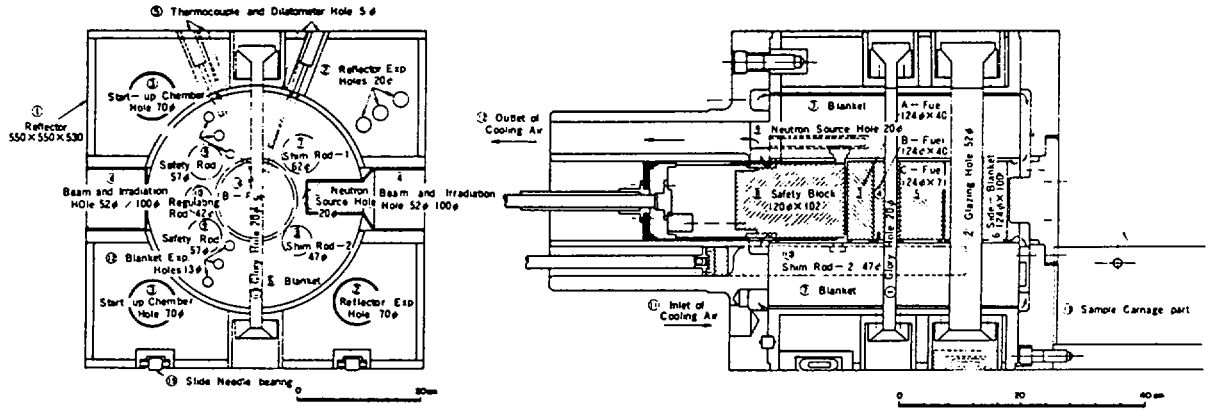

Fig. 1. Core Assembly of Fast Neutron Source Reactor.

An octagonal intermediate neutron column is also installed, a lead pile 2.5 m high and with a thickness of about 2.5 m face to face distance, with many experimental holes.

Two safety rods, two shim rods, and one regulating rod are provided in the blanket, and one safety block facing the core. All these control elements are made of depleted uranium.

The reactor core is cooled by air, which is exhausted to out-door through filters.The blower is located in an auxiliary machinery room adjoining the concrete shield.

The instrumentation and control system includes nuclear instrumentation, process instrumentation, and safety devices. The nuclear instrumentation incorporates two fission chamber start-up channels, two C.I.C. linear safety channels and two C.I.C. log safety channels. The reactor room is covered by closed-circuit television surveillance. This and other electronic information devices provide a complete system of collective centralized control for reactor operation.

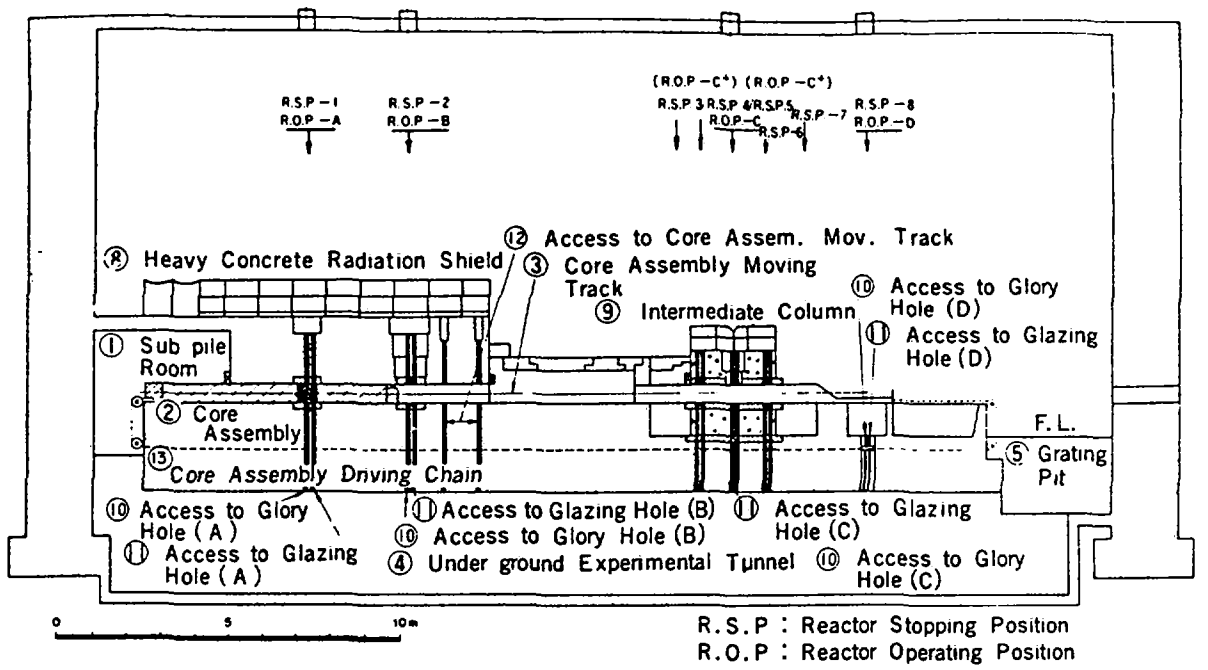

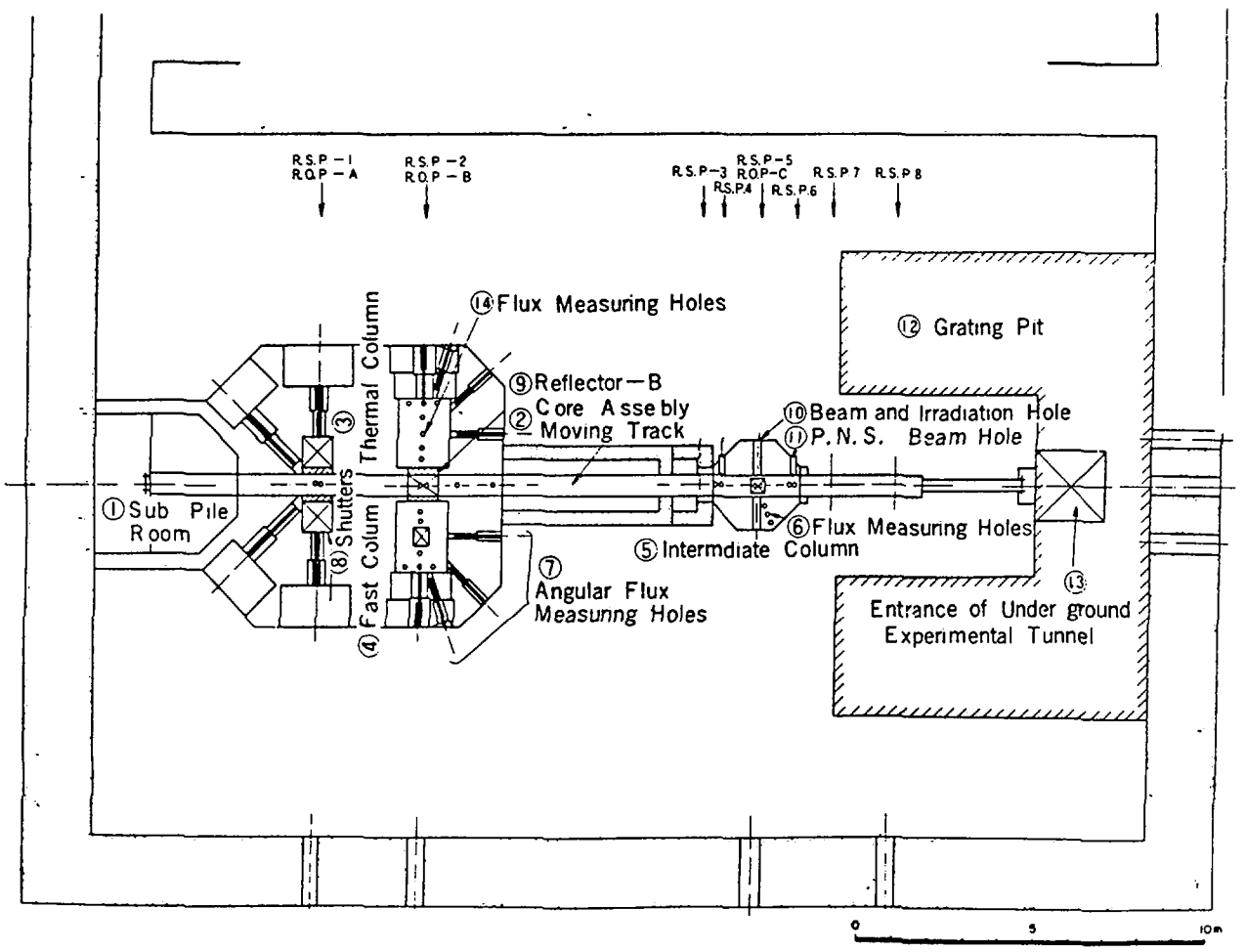

Fig 2 Layout of 「YAYOI」 of University of Tokyo

Appendix (2) Improved Hughes' Method Based on the General Unfolding Technique.

Many studies on the foil data unfolding technique have been made since the early Hughes' work, and the recent refined techniques of SPECTRA (Greer and Walker), SAND-II (McErlory), CRYSTAL-BALL (Stalmann and Kam) and several versions based on a linear programming technique have been successfully applied to practical analysis.

The proposed technique here is a general unfolding method which is able to apply to the determination of spectrum, dose or any other quantities depending on the object of measurement. Furthermore, error range of the results can be introduced from the accuracy of guess spectrum and from the error of reaction rates and cross sections.

Obtained reaction-rates by the measurement, Ri(i = 1 - n) and a desired quantity I are related to an unknown neutron differential flux $\phi(E)$ in the following manner.

$$Ri = \int_0^\infty \sigma_i(E)\phi(E)\,dE, \quad i = 1, n \qquad \ldots(1)$$

$$I = \int_0^\infty W(E)\phi(E)\,dE, \qquad \ldots(2)$$

where $\sigma_i(E)$ is cross-section of i-th reaction. W (E) is usuallv called as a window function in the spectrometry, and is equivalent to a damage function or a KERMA factor in the dosimetry.

For the estimation of the value of I, the following functional J is introduced in which a new parameter c is determined by the least square technique.

$$J[\phi, c] = \int_0^\infty W(E)\phi(E)\,dE + \sum_{i=1}^{n} c_i \left(R_i - \int \sigma_i(E)\phi(E)\,dE\right) \qquad \ldots(3)$$

When we assume the guess spectrum is characterized by average $\phi_0(E)$ and covariance $V_0(E, E')$, avarage and variance of th value of I are given in the following equation using a statistical treatment of functional J.

$$\text{Ave. } I = \int_0^\infty W\phi_0 dE + \sum_i c_i \left(R_i - \int \sigma_i \phi_0(E)\,dE\right) \qquad \ldots(4)$$

and

$$\text{Var. I} = \int_0^\infty dE \int_0^\infty dE' \left[W(E) - \sum_{i=1}^{n} c_i \sigma_i(E)\right]\left[W(E') - \sum_{i=1}^{n} c_i \sigma_i(E')\right] V_0(E, E') + \sum_{i=1}^{n} c_i^2 \left[(\Delta R_i)^2 + \int (\Delta\sigma_i)^2 \phi_0^2(E)\, dE\right] \quad \ldots(5)$$

where ΔR_i, $\Delta\sigma_i$ mean a standard deviation of R_i and σ_i. Here, coefficients c_i are selected to minimize Var. I.

This technique is considered to be the extension of SPECTRA in a point of error analysis. That is the generalization of window function and the estimation of error due to the initial guess of spectra are possible in the present technique.

In addition, other functionals are also useful. For example,

$$J = \int W(E) \ln\phi(E)\, dE + \sum_i c_i \left(\ln R_i - \ln \int \sigma_i \phi\, dE\right)$$

In the above expression, non-linear forms are used to avoid a negativity of flux $\phi(E)$.

Here, the improved values of the threshold energy Eeff and the effective cross-section σeff of the threshold foil can be obtained by using the generalized unfolding technique described above. In this application, the window function in Eq. (2) is selected as a step function:

$$W(E) = \begin{cases} 1, & E \geq \text{Eeff} \\ 0, & \text{otherwise} \end{cases}$$

The covariance of guess spectrum is assumed to be the following simple form:

$$V_0(E, E') = \varepsilon^2 \phi_0^2(E)\, \delta(E, E'),$$

where ε is a relative deviation to be assigned with respect to the degree of physical knowledge on the neutron spectrum in question, and $\delta(E, E')$ is the Dirac delta function.

Based on the above assumption, coefficients c_i in Eq. (4) and (5) can be calculated corresponding to the assigned values of Eeff. Among those c_i values, the minimum value of Var. I is utilized for the determination of the

best value of Eeff.

As a result, average I and relative variance of I can be arranged in the following manner.

$$I = \int_{Eeff}^{\infty} \Phi(E)\, dE = \frac{R}{\sigma_{eff}}$$

$$\left(\frac{\sqrt{Var.I}}{I}\right)^2 = \left(\frac{\Delta\sigma_{eff}}{\sigma_{eff}}\right)^2 + \left(\frac{\Delta R}{R}\right)^2$$

When we apply this technique to the dose measurement in the reactor core of 'YAYOI', a guess spectrum is referred to the core center spectrum described as a parameter representation. Corresponding to this case, values of Eeff, σeff and $\Delta\sigma$eff for typical eight reactions are summarized in Table 1. These values have been successfully applied to determine the neutron spectra in different positions in the reactor.

Another exercise of the technique has been done by unfolding the reported reaction-rate data of Mol $\Sigma\Sigma$-facility. With the assumption of $\mathcal{E}$ value to be 0.3, differential of integrated flux are agreed well with the evaluated spectrum contained in the report.

Table 1 Improved effective threshold cross-sections for typical reactions

Reaction type	Cross-section Data*	Error	Effective-Thresh. Energy : Eeff	σ_{eff} (mb)	$\Delta\sigma_{eff}/\sigma_{eff}$ (%) $\mathcal{E}$ = 1	$\mathcal{E}$ = 0.5
$^{27}Al(n,\alpha)^{24}Na$	(1)	10%	7.2 MeV	65.5	91	51
$^{24}Mg(n,p)^{24}Na$	(1)	10	6.6 MeV	88.3	78	44
$^{27}Al(n,p)^{27}Mg$	(3)	10	4.4 MeV	46.1	77	43
$^{58}Ni(n,p)^{58}Co$	(1)	10	2.6 MeV	384	48	27
$^{115}In(n,n')^{115m}In$	(1)	10	1.3 MeV	310	29	17
$^{232}Th(n,f)$	(2)	10	1.5 MeV	131	23	14
$^{238}U(n,f)$	(1)	5	1.5 MeV	587	17	9.3
$^{237}Np(n,f)$	(2)	10	0.6 Mev	1,450	18	11

* (1) A. M. Bresesti et. al., Nucl. Sci. & Eng. 40, 331-348 (1970)
(2) W. G. Davey, ibid: 26, 149-169 (1966)
(3) H. Liskin and A. Paulsen, EUR 119e (1966)

I.9. Thermal Neutron Standard Fields with the KUR Heavy Water Facility

by

Keiji Kanda, Keiji Kobayashi and Toshikazu Shibata

Research Reactor Institue, Kyoto University,
Kumatori-cho, Sennan-gun, Osaka, Japan

Abstract

A heavy water facility attached to the KUR(Kyoto University Reactor, swimming pool type, 5 MW) yields pure thermal neutrons in the Maxwellian distribution.

The facility is faced to the core of KUR and it contains about 2 tons of heavy water. The thickness of the layer is about 140 cm.

The neutron spectrum was measured with the time of flight technique using a fast chopper. The measured spectrum was in good agreement with the Maxwellian distribution in all energy region for thermal neutrons. The neutron temperature was slightly higher than the heavy water temperature.

The contamination of epithermal and fast neutrons caused by photo-neutrons of the γ-n reaction of heavy water was very small. The maximum intensity of thermal neutrons is 3×10^{11} n/cm^2 sec. When the bismuth scatterer is attached, the gamma rays contamination is eliminated by the ratio of 0.05 of gamma rays to neutrons in rem.

This standard neutron field has been used for such experiments as thermal neutron cross section measurement, detector calibration, activation analysis, biomedical purposes etc.

1. Introduction

It is desirable that the neutron standard field satisfies the following conditions in order to offer a universal data convenient for inter-comparison between one experiment and others or between calculation and experiment. In the case of thermal neutron field:

a. to be capable to offer only neutrons of a certain energy group,
b. the neutron spectrum has to be known,
c. the spectrum does not depend on a certain facility itself, in other words it must be common, universal and reproducible,
d. the spectrum can be expressed in analytical form, if possible,
e. the absolute value of neutron fluence is to be known,
f. the intensity of neutron fluence is variable in a wide range,
g. the direction of neutron current is to be known, e.g. beam or isotropic field etc.,
h. the contamination of other rays, e.g. gamma rays, fast neutrons etc., is reduced as low as possible to eliminate nonobjective nuclear reactions.

The thermal neutron fields obtained in our institute are tabulated in Table 1., which shows the superiority of the heavy water facility. It is mainly due to the characteristics of moderators, as shown in Table 2. Since such solid moderators as graphite and beryllium have crystalline structure in neutron cross section, the spectrum of neutrons from these moderators has a discontinuous structure in low energy side.

In the present paper, the characteristics of KUR heavy water facility[1] is described, which has served as the standard neutron field for such experiments as thermal neutron cross section measurement, detector calibration, activation analysis, biomedical purposes.

2. Facility

The heavy water tank containing 2 tons of heavy water is faced to the core of KUR. (Fig.1.) The thickness of heavy water layer is about 1.4 m. The tank is a shape of trapezoid cone and is made of aluminum, of which thickness on neutron outlet side is 10mm. (Fig.2.)

The purity of heavy water is 99.75%. The temperature is continuously measured by a thermocouple, and it is usually kept in about 40°C.

At the outside of the heavy water layer, a removable graphite layer of 48 cm thick and a removable bismuth layer of 15 cm thick are placed. For the irradiation purpose, there is an irradiation room of 2.4 m x 2.4 m , surrounded by a 90 cm thick heavy concrete.

In the graphite layer, the bismuth scatterer[2] can be attached, which reduces the gamma ray contamination by the ratio of 0.05 of gamma-rays to neutrons in rem. (0.96×10^9 neutrons = 1 rem,)

A fission plate of 90% enriched uranium of 29 cm in diameter is attachable to offer a fission neutron field.[3]

3. Experiments

3.1. Neutron Spectrum Measurement

The experimental arrangement is shown in Fig.3. The detail of the neutron collimator is shown in Fig.4. The neutron spectra yielded from the facility and heavy water samples were measured with the time of flight technique using a fast chopper with a perpendicular rotor of K-monel as shown in Fig.5. The block diagram of electronic circuit is shown in Fig.6. The length and diameter of the flight tube was 5 m and 10 cm respectively. A BF_3 shielded with boric anhydride and cadomium sheet was used as a neutron detector.

The measured spectra were on neutrons (i) from the surface of the heavy water tank, (ii) from the graphite layer, (iii) from the heavy water can of 60 cm in diameter and 100 cm in height and (iv) from the can of 15 x 15 x 10 cm^3, both placed at the

irradiation room.

3.2 Neutron Flux and Gamma Ray Dose Rate Measurement

The intensity of neutron flux, namely neutron fluence rate, was measured with gold foils of 3 mm in diameter and 0.05 mm thick. The induced activity was counted by a β-γ coincidence equipment and a well type NaI(Tl) scintillator. The gamma ray dose was measured with thermo-luminescence detectors of $CaSO_4$ cased into polyethelene pipe of 1 mm in diameter and 10 mm long, which were insensitive to thermal neutrons.

4. Results and Discussions

4.1 Neutron Spectrum

The obtained time spectrum was deduced to the energy spectrum after several corrections: (i) a chopper trasmission, (ii) the neutron arrival probavility to the detector, (iii) the detector efficiency, (iv) background (v) the dead time of the multichannel analyzer.

Fig.7 shows the neutron spectra from the heavy water tank and the graphite layer. The former is in good agreement with a Maxwellian distribution of 60°C, which is slightly higher than heavy water temperature of 40°C, while in the latter several structures due to crystal of graphite is observed. Anyway in both cases apparent epithermal neutrons were not observed. It is also found from the fact that cadmium ratio of gold foil for (a) and (b) were 5×10^3 and 10^4 respectively. In the case of the heavy water(a), however, a little contamination of fast neutrons was observed, which may be due to the photo-neutrons from deuterium.

The neutron temperatures for both spectra were checked by the foil activation method using several detectors with and without filter of gadolinium of 0.025 mm thick. (See Table 3.) The neutron temperatures for neutrons from the heavy water and the graphite layer correspond to 60°C and 20°C, respectively, as shown in Fig.8.

The former experiment using a heavy water can of 60 cm

in diameter and 100 cm in height pointed out that the spectrum of neutrons emerging from the can was largely distorted upward from the Maxwelliam distribution at the energy range less than 0.025eV[4], as shown in Fig.9. However, according to our experiment using the can of the same size, the distortion is not so remarkable. Fig.10 shows the spectrum of neutrons from the smaller can of 15 x 15 x 10 cm^3 for reference of the extreme case, but the distortion is not so large as the former data. The calculation using ANISN, one dimentional multi-group transport code, shows the same tendency as our experiment. (See Fig.11.)

4.2 Neutron Fluence Rate and Gamma Ray Dose Rate

The neutron fluence rate and gamma ray dose rate measured at several irradiation positions were tabulated in Table 4.

5. Concluding Remarks

The characteristics of the KUR heavy water facility are as follows:

(i) The layer of heavy water is so thick that pure Maxwellian neutrons are obtained.

(ii) As the heavy water tank is faced directly to the KUR core, high neutron fluence rate is available.

(iii) The irradiation room is so wide that a large sample (e.g. a cow) can be irradiated.

(iv) As the removable neutron collimator is equipped, the experiment using beam neutrons is possible.

(v) By means of the time of flight technique using the chopper, neutron spectrum measurement and neutron cross section measurement are performed.

(vi) As the fission plate is equipped, a standard field of fission neutrons is also offered.

(vii) By means of the bismuth scatterer, high qualitative thermal neutrons eliminating gamma ray contamination are available.

The standard neutron field has been used for such experiments as thermal neutron cross section measurement[5,6], detector calibration, activation analysis[7], biomedical purposes[8] including neutron capture therapy[9] etc. The fission plate has been used for such experiments as fission neutron cross section,[10,11] neutron slowing down[12] etc.

Acknowledgment

The design of the heavy water facility was mainly made by Prof. S. Okamoto of Kyoto University.

The authors wish to acknowledge Prof. I. Kimura of Kyoto University for his valuable suggestions and discussion, and they are also indebted to Mr. T. Kozuka of Kyoto University, Mr. T. Kawamoto of Hitachi Ltd. and Dr. T. Mizuno of Hokkaido University for their assistance in carrying out the experiments.

They also thank to Mr. H. Kadotani of Century Research Center for calculating neutron spectra.

Reference

(1) Shibata T. et al., "KUR Heavy Water Thermal Neutron Facility" (in Japanese), KURRI-TR-28 (1967)

(2) Kanda K. et al., "Elimination of Gamma Rays from a Thermal Neutron Field for Medical and Biological Irradiation Purposes", *Biomedical Dosimetry*, IAEA (1975) 205

(3) Kanda K., Kobayashi K. et al., "Neutron Energy Convertor" (in Japanese), KURRI-TR-96 (1972)

(4) Ramanna R. et al., "On the Spectrum of Neutrons Emerging from Moderators", 2nd Geneve Conf. P/1636 (1958)

(5) Kanda K. et al., "Effect of Temparature on Total Cross Section of Beryllium for Thermal Neutrons", J. Nucl. Sci. Technol. 12 (1975) 601

(6) Kanda K. and Aizawa O., "Total Neutron Cross Section of Lead", Nucl. Sci. Eng. 60 (1976) 230

(7) Takeuchi T. and Hayashi T., "A Method for Automatic Analysis of Gamma-ray Spectra and Its Application to Activation on Analysis(IV)", Annu. Rep. Res. Reactor Inst. Kyoto Univ. 6 (1972) 68

(8) Mishima Y., "Neutron Capture Treatment of Malignant Melanoma Using ^{10}B-Chlorpromazine Compound", Pigment Cell 1 (1973) 215

(9) Hatanaka H. et al., "Slow Neutron Capture Therapy for Malignant Tumors", *Biomedical Dosimetry*, IAEA (1975) 147

(10) Kimura I. et al., "Integral Check of the Fission Neutron Spectrum through Average Cross Sections for Some Threshold Reactions", *Prompt Fission Neutron Spectra*, IAEA (1972)113

(11) Kanda K. et al., "Measurement of the Averaged Neutron Cross Section of Some Threshold Reactions for Fission Neutrons", Annu. Rep. Res. Reactor Inst. Kyoto Univ. 4 (1971) 94

(12) Kanda K. et al., "The Age of Fission Neutrons to Indium Resonance in Water and Polyethylene", ibid 3 (1970) 93

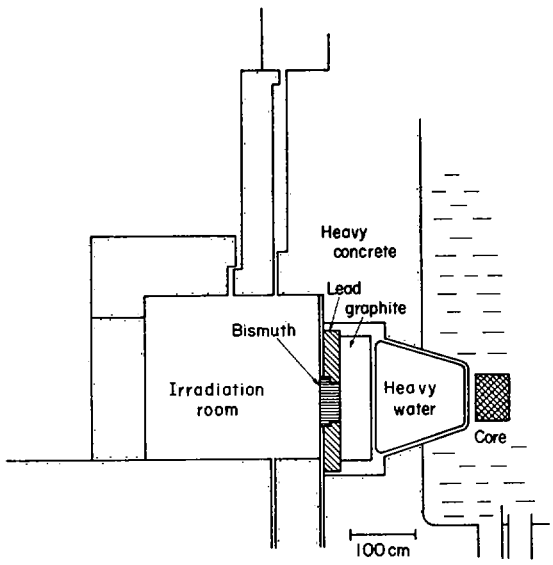

Fig 1 Kyoto University Reactor (KUR)
Heavy Water Facility

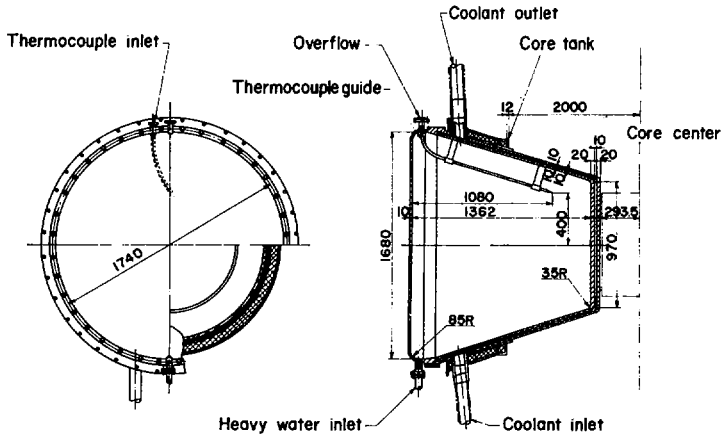

Fig 2 Detail of Heavy Water Tank

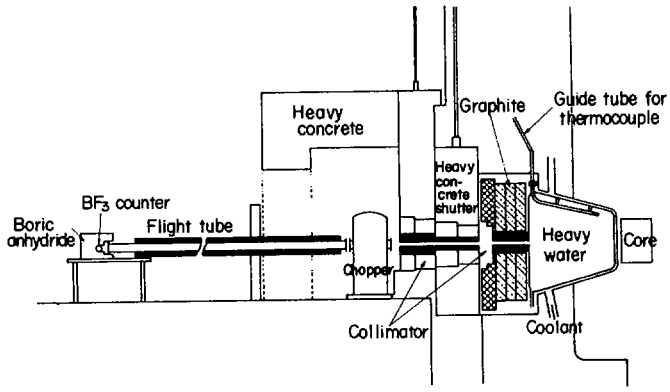

Fig.3 Experimental Arrangement of Time-of-Flight
Measurement

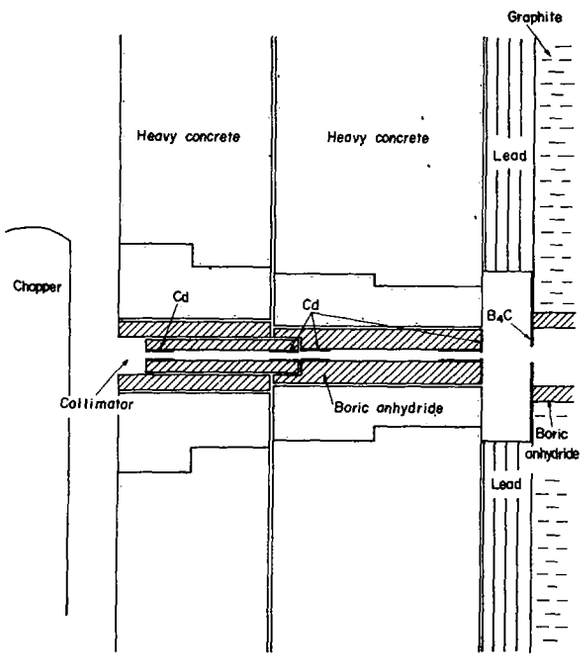

Fig. 4 Collimator System

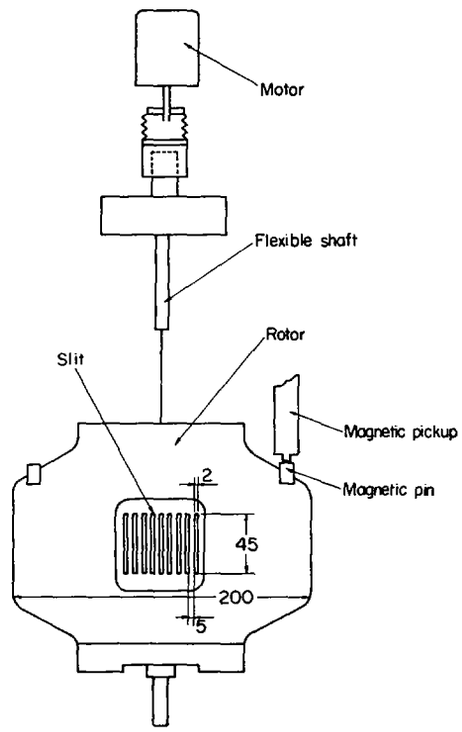

Fig. 5 Fast Chopper

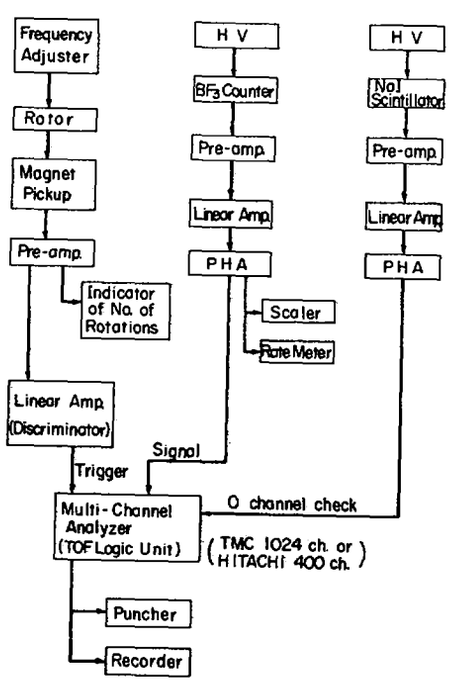

Fig. 6 Block Diagram of Time-of-Flight Measurement

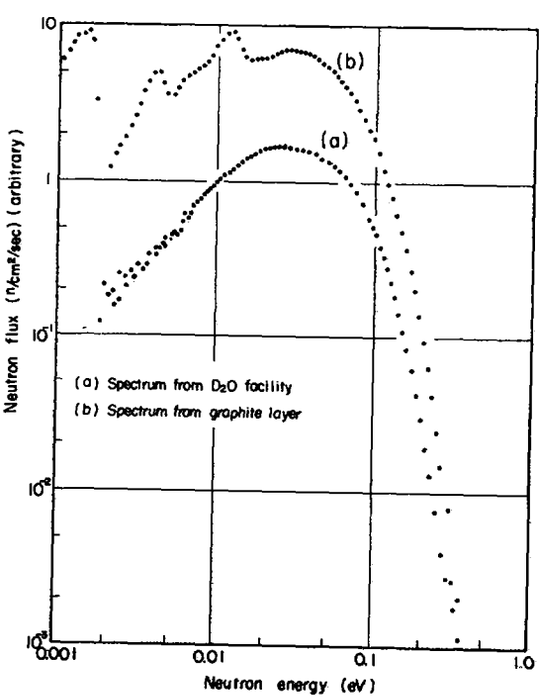

Fig. 7 Neutron Spectra Yielded from KUR D_2O Facility and Graphite Layer

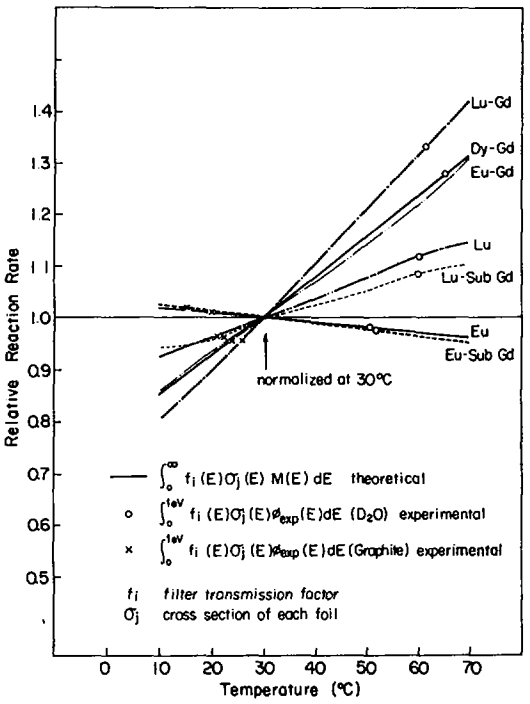

Fig.8 Sensitivity of Activation Foils for Neutron Temperature

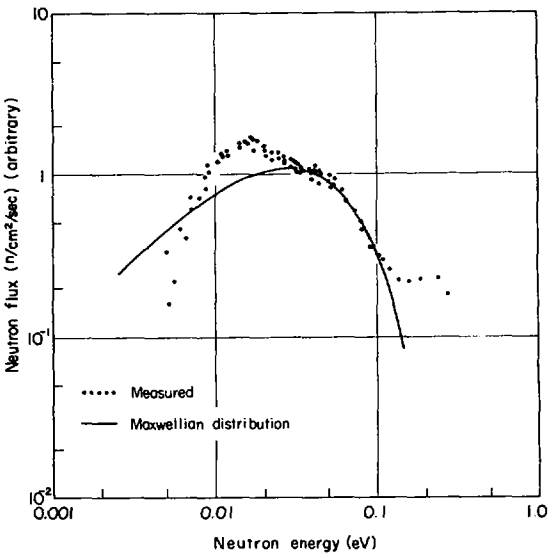

Fig.9 The Former Experiment Performed in India

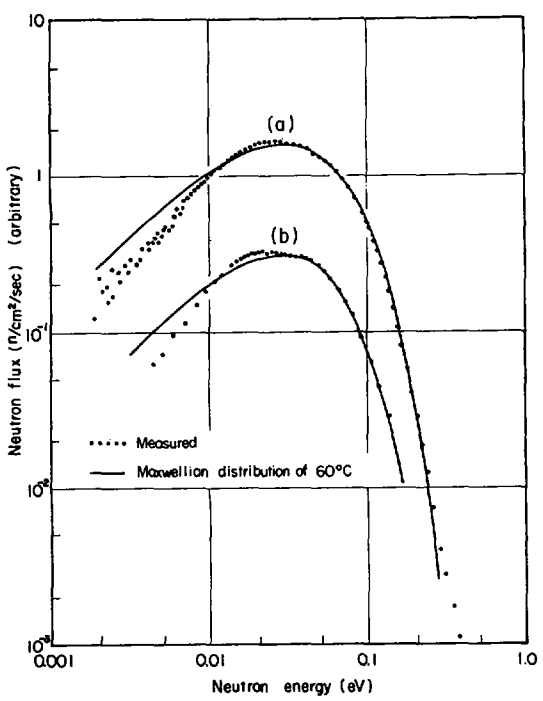

Fig.10 Neutron Spectra Yielded from KUR D_2O Facility (a) and from Small D_2O Can (b)

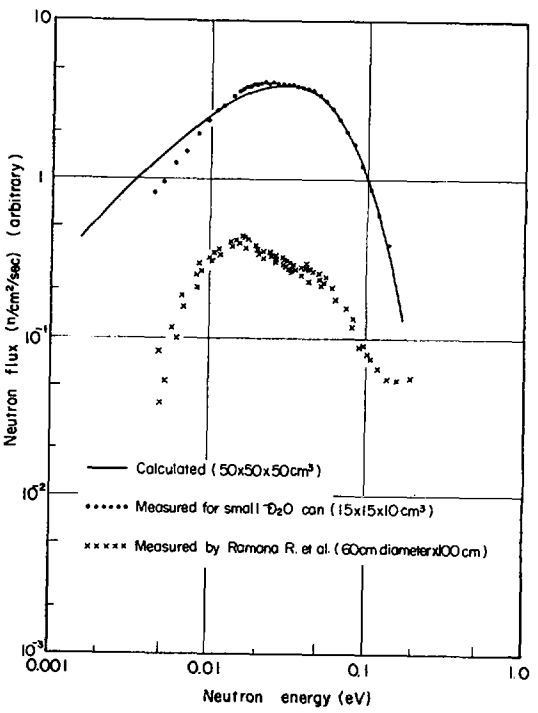

Fig.11 Comparison between Calculated Spectra with Measured One

I.10. THE COUPLED FAST REACTIVITY MEASUREMENTS FACILITY (CFRMF)*

JW Rogers, Y. D. Harker and D. A. Millsap

EG&G Idaho, Inc.
Idaho National Engineering Laboratory
Idaho Falls, Idaho 83401

Compiled by JW Rogers

Abstract

This is a description, application and performance evaluation of the Coupled Fast Reactivity Measurements Facility in relation to reactor dosimetry. Methods and data related to physical description, flux spatial distribution, integral testing of the spectrum, spectrum measurements, theoretical calculations and measured vs calculated reaction rates are covered. More detailed information may be found in Nuclear Technology, Volume 25, Number 2, February, 1975.

Prepared for the IAEA Consultants Meeting on Integral Cross-Section Measurements in Standard Neutron Fields for Reactor Dosimetry. Vienna, Austria, November 15-19, 1976.

*Work performed under the auspices of the US Energy Research and Development Administration.

ACKNOWLEDGEMENTS

The authors would like to acknowledge the operations and maintenance staff of CFRMF for their part in helping to obtain this information. We would like to recognize the leadership and direction of E. Fast. R. G. Fluharty, R. M. Brugger and R. L. Heath throughout the 8 years that CFRMF has been in use; the design efforts of R. R. Piscatella; the contributions of R. G. Helmer, R. C. Greenwood, C. H. Hogg, R. G. Nisle and J. J. Scoville to some of the results presented here. W. N. McElroy and L. S. Kellogg of HEDL provided planning, dosimetry materials, measurements and analyses of many results included here. J. A. Grundl and D. M. Gilliam of NBS provided the fission chambers and data analyses of the fission rates. H. Farrar IV of AI provided the materials, measurements and analyses of the helium production results. N. D. Dudey and R. R. Heinrich of ANL also contributed results incorporated into this report. G. and S. De Leeuw of CEN/SCK (Belgium) conducted the ^{6}Li spectrometry measurements and provided some detectors and all data analyses. C. D. Kemshall of A.W.R.E. (England) and H. Werle of K.F.K. (W. Germany) provided the spherical proportional counters used in the proton recoil spectrometry results and many valuable suggestions for their use.

THE COUPLED FAST REACTIVITY MEASUREMENTS FACILITY (CFRMF)

Idaho National Engineering Laboratory (INEL)
Idaho Falls, Idaho 83401

I. Physical Description of the CFRMF

The CFRMF is a zoned-core critical assembly with a fast-neutron spectrum zone in the center of an enriched ^{235}U, water-moderated thermal "driver" and the core is contained in a large pool about 4.5 m beneath the surface. The concept, preliminary considerations, and most details of the CFRMF have been documented. [1-5] The CFRMF was originally designed to be a high precision static reactivity measurements facility to operate at a flux level of approximately 10^8 n/(cm^2 sec), but has more recently found much use in the fast breeder reactor program as a fast-neutron field for the irradiation of materials of interest at flux levels up to approximately 10^{12} n/(cm^2 sec).

Figure 1 is a cutaway pictorial diagram of the CFRMF. The core has quadrantal symmetry with respect to structural assembly and fuel loading as shown in Fig. 2, which is a midplane cross-sectional diagram of the CFRMF. The thermal driver zone fuel elements are conventional plate-type elements of fully enriched (approximately 93% ^{235}U clad in aluminum. The fueled portion of the core is 60.96 cm long, and each element is 8.283 cm square. The fast zone is constructed of materials for keeping the zone water-free and to "filter" or "tailor" the neutron energy spectrum. Figure 3 is a horizontal midplane cross-sectional diagram of the fast zone assembly. The 0.317-cm-thick stainless-steel housing is sealed waterfree and provides the minimal thickness required to provide the strength necessary to support the large mass of uranium. The 0.635-cm-thick 50 wt% boral side and end plates completely shroud the assembly

except where the boral end plates have 4.20-cm-diam holes through which the experiment access tube passes. Outside each boral end plate are 2.697-cm-thick aluminum spacers through which the access tube also extends. The lower aluminum plate positions the uranium block and the upper one is for symmetry. The ^{238}U(99.7%) block (14.52 cm square x 60.96 cm long and weighing approximately 217 kg) with a 5.295-cm-diam hole drilled through its axial center is vertically aligned with the core fuel. The 0.635-cm-thick annulus of enriched ^{10}B (90%) and 0.0889-cm-thick annulus of enriched ^{235}U (93%) are clad with 0.0305-cm-thick stainless steel and slip-fit together into the ^{238}U block. The ^{235}U and ^{238}U materials are solid metal, and the stainless steel is either Type 304 or 321. The ^{10}B is of crystalline powder form and is vibrocompacted to a density of 1.355 g/cm^3. The stainless-steel access tube, with 0.147-cm-thick walls in the core region, slip-fits inside the ^{235}U annulus and will accept objects with effective diameters up to 3.78 cm. The distance from the bottom of the access tube to the core midplane is 31.11 cm; it is approximately 6.1 m from the core midplane to the top of the access tube above the pool surface. Some asymmetry exists in the fast zone vertical plane because above the top end aluminum spacer plate there is a 15.75-cm cube-shaped void capped with a 2.54-cm-thick stainless-steel cover plate through which the access tube passes. Below the bottom end aluminum spacer plate is the 1.27-cm-thick stainless steel end plate of the housing which rests on the aluminum grid support structure of the reactor with a metal-to-water ratio of approximately 0.6 by volume.

The thermal driver zone neutron energy spectrum is filtered or tailored by the materials in the fast zone in the following general

manner. The boron in the boral plates attenuates the neutrons below approximately 1 keV by absorption. The ^{238}U block degrades the energy of the fission neutrons by inelastic scattering. The ^{10}B annulus attenuates the neutrons below approximately 1 keV even further and ensures that all thermal neutrons are removed. The ^{235}U annulus has no significant effect on the real flux spectrum other than supplying some fast-fission neutrons but does affect the importance function (adjoint flux) which is of concern only in reactivity measurements.

In the use of the CFRMF as a high precision irradiation facility it is very important that the power level control system reproducibly establish the desired neutron level and the energy specturm without changing the flux distribution at the location of the experiment. The locations of the control devices are shown in Fig. 2. The safety rods are not used for normal operation control purposes and are completely out-of-core during irradiations. The shim rod (a 1-mm-thick, 15.24- x 60.96-cm cadmium plate on a flat surface parallel to the core) is always set at the same position for related irradiations and can be repositioned to within $\pm 5 \times 10^{-4}$ of a degree of rotation (equivalent to 1.5×10^{-7} $\Delta k/k$) which causes no detectable changes in the flux distribution in the experiment region. The power of the CFRMF is maintained at a constant and preset level by means of a conventional dc servo system shown in Fig. 4. This servo system is composed of a boron-lined compensated ion chamber (CIC), appropriate amplifiers, reference voltage source, and a torque motor-driven regulating rod (a 1-mm-thick, 6.0- x 60.96-cm cadmium plate on a 6.35-cm-diam curved surface parallel to the core). The signal applied to the first-stage amplifier is the difference between a current porportional to the reactor power level as produced by the servo

CIC and a current obtained from the reference voltage source. The power level error signal is then amplified and used to drive the regulating rod to correct for any power level deviation. The regulating rod is capable of holding the power level steady with a total motion corresponding to a reactivity of $\pm 8.4 \times 10^{-8}$ $\Delta k/k$ at low power levels where thermal heating causes no problems. At the power levels normally used for irradiations, the reactivity changes observed are approximately 1×10^{-4} $\Delta k/k$, which also does not produce detectable changes in the flux distribution in the core. The servo CIC, reference voltage, and first-state dc amplifier determine the reproducibility and linearity of multiples of the power level. The servo CIC positioning reproducibility has been measured to $<\pm 0.5\%$. The long-term (several years) overall stability of chambers like the CFRMF servo CIC in neutron fields equal to or greater than the CFRMF has been very good in that no detectable changes have been observed. Routine checks on the compensation and bias voltages of the servo CIC ensure that they are at the proper levels and are stable. The reference voltage unit, used to preset the level at which the power is controlled, consists of a voltage power supply potentiometer, and two switchable precision resistors (100x and 1000x). The stability of this devise is $\pm 0.01\%$ or better over the normal range of ambient temperatures. The linearity of the CFRMF power level control system has been checked against foil activations and fission rates in the fast zone center. A factor-of-10 change (0.6 to 6.0 kW) on the power level setpoint produces a change of 9.6 or a nonlinearity of 4%. This nonlinearity, however, is reproducible and stable. Measurements of the output of the reference voltage supply each of these setpoints shows no more than 1% nonlinearity for each range of the system. Consequently, the reason for the nonlinearity is likely due to imperfect CIC compensation at either or both levels.

II. Neutron Flux Spatial Distribution

The spatial distribution of the neutron flux in the CFRMF fast zone has been investigated using activation and fission rate measurement techniques. These measurements establish the relative flux along the vertical axis of the experiment region to ± 1-2% and follow a "typical cosine" distribution over the central 40 cm. The peak of the flux at the center of CFRMF is approximately 8.5 X 10^{11} $n/cm^2/sec$ at the maximum permissable power level of 100 kW thermal output. The total fluence available is dependent on the amount of time that is practical for a given experiment since the neutron level can be held constant for whatever time is found to be optimum.

Devices were fabricated from stainless steel that would hold samples for activation along the vertical axis of the CFRMF test region and allow end plugs to be located at the ends of the access hole. A diagram of these devices as located in the CFRMF unit is shown in Figure 5. The larger tubing between the end plugs is for supporting and positioning the plugs and the smaller tubing inside is for holding the activation samples. Two identical sets of end plugs were fabricated, one set (top and bottom) being empty and the other filled with enriched ^{10}B powder. The 99.9% pure B enriched to 92 atom percent ^{10}B was vibrocompacted into the end plugs to a density of 1.06 g/cm^3. The walls of the end plugs were made as thin (0.5 mm) as fabrication procedures would allow in order to minimize any neutron leakage around the plugs. This device allows the vertical position of the activation samples to be known to ±1 mm relative to the bottom of the experimental access tube.

Two materials, pure Au and Al alloy of 10 w/o ^{235}U (93% enriched), have been irradiated with the empty and ^{10}B filled end plugs in CFRMF.

The activation samples were short wires (6.35 mm long and 1 mm diameter) which were stacked end-to-end the full length of the sample holding tube for each irradiation. In each irradiation 83 samples were exposed and each was counted by gross beta counting techniques. From the $^{197}Au(n,\gamma)^{198}Au$ reaction an activity due to the capture of resonance energy neutrons was obtained. From the $^{235}U(n,f)FP$ reaction an activity due to the fission of a very broad energy range of neutrons was measured.

From these activities profiles of the activation responses of these samples in the CFRMF neutron flux have been drawn and are shown in Figures 6 and 7. From these profiles the peak of the CFRMF flux is found to be 30.6 $\pm$ 0.1 cm from the bottom of the experimental access tube (the geometrical midplane is 31.1 cm from the bottom). The shapes of these profiles are nearly identical and have no irregularities which suggest that the filter materials are very uniformly dispersed. The ^{10}B end plugs cause no detectable changes in either the absolute or relative reaction rates of these materials along the central 30 cm of the fast zone vertical axis. In the end regions beginning 15 cm above or below the peak of the flux the profiles show changes due to the presence of the ^{10}B end plugs. These changes are assumed due to spectral perturbations of the flux in these regions. The reduced reaction rates in the end regions when the ^{10}B end plugs are installed imply that more resonance and/or thermal energy neutrons are present there without the end plugs.

The absolute fission rates at the flux peaks of $1.218\pm0.016\times10^{13}$ and $1.232\pm0.016\times10^{-13}$ fissions/sec-nucleus for the plugged and unplugged measurements respectively are based upon a thermal flux fission rate calibration. The difference ($\pm$0.6%) between these fission rates is well within their associated uncertainties. The corresponding absolute Au

reaction rates are $2.525 \pm 0.025 \times 10^{-10}$ and $2.508 \pm 0.025 \times 10^{-10}$ d/sec-atom which agree to ± 0.15%. These differences are well within statistical uncertainties and are regarded as insignificant. The relative activities used to describe the profiles are of the same accuracy. These measurements have not been corrected for neutron self-shielding and gamma self-absorption. Based upon least squares fitting of these data there is no difference in the shapes of the profiles over the central 30 cm and the scatter of the data relative to the fitted curves is less than the estimated uncertainties. Fission chambers containing ^{235}U, ^{238}U, ^{239}Pu, and ^{237}Np have also been used to observe the fission rate along selected portions of the CFRMF vertical axis. The fission chambers contain microgram quantities of the fissionable materials. These measurements are summarized in Table I, where the results are presented relative to the measurement at the centerline of the assembly.

The central 25 mm along the vertical axis and the horizontal plane 38 mm above the centerline are often the locations of the primary test specimens and the power level normalization monitors, respectively. The flux distributions in these locations have been examined in much greater detail than the previous measurements show. The $^{197}Au(n,\gamma)^{198}Au$ reaction rates from 0.127-mm-thick, 4-mm-diam foils spaced along the 55 mm above the CFRMF centerline were measured by gamma-ray spectroscopy techniques. These results are shown in Fig. 8 and indicate that the gradient for this reaction along the central 25 mm is probably about 0.3%. The uncertainties in these data represent only counting statistics.

At the CFRMF centerline, diametric profiles of the $^{197}Au(n,\gamma)^{198}Au$ and $^{115}In(n,n')^{115m}In$ reaction rates were measured in the north-south and west-east directions (see Fig. 2). The foils were approximately 2.7 mm

square, and the gold was 0.05 mm thick, whereas the indium foils were 0.127 mm thick. The results from these measurements are shown in Figs. 9 and 10. Also shown in Fig. 9 are results from 0.127-mm-thick, 4-mm-diam. gold foils oriented in the north-south direction and activated at a different time. The uncertainties on the thicker foils represent only counting statistics (one measurement, one analysis) and on the thinner foils the bars represent the span of dual analyses of two activity measurements (four values). The end points on the north-south profile suggest that there may be some neutron self-shielding at these locations but a different normalization within the limits of uncertainty could completely obscure such analogy. The west-east profile shows a gradient for this reaction of approximately 5%, whereas the the north-south profile shows approximately 3%.

The profiles of the $^{115}In(n,n')^{115m}In$ reaction which is sensitive to neutron energies in excess of approximately 0.5 MeV show no statistically significant gradients in either direction (see Fig. 10). The bars for the data points represent the same span of measurements as described for the gold data.

In the horizontal plane 38 mm above the CFRMF centerline 0.05-mm-thick, 4-mm-diam gold foils were positioned tangent to one another around the perimeter of the experimental area and activated. The perimetric profile of the $^{197}Au(n,\gamma)^{198}Au$ reaction rate obtained from these foils is shown in Fig. 10. It is observed that this profile has two fold asymmetry about the axis of the CFRMF and follows a sine wave distribution. These results show that the reaction rate has a maximum at approximately 150 and approximately 345 deg. and a minimum at approximately 70 and approximately 255 deg. relative to north. The shim and regulating rods are located on

the west and east sides of the CFRMF core, respectively, and probably cause this asymmetry. These results, when compared with the corresponding (north, south, east, and west) reaction rates of the diametric profiles, and relative to the reaction rate at the north position, show the gradient at the east location to be approximately 1% less than at the west and south locations. These results show that at a constant power level the gold power level monitor foils could, if randomly positioned, give reaction rates which differ up to approximately 1%.

The gamma ray dose is approximately 1860 R/ hr at a fast neutron level of 5.75×10^8 $n/cm^2/sec$ at the center of CFRMF and based on available data the gamma dose is directly proportional to the neutron level.

III. Integral Tests of Neutron Spectrum

Several integral measurements have been made to test for the possibility of the streaming of thermal and resonance energy neutrons from the ends of the fast zone. Gold cadmium ratios taken at the centerline have a value of 1.00 ± 0.02, which indicates that there is no thermal-neutron flux at this location. Gold foils, 0.127 mm thick, and cadmium covers, 1 mm thick, were used for these measurements. Copper and gold cadmium ratios taken about 19 cm above and below the centerline gave values of 1.00 ± 0.05 which show no thermal-neutron effects, although the uncertainties of these measurements are quite large.

Plugs for each end of the CFRMF fast zone, consisting of aluminum, boral, and ^{238}U were used to test for neutrons streaming from the ends. Vertical profiles of the gold reaction rate with and without these plugs were measured, and the results show no difference in the shape of the profile in the section where it was possible to compare the activities. Stacks of twenty 0.127-mm-thick gold foils were activated at the centerline, and the activities of each foil were measured to observe the reaction rate through the stacks. A comparison of the ratio of the activity of the end foils to the center foils of the stacks, activated with and without the end plugs, provides a test for any changes in the relative amounts of thermal and/or resonance neutron streaming from the ends of the assembly. The results of such measurements are summarized in Table II. These results do not indicate any measureable streaming of thermal and resonance neutrons from the ends of CFRMF fast zone assembly above the 1 to 2% level.

Another study in the CFRMF was made on the effect of cadmium metal of different thicknesses on the activation of gold foils. This study was done to test for the presence of thermal neutrons and to investigate scattering-in-Cd effects on reaction rates in the CFRMF neutron spectrum.

For this study a 0.5 mm cadmium foil strip was rolled to produce strips of various thicknesses. These strips were used to fabricate the cadmium covers. The cadmium cover was made by cutting two pieces 1.27 cm by 1.9 cm from one of these strips. The two pieces were placed one on top of the other with the long axis of the pieces at right angles to each other. A gold foil enclosed in a 0.013 mm aluminum foil packet 1.27 cm square was placed between the two cadmium pieces. The overlapping edges of each cadmium piece were bent over the edges of the other cadmium piece. This resulted in a packet with the gold foil in the center. To eliminate any possibility of neutron leakage the corners of the packet were crimped.

A 0.05 mm gold foil was mounted in a 0.013 mm aluminum foil packet 3.81 cm above the gold packet being tested. This foil was attached using 0.089 mm diameter copper wire. These foils were used to normalize power level variation between the bare and cadmium covered runs. Two irradiations were made using gold foils of the same thickness and both enclosed in 0.013 mm aluminum foil covers. One irradiation was made with the gold foil in the cadmium covered packet and the other without the cadmium cover. For the irradiations the packets were mounted on an aluminum metal strip (3.81 cm x 13.97 cm x 0.068 cm) using 0.089 mm diameter copper wire. Mounting of the packet was done so that when the mounting strip rested on the pedestal in the CFRMF experimental access tube the gold was located at the reactor centerline with the plane of the sample vertically oriented. Tests were made using 0.05 mm gold and varying the thickness of the cadmium and a test was made using a 0.0005 mm gold foil to study the effect of gold thickness. One test was also made with the ^{10}B end plugs installed.

Results of the irradiations are expressed as a cadmium ratio. This is the ratio of the bare gold foil activity (normalized to the cadmium covered run) to the cadmium covered gold foil activity. Table III is a summary of these measurements. These are estimated to have an uncertainty of $\pm 2\%$. Most of this arises from the normalization procedures used. Reproducibility was of the order of $\pm$ 0.5%.

Cadmium thickness and gold thickness gave no indication of having any effect on the cadmium ratio for gold in the CFRMF experimental access facility tube. The plugging of the ends of the test region with ^{10}B end caps showed no appreciable effect.

IV. Neutron Spectrum Measurements

Proton Recoil Measurements

The spectrum of the CFRMF has been measured three times by the proton recoil method. The first series of measurements was made using two cylindrical detectors, one predominantly hydrogen filled, the other methane filled. Pulse shape analysis (rise-time) was used to discriminate against gamma events so that the applied energy ranges of these two detectors were extended to lower neutron energies and the lower limit of the methane detector overlapped the upper limit of the hydrogen detector. The gamma background during these measurements was the lowest because the CFRMF had not been operated at high neutron flux levels ($< 10^8$ n/cm^2/sec).

The second series of measurements was made using five cylindrical detectors, three predominantly hydrogen filled and two methane filled. Gas pressure was used as the parameter to discriminate against gamma events and also to cover neutron energy ranges with energy overlap between detectors of different pressures. The cylindrical detectors are described in Table IV. The gamma background during these measurements was much higher because the CFRMF had been operated at high flux levels ($> 10^{11}$ n/cm^2/sec).

The third series of measurements consisted of a repeat of the second series plus additional measurements with four spherical detectors filled with hydrogen. The spherical detectors are described in Table V. These measurements were for the purpose of comparing the results from detectors of different geometries to test for anisotropy effects upon the measured spectrum. The gamma background was even higher for these measurements due to additional high power operation of CFRMF. Figure 12 is a photograph of the detectors used in these measurements.

The results of the first series of measurements are excluded because it was found that these measurements were very sensitive to a bias setting in the stretcher of the pulse shape discrimination circuitry. It is not known that this was properly set during the first series of measurements. Also, during the first series of measurements it was not possible to check the energy calibration (gas gain) during the course of the measurements and nonreproducibility was later observed in the high voltage power supply. The results of the second and third series of measurements are accepted since the uncertainties of the first series of measurements were avoided by using gas pressure discrimination against gamma rays and checking the calibrations during the measurements. Pulse pile-up rejection tests indicated that no spectral distortions were encountered due to the high gamma ray backgrounds. Figure 13 illustrates the results from the third series of measurements comparing the results of the cylindrical and spherical detectors. The results of both measurements with the cylindrical detectors agree within statistical error.

^{6}Li-Semiconductor Sandwich Measurements

The CFRMF spectrum has been measured with two ^{6}Li semiconductor sandwich detectors, one with 4π geometry where the diodes are separated by 0.24 mm and the other with energy independent collimation geometry where the diodes are separated by 10 mm. Figure 14 is a sketch of these detector assemblies. These detector assemblies were positioned in CFRMF so that the ^{6}Li deposit was located at the center of the core with the surface of the deposit perpendicular to the vertical axis of the core. The neutron spectrum is derived below approximately 500 keV from the triton energy responses from each of the diodes in each detector assembly whereas above 500 keV it is from the energy response of the sum of the triton and alpha.

In the present measurements the triton energy responses from each diode of a detector assembly are not identical, suggesting a forward-backward anisotropy in the neutron energy distribution. Figure 15 compares the results obtained in the collimated and 4 geometries, omitting for clarity purposes, one diode response in each case. The same unfolding code and cross section set were used to derive the results which came from the similar experimental conditions. The disagreement between the two measurements is thought to be due to neutron spectrum anisotropy for which the collimated detector is more sensitive[6].

In comparing the H(n,p) and ^{6}Li measurements rather significant discrepancies are observed between the two measurements techniques especially between 200 keV and 500 keV. At this time these discrepancies have not been resolved. There have not been enough measurements conducted to resolve some of the remaining questions of each technique. The gamma ray background in CFRMF presents conditions nonideal for conducting neutron energy spectrometry. If another CFRMF assembly were assembled with a very low gamma ray background more spectrometry measurements could be conducted which should establish the neutron spectrum more accurately and resolve some of the existing discrepancies between techniques.

The estimated uncertainties on the proton recoil measurements are $\pm$5% assuming there are no systematic errors and the possibility of improving the accuracy of these measurements would be to discover and correct any systematic errors. The errors on the ^{6}Li measurements involve the errors on the ^{6}Li(n,α) cross section over the applied energy range and in the energy range of triton analysis also includes the errors on the angular distributions for the ^{6}Li(n,α)t reaction.

Theoretical Calculations

In the effort to characterize the CFRMF spectrum calcualtional techniques have been applied using transport, Monte Carlo and resonance

theory computerized methods. The versatility of the transport code (SCAMP, ID, P1, S6) with its many options and relatively short computation time made it quite useful for most of the calculations. The Monte Carlo calculations were used to test for smoothing effects in the cross section processing and only minor differences were observed. The resonance theory spectrum also showed only minor differences in comparison with the transport theory in the resonance energy region. Extensive tests of the cylindrical model to give the best representation of the complex CFRMF assembly have shown the best compromise between neutron energy group structure and material regions to be 71 energy groups with 0.25 lethargy spacing from 21 MeV down. Both cell and full core models have been used in the calculations with only minor differences between these. Both ENDF/B Versions III and IV have been used and Version IV data produces more relative flux above 0.5 MeV due primarily to the Version IV changes in ^{238}U inelastic scattering. At this time the recommended spectrum for CFRMF is the full core cylindrical model calculation using ENDF/B Version IV cross section data. This spectrum is tabulated in Table VI. This spectrum is recommended because it agrees very well in shape with the measurements in the energy regions where the various measurements are considered to be most credible and because it is impossible to make spectrum measurements over the entire energy range of interest. Figures 16, and 17 show the comparisons of the measurements with the calculation. These measurements and calculations have been normalized by making the fluxes equal between 0.5 and 0.6 MeV.

V. Flux Level Monitoring

Flux level monitoring and control methods incorporated in the reactor control system have been described in Section I. This flux level control will hold a prescribed level to approximately ± 0.3% at flux levels of up to $7x10^{10}$ $n/cm^2/sec$ for time durations up to 30 hrs. The run-to-run reproducibility for a given power level in this range has been shown to be ± 0.5% based on fission chamber (^{235}U and ^{238}U) measurements at the center of CFRMF. Activation measurements of the $^{197}Au(n,)^{198}Au$ and $^{115}In(n,n')^{115m}In$ reactions near the center of CFRMF (2.54 cm above) show run-to-run reproducibility of ± 0.5% if the azimuthal position of the foils is fixed. This activation method of determining the integrated flux may be as great as ± 1.0% if the azimuthal positioning is not fixed due to the $^{197}Au(n,\gamma)^{198}Au$ reaction rate gradients in the flux where these foils are normally located. These methods of determining the flux levels have minimum detection sensitivities of 0.1% to 0.2%. The fission chamber measurements have been used to monitor the flux level immediately before and after the irradiations. The activation measurements have been used to monitor the integrated flux (fluence) throughout the irradiations.

The precision attained on relative flux levels of twenty irradiations conducted over a period of over two years ranged from ± 0.3% to ± 1.0%. These results are summarized in Table VII. During this time period when the monitoring methods indicated level changes outside their estimated precision positive reasons were identified for causing the level change. These reasons were such things as failure to properly reposition the power level control reference chamber and the perturbation of flux at the reference chamber by water leakage into an adjacent instrument tube. These types of problems illustrate the critical need to have several

independent methods of monitoring the flux level in any standard reference neutron field. It also illustrates the critical need of maintaining cognizant surveillance over the facility control equipment and all activities at or around the facility that may cause any changes or perturbations to the neutron field.

The availability of the CFRMF for interlaboratory experiments is dependent upon the programmatic and support work loads which vary from time to time. Based on recent experience the CFRMF should be available about 20% of the time. The availability will also depend to some extent on the flux level required for the experiments because the more the reactor is run at high power the sooner it will use up the core excess reactivity.

VI. Results of Reaction Rate Measurements and Calculations

Integral reaction rates have been obtained for fissionable and non-fissionable dosimeter materials irradiated in the CFRMF neutron field. Fission chamber, solid state track recorder, gamma-ray spectrometry and helium mass spectrometry measurements and analyses techniques have been used to determine these reaction rates. Several laboratories have been involved in the planning, preparation and execution of these measurements and the results summarized here represent the efforts of many people associated with these laboratories. Table VIII summarizes the measured reaction rates in CFRMF at the 6 kW power level which corresponds to approximately 7.5×10^{10} $n/cm^2/sec$.

Using the calculated neutron spectrum from Section IV the reaction rates have been calculated for those reaction rates which have been measured. Table IX lists these reaction rates relative to the ^{235}U fission rate and compares them by the ratios of measured to calculated.

References

1. E. Fast, C. L. Beck, D. A. Millsap, R. G. Nisle, JW Rogers and J. J. Scoville, "Use of ARMF for a Fast Reactor Support Program," IN-1143 (November, 1967).

2. E. E. Burdick, E. Fast and D. W. Knight, "The Advanced Reactivity Measurements Facilities," IDO-17005 (October, 1964).

3. JW Rogers, D. A. Millsap and Y. D. Harker, "CFRMF Neutron Field Flux Spectral Characterization," Nuclear Technology 25, 330 (February, 1975).

4. JW Rogers, Y. D. Harker and D. A. Millsap, "Fast Neutron Spectrum and Dosimetry Studies in the CFRMF," First ASTM-EURATOM Symposium on Reactor Dosimetry, (September, 1975) to be published.

5. G. DeLeeuw-Gierts, S. DeLeeuw, H. H. Helmick and JW Rogers, "Neutron Spectrometry Data in LMFBR Benchmark and Standard Neutron Fields," First ASTM-EURATOM Symposium on Reactor Dosimetry, (September, 1975) to be published.

6. G. and S. DeLeeuw, private communication (August, 1976).

TABLE I

Relative Fission Rates Along the CFRMF Vertical Axis

Distance from Core Midplane (cm)	^{235}U Fission Chamber	^{238}U Fission Chamber	^{239}Pu Fission Chamber	^{237}Np Fission Chamber
+10.16	0.922	0.904	0.910	0.905
+ 7.62	0.966	0.942	0.948	0.942
+ 5.08	0.983	0.979	0.976	0.969
+ 2.54	0.993	0.991	0.997	0.995
0	1.000	1.000	1.000	1.000

TABLE II

Stacked Gold Foil Activity Ratios from CFRMF

Ends Unplugged Foils Horzontal	Ends Plugged Foils Horizontal	Ends Plugged Foils Vertical
1.179 $\pm$ 0.010	1.176 $\pm$ 0.010	1.185 $\pm$ 0.010

TABLE III

Cd Ratio Measurements in the CFRMF

Cd (mm)	Au (mm)	Cd Ratio
0.127	0.05	1.02
0.229	0.05	1.00
0.508	0.05	1.00
0.508	0.0005	1.02
0.508*	0.0005*	0.98*

*With ^{10}B end plugs installed.

TABLE IV

Description of Cylindrical Proportional Counter Detectors

	1 atm H_2	2.63 atm H_2*	5 atm H_2	2.63 atm CH_4	5 atm CH_4*
Inside Diameter	2.46 cm	2.23 cm	2.46 cm	2.46 cm	2.23 cm
Body Length	12.7 cm	11.43 cm	12.7 cm	12.7 cm	11.43 cm
Center Wire Diameter	25.4 μm	25.4 μm	25.4 μm	25.4 μm	25.4 μm
Sensitive Length	7.62 cm	7.62 cm	7.62 cm	7.62 cm	7.62 cm
Field Tube Diameter	127.0 μm	127.0 μm	127.0 μm	127.0 μm	127.0 μm
Field Tube Lengths	2.38 cm	1.9 cm	2.38 cm	2.38 cm	1.9 cm
Sensitive Volume	36.7 cm^3	29.73 cm^3	36.7 cm^3	36.7 cm^3	29.73 cm^3
H_2 Pressure	76 cm Hg	200 cm Hg	380 cm Hg		
CH_4Pressure	4 cm Hg	20 cm Hg	19 cm Hg	200 cm Hg	380 cm Hg
N_2 Pressure	4 cm Hg	10 cm Hg	19 cm Hg	10 cm Hg	19 cm Hg
Stainless Steel Body	40.6 μm Thick	76.2 μm Thick	40.6 μm Thick	40.6 μm Thick	76.2 μm Thick
Resolution †	5% FWHM	5% FWHM	6% FWHM	6% FWHM	8% FWHM
Minimum Energy	68 keV	120 keV	170 keV	280 keV	440 keV
Maximum Energy	350 keV	450 keV	620 keV	970 keV	2000 keV

* Detectors used in pulse shape discrimination measurements.

† Full width at half maximum resulting from $^{14}N(n,p)^{14}C$ reaction at 585 keV.

TABLE V

Descriptions of Spherical Proportional Counter Detectors

	1.4 atm H_2	4.22 atm H_2	4 atm H_2	5.22 atm H_2
Inside Diameter	32 mm	22.73 mm	32 mm	22.73 mm
Body Length	134 mm	95 mm	134 mm	95 mm
Center Wire Diameter	22 μm	22 μm	22 μm	22 μm
Sensitive Volume	17.2 cm^3	6.15 cm^3	17.2 cm^3	6.15 cm^3
H_2 Pressure	106.4 cm Hg	320.7 cm Hg	304 cm Hg	396.7 cm Hg
CH_4 Pressure		32.7 cm Hg		
^3He Pressure		0.10 cm Hg		0.40 cm Hg
Stainless Steel Body	0.51 mm Thick	0.51 mm Thick	0.51 mm Thick	0.51 mm Thick
Resolution	∿7% †	∿4% *	∿9% **	∿6% *
Minimum Energy	48 keV	132 keV	146 keV	107 keV
Maximum Energy	236 keV	578 keV	787 keV	578 keV

† Full width at half maximum resulting from ^{239}Pu alpha particles (Eeff = 260 ± 3 keV).
* Full width at half maximum resulting from ^3He (n,p)T reaction (Eeff = 770 ± 10 keV).
** Full width at half maximum resulting from ^{239}Pu alpha particles (Eeff - 1.01 ± 0.01 MeV).

TABLE VI

CFRMF Calculated Neutron Energy Spectrum, ID Transport, P1-S6 Approximation, ENDF/B IV Data

Group #	Lower Energy (eV)	Relative Real Flux $\phi(u)\Delta u$	Group #	Lower Energy (eV)	Relative Real Flux $\phi(u)\Delta u$
1	1.6487×10^{7}	2.7818×10^{-6}	36	2.6126×10^{3}	3.1659×10^{-3}
2	1.2840	4.0995×10^{-5}	37	2.0347	2.8491
3	9.9990×10^{6}	2.9946×10^{-4}	38	1.5846	2.9647
4	7.7880	1.4513×10^{-3}	39	1.2341	2.4583
5	6.0653	4.2566	40	9.6112×10^{2}	1.7658
6	4.7237	8.9123	41	7.4851	1.8431
7	3.6788	1.4549×10^{-2}	42	5.8294	1.4216
8	2.8650	2.1374	43	4.5400	1.3335
9	2.2313	2.8616	44	3.5357	8.9206×10^{-4}
10	1.7377	3.2166	45	2.7536	7.4516
11	1.3533	3.6963	46	2.1445	5.8312
12	1.0540	4.5966	47	1.6702	4.7521
13	8.2085×10^{5}	5.8769	48	1.3007	4.2541
14	6.3928	7.4516	49	1.0130	1.8149
15	4.9787	8.3137	50	7.8893×10^{1}	2.2322
16	3.8774	7.9180	51	6.1442	1.0209
17	3.0197	7.9354	52	4.7851	1.0517
18	2.3518	7.0509	53	3.7266	4.8777×10^{-5}
19	1.8316	6.0150	54	2.9023	3.2889
20	1.4264	4.8486	55	2.2603	2.3910
21	1.1109	4.4753	56	1.7603	5.1395×10^{-6}
22	8.6517×10^{4}	3.3562	57	1.3709	8.7709
23	6.7379	3.3222	58	1.0677	4.1776
24	5.2475	2.4791	59	8.3153×10^{0}	1.3859
25	4.0868	1.8273	60	6.4759	1.8581×10^{-7}
26	3.1828	1.4848	61	5.0435	8.0185×10^{-8}
27	2.4787	1.3992	62	3.9278	7.1747
28	1.9304	1.0583	63	3.0590	2.2289
29	1.5034	7.2421×10^{-3}	64	2.3824	6.3475×10^{-9}
30	1.1709	6.8513	65	1.8554	1.1273
31	9.1188×10^{3}	5.6633	66	1.4449	1.9803×10^{-10}
32	7.1017	4.3015	67	1.1253	2.7826×10^{-11}
33	5.5308	3.9449	68	8.7642×10^{-1}	5.9817×10^{-12}
34	4.3074	3.6821	69	6.8256	2.9788
35	3.3546	3.9291	70	5.3157	1.7941×10^{-13}
			71	4.1399	1.0053×10^{-14}

TABLE VII

CFRMF Run-to-Run Flux Level Monitor Measurements

Test	Date	^{235}U	^{238}U	AVG.	Au	In	AVG.
ARHCO-I	2-8-72				1.654 ±1.8%	1.672 ±1.1%	1.663 ±1.0%
ANL-I	2-15-72				1.613 ±1.6%	1.618 ±1.0%	1.616 ±0.8%
HEDL-I	2-16-72				1.594 ±1.6%	1.626 ±1.2%	1.610 ±1.0%
ANC-I	2-29-72				1.627 ±1.0%	1.636 ±0.3%	1.631 ±0.6%
AI-I	4-11-72				1.612 ±1.5%	1.631 ±0.6%	1.623 ±0.7%
HEDL-V	11-6-72	0.9989	0.9997	0.9993 ±0.2%	0.9945 ±0.3%	0.9962 ±0.3%	0.9954 ±0.2%
HEDL-VI	11-7-72	1.000 (158982)*	1.000 (365547)*	1.000	1.000 (300.8)*	1.000 (38.36)*	1.000
ANL-SSTR	11-8-72	0.1038	0.1036	0.1037 ±0.3%	0.1043 ±0.6%	0.1036 ±0.8%	0.1039 ±0.5%
ANL-SSTR	3-7-73	0.1037	0.1037	0.1037 ±0.3%	0.1047 ±0.5%	0.1039 ±1.0%	0.1043 ±0.5%
SS-I	3-13-73	1.792	0.798	1.795 ±0.2%	1.785 ±0.3%	1.783 ±0.7%	1.784 ±0.3%
SS-II	3-14-73	1.792	1.798	1.795 ±0.2%	1.788 ±0.4%	1.793 ±0.6%	1.791 ±0.3%
SS-III	3-14-73	1.792	1.798	1.795 ±0.2%	1.800 ±0.5%	1.797 ±0.7%	1.798 ±0.4%
AI-II	5-24-73	1.026	1.024	1.025 ±0.2%	1.014 ±0.4%	1.027 ±1.0%	1.021 ±0.6%
ANC-IV	1-15-74	1.051	1.051	1.051 ±0.2%	1.046 ±1.8%	1.040 ±1.7%	1.043 ±1.2%

Table VII (continued)

Test	Date	^{235}U	^{238}U	AVG.	Au	In	AVG.
ANC-V	1-17-74	1.049	1.048	1.049 ±0.2%	1.058 ±0.8%	1.061 ±0.2%	1.059 ±0.4%
HEDL-VI A	1-21-74	1.050	1.045	1.048 ±0.2%	1.057 ±0.8%	1.055 ±0.4%	1.056 ±0.5%
HEDL-VI B	1-22-74	1.051	1.046	1.049 ±0.2%	1.058 ±1.0%	1.055 ±0.4%	1.056 ±0.5%
ANL-VII A	1-24-74	1.048	1.046	1.047 ±0.2%	1.057 ±0.7%	1.058 ±0.3%	1.056 ±0.4%
ANL-VII B	1-24-74	1.051	1.047	1.049 ±0.2%	1.059 ±0.7%	1.061 ±0.5%	1.060 ±0.5%
AI-III	6-25-75	1.016	1.014	1.015 ±0.2%	1.017 ±0.9%	1.026 ±0.1%	1.023 ±0.5%

* Reference values.

TABLE VIII

CFRMF Measured Reaction Rates

Reaction	Reaction Rate [reactions/(sec atom)] $\times 10^{15}$	
$^{235}U(n,f)$	122.1	$\pm$ 1.4%
$^{238}U(n,f)$	5.96	$\pm$ 1.9%
$^{239}Pu(n,f)$	142.3	$\pm$ 1.6%
$^{237}Np(n,f)$	43.5	$\pm$ 1.9%
$^{45}Sc(n,\gamma)^{46}Sc$	1.845	$\pm$ 1.8%
$^{58}Fe(n,\gamma)^{59}Fe$	0.481	$\pm$ 1.5%
$^{59}Co(n,\gamma)^{60}Co$	7.197	$\pm$ 2.3%
$^{63}Cu(n,\gamma)^{64}Cu$	3.56	$\pm$ 4.5%
$^{115}In(n,\gamma)^{116m}In$	22.1	$\pm$ 2.5%
$^{197}Au(n,\gamma)^{198}Au$	33.3	$\pm$ 1.0%
$^{238}U(n,\gamma)^{239}U$	14.5	$\pm$ 2.4%
$^{27}Al(n,\gamma)^{24}Na$	0.0127	$\pm$ 1.2%
$^{27}Al(n,p)^{27}Mg$	0.0687	$\pm$ 2.0%
$^{46}Ti(n,p)^{46}Sc$	0.205	$\pm$ 2.0%
$^{47}Ti(n,p)^{47}Sc$	0.328	$\pm$ 4.0%
$^{48}Ti(n,p)^{48}Sc$	0.00541	$\pm$ 2.0%
$^{54}Fe(n,p)^{54}Mn$	1.371	$\pm$ 1.0%
$^{58}Ni(n,p)^{58}Co$	1.900	$\pm$ 1.0%
$^{115}In(n,n')^{115m}In$	3.90	$\pm$ 4.4%
$^{6}Li(n, \text{total } ^{4}He)$	76.07	$\pm$ 1.0%
$^{10}B(n, \text{total } ^{4}He)$	145.8	$\pm$ 1.6%

TABLE IX

Comparison of Measured and Calculated Reaction Rates in CFRMF

Reaction	Measured*	Calculated	Measured/Calculated
$^{235}U(n,f)$	1.00 (Ref.)	1.00 (Ref.)	1.00 (Ref.)
$^{238}U(n,f)$	0.0488	0.0481	1.014
$^{239}Pu(n,f)$	1.165	1.117	1.043
$^{237}Np(n,f)$	0.356	0.363	0.981
$^{45}Sc(n,\gamma)^{26}Sc$	0.0151	0.0126	1.198
$^{58}Fe(n,\gamma)^{59}Fe$	0.00394	0.00386	1.021
$^{59}Co(n,\gamma)^{60}Co$	0.0589	0.0566	1.041
$^{63}Cu(n,\gamma)^{64}Cu_m$	0.0292	0.0299	0.977
$^{115}In(n,\gamma)^{116m}In$	0.181	0.190	0.953
$^{197}Au(n,\gamma)^{198}Au$	0.273	0.261	1.046
$^{238}U(n,\gamma)^{239}U$	0.119	0.146	0.815
$^{27}Al(n,\alpha)^{24}Na$	0.000104	0.000111	0.937
$^{27}Al(n,p)^{27}Mg$	0.000563	0.000590	0.954
$^{46}Ti(n,p)^{46}Sc$	0.00168	0.00143	1.175
$^{47}Ti(n,p)^{47}Sc$	0.00269	0.00321	0.838
$^{48}Ti(n,p)^{48}Sc$	0.0000443	0.0000274	1.617
$^{54}Fe(n,p)^{54}Mn$	0.0112	0.0111	1.009
$^{58}Ni(n,p)^{58}Co$	0.0156	0.0148	1.054
$^{115}In(n,n')^{115m}In$	0.0319	0.0300	1.063
$^{6}Li(n,$ total $^{4}He)$	0.623	0.608	1.025
$^{10}B(n,$ total $^{4}He)$	1.194	1.064	1.122

* Relative to ^{235}U fission rate.

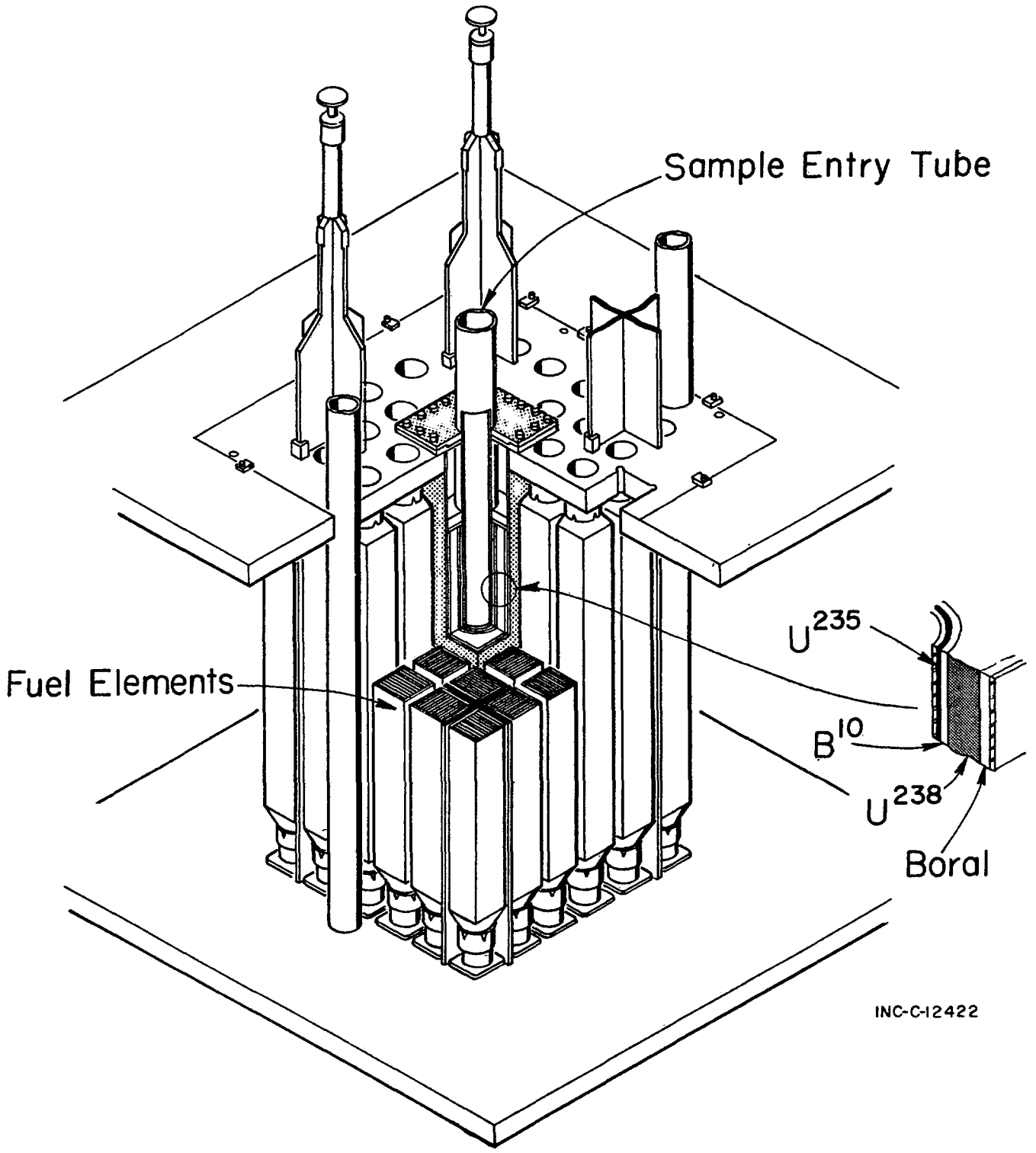

Figure 1. Cutaway pictorial diagram showing general assembly of the CFRMF.

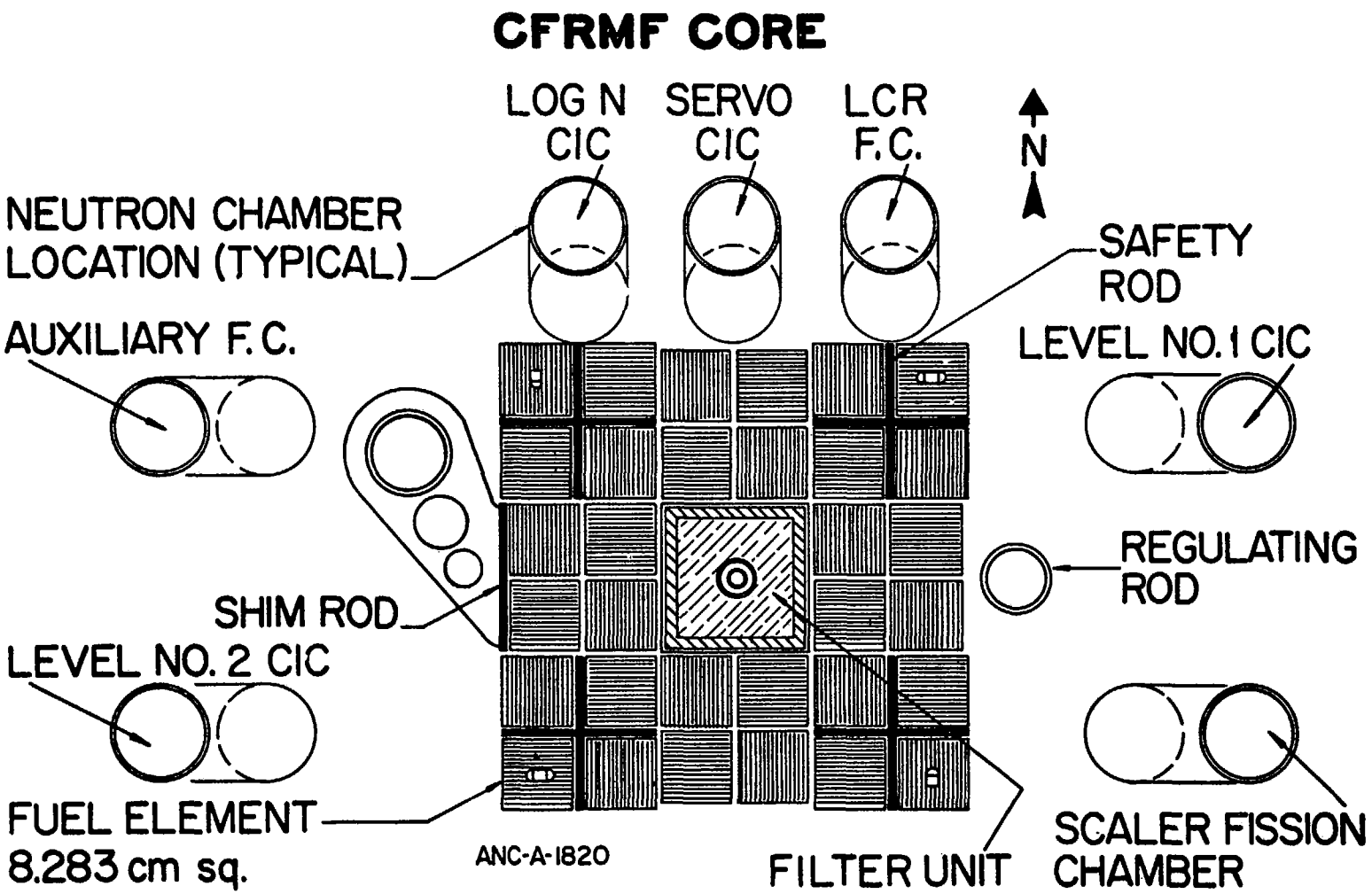

Figure 2. Midplane cross-sectional diagram of CFRMF core, control devices, and chamber locations.

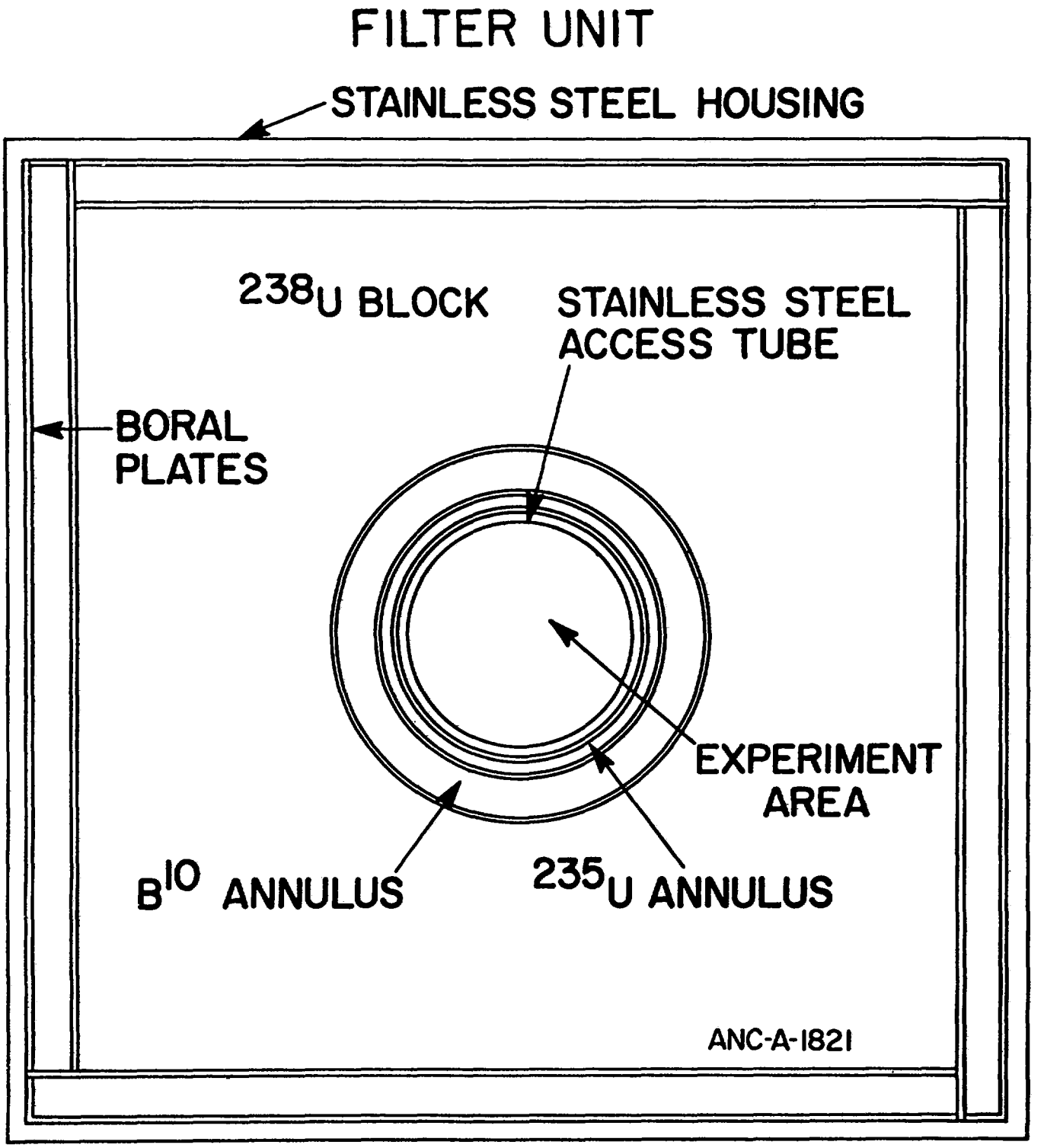

Figure 3. Midplane cross-sectional diagram of filter unit which forms the CFRMF fast zone.

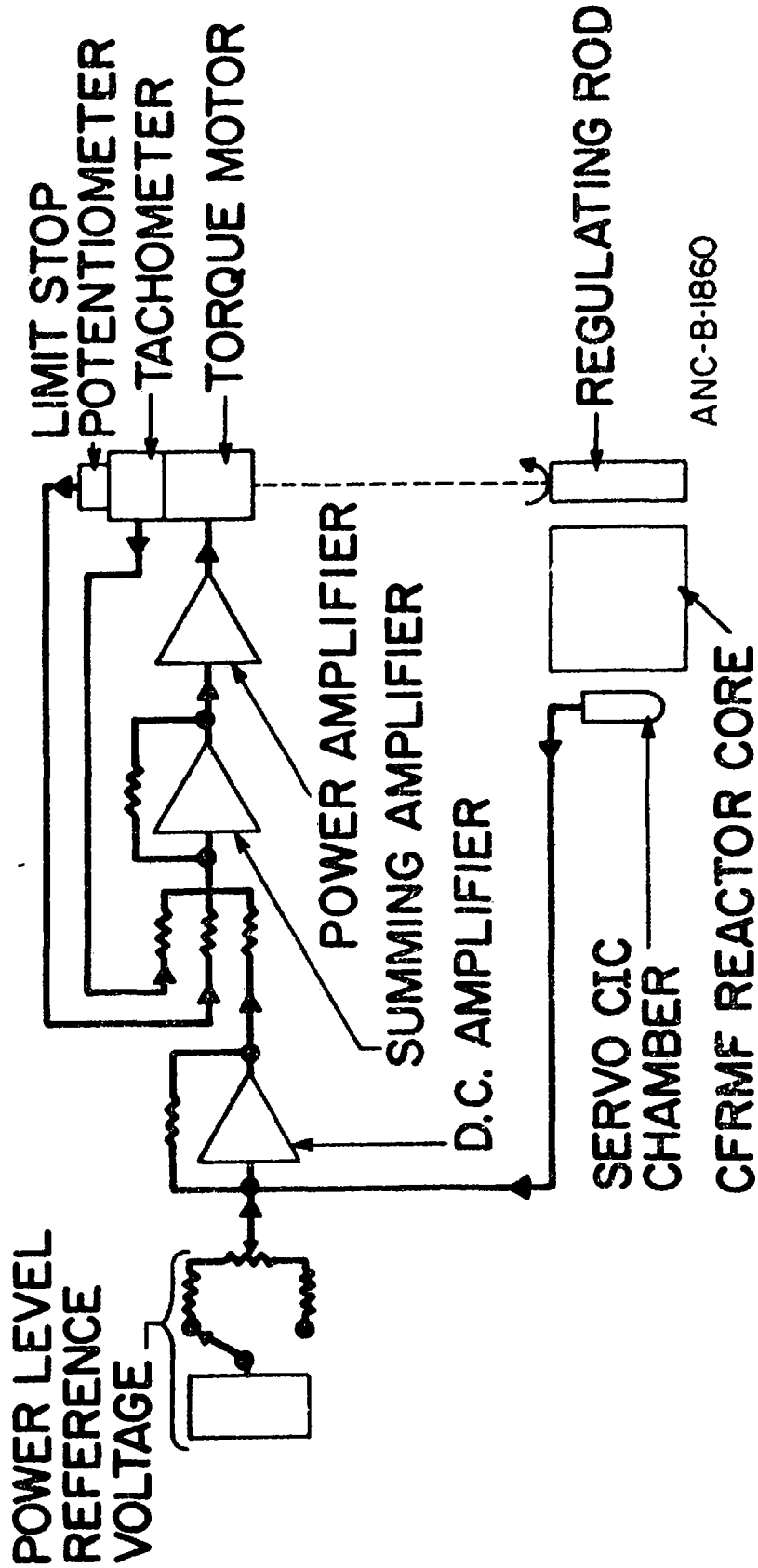

Figure 4. CFRMF power level control servo system used for maintaining a fixed neutron level.

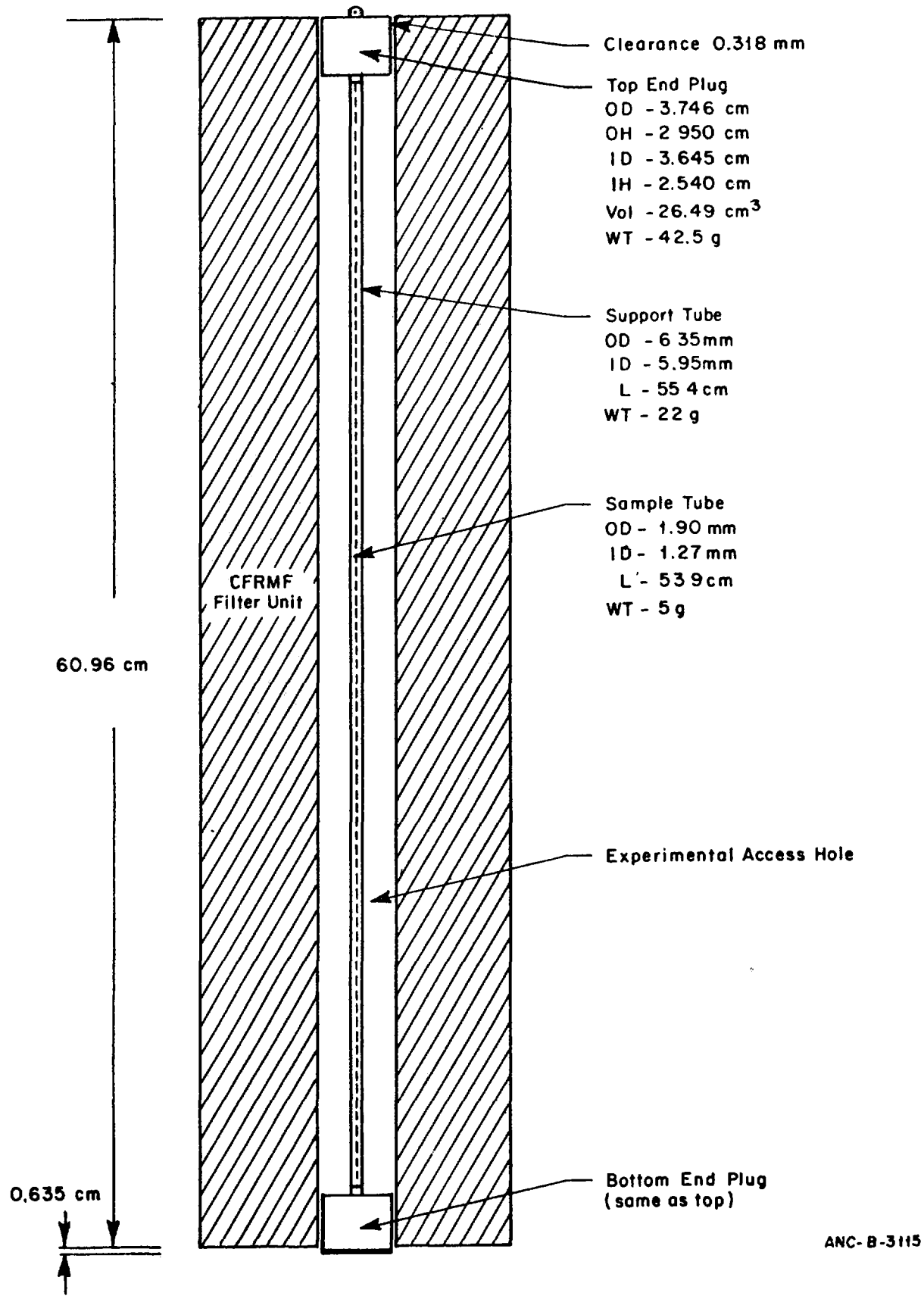

Figure 5. Diagram of device used to position end plugs and flux monitors in CFRMF fast neutron spectrum zone.

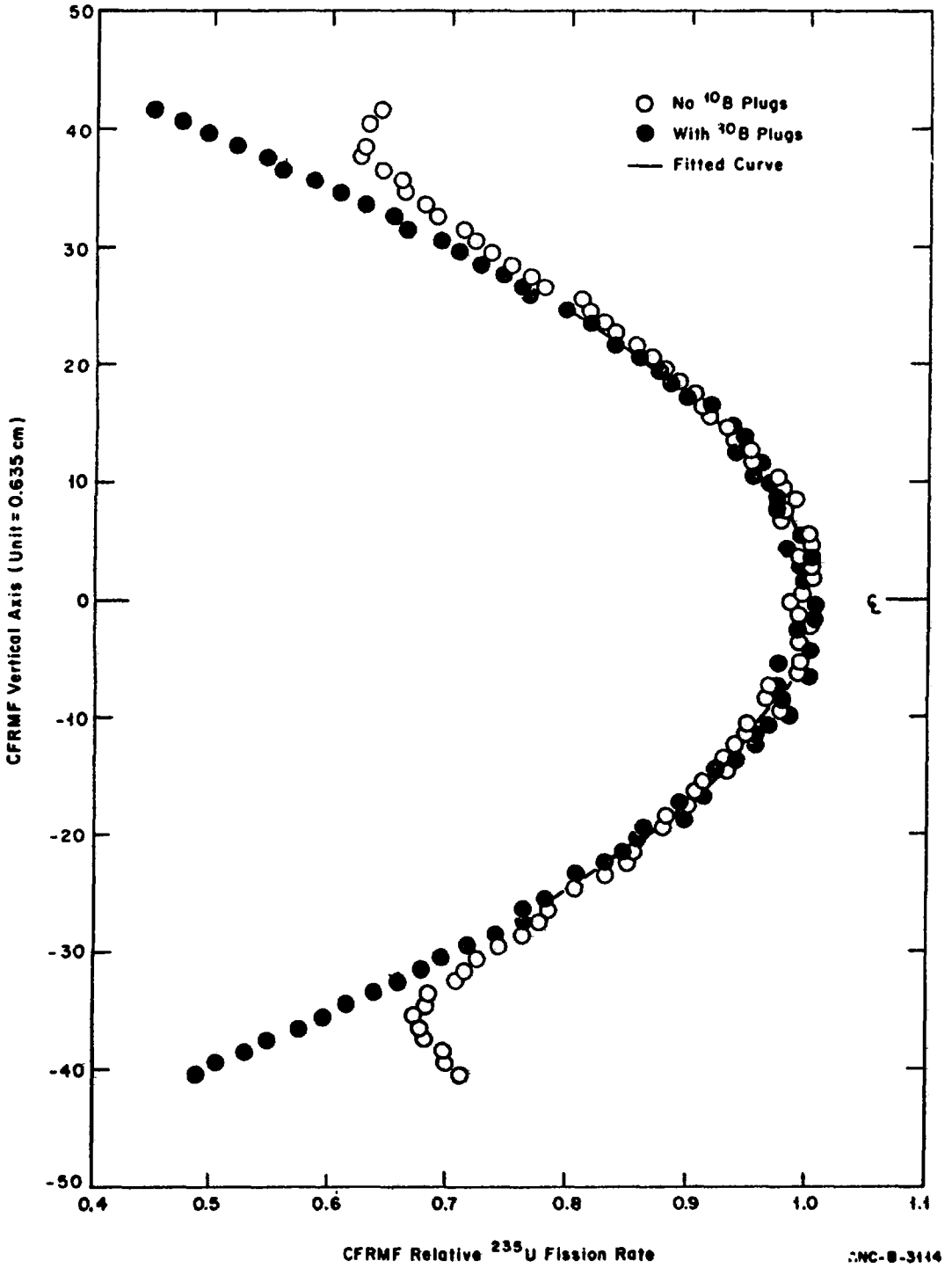

Figure 6. Profiles of ^{235}U fission rate along the vertical axis of CFRMF fast neutron spectrum zone with and without ^{10}B end plugs.

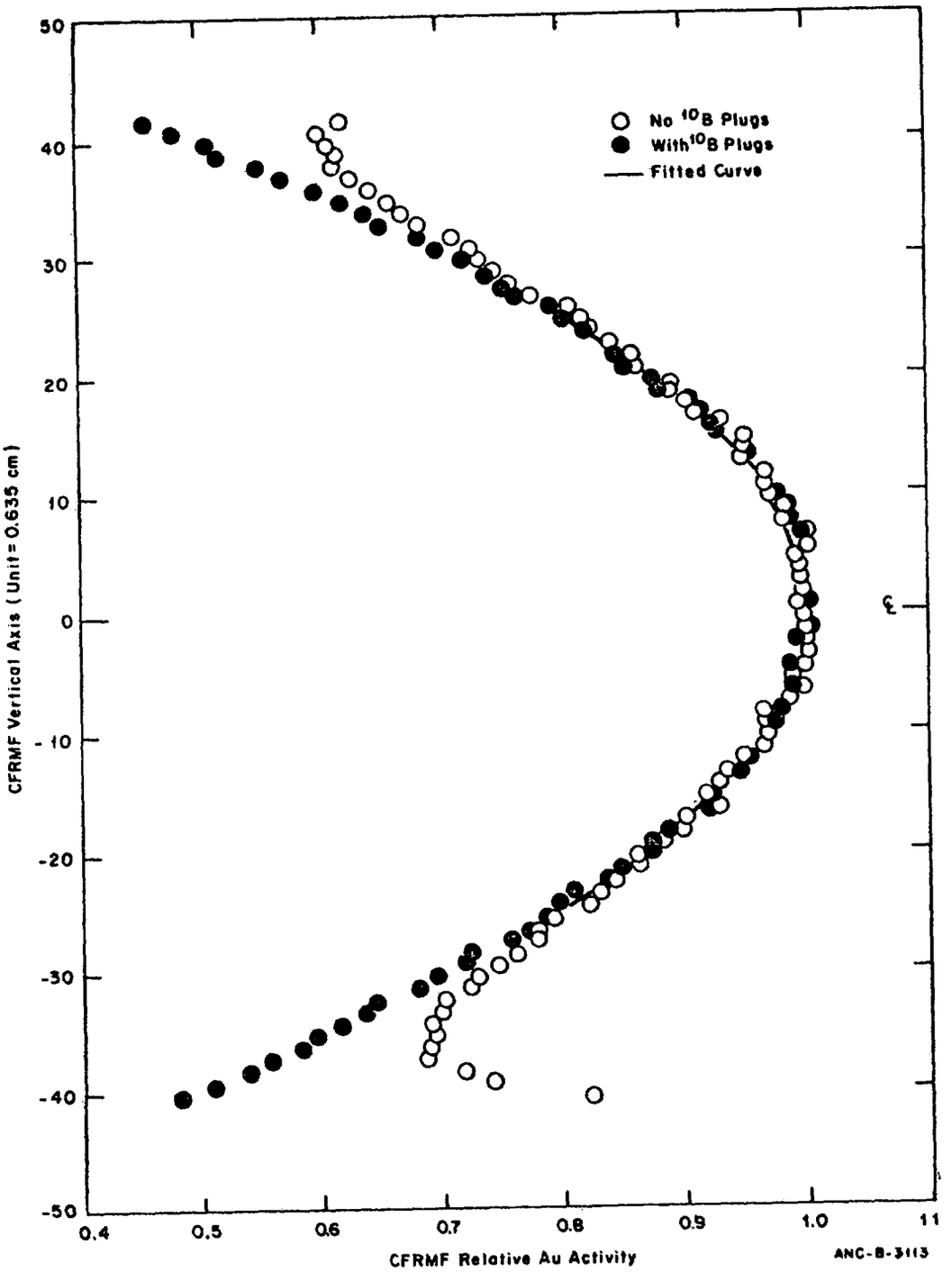

Figure 7. Profiles of ^{198}Au activity along the vertical axis of CFRMF fast neutron spectrum zone with and without ^{10}B end plugs.

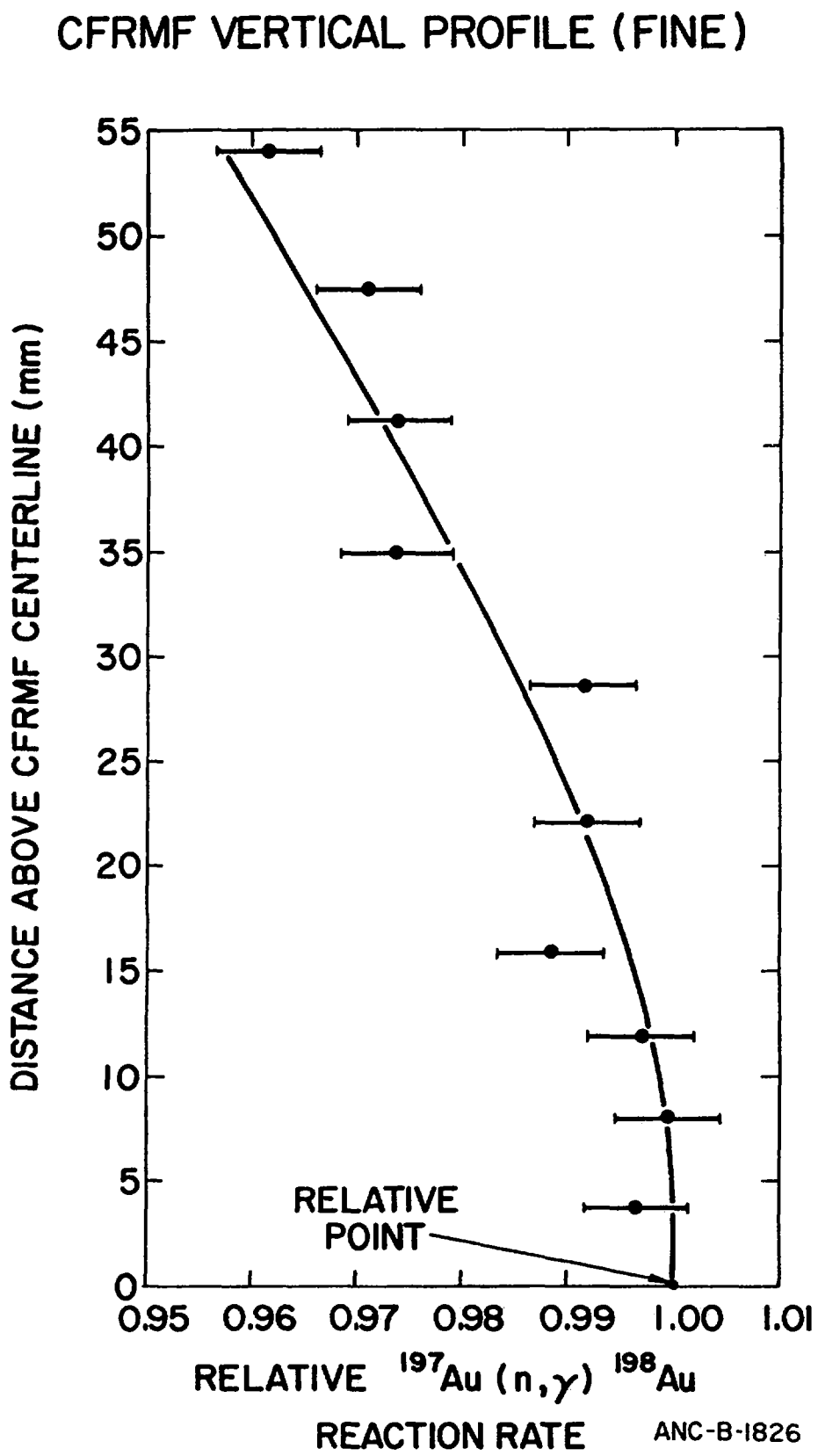

Figure 8. Vertical axis profile of gold (n,γ) reaction rate near the centerline of the CFRMF fast zone.

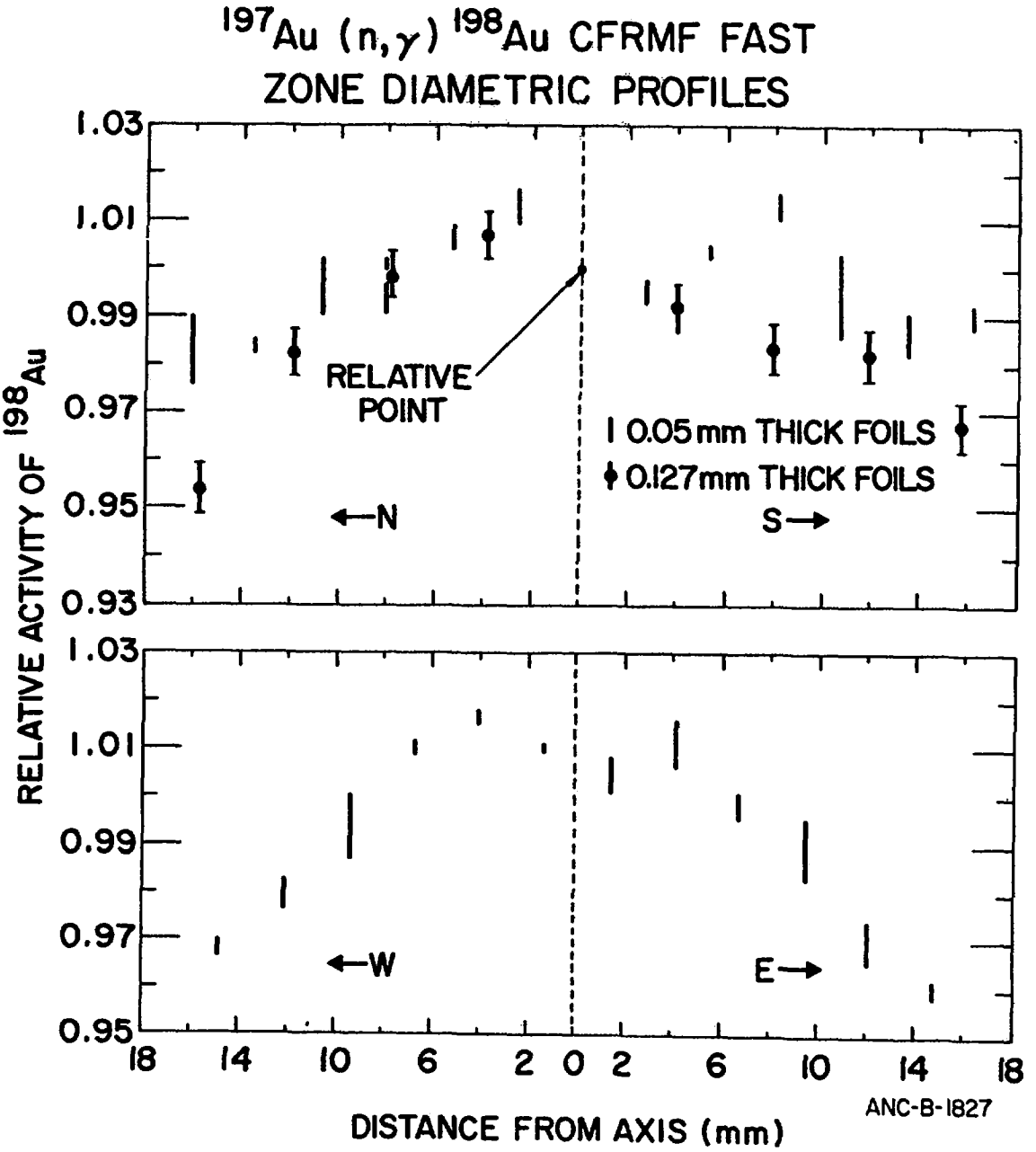

Figure 9. Diametric profiles of gold (n,γ) reaction rate inside the fast zone at CFRMF centerline in the north-south and east-west directions.

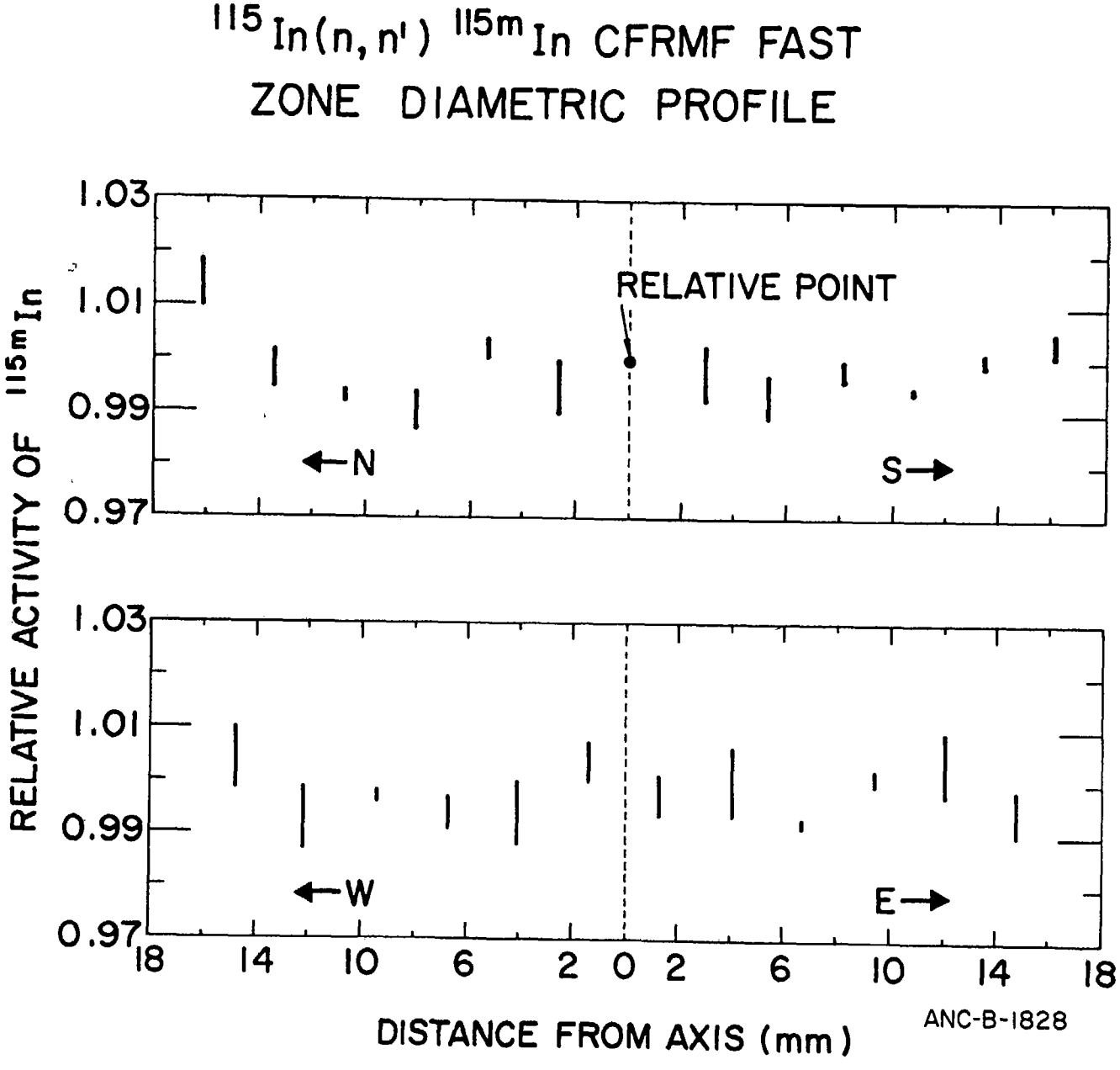

Figure 10. Diametric profiles of indium (n,n') reaction rate inside the fast zone at CFRMF centerline in the north-south and east-west directions.

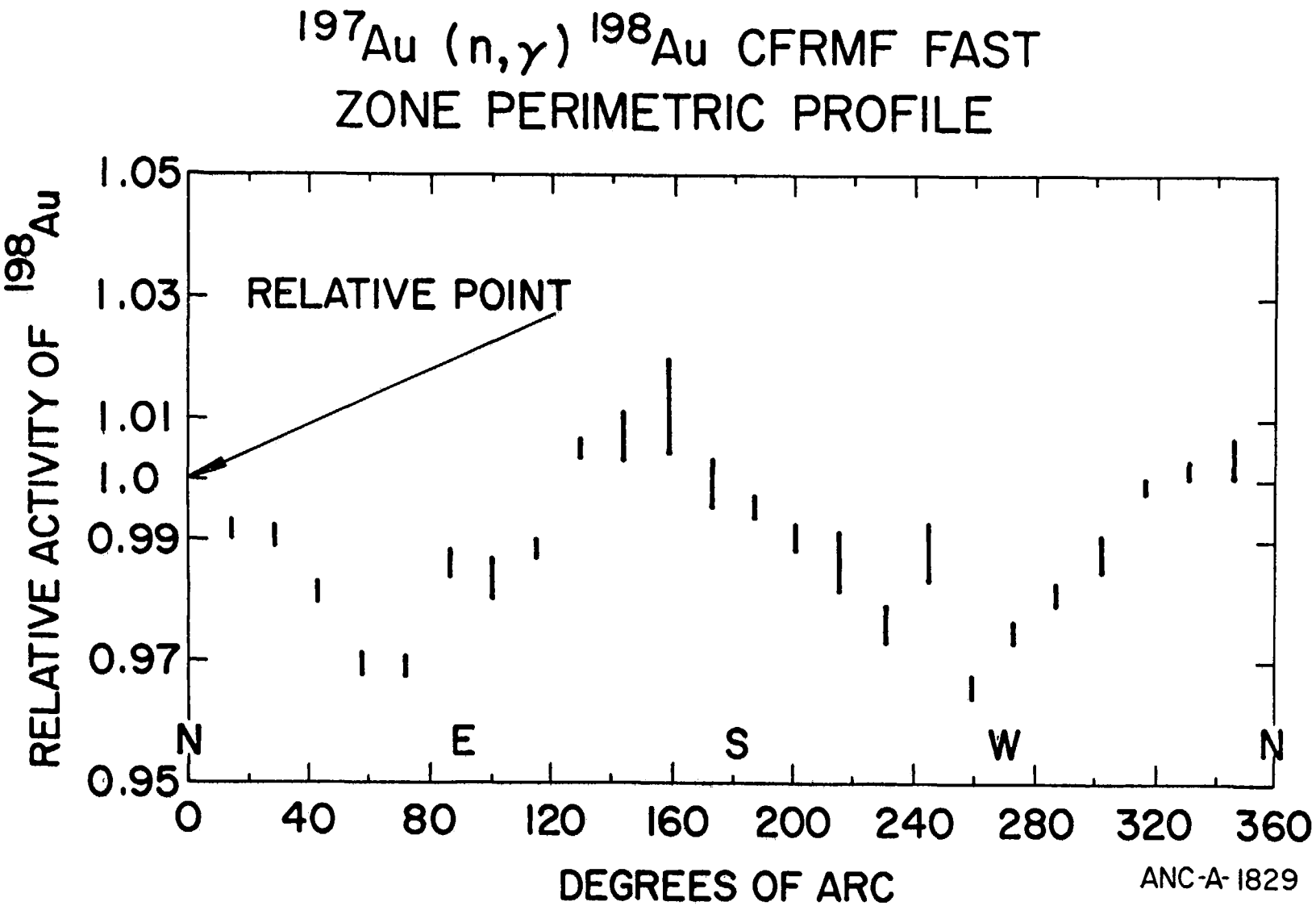

Figure 11. Perimetric profile of gold (n,γ) reaction rate 38 mm above CFRMF centerline inside the fast zone.

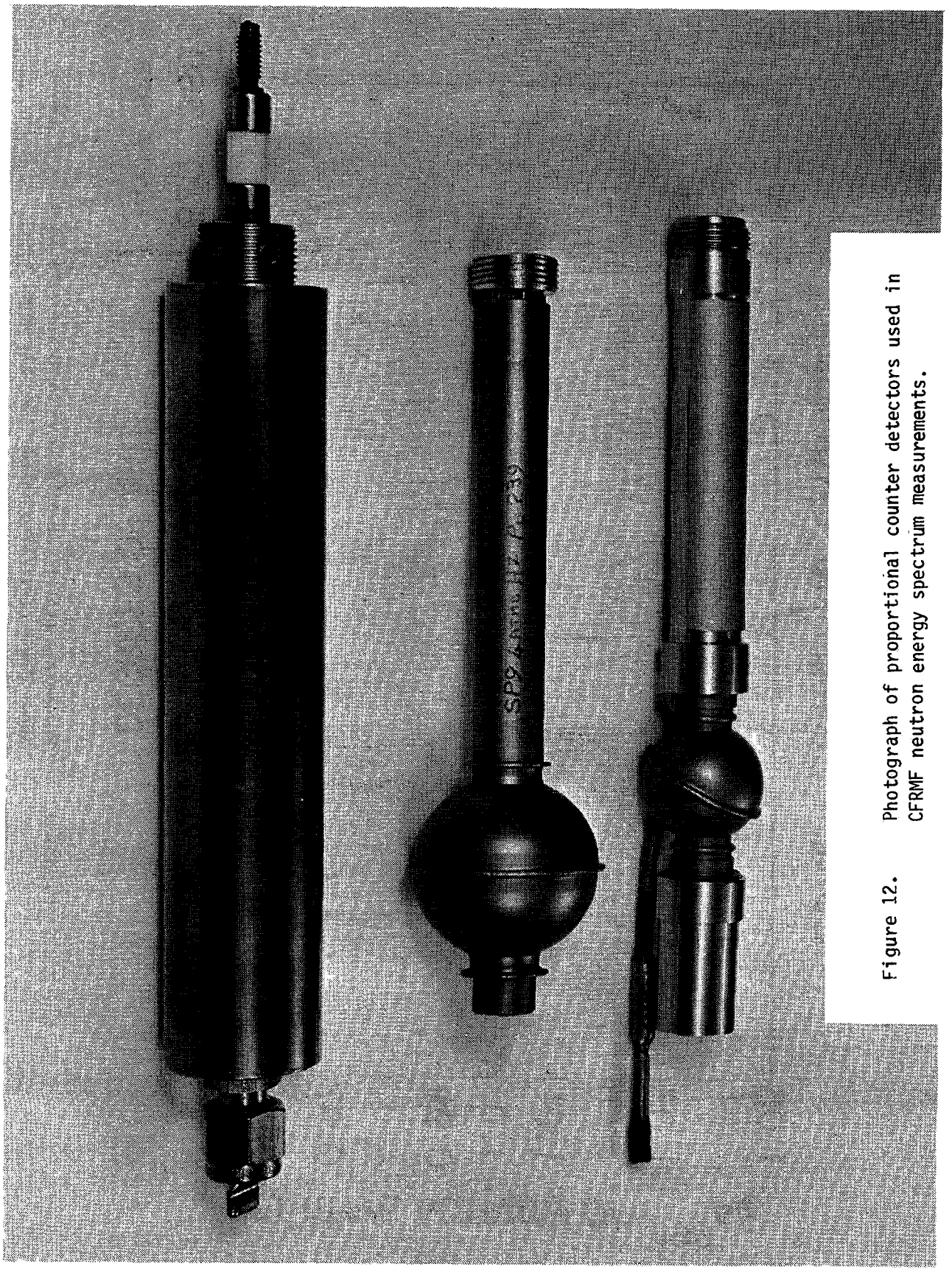

Figure 12. Photograph of proportional counter detectors used in CFRMF neutron energy spectrum measurements.

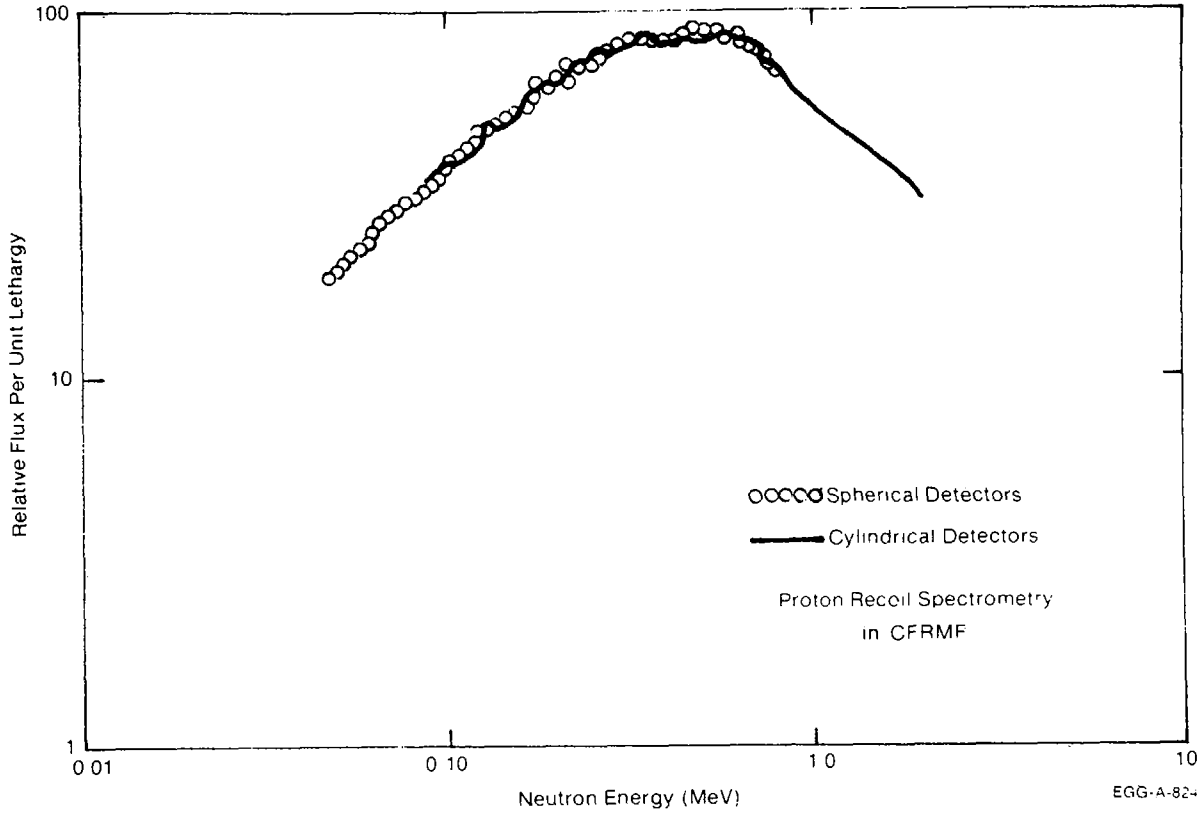

Figure 13. Neutron energy spectrum of CFRMF obtained from the cylindrical and spherical detector proton-recoil spectrum measurements.

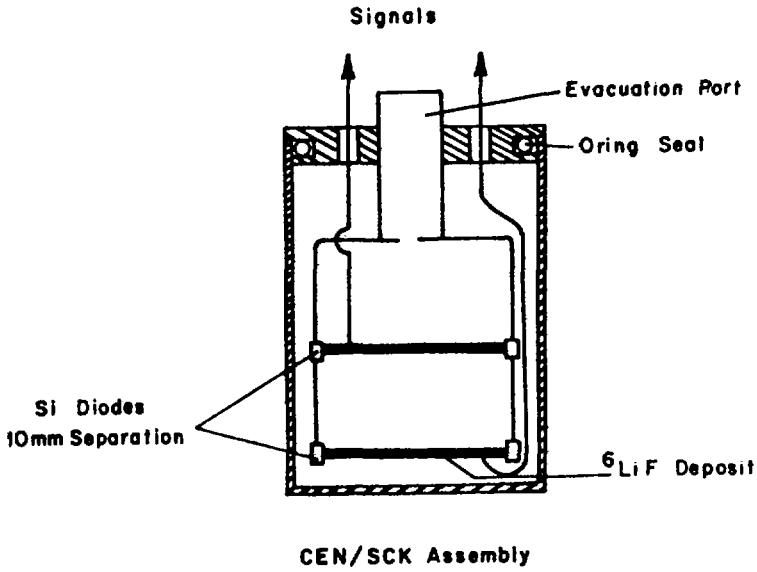

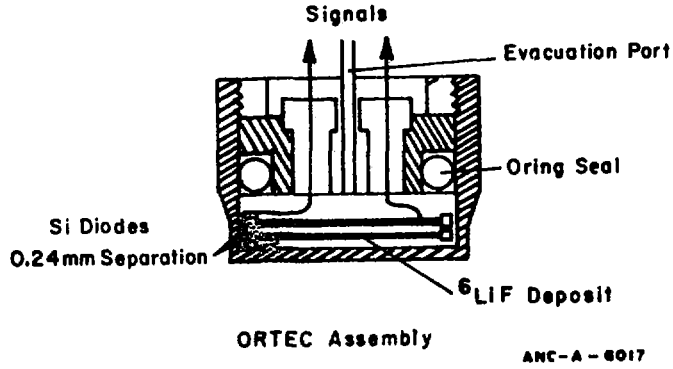

Figure 14. Sketches of the ^{6}Li detector assemblies used in the CFRMF ^{6}Li spectrometry measurements.

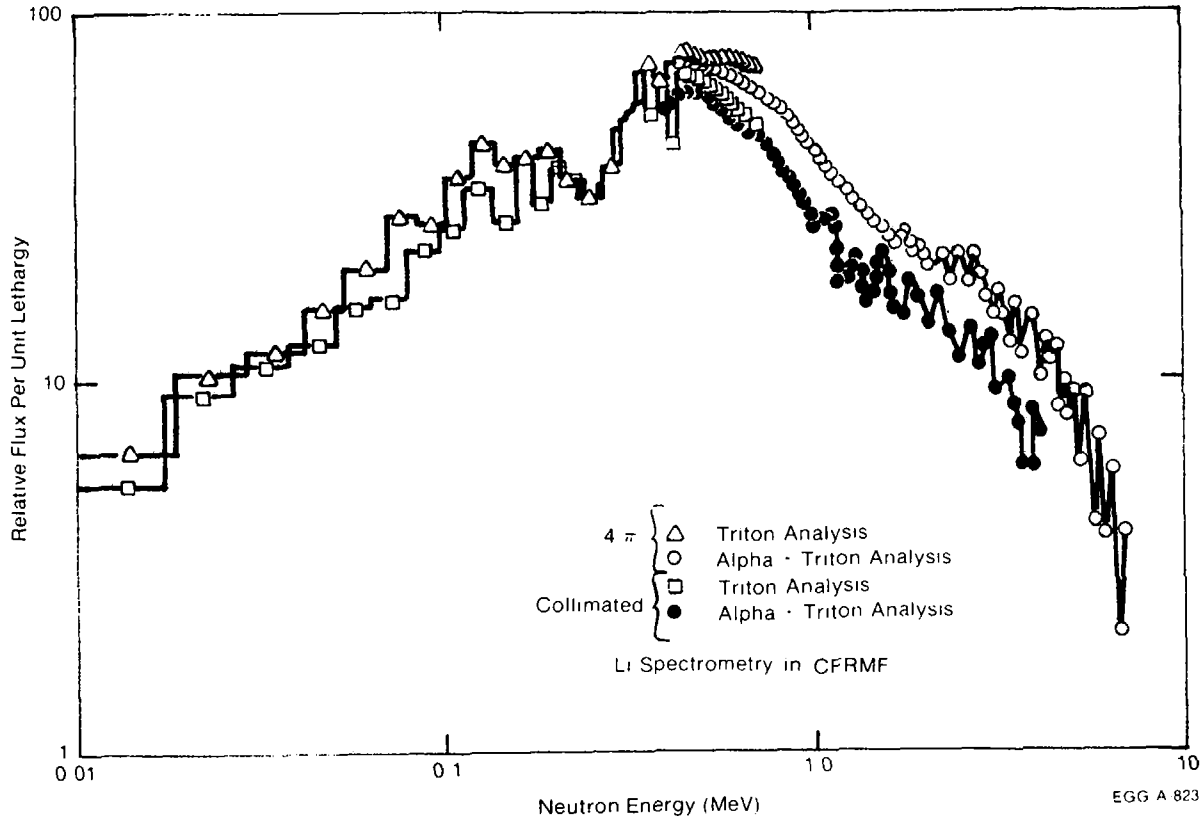

Figure 15. Neutron energy spectrum of CFRMF obtained from ^{6}Li semiconductor sandwich detector ^{6}Li (n,α)T reaction measurements (4π and collimated geometries).

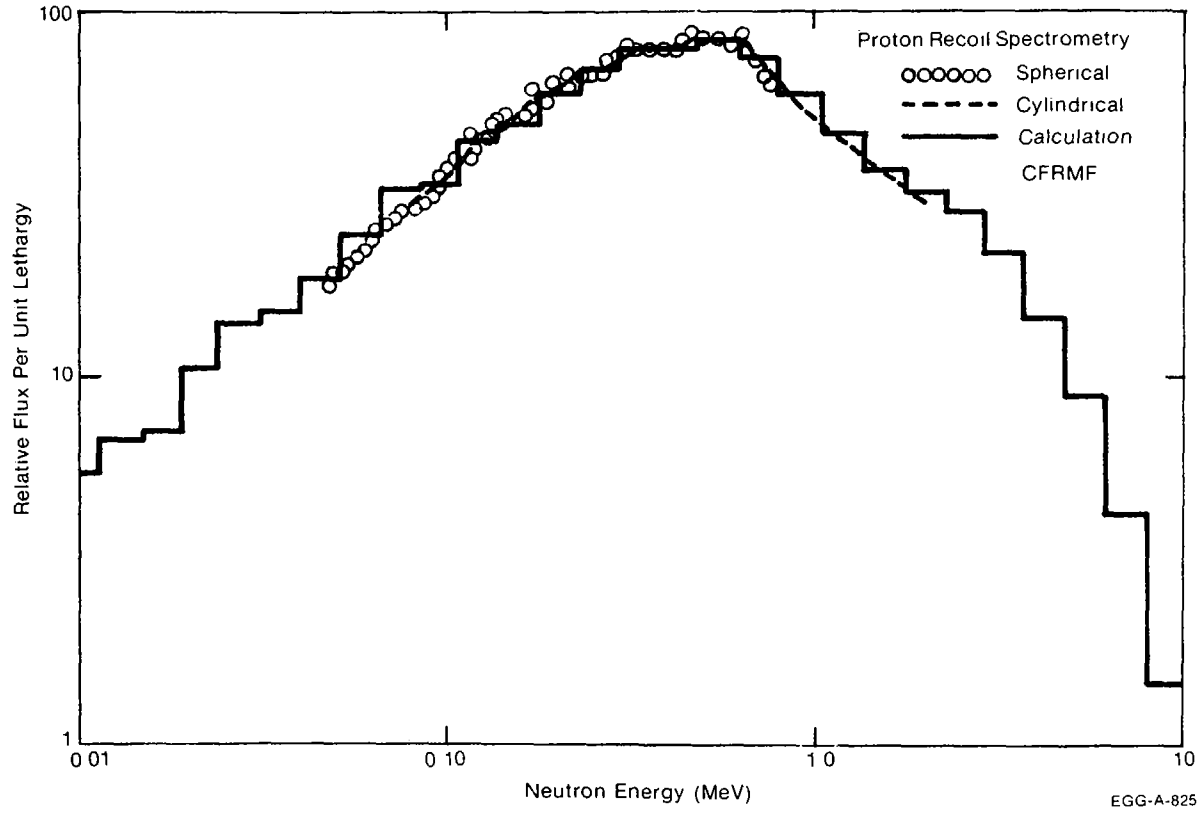

Figure 16. Comparison of neutron spectra from proton-recoil measurements with calculated spectrum.

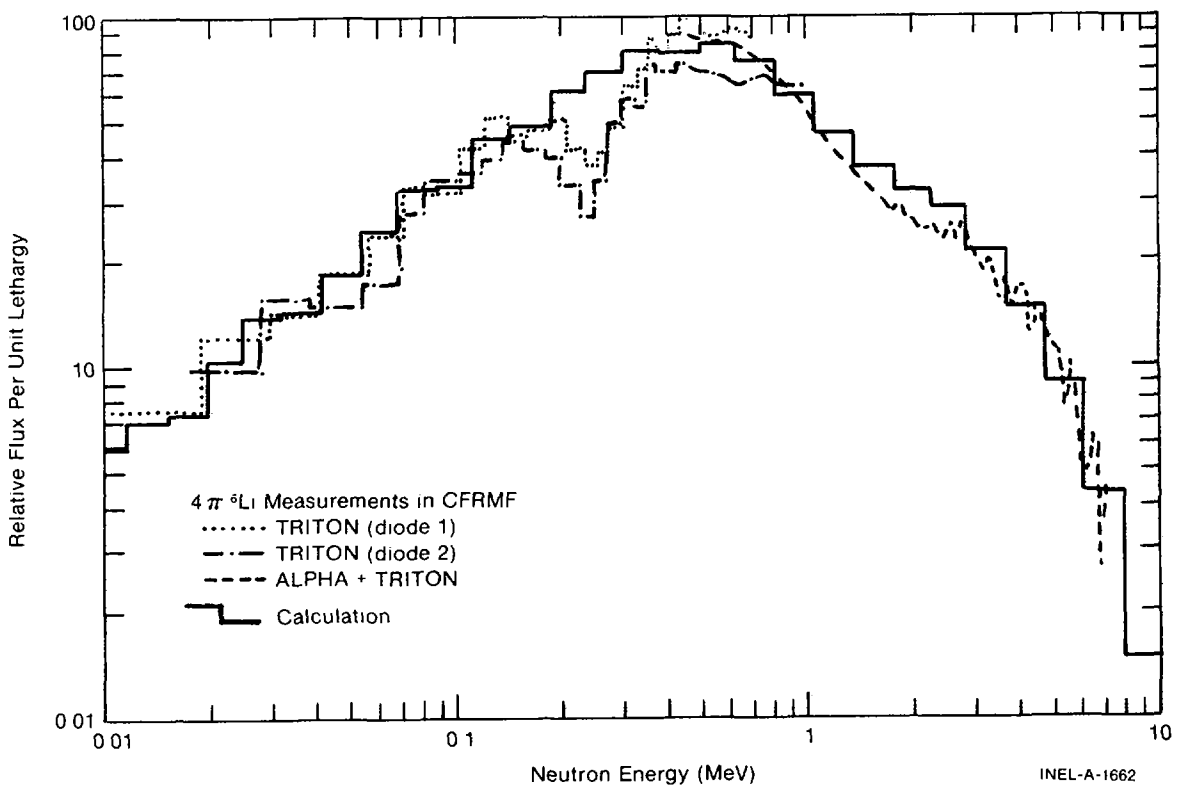

Figure 17. Comparison of neutron spectra from 4π geometry ^{6}Li measurements with calculated spectrum.

APPENDIX A

Dimensional Specifications Necessary for R,Z Neutronic Calculations for the CFRMF

Introduction

The central measurement position of the Coupled Fast Reactivity Measurements Facility (CFRMF) at the Idaho National Engineering Laboratory (INEL) is being used to obtain a variety of integral measurement data (reaction rates, reactivities, etc.) for reactor materials of interest to the LMFBR and other fast reactor programs. Of major importance in the analysis of these data is accurate knowledge of the neutron spectrum in the measurement position of the CFRMF. In order to provide this knowledge an extensive program of spectrum measurements and calculations was undertaken during the construction of the facility and has continued until the present. Because there are continued improvements in measurement techniques, cross section evaluations and reactor physics codes, a sizeable effort in measurements and calculations is maintained in order to give the most up to date characterization possible of the central spectrum of the CFRMF.

The CFRMF is a zoned-core critical assembly with a fast neutron spectrum zone in the center of an enriched uranium, water moderated thermal "driver" zone. Efforts were made in the design and critical loading of the core to retain transverse and axial symmetry. However, practical limitations have necessitated certain departures from this ideal. Because of these departures from symmetry it is necessary to make radial and axial measurements and/or calculations in order to determine the magnitude and nature of any effect they may have on the spectrum in the central measurement position. It is the purpose of this report to present as accurately as possible the dimensional specifications sufficient to make r,z calculations for the study of axial flux distributions in the central spectrum of the CFRMF.

The Calculational Model

Since the CFRMF thermal driver zone and several of the important features of the fast zone are rectangular in shape it is obviously impossible to give an exact r,z representation of the reactor. Furthermore there are sufficient structural complexities that even a cylindrical version of the transverse dimensions requires considerable homogenization in order to make a calculation practicable. The calculational model presented here has homogenized most of the thermal driver region, and gives a fuel composition which preserves the masses of uranium, aluminum and water actually present in the reactor. However, it should be noted that in fact the core contains fuel elements in the driver with six different fuel compositons. This homogenization of the fuel region will therefore give a somewhat inaccurate source distirubtion in the driver. This will effect the eigenvalue but should not bias axial flux distributions to any appreciable extent. The "fast zone" is, however, more explicitly represented. The axial representation has included all pertinent features above and below the core both for the fast region and the thermal driver zone which might influence the axial flux distributions of the central measurement position.

The details of the r,z calculational model are given in Tables I through V. Table I lists the dimensions of the interfaces which are used to define the regions of the model and their coded number designations (arabic numerals for the radial direction, roman numerals for the axial direction). For the purpose of identifying each region numerically, the combined number of the axial and radial interfaces forming the upper

left-hand boundary of each region is used to designate that region. This can be perceived more easily by referring to Figure 1 which shows the reactor model. The dimensions in this figure have not been drawn to scale. All regions are represented as either simple cylinders or cylindrical shells. Table II is a tabulation of the various regions in the model including a brief description of the reactor components contained in each region, and the code number for the composition contained in each region. Table III gives the volume fractions of the various materials contained in each composition code. Table IV lists the elements or isotopes contained in each of the materials along with their atom densities and the pertinent parameters used to calculate those atom densities. The material atom densities given were calculated by the relation

$$N = \rho \frac{M}{M_T} \frac{N_A}{A}$$

where

N = material atom density (atom/cm^3)

ρ = material density (gm/cm^3)

M/M_T = elemental or isotopic mass divided by the total mass of the material

N_A = Avagadro's number (atoms/mole)

A = atomic weight of the element or isotope (gm/mole)

When a compostion atom density rather than material atom density is desired, the results of the expression above must be multiplied by the respective volume fractions given in Table III. If an isotope occurs in more than one material of a particular composition then the composition atom density for that isotope is found by adding the material atom densities weighted by the appropriate volume fractions.

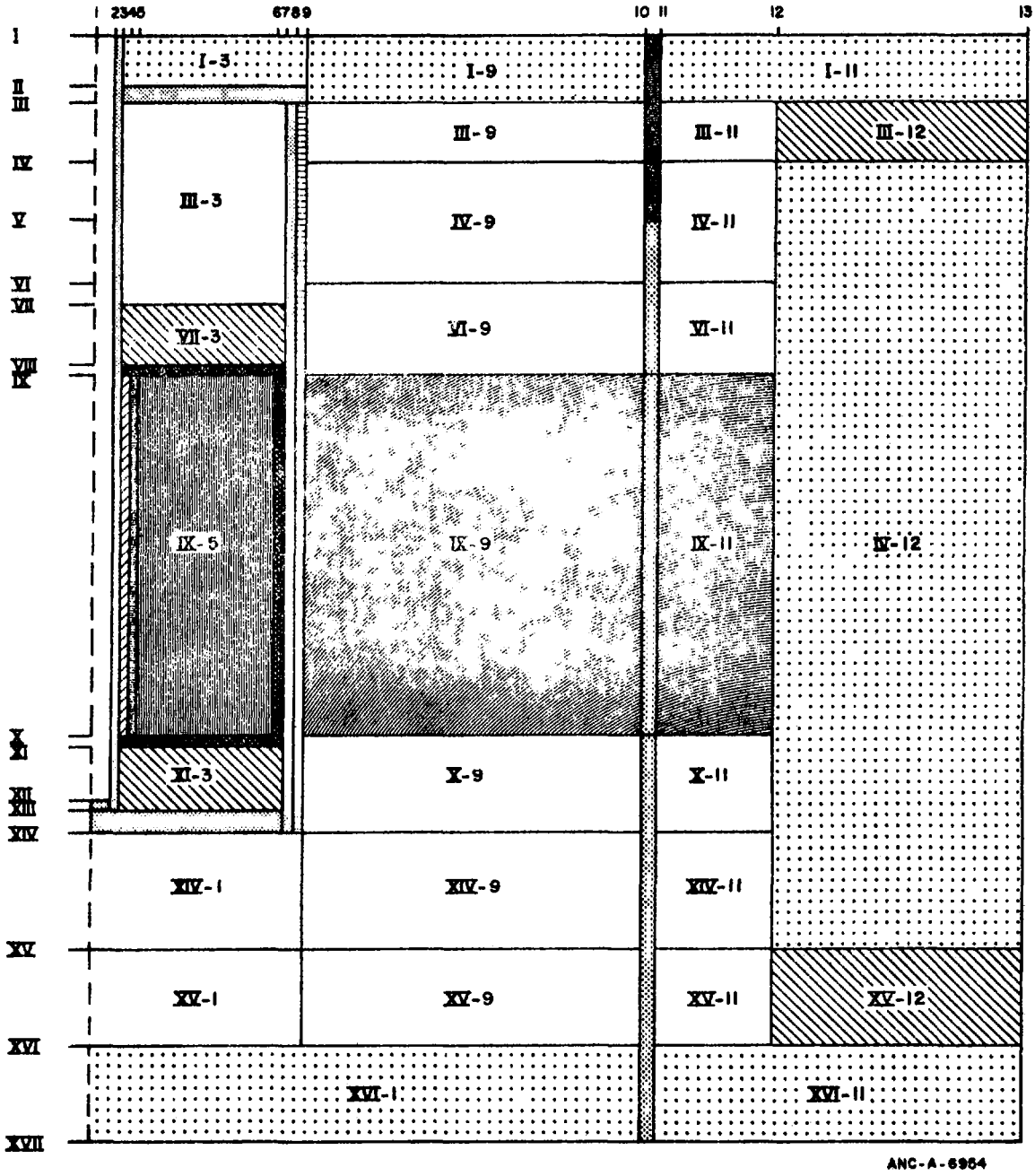

Figure 1. Diagram of CFRMF R,Z Calculational Model
(Not drawn to scale)

Additional Information

If more calculations for resonance and/or thermal cross sections are desired the information given in Table V will be required. Additional information for the fuel element plates and the heavily shielded compositions are given there. Figure 2 will aid in interpreting the information given in Table V.

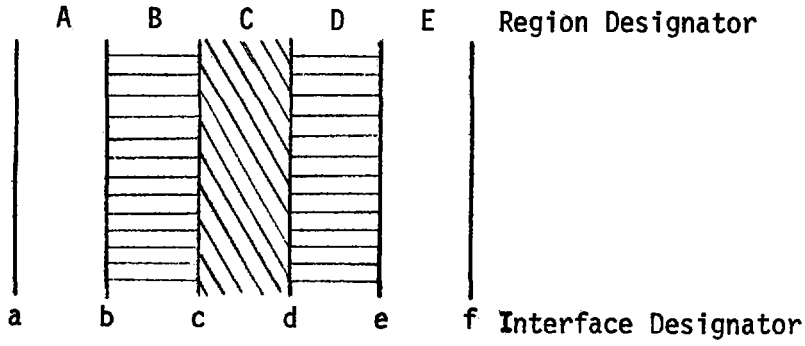

Figure 2 Generalized Diagram for Clad Regions

For cross checks other information may also be of use. It should be noted that the material volume fractions given in Table III can be derived from the data given in Table V for composition No.'s 3, 4, 6, and 8b; however the dimensional data for compositions 3 and 4 are for cylindrical shells, compositions 6 and 8b are for slabs (as is No. 18). Composition No. 8b is for a single fuel plate. There are 15 plates in each fuel element with 32 fuel elements in the core. The cross sectional area occupied by each fuel element is 69.4512 cm^2 . Total fuel loading is 5698.9 gm U-235 (93.16% enriched). The total cross sectional area of the four cruciform-shaped safety rods is 86.2837 cm^2 . The area of the assembly to the reflector is equivalent to 36 fuel elements plus the area of the safety rods. The weight of enriched uranium in the U-235 sleeve is 1494.7 gm, and the weight of enriched boron in the B-10 sleeve is 437.05 gm.

Table I

RZ Model Dimensions

Interface Number	r (cm)	Δr(cm)
1	0.0	--
2	1.91643	1.91643
3	2.06375	0.14732
4	2.25996	0.19621
5	2.69748	0.43752
6	8.19129	5.49381
7	8.97084	0.77955
8	9.39210	0.42126
9	9.40362	0.01152
10	23.03407	13.63045
11	23.62263	0.58866
12	28.69351	5.07078
13	43.69351	15.00

Interface Number	z (cm)	Δz (cm)
I	0.0	--
II	9.04875	9.04875
III	11.58875	2.54
IV	16.66875	5.08
V	21.035	4.36625
VI	26.035	5.00
VII	27.14625	1.11125
VIII	29.845	2.69875
IX	30.48	0.635
X	91.44	60.96
XI	92.075	0.635
XII	94.059375	1.984375
XIII	94.77375	0.7143758
XIV	95.885	1.11125
XV	105.25125	9.36625
XVI	112.87125	7.62
XVII	121.92	9.04875

Table II

Region Specifications

Region Number	Description	Compostion Number
I-1	Measurement Hole	1
I-2	Dry Tube Wall	2
IX-3	Uranium Sleeve	3
IX-4	Boron-10 Sleeve	4
IX-5	Depleted Uranium Block	5
IX-6	Boral Liner (Sides)	6
III-7	Fast Assembly Containment Vessel (Sides)	2
III-8	Water Annulus	7
IX-9	Homogenized Reactor Fuel (Or Side Plates and Homogenized Fuel Plates)	8 (Or 8a & 8b)
IX-10	Safety Rod Followers (Core Section)	9
IX-11	Homogenized Reactor Fuel	8
IV-12	Reflector	7
XII-1	Bottom of Dry Tube	2
VIII-3	Boral Liner (Top)	6
X-3	Boral Liner (Bottom)	6
VII-3	Spacer Block (Top)	10
XI-3	Spacer Block (Bottom)	10
III-3	Empty Space	1
II-3	Fast Assembly Containment Vessel (Top)	2
XIII-1	Fast Assembly Containment Vessel (Bottom)	2
VI-9	Ends of Fuel Elements (Top, Inner)	11
V-10	Safety Rod Followers (Above Core)	19
VI-11	Ends of Fuel Elements (Top, Outer)	11
X-9	Ends of Fuel Elements (Bottom, Inner)	11
X-10	Safety Rod Followers (Below Core)	19
X-11	Ends of Fuel Elements (Bottom, Outer)	11
IV-9	Fuel Element Adapters & End Boxes (Top, Inner)	12
IV-11	Fuel Element Adapters & End Boxes (Top, Outer)	12
XIV-1	Special Adapters & Vessel Positioning Pins	13
XIV-9	Fuel Element Adapters & End Boxes (Bottom, Inner)	14
XIV-11	Fuel Element Adapters & End Boxes (Bottom, Outer)	14

Table II (Continued)

Region Number	Description	Composition Number
III-9	Grid (Top, Inner)	15
III-11	Grid (Top, Outer)	15
III-12	External Portion of Grid (Top)	10
XV-1	Grid Below Fast Assembly	16
XV-9	Grid (Bottom, Inner)	17
XV-11	Grid (Bottom, Outer)	17
XV-12	External Portion of Grid (Bottom)	10
I-3	Reflector	7
I-9	Reflector	7
I-10	Safety Rods	18
I-11	Reflector	7
XVI-1	Reflector	7
XVI-11	Reflector	7

Table III

Composition Specifications

Composition Number	Material Number	Description	Volume Fraction
1	1	Void	1.0
2	2	Stainless Steel, Type 304	1.0
3	1	Void	0.19337
	2	Stainless Steel, Type 304	0.31988
	3	Enriched Uranium (Sleeve)	0.48675
4	1	Void	0.0557
	2	Stainless Steel, Type 304	0.1443
	4	Enriched Boron Powder	0.8000
5	5	Depleted Uranium	1.0
6	1	Void	0.08088
	6	Boral Core Material (50 wt% B C in Al)	0.61765
	7	Aluminum	0.30147
7	8	Water	1.0
8*	7	Aluminum	0.27445
	8	Water	0.62501
	9	Enriched Uranium (in an aluminum Matrix)	0.10053
8a*	7	Aluminum	0.94358
	8	Water	0.05642
8b*	7	Aluminum	0.18287
	8	Water	0.70284
	9	Enriched Uranium (in an Al Matrix)	0.11429
9	7	Aluminum	0.4340
	8	Water	0.5660
10	7	Aluminum	1.0
11	7	Aluminum	0.3682
	8	Water	0.6318
12	7	Aluminum	0.1227
	9	Water	0.6734
	10	Stainless Steel, Type 17-4 PH	0.2039
13	7	Aluminum	0.2257
	8	Water	0.5802
	10	Stainless Steel, Type 304	0.1941
14	7	Aluminum	0.1227
	8	Water	0.6516
	10	Stainless Steel, Type 17-4 PH	0.2257

Table III (Continued)

Composition Number	Material Number	Description	Volume Fraction
15	7	Aluminum	0.5505
	8	Water	0.3547
	10	Stainless STeel, Type 17-4 PH	0.0948
16	7	Aluminum	0.4283
	8	Water	0.5717
17	7	Aluminum	0.5205
	8	Water	0.4163
	10	Stainless Steel, Type 17-4 PH	0.0632
18	7	Aluminum	0.6057
	8	Water	0.2470
	11	Cadmium	0.1473
19	7	Aluminum	0.7530
	8	Water	0.2470

* Composition Number 8 contains 12.039% 8a (Fuel element side plates) and 87.961% 8b (Homogenized fuel plates).

Table IV

Material Specifications

Material Number	Material Density (gm/cm^3)	ENDF/B Number	Element or Isotope	Elemental or Isotopic Mass Fraction	Elemental or Isotopic Mass (gm/mole) (Carbon-12 Scale)	Atom Density (Atoms/$cm^3 \times 10^{-24}$) $N_A = 6.022045 \times 10^{23}$
1	--	--	--	--	--	--
2	7.92	1190	Nickel	0.0913	58.71	0.00742
		1191	Chromium	0.1805	51.996	0.01656
		1192	Iron	0.7072	55.847	0.06040
		1194	Silicon	0.0044	28.086	0.00075
		1197	Manganese-55	0.0160	54.938	0.00139
			Other	0.0006	--	--
3	18.9	1034	Uranium-234	0.0100	234.041	0.00049
		1261	Uranium-235	0.93115	235.044	0.04509
		1163	Uranium-236	0.00415	236.046	0.00020
		1262	Uranium-238	0.0547	238.051	0.00262
4	1.3152	1273	Boron-10	0.9071	10.0129	0.07175
		1160	Boron-11	0.0929	11.0093	0.00668
5	18.876	1261	Uranium-235	0.00193	235.044	9.334-5
		1262	Uranium-238	0.99782	238.051	0.04765
			Other	0.00025	--	--
6	2.61	1273	Boron-10	0.07748	10.0129	0.01216
		1160	Boron-11	0.31384	11.0093	0.04481
		1274	Carbon	0.10868	12.011	0.01422
		1193	Aluminum	0.5	26.9815	0.02913
7	2.699	1193	Aluminum	1.0	26.9815	0.06024

Table IV (Continued)

Material Number	Material Density (gm/cm^3)	ENDF/B Number	Isotope	Isotopic Mass Fraction	Isotopic Mass (gm/mole) (Carbon-12 Scale)	Atom Density (Atoms/$cm^3 \times 10^{-24}$) $N_A = 6.022045 \times 10^{23}$
8	0.998595 (18°C)	1269	Hydrogen	0.111894	1.0079	0.06676
		1276	Oxygen	0.888106	15.9994	0.03338
9	3.0840	1193	Aluminum	0.85437	26.9815	0.058808
		1034	Uranium-234	0.00150	234.041	1.190-5
		1261	Uranium-235	0.13567	235.044	1.0720-3
		1163	Uranium-236	0.00029	236.046	2.282-6
		1262	Uranium-238	0.00817	238.051	6.374-5
10	7.78	1190	Nickel	0.0425	58.71	0.00339
		1191	Chromium	0.1700	51.996	0.01532
		1192	Iron	0.7365	55.847	0.06187
		1194	Silicon	0.0050	28.086	0.00083
		1197	Manganese-55	0.0050	54.938	0.00043
		1295	Copper	0.0400	63.546	0.00295
			Other	0.0010	--	--
11	8.62	1281	Cadmium	1.0	112.40	0.04618

Table V-A

Detailed Specifications for Selected Compositions (Cylindrical Geometry)

Region Designator	Material Number	Description	Thickness of Annulus (cm)	Interface Designator	Radius In Core (cm)
Uranium-235 Sleeve (Composition No 3)					
A	1	Void	0.02777	a	2.06375
B	2	Stainless Steel, Type 304	0.03340	b	2.09152
C	3	Enriched Uranium	0.09504	c	2.12492
D	2	Stainless Steel, Type 304	0.02921	d	2.21996
E	1	Void	0.01079	e	2.24917
				f	2.25996
Boron-10 Sleeve (Composition No. 4)					
A	1	Void	0.01080	a	2.25996
B	2	Stainless Steel, Type 304	0.02921	b	2.27076
C	4	Enriched Boron Powder	0.35052	c	2.29997
D	2	Stainless Steel Type 304	0.03364	d	2.65049
E	1	Void	0.01335	e	2.68413
				f	2.69748

Table V-B

Detailed Specifications for Selected Compositions (Slab Geometry)

Region Designator	Material Number	Description	Thickness of Slab (cm)
Boral (Composition No. 6)			
A	1	Void	0.02794
B	7	Aluminum	0.10414
C	6	Boral Core Material	0.42672
D	7	Aluminum	0.10414
E	1	Void	0.02794
Typical Fuel Plate (Composition No. 8b)			
A	8	Water	0.19524
B	7	Aluminum	0.05080
C	9	Enriched Uranium (in Al)	0.06350
D	7	Aluminum	0.05080
E	8	Water	0.19524
Typical Safety Rod Blade (Related to Composition No. 18)			
A	8	Water	0.07620
B	7	Aluminum	0.19050
C	11	Cadmium	0.10160
D	7	Aluminum	0.19050
E	8	Water	0.07620

I.11. Preliminary Report on an Intercomparison of Methods for Processing Ge(Li) Gamma-ray Spectra

by

R.M. Parr, H. Houtermans and K. Schaerf
International Atomic Energy Agency, Vienna

ABSTRACT

An intercomparison has been organized by the IAEA for the purpose of evaluating methods for processing Ge(Li) gamma-ray spectra. These spectra cover an energy range of about 1 MeV and, with one exception, contain only well separated single peaks; another spectrum contains double peaks with various relative intensities and degrees of overlap. The spectra were prepared in such a way that the areas and positions of all peaks, relative to a standard spectrum which is also provided, are known exactly. The intercomparison enables the user to test the ability of his methods (1) to detect small peaks near the limit of detectability; (2) to determine the position and area of more easily detectable peaks, and (3) to determine the position and area of overlapping double peaks. The method of preparation of the spectra and the organization of the intercomparison are described in this report.

INTRODUCTION

As part of its 1976 analytical quality control services programme, the IAEA decided for the first time to offer an intercomparison dealing with the evaluation of methods for processing Ge(Li) gamma-ray spectra. The need for such a service had been verified by expressions of interest from scientists representing a number of different fields such as nuclear physics, radiochemistry, activation analysis and nuclear safeguards, and was further confirmed by the fact that approximately 200 laboratories from 37 Member States of the Agency applied to take part in it.

A number of gamma-ray spectra recorded with a Ge(Li) detector of average performance (defined below) were offered on magnetic tape, paper tape or punched cards. Participants were requested to evaluate the photopeaks in the spectra as best they could and to report their results to the Agency together with details of the methods used.

The purposes of the intercomparison are twofold: first to permit each participant to test the validity of his own evaluation methods, and second, to permit a comparison of different evaluation methods with a view to helping any worker in this field to select the algorithm and/or computer program most appropriate to his own needs and possibilities.

PRODUCTION OF THE SPECTRA

Spectra of a number of pure radionuclides were recorded experimentally with the highest precision possible (i.e. just below 10^6 counts in the channel with the highest number of counts) using a Ge(Li) γ-ray detector of "average" performance. The detector actually used was one of 60 cm^3 volume providing a resolution (FWHM) of about 2.8 keV and a peak-to-Compton ratio of about 40:1 for the 1.332 keV ^{60}Co gamma-ray. The total number of channels per spectrum was 2048, at ~ 0.5 keV/channel.

The experimental spectra thus recorded were then manipulated and combined in various ways in a large computer, e.g. multiplication of the channel contents by a constant factor; shifting the whole spectrum by a few channels to the left or right; simple arithmetic addition of two or more spectra. In addition, some of the complex spectra so obtained were superimposed on a synthetic Compton continuum. The latter was constructed in the form of a step function providing around 10^4 counts per channel in the lower half of the spectrum (below around channel No. 1000) and around 200 counts per channel in the upper half of the spectrum (above channel No. 1100); between these two regions the number of counts per channel varies smoothly in a fashion which is intended to simulate a Compton edge.

The number of counts in each channel of the resulting complex spectra were all finally subjected to a random number generation process to simulate the effects of counting statistics. The latter was done in such a way that, for all the spectra distributed, the expected variance of each channel content is the same as the channel content, i.e. the channel contents all conform to Poisson statistics.

As regards the photopeaks, these spectra therefore have all the characteristics of "real" spectra recorded with a typical Ge(Li) γ-ray detector. However, the relative intensities of the peaks as well as their relative positions (for the test spectra as compared with the standard spectrum) are known exactly to IAEA (i.e. without experimental error) since they depend

only on the way in which the original experimental spectra were combined and manipulated in the computer.

TYPES OF SPECTRA DISTRIBUTED FOR EVALUATION

Four types of spectra are included in the data distributed for evaluation.

Reference spectrum

Data are provided for 20 individual photopeaks which are to be regarded as 20 independent radionuclides. The spectrum provided (Fig. 1) contains the complete spectra of all 20 radionuclides summed together across the whole channel range. The statistical precision is as good as possible, i.e. just below 65536 counts per channel in the peaks.

Test spectrum for peak detection (single peaks)

This contains a number of small photopeaks close to the limit of detectability (Fig. 2). Their positions are generally different from those in the reference spectrum, but the peak shapes and the variability of peak shape parameters with channel position are the same. Participants are asked to detect the largest number of true peaks and the smallest number of spurious peaks.

Test spectra for peak position and area (single peaks)

Six test spectra are provided containing the same 20 photopeaks as the standard spectrum with the addition of 2 photopeaks for which no standards are provided. All six test spectra are identical (Fig. 3) except for differences due to counting statistics. Participants are requested to report results for all 6 test spectra so that the effects of counting statistics may be evaluated.

Test spectrum for peak position and area (double peaks)

This contains 9 double peaks with various relative intensities and degrees of overlap (Fig. 4). Their positions are generally different from those in the reference spectrum, but the peak shapes and the variability of peak shape parameters with channel position are the same.

FORMS OF DATA

The data are offered in three forms, punched paper tape, punched cards and magnetic tape. The spectrum length is 2048 channels and the number of counts in one channel is always less than 65536 (i.e. the word length required

for storage need not be greater than 16 bits). A complete listing of the data, and computer plots of the spectra, are also provided.

The punched paper tape is a standard eight-hole one-inch paper tape with ASCII code; the punched cards are standard 80-column cards; and the magnetic tape is an industry-compatible one (9-track; 800 bpi) containing the data in card image form. Participants may request the data in any one of these forms for which they are charged a small fee to cover the cost of the data carrier.

REPORTING OF RESULTS

Only the results for peak position and peak area have to be reported, together with their standard deviations if these are provided by the algorithm used. Participants are also requested to provide the answers to a questionnaire on the spectrum analysis methods used.

EVALUATION OF RESULTS

The results submitted by the participants are evaluated by the Agency using a computer program. The results to be compared are, in the case of peak position, the shift in peak position relative to the standard, and in the case of peak area, the ratio of the test peak area to the standard peak area. The true values of these quantities are known to IAEA from the way in which the data were prepared. Conventional statistical tests are used in carrying out this evaluation.

At the time of submission of this report, the intercomparison is still in progress. A detailed evaluation report for all participants is planned, and a summary of the results obtained is also being considered for publication in the open literature. The intercomparison will continue to form part of the Agency's Analytical Quality Control Services Programme in future years, provided that a demand for it exists, though it will henceforth be offered as a reference service rather than as an intercomparison.

Figure Legends

1. Computer plot of the standard spectrum containing 20 photopeaks.
2. Computer plot of the test spectrum for peak detection (single peaks).
3. Computer plot of the test spectrum for peak position and area (single peaks).
4. Computer plot of the test spectrum for peak position and area (double peaks).

Figure 1

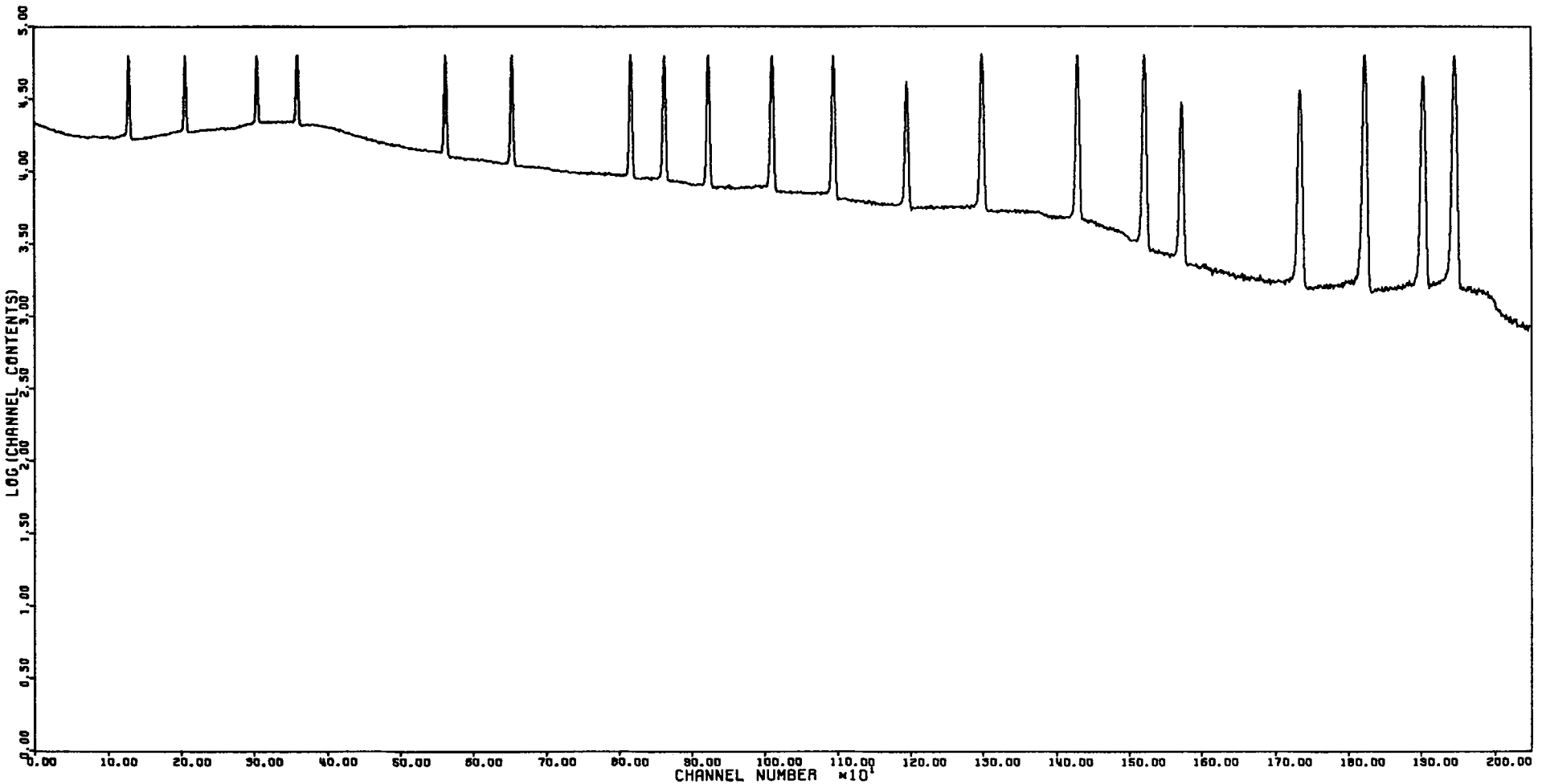
LOG(CHANNEL CONTENTS)
0.00
0.50
1.00
1.50
2.00
2.50
3.00
3.50
4.00
4.50
5.00
0.00
10.00
20.00
30.00
40.00
50.00
60.00
70.00
80.00
90.00
100.00
110.00
120.00
130.00
140.00
150.00
160.00
170.00
180.00
190.00
200.00
CHANNEL NUMBER ×10¹

Figure 2

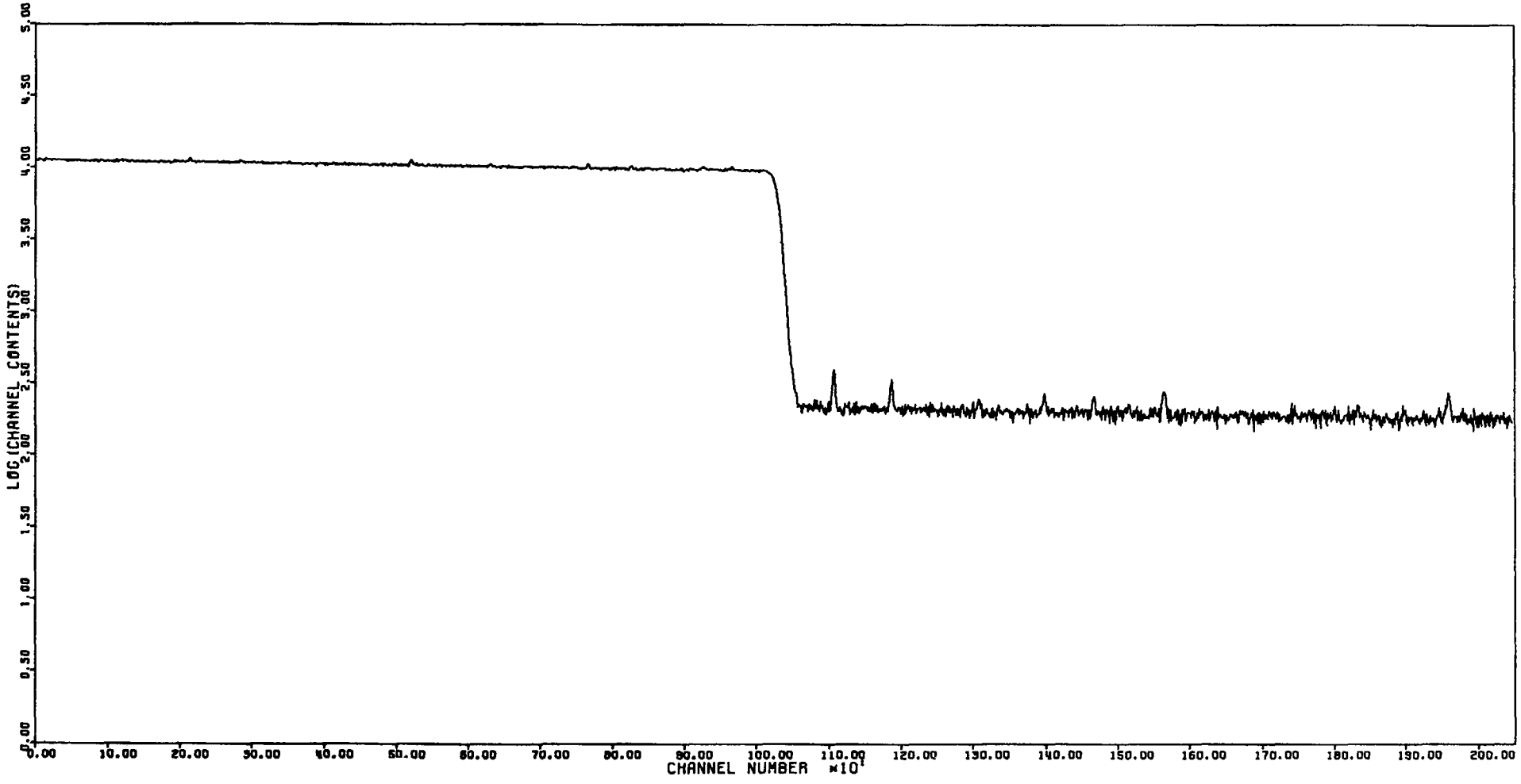
LOG(CHANNEL CONTENTS)
0.00
0.50
1.00
1.50
2.00
2.50
3.00
3.50
4.00
4.50
5.00
0.00
10.00
20.00
30.00
40.00
50.00
60.00
70.00
80.00
90.00
100.00
110.00
120.00
130.00
140.00
150.00
160.00
170.00
180.00
190.00
200.00
CHANNEL NUMBER ×10¹

Figure 3

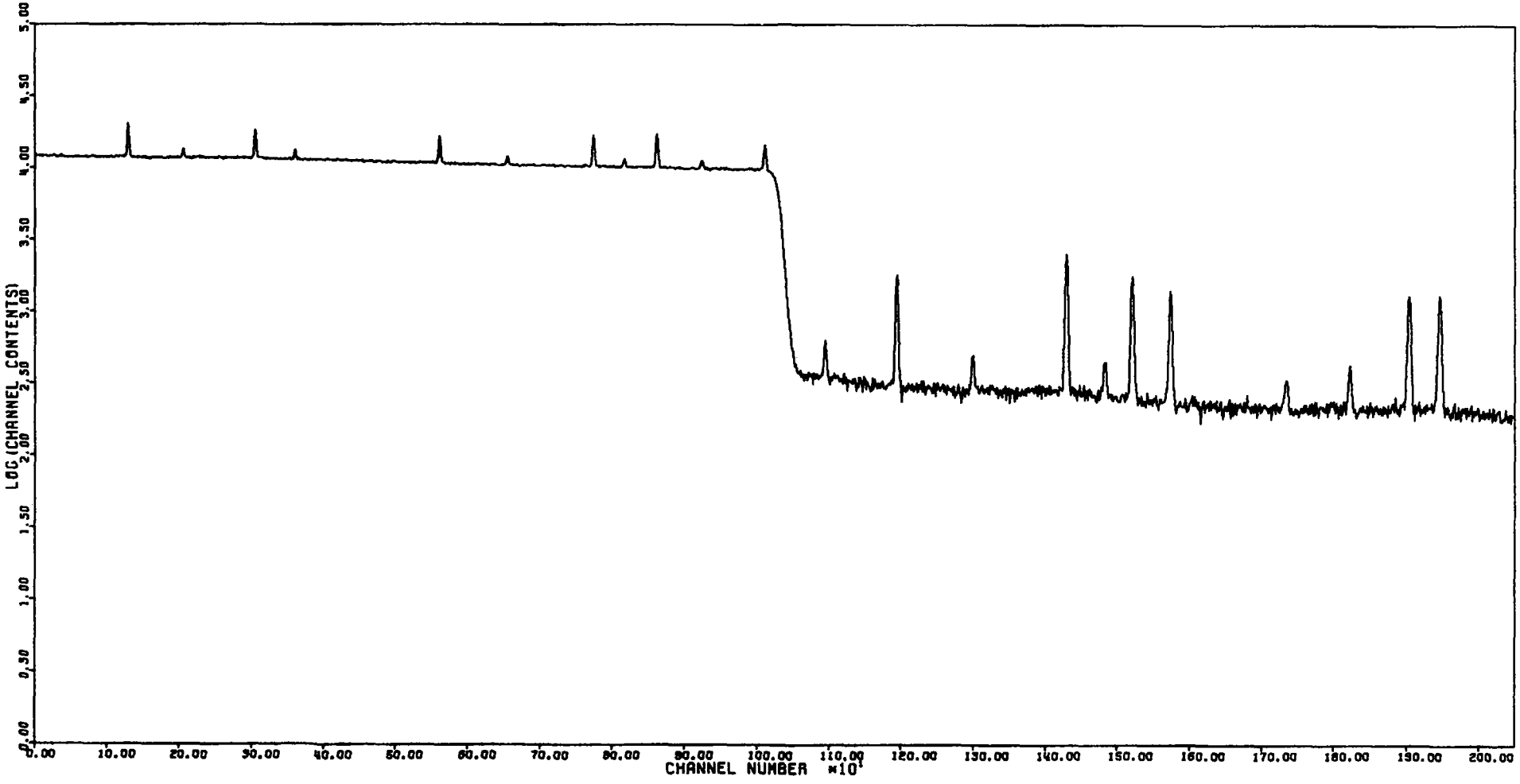
LOG (CHANNEL CONTENTS)
0,00
0,50
1,00
1,50
2,00
2,50
3,00
3,50
4,00
4,50
5,00
0.00
10.00
20.00
30.00
40.00
50.00
60.00
70.00
80.00
90.00
100.00
110.00
120.00
130.00
140.00
150.00
160.00
170.00
180.00
190.00
200.00
CHANNEL NUMBER ×10¹

Figure 4

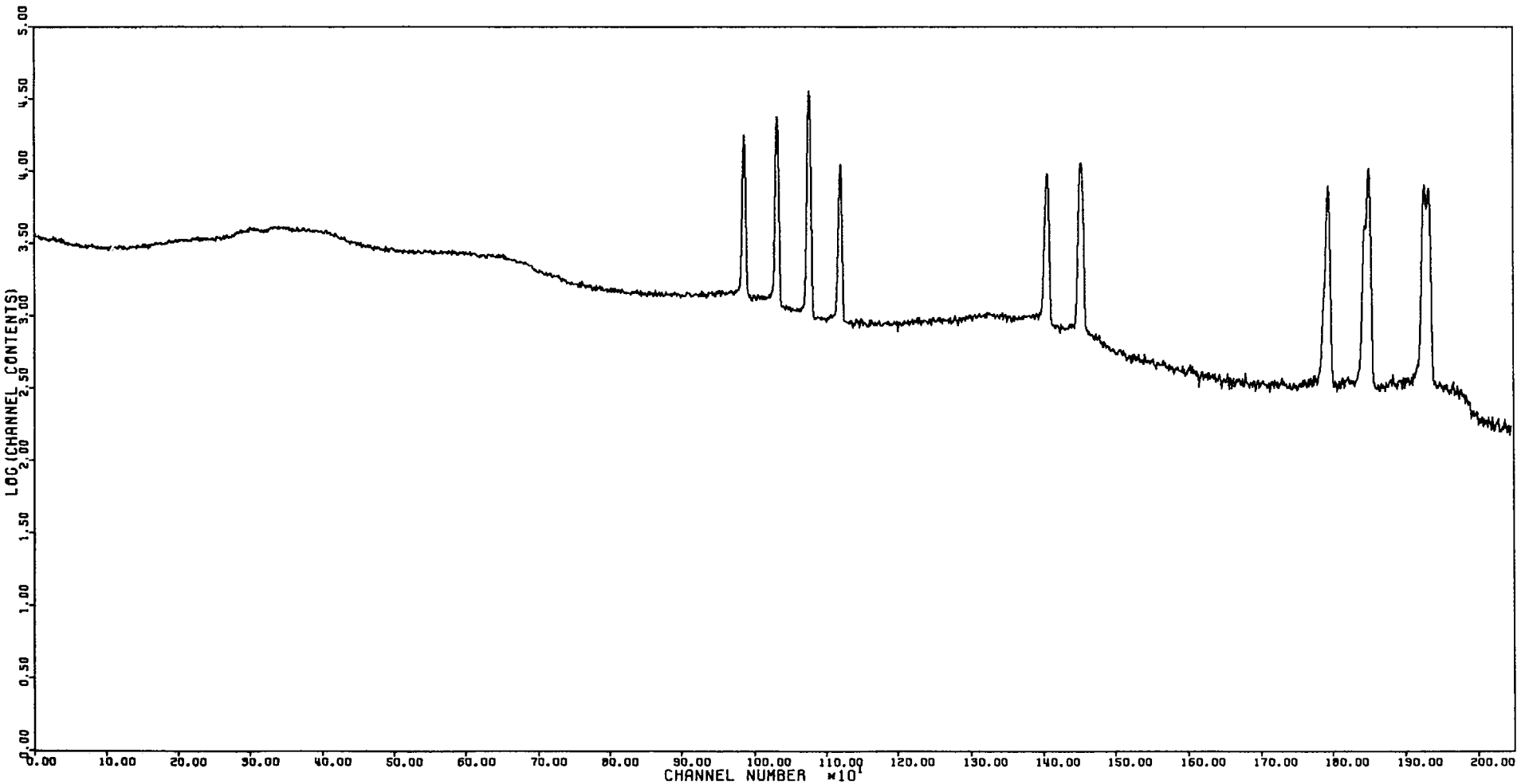
LOG(CHANNEL CONTENTS)
0.00
0.50
1.00
1.50
2.00
2.50
3.00
3.50
4.00
4.50
5.00
0.00
10.00
20.00
30.00
40.00
50.00
60.00
70.00
80.00
90.00
100.00
110.00
120.00
130.00
140.00
150.00
160.00
170.00
180.00
190.00
200.00
CHANNEL NUMBER ×10¹

II. INTEGRAL DATA IN BENCHMARK NEUTRON FIELDS

II.1. General Remarks on the Benchmark Studies

W.L. Zijp

Stichting Energieonderzoek Centrum Nederland

Insufficiency of cross section data:

At the Petten Symposium Paulsen and Magurno concluded that the situation in the field of cross section data for reactor radiation measurements is still unsatisfactory with respect to accuracy and completeness.

The reasons for this unsatisfactory situation are the following (see 1973 Consultants Meeting):

a. The lack of agreement for a limited set of reactions on which all measuring effects should be concentrated;
b. The failure to concentrate the differential measurements on the most sensitive energy region for dosimetry purpose;
c. The lack of a sufficient number of laboratories equipped with accelerator which can produce monoenergetic neutrons in the 6 - 12 MeV region, and which are used for neutron measurements.

How inconsistencies may arise:

The consistency between measured and calculated reaction rates may be influenced by various effects or procedures:

- The group structure chosen for presentation of the final spectrum;
- The discontinuity or extrapolation at the lower and upper energy bounds of the spectrum;
- The group structure of the cross section libraries, and especially the detailed structure in the resonance region (e.g. important for (n,γ) reactions);
- The adjustments sometimes made to a spectrum from reactor physics calculations to obtain a better fit for experimental data;
- The accuracy and precision of the experimentally determined reaction rates;
- The perturbation of the neutron field by the presence of one or more activation and fission detectors, or their encapsulations;
- The uncertainty in the selfshielding effect in the activation and fission detector applied.

How to improve the situation:

The present situation of the cross sections for reactor radiation measurements can be improved by a series of actions:

- Application of recommended evaluated cross section libraries, both in reactor physics calculations and in spectrum unfolding;
- Application of a reference group structure and application of recommended procedures for arriving at other group structures or a series of point values;
- Recalculation of neutron spectra using well established reactor physics computer programs under well defined and imporved conditions;
- Selection of a few well known spectra (serving as benchmark spectra) with different shapes;
- Careful definition of the neutron spectra in the benchmark facilities;
- Accurate determination of experimental activities, using enlarged series of detectors;
- Adoption of agreed procedures for adjustment and extrapolation of neutron spectra based on reactor physics calculations;
- Intercalibration of counting equipment, based on distribution of calibrated radionuclide samples;
- Adoption of agreed nuclear data (half-lives, decay schemes, gamma abundances, fission product yields, etc.).

II.2. Intercomparison of the Intermediate-Energy Standard Neutron Fields at the NISUS and MOL-ΣΣ Facilities by Means of Absolute Fission Chambers

by A. Fabry, CEN-SCK, Mol, Belgium;
J.G. Williams, A.H.M.A. Hannan, University of London Reactor Centre;
and D. Azimi-Garakani, Tehran University, Institute of Nuclear Science and Technology, Tehran, Iran.

ABSTRACT

Intermediate-energy standard neutron fields simulating core neutron spectra of fast breeder reactors are in operation at the Mol-ΣΣ (Belgium), ITN-ΣΣ (Rumania) and NISUS (Great Britain) facilities. These three assemblies are implemented within 50 cm diameter spherical cavities hollowed out from conventional graphite thermal columns; the standard configuration consists of an ∿ 5 cm thick natural uranium spherical source, ∿ 25 cm outer diameter, surrounding a concentric natural boron carbide shell at the centre of which the standard neutron field is generated.

Measurements of absolute fission rates and ratios have been performed in NISUS by means of NBS-type, double gas-flow ionization fission chambers previously exposed in Mol-ΣΣ and ITN-ΣΣ.

Leakage of subcadmium neutrons through the access hole into the NISUS standard field has been detected and eliminated.

Expected, small neutronic differences between the ΣΣ and NISUS assemblies have been assessed by transport theory computations for comparison with experimental data.

The unperturbed fission cross section ratios measured at NISUS centre are (1.000: 1.175 ± 0.027: 0.0568 ± 0.0015: 0.383 ± 0.011) for ^{235}U: ^{239}Pu: ^{238}U: ^{237}Np respectively; they agree with similar data obtained at the centre of the Mol-ΣΣ and ITN-ΣΣ facilities.

1. INTRODUCTION

The concept of intermediate-energy standard neutron fields and their importance in terms of fast reactor physics and fuels and materials neutron dosimetry have been discussed in a number of publications |1| |2| |3| |4| |5|. In particular, these neutron fields are well suited for the validation of techniques needed for absolute fission rate measurements as well as for the testing of differential-energy fission cross sections by confrontation with accurate measurements of integral microscopic cross section ratios.

Secondary intermediate-energy standard neutron fields are presently in operation at the NISUS facility |4|, University of London Reactor Centre, England, at the MOL-ΣΣ facility |5|, C.E.N.-S.C.K., Belgium, and at the ITN-ΣΣ facility |6|, Bucharest, Rumania. The last two neutron fields are geometrically and physically exact duplicates of each other, while the first one departs from them in a few design details. Basically, the three facilities are implemented within 50 cm diameter spherical cavities hollowed out of conventional graphite thermal columns. The standard configuration consists of an $\sim$ 5 cm thick natural uranium spherical shell, $\sim$ 25 cm outer diameter, surrounding a concentric natural boron carbide shell at the centre of which the standard neutron field is generated. A direct experimental comparison between the NISUS and MOL-ΣΣ facilities is essential to establish in practice the conceptually obvious reproducibility of such secondary standard neutron fields and to assess the neutronic implications of the existing, small, geometrical and physical differences (table I). The need for such comparison has even increased since these neutron fields have been identified as benchmarks |7| for the testing and improvement of dosimetry cross section files. Significant discrepancies between integral cross section ratios independently measured |5| |8| in the two facilities tend to obscure the crucial reproducibility

issue. Extensive experience |9| at the MOL-ΣΣ facility has suggested that carbon wall return-and thermal neutron-flux leakage through the access hole to the centre of NISUS might be responsible in part for the above disagreements. Such neutron leakage effects are particularly critical (and thus best investigated) in fission chamber fission rate measurements, because signal cables and other instrumental components render most delicate the adequate shielding of the hole.

On another hand, fission rate measurements are of basic importance while simultaneously affording a relevant integral comparison of the neutron spectral shapes.

Two NBS-type, double, absolute ionization fission chambers |10| associated with five fissionable deposits previously exposed at the centre of the MOL-ΣΣ facility, have been used as probes to

(a) assess the spectral integrity at NISUS centre,

(b) intercompare fundamental fission rate ratios at MOL-ΣΣ and NISUS centres.

These chambers have also been applied for similar purposes at the centre of the ITN-ΣΣ facility |6|.

2. EXPERIMENTAL DETAILS

2.1 Fission chambers performance and operation

The NBS-type fission chambers have been loaded sequentially with the five high quality fissionable NBS deposits whose major specifications are gathered in table II. These deposits were exposed also in MOL-ΣΣ |9| and in the Mol cavity uranium-235 fission spectrum neutron field |11|.

The NBS double fission chamber has been operated in a way extensively described elsewhere |10|. Dual triple-scaler counts were recorded simultaneously with multichannel analyser pulse-height distributions. The chamber performance was found excellent in all but two runs, during which the gas-flow throught the bottom chamber was considerably reduced by an accidental leak at the inlet connector. Run-to-run flux power level normalization has been achieved by means of two redundant fission chamber monitors installed within the thermal column. The so-called principal monitor displayed a slight gain drift, and the ancillary monitor was lost in part of the runs due to discriminator level and/or scaler malfunctioning. Nevertheless, the monitoring accuracy over the five days campaign of measurements was of ± 0.4% or better, and the stability as a function of time was found to be excellent.

Further control and relationship to past and future NISUS irradiations has been provided by gold and $^{115}In(n,n')$ activation foils.

2.2 Mounting of fission chambers in NISUS

The cavity constituting the NISUS standard neutron field is normally accessible through a 45 mm diameter right cylindrical hole. The NBS-type fission chamber has first been mounted at NISUS centre in the way sketched in fig. 1. In this mounting, called A, as well as in the modified ones discussed below, the fissionable deposits lie back-to-back in the horizontal plane, at the centre of the assembly. The chamber is held within a natural uranium plug by an insulating teflon piece; this plug is used to reduce the NISUS normal access hole to the optimized ΣΣ diameter of 15.5 mm and is shielded by 1 mm thick cadmium screen arranged according to a design thoroughly investigated |9| in the MOL-ΣΣ facility. It has been demonstrated experimentally that in this way, the aperture of the

hole along the chamber stem is so small that no thermal leakage effect can be detected at any position in the central exposure zone. There is however an important difference between the displayed mounting and the one routinely applied in ΣΣ. Because the flange of the inner cadmium screen has a diameter selected for the ΣΣ conditions, it is apparent that subcadmium leakage neutrons partly filtered by the uranium shell may still hit centred detectors through a conical aperture subtended by the aluminium edge of the boron carbide shell.

The importance of this weak point was realized only in the course of the experiments and was suggested by the observation of a plutonium-239 fission rate 4-5% higher than expected. In order to confirm the explanation forwarded for this effect, runs were also performed.

- by surrounding the chamber with a 1 mm thick cadmium box (termed as mounting B)
- by moving the inner cadmium screen closer to NISUS centre so that its flange would intersect entirely the identified streaming cone (mounting C).

2.3 Presentation of raw experimental results

Seven irradiations of about 1-1/2 hours duration each, have been performed in five days at a reactor power level of 100 kW, and the individual main observations collected are gathered in Table III. As indicated, the fission rates are not corrected for access hole and instrumental neutron field perturbations, which are considered separately later. The corrections typically applied to the observed count rates so as to derive the quoted fission rates are summarized in Table IV together with their assigned uncertainties. Though the main and redundant chamber signals are

the scaler count rates above the two discriminator levels placed at 54% and 36% of the peak in the fragment pulse-height distributions |10|, the amount of fission fragment losses below the alpha cut-off is a more realistic measure of the extrapolation-to-zero pulse-height corrections effectively applied after combination of the multichannel analyzer data with the scaler counts. For practical reasons, nevertheless, the nominal extrapolation-to-zero values given in Table IV are for the upper discrimination level and are slightly more than twice the extrapolation from the alpha cut-off; the quoted uncertainties however are typical of corrections from the lower discriminator.

2.4 Intrinsic neutron field perturbation and flux gradient corrections

Neutron scattering and absorption within the fission chamber components, in particular the fission foils backings, may alter central fission rates from the values that would be observed with an ideal, point-wise instrument.

Such perturbation has been computed by means of a single-scattering, but geometrically exact model |12|, at the centre of the CFRMF fast-thermal coupled facility |13|. Because the ΣΣ, NISUS and CFRMF neutron spectra are close to each other and angular flux spectrum anisotropies are not severe, it may be accepted that the same correction applies to the NBS fission chamber in any of these fields. For ^{235}U and ^{239}Pu fission rates, this correction is taken as 1.000 ± 0.001 and for ^{238}U and ^{237}Np as 1.006 ± 0.003.

It is known however that surrounding the fission chamber head by 1 mm thick cadmium entails slight additional decreases of the threshold central fission rates; this explains the ^{237}Np fission rate change in run 17-6/2 as compared to run 17-6/1, Table III.

Inspection of an array of recent activation rate traverses through the central exposure zone indicates that the neutron flux spectrum gradients in the energy response range of present interest are similar in NISUS and MOL-ΣΣ. The linear superposition property of fine and macroscopic gradients as established in ΣΣ applies thus to NISUS as well and no gradient correction is necessary for centred foils. In run 16-6/1, the chamber was accidentally off-centred by 2.5 mm; corrections of 0.2% and 0.4% had consequently to be applied to the ^{239}Pu and ^{238}U fission rates respectively observed in this run.

2.5 Access hole perturbations

A method to provide adequate shielding of the access hole against reentrant thermal neutrons for exposure of fission chambers in the ΣΣ - NISUS facilities has been developed and tested |9|. In terms of the fission chamber mountings presented above, the ideal set-up would correspond to case A if the aluminium edge at the hole in the boron carbide shell was covered by an appropriate cadmium ring; case C is nearly equivalent, except that the proximity of the flange may depress the uranium-238 fission rate in the chamber by a few tenths of a percent.

Epicadmium leakage effects are the superposition of collided (fundamental mode) and uncollided components |5|. The former are dominates for fission chamber experiments and encompasses a correction of (0.995 ± 0.005) for ^{235}U and ^{239}Pu fission rates in ΣΣ. This figure cannot be applied straight-away to NISUS because the hole in the boron carbide shell is much bigger than in ΣΣ while the hole in the uranium shell is identical; in the energy range of interest, the attenuation of neutrons returning from the carbon cavity walls is of the same order of magnitude within the uranium and the boron

carbide shells so that it is difficult to extrapolate accurately the ΣΣ correction to the NISUS case. A separate measurement has thus been performed by means of activation fission foils. These foils have been irradiated in conditions imilar to the ones of NBS fission chamber exposures, as well as in a fully closed configuration. The resulting correction was found to be (0.995 ± 0.005) for ^{235}U which, within errors, is identical with that found for ΣΣ. Replacing the standard Mol-ΣΣ boron shell access hole (17 mm diameter) by a hole of 27 mm diameter does not affect the hole perturbation correction ever. This can be understood easily in terms of subtended solid angles for the collided mode neutrons |5|.

The relative importance of the uncollided access hole perturbation observed in NISUS, mounting A, may be understood physically as follows. In the energy range below a few keV, unperturbed central neutron flux spectra at ΣΣ - NISUS centres are dominated by neutrons multiply scattered from the cavity walls and filtered by the source and absorber shells. In this energy range, the neutron wall return spectrum at the cavity - carbon boundary is grossly speaking close to a 1/E shape and is nearly isotropic. Direct streaming from the wall to the assembly centre through a hole thus results predominantly in a pick-up of response by the first positivie energy resonance of the exposed detector; the higher the energy of this first resonance, the lower is the proportion of uncollided hole leakage response. For ^{235}U and ^{239}Pu under cadmium, such pick-up is negligibly small as compared to the response to higher energy neutrons multiply scattered within the boron carbide shell (collided-mode component).

Such is not the case if complete cadmium shielding is not provided; in addition to thermal neutron response sensitivity, for both ^{235}U and ^{239}Pu foils, the latter are also extremely sensitive to uncollided neutrons at the energy of ∿ 0.3 eV, the

first positive energy resonance in ^{239}Pu: indeed, more than 90% of the ^{239}Pu response above the energy range of the joining function between slowing-down and nearly maxwellian neutron spectra is due to the 0.3 eV resonance for cavity wall return neutron flux spectra |14|. These arguments, based on discrete-ordinates computations, have led us to perform the runs 19-6/2 and 19-6/3, Table III, in order to unambiguously explain the 4-5% excess in the plutonium-239 fission rate observed in run 16-6/1; note from run 19-6/1 that such excess response is extremely sensitive to exact chamber positioning, as expected for an uncollided access hole perturbation. The $\sim$ 1.5% excess response of ^{235}U in runs 17-6/1 and 17-6/3 is also due to a similar leakage of neutrons below the cadmium cut-off.

2.6 Run-to-run flux level normalization

The data in Table III, columns 3 to 6, are expressed in terms of the monitor arbitrarily called "principal". As already mentioned, this monitor displayed a slight gain drift with time. The final run-to-run normalization factors have thus been obtained from a weighted combination of the responses of the two monitors. The run-to-run normalization uncertainty is estimated not to exceed ± 0.4%.

2.7 Unperturbed fission rates at NISUS centre

Final unperturbed fission rate ratios at the centre of NISUS are given in Table V, column 2. They are derived from the underlined figures in Table III, on basis of the analysis discussed above.

The uncertainties, quoted at the 1σ confidence level, encompass propagation of:

statistical errors (Table III)
fission foil mass assay errors (Table II)
uncertainties in corrections:

a) intrinsic of the fission chambers (Table IV)
b) related to the neutron field integrity (first and second paragraphs above).

errors in run-to-run flux level normalization (± 0.4%).

The maximum power of the reactor used to drive NISUS is presently 100 kW. The maximum absolute fission rates for ^{235}U in Mol-ΣΣ, NISUS, and ITN-ΣΣ compare as follows:

Mol-ΣΣ	2.8, 10^{-15} fission/nucleus sec.
NISUS	0.2, 10^{-15} fission/nucleus sec.(*)
ITN-ΣΣ	6.2, 10^{-15} fission/nucleus sec.

3. DISCUSSION OF RESULTS

Table I summarizes the physical and geometrical differences between the Mol-ΣΣ and NISUS facilities. On this basis, discrete-ordinates transport theory computations of the two facilities have been performed in the S_8P_3 approximation, using |15| the ENDF/B-III nuclear data files, except for the response of the fissionable isotopes, for which the ENDF/B-IV dosimetry cross section file |16| was selected instead. The computed differences in reaction rate ratios for Mol-ΣΣ and NISUS are given in the last column of Table V. Within uncertainties, they agree well with the measured differences. Experiment, however, seems to indicate a closer neutronic identity of the two facilities than calculations do.

According to transport theory, the Mol-ΣΣ and NISUS spectral shapes are the same to within ± 1-2% in the energy range 0.1 - 10 MeV, a range that encompasses ∿ 70-75% of the ^{235}U and ^{239}Pu fission responses. Below 100 keV, shape differences increase up to a max-

---

* The exact figure is 0.197, 10^{-15}(± 1.7%).

imum of ∿10% between 1 and 10 keV, but fission reactions are largely insensitive to such departures (∿ 90% response above 10 keV).

Further measurements and calculations, especially for reactions sensitive to the low energy tail of the neutron spectrum, are necessary if the small neutronic differences as predicted by theory are to be fully understood.

4. CONCLUSIONS

By the present work, a first experimental link has been established between the intermediate-energy standard neutron fields at the companion facilities NISUS and Mol-ΣΣ. The accurate absolute fission rate scale previously determined for Mol-ΣΣ |9| has been transferred to NISUS by means of NBS-type fission chambers and has been related to the scale for activation reaction rate measurements in the two assemblies.

Within uncertainties of the order of 1-2%, it has been experimentally demonstrated (this work and reference |6|), that the standard neutron fields at three facilities, Mol-ΣΣ in Belgium, ITN-ΣΣ in Rumania and NISUS in Great Britain, are neutronically identical in terms of central fission rates and threshold reaction rates.

Such achievements are of utomost relevance in views of the current, international efforts |2| |3| |7| to standardize fundamental reaction rate and reactor dosimetry measurement practices.

REFERENCES

|1| A. Fabry, P. Vandeplas - Fast Reactor Physics, Vol. I, p. 389, IAEA (1968).

|2| M.F. Vlasov, C. Dunford - Proc. Consultants Meeting on Nuclear Data for Reactor Neutron Dosimetry, IAEA report INDC(NDS)-56/U (1973).

|3| M.F. Vlasov, A. Fabry, W.N. McElroy - "Status of Neutron Cross Sections for Reactor Dosimetry", Lowell Conference on Interactions of Neutrons with Nuclei, Lowell, Massachusetts, July 8 (1976).

|4| C.B. Besant et al. - Nucl. Eng. Intern. 425 (May 1973).

|5| A. Fabry, G. and S. De Leeuw - Nucl. Techn. 25, 349 (1975).

|6| I. Girlea, C. Miron, A. Fabry - Report Blg 512 (1976).

|7| Proceedings, First ASTM-Euratom Symposium on Reactor Dosimetry, Petten, Netherlands, Sept. 22-26 (1975).

|8| S. Azad - Nucl. Instr. Meth. 121, 591 (1974).

|9| M. Pinter et al - Nucl. Cross Sections and Techn. Conf., NBS Special Pubication 425, 258-261, Washington D.C., March (1975).

|10| J.A. Grundl et al - Nucl. Techn. 25, 237 (1975).

|11| A. Fabry, J.A. Grundl, C. Eisenhauer - Nucl. Cross Sections and Techn. Conf., NBS Special Publication 425, p. 254-257, Washington D.C., March (1975).

|12| C. Eisenhauer - Private communications, National Bureau of Standards.

|13| J.W. Rogers, D.A. Millsap, Y.D. Harker - Nucl. Techn. 25, 330 (1975).

|14| A. Fabry, J.D. Jenkins - Trans. ANS 15, 975 (1972).

|15| A. Fabry, J.D. Jenkins - Trans. ANS 15, 940 (1972).

|16| B.A. Magurno, editor - "ENDF/B-IV Dosimetry File", Report BNL-NCS-50446, April (1975).

TABLE I PHYSICAL AND GEOMETRICAL DIFFERENCES BETWEEN THE MOL-ΣΣ AND NISUS STANDARD NEUTRON FIELDS

TYPE OF DATA	MOL-ΣΣ	NISUS
CARBON DENSITY (gr/cm^3)	1.60 ± 0.02	1.72_2
BORON CARBIDE SHELL		
• DENSITY (gr/cm^3)	1.499± 0.005	1.58 ± 0.01
• THICKNESS (cm)	1.50 ± 0.01	1.50 ± 0.01
• INNER DIAMETER (cm)[a]	11.0 ± 0.01	12.34 ± 0.01
• OUTER DIAMETER (cm)[a]	14.4 ± 0.01	15.74 ± 0.01
• ACCESS HOLE DIAMETER (cm)	1.70 ± 0.01	4.57_5 ± 0.005
• ^{10}B ABUNDANCE	18.37 ± 0.04%	19.78%
NATURAL URANIUM SHELL		
• THICKNESS (cm)	5.0 ± 0.01	4.825 ± 0.01
• INNER DIAMETER (cm)	14.5 ± 0.02	15.75 ± 0.02
• OUTER DIAMETER (cm)	24.5 ± 0.02	25.4 ± 0.02
• ACCESS HOLE DIAMETER (cm)	1.55 ± 0.01	4.57_5 ± 0.005

[a] Including aluminium cladding, 1 mm thick.

TABLE II. THIN NBS FISSIONABLE DEPOSITS[a] EXPOSED AT THE CENTER OF THE NISUS STANDARD NEUTRON FIELD

Foil identification and principal isotope	Isotopic concentrations (atom percent)[b]	Mass of Principal Isotope ($\mu gr/cm^2$)
28N-5-2 ^{238}U (natural)	^{238}U : 99.275; ^{235}U : 0.720(1)	541.5 (±1.4%)
28HD-5-1 ^{238}U (depleted)	^{238}U : 99.999; ^{235}U : ∿0.0001	514 (±2.2%)
25S-2-3 ^{235}U	^{235}U : 99.748(3); ^{238}U : 0.1261(7); ^{234}U : 0.0608(12); ^{236}U : 0.0652(12)	175 (±1.4%)
49I-1-1 ^{239}Pu	^{239}Pu : 99.11(1); ^{240}Pu : 0.880(5); ^{241}Pu	83 (±1.4%)
37-5-1 ^{237}Np	^{237}Np : 99.3(1); ^{239}Pu : 0.68(2)	497 (±1.8%)

[a] All deposits are 12.7 mm diameter fissionable oxides prepared by vacuum evaporation. Deposit backings are 19.0 mm diameter polished platinum 0.13 mm thick.

[b] Figures within brackets are 1 σ uncertainties. For example, 6.07(11) means 6.07 ± 0.11.

TABLE III. INDIVIDUAL RESULTS OF THE NBS-TYPE FISSION CHAMBER IRRADIATIONS AT NISUS CENTER [a]

Run Identification	Mounting Type [b]	Raw Fission Rate of Principal Isotope [c] Per Monitor [d] Count Rate (fission/sec. nuclide cps) X10^{19} For Fission Foil:				Count Rate of Fission Monitor (cps)	
		49I-1-1 [e]	25S-2-3 [e]	28N-5-2 (or 28HD-5-1) [e]	37-5-1 [e]	Principal	Ancillary
16-6/1	A	1.857(±0.2%)		<u>0.0839</u>(±0.3%)	-	1319	-
17-6/1	A		1.519(±0.15%)		<u>0.569</u>(±0.2%)	1323	548.1
17-6/2	B		<u>1.500</u>(±0.15%)		0.566(±0.3%)	1323	548.4
17-6/3	A		1.521(±0.15%)	<u>0.0848</u>[±0.4%]		1322	547.8
19-6/1	A	1.812(±0.3%)		(f)		1317	-
19-6/2	B	<u>1.754</u>(±0.3%)		(f)		1313	546.7
19-6/3	C	<u>1.773</u>(±0.3%)		0.0835(±0.4%)		1315	547.3

(a) All uncertainties random at the 1 σ confidence level. Reflect only counting statistics.

(b) A : see fig. 1; B : additional cadmium box placed around chamber head; C : inner cadmium screen moved inwards so that flange is at ∿ 2 cm from NISUS center.

(c) Uncorrected for access hole and intrinsic instrumental neutron field perturbation.

(d) Weighted combination of the two fission chamber monitors expressed in terms of the principal monitor count rate.

(e) Underlined figures only have been used to derive final data (see text).

(f) Chamber malfunctions.

TABLE IV. TYPICAL CORRECTIONS OF CHAMBER PULSE RATES TO ISOTOPIC FISSION RATES

CORRECTION / ISOTOPE → / FOIL →	^{238}U		^{235}U	^{239}Pu	^{237}Np
	28N-5-2	28HD-5-1	25S-2-3	49I-1-1	37-5-1
Dead-time loss	negligible	negligible	negligible	negligible	negligible
Fragments undetected					
• Extrapolation-to-zero[(a)]	1.050 ± 0.015	1.036 ± 0.013	1.015 ± 0.005	1.008 ± 0.004	1.037 ± 0.013
• Absorption in deposit	1.0375 ± 0.0095	1.035 ± 0.009	1.012 ± 0.0035	1.0055 ± 0.0035	1.034 ± 0.009
Fission in other isotopes	0.885 ± 0.005	1.000 ± 0.000	0.9995 ± 0.0002	0.997 ± 0.001	0.980 ± 0.008
Estimated combined uncertainty of corrections	±1.8%	±1.5%	±0.6%	±0.6%	±1.7%

(a) Nominal extrapolation from upper discriminator level, as derived from the values given for the lower discriminator level in Figure 4 of reference (10).

TABLE V. FISSION CROSS SECTION RATIOS FOR MOL-ΣΣ AND NISUS

Ratio	NISUS	MOL-ΣΣ[a]	Ratio NISUS/MOL-ΣΣ	
			Measured[b]	Computed
$\frac{\overline{\sigma}_f(^{239}Pu)}{\overline{\sigma}_f(^{235}U)}$	1.175 (±2.3%)	1.173 (±2.1%)	1.002 (±1.0%)	0.994
$\frac{\overline{\sigma}_f(^{238}U)}{\overline{\sigma}_f(^{235}U)}$	0.0568 (±2.7%)	0.0564 (±2.5%)	1.007 (±1.2%)	0.996
$\frac{\overline{\sigma}_f(^{237}Np)}{\overline{\sigma}_f(^{235}U)}$	0.383 (±3.0%)	0.381 (±2.8%)	1.005 (±1.1%)	0.989

(a) NBS-type fission chamber results only. Interlaboratory values[9] are 1.000: 1.167 (±2%): 0.0561 (±1.5%): 0.388 (±2.5%) for ^{235}U: ^{239}Pu: ^{238}U: ^{237}Np respectively.

(b) Systematic errors (such as mass assay uncertainties) common to the data in the two facilities are not propagated.

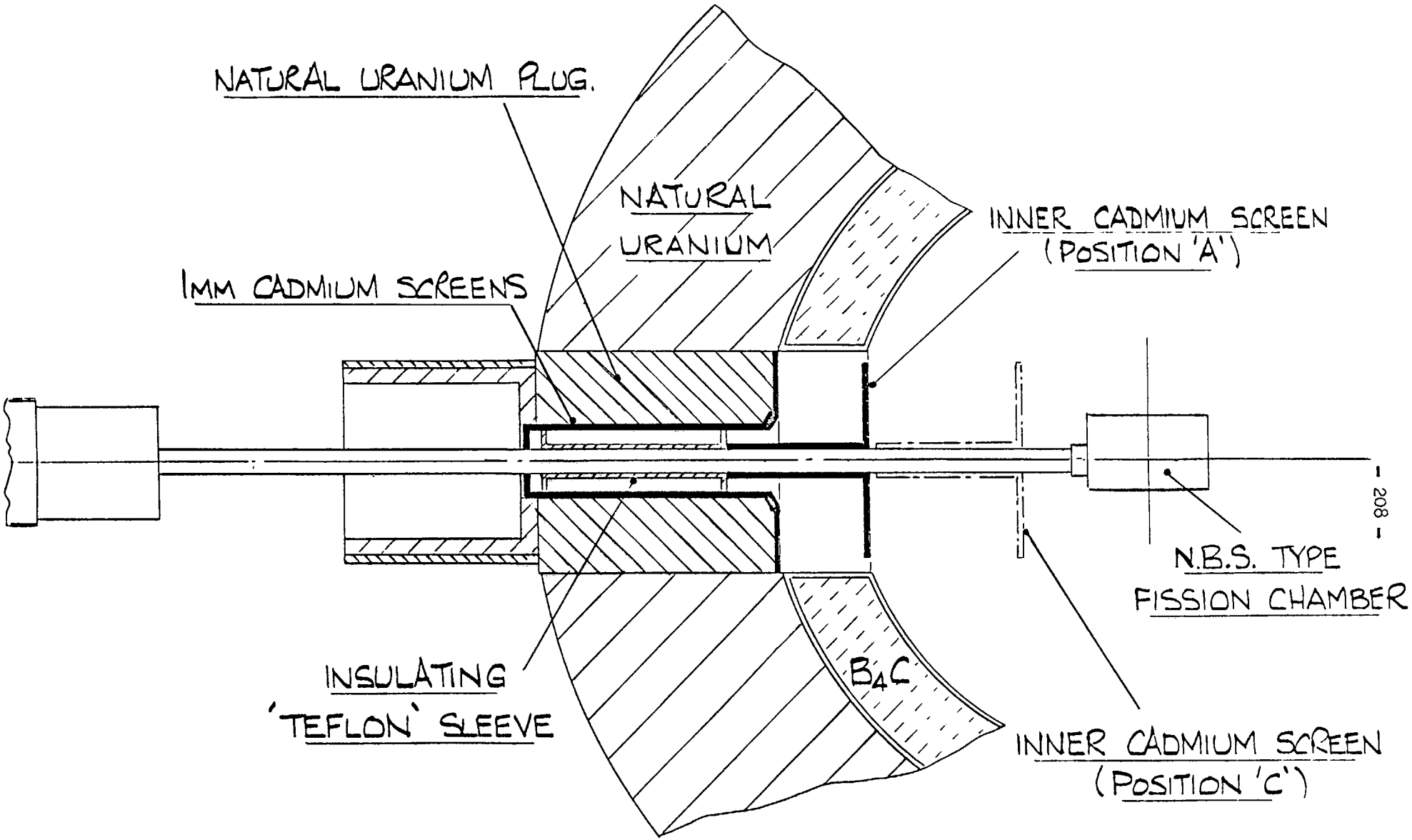

Fig. 1. Mounting of Fission Chambers in NISUS

II.3. Activation Foil Data for Nisus, MOL-ΣΣ and ^{235}U Fission Spectrum

A.H.M.A. Hannan and J.G. Williams

University of London Reactor Centre
Imperial College of Science and Technology
Silwood Park, Sunninghill
Ascot, Berkshire SL5 7PY, U.K.

ABSTRACT

Measurements of reaction rates using activation foils have been made in the standard fast neutron fields NISUS, Mol-ΣΣ and the Mol ^{235}U thermal neutron induced fission spectrum (Mol-χ_{25}). Reactions included in the work were $^{55}Mn(n,\gamma)^{56}Mn$, $^{115}In(n,\gamma)^{116m}In$, $^{197}Au(n,\gamma)^{198}Au$, $^{115}In(n,n')^{115m}In$, $^{58}Ni(n,p)^{58}Co$, $^{64}Zn(n,p)^{64}Cu$, $^{27}Al(n,p)^{27}Mg$, $^{56}Fe(n,p)^{56}Mn$, $^{24}Mg(n,p)^{24}Na$, $^{27}Al(n,\alpha)^{24}Na$.

Intercomparison of the reaction rates obtained in NISUS and Mol-ΣΣ shows that these are two identical fields so far as these reaction rate measurements are concerned. Comparison of the present data with evaluated data for Mol-ΣΣ and Mol-χ_{25} shows that agreement is generally within 2 - 3% except for $^{27}Al(n,\alpha)^{24}Na$ in Mol-ΣΣ and $^{64}Zn(n,p)$ in Mol-χ_{25}.

Average cross-sections obtained for NISUS are presented.

Activation foil data for NISUS, Mol-ΣΣ and ^{235}U fission spectrum

1. INTRODUCTION

Measurements of reaction rates using activation foils have been made in the standard neutron fields NISUS[1], Mol-ΣΣ[2] and the Mol ^{235}U thermal neutron induced fission spectrum[3] (Mol-χ_{25}).

These measurements have been made with the following interrelated objectives in mind:

(1) to intercompare the reaction rates, obtained under identical counting conditions, of foils exposed in NISUS and Mol-ΣΣ and thereby to investigate further the neutronic identity of the two fields already established for central fission rates using NBS-type fission chambers[4].

(2) to intercompare the reaction rates measured in Mol-ΣΣ and Mol-χ_{25} with data obtained by workers in other laboratories[5], and thereby to establish the capability of measuring reaction rates from non-fissile materials with an accuracy of ± 2-3% (1σ).

(3) to provide new independent and reliable data which may be used for spectral characterization of the fields and for testing and evaluation of the cross section data files for these dosimetry reactions.

The application of the data to spectral characterization will predominate in the case of the reactions with the best known cross sections induced in fields with less well characterized spectra,

and the data testing application will be most significant for the less well known cross sections, especially for data obtained in well characterized fields. These criteria are liable to change with time as differential energy spectrometry data and differential energy cross section data improve. A unified approach to spectral characterization and data testing involves the use of simultaneous evaluation techniques such as that described by the present authors in another paper[6].

2. NISUS IRRADIATIONS

The central reaction rates in NISUS for each of ten non-fission reactions have been measured two or three times between February 1975 and May 1976. Foils were mounted on a holder consisting of a hemi-cylinder of aluminium made from sheet material 0.5 mm thick and weighing approximately 5g (Fig. 1) and loaded into the central cavity of NISUS through a horizontal access hole of 45 mm diameter which was closed by means of uranium and boron carbide plugs. In some of the earlier measurements foils were exposed at the centre of NISUS and simultaneously at four other positions displaced + 4 cm, + 2 cm, - 2 cm and - 4 cm from the centre in the direction of the University of London Reactor core. The principal conclusions from these scans were as follows:

(1) The Mn(n,γ) and Au(n,γ) reactions showed some evidence for a residual streaming of uncollided thermal neutrons through the aluminium cladding of the boron carbide plug, producing reaction rates increased by 2-3% at the position nearest to the plug. This streaming path was subsequently closed by means of small cadmium rings. Only data taken after this modification was made have been accepted in the present work, although no significant change in central reaction rate values has been found.

(2) The flux gradient found for the In(n,n') reaction at the centre of NISUS was approximately 2.2% per cm. This value is consistent with that given by Fabry et al[2] for threshold reactions in Mol-ΣΣ.

(3) Flux gradients for higher threshold reactions were found to increase systematically with increasing energy of response[7], indicating a gradual hardening of the spectrum at positions closer to the reactor core. The gradient found for Al(n,α) was 3.6% per cm.

In later experiments single foils were loaded for each irradiation together with monitoring foils as follows: one indium foil at a distance of 3 cm (towards the core) from the centre of NISUS, within the central exposure zone; and two gold foils in the graphite of the NISUS thermal column at 90 cm and 102 cm from the centre of NISUS for positions A and B respectively. Additional monitoring was provided by two ½ inch diameter ^{235}U pulse fission chambers position 72 cm and 110 cm from the centre of NISUS for the principal and auxilliary fission chambers respectively.

The data presented in this paper are for reactions per nucleus per second at the centre of NISUS relative to $^{197}Au(n,\gamma)$ reactions per nucleus in a .05 mm thick foil at position A (uncorrected for self shielding and flux depression). This monitor has been found to give results consistent within a precision of ± 1.1% (1σ). The fission chamber monitors provide better precision over short periods and have been used for fission rate measurements with NBS-type fission chambers[4]. The reaction rate for the gold monitor at position A relative to the principal fission chamber was 7.955×10^{-19} ± 1.0% reactions per nucleus per monitor fission chamber count.

Specifications of the foils used and data used for each reaction studied are given in Table 1. Similar foils were used for the irradiations in Mol-ΣΣ and Mol-χ_{25}. The duration of each irradiation in NISUS was 7 hours, controlled by means of a cadmium shutter in the thermal column.

3. MOL-ΣΣ IRRADIATIONS

Irradiations in Mol-ΣΣ were made during a period of three days during April 1976. Eight non fission reactions were studied by placing sets of foils in a flanged cylindrical aluminium foil holder as shown in Fig. 2. This was mounted at the centre of ΣΣ by means of a light aluminium tube. No access holes were needed in the boron carbide or uranium shells. Monitoring information was provided by means of two installed fission chambers and indium and gold foils at several positions in the ΣΣ uranium shells. The monitoring foils were counted and the data processed by F. Cops and A. Fabry of C.E.N./S.C.K., Mol. Mol indium foils were also exposed with the U.L.R.C. foils at the central exposure position and counted by the Mol experts. Reaction rates in this work are quoted relative to the In(n,n') reaction rate measured using the U.L.R.C. foils and counting methods. The absolute value of the In(n,n') reaction rate obtained at U.L.R.C. agreed precisely (within less than 0.1%) with the reference value calculated by A. Fabry from the monitoring data and the Mol indium foils exposed at the centre of ΣΣ with the U.L.R.C. foils.

Details of the foils used in each exposure in ΣΣ were as follows:

Run 1. One gold foil and two Mol indium foils

Run 2. One each zinc and aluminium foils, three iron foils and three Mol indium foils.

Run 3. One each indium and nickel foils, three magnesium foils and three Mol indium foils.

The specification of the U.L.R.C. foils was the same as given in Table 1. except that the diameter of the gold foil was 12.7 mm. The reactor power was 600 kW and each exposure was of approximately 8 hours. The effective duration of the irradiation was calculated from the reactor instrumentation data by F. Cops using a correction program developed by A. Fabry[8] for non uniform irradiations.

4. MOL-χ_{25} IRRADIATIONS

Irradiations in Mol-χ_{25} were made during a period of two days during April 1976. Six non fission reactions were studied by placing sets of foils in a holder similar to the one used in ΣΣ (Fig. 2). This was mounted at the centre of the BR1 1 m graphite cavity by means of a light aluminium tube. The fission source consisted [2] of a 93% enriched, 0.1 mm thick and 7.7 cm long metallic uranium sheet clad in aluminium (< 0.02 mm thick) wrapped around a 1 mm thick cadmium tube of inner diameter 3.1 cm.

The irradiations were simultaneous with Runs 2 and 3 in ΣΣ and the same types of monitoring data were applied. Foil loadings were identical with those used for Runs 2 and 3 in ΣΣ. The Mol

indium foils were used to check for any flux gradients, which were not found, and to provide a reference reaction rate for the exposures. Data presented in this work are reaction rate ratios relative to In(n,n') as measured using the U.L.R.C. foils and counting methods. The absolute value for the In(n,n') reaction found at U.L.R.C. was 1.6% lower than the reference value supplied by the Mol experts.

5. ACTIVITY MEASUREMENTS

All foils used in this work were counted under standardized conditions using a 43 c.c. coaxial Ge(Li) detector having a resolution of ∿ 2.2. keV at 1.332 MeV. The spacing between the sources and the crystal was 1.77 cm in all measurements. This small spacing was necessary because of the low activity of some of the foils.

Photopeak areas were determined by means of a simple subtraction of a trapezoidal background contribution from the multichannel data. This was done using standard settings of the energy calibration per analyser channel and a standard number of channels for inclusion in each peak. This technique was found to give results at least as reproducible as those obtained using multiparameter fits to the data. The photopeak efficiency of the detector was determined under the same conditions using ∿ 1μCi standard sources supplied by the Radiochemical Centre, Amersham. Both the standard sources and the activation foils were held in aluminium trays during the measurement. The thickness of aluminium between source and detector was 1.48 mm for the activation foils and 1.12 mm for the standard sources. The difference of 0.36 mm is very nearly compensated by the 0.5 mm polystyrene windows of the standard sources. The net external absorber correction for foils relative to standard sources was 1.002 ± 0.005. In addition

to the Radiochemical Centre sources a ^{110m}Ag source consisting of a very small metal foils was manufactured at U.L.R.C. and used in efficiency measurements to provide additional coverage of the energy range of the photopeaks used in the experiment. This source was calibrated by interpolation of the efficiency curve obtained with the Radiochemical Centre sources for three energies at which ^{110m}Ag has gamma rays of nearly equal energy with those of ^{137}Cs, ^{54}Mn and ^{88}Y. The photopeak efficiency data for all measured energies were plotted and interpolated by means of a hand drawn line for the energy range 279 keV to 1.836 MeV. The data were also interpolated by means of a polynomial least squares fitting. Efficiency values interpolated by the two methods agreed within ± 2%. The uncertainties in the activity of the Radiochemical Centre sources were in the range 1.4% - 2.3% (1σ). The uncertainty assigned to the final efficiency curve was ± 2%.

A correction factor of 1.019 ± .003 was applied to the measured count rates to allow for the reduction of detection efficiency for 1.27 cm diameter foils relative to that for point sources. This correction was obtained by measurement using the small ^{110m}Ag source. Correction for gamma self absorption in the foils was done using a first order (axial) formula, which is not strictly correct for the geometry employed, but was accepted because the largest correction factor obtained (for In(n,n')) was 1.013. Correction for true coincidence summing was made for ^{58}Co by assuming the following data[9] :

γ_1 , E = 0.811 MeV , I = 0.9945 ± 0.0001 (this photopeak was counted)

γ_2 , E = 0.864 MeV , I = 0.0069 ± 0.0002 (coincident with γ_1)

β^+_1 , Annihilation quanta 0.511 MeV, I = 0.1500 ± 0.0005 (coincident with γ_1)

The correction factor obtained for the experimental geometry was 1.029 ± 0.003.

6. RESULTS

Reaction rate ratios in each of the three fields are presented in Table 2 relative to $^{115}In(n,n')$ reaction rate. The error shown in the table for $^{115}In(n,n')$ is the original total error assigned to the absolute reaction rate. This value has been combined in quadrature with the errors in the other reaction rates to give the errors on the ratios shown in the table.

Data in all cases are for reaction rates actually induced in the foils except that the $^{197}Au(n,\gamma)$ results carry a correction factor of 1.125±.01 for self shielding. This value was taken from Fabry et al[2]. The $^{115}In(n,\gamma)$ carries no correction for self shielding, and according to Fabry[2] none is needed. The $^{55}Mn(n,\gamma)$ reaction rate is uncorrected and therefore not useful, since a large $\sim$ 20% correction is required, but no experimental data are available for this.

No corrections have been applied for the effects of foil holders, foil to foil effects or the intrinsic field perturbations. These effects are expected to be less than 1%, except for the correction to true ^{235}U fission spectrum from the Mol-χ_{25} results due to scattering in cadmium. The latter correction may amount to 1 - 2% in some reactions.

Table 3 shows cross sections for NISUS calculated on the basis of a total neutron flux of 1.352×10^{8} at a reactor power of 100 kW and gold monitor A reaction rate of 1.0669×10^{-15} reactions per nucleus per second. This normalization was obtained from SIMMM[6] on the basis of eight reaction rates, the ENDF/BIV dosimetry file and NISUS evaluated spectrometry.

7. CONCLUSIONS

The result of the comparison between NISUS and Mol-ΣΣ is very gratifying. No significant difference between the two fields is found. Since a very wide range of neutron energies is included in the response of the detectors used we can conclude that NISUS and Mol-ΣΣ are two identical neutron fields, so far as reaction rate measurements are concerned.

Comparison between ULRC and CEN-SCK measurements in Mol-ΣΣ has been made by Fabry et al[10] in another paper to this meeting. The conclusion is that agreement is very good, except for $^{27}Al(n,\alpha)$ for which the ULRC data are $\sim$ 12% lower than the CEN-SCK data.

Comparison between the present data for Mol-χ_{25} and Fabry's[5] evaluation shows that agreement is generally good (within 3%), including $^{27}Al(n,\alpha)$, but that the ULRC value for $^{64}Zn(n,p)$ is 9.5% higher than the evaluation.

The results of the above comparisons give confidence in the measured data, except perhaps for $^{27}Al(n,\alpha)$ and $^{64}Zn(n,p)$ for which more work is needed.

REFERENCES

1) BESANT,C.B., EMMETT,J., CAMPBELL,C.G., KERRIDGE,M., and JONES,T.C., Nucl. Eng. Int. , 18 ,425 May (1973).
2) FABRY,A., DeLEEUW,G. and DeLEEUW,S.,Nucl. Tech., 25 ,349 (1975).
3) FABRY,A., GRUNDL,J.A., and EISENHAUER,C., Conf. on Nucl. Cross Sections and Technology, Washington,D.C.,March (1975).
4) FABRY,A., WILLIAMS,J.G., HANNAN,A.H.M.A., AZIMI-GARAKANI,D., This Meeting Vienna 15th-19th November (1976).
5) FABRY,A., CEULEMANS,H., VANDEPLAS,P., McELROY,W.N.,LIPPINCOTT,E.P., First ASTM-EURATOM Symposium on Reactor Dosimetry, Petten September 22-26 (1976).
6) WILLIAMS,J.G., and HANNAN,A.H.M.A., This meeting, Vienna 15th-19th November (1976).
7) HANNAN,A.H.M.A., Ph.D. Thesis , University of London, I.C. (1976).
8) FABRY,A., Private Communication (1976).
9) FABRY,A., Private Communication (1976).
10) FABRY,A., McELROY,W.N., KELLOGG,L.S., LIPPINCOTT,E.P., GRUNDL,J.A., GILLIAM,D.M., HANSEN,G.E., Invited paper, This meeting, 15th-19th November (1976).
11) Vendor Certificate, Reactor Experiments Inc., California, U.S.A.
12) SMITH,Donald L., and MEADOWS,James W., Nucl. Sci. & Eng.., 58 , 314-20 (1975).
13) Handbook of Chemistry and Physics (CRC), "Table of Isotopes," 51st Edition (1970-71).
14) HELMER,R.G., GREENWOOD,R.C., Nucl. Tech., 25 , 258 (1975).
15) PETR,J., Ph.D. Thesis, University of London, I.C. (1973).
16) FABRY,A., and CZOCK,K.H., INDC(IAEA)-005/G., IAEA/RL/27, December (1974).

TABLE 1.

Specification and dimension of foils

Target nucleus (type of reaction)	Reaction product	Abundance (%)	Half life	Branching ratio (%) [g]	Foil thickness (mm)	Foil diameter (mm)	Material purity (%)
$^{55}Mn(n,\gamma)$	^{56}Mn	81.30 [c]	2.580 h [b]	98.80 [b]	0.0508 [a]	12.70 [a]	99.90 [a]
$^{115}In(n,\gamma)$	^{116m}In	95.72 [c]	54.03 min [d]	83.40(15) [d]	0.2540 [a]	12.70 [a]	99.90 [a]
$^{197}Au(n,\gamma)$	^{198}Au	100.0 [c]	2.696d [d]	95.48(10) [d]	0.0508 [e]	9.00 [e]	99.99 [e]
$^{115}In(n,n')$	^{115m}In	95.72 [c]	4.500h [d]	45.9(1) [h]	0.254 [a]	12.70 [a]	99.90 [a]
$^{58}Ni(n,p)$	^{58}Co	67.88 [c]	70.78d [i]	99.45(1) [i]	0.254 [a]	12.70 [a]	99.90 [a]
$^{64}Zn(n,p)$	^{64}Cu	48.89 [c]	12.70h [d]	36.80(16) [d]	0.254 [a]	12.70 [a]	99.90 [a]
$^{27}Al(n,p)$	^{27}Mg	100.0 [c]	9.460 min [d]	71.40(5) [d]	1.170 [e]	12.70 [e]	-
$^{56}Fe(n,p)$	^{56}Mn	91.66 [c]	2.580h [b]	98.80 [b]	0.381 [a]	12.70 [a]	99.90 [a]
$^{24}Mg(n,p)$	^{24}Na	78.70 [c]	15.00h [d]	99.99(2) [d]	0.381 [a]	12.70 [a]	99.90 [a]
$^{27}Al(n,\alpha)$	^{24}Na	100.00 [c]	15.00h [d]	99.99(2) [d]	1.170 [e]	12.70 [e]	-

(a) These values are taken from the certificate of vendor (Reactor Experiment Inc.), Ref. 11.

(b) These data are taken from Ref. 12.

(c) Handbook of Chemistry and Physics (CRC), Ref. 13.

(d) Evaluated decay scheme data, Ref. 14.

(e) These foils were made at the University of London Reactor Centre. Foil thickness, diameter and material purity obtained from Ref. 15.

(g) The numbers in parenthesis indicate uncertainties (1σ) in the last digit(s) Ref. 14.

(h) Branching ratio of $^{115}In(n,n')$ and its uncertainty (1σ level) are taken from Ref. 16.

(i) Gamma ray energy, branching ratio and half life of $^{58}Ni(n,p)^{58}Co$ reaction are taken from Ref. 16.

Footnotes to TABLE 1.

TABLE 2.

Measured reaction rate ratios in NISUS, Mol-ΣΣ and Mol-χ_{25}

Reaction	Reaction rate ratio		
	NISUS[a]	Mol-ΣΣ	Mol-χ_{25}
$^{55}Mn(n,\gamma)^{56}Mn$	(0.5415 ± 3.8%)[b]	-	-
$^{115}In(n,\gamma)^{116m}In$	4.366 ± 4.0%	4.342 ± 3.4%	-
$^{197}Au(n,\gamma)^{198}Au$	7.1768 ± 3.9%	7.209 ± 3.3%	-
$^{115}In(n,n')^{115m}In$	1.000 Ref. ± 2.8%	1.000 Ref. ± 2.3%	1.000 Ref. ± 2.1%
$^{58}Ni(n,p)^{58}Co$	0.4713 ± 4.1%	0.4679 ± 3.5%	0.556 ± 3.3%
$^{65}Zn(n,p)^{64}Cu$	0.1425 ± 4.0%	0.1415 ± 3.4%	0.173 ± 3.2%
$^{27}Al(n,p)^{27}Mg$	0.0170 ± 5.6%	-	
$^{56}Fe(n,p)^{56}Mn$	0.00452 ± 4.2%	0.00466 ± 4.0%	0.00547 ± 3.9%
$^{24}Mg(n,p)^{24}Na$	0.00633 ± 4.3%	0.00610 ± 3.9%	0.00785 ± 3.7%
$^{27}Al(n,\alpha)^{24}Na$	0.00279 ± 4.1%	0.00274 ± 3.6%	0.00367 ± 3.3%

(a) $^{115}In(n,n')^{116m}In$ reaction rate = 7.0189×10^{-3} ± 2.8% reactions per $^{197}Au(n,\gamma)$ reaction at monitor position A.

(b) Uncorrected for self shielding.

TABLE 3.

Cross sections in NISUS

Reaction	$\bar{\sigma}$ mb[(a)]	
$^{115}In(n,\gamma)^{116m}In$	242	± 6.9
$^{197}Au(n,\gamma)^{198}Au$	397	±10.8
$^{115}In(n,n')^{115m}In$	55.3	± 1.5
$^{58}Ni(n,p)^{58}Co$	26.1	± 0.8
$^{64}Zn(n,p)^{27}Mg$	7.89	± 0.23
$^{27}Al(n,p)^{27}Mg$	0.942	± 0.046
$^{56}Fe(n,p)^{56}Mn$	0.250	± 0.008
$^{24}Mg(n,p)^{24}Na$	0.350	± 0.011
$^{27}Al(n,\alpha)^{24}Na$	0.1546	± 0.0046

(a) Based on an absolute flux of 1.352×10^{8} $n.cm^{-2}.s^{-1}$ at 100 kW, equivalent to $1.267 \times 10^{23} n.cm^{-2}.s^{-1}$ per ($^{197}Au(n,\gamma)^{198}Au$ reaction per atom per second at position A). This value was obtained from SIMMM using ENDF/BIV dosimetry cross-sections, NISUS evaluated spectrometry and the reaction rates for the reactions with cross-sections underlined, together with fission rates of ^{239}Pu, ^{237}Np and ^{238}U. Errors attributable to normalisation, not included in the table, are estimated at ± 3%.

DIMS. IN CM.

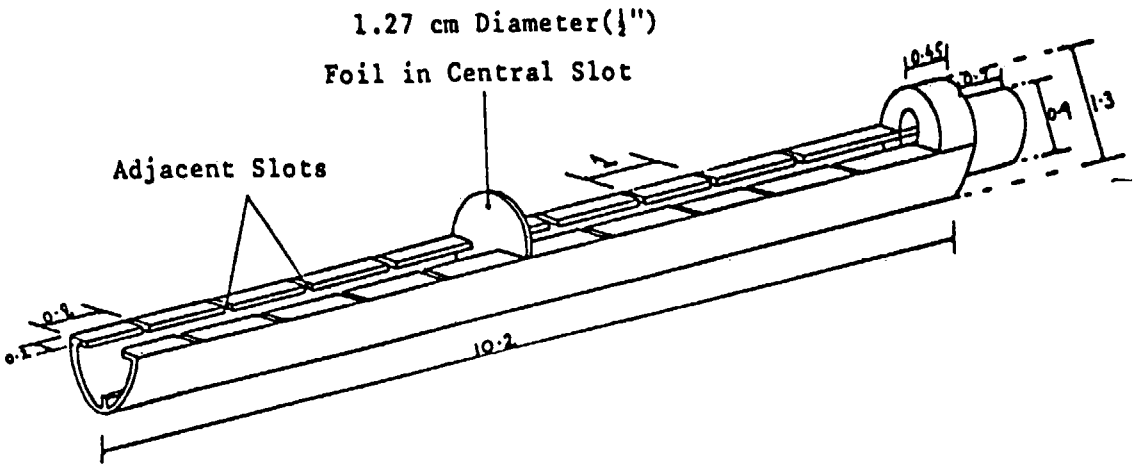

Fig.1. Aluminium foil holder used in NISUS.

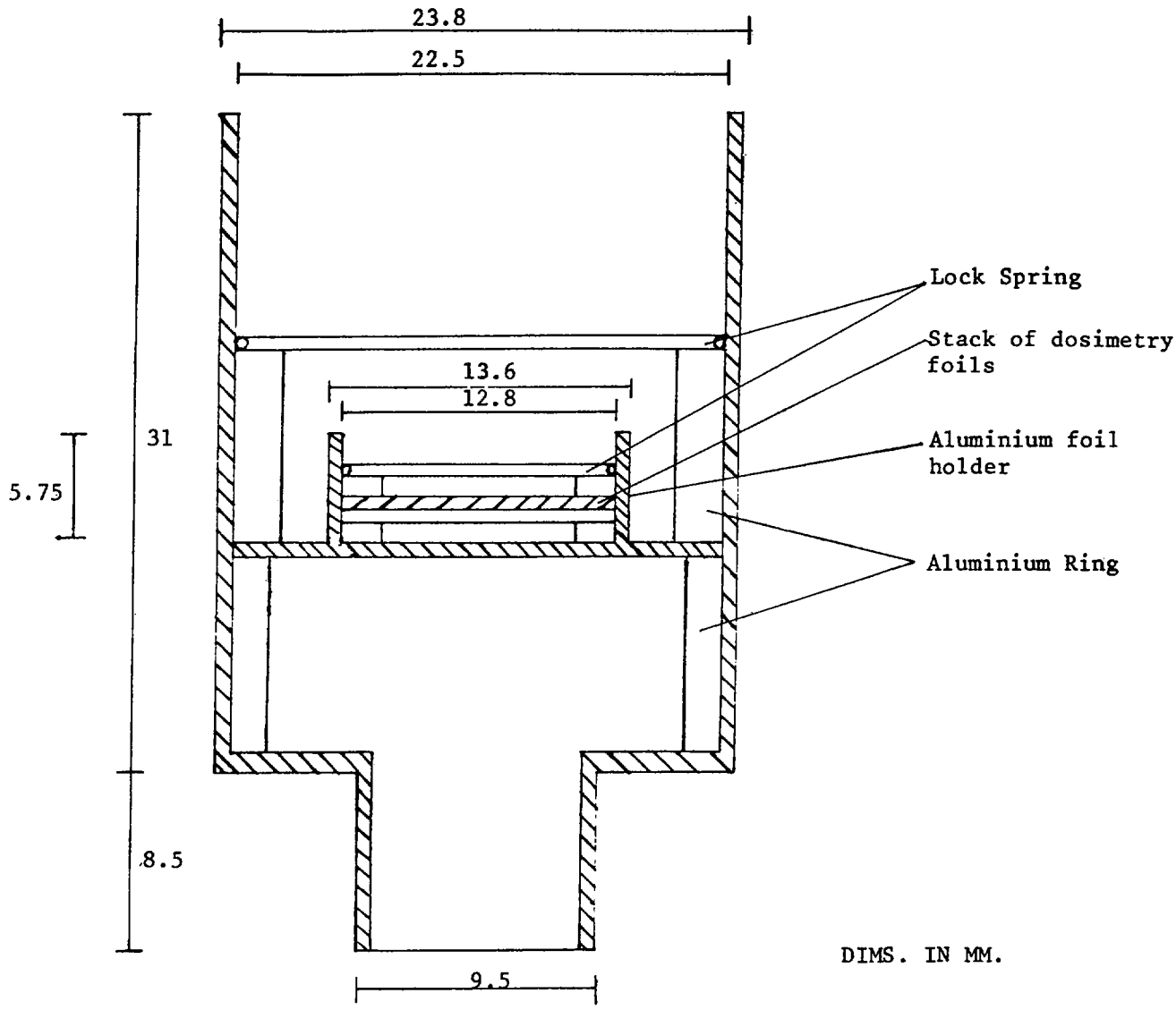

Fig.2. Schematic diagram of an aluminium tube with aluminium foil holder positioned inside.

II.4. MEASUREMENT OF AVERAGE CROSS SECTIONS WITH REGARD TO THE LOW AND HIGH ENERGY PART OF THE CALIFORNIUM-252 NEUTRON SPECTRUM

W. Mannhart
Physikalisch-Technische Bundesanstalt
D-3300 Braunschweig
Federal Republic of Germany

Abstract:

To investigate the low energy part of the ^{252}Cf-neutron spectrum the reactions $^{197}Au(n,\gamma)^{198}Au$ and $^{115}In(n,\gamma)^{116}In^{m}$ were used. The resulting averaged cross sections are (76.2 ± 1.8)mb and (124.1 ± 3.6)mb respectively. The fair agreement between these measurements and calculated average cross sections confirms that there is probably no intrinsic structure in the neutron spectrum. Above 8.1 MeV, the neutron spectrum was tested by the reaction $^{197}Au(n,2n)^{196}Au$. The cross section obtained is (5.50 ± 0.14)mb and in good agreement with an adopted pure Maxwellian neutron spectrum with a temperature parameter of (1.41 ± 0.01) MeV.

Moreover, the average cross sections for $^{113}In(n,n')^{113}In^{m}$ of (160 ± 4)mb and for $^{115}In(n,n')^{115}In^{m}$ of (195 ± 5)mb were measured. The latter value is comparable to the earlier PTB-value of (198 ± 5)mb, determined by a slightly modified method for activity measurement. All the results are compared with recent measurements and calculations. In addition, future activities in neutron cross section data measurement at the PTB are discussed.

1. Introduction

The applicability of reference neutron fields for checking experimentally determined energy-dependent neutron cross section data is well known (Ref. /1/, for example). However, for the comparison of measured average cross sections with $\sigma(E)$-data, averaged over the energy distribution of fission neutrons, the validity of these comparisons is strongly dependent upon a correct description of the neutron spectrum.

The spectrum of prompt neutrons emitted in the spontaneous fission of ^{252}Cf may be generally described by a Maxwellian. However, three areas of uncertainty remain: 1) The range below some 100 keV, 2) the range at energies of the order of MeV and 3) the spectral shape at high energies. In the low energy portion of the neutron spectrum of ^{252}Cf, excess neutron intensity is expected, which is confirmed by spectrum unfolding results /2/ and, in particular, by measurement of a very high average cross section for gold /3/. The structure in the MeV-range, determined by time-of-flight measurements /4/, can probably be explained by air scattering effects, described in recent work /5/. Above 8-10 MeV, lower neutron intensities compared with those for a Maxwellian are expected.

In order to improve the above information, the average cross sections of the non-threshold reactions $^{197}Au(n,\gamma)$ and $^{115}In(n,\gamma)$ and of the high-threshold reaction $^{197}Au(n,2n)$ were measured in the ^{252}Cf-spectrum. In addition, the average cross section of $^{113}In(n,n')$ and $^{115}In(n,n')$ were also determined. The result for $^{113}In(n,n')$ allows comparison with recently determined energy-dependent data /6/, and the remeasurement of $^{115}In(n,n')$ confirms an earlier result /7/.

2. Experimental Procedure

Irradiation was carried out using the low-scattering irradiation facility at the PTB. Metallic foils of gold and indium of high purity and 50 µm thick, were irradiated in 4π-geometry, i.e. cylindrical samples enclosing completely two combined ^{252}Cf-sources. The general procedure has already been described in detail elsewhere /7,8/. The total source strength, $(1.33 \pm 0.02) \cdot 10^9 s^{-1}$ on January 1st, 1976, was determined using the waterbath method /9/.

For the measurement of the average cross sections of the non-threshold reactions, irradiation was done without cadmium shielding. This is justified since the 90%-energy-response range of both reactions between about 50 keV and 3 MeV lies at a good distance from the dominant resonances in the neutron cross section. For the reaction ^{197}Au(n,γ), which in this case is more sensitive than ^{115}In(n,γ), an additional measurement was made with thinner samples (10 µm). No indication of losses due to foil self-shielding was found.

In earlier measurements of average cross sections at the PTB /7/, the activity measurement was usually performed on chemically dissolved samples. In the present work, the activity determination was carried out on solid samples only. The activity was measured with a calibrated 70 cm^3-Ge(Li)-detector, the samples being at a distance of 5 cm from the detector face. Data was collected in a 4096-channel pulse-height analyzer and photopeaks were analyzed. Counting losses by dead-time and random coincidences, 0.5 % for gold and 4.5 % for indium, were corrected for by analyzing the spectral response of a periodic amplitude-stabilized pulser /10/. Real coincidences could not be neglected in the

geometry chosen. They were of the order of 1-3 % and were corrected using experimentally determined total efficiencies. The cylindrical samples were cut into 10 pieces of almost identical area (10 x 10 mm) and the activity of the total foil package was measured. The gamma ray absorption correction of the foil package was between 1-2 %, for indium foils of 50 µm and gold foils of 10 µm thickness. The correction was based on theoretical gamma absorption coefficients /11/. In addition, the absorption losses were measured with different gold foil packages of 50, 100, 250 and 500 µm thickness The results confirmed the validity of the corrections used.

The reactions and the decay properties of the reaction products are summarized in table 1. In the case of $^{197}Au(n,2n)^{196}Au$, the activity of the 9.7h-isomer was allowed to decay before measurements were started.

3. Results and conclusions

The average cross sections measured in this work are given in table 2. The quoted uncertainties correspond to a confidence level of 68 %. They were calculated by quadratic summation of all contributions. The individual contributions were: 0.3 -0.7 % for the counting statistics, for the gamma emission probability as given in table 1, 1.0 % for the photopeak efficiencies, 1.7 % for the source strength determination and 1.2 % for the effective neutron path length through the sample. Further contributions were of negligible order of magnitude compared to the values quoted above. It should be observed that the average cross sections in this paper are based on absolute measurements. The source strength determination, and the efficiency calibration of the

γ-detector, are both based on the $4\pi\beta$-γ-coincidence method.

The results, given in table 2, are compared with other measurements and calculations. For the calculated average cross section the spectral flux density $\chi(E)$ used and the energy-dependent cross section $\sigma(E)$ are given. $\chi(E)$ is either described by a Maxwellian with the given temperature parameter T, or by the evaluated spectral form (NBS) of Grundl and Eisenhauer /16/. The energy-dependent cross section data is mainly from the ENDF/B-IV file /17/ or from the SAND-II cross section library /18/. Where necessary and possible the average cross sections were renormalized (quoted as RN) to the gamma emission probabilities of table 1.

For both non-threshold reactions, $^{197}Au(n,\gamma)$ and $^{115}In(n,\gamma)$, which are most sensitive in the low energy part of the fission spectrum, our measured cross sections agree quite well with the results calculated from the ENDF/B-IV file using the NBS spectral distribution /16/. One should remember that the uncertainty of the calculated values is of the order of magnitude of 10-20 % /14/. But one should also observe that the calculated response, in a ^{252}Cf neutron spectrum, of the ENDF/B-IV data /2/ for both (n,γ)-reactions is higher by nearly the same amount (about 5 %) than the measured average cross sections in this paper. For the reaction $^{197}Au(n,\gamma)^{198}Au$ the good agreement of our measurement with recent work of Green /12/ indicates that the high average cross sections measured by Pauw and Aten /3/, and recently also by Buczkó et al. /13/, must be incorrect. This is all the more valid since for $^{115}In(n,\gamma)$ our result confirms the measurement of ref. /3/. The assumption, based on the high average cross section of (95.5 ± 2.3) mb /3/ for gold, that an excess of low energy neutrons compared with a Maxwellian, may exist in the fission spectrum would now

appear unjustified.

The measurement of the average cross sections of both non-threshold reactions has also been of particular interest to us. Because of the special form of our sources, we could not exclude a priori spectrum deformation by scattering processes in the low energy range. The sources comprise Al_2O_3-ceramic cylinders, with a diameter of 6 mm and height of 4 mm, surrounded by a zirconium alloy mantle 1.5 mm thick. The californium is implanted in the ceramics. Because of the 4π-geometry of our irradiation arrangement, elastic scattering within the source should not affect the measured cross sections. Inelastic scattering, however, should become detectable and give an increase in the measured $\langle\sigma\rangle$-value, owing to the higher response of the lower energy neutrons because of the increasing reaction cross section on going to lower energies. The present measurements confirm that such a disturbance of the neutron spectrum must be of negligibly low order of magnitude.

The average cross section of the reaction $^{197}Au(n,2n)^{196}Au$ gives an indication of the form of the fission neutron spectrum above 8.1 MeV. Our result agrees with the measurement of Buczkó et al. /13/ but is about 10 % higher than the value given in ref. /3/. The $\langle\sigma\rangle$-value is very sensitive to the temperature parameter T of the adopted Maxwellian, which may be used to describe the fission spectrum in the high energy range. A change in $\langle\sigma\rangle$ of 10 % corresponds to a change in T of about 0.02 MeV. From our measurement a value of (1.41 $\pm$ 0.01) MeV for the T-parameter was deduced, which is in good agreement with the recent result of (1.42 $\pm$ 0.01)MeV confirmed by ref. /5/.

The measurement of $\langle\sigma\rangle$ for the reaction $^{113}In(n,n')^{113}In^{m}$ was mainly carried out to allow comparison with the recent work of Smith and Meadows /6/. The average of their $\sigma(E)$-data taken over the ^{252}Cf-spectrum gives a result about 10 % lower than our measurement. Part of this discrepancy may be due to the uncertainties of the fission cross sections, used in ref. /6/ as flux density monitor cross sections. For the reaction $^{115}In(n,n')^{115}In^{m}$ a new measurement was made. The result of this work confirms the earlier PTB-value of (198 $\pm$ 5)mb /7/. For this reaction the calculated spectral response of the $\sigma(E)$-data from Smith and Meadows /6/ also lies at about 6 % below our measurement. If the renormalization of the ENDF/B-IV data to a gamma emission probability of 45.9 % /19/ which was done by Fabry /2/, is justified, then good agreement of our measured average cross section with the response of the ENDF/B-IV data in a ^{252}Cf-spectrum is achieved.

4. Future Activities in Neutron Cross Section Data Measurement at the PTB

The intention of this chapter is not to present a complete programme, but to demonstrate in a few examples some possibilities for future work. Up to now the two new accelerators at the PTB, a 3.7 MV Van-de-Graaf accelerator and a compact cyclotron, will mainly be used for dosimetry work, i.e. the calibration of neutron dosimeters (see also ref../20/). The determination of elastic and inelastic neutron scattering cross sections is also planned. The wide neutron energy range of about 10 keV to 30 MeV covered by the combination of both accelerators, and the large available beam intensities of 70 to 500 µA, depending on energy, for protons between 0.3 and 24 MeV and also for deuterons between 0.3 and 14 MeV, make the accelerators very suitable for the mea-

surement of excitation functions of neutron activation reactions. In particular the possibility of parallel work, by measuring energy-dependent neutron cross sections at the accelerators and determining average cross sections for the same reactions in the ^{252}Cf-neutron spectrum, would appear to be most promising.

The usefulness and the limitations of these comparisons between both different methods of measurement are shown in the example of the reaction ^{48}Ti(n,p)^{48}Sc (fig. 1). The 90 %-energy-response range of $\langle\sigma\rangle$, measured in a ^{252}Cf-spectrum, covers the neutron energies between 5.9 and 12.7 MeV. In this range, the σ(E)-data from a new measurement /1/, from two evaluated files /17,18/ and from a model calculation, show strong divergence. Table 3 shows a comparison between a measured $\langle\sigma\rangle$-value /7/ and the average taken over the ^{252}Cf-spectrum, with the diverse σ(E)data. As the data of Smith and Meadows /1/ only extends to 10 MeV, and therefore fails to cover the total energy-response range, interpolation between their values and an experiment performed at about 14 MeV neutron energy /22/ was attempted. The results of the comparison given in table 3 demonstrate that the data of the ENDF/B-IV file (of the SAND-II file), and of the statistical model calculation, clearly fail to describe the energy-dependent cross sections in this energy range. One should notice further that the calculated $\langle\sigma\rangle$-results do not depend upon the value of the maximum of the excitation function (at about 14.5 MeV), but mainly upon the slope of the function near threshold.

In general one can say that the neutron energy range covered by the response of threshold reactions in a ^{252}Cf-spectrum, lies between the reaction threshold and about 6 MeV above threshold. Only for a few very high threshold reactions does the comparison of average

cross sections with $\sigma(E)$-data allow conclusions to be drawn concerning the quality of cross sections measured around 14 MeV neutron energy. On the other hand, a relatively large number of often strongly divergent cross section measurements is concentrated at this energy, more so because of the easy production of monoenergetic neutrons here. Fig. 2 gives an example of this. For $^{65}Cu(n,2n)^{64}Cu$ recent measurements carried out with Vonach /22/ are about 10 % lower than the ENDF/B-IV data. The contribution to a $\langle\sigma\rangle$-measurement using ^{252}Cf is about 65 % up to the lower limit of the neutron energy range of 13.6 to 14.7 MeV, covered by the experiment /22/. A deviation of 10 % in the cross section data above 13.6 MeV corresponds to a deviation in the average cross section measurement of 3.5 %. Assuming that the deviation of 10 % is valid over a larger neutron energy range, the influence on $\langle\sigma\rangle$ may increase further up to a maximum of 10 %. Unfortunately, the measurement of $\langle\sigma\rangle$ for $^{65}Cu(n,2n)^{64}Cu$ is complicated by a parallel reaction, $^{63}Cu(n,\gamma)^{64}Cu$, forming the same product nucleus.

In the measurement of $\sigma(E)$-data, there is always a large amount of uncertainty due to the determination of neutron flux density. Apart from a few absolute measuring methods, the flux density measurement is (for practical reasons) often related to a monitor reaction. The calibration of these monitor reactions has been attempted in a few cases with high precision. Table 4 gives an example for such absolute measurements of neutron monitor reactions. For the reaction $^{27}Al(n,\alpha)^{24}Na$ a measurement with a proton recoil counter performed at the NPL by Robertson et al. /24/ gives a neutron cross section of (115.5 $\pm$ 3.0) mb at 14.78 MeV. Another absolute measurement, based on the associated particle method of Vonach et al. /25/ was carried out at 14.43 MeV neutron

energy with the result (117 ± 0.8)mb. By means of a relative excitation function (uncertainty 1 %) /26/, one abtains a cross section of (110.6 + 1.3)mb at 14.78 MeV which should be compared with the result of Robertson et al. Both authors quote a confidence level of 99.5 % (3σ-errors), although no overlap of both absolute measurements is given. A second monitor reaction is $^{56}Fe(n,p)^{56}Mn$. To allow a direct comparison with ref. /24/, extrapolation of the result of Vonach et al. /26/ with the slope of an excitation function (measured between 13.6 to 14.7 MeV /26/) from 14.70 to 14.78 MeV was carried out. In the second example too the data fail to agree. Thus, further attempts at absolute measurement of both reactions would seem to be very important. The experience gained from participation in an international comparison of neutron fluences (organized by the BIPM), should constitute a sound basis for such work in the future.

References

/1/ D.L. Smith, J.W. Meadows: ANL/NDM-13 (June 1975)

/2/ A. Fabry, H. Ceulemans, P. Vandeplas, W.N. McElroy, E.P. Lippincott: First ASTM-EURATOM Symposium of Reactor Dosimetry, Petten, Sept. 22-26, 1975

/3/ H. Pauw, A.H.W. Aten: J.Nucl.Energy 25, 457 (1971)

/4/ L. Green, J.A. Mitchell, N.M. Steen : Nucl.Sci Eng. 50, 257 (1973)

/5/ P. Guenther, D. Havel, R. Sjoblom, A. Smith : ANL/NDM-19 (March 1976)

/6/ D.L. Smith, J.W. Meadows: ANL/NDM-14 (July 1975)
D.L. Smith, J.W. Meadows: Nucl.Sci.Eng. 60, 319 (1976)

/7/ W.G. Alberts, E. Günther, M. Matzke, G. Rassl: First ASTM-EURATOM Symposium of Reactor Dosimetry, Petten, Sept. 22-26, 1975

/8/ W.G. Alberts, J. Bortfeldt, E. Günther, K. Knauf, M. Matzke, G. Rassl, V. Siegel, K.F. Walz: Proceedings of the Conference on Nuclear Cross Sections and Technology, Washington D.C., March 3-7, 1975. NBS Special Publication 425, p. 273 (1975)

/9/ J. Bortfeldt, M. Matzke: PTB-Mitt. 84, 254 (1974)

/10/ K. Debertin: Atomkernenergie 17, 97 (1971)

/11/ W.J. Veigele: Atomic Data Tables 5, 51 (1973)

/12/ L. Green: Nucl.Sci.Eng. 58, 361 (1975)

/13/ M. Buczkó, Z.T. Bödy, J. Csikai, Z. Dezsö, S. Juhász, H.M. Al-Mundheri, G. Petö, M. Várnagy: International

Symposium of Californium-252 Utilization, Paris, April 26-28, 1976

/14/ S.F. Mughabghab, A. Prince, M.D. Goldberg, M.R. Bhat, S. Pearlstein: BNL-50439 (October 1974)

/15/ G.J. Kirouac, H.M. Eiland, C.J. Slavik: Proceedings of the Topical Meeting on Irradiation Experimentation in Fast Reactors, Jackson Lake Lodge, p. 412 (1973)

/16/ J. Grundl, C. Eisenhauer: First ASTM-EURATOM Symposium of Reactor Dosimetry, Petten, Sept. 22-26, 1975

/17/ B.A. Magurno: BNL-NCS-50446 (April 1975)

/18/ R.L. Simons, W.N. McElroy: BNWL-1312 (May 1970)

/19/ H.H. Hansen, E. de Roost, W. van der Eijk, R. Vaninbroukx: Z. Physik 269, 155 (1974)

/20/ S. Wagner: This meeting

/21/ M. Vlasov: INDC(NDS)-47/L Part II (September 1975)

/22/ W. Mannhart, H. Vonach: Z. Physik A272, 279 (1975)

/23/ A. Paulsen, B.A. Magurno: First ASTM-EURATOM Symposium on Reactor Dosimetry, Petten, Sept. 22-26, 1975

/24/ J.C. Robertson, B.N. Audric, P. Kolkowski: J.Nucl. Energy 27, 139 (1973)

/25/ H. Vonach, M. Hille, G. Stengl, W. Breunlich, E. Werner: Z. Physik 237, 155 (1970)

/26/ H.K. Vonach, W.G. Vonach, H. Münzer, P. Schramel: Neutron Cross Sections and Technology. Proceedings of a Conference, Washington, March 1968. NBS Special Publ. 299, Vol. II, p. 885 and private communication (1976)

Table 1: Reactions and Decay Properties

Reaction	Sample	Reaction product		
	Isotopic abundance	Half-Life	Gamma-Ray Detected	Gamma-Emission Probability
$^{197}Au(n,\gamma)\ ^{198}Au$	100 %	2.6965(15)d [a]	411.8 keV	0.9553(5) [a]
$^{197}Au(n,2n)\ ^{196}Au$	100 %	6.183(10)d [b]	333.0 keV 355.7 keV	0.231(5) [b] 0.876(9) [b]
$^{113}In(n,n')\ ^{113}In^{m}$	4.28 %	99.48(24)m [c]	391.7 keV	0.6490(20) [d]
$^{115}In(n,n')\ ^{115}In^{m}$	95.72 %	4.486(4)h [e]	336.3 keV	0.459(1) [e]
$^{115}In(n,\gamma)\ ^{116}In^{m}$	95.72 %	54.15(6)m [f]	416.9 keV 1097.3 keV 1293.5 keV	0.292(15) [d] 0.562(12) [d] 0.844(18) [d]

a) M.J. Martin, P.H. Blichert-Toft: Nuclear Data Tables A8, 1 (1970)
b) Nuclear Data Sheets B7, no. 4 (April 1972)
c) Nuclear Data Sheets B5, no. 2 (February 1971)
d) M.J. Martin, ORNL-5114 (March 1976)
e) H.H. Hansen et al.: Z. Physik 269, 155 (1974)
f) Nuclear Data Sheets 14, no. 3 (March 1975)

Table 2: Average cross sections in the ^{252}Cf-fission spectrum

Reaction	<σ> (mb)					Author(s)	Ref.
	This Work	Others					
		MEAS.	CALC.	χ(E)	σ(E)		
$^{197}Au(n,\gamma)\ ^{198}Au$	76.2 ± 1.8	95.5 ± 2.3				Pauw, Aten (1971)	/3/
		79.9 ± 2.9				Green (1975)	/12/
		110 ± 11				Buczkô et al. (1976)	/13/
			81.8	T = 1.39	ENDF/B-IV	Mughabghab et al.(1974)	/14/
			79.9	NBS	ENDF/B-IV	Fabry et al. (1975)	/2/
			82.2	NBS	SAND-II	Fabry et al. (1975)	/2/
$^{115}In(n,\gamma)\ ^{116}In^{m}$	124.1 ± 3.6	125.3 ± 4.3				Pauw, Aten (1971)	/3/
		132 ± 14[RN]				Buczkô et al. (1976)	/13/
			130.3	NBS	ENDF/B-IV	Fabry et al. (1975)	/2/
			141.4	NBS	SAND-II	Fabry et al. (1975)	/2/
$^{197}Au(n,2n)\ ^{196}Au$	5.50 ± 0.14	4.93 ± 0.14				Pauw, Aten (1971)	/3/
		6.2 ± 0.6[RN]				Buczkô et al. (1976)	/13/
			5.11	T = 1.39	ENDF/B-IV	Mughabghab et al.(1974)	/14/

[RN] The values were renormalized to the gamma emission probability given in Tab. 1.

Table 2 (continued)

Reaction	<σ> (mb) This Work	Others MEAS.	Others CALC.	Others χ(E)	Others σ(E)	Author(s)	Ref.
$^{113}In(n,n')\ ^{113}In^{m}$	160 ± 4	178 ± 18				Buczkó et al. (1976)	/13/
			143 ± 10	T = 1.42	MEAS.	Smith, Meadows (1975)	/6/
$^{115}In(n,n')\ ^{115}In^{m}$	195 ± 5	188 ± 8				Pauw, Aten (1971)	/3/
		202 ± 11 RN				Kirouac et al. (1973)	/15/
		198 ± 5				Alberts et al. (1975)	/7/
		221 ± 20 RN				Buczkó et al. (1976)	/13/
			183 ± 13 RN	T = 1.42	MEAS.	Smith, Meadows (1975)	/6/
			191.1 a)	NBS	ENDF/B-IV	Fabry et al. (1975)	/2/
			190.7 b)	NBS	SAND-II	Fabry et al. (1975)	/2/

RN The values were renormalized to the gamma emission probabilities given in Tab. 1.

a) Normalized by the author for a gamma emission probability of 45.9 %. Without the normalization the value is 175.5 mb.

b) Analogous to a).

Table 3: Cross sections of $^{48}Ti(n,p)^{48}Sc$ averaged over the ^{252}Cf-fission neutron spectrum

	$\langle\sigma\rangle$ (mb)	$\sigma(E)$	$\chi(E)$
CALC.	0.265	ENDF/B-IV	NBS
	0.383	SAND-II	NBS
	(0.53)*	Menapace (1974)	T = 1.42
	0.315	Smith, Meadows (1975) [$E_n \leq 10$ MeV]	T = 1.42
	(0.43)*	Smith, Meadows [+ Interpolation]	T = 1.42
MEAS.	0.42 ± 0.01	Alberts et al. (1975)	

*Values given in brackets are rough estimates.

Table 4: Fast Neutron Flux Density Monitor Reactions

Reaction	E_n (MeV)	σ(mb)*	Method of Measurement	Authors
$^{27}Al(n,\alpha)\ ^{24}Na$	14.78	115.5 ± 3.0	Proton Recoil	Robertson et al. (1973)
	14.78	110.6 ± 1.3	Assoc. Particles	Vonach et al. (1970)
$^{56}Fe(n,p)\ ^{56}Mn$	14.78	109.8 ± 2.9	Proton Recoil	Robertson et al. (1973)
	14.70	100.4 ± 3.2	rel. $^{27}Al(n,\alpha)$	Vonach et al. (1968)
	14.78	99.4 ± 3.4	+ extrapol. excit. Funct.	Vonach et al. (1968)

*All quoted uncertainties are 3σ-errors (99.5 %)

Figure captions:

Figure 1: Neutron cross section for $^{48}Ti(n,p)^{48}Sc$ (from ref. /21/)

Figure 2: Excitation function of $^{65}Cu(n,2n)^{64}Cu$ (from ref. /23/)

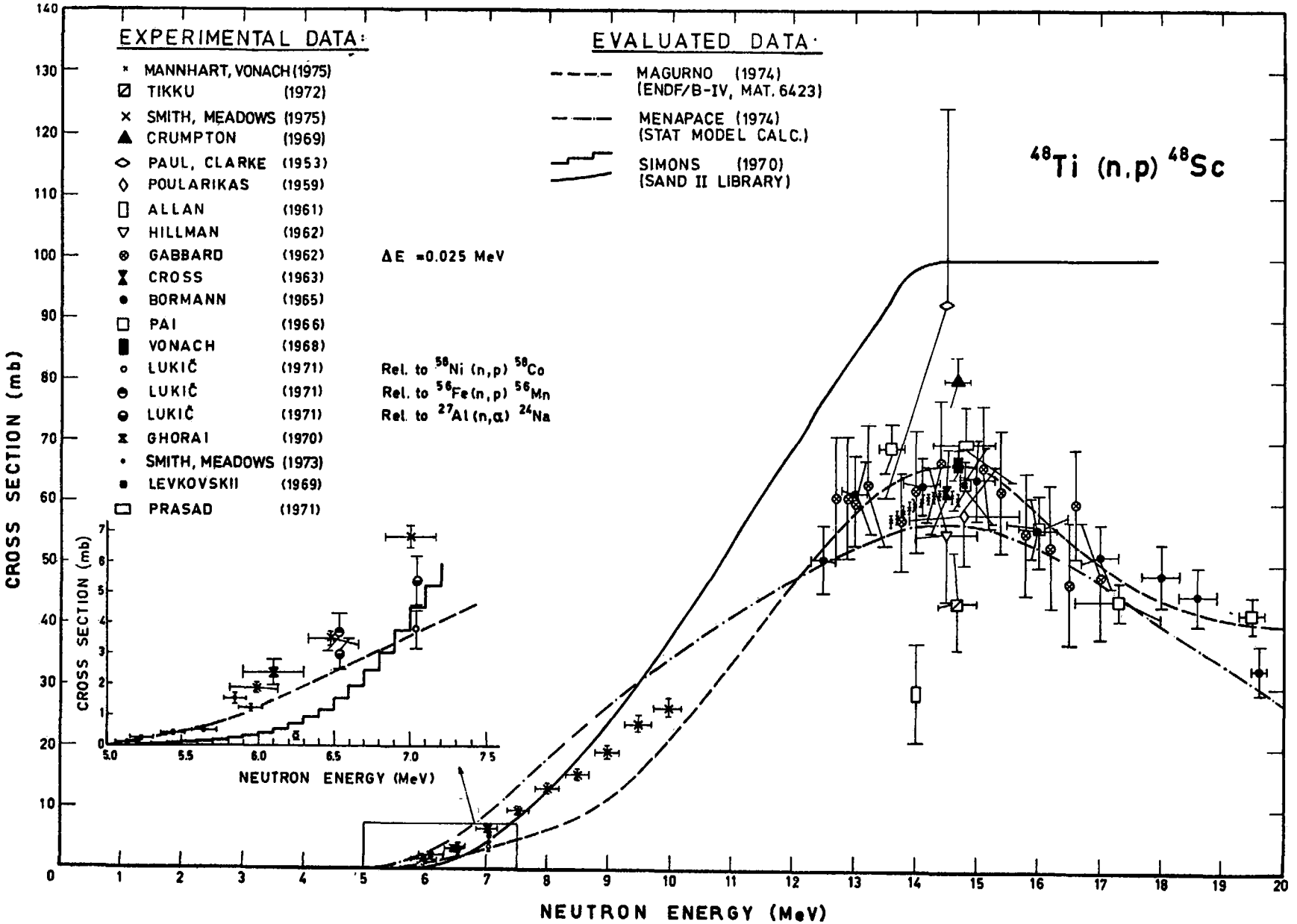
EXPERIMENTAL DATA:
MANNHART, VONACH (1975)
TIKKU (1972)
SMITH, MEADOWS (1975)
CRUMPTON (1969)
PAUL, CLARKE (1953)
POULARIKAS (1959)
ALLAN (1961)
HILLMAN (1962)
GABBARD (1962)
CROSS (1963)
BORMANN (1965)
PAI (1966)
VONACH (1968)
LUKIČ (1971)
LUKIČ (1971)
LUKIČ (1971)
GHORAI (1970)
SMITH, MEADOWS (1973)
LEVKOVSKII (1969)
PRASAD (1971)
EVALUATED DATA:
MAGURNO (1974) (ENDF/B-IV, MAT. 6423)
MENAPACE (1974) (STAT MODEL CALC.)
SIMONS (1970) (SAND II LIBRARY)
ΔE =0.025 MeV
Rel. to 58Ni (n,p) 58Co
Rel. to 56Fe(n,p) 56Mn
Rel. to 27Al(n,α) 24Na
48Ti (n,p) 48Sc
CROSS SECTION (mb)
NEUTRON ENERGY (MeV)

Fig. 1

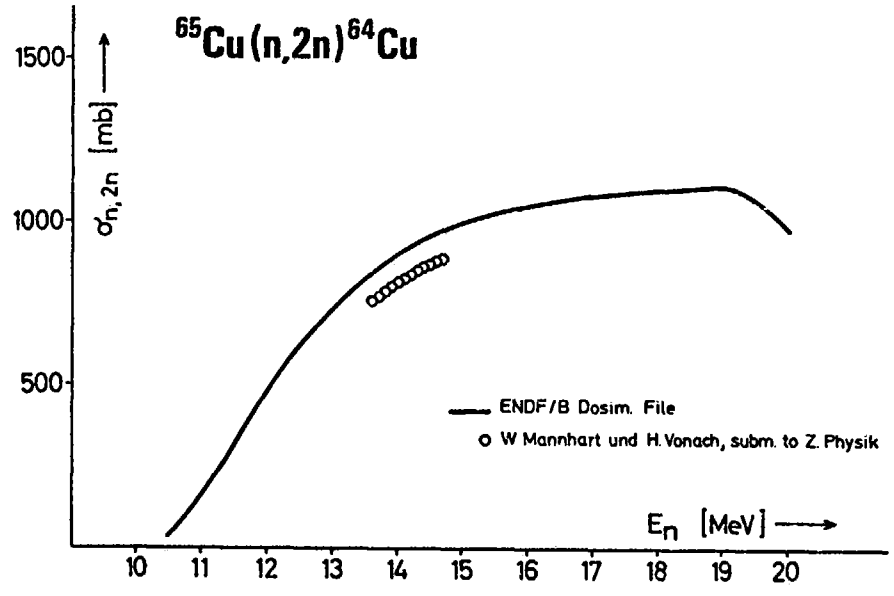
65Cu(n,2n)64Cu
1500
1000
500
σn,2n [mb]
ENDF/B Dosim. File
W Mannhart und H. Vonach, subm. to Z. Physik
En [MeV]
10
11
12
13
14
15
16
17
18
19
20

Fig. 2

II.5. Spectrum Averaged Cross-Section Measurements in the Fast Neutron Field of a Uranium Fission Plate

M. Najzer and J. Rant

University of Ljubljana
J. Stefan Institute

Abstract

Neutron Cross-Section averaged over the ^{235}U fission spectrum for $^{115}In(n,n')^{115}In$, $^{64}Zn(n,p)^{64}Cu$, $^{27}Al(n,p)^{27}Mg$, $^{56}Fe(n,p)^{56}Mn$, $^{24}Mg(n,p)^{24}Na$ and $^{19}F(n,2n)^{18}F$ reactions have been measured relative to the $^{27}Al(n,\alpha)^{24}Na$ reaction for which the averaged cross-section of 0,705 mb was assumed. The values obtained are 184±7,4; 30,1±0,8; 3,7±0,2; 0,98; 1,49±0,04 and (6,5±0,3)$\times 10^{-3}$ mb respectively. Characteristics of a neutron field of a 20 % enriched uranium converter plate driven by the thermalizing column neutron beam and suspended in the large exposure room of the TRIGA Mark II reactor are described. The induced gamma or positron-annihilation activities were measured by a calibrated 3"×3" NaJ(Tl) scintilation spectrometer and calculated by analyzing the resulting spectra by an unfolding code. The accuracy of measuring the activities was at the 2 % level, except for the ^{24}Na activity, where it was about 0,5 %. The measured cross-section values are compared with the previous results of present authors as well as with recent evaluations of Fabry.

1. Introduction

It is well known that evaluation of energy dependent cross-section of threshold reactions can be improved by measuring their integral cross-sections i.e. cross-sections averaged over a well defined fast neutron induced fission spectrum of ^{235}U.

Several well documented measurements of ^{235}U fission spectrum averaged cross-sections for a substantial number of threshold reactions have been performed in various experimental conditions, such as spherical fission cavities /1/, cores of thermal /2,3/ or fast reactors /4/ and uranium fission plates /5,6,7,2,3/. The accuracy of these measurements is on average 2-10% in absolute and 2-5% in relative scale /8,9/. In order to resolve the discrepancies between the calculated and measured fission spectrum averaged cross-sections and to clarify differences between the measurements of different authors, new measurements of cross-sections of threshold reactions averaged over ^{235}U reference fission spectrum and in reasonably well defined experimental conditions are strongly encouraged. According to the recommendations of the INDC /10/ the accuracy of these measurements should be about 2-5%.

The aim of the present report is to briefly describe measurements of the ^{235}U fission spectrum averaged cross-sections for the following set of threshold reactions: $^{115}In(n,n')^{115m}In$, $^{64}Zn(n,p)^{64}Cu$, $^{27}Al(n,p)^{27}Mg$, $^{56}Fe(n,p)^{56}Mn$, $^{24}Mg(n,p)^{24}Na$, $^{27}Al(n,\alpha)^{24}Na$ and $^{19}F(n,2n)^{18}F$. A detailed description of these measurements can be found in a reference /11/.

The measurements were performed in the fast neutron field of an ^{235}U fission converter plate and in experimental conditions which assurred that only minor distortions of the fission

spectrum were present. An assessment of fission spectrum distortions, partly experimental, partly numerical will be briefly described later on.

The present authors measured ^{235}U fission spectrum averaged cross-section for a set of selected threshold reactions previously /7/. In comparison with previous measurements the present ones have been performed in somewhat better experimental conditions due to the reconstructed thermalizing column, offering nearly 3 times greater driving thermal flux. In addition the method of measuring induced gamma and positron-annihillation activities has been improved so that an accuracy in measuring the activities better of 2 % was achieved.

2. Characteristics of the Fast Neutron Field of the Uranium Fission Plate.

As a fast neutron source ^{235}U enriched circular converter plate has been used. The converter plate is mounted in the middle of the TRIGA Reactor exposure room (dimensions 2,4 × 2,4 × 3,5 m) and is positioned 0,85 m above the floor and 1,10 m from the walls and the rear end of graphite thermalizing (60 × 60 cm) column. The details of the irradiation facility and converter plate mounting have been described elsewhere /12/.

The characteristics of the neutron soutce are listed in Table I.

Table I: Characeristics of the neutron source

the shape of the source	circular disk (Ø260 × 3,1mm)
thickness of Uranium	1,5 mm
^{235}U enrichment	20 %
Thickness of the Al-cladding	0,8 mm
Fast neutron flux on the converter surface ($^{115}In(n,n')$ detector)	$4,3 \times 10^7$ n/cm^{2}sec
Thermal neutron flux incident on the converter surface	$3,3 \times 10^7$ n/cm^{2}sec
Surface distribution of the incident thermal neutron beam	homogeneous within 1,5 %
Transmitted thermal neutron flux	$1,3 \times 10^7$ n/cm^{2}sec
Cadmium ratio of the incident neutron flux (Au detector)	110

A detector foil holder is positioned in the axis of the converter plate and enables irradiations at 10 different distances from the converter plate as represented on Fig. 1. The axial variation of the fast neutron flux has been experimentally determined by measuring the relative activation of $^{115}In(n,n')$, $^{64}Zn(n,p)$ and $^{27}Al(n,\alpha)$ detectors as a function of the distance from the converter plate. The axial decrease in the activation of $^{27}Al(n,\alpha)$ detector is represented in Fig. 2. The fast neutron flux gradient is about 1,5 % over a distance of 1 mm.

The radial distribution of the fast neutron flux has also been found constant over a surface area of 50 mm diam. detector foils to within less then 1 %.

The spectrum shape of the fast neutron converter field slightly deviates from the ^{235}U fission spectrum.

These distortions are caused by:

i. Fast neutron background due to the fast neutron leakage through the thermalizing column.

ii. Return flux from the walls of the exposure room

iii. Elastic and inelastic scattering of fast neutrons in the converter plate, support structures, detector foils and cadmium box.

The greatest contribution to the fission spectrum distortion is due to the fast neutron background, whose spectrum significantly differs from the fission spectrum. The contribution of fast neutron background to the activation of detector foils has been experimentally determined by irradiating detector foils with the converter plate in the"out of beam" condition. It has been also found, that the activation of the detectors in the fast neutron background does not vary significantly with the axial distance from the converter plate. The relative contribution of the fast neutron background to the activation of detectors in the fast neutron field of the converter plate, given for a distance of 26 mm from the fast neutron source,is quoted in Table II.

Table II. The experimental ratios of detector activities obtained with the converter plate in the "out of beam" and "in the beam" condition

Reaction	A background/A fiss. plate
$^{115}In(n,n')$	0.012
$^{64}Zn(n,p)$	0.030
$^{27}Al(n,p)$	0.049
$^{56}Fe(n,p)$	0.064
$^{24}Mg(n,p)$	0.069
$^{27}Al(n,\alpha)$	0.057
$^{19}F(n,2n)$	0.038

Distortion of the fission spectrum due to the fast neutron scattering on the walls of the exposure room has not been calculated due to the complicated geometry. From a simple and a very conservative calculation is evident that the wall returned flux is less than 0,3 % of the total fast neutron flux at the normal irradiation position and hence these distortions were neglected.

However, fission spectrum distortions due to the elastic and inelastic scattering of fast neutrons in the uranium converter plate, aluminium cladding, cadmium box and aluminium support structures cannot be neglected. This type of distortions were not estimated accurately, since no computer code, suitable for that purpose, has been available. Only the upper limit for the fission spectrum distortion has been calculated using the method of first collisions and neglecting the contribution of the neutrons, scattered into the effective beam. The influence of calculated distortion on the detector activities ranges between 0,0 and 4,9 % for $^{27}Al(n,\alpha)$ and $^{115}In(n,n')$ detector respectively.

Fission spectrum distortion is larger near the fission plate where also the effective thickness of the plate is greater. Variation of the distortion with the distance was determined experimentally by measuring the In/Al spectral index which is most sensitive to this effect. Results are shown in Fig. 3. It can be seen that within the experimental error of about 2 % only the point at 10 mm distance is below the average value of 262. Calculated values of spectral index for the disturbed fission spectrum, normalized to the value of 262 assumed for the undisturbed fission spectrum are shown in the same figure. The experimental and calculated values are in accordance. Knowing that calculated values are too low because in beam scattering has been neglected one can conclude that the measured In/Al spectral index is probably not in

error for more than 2 to 3 % due to fission spectrum distortions. For other detectors the corresponding errors in spectral indices are lower.

3. Measurements of Fission Spectrum Averaged Cross-Sections

The actually measured quantities were not fission spectrum averaged cross-sections $\langle\sigma\rangle$ of threshold reactions, but merely their spectral indices R_i, measured relative to the averaged cross-section $\langle\sigma\rangle_R$ of the reference reaction $^{27}Al(n,\alpha)$. The $^{27}Al(n,\alpha)$ reaction has been selected as a reference, as it possesses a reasonably well known cross-section and as it was possible to measure the specific activity of this detector very accurately.

Normally, detector foils were irradiated so that a set of detector foils is stacked together, sandwiched between two aluminium foils, mounted into foil holder and covered by a cylindrical cadmium box with 1 mm thick walls. The irradiation arrangement is shematically represented in Fig. 1.

For the detector foils metals* of highest purity (99.999) have been used, except for $^{18}F(n,2n)$ detector, where gaflon** $((C_2F_4)_n)$ has been found suitable material. All the foils were circular discs with the diameter of 50 mm. The properties of detector foils as well the data needed to convert measured activities into specific activities are listed in Table III. Data about half life and branching ratios were taken from reference /13/ except for the conversion factor of 335 MeV

---

* Supplied by Johnson Matthey, England

** Supplied by Appareille Gachot, France

line of ^{115m}In, where the value of Misra and Meritt /14/ has been retained.

The gamma activities induced in irradiated detector foils were measured by a low-background 3"×3" NaI(Tl) gamma--ray spectrometer. Since the foil materials were of natural isotopic composition, the epithermal and fast neutrons induced several parasitic activities. Due to properly selected waiting time and due to good energy resolution of the spectrometer only a small overlap of parasitic acitvities and gamma rays of interest was observed. To increase the accuracy of computations of specific activities, the spectra were fitted with an appropriate set of scintillator response functions using GAMA 2 /15/ unfolding code, patterned after similar method of Echhoff /16/ and Heath /17/. This code incorporates also a gain shifting procedure what significantly improves the quality of fit.

The accuracy with which the intensities of gamma lines were calculated using the GAMA 2 unfolding code were typically about 0,3 %, except for the ^{24}Na and ^{18}F where these values were 0,2 % and 1,3 % respectively. The response functions, as well as the efficiency of the spectrometer were determined, using ^{203}Hg, ^{52}Cr, ^{198}Au, ^{18}F, ^{137}Cs, ^{54}Mn, ^{65}Zn, ^{22}Na, ^{88}Y and ^{24}Na sources, calibrated with $4\pi\beta$-γ method. The accuracy of experimentally determined spectrometer efficiency was at the 2 % level. An exception was the efficiency of the ^{24}Na activity, which for itself represented a response function of the spectrometer where the accuracy was 0,5 %.

4. Results and Discussion

In Table IV the spectral indices R_i as obtained in four independent experimental runs are given uncorrected for the fission spectrum distortions. The fission spectrum averaged cross-sections are quoted relative to the assumed value of 0,705 mb for the averaged cross-section of the $^{27}Al(n,\alpha)$ reaction. The quoted error bounds (1σ) include the errors in measuring the detector activities as well as the statistical scatter of results as obtained in independent experimetal runs. The value for the averaged cross-section of $^{56}Fe(n,p)^{50}Mn$ reaction is given without error bounds, since for this reaction only one measurement has been performed.

In Table IV the present results are compared with our previous measurements /7/ and with the recent evaluation of Fabry /18/. The present values agree well within experimental errors with Fabry's evaluation. An exception is the $^{56}Fe(n,p)^{56}Mn$ reaction. The present as well as previous value for this reaction is significantly lower from the value given by Fabry, however both our values are still within the error bounds given by Fabry for this reaction.

Table III; Properties of detector foils used for measurements of ^{235}U fission spectrum averaged cross-sections.

reaction	material	foil thickness {mm}	isotopic abundance {%}	half life	measured γ-ray {KeV} and its branching ratio {%}
$^{115}In(n,n')^{115m}In$	metal	0,121±2%	95,7	$4,53^{h}$	335(46)
$^{64}Zn(n,p)^{64}Cn$	metal	0,247±0,5%	48,9	$12,71±0,01^{h}$	β^{+} (19)
$^{27}Al(n,p)^{27}Mg$	metal	0,131±0,5%	100	$9,40^{m}$	and $^{835}_{1015}$(100)
$^{56}Fe(n,p)^{56}Mn$	metal	0,258±0,5%	91,6	$2,587±0,006^{h}$	846,7(99)
$^{24}Mg(n,p)^{24}Na$	metal	0,845±0,5%	78,8	$15,030±0,006^{h}$	*(100)
$^{27}Al(n,\alpha)^{24}Na$	metal	0,131±0,5%	100		
$^{19}F(n,2n)^{18}F$	gaflon	1,040±2%	75,9**	112^{m}	β^{+} (97)

* The spectrum of ^{24}Na constituted for itself a response function with known absolute activity.

** Chemical composition.

Table IV; Comparison of measured fission spectrum averaged cross-sections with the recent evaluation of Fabry /18/

Reaction	Measured Spectral Index	Fission Spectrum Averaged Cross-Section		
		Present work {mb}	NAJZER 70 {mb}	FABRY 75 {mb}
$^{115}In(n,n')$	261,9(1±0,134)	184± 7,4	180,3±6	189 ±8
$^{64}Zn(n,p)$	42,72(1±0,012)	30,1±0,8	29,1±1,5	29,9±1,6
Al(n,p)	5,25(1±0,043)	3,7±0,2	3,4±0,3	3,84±0,25
Fe(n,p)	1,392	0,98	0,98±0,06	1,035±0,075
Mg(n,p)	2,11(1±0,026)	1,49±0,06	1,51±0,06	1,48±0,082
Al(n,α)	1	0,705	0,705*	0,705±0,40
F(n,2n)	$8,9.10^{-3}$(1±0,047)	(6,5±0,3)**	(6,1±0,6)**	

* Fission spectrum averaged cross-section have been measured relative to this value

** Values to be multiplied by a factor 10^{-3}

References

/1/ Fabry et al., Proc. IAEA Conf. on Nuclear Data for Reactors, Vol. 2, 535-569, Helsinki (1970)

/2/ Kimura I., Kobayshi K., Shibata T., J. Nucl. Sci. Technol. 8, No. 2, 59 (1971)

/3/ Kimura I. et al., Ibid, 10, No. 9, 574 (1973)

/4/ Kobayashi K. et al., Ibid., 13, No. 10, 561 (1976)

/5/ J.W. Boldeman, J. Nucl. Energy A/B 18, 417 (1964)

/6/ A.M. Bresesti et al., Nucl. Sci. Engng. 40, 331 (1970)

/7/ Najžer M., Rant J., Šolinc H., Proc. IAEA Conf. on Nuclear Data for Reactors, Vol. 2, 571, Helsinki (1970)

/8/ Liskien H., Paulsen A., IAEA Consultants Meeting on Nuclear Data for Reactor Neutron Dosimetry, INDC (NDS)--56/U, 79, Vienna (1973)

/9/ Fabry A., BLG-465 (1972)

/10/ IAEA Consultants Meeting on Nuclear Data for Reactor Neutron Dosimetry, INDC(NDS)-56/U, 1, Vienna (1973)

/11/ Rant J., Measurement of ^{235}U fission spectrum averaged cross-sections for a selected set of threshold Reactions, M.S. Thesis, University of Ljubljana (1974)

/12/ Najžer M., Rant J., IAEA Conf. "Irradiation Facilities for Research Reactors", 161, Teheran (1973)

/13/ Nuclear Data Sheets, National Academy of Sciences, NRC, Washington D.C., (1965)

/14/ Misra, S.C., Merritt, J.S., AECL-2044 (1964)

/15/ Rant J., GAMA2 - A Computer Code for Analysis of Complex Gamma-Ray Spectra; IJS-DP-642 Report (1973)

/16/ Eckhoff N.D., Nucl. Instr. and Methods 74, 77 (1969)

/17/ Heath R.L., Helmer R.C., Nucl. Instr. and Meth., 47, 305 (1967)

/18/ Fabry A. et al., Reactor Dosimetry Integral Reaction Data in LMFBR Benchmark and Stadard Neutron Fields; Status, Accuracy and Implications, 1st ASTM-EURATOM Symposium on Reactor Dosimetry, Petten (1975).

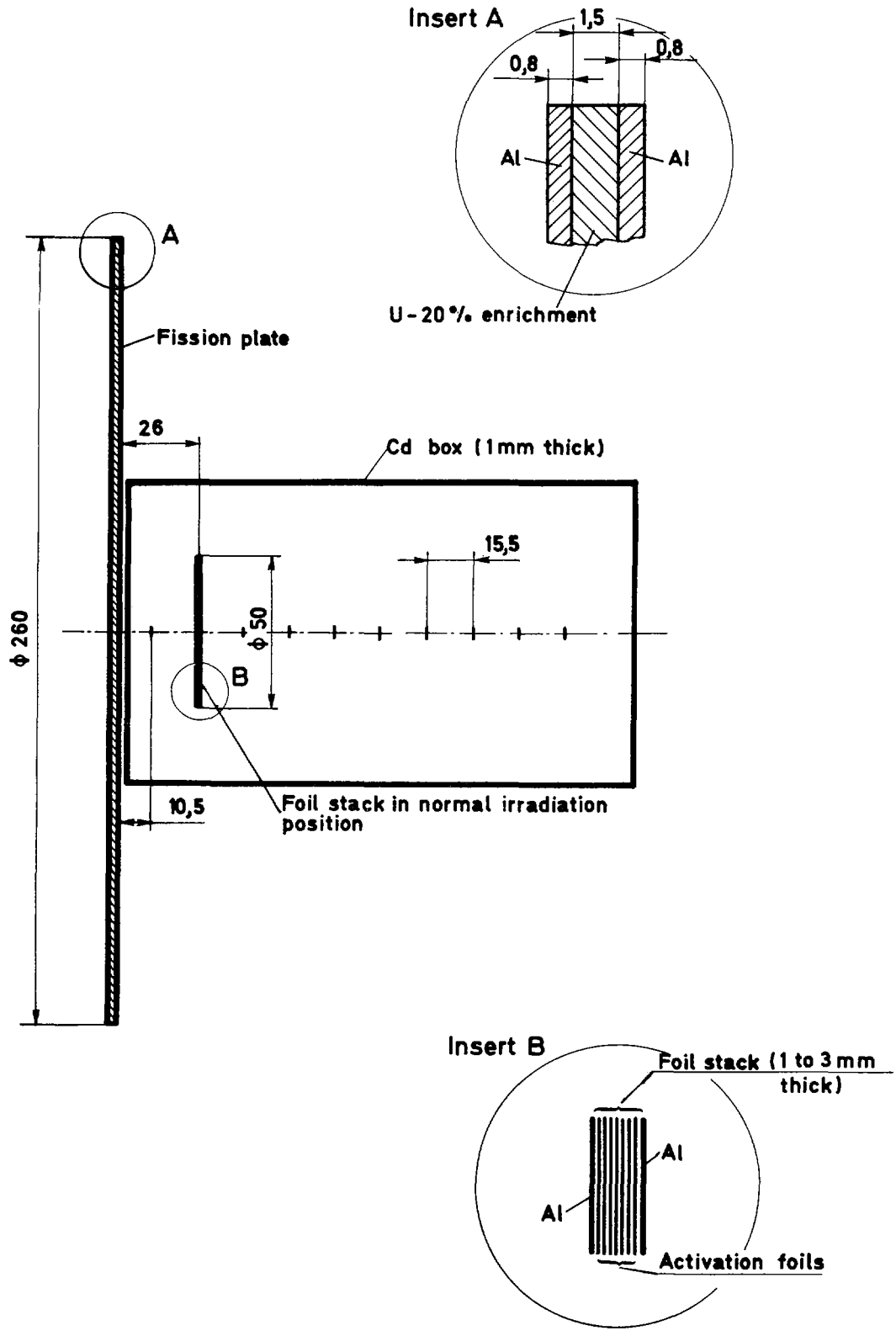

Fig 1 Irradiation arrangement; All measures in mm

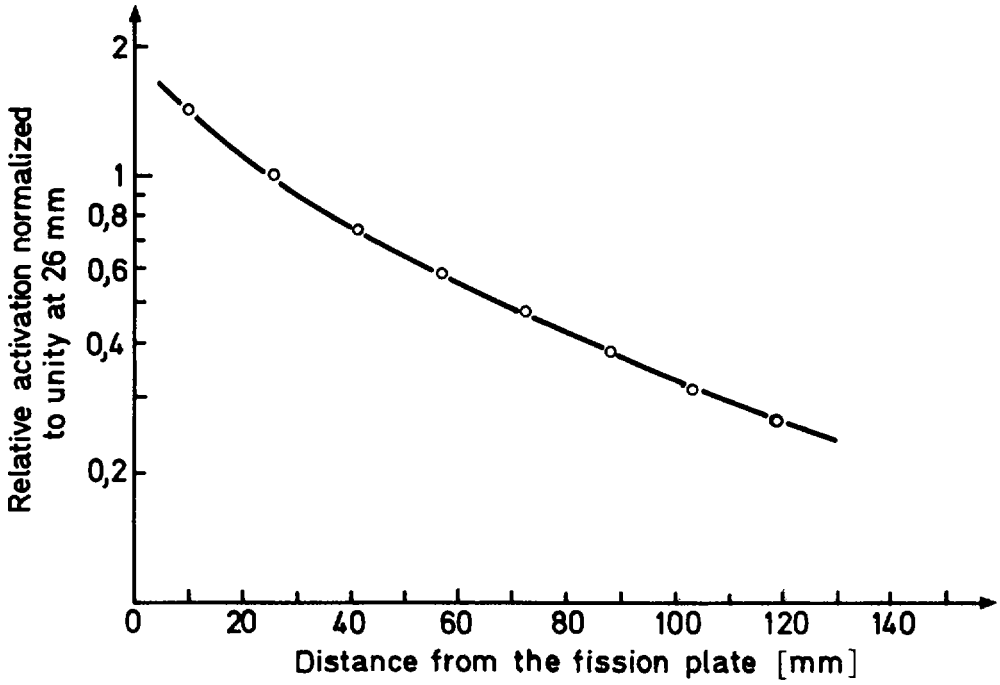

Fig. 2 Variation in the activation of $^{27}Al(n,\alpha)$ detector with the distance in the axial direction.

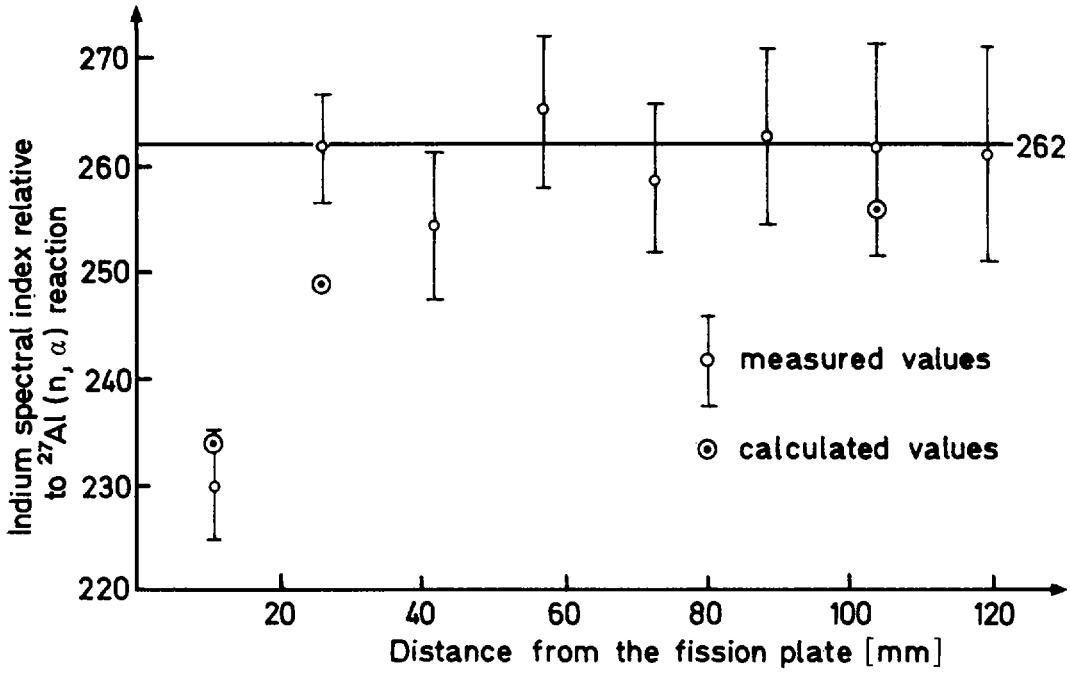

Fig. 3 Variation of spectral index of $^{115}In(n,n')$ reaction (relative to $^{27}Al(n,\alpha)$ reaction) with the distance from the converter plate.

II.6. Fission Product Yield Ratios for Uranium-235 Fission by Thermal and Californium-252 Neutrons

S.R. Wagner reporting on work performed by K. Debertin.
Physikalisch-Technische Bundesanstalt (PTB), Braunschweig
Federal Republic of Germany

Abstract:

Fission yields of ^{235}U in the pure fission neutron spectrum of a ^{252}Cf source relative to thermal neutron fission yields were determined for ^{95}Zr, ^{97}Zr, ^{99}Mo, ^{103}Ru, ^{131}I, ^{132}Te, $^{140}Ba/^{140}La$ and ^{143}Ce by means of Ge(Li) gamma-ray spectrometry.

In connection with the development of fast reactors, the neutron energy dependence of fission product yields is of interest. Until now fast neutron fission yields have been determined in more or less well defined reactor spectra, the shapes of which were, in most cases, only little known. No serious variations of the yields of the fission products are to be expected in the maxima of the mass yield curve. In the valley and on the wings of the curve, however, an appreciable energy dependence has been observed.

Hence K. Debertin /1/ of PTB took advantage of the pure fission-neutron spectrum of californium-252 sources to determine fast neutron fission yields from uranium-235 relative to thermal neutron fission yields. The uranium samples (discs of 10 mm diameter and 0.2 mm thickness, ^{235}U enriched to 93 %) were irradiated during a period of 2 hours to 12 days with ^{252}Cf-fission neutrons in an open air low scatter arrangement /3/ and with thermal neutrons in the reactor FMRB of PTB. Gamma-ray spectra of the irradiated samples were taken by means of a Ge(Li)-spectrometer. As the number of fissions in the irradiated samples were not known, only relative cumulative yields of the fission products could be extracted from each spectrum. In order to make the results obtained, comparable to the tabulation of evaluated fission product yields by Meek and Rider /2/, the ratios of the observed relative cumulative yields for fast and thermal fission were normalized to the evaluated chain yield ratio for zirconium-95. The results are given in the table.

They show that the differences between the fission spectrum and the reactor spectrum results are largest where a marked energy dependence of fission product yields is to be expected, their signs being such as to confirm the assumption that the reactor spectra were appreciably moderated fission spectra. However, final conclusions cannot be drawn until results for all fission products measured (^{88}Kr, ^{91}Sr, ^{105}Rh, ^{133}I, ^{125}I; possibly ^{127}Sb, ^{134}I, ^{138}Cs, ^{142}La) will be available.

Fission product	$\left[Y_c^{Cf} / Y_c^{th}\right]_{rel}$ *) Debertin, 1976	Y_t^r / Y_t^{th} Meek and Rider, 1974
^{95}Zr	0.990 (± 0.011) **)	0.990 ± 0.012
^{97}Zr	1.025 ± 0.007	1.004 ± 0.020
^{99}Mo	1.014 ± 0.025	0.930 ± 0.016
^{103}Ru	1.102 ± 0.009	1.051 ± 0.030
^{131}I	1.261 ± 0.019	1.143 ± 0.023
^{132}Te	1.145 ± 0.012	1.106 ± 0.019
$^{140}Ba/^{140}La$	0.963 ± 0.010	0.954 ± 0.014
^{143}Ce	0.900 ± 0.006	0.946 ± 0.011

*) normalized to the ratio for ^{95}Zr from Meek and Rider

**) not included in the uncertainties of the other ratios.

Ratios of fission product yields Y from ^{235}U fission by fast neutrons (Cf: ^{252}Cf fission neutrons, r reactor spectrum neutrons) to the yields Y^{th} from thermal neutron induced fission (Y_c cumulative yield, Y_t total yield). The uncertainties quoted in column 2 are mainly statistical ones and relate to a confidence level of 68 %.

References:

/1/ K. Debertin: Spaltproduktausbeuten bei der Spaltung von ^{235}U durch thermische und schnelle Neutronen.
PTB-Jahresbericht für 1976. Braunschweig, to be published.

/2/ M.E. Meek and B.F. Rider: Compilation of Fission Product Yields. Report NEDO-12154-1, January 26, 1974, Vallecitos Nuclear Center, Pleasanton, California

/3/ W.G. Alberts, J. Bortfeldt, E. Günther, K. Knauf, M. Matzke, G. Rassl, V. Siegel, K.F. Walz: Measurement of Cross Sections for Threshold Reactions induced by Californium-252 Spontaneous Fission Neutrons.
Proceedings of the Conference on Nuclear Cross Sections and Technology, Washington D.C., March 3 - 7, 1975. NBS Special publication 425, p. 273 (1975)

II.7. MEASUREMENT AND EVALUATION OF THRESHOLD REACTION CROSS SECTIONS IN STANDARD NEUTRON FIELDS

Itsuro Kimura, Katsuhei Kobayashi, Shu A. Hayashi
Shuji Yamamoto
(Research Reactor Institute, Kyoto University
Kumatori-cho, Sennan-gun, Osaka-fu, JAPAN)
and
Hiroshi Gotoh and Hideyuki Yagi
(Japan Atomic Energy Research Institute
Tokai-mura, Naka-gun, Ibaraki-ken, JAPAN)

Abstract

Review and discussion are given on standard fields of neutrons, mainly fast neutrons, which have been studied by the authors. Some other standard neutron fields in Japan are also introduced. Thereafter, the measured results of cross sections for some threshold reactions are compared with those measured or evaluated by other groups.

I. INTRODUCTION

Precise knowledge of cross sections for neutron induced threshold reactions is of much importance from the standpoint of not only using them as fast neutron detectors for neutron dosimetry but also evaluation of radiation damage, nuclear transformation and so forth. Although a large number of experimental works to measure energy dependent cross sections for many threshold reactions have been carried out so far and theoretical predictions of them have been performed by several workers recently, accuracy and reliability in the cross section data are not always enough to satisfy the requirement for utilizing them in practice[1].

Measurement of average cross sections, if they are obtained in a well defined fast neutron standard spectrum field, makes it possible to assess energy dependent cross sections. Furthermore, we can obtain cross sections with extremely small values by this integral method, since fast neutron flux in the standard spectrum field is usually much more intense than those of neutron generators for energy dependent cross section measurement. As a fast neutron standard spectrum field, spontaneous fission sources, simple fission plate or specially designed facilities, such as a spherical shell of fission material placed in a thermal neutron field in a reactor, have been proposed and used by several workers. On the other hand, we can use a reactor core itself as a standard fast neutron spectrum field, if the shape of the fast neutron spectrum is determined accurately. A neutron spectrum produced by the combination of a pile of some reactor material and a neutron generator, such as an electron linear accelerator, can be also useful for a standard neutron spectrum field. A monochromatic fast neutron source with a Cockcroft-Walton type accelerator or a Van de Graaff accelerator can be also regarded as a standard fast neutron field, however it is usually excluded from this category.

In this paper, standard fast neutron fields including monochromatic neutron sources, used by the authors and by

some other groups in Japan are reviewed. Thereafter, the measured results of some cross sections for neutron threshold reactions are compared with previous published values which were experimentally and theoretically obtained and were evaluated.

II STANDARD NEUTRON FIELDS

Standard fast neutron fields, including monochromatic neutron sources, used by the authors and by some other groups in Japan are tabulated in Table I.

1. Core and Beam Tube of a Thermal Reactor

Fast neutron spectrum in the core of a reactor with highly enriched uranium as a plate type fuels and with almost homogeneously distributed light water as a moderator, is close to that of fission neutrons. The core of the MTR type reactor, such as Kyoto University Reactor(KUR), places under this category. The shape of the fast neutron spectrum in the core is practically very close to that of fission neutrons for $E > 1.5$ MeV. And the angular distribution of fast neutrons is almost isotropic. Therefore, we can use it as a standard neutron field with a fission-type fast neutron spectrum. Using the reactor core, available fast neutron flux is very high and is about 5×10^{13} n/cm^2/sec for a 5 MW reactor, in KUR.

A thermal reactor generally accompanies thermal and epithermal neutrons of equivalent level to fast neutrons. For that reason, we must be careful for the interference by thermal and epithermal neutrons when we measure threshold reaction cross sections in the core of the thermal reactor. Furthermore, the shape of the fast neutron spectrum is, strictly speaking, not the very same as that of fission neutrons, especially in lower energy range, around 1 MeV or less. Therefore, errorneous result is apt to be obtained in the cross section measurement for a threshold reaction with lower threshold energy.

According to the classification of benchmark neutron fields identified at a work shop held during the Petten Symposium[2], the core of a thermal reactor does not belong under the standard field, but under the reference neutron field. Nevertheless, the core of a thermal reactor is frequently used for the measurement of threshold reaction cross sections.

A large number of threshold reaction cross sections have been measured in the core of KUR. The configuration of KUR is shown in Fig. 1. The details are given elsewhere[3)4)].

In addition to the core, an experimental beam tube of KUR can be also used for the measurement of threshold reaction cross sections. A ^{237}Np fission counter with a silicon detector was manufactured and the cross section for the ^{237}Np (n,f) reaction was obtained[5]. Experimental arrangement is shown in Fig. 2. In this measurement, fast neutron flux was monitored with the $^{115}In(n,n')^{115m}In$ reaction whose average cross section was 175 $\pm$ 6 mb[6].

2. Core and Reflector of a Fast Reactor

The core of a fast source reactor with metallic enriched uranium fuels can be utilized for the measurement of threshold reaction cross sections[3)7)~9)]. Similar works have been achieved by making use of a fast critical assembly[10] and a coupled system composed of a fast zone and a thermal driver[11].

In comparison with the core of a thermal reactor, the fast reactor core is superior to the other in non-interference by thermal and epithermal neutrons and in higher fast neutron flux at the same reactor power. Furthermore, we can tailor various fast neutron spectra to simulate those in a large fast reactor. The core of a fast reactor, as same as that of a thermal reactor, is thought to belong to the reference neutron field.

A large number of threshold reaction cross sections have been measured in the core of YAYOI, a fast source reactor of the University of Tokyo. The experimental arrangement

at YAYOI is shown in Fig. 3. The details were described in the previous papers[3)9)]. Recently, A. Sekiguchi et al. have applied several neutron spectrometers to measure fast neutron spectra in YAYOI[12)].

The core of YAYOI can be moved to three locations: (1) the ordinary position in the heavy concrete shield, (2) the central position in a large lead pile and (3) the position without reflector and shield for the bare core experiment. Although we used only the first position previously, the second or the third must also be an excellent standard fast neutron standard spectrum field for the neutron cross section measurement.

Formation of a standard neutron spectrum field with Kyoto University Critical Assemblies(KUCA) is planned to carry out[13)].

3. Fission Plate, Neutron Energy Converter

A fission plate, of preferably highly enriched uranium, which is installed in a thermal neutron field of a reactor, can give us an excellent thermal neutron-induced fission spectrum, which is more clean standard fast neutron spectrum field. By conbination of a pile or a shell of reactor materials, we can tailor various fast neutron spectra to simulate those in a large fast reactor.

At the heavy water thermal neutron facility of KUR, we made use of (1) a neutron energy converter of fission plate type, 27 cm in effective diameter with 90 % enriched uranium of 1.1 kg[14)] and (2) a small fission foil of 90 % enriched U-Al alloy about 0.5 mm thick and 10 mm in diameter fixed on the periphery of a rotor plate, as shown in Fig. 4[15)]. With the highly enriched uranium fission plate, we could obtain fast neutron flux of order of 10^8 n/cm^2/sec. For the case of the small fission foil, fast neutron flux entering into a sample foil placed beside the fission foil, can be obtained by fission rate and shape factor. The fission rate was determined by measuring the activity of ^{140}La-^{140}Ba in the uranium foil. By this method, we measured the cross sections for the ^{115}In(n,n')^{115m}In, ^{58}Ni(n,p)^{58}Co and ^{27}Al(n,α)

^{24}Na reactions, which were used as reference reactions for monitoring absolute value of fast neutron flux in the cores of KUR and YAYOI and on the big fission plate.

Besides KUR, several groups previously used fission plates at HTR, JRR-4 and so forth in Japan. Very recently, K. Kudo et al. of Electrotechnical Laboratory made a spherical shell of 93 % enriched uranium in order to make a fast neutron standard spectrum field[16]. Powder of UO_2, about 2.1 kg in weight, was packed into an aluminum shell, whose inner diameter and outer diameter are 16 cm and 18.7 cm respectively. A tritium target of a Cockcroft-Walton type accelerator can be placed at the center of the shell.

4. ^{6}LiD Plate, 14 MeV Neutron Converter

With a plate of ^{6}LiD installed in a thermal neutron field, 14 MeV neutrons are produced by the following processes[17];

$$^{6}Li + n_{th} \longrightarrow {}^{4}He + {}^{3}T \quad ,$$

$$^{2}D + {}^{3}T \longrightarrow {}^{4}He + n_{14\ MeV} \cdot$$

In contrast to that neutrons are directly originated by fission in a fission plate, 14 MeV neutrons are generated by the interaction of deuterons and tritons which are produced by the first reaction. Therefore, the conversion efficiency from thermal neutrons to fast neutrons for the ^{6}LiD plate is much smaller than that for the fission plate.

We have carried out preliminary study with the ^{6}LiD plate at the heavy water thermal neutron facility of KUR. A powder sample of ^{6}LiD, about 1 mm thick, packed into a polyethylene case was attached on the periphery of the rotor plate which was described before. The 14 MeV neutrons were measured by the $^{58}Ni(n,p)^{58}Co$ reaction. The result of the conversion efficiency from thermal neutrons to fast neutrons was about 1×10^{-4} and this value agreed with the predicted. Even with a relatively intense thermal neutron field, of which neutron flux is order of 10^{11} $n/cm^2/sec$, the flux of 14 MeV neutrons may be much lower than that of a Cockcroft-Walton type accelerator. However, we can make a plane source of

14 MeV neutrons with a ^{6}LiD plate placed in a large thermal neutron field. This can be also used as a fast neutron standard spectrum field.

5. T(p,n)^{3}He, D(d,n)^{3}He and T(d,n)^{4}He Reactions

Monochromatic fast neutrons are generated by the T(p,n)^{3}He, D(d,n)^{3}He and T(d,n)^{4}He reactions with a Cockcroft-Walton type accelerator, a Van de Graaff accelerator and so forth. They are often excluded from the fast neutron standard spectrum field. However, we deal with them inclusively in this paper. And the emphasis is laid on the measurement of absolute neutron flux.

Perry reviewed the fast neutron flux measurements and classified them to three methods[18]; (1) production of known flux, (2) recoil proton methods and (3) neutron moderation methods. A large number of groups have studied and are still studying the absolute measurement of fast neutron flux. Some groups use different method from the Perry's review, such as a fission counter method by Smith et al.[19]. Recently international intercomparison of fast neutron flux or fluence was performed by Bureau International des Poids et Measures (BIPM) and its result will be reported in May, 1977[20].

Table II shows a few examples of the methods of the absolute neutron flux determination to measure threshold reaction cross sections with a Cockcroft-Walton type accelerator or a Van de Graaff accelerator.

Two types of recoil proton counters, as shown in Fig. 5, were manufactured by the authors. The counters are composed of a thin recoil proton radiator of polyethylene and either a silicon surface barrier detector or a CsI(Tl) scintillation counter. The former counter is mainly used for fast neutrons with lower energy $E < 6\sim7$ MeV and the latter for higher energy. The uncertainty in the absolute neutron flux measurement with these counters was evaluated and the results are given in Table III.

6. Electron Linear Accelerator

Various types of fast neutron standard fields can be

made by using an electron linear accelerator which produces a pulsed neutron source. By making use of it, we can obtain quasi-monochromatic neutrons by the time-of-flight method. Although few integral cross section measurements have been attempted with them before, there is a possibility to utilize them for integral measurements.

By a combination of a thin bremsstrahlung target and a compound of deuterium such as heavy water, we can establish a fast neutron standard spectrum field with an electron linear accelerator. Kaushal et al. used this type of neutron field to calibrate the detection efficiency of a scintillation counter[28].

Another method employs to use a pile of simple geometry and of elemental constituents of which neutron cross section data are accurately known. A borated graphite pile was designed and used by the authors[29] to calibrate the neutron detection efficiency of a ^{6}Li glass scintillation counter bank and a ^{10}B-vaseline plug NaI(Tl) counter in the keV region. The experimental configuration and the predicted neutron spectra in the pile are shown in Fig. 6 and Fig. 7. The spatial neutron distributions in the pile measured by the $^{58}Ni(n,p)^{58}Co$ and $^{197}Au(n,\gamma)^{198}Au$ reactions were nearly isotropic around the photoneutron source, and agreed with the predicted. Similar integral test can be achievable for various neutron cross sections by making use of the standard pile with not only electron linear accelerator but also a steady neutron source.

Fast neutron spectra in the piles of several reactor materials have been measured and analyzed by the authors[30]. The spectrum in a sample pile shows the proper shape to the sample material and may be applicable to integral test of neutron cross sections in future.

In order to save the quantity of sample of expensive materials, we used a lead reflector around the sample pile and could obtain almost the same spectrum in a much larger sample pile[31]. This neutron field might be also used for the same purpose.

III EVALUATION OF CROSS SECTIONS

For the purpose of obtaining threshold reaction cross sections accurately in a standard neutron field with absolutely known neutron flux spectrum, we must know the following values, as precise as possible, which are mainly related to the detector; (1) decay scheme data[32] such as half life, energy and branching ratio of the measured radiation, (2) counting efficiency of the radiation detector and its background and (3) irradiation time, waiting time and counting time. One should explicitly describe these values in a publication, by which other group can check and evaluate the result.

On the other hand, for the comparison with the measured or evaluated energy dependent cross section, it is important that what type of fission neutron spectrum is adopted to calculate the average cross section. The fission neutron spectrum itself can be evaluated by average cross sections for some threshold reactions[33].

1. $^{115}In(n,n')^{115m}In$

The energy dependent cross section and the average cross section for this reaction were measured with a Van de Graaff accelerator at JAERI, the big fission plate and the small fission foil at KUR. The results are tabulated in Table IV and are compared with those of other groups. From this table it can be seen that all data of the present authors agree with those of Bresesti et al.[35] and with the calculated values using the energy dependent cross sections of Smith and Meadows[24] and of Santry and Butler[23]. The value calculated with ENDF/B-IV (T=1.32) is slightly small but agrees with the authors' within the experimental error. All of the Fabry's values exceed others.

Present authors adopted the intensity of the 0.336 MeV gamma-ray I_γ being 50 %, however, Fabry and Santry took I_γ to be 45.9 %[40]. If we take this value for I_γ, the cross section for this reaction becomes about 193 mb which satisfactorily agrees with the third value of Fabry. In the core of fast source reactor YAYOI, the fast neutron flux monitored

by the $^{115}In(n,n')^{115m}In$ reaction whose average cross section was taken to be 177 mb agreed with those obtained by the $^{58}Ni(n,p)^{58}Co$ and $^{27}Al(n,\alpha)^{24}Na$ reactions in 2 to 3 %. Accodingly, if we use the larger cross section value for the $^{115}In(n,n')^{115m}In$ reaction, those for the above two reactions should be increased by the same factor. Furthermore, all of the obtained cross sections for other reactions should be also changed by the same factor. By this increment, most of the cross sections measured by the authors approach to those of Fabry[37]. But this increment of the cross section for the $^{115}In(n,n')^{115m}In$ reaction causes remarkable discrepancy from those calculated with energy dependent cross sections. This discrepancy might be explained by different fission neutron spectrum. More studies are required.

2. $^{58}Ni(n,p)^{58}Co$

The absolute cross section for this reaction was measured with the small fission foil. The result is compared with other published values in Table V. The tendency found for the $^{115}In(n,n')^{115m}In$ reaction is also seen for the present case.

3. $^{27}Al(n,\alpha)^{24}Na$

The absolute cross section for the $^{27}Al(n,\alpha)^{24}Na$ reaction was measured with the small fission foil. The result is compared with other published values in Table VI. The situation for this reaction is rather different from the above two reactions.

4. Ti(n,p)Sc

The cross sections for three (n,p) reactions were measured and the results are tabulated in Table VII. In these measurements, fast neutron flux was monitored by the $^{58}Ni(n,p)^{58}Co$, $^{27}Al(n,\alpha)^{24}Na$ and $^{24}Mg(n,p)^{24}Na$ or $^{115}In(n,n')^{115m}In$ reactions. The $^{24}Mg(n,p)^{24}Na$ and $^{115}In(n,n')^{115m}In$ reactions were used for the measurement at KUR and for that at YAYOI respectively.

Present results show smaller values than those of Fabry probably due to different monitors. The values calculated with ENDF/B-IV (T=1.32) and Smith and Meadows' data agree for the $^{46}Ti(n,p)^{46}Sc$ reaction and are not very different for the $^{47}Ti(n,p)^{47}Sc$ reaction, but are remarkably smaller than the integral values for the $^{48}Ti(n,p)^{48}Sc$ reaction. This reason should be investigated in future.

5. Some Fission Cross Sections

The cross sections for the $^{232}Th(n,f)$, $^{237}Np(n,f)$ and $^{238}U(n,f)$ reactions were measured and the results are tabulated in Table VIII. The cross section for the $^{237}Np(n,f)$ reaction was measured by two different methods[5]; one by direct counting method with a fission counter shown in Fig. 2 and the other, by activation method with the big fission plate. Both results satisfactorily agree each other and the calculated values with the ENDF/B as seen in Table VIII. In this case, our results agree with the Fabry's value. However, the cross sections for the $^{232}Th(n,f)$ and $^{238}U(n,f)$ reactions are slightly smaller than the Fabry's values.

6. Concluding Remarks

A large number of threshold reaction cross section were measured at the standard fast neutron fields described in the previous section. Results and discussion are given elsewhere[3)9)]. As described both in this paper and in the previous paper[9)], systematic discrepancy exists between the results of the present authers and those of Fabry's. Parts of the discrepancies may be mainly attributed to the reference cross section values used for monitoring fast neutron flux. We must investigate the reason of this discrepancy in future.

Fortunately, IAEA is going to support to carry out the international inter-laboratory* study to seek the reason of the above discrepancy[45)].

---

* CEN-SCK, Mol, Belgium
RRI, Kyoto University, Osaka, Japan
(IAEA Seibersdorf Laboratory)

REFERENCES

[1] VLASOV,M.F., FABRY,A., McELROY,W.N., Status of Neutron Cross Sections for Reactor Dosimetry, Paper presented at the 1976 International Conference on the Interactions of Neutrons with Nuclei, July 6-9, 1976, Lowell, Mass., U. S. A.

[2] Proc. First ASTM-EURATOM Symposium on Reactor Dosimetry, Petten, Netherlands, Sept. 22-26 (1975).

[3] KIMURA,I., KOBAYASHI,K., Intercomparison of Reactor Dosimetry Cross Sections Measured in a Thermal Reactor, in a Fast Reactor and with an Enriched Uranium Fission Plate, paper in (2).

[4] KIMURA,I., KOBAYASHI,K., SHIBATA,T., J. Nucl. Sci. Technol., 8 (1971) 59.

[5] KOBAYASHI,K., KIMURA,I., GOTOH,H., YAGI,H., Annu. Repts, of Res. Reactor Inst., Kyoto Univ., 6 (1973) 1.

[6] KOBAYASHI,K., KIMURA,I., GOTOH,H., YAGI,H., J. Nucl. Energy, 27 (1973) 741.

[7] GRUNDL,J.A., HANSEN,G.H., Proc. IAEA Conf. on Nucl. Data for Reactors, Vol.1 (1967) 321.

[8] MARTINI,M., BELLI,M., SIRITO,M.F., The TAPIRO Fast Source Reactor as a Benchmark to Test Activation Detector Cross Sections, paper in (2).

[9] KOBAYASHI,K., KIMURA,I., NAKAZAWA,M., AKIYAMA,M., J. Nucl. Sci. Technol., 13 (1976) 531.

[10] DOWDY,E.J., LOZITO,E.J., PLASSMANN,E.A., Nucl. Technol., 25 (1975) 381.

[11] ROGERS,J.W., MILLSAP,D.A., HARKER,Y.D., ibid. 25 (1975) 330.

[12] SEKIGUCHI,A., WAKABAYASHI,H., NAKAZAWA,M., AKIYAMA,M., KOSAKO,T., Several Studies of Neutron Standard Fields in the Fast Reactor, YAYOI, to be presented at this meeting.

[13] KANDA,K., private communication.

[14] KANDA,K., KOBAYASHI,K., CHATANI,H., SHIBATA,T., Neutron Energy Converter (in Japanese), KURRI-TR-96 (1972).

[15] KIMURA,I., KOBAYASHI,K., SHIBATA,T., J. Nucl. Sci. Technol., 10 (1973) 574.

[16] KUDO,K.(ETL), private communication.
[17] HUGHES,D.J., Pile Neutron Research, p.117, Addison-Wesley (1953).
[18] PERRY,J.E., Jr., Fast Neutron Physics (ed. J.B. Marion and Fowler) Part I, 623, Interscience (1960).
[19] SMITH,D.L., MEADOWS,J.W., Nucl. Sci. Eng., 58 (1975) 314.
[20] MICHIKAWA,T.(ETL), private communication.
[21] LISKIEN,H., PAULSEN,A., Nucl. Phys., 63 (1965) 393.
[22] BAYHURST,B.P., et al., Phys. Rev. C, 12 (1975) 451.
[23] SANTRY,D.C., BUTLER,J.P., Can. J. Phys., 54 (1976) 757.
[24] SMITH,D.L., MEADOWS,J.W., Nucl. Sci. Eng., 58 (1975) 314.
[25] KUDO,K., Nucl. Instr. Meth., in print.
[26] SATO,T., KANDA,Y., KUMABE,I., J. Nucl. Sci. Technol., 12 (1975) 681.
[27] KATOH,T., et al., unpublished.
[28] KAUSHAL,N.N., et al., Phys. Rev., 175 (1968) 1330.
[29] KIMURA,I., et al., Nucl. Instr. Meth., 137 (1976) 85.
[30] KIMURA,I., et al., Proc. Neutron Cross Sections and Technol., NBS, SP 425, Vol.1 (1975) 184.
[31] KIMURA,I., et al., Measurement of Neutron Spectrum in a Small Iron Pile Surrounded by a Lead Reflector, to be published.
[32] HELMER,R.G., GREENWOOD,R.C., Nucl.Technol, 25 (1975) 258.
[33] KIMURA,I., KOBAYASHI,K., SHIBATA,T., Proc. IAEA Specialist Meeting on the Status of Prompt Fission Neutron Spectra, IAEA (1972) p.113.
[34] KIMURA,I., KOBAYASHI,K., SHIBATA,T., J. Nucl. Sci. Technol., 6 (1969) 485.
[35] BRESESTI,A.M., et al., Nucl. Sci. Eng.,40 (1970) 331.
[36] FABRY,A., Nukleonik, 10 (1967) 280.
[37] FABRY,A., BLG-465 (1972).
[38] FABRY,A., private communication (1976).
[39] MAGURNO,B.A., OZER,O., Nucl. Technol., 25 (1975) 376.
[40] HANSEN,H.H., et al., Z. Phys., 269 (1974) 155.
[41] SMITH,D.L., MEADOWS,J.W., ANL/NDN-13 (1975).
[42] ASAMI,T., Evaluation of $^{27}Al(n,\alpha)^{24}Na$, $^{27}Al(n,p)^{27}Mg$ and $^{58}Ni(n,p)^{58}Co$ Cross Sections, to be presented at this meeting.
[43] BRUGGEMAN et al., J. Radioanal. Chem., 23 (1974) 131.
[44] PEARLSTEIN,S., Nucl. Sci. Eng., 23 (1965) 238.
[45] CZOCK,K.H., private communication.

Table I Standard fields of fast neutrons for the measurement of threshold reaction cross sections in Japan

Name of field(place)		Neutron spectrum	Available fast neutron flux	Determination of neutron flux
Core of thermal reactor (KUR)		Fission-type,MeV 1/E-type, keV much thermal n	$< 5 \times 10^{13}$ (5MW) $\sim 10^{12}$ (100 kW)	Foil
Beam tube of thermal reactor (KUR)		Fission-type,MeV 1/E-type, keV much thermal n	$\sim 10^{8}$ (5 MW)	Foil ^{6}Li and ^{3}He sandwich counters
Core in fast reactor (YAYOI, UT *)		Fission-type,MeV slightly moderated no thermal n	5×10^{11} (2 kW)	Various neutron spectrometer Foil
Reflector or pile around fast reactor (YAYOI, UT *)		Lead moderated-type no thermal n		Various neutron spectrometer Foil
Fission plate	Big enriched U-235 plate(KUR)	Fission	$\sim 10^{8}$ (5 MW)	Foil
	Small enriched U-235 foil (KUR)	Fission	$\sim 10^{6}$	FP (^{140}La-^{140}Ba)

Table I -- continued --

Fission plate	Enriched U-235 spherical shell (ETL **)	Fission and others		
^{6}LiD plate (KUR)		14 MeV,monoch.	$\sim 10^{5}$	Foil
Cockcroft & Walton accelerator,D-T (ETL **) (JAE ***) (NU +) (KYU ++)etc.		14 MeV,monoch.		Proton recoil counter with a CsI(Tl) scintillator, Associated particle, Foil
Van de Graaff accelerator, P-T, D-D (JAE ***)		Several hundred keV $\sim$ 8 MeV monoch.	$10^{4} \sim 10^{5}$	Proton recoil counter with a Si detector or CsI(Tl), Foil
Electron linear accelerator	Borated graphite (KUR)	1/E-type, keV		Foil TOF
	Other sample piles(KUR)	Proper type to sample		Foil TOF
	Sample with reflector (KUR)	Proper type to sample		Foil TOF

* University of Tokyo, ** Electrotechnical Laboratory, *** Japan Atomic Energy Research Institute, + Nagoya University, ++ Kyushu University, KUR: Kyoto Univ., Res. Reactor Institute.

Table II Methods of absolute neutron flux determination in threshold reaction cross section measurement with accelerator neutron sources

Group	Accelerator	Neutron fluence determination
Present authors Kyoto Univ. & JAERI	VdG* (C-W**)	Proton recoil counter $^{115}In(n,n')^{115m}In$
Liskien & Paulsen[21] (Geel)	VdG	Proton recoil counter
Bayhurst et al.[22] (Los Alamos)	VdG C-W	Proton recoil counter $^{27}Al(n,\alpha)^{24}Na$ $^{90}Zr(n,2n)^{89}Zr$
Santry & Butler[23] (Chalk River)	VdG	Long counter $^{32}S(n,p)^{32}P$
Smith & Meadows[24] (ANL)	VdG	Fission counter
Kudo[25] (ETL; Japan)	C-W	Associated particle
Sato et al.[26] (Kyushu Univ. Japan)	C-W	$^{27}Al(n,\alpha)^{24}Na$
Katoh et al.[27] (Nagoya Univ. Japan)	VdG	$^{27}Al(n,\alpha)^{24}Na$

* Cockcroft-Walton type accelerator

** Van de Graaff type accelerator

Table III Estimated uncertainties in absolute fast neutron flux determination with the proton recoil counters*

Source of error	Uncertsinty (%)
Total cross section of (n,p) scattering	0.5
Anisotropy of (n,p) scattering	1.2
Number of hydrogen atoms	0.3
Geometry of counter	1.2
Contribution of scattered neutrons	1.0
Contribution of D-D neutrons (C-W)	1.0
Contribution of C(n,n')3α reaction	Very small
Statistical error	0.3
Total — With D-D neutrons	2.3
Total — Without D-D neutrons	2.1

* The absolute fast neutron flux at the Cockcroft-Walton type accelerator of ETL measured with these counters agreed within 2 to 3 % with that obtained by the associated particle method.

Table IV Average cross section for $^{115}In(n,n')^{115m}In$

Reference		Cross section (mb)
Present authors	Small fission foil[15]	176.5 ± 8.8 177.4 ± 9.8 177 (av.)
	Big fission plate[33]	176 ± 10
	Calculated by using energy dependent cross section 6) 34)	176 177
Bresesti et al.[35]		177 ± 6.0
Fabry	Nukleonik[36]	200 ± 10
	BLG-465[37]	188 ± 4
	Private commun.[38]	193 ± 8.5
ENDF/B[39]	T=1.29	163.9
	T=1.32	166.8
Smith & Meadows[24] ($\bar{E}$=1.97)		179 ± 13
Santry & Butler[23]	T=1.29	166 ± 9
	T=1.31	168 ± 9

Table V Average cross section for $^{58}Ni(n,p)^{58}Co$

Reference		Cross section (mb)
Present authors[15]		102.6 ± 5.2 101.6 ± 5.6 102.1 (av.)
Bresesti et al.[35]		104.5 ± 4.0
Fabry	BLG-465[37]	113 ± 2.5
	Private commun.[38]	111 ± 5.2
ENDF/B[39]	T=1.29	97.2
	T=1.32	101.5
Smith & Meadows[41] ($\bar{E}$=1.97)		99.4
Asami[42]	Maxwellian	99.7
	Watt	101

Table VI Average cross section for $^{27}Al(n,\alpha)^{24}Na$

Reference		Cross section (mb)
Present authors[15]		0.635 ± 0.036 0.653 ± 0.036 0.644 (av.)
Bresesti et al.[35]		0.695 ± 0.02
Fabry	BLG-465[37]	0.725 ± 0.02
	Private commun.[38]	0.710 ± 0.04
ENDF/B[39]	T=1.29	0.709
	T=1.32	0.801
Asami[42]	Maxwellian	0.790
	Watt	0.684

Table VII Average cross sections for Ti(n,p)Sc

Reference		Cross section (mb)		
		$^{46}Ti(n,p)^{46}Sc$	$^{47}Ti(n,p)^{47}Sc$	$^{48}Ti(n,p)^{48}Sc$
Present authors	Core of KUR	11.2±0.63	19.0±1.2	0.294±0.025
	Fission plate	10.8±0.6	17.3±0.90	0.272±0.016
	Core of YAYOI	10.9±0.59	18.9±0.87	0.256±0.013
Fabry[37] (BLG-465)		12.5±0.5	20±2	0.315±0.02
Bruggeman et al.[43]		10.5±0.4	16.3±0.6	0.272±0.005
ENDF/B[39]	T=1.29	9.5	20.6	0.171
	T=1.32	10.2	21.4	0.194
Smith & Meadows[24] ($\bar{E}$=1.97)		10.0	21.0	0.227
Pearlstein[44]		11.3	17.2	0.236

Table VIII Average cross sections for some fission reactions

Reference		Cross section (mb)		
		$^{232}Th(n,f)$	$^{237}Np(n,f)$	$^{238}U(n,f)$
Present authors	Beam tube of KUR		1320±70	
	Fission plate		1330±110	
	Core of YAYOI	78.6±3.9		294±15
Fabry[37] (BLD-465)		83±3.5	1370±75	328±10
ENDF/B[39]	T=1.29	67.3	1313	289
	T=1.32	69.0	1323	295

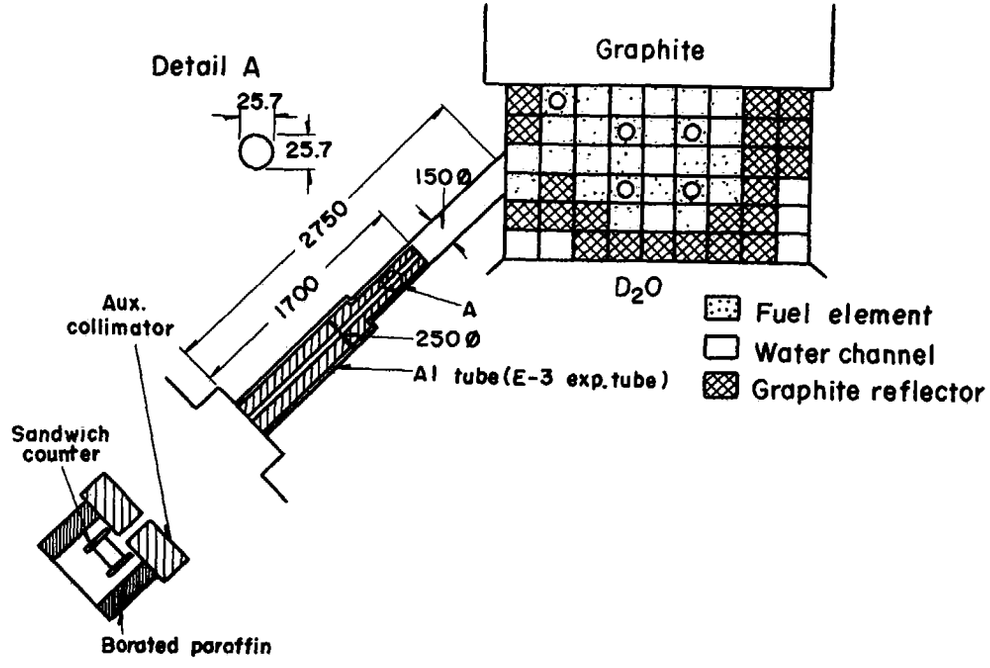

Fig. 1 The core and an experimental hole of KUR, where average cross sections for some threshold reactions were measured by the authors(4).

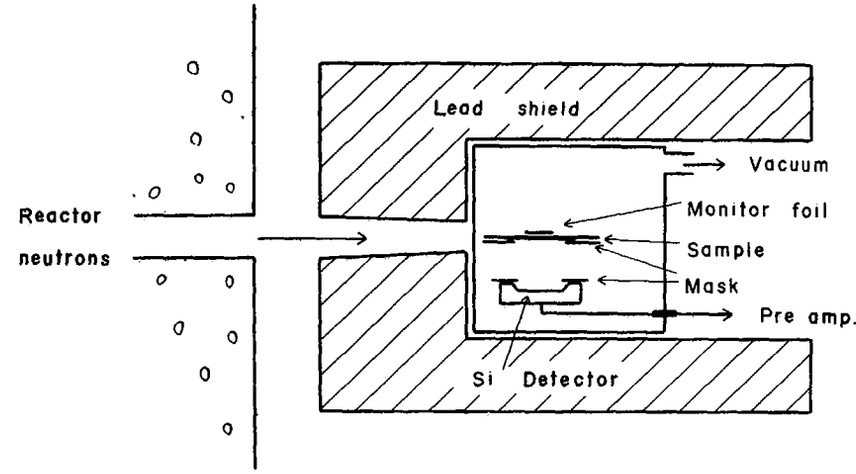

Fig. 2 Schematic figure of a ^{237}Np fission chamber used for the measurement of the cross section for the $^{237}Np(n,f)$ reaction at the experimental hole of KUR.

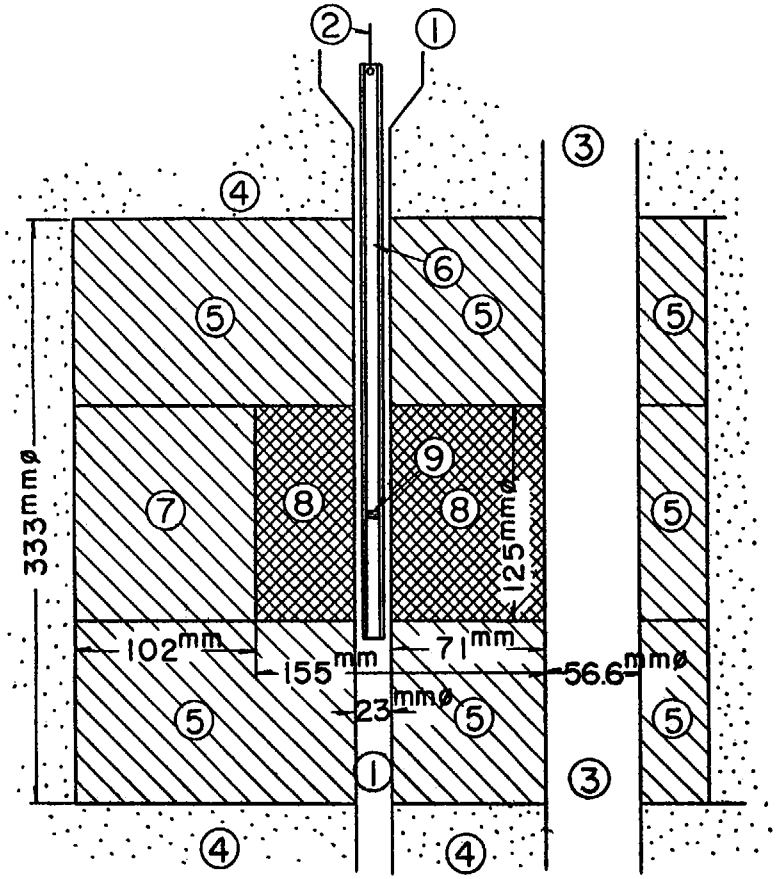

Fig. 3 The experimental arrangement at YAYOI. (1) Glory hole where a number of threshold reaction cross sections were measured by the authors, (2) string for hanging foil holder(6), (3) grazing hole, (4) lead reflector, (5) depleted uranium blanket, (7) safety block of depleted uranium, (8) 90 % enriched uranium fuel of cylindrical shape, (9) sample and monitor foils.

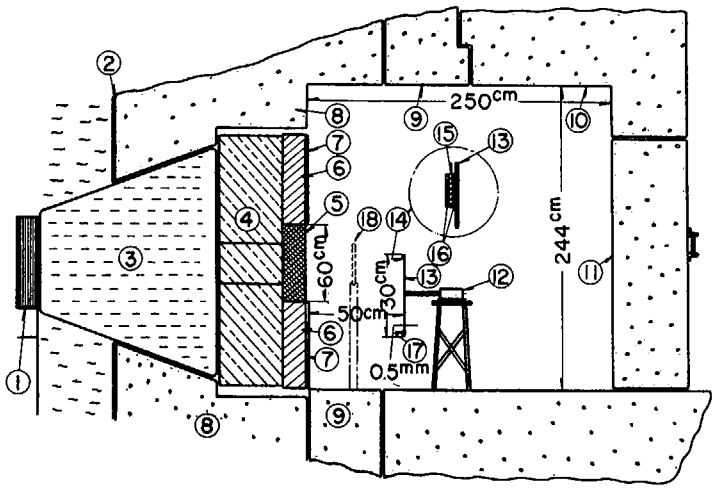

Fig. 4 Experimental arrangement for irradiation of threshold foils in company with a small fission foil or a large fission plate in the heavy water thermal neutron facility of KUR. (1) Core, (2) reactor tank, (3) heavy water, (4) graphite, (5) bismuth, (6) lead, (7) boral, (8) reactor shield of heavy concrete, (9) shutter, (10) heavy concrete blocks, (11) door, (12) geared motor, (13) rotor, (14) sample foils with the fission foils, (15) fission foil,. (16) sample foils, (17) sample foils with a fission foil, (18) large fission plate.

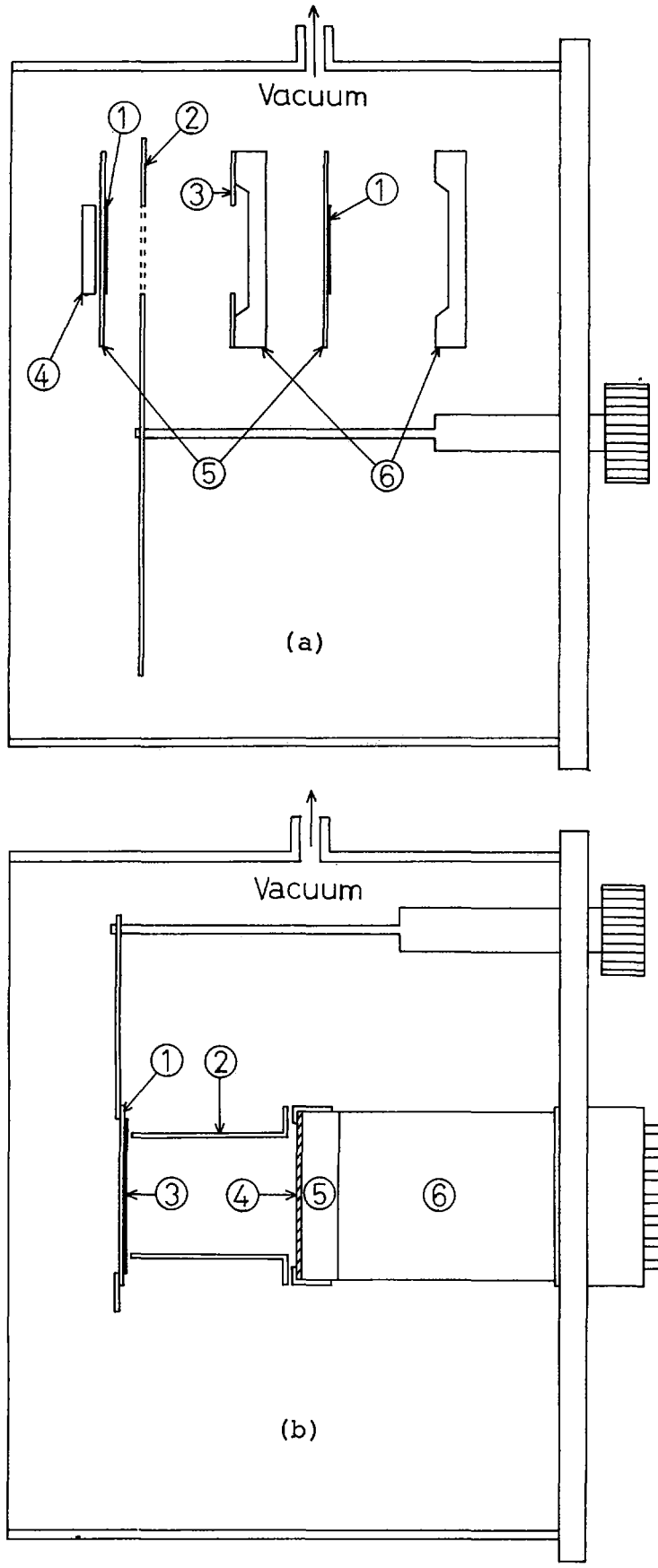

① Radiator
② Shutter
③ Mask
④ Sample
⑤ Au Backing
⑥ Si Detector

Fig. 5 Two types of proton recoil counters to measure the absolute fast neutron flux from a neutron generator. (a) A counter composed of a radiator and a surface barrier silicon detector, and (b) a counter composed of a radiator and a CsI(Tl) scintillation counter.

① Au Backing
② Au Collimator
③ Radiator
④ CsI(Tl) Scintillator
⑤ Light Guide
⑥ Photo Multiplier

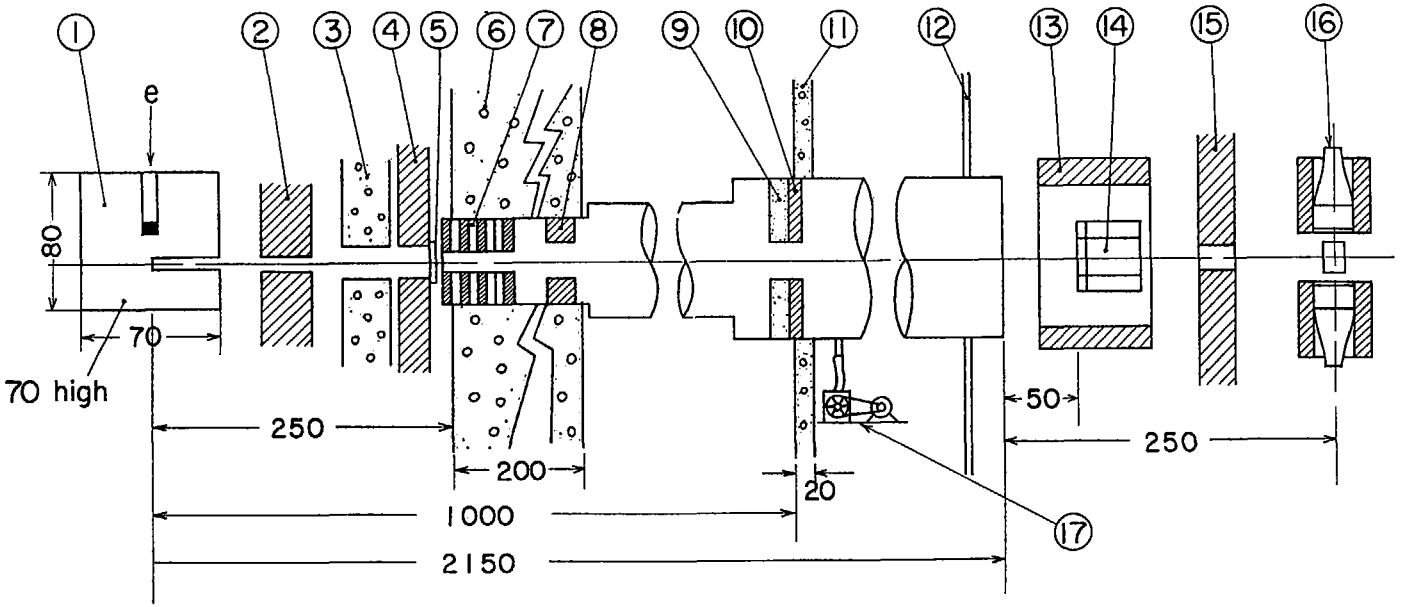

Fig. 6 Experimental arrangement of the borated graphite standard neutron spectrum pile. (1) Borated graphite pile, (2) (4) (8) (10) (15) lead collimators, (3) heavy concrete collimator, (5) uranium plate for eliminating gamma flash, (6) (11) concrete wall, (7) (9) B_4C collimator, (12) wall of the hut, (13) lead shield, (14) Li-6 glass scintillation counter bank, (16) B-10 vaseline plug detector.

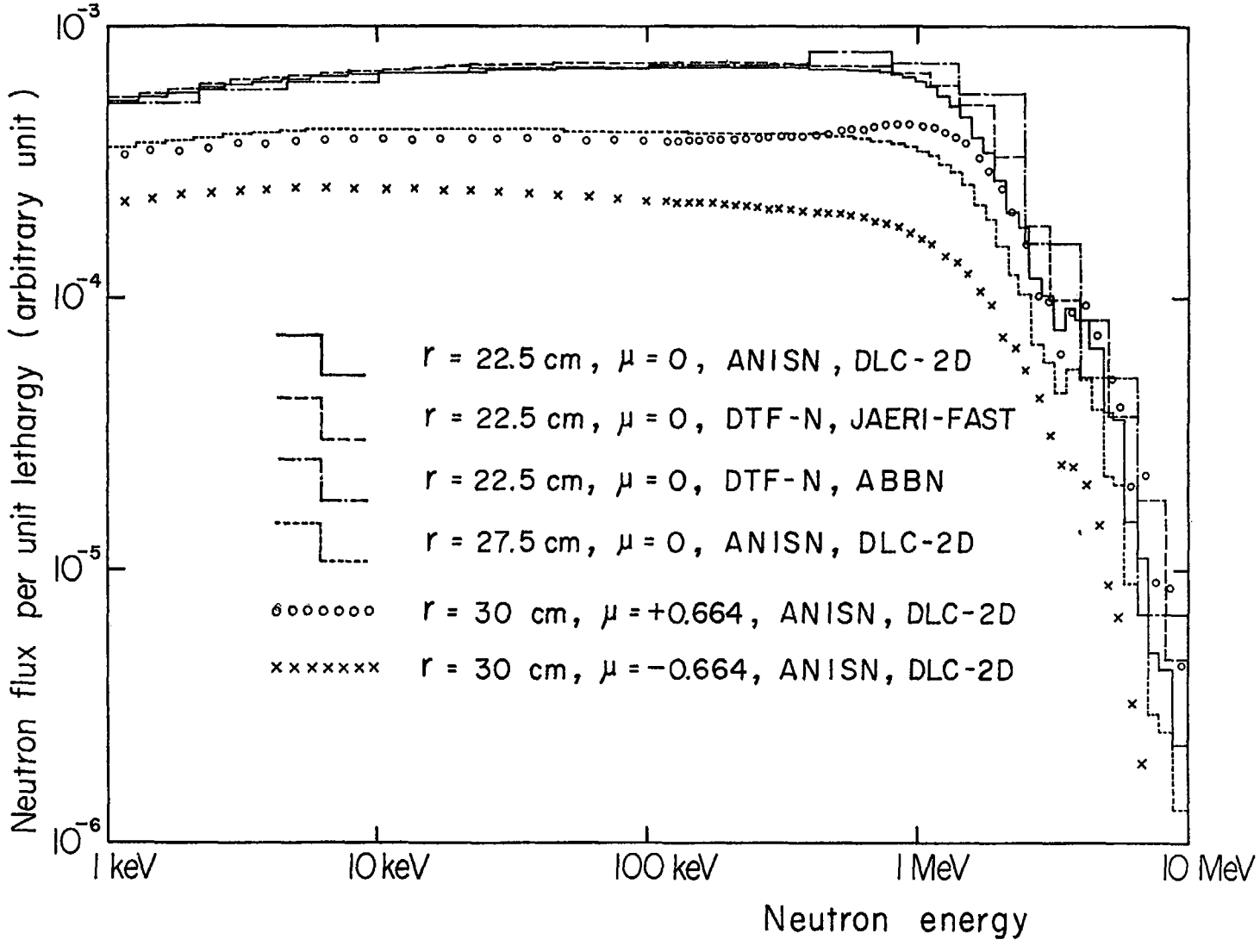

Fig. 7 Theoretically predicted neutron spectra in the borated graphite pile.

II.8. QUALITY CONTROL AND CALIBRATION OF MINIATURE FISSION CHAMBERS BY EXPOSURE TO STANDARD NEUTRON FIELDS. APPLICATION TO THE MEASUREMENT OF FUNDAMENTAL INTEGRAL CROSS SECTION RATIOS

A. FABRY

Reactor and Energy Development Division
C.E.N.-S.C.K., MOL, BELGIUM

I. GÂRLEA

Reactor Development Section
ITN, BUCHAREST, RUMANIA

SUMMARY

The intermediate-energy standard neutron field at the MOL-ΣΣ facility and an associated reference Maxwellian thermal neutron field have been used for quality control and calibration of ten miniature commercial absolute ionization fission chambers containing the fissionable isotopes ^{235}U, ^{239}Pu, ^{233}U, ^{241}Pu, ^{238}U, ^{237}Np and ^{232}Th.

The performance of the chambers is found very good, but the fission foil mass assay data as provided by the supplier are generally inaccurate and sometimes grossly in error.

Using these chambers on basis of the present calibrations, high-accuracy microscopic integral fission cross section ratios are determined; for the MOL-ΣΣ neutron field, they are (1.000 : 1.173 ± 0.025 : 1.543 ± 0.032 : 1.365 ± 0.030) for ^{235}U : ^{239}Pu : ^{233}U : ^{241}Pu respectively; for another fundamental neutron field, the thermal-neutron induced uranium-235 fission neutron spectrum, they are (1.000 : 1.504 ± 0.032 : 1.564 ± 0.036 : 1.342 ± 0.036 : 0.254 ± 0.009 : 1.109 ± 0.039) for ^{235}U : ^{239}Pu : ^{233}U : ^{241}Pu : ^{238}U : ^{237}Np respectively. These new measurements compare most favourably with previous interlaboratory data whenever available. The ^{233}U and ^{241}Pu fission cross sections are measured for the first time in these standard neutron fields. In the thermal neutron induced uranium-235 fission neutron spectrum, the corresponding integral microscopic cross sections are (1881 ± 64) mb and (1614 ± 60) mb for the $^{233}U(n,f)$ and $^{241}Pu(n,f)$ reactions respectively, accepting a value of (1203 ± 30) mb for $^{235}U(n,f)$.

SCOPE AND OBJECTIVES

The accurate determination of absolute fission rates and of microscopic fission cross sections is of mandatory importance in many areas of nuclear science and technology, e.g. reactor physics, fuel burn up, safeguards, fuels and materials dosimetry, ...

Such measurements are generally performed by means of (or are related to) absolute fission chambers. The accuracy goals are of $\pm$ 1 - 3 % (depending on the isotope) at the 68.3 % (1 σ) confidence level, and meeting them is not a trivial task. In particular, the mass assay of the fissionable deposits - used in the chambers or applied with other detecting devices, such as solid state track recorders - is a demanding undertaking and may require the use of different methods : mass isotopic dilution, quantitative deposition, gravimetric analysis, absolute alpha and/or fission counting, ... Ideally, all of the above methods should be applied independently so as to eliminate systematic errors, but in practice, this is seldomly done, except for the establishement of standard fissionable deposits. Relative alpha and/or fission counting comparisons with respect to the standards allow then to derive the masses of the working deposits.

If often happens however that the fissionable material is not accessible for alpha measurements because it is conceiled within the chambers at the time of their manufacture. Such sealed chambers are available commercially or on a semi-commercial basis; whether they are sold as absolute or as relative instruments, it is necessary to check their performances and, in addition, their calibration if absolute fission rates are to be measured routinely. Relevant quality controls and calibrations (or calibration checks) may be achieved by exposure of these chambers to a standard neutron field in which the fission rates to be expected for any given isotope are well known, from literature or because they have been previously assessed with standard deposits.

Monochromatic thermal neutron beams or Maxwellian thermal neutron fields of known intensity may be used for such purposes, but display the following shortcomings :

they are not applicable to the case of threshold fission reactions

systematic errors may be serious, unless the fission counting involves only the intercomparison of chambers very similar in design.

For threshold reactions, the solution may be exposure to a fission spectrum neutron field such as, for example, the one of a californium-252 point source of known strength.
The intermediate-energy standard neutron field at the MOL-ΣΣ facility [1] provides an ideal test bed for all fissionable isotopes of current interest. This facility (Fig. 1) is implemented within a 50 cm diameter spherical cavity hollowed out from a conventional graphite thermal column; the standard configuration is constituted by a ~ 5 cm thick natural uranium spherical source, ~ 25 cm outer diameter, surrounding a concentric natural boron carbide shell at the centre of which the standard neutron field is generated. Interlaboratory and international comparisons of absolute reaction rate measurements in MOL-ΣΣ are currently pursued and have already established [2] central fission rate scales for ^{235}U, ^{239}Pu, ^{238}U and ^{237}Np with accuracies of $\pm$ 1.3 %, $\pm$ 1.6 %, $\pm$ 1.8 % and $\pm$ 2.5 % respectively; these scales are relative to a highly redundant run-to-run flux level monitoring system whose long as well as short term precision is better than $\pm$ 0.5 % . The MOL-ΣΣ standard is permanently available and is reproducible; it has indeed been duplicated at other laboratories and experimental demonstration of its neutronic reproducibility has been achieved [3][4] .

In addition to the MOL-ΣΣ facility, two other standard neutron fields have been used for this work :

a Maxwellian thermal neutron field, of neutron temperature 20°C [5] , existing at the centre of the 50 cm spherical cavity when ΣΣ is removed from the BR1 reactor horizontal thermal column

a thermal-neutron induced uranium-235 fission neutron spectrum, the Mol Cavity Fission Spectrum Neutron Field [6], consisting (Fig. 2) of a cylindrical, thin uranium-235 source shell centered in a one-meter diameter spherical cavity of BR1 vertical thermal column; this source is concentric to a long cadmium tube aimed at suppressing the thermal neutron background; the fission chambers are easily inserted at any position into this tube, as shown on Fig. 2.

Once calibrated with suitable accuracy, the commercial fission chambers may be used for the measurement of absolute fission cross sections and ratios. This has been done in the course of this work and the results are reported below.

EXPERIMENTAL DETAILS

This work involves a set of 10 commercial, parallel-plate, gas ionization sealed fission chambers purchased from CEA, Saclay [7], and to be used for the Belgian and Rumanian fast reactor physics and neutron dosimetry programs.
Two models of chambers, I and II, have been studied; they essentially differ in diameter only. Table 1 gathers the major nominal data relative to these chambers.

The fission chambers have been operated by means of the triple scaler counting system described by GRUNDL et al. [8]. Pulse-height distributions have furthermore been recorded by means of a 400 channel analyser.
For all chambers, the fission layer thicknesses ($\mu gr/cm^2$) differ relatively little. It has been found that a same extrapolation-to-zero pulse height (ETZ) correction could be applied in all cases within uncertainties. For a discriminator level set at ~ 54 % of the fission fragment main peak, this correction is 1.0135 ± 0.0015, after proper consideration of dead time (dead time : 4.4 μsec for a bias at 36 % of the peak, 4.0 μsec at 54 % of the peak) and alpha pile-up effects, including pile-up between alpha and true fission fragment pulses in the valley of the pulse-height distribution. Such ETZ correction is about twice as much as would be

expected [8] for perfectly absolute chambers; it is believed that this departure is due to fragments emerging from the fission layers under small or grazing angles and for which only part of the associated gas ionization is effectively collected because these fragments escape the zone of strong electric field after crossing a fraction only of their range.

Table 2 gathers all raw count rates observed in the three neutron fields. Quoted uncertainties are statistical only (1 σ confidence interval). These results are averaged over a number of independent runs for which internal and external errors were found consistent.

The major corrections and uncertainties involved in transforming the observed chamber count rates into isotopic fission rates per nucleus are listed in table 3.
The corrections for fission of impurity isotopes in thermal neutron field irradiations are negligible for all exposed chambers. In this neutron field, only fission rate ratios between various of the considered chambers have been looked at, so that the instrumental perturbation can be assumed unity for all chambers with a same diameter, say model I; the change in this perturbation when comparing model I and II chambers is 1.1 %, and has been measured by comparing ^{233}U chambers n° 30 (model II) and n° 1384 (model I).

The chamber responses in the Cavity Fission Spectrum Neutron Field differ from the ones that would be observed in an ideal thermal neutron-induced uranium-235 fission neutron spectrum. The corrections necessary to account for such differences have been extensively studied [6], both experimentally and theoretically. They are summarized in table 4.
Table 5 shows that for what concerns the dominating correction, e.g. cavity wall return neutron backgrounds, excellent agreement is obtained between measured and computed (discrete-ordinates transport theory [9]) data : the table compares measured and predicted ratios

$$\frac{\bar{\sigma}_W}{\bar{\sigma}_\chi} = \frac{\int_{E_{Cd}}^{\infty} \Phi_W(E)\, \sigma(E)\, dE}{\int_0^{\infty} \chi_5(E)\, \sigma(E)\, dE}$$

The discrepancies are catastrophic for ^{238}U and ^{232}Th, bad for ^{235}U, acceptable for ^{241}Pu. Agreement is good for one of the ^{233}U chambers and bad for the other.

The conclusion is that nominal foil mass assay data for commercial fission chambers are generally not trustworthy and this is confirmed by the data obtained in the Cavity Fission Spectrum Neutron Field; these data also confirm that the calibration data obtained from exposure of the chambers in Mol-ΣΣ are of good accuracy, e.g. of the order of $\pm$ 1 - 1.5 % or better insofar as mass ratio data are concerned.

As already noticed, no concensus interlaboratory fission cross section data are available for ^{233}U and ^{241}Pu in the ΣΣ neutron spectrum. Therefore, the recommanded fission foil masses have been derived from the thermal neutron field exposures, accepting

- the ^{235}U mass as established in ΣΣ for chamber 23
- the recent "Third IAEA Evaluation of the 2200 m/sec and 20° C Maxwellian Neutron Data for ^{233}U, ^{235}U, ^{239}Pu and ^{241}Pu" [11] .

The reliability of such approach has been verified by applying it also to the ^{239}Pu over ^{235}U fission rate ratio. This ratio can be compared to the interlaboratory data in both the Mol-ΣΣ and the Mol Cavity Fission Spectrum Neutron Fields : this is done in the first line of experimental results, table 7. Remarkable confirmation of the accuracy of this method is obtained.

For threshold reactions, it is as well easy to define integral cross section ratios in the fission spectrum on basis of the fission foil masses derived from Mol-ΣΣ irradiations.

Table 7 presents a summary of all the integral fission cross section ratios obtained in this work and compares them with interlaboratory results when available.
The agreement is gratifying.

for the carbon wall return average cross section $\bar{\sigma}_W$ to the fission spectrum average cross section $\bar{\sigma}_\chi$, where

$\Phi_W(E)$: wall return neutron flux spectrum, normalized : $\int_{E_{Cd}}^{\infty} \Phi_W(E)\, dE = 1$

$\chi_5(E)$: uranium-235 fission spectrum, normalized : $\int_0^{\infty} \chi_{25}(E)\, dE = 1$

E_{Cd} : cadmium cut-off energy for 1 mm thick cadmium in cylindrical geometry.

An error of $\pm$ 5 % in this ratio entails an uncertainty smaller than $\pm$ 0.5 % in the wall return correction factors given in table 4.

RESULTS AND CONCLUSIONS

Table 6 summarizes the calibration data for the 10 chambers as obtained from analysis of the exposures at center of the Mol-ΣΣ Standard Neutron Field. Recommanded foil masses, presented as number of nuclides in the last column of the table, have been derived by imposing that the fission rate for each principal isotope as deduced from observed count rates and nominal foil masses, should be equal to the expected one . For the nuclides ^{235}U, ^{238}U, ^{239}Pu and ^{237}Np, the expected fission rates are the ones recommanded as result of the sustained and systematic interlaboratory comparison in Mol-ΣΣ [2]; for ^{232}Th, preliminary RCN data [10] in ΣΣ have been taken as reference and uncertainties here are of the order of ~ $\pm$ 3%, in contrast to uncertainties ranging from $\pm$ 1.2 % to $\pm$ 2 % for the previous nuclides. For ^{233}U and ^{241}Pu, the expected values have been determined from the thermal neutron field irradiations performed in the course of the present work (see below).

It is assumed here that all chambers have a fission fragment collection efficiency of 100 % after correction for absorption within deposits and extrapolation to zero pulse height.

For the nuclides ^{239}Pu and ^{237}Np, the deduced foil masses agree well with the ones provided by the supplier.

REFERENCES

[1] FABRY A., DE LEEUW G. and S. - Nucl. Techn. 25, 349 (1975).

[2] PINTER M. et al. - Nuclear Cross Sections and Technology Conference, paper DB 8, Washington D.C., March (1975).

[3] GIRLEA I., MIRON C. and FABRY A. - Report BLG 512, CEN-SCK Belgium/ ITN Rumania (February 1976).

[4] FABRY A., WILLIAMS J.G. et al. - Paper to be presented at the IAEA Consultants' Meeting on "Cross Sections Measurements in Standard Neutron Fields" Vienna, November 15-19 (1976).

[5] POORTMANS F., GIRLEA I. and FABRY A. - Nucl. Phys. A 172, 489 (1971).

[6] FABRY A., GRUNDL J.A., EISENHAUER C. - Nuclear Cross Sections and Technology Conference, paper DB 7, Washington D.C., March (1975).

[7] GUERY M. and JARRIGE A. - Revue de Physique Appliquée, tome 6, 121, Juin (1971).

[8] GRUNDL J.A., GILLIAM D.M., DUDEY N.D., POPEK R.J. - Nucl. Techn. 25, 237 (1975).

[9] FABRY A., JENKINS J.D. - Trans. ANS, 15, 940 (1972).

[10] VAN DER KAMP H.A.J., QUAADVLIET W.H.J. - STEK Memo n° 40, Reactor Centrum Nederland, Private Communications (1972 - 1974).

[11] LEMMEL H.D. - Nuclear Cross Sections and Technology Conference, paper EA 2, Washington D.C., March (1975).

[12] FABRY A. - Report NEACRP - L-140 (1975).

[13] FABRY A. - Report BLG 465 (1972).

TABLE 1. MAJOR FEATURES OF THE COMMERCIAL MINIATURE FISSION CHAMBERS

1. MAIN GEOMETRICAL AND PHYSICAL SPECIFICATIONS

TYPE OF CHAMBERS : gas ionization, parallel-plate, sealed.

CHAMBER SIZE : MODEL I : 20 mm O.D., 5.5 mm thick
MODEL II : 12 mm O.D., 5.5 mm thick.

MATERIAL : zircalloy except insulators (steatite); deposit backings : zircalloy.

TOTAL CHAMBER WEIGHTS : 6.5 gr (model I) and 2.3 gr (model II).

FILLING GAS : argon (12 bars) INTERELECTRODE DISTANCE : 0.5 mm.

DIAMETER OF FISSIONABLE DEPOSITS : 15 mm (model I) and 8 mm (model II).

2. MAIN NUCLEAR SPECIFICATIONS, NOMINAL

PRINCIPAL ISOTOPE	CHAMBER IDENTIFICATION	TOTAL DEPOSIT MASS (μgr)	ISOTOPIC COMPOSITION, atom percent
	MODEL I		
^{235}U	23	96.6 (± 1.7%)	99.89% ^{235}U, 0.02% ^{234}U, 0.04% ^{236}U, 0.07% ^{238}U
^{239}Pu	24	95.24 (±0.15%)	99.88% ^{239}Pu, 0.12% ^{240}Pu
^{239}Pu	1383	92.17 (± 0.3%)	"
^{237}Np	25	83.5 (± 0.3%)	~ 100% ^{237}Np, 0.4 ppm ^{239}Pu
^{238}U	26	95.75 (± 0.9%)	~ 100% ^{238}U, 200 ppm ^{235}U
^{238}U	27	84 (± 0.9%)	~ 100% ^{238}U, 400 ppm ^{235}U
^{232}Th	1381	116.1 (± 3.2%)	~ 100% ^{232}Th, < 0.16% natural uranium
^{233}U	1384	89.10 (± 0.6%)	99.44% ^{233}U, 0.522% ^{234}U, 0.016% ^{235}U, 0.018% ^{238}U
	MODEL II		
^{233}U	30	73.51 (±0.41%)	99.44% ^{233}U, 0.522% ^{234}U, 0.016% ^{235}U, 0.018% ^{238}U
^{241}Pu	19	55.02 (± 0.2%)	98.55% ^{241}Pu

TABLE 2. RAW FISSION CHAMBER COUNT RATES IN THE THREE STANDARD NEUTRON FIELDS

CHAMBER IDENTIFICATION AND PRINCIPAL ISOTOPE		RELATIVE CHAMBER COUNT RATE[a]		
		THERMAL[b] FIELD	MOL-ΣΣ[b]	FISSION SPECTRUM
^{235}U	23	79.07 (± 0.2%)	0.1700 (± 0.2%)	1 [c]
^{239}Pu	24	113.1 (± 0.4%)	0.2064 (± 0.3%)	1.520 (± 0.4%)
^{239}Pu	1383	109.9 (± 0.7%)	0.2015 (± 0.4%)	-
^{238}U	26	-	0.00902_5 (± 1.2%)	-
^{238}U	27	-	0.00735_5 (± 0.8%)	0.1655 (± 0.5%)
^{237}Np	25	-	0.0607_4 (± 0.3%)	0.8764 (± 0.3%)
^{232}Th	1381	-	0.002104 (± 2.6%)	0.0487 (± 2.5%)
^{233}U	30	57.03 (± 0.3%)	0.2020 (± 0.3%)	1.328 (± 0.7%)
^{233}U	1384	72.84 (± 0.4%)	0.2608 (± 0.3%)	1.716 (± 0.5%)
^{241}Pu	19	85.10 (± 0.2%)	0.1327 (± 0.3%)	0.8256 (± 1%)

[a] Count rates above main discriminator bias, corrected for dead-time losses and alpha pile up (if any), given with respect to reference indicated by appropriate footnote.

[b] Reference : long-term fission chamber flux level monitor installed at the Mol-ΣΣ facility in June 1974.

[c] Reference.

TABLE 3. CORRECTIONS AND UNCERTAINTIES [a]

SOURCE OF CORRECTION AND/OR UNCERTAINTY	CORRECTION	UNCERTAINTY [b]
Counting statistics	-	± 0.2 - ± 2.5%
Dead-time losses	1.000 - 1.004	0 - ± 0.05%
Undetected fission fragments:		
· extrapolation-to-zero pulse height	1.007 [c]	± 0.4%
· absorption in deposit	0.66 - 0.69% for 100 μgr/cm^2	± 0.35%
Fission of impurity isotopes	1.000 - 0.992$_9$	0 - ± 0.2%
Instrumental perturbation [d]	0.995 - 1.006	± 0.3 - 0.6%
Chamber positioning	-	± 0.2 - 0.3%
Flux level :		
· run-to-run monitoring	-	± 0.5% or better
· long-term normalization	-	± 0.5% (ΣΣ)

[a] Applies to both Mol-ΣΣ and the cavity fission spectrum neutron source, but, for the later case, additional corrections are needed for backgrounds and for perturbations due to the neutron field structural components; the associated uncertainty is ± 1% but is not propagated for quality control purposes (see text)..

[b] For a 68.3% confidence interval (1 σ).

[c] Except for ^{239}Pu, ^{233}U and ^{241}Pu, where the alpha cut-off is much higher : the main discriminator bias has been placed at about half the fission fragment peak in the pulse-height distribution and the extrapolation-to-zero was then 1.014 (± 0.5%); even at this bias, a correction for alpha pile-up must be applied (0.5 - 1.4% in ΣΣ, 3 - 4% in cavity fission source, depending on reactor power; measured at shutdown) ; the uncertainty due to this correction is included in the counting statistics.

[d] Encompasses all neutron field perturbations due to insertion of the instrument, e.g. perturbation due to neutron scattering and absorption by the chambers(1.003 - 1.006 ± 0.003 for threshold reactions, 1.000 ± 0.003 for non-threshold ones), and access hole perturbation for ^{233}U, ^{235}U, ^{239}Pu and ^{241}Pu chambers in ΣΣ (0.995 ± 0.005).

TABLE 4. CORRECTION FACTORS FOR BACKGROUND RESPONSES AND NEUTRON FIELD PERTURBATIONS IN THE CAVITY FISSION SPECTRUM NEUTRON FIELD MEASUREMENTS

TYPE OF CORRECTION	NUCLIDE					
	^{235}U	^{233}U	^{239}Pu	^{241}Pu	^{237}Np	^{238}U
Wall return background	0.8636	0.7810	0.8923	0.7995	0.9975	0.9978
Photofission, epithermal and thermal neutron penetration	0.9907	0.9939	0.9840	0.9939	0.9967	0.9935
Impurity isotopes	0.9992	0.9968	0.9991	1.000	1.000	0.9984[a]
Cadmium sleeve perturbation	0.991	0.991	0.991	0.991	1.001	1.010
Instrumental perturbation	1.000	1.000	1.000	1.000	1.003	1.006
Net correction	0.8472	0.7668	0.8693	0.7875	0.9982	1.0056

[a] Chamber 27.

TABLE 5. $\bar{\sigma}_W/\bar{\sigma}_\chi$: INTEGRAL CROSS SECTION RATIO FOR FISSION BY GRAPHITE WALL RETURN AND FISSION SPECTRUM NEUTRONS (MOL 1 METER SPHERICAL CAVITY).

NUCLIDE	MEASURED	COMPUTED	DIFFERENCE
^{235}U	9.07(± 4%)	9.37	- 3.3%
^{239}Pu	6.93 (± 4%)	6.67	+ 3.9%
^{233}U	16.1 (± 5%)	15.9	+ 1.3%
^{241}Pu	14.4 (± 5%)	14.8	- 2.8%

TABLE 6. MASS ASSAY DATA FOR THE MINIATURE COMMERCIAL FISSION CHAMBERS : CALIBRATION BY EXPOSURE AT CENTER OF THE MOL-ΣΣ STANDARD NEUTRON FIELD

CHAMBER IDENTIFICATION AND PRINCIPAL ISOTOPE		ΣΣ CENTRAL FISSION RATE PER NUCLEUS OF PRINCIPAL ISOTOPE PER $^{115}In(n,n')^{115m}In$ NORMALIZATION COUNT[a][b]		ERROR IN NOMINAL DEPOSIT MASS	NUMBER OF PRINCIPAL ISOTOPE NUCLIDES IN FISSIONABLE DEPOSIT, ΣΣ RECOMMANDATION[b] ($\times 10^{17}$)
		FROM NOMINAL FISSIONABLE DEPOSIT MASS	EXPECTED		
^{235}U	23	24.88	26.98 (± 1.3%)[2]	+ 8.4%	2.281 (± 1.6%)
^{239}Pu	24	31.15	31.56 (± 1.8%)[2]	+ 1.3%	2.367 (± 1.8%)
	1383	31.38	"	+ 0.6%	2.310 (± 1.8%)
^{238}U	26	1.358	1.512 (± 1.6%)[2]	+ 11.3%	2.178 (± 3.0%)
	27	1.257	"	+ 20.3%	1.768 (± 2.4%)
^{237}Np	25	10.47	10.47 (± 2.5%)[2]	0%	2.123 (± 2.4%)
^{233}U	30	38.86	41.63 (± 1.8%)[c]	+ 7.1%	1.764 (± 1.8%)
	1384	40.93	"	+ 1.7%	2.265 (± 1.8%)
^{241}Pu	19	35.58	36.83 (± 2.0%)[c]	+ 3.5%	1.310 (± 1.9%)
^{232}Th	1381	0.254	0.356 [d] [10]	+ 40%	2.153 (± 6.0%)

[a] Normalization procedure discussed in references [1][2] .

[b] Quoted uncertainties are for a 68.3% confidence interval.

[c] This work, thermal neutron field calibrations.

[d] No final assessment of error yet available but the magnitude is < 5%.

TABLE 7. INTEGRAL FISSION CROSS SECTION RATIOS IN TWO STANDARD NEUTRON FIELDS

CHAMBER IDENTIFICATION AND PRINCIPAL ISOTOPE		INTEGRAL CROSS SECTION RATIO $\bar{\sigma}/\bar{\sigma}_f$ (^{235}U)			
		MOL-ΣΣ		^{235}U FISSION SPECTRUM	
		This work[a]	Literature[b]	This work[a]	Literature
^{239}Pu	24	1.170 (± 0.6/1.5%)	1.167 (± 2.0%) [2]	1.504 (± 0.6/1.5%)	1.505 (± 2.2%)[6]
	1383	1.176 (± 0.8/1.5%)		-	
^{233}U	30	1.543 (± 0.5/1.5%)	-	1.563 (± 0.8/1.6%)	-
	1384	1.543 (± 0.6/1.5%)		1.564 (± 0.7/1.6%)	
^{241}Pu	19	1.365 (± 0.5/1.7%)	-	1.342 (± 1.0/1.7%)	-
^{238}U	26	-	[0.0561 (± 1.5%)][2]	-	0.254 (± 2.0%)[6]
	27	-		0.254 (± 1.0/2.5%)	
^{237}Np	25	-	[0.388 (± 2.5%)][2]	1.109 (± 0.5/3.0%)	1.091 (± 3.0%)[6](c)
^{232}Th	1381	-	[(0.0132[10])]	0.0612 (± 3.6/1.9%)[d]	0.0664 (± 4.5%)[13]

[a] Uncertainties for a 68.3% confidence interval. Respectively, random and systematic errors.

[b] Data within brackets used as reference to derive corresponding ratios in fission spectrum.

[c] Corrected according to reference [12] .

[d] Systematic error does not include the yet unknown contribution from ΣΣ reference data, last line, column 3.

TITLES OF FIGURES

Fig. 1 Cross-sectional sketch of the reference setup for fission chamber fission rate measurements in $\Sigma\Sigma$.

Fig. 2 Cross-sectional sketch of the setup for fission chamber fission rate measurements in the thermal-neutron induced uranium-235 fission neutron spectrum.

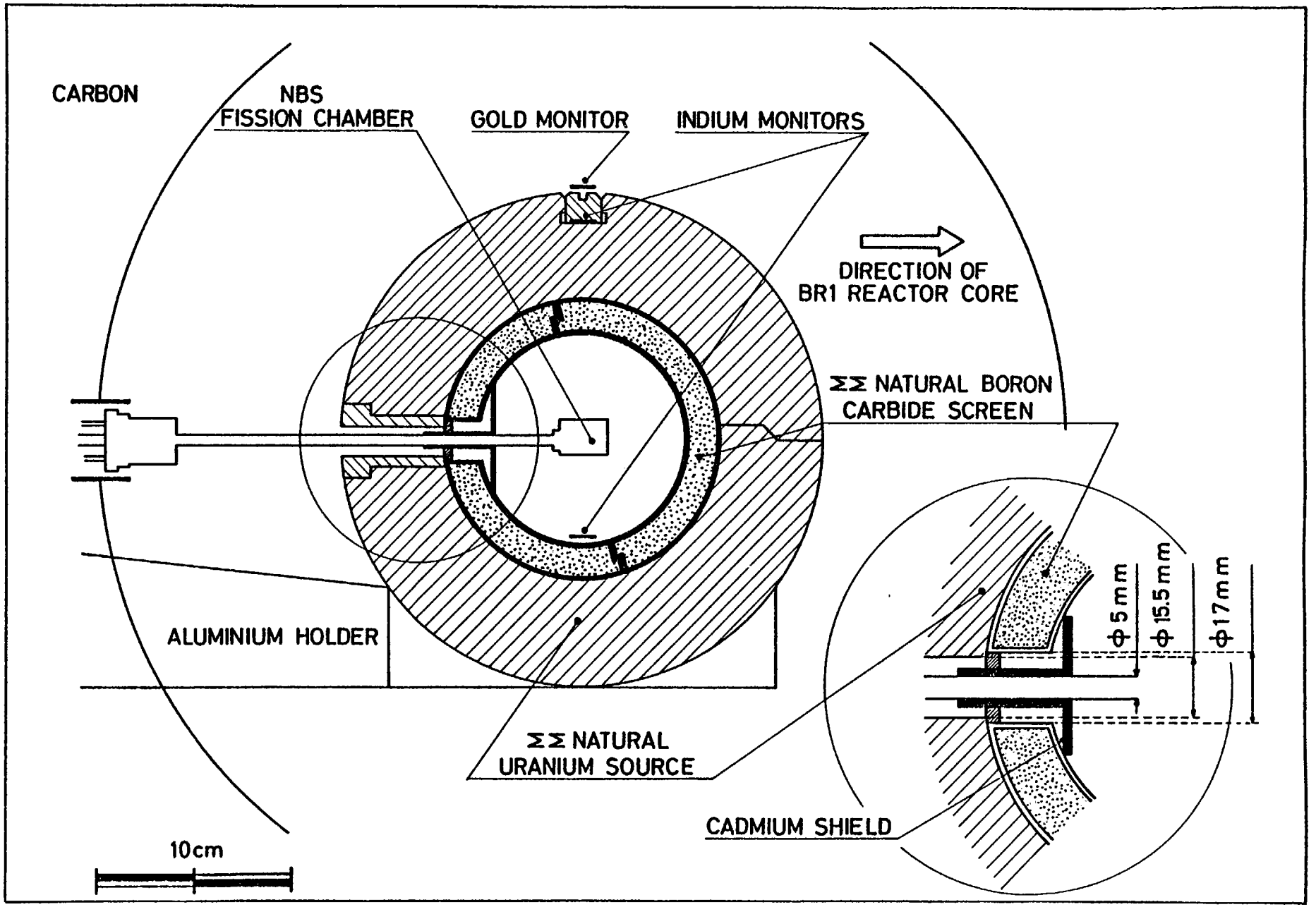
CARBON
NBS
FISSION CHAMBER
GOLD MONITOR
INDIUM MONITORS
DIRECTION OF
BR1 REACTOR CORE
ΣΣ NATURAL BORON
CARBIDE SCREEN
ALUMINIUM HOLDER
ΣΣ NATURAL
URANIUM SOURCE
CADMIUM SHIELD
φ5mm
φ15.5mm
φ17mm
10cm

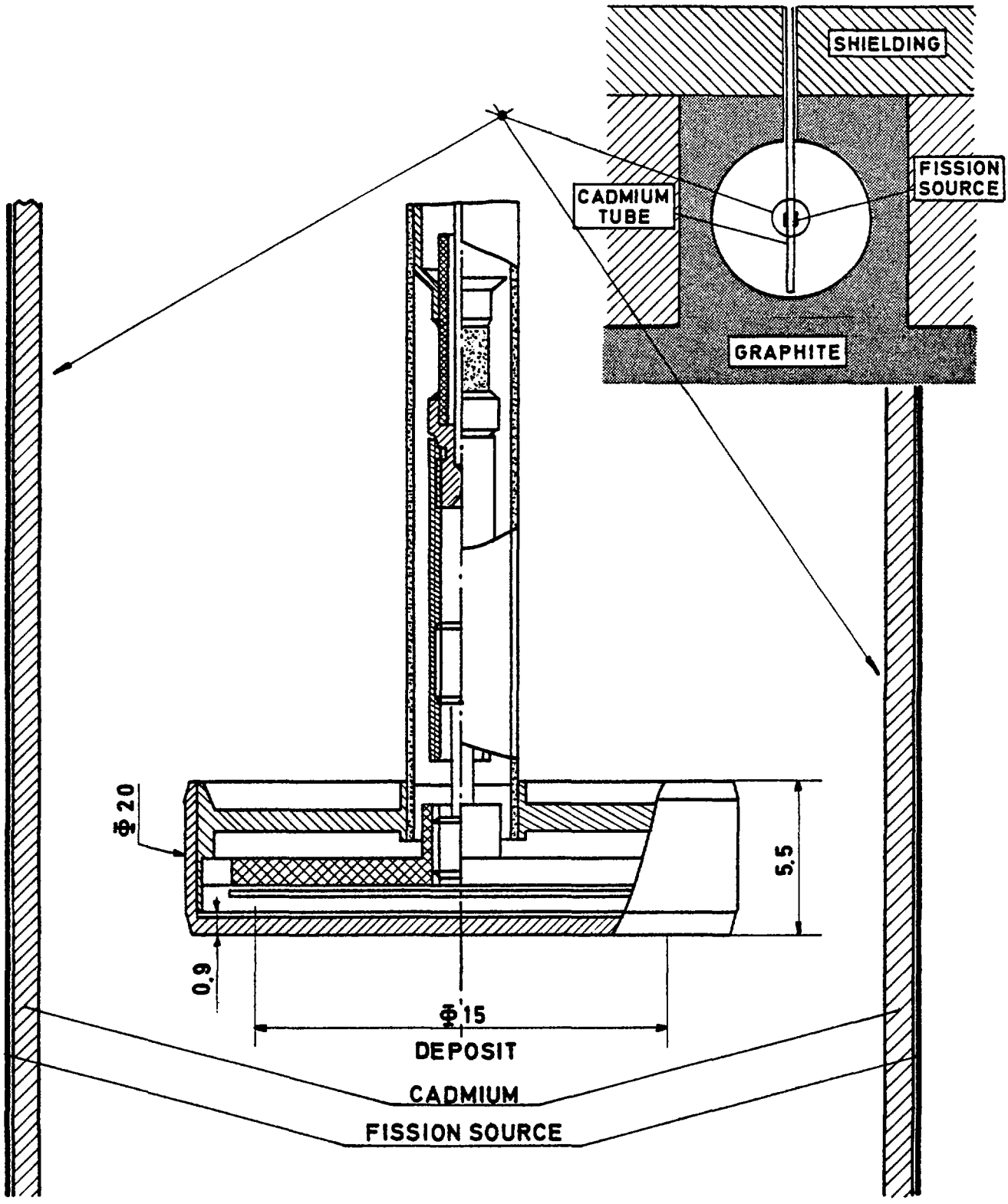
SHIELDING
FISSION SOURCE
CADMIUM TUBE
GRAPHITE
Φ 20
5.5
0.9
Φ 15
DEPOSIT
CADMIUM
FISSION SOURCE

II.9. MEASURING OF A FEW INTEGRAL DATA IN THE ΣΣ NEUTRON FIELD

I.Gârlea,C.Miron,M.Lupu,P.Ilie,A.Thurzó,N.Stănică,F.Popa
Institute for Nuclear Technology , Romania
and
G.Fodor
Institute of Atomic Physics, Romania

Abstract : Measurements of absolute reaction rates for the nonfissionable isotopes were obtained ,at Institute for Nuclear Technology (ITN) Romania, using activation detector foils exposed at the centre of ΣΣ. The average microscopic integral cross sections $\bar{\sigma}$ were obtained for the following reactions : $^{197}Au(n,\gamma)$, $^{115}In(n,\gamma)$, $^{115}In(n,n')$, $^{27}Al(n,\alpha)$, $^{46}Ti(n,p)$, $^{47}Ti(n,p)$, $^{48}Ti(n,p)$ and $^{58}Ni(n,p)$.

The same data, the absolute reaction rates and the average microscopic integral cross sections, for the principal fissionable isotopes were performed in the ΣΣ-ITN facility by means of absolute fission chambers. These average fission cross sections for ^{235}U, ^{239}Pu, ^{238}U, ^{237}Np, ^{232}Th, ^{233}U, ^{241}Pu were determined.

INTRODUCTION

In order to develop and to improve the neutronic measure - ments in the material testing and fast reactors, at the Institute for Nuclear Technology, the ΣΣ-ITN system was performed in cooperation with C.E.N./S.C.K. Mol Belgium.

In reference /1/ there are given the detailed description of the system and its neutronic characterization made by means of the ANISN code and ENDF/B III library. The identity between the ΣΣ-Mol and ΣΣ-ITN systems was demonstrated by calculations.

The measurements of the reaction rates /2/, fission densi - ties /3/ and neutron spectra /4/ confirmed this identity.

The existence of the ΣΣ facility allows the improvement of the experimental techniques and the obtaining of new integral data on the ΣΣ spectrum.

MEASUREMENT OF MICROSCOPIC INTEGRAL CROSS SECTIONS FOR NONFISSIONABLE ISOTOPES

1. Experimental details

The maximum thermal flux available in the ΣΣ-ITN (5.0×10^9 neutrons/ cm^2 s) allowed the beginning of a programme for measuring reaction rates for nonfissionable isotopes used in reactor dosimetry. In order to manipulate the multishell source of irradiated Uranium , there was constructed a cell with led blindage and vaccum devices for moving the shells. This permitted long time irradiations (~10 h), at the reactor nominal power (2 MW).

Figure 1 presents a transversal section in the thermal column of the VVRS-IFA reactor, with the ΣΣ-ITN facility inside.The positions of the principal monitors (two fission chambers) are indi-

cated. All detector foils were exposed at the centre of the ΣΣ-ITN using a boron carbide shell without access hole. In order to diminish the support effects, the foils were hung by means of a very thin wire (Ø = 50 um). There were exposed single-foils and packets of 3 foils to appraise the selfshielding effects in the ΣΣspectrum.

The fission chamber monitoring system is permanent and it is considered the principal reference for long time activation and fission chamber measurements. It allows both the flux determination for a certain irradiation and the correct obtainance of the flux profile needed in calculations. In the performed exposures, the gold foils placed on the fission chamber supports were also utilized as activation monitors.

The gamma induced activity was measured with a high-resolution Ge(Li) spectrometer (100 c.c.) coupled with a multichannel analyzer (4096 channels). The spectrometer is mounted in a low background shielding (1 m x 1 m x 1 m). In these measurements the distance source-crystal surface was 10 cm, the detectors being positioned on a special support. The absolute calibration was made by means of two reference source sets : one delivered by Amersham (England) and the other of ОГИС type (Soviet Union). The absolute activity of the reference source sets is known with errors varying from 1% to 2.5%, in the energy range 60 keV - 1.8 MeV.

The experimental values of the efficiency versus energy $\varepsilon(E)$ were fitted with a function

$$\varepsilon(E) = \sum_i a_i \, e^{b_i E} \qquad (i=5)$$

where the coefficients a_i and b_i were determined.

The gamma spectra were processed, using a code system which allowed the peak fitting, its area determination and the appraisal of the associated errors, where the Compton background substracted lineary or parabolically.

2. Experimental results

The used detectors and their physical characteristics are gathered in Table I. The impurities given in the table (indicated by the suppliers) do not alter significantly the experimental results (the application of the impurity correction improves the results by less than 0.3%).

The choice of detectors with certain geometrical characteristics was necessary in order to obtain gamma induced activities allowing their sufficiently accurate measuring with our spectrometer.

In Table III there are given the used reactions, the absolute reaction rates for 1 thermal neutron available in the system and the average microscopic integral cross sections for the $\Sigma\Sigma$spectrum . The $\bar{\sigma}$ values are compared with the calculated values using the ENDF/B IV library - Dosimetry file and normalized fluxes recommended for the $\Sigma\Sigma$ system in reference /5/. The values presented in Table III were determined by single-foil experiments.

The gamma selfabsorption and spread-source corrections were applied for absolute reaction rates. Figure 3 gives the gamma self-absorption curve. The spread-source corrections were determined experimentally with a point-wise source and they were compared with the calculations (see Fig.4).

The neutron selfshielding correction given in reference /5/ was applied only for the reaction $^{197}Au(n,\gamma)$. The single-foil and sandwich experiments made obvious that the neutronic selfshielding correction for used reactions(except $^{46}Ti(n,p)$, $^{47}Ti(n,p)$, $^{48}Ti(n,p)$ $^{197}Au(n,\gamma)$ and $^{115}In(n,\gamma)$) had not important values. For example , for $^{197}Au(n,\gamma)$ reaction $\bar{\sigma}_{single\text{-}foil}$ is 329.7 mb and $\bar{\sigma}_{sandwich}$ is 310.1 mb. The value 395 mb for a single-foil was obtained by applying the correction proposed in reference /5/. For the reactions $^{27}Al(n,\gamma)$, $^{58}Ni(n,p)$ and $^{115}In(n,n')$ the differences between cross

section values measured for single-foil and sandwich are about 1%-2%. This difference for reaction $^{115}In(n,\gamma)$ is about 4 %. This fact allows one to conclude that there is a neutronic selfshielding effect for the utilized detectors. There are discrepancies up to 6% between $\bar{\sigma}_{single\text{-}foil}$ and $\bar{\sigma}_{sandwich}$ for Ti due to the use of thick foils (1.2 mm thickness).

The appraised errors for the values in Table III are :

- statistical errors
- errors due the uncertainties in the absolute activity of the reference sources
- errors due the interpolation by the square least fitting method
- errors due the determination of gamma selfabsorption and spread-source correction values
- errors related to edge-correction determination.

The reaction rates are given with errors up to 3.5% - 4% , except Ti which has large associated errors (about 10 %).

The discrepancies between the measured and calculated values of microscopic integral cross sections are from 1% to 10%, except ^{46}Ti where there are 67%. The results for Ti are preliminary and a careful examination will be carried on by the authors.

FISSION RATE MEASURING IN THE ΣΣ-ITN NEUTRON FIELD BY MEANS OF ABSOLUTE FISSION CHAMBERS

The fission chambers used in this programme are given in Table II. They contain main fissionable isotopes : ^{235}U, ^{239}Pu, ^{237}Np , ^{233}U, ^{241}Pu, ^{232}Th, ^{238}U. These fission chambers (Saclay-type) have been calibrated by exposure in standard neutron spectra /6/. The uncertainties on the main isotope mass vary from 1.6% up to 3% (except ^{232}Th with an error about 5%).

1. Experimental arangement

The fission chambers were exposed at the centre of the ΣΣ-ITN system (Fig.2). To stop the penetration of thermal neutrons into the system by the access hole a Cadmium screen (1 mm thickness) shown in the figure detail has been used.

The used monitors were two fission chambers placed one in the ΣΣ-cavity and the other in the second vertical thermal channel (CT2) of the reactor graphite column. Both monitors were 4 mm diameter chambers containing depleted Uranium deposits. The first chamber placed in cavity wall contains 72 µg ^{238}U (+ 400 ppm ^{235}U) and the second - placed in CT2 - has 70 µg ^{238}U (+ 200 ppm ^{235}U). The counting rates (at the reactor power to 1 MW) were about 70 cps (for the first monitor fission chamber) and 600 cps (for the second).

The used associated electronic system for the processing is that proposed by Grundl /7/. A charge-sensitive preamplifier (coupled with a spectroscopy amplifier with 1 µs FHWM) was utilized. The setting is made by means of a precision pulse generator on the multichannel analyzer (parallely coupled with the amplifier output). The system has also three discriminators (100 MHz). The discrimination levels were fixed to $V_L = 0.36\ V_{PEAK}$, $V_U = 0.54\ V_{PEAK}$ and $V_{GC} = 1.4\ V_{PEAK}$. The V_{PEAK} value corresponded to the maximum of fission fragment spectrum.

2. Results and corrections

The dead-time of the measuring chain was determined for a range up to 5.10^4 cps and was 3.2 ± 0.5 µs, for the both count rates S_L and S_U.

For each set of observed values of S_L / S_U ratio the extrapolation to zero pulse-height (ETZ) correction /8/ was applied:

$$ETZ_{applied} = ETZ_{nominal} + 0.5\ (\ 3\ (S_L / S_U - 1) - ETZ_{nominal}\ )$$

slightly adjusted for small deparature from nominal expectations. The

nominal ETZ values exist in the reference /7/ and represent the result of a measurement under ideal count rate and signal-to-noise ratio conditions.

The impurity correction was calculated for every fission chamber. The impurity content taken into account is that given in Table II.

In Table III there are given the fission reactions for which there were determined the reaction rates and the average microscopic integral fission cross sections for the$\Sigma\Sigma$spectrum. The determined values are compared with the ones calculated by means of the ENDF/B IV library - Dosimetry file and of the normalized spectrum recommended in reference /5/.

The errors affecting the measurements do not exceed 4 %, except ^{232}Th (with an error of 6%) and they are:

- statistical errors about 0.5 %
- calibration errors (see Table II)
- run-to-run monitor level errors
- errors related to correction application.

The differences between measured and calculated values are up to 3 %.

The Table IV presents spectral index values (reffered to ^{235}U) determined in the $\Sigma\Sigma$-ITN şi $\Sigma\Sigma$Mol facilities. The obtained results for the$\Sigma\Sigma$Mol are those reported in references /9/ and /10/ and they were determined by means of various types of fission chambers. For the$\Sigma\Sigma$-ITN fission chambers Saclay and N.B.S. type there were utilized /2/. Between the fission rate ratio values for both systems there is a good agreement, except the $\overline{\sigma}_{237_{Np}} / \overline{\sigma}_{235_U}$ ratio for which the values obtained in this work are greater than those in all the other determinations.

REFERENCES

/ 1/. I.GIRLEA et al. - Standartnii spectr neitronov v oblasti promejutocinoi energii Instituta Iadernoi Tehnologii Śymposium , Predeal (1974) , Romania, p.982 (in Russian)

/ 2/. I.GIRLEA,C.MIRON,A.FABRY - Intercomparison of Fundamental Fission Rates and Ratios in the Intermediate Energy Standard Neutron Fields at ITN-ΣΣ and Mol- ΣΣFacilities BLG 512

/ 3/. I.GIRLEA,C.MIRON,P.ILIE - Măsurarea distribuţiei densităţii de fisiune prin metoda traselor în dielectrici(SSTR) Colocviul Naţional al Tineretului,Bucureşti,România,septembrie 1976

/ 4/. I.GIRLEA et al. - Neutron Spectrum Measurements Performed in ΣΣ-ITN Facility by Means of the Proton Recoil Counters To be published

/ 5/. A.FABRY,G.de LEEUW and S.de LEEUW - The Secondary Intermediate - Energy Standard Neutron Field at the Mol- ΣΣFacility , Nucl.Tech., vol.25 - Feb.1975

/ 6/. A.FABRY,I.GIRLEA - Quality Control and Calibration of Miniature Fission Chambers by Exposure to Standard Neutron Fields. Application to the Measurements of Fundamental Integral Cross Section Ratios
Paper presented at the IAEA Consultants´ Meeting on Integral Cross Section Measurements in Standard Neutron Fields, Vienna, Nov. 15-19,1976

/ 7/. J.GRUNDL et al. - Measurements of Absolute Fission Rates Nucl.Tech., vol. 25, no.2 (1975)

/ 8/. A.FABRY - Private comunication (1975)

/ 9/. M.PINTER et al. - Nuclear Cross Sections and Technology. Conf.paper DB 8, Washington D.C., March (1975)

/10/. A.FABRY,F.COOPS,J.GRUNDL,D.GILLIAM - Contribution to the 10^{th} ILRR Progress Report, unpublished (1975)

TABLE I : SPECIFICATION AND DIMENSION OF FOILS

Material	Thickness (mm)	Diameter (mm)	Purity %	Impurity (maximum percent)
Al	0.762	19.01	99.994	Mg(0.001), Cu(0.001), Fe(0.002), Ca(0.002)
Ni	0.254	12.70	99.981	Mg(0.001), Co(0.001), S(0.001), Si(0.001), Cu(0.001), Cr(0.001), Ti(0.001), C(0.001), Fe(0.001), Mn(0.001)
Au	0.127	19.00	99.998	
Ti	1.200	19.00	99.729	Cu(0.005),Sn(0.005), Cr(0.040), Mg(0.001), Ni(0.004) V(0.020), Si(0.005), Fe(0.120), Al(0.070), Mn(0.001)
In	0.127	19.00	99.9959	Cu(0.002), Pb(0.0018), Sn(0.0014), Cd(0.0007)

Au and In foils are received from C.E.N./S.C.K. Mol Belgium.

Al and Ni foils are delivered by Reactor Experiments, Inc. - U.S.A. and Ti foils by Koch-Light Lab.Ltd. (England).

TABLE II : MAIN NUCLEAR SPECIFICATIONS OF THE FISSION CHAMBERS

Principal isotope	Chamber identification	Total mass recomandation (µg)	Mass of principal isotope (µg/cm^2)	Number of principal isotope nuclid in fissionable deposit $\Sigma\Sigma$recomandation (x 10^{17})	Chamber isotopic composition atom percent
	MODEL I				
^{235}U	23	89.10 (±1.6%)	50.34	2,281 (±1.6%)	99.89% ^{235}U, 0.02% ^{234}U, 0.04% ^{236}U, 0.07% ^{238}U
^{239}Pu	24	94.04 (±1.8%)	53.13	2.367 (±1.8%)	99.88% ^{239}Pu, 0.12% ^{240}Pu
^{237}Np	25	86.06 (±2.4%)	48.70	2.123 (±2.4%)	~100% ^{237}Np, 0.4 ppm ^{239}Pu
^{238}U	26	83.54 (±3.0%)	47.30	2.178 (±3.0%)	~100% ^{238}U, 200 ppm ^{235}U
^{238}U	27	69.86 (±2.4%)	39.50	1.768 (±2.4%)	~100% ^{238}U, 400 ppm ^{235}U
	MODEL II				
^{233}U	30	68.62 (±1.8%)	135.70	1.764 (±1.8%)	99.44% ^{233}U, 0.522% ^{234}U, 0.016% ^{235}U, 0.018% ^{238}U
^{241}Pu	19	53.19 (±1.9%)	104.30	1.310 (±1.9%)	98.55% ^{241}Pu
^{232}Th	17	65.49 (±3.5%)	130.35	1.700 (±3.5%)	~100% ^{232}Th, <0.16% natural Uranium

MODEL I : 20 mm O.D., 5.5 mm thickness, 15 mm diameter of fissionable deposit

MODEL II : 12 mm O.D., 5.5 mm thickness, 8 mm diameter of fissionable deposit

TABLE III : MICROSCOPIC INTEGRAL CROSS SECTIONS IN THE ΣΣ-ITN BENCHMARK

REACTION	REACTION RATE[a] (x 10^{27})	$\bar{\sigma}_{measured}$ (mb)	$\bar{\sigma}_{calculated}$ $\int_0^\infty {}^i_r\sigma(E)\phi(E)dE$[b] (mb)	MEASURED/CALCULATED
$^{197}Au(n,\gamma)^{198}Au$	291 ± 3.5 %	395 ± 13	373.5	1.058
$^{115}In(n,\gamma)^{116m}In$	191.6 ± 3.5 %	260.2 ± 9	285.0	0.913
$^{115}In(n,n')^{115m}In$	40.4 ± 3.5 %	54.8 ± 1.9	55.2	0.993
$^{58}Ni(n,p)^{58}Co$	18.65 ± 3.5 %	25.32 ± 0.9	23.3	1.087
$^{27}Al(n,\alpha)^{24}Na$	0.116 ± 4 %	0.158 ± 0.07	0.152	1.039
$^{46}Ti(n,p)^{46}Sc$	1.695 ± 10 %	2.30 ± 0.2	2.070	1.111
$^{47}Ti(n,p)^{47}Sc$	3.68 ± 10 %	5.00 ± 0.5	5.150	0.971
$^{48}Ti(n,p)^{48}Sc$	0.046 ± 10 %	0.062 ± 0.006	0.037	1.675
^{235}U (n,f)	1114 ± 3.5 %	1512 ± 53	1525	0.991
$^{239}Pu(n,f)$	1311 ± 3.5 %	1780 ± 62	1735	1.026
$^{237}Np(n,f)$	444 ± 3.5 %	603 ± 22	607	0.993
^{238}U (n,f)	61.5 ± 4 %	83.46 ± 3.3	81.2	1.028
^{233}U (n,f)	1713 ± 4 %	2325 ± 93	-	-
$^{241}Pu(n,f)$	1493 ± 4 %	2026 ± 81	-	-
$^{232}Th(n,f)$	14.59 ± 6 %	19.8 ± 1.2	-	-

(a) Absolute central reaction rate per nuclid for a unit available thermal-neutron flux (calculated by transport theory).

(b) ${}^i_r\sigma$ (E) : ENDF/B IV Dosimetry file, $\phi(E)$ as recommended in /5/, normalized $\int_0^\infty \phi(E)dE=1$

TABLE IV : COMPARISON OF FISSION RATE RATIOS MEASURED IN THE ΣΣ-MOL AND ΣΣ-ITN BY MEANS OF FISSION CHAMBERS

RATIOS	ΣΣ- Mol		ΣΣ-ITN	
	INTERLABORATORY[9]	NBS CHAMBERS[10]	NBS CHAMBERS[2]	THIS WORK
$\frac{\bar{\sigma}(^{238}U)}{\bar{\sigma}(^{235}U)}$	0.0561 (±1.5%)	0.0564 (±2.5%)	0.0566 (±2.5%)	0.0552 (±2.5%)
$\frac{\bar{\sigma}(^{233}U)}{\bar{\sigma}(^{235}U)}$	1.543 (±0.5% / 1.5%)[6]		-	1.538 (±2.5%)
$\frac{\bar{\sigma}(^{239}Pu)}{\bar{\sigma}(^{235}U)}$	1.167 (±2%)	1.173 (±2.1%)	1.169 (±2.3%)	1.177 (±2.5%)
$\frac{\bar{\sigma}(^{237}Np)}{\bar{\sigma}(^{235}U)}$	0.388 (±2.5%)	0.381 (±2.9%)	0.380 (± 3%)	0.399 (± 3%)
$\frac{\bar{\sigma}(^{241}Pu)}{\bar{\sigma}(^{233}U)}$	1.365 (±0.5% / 1.7%)[6]		-	1.340 (±2.5%)
$\frac{\bar{\sigma}(^{232}Th)}{\bar{\sigma}(^{235}U)}$	0.0132[9]		-	0.0131 (± 7%)

II.10. Progress Report on Detector Cross Section Benchmark Measurements in the TAPIRO Reactor

M. Martini, P. Moioli, F. Sirito,

C.N.E.N.
Department of Technological Research
C.S.N. Casaccia, Rome

ABSTRACT

A program of irradiation of activation detectors aimed to improving the knowledge of their cross sections in under way in the core and reflector of the TAPIRO reactor.
This program follows the recommendations of the first IAEA Consultants' Meeting on detector cross sections, where TAPIRO was identified as a candidate benchmark spectrum for dosimetry reactions.
This report presents a comparison between activation measurements and predictions based on differential data for Category 1 and Category 2 reactions, some preliminary conclusions and the Suture program.

1. INTRODUCTION

This paper contains a provisional comparison between calculated and measured values of reaction rates for Category 1 and 2 detectors irradiated in the TAPIRO reactor at CNEN Casaccia, a first analysis of the discrepancies and a programme for future analysis.

2. CALCULATIONS OF THE NEUTRON SPECTRA

Two-dimensional transport calculations have been carried out in cylindrical geometry, with a very detailed geometrical description of the reactor. The geometry extends from the core through the copper reflector into the concrete biological shield. The energy group structure used is given in Table 1; 27 groups have been used throughout. The results of the spectrum calculations for the various experimental positions are given in Table 2.

3. MEASUREMENTS

Irradiations have been carried out in several positions in the core and the reflector; the normalization between calculated and measured value has been performed on U-235 fission rate at the core centre.

4. CATEGORY 1 DETECTORS

The comparison for category 1 detectors is given in Table 3; references for detector cross sections are given in table. Discrepancies are present especially inside the reflector. It should be noted for Mn that by re-normalizing the reaction rate at the first position in the reflector (r=10) there is a good agreement with further values calculated with ENDF/B-IV. On the whole it seems that, apart from the low-energy component at the outer part of the reflector, there is a reasonable agreement between the calculated and the measured reaction rates for Category 1 detectors.

5. CATEGORY 2 DETECTORS

The comparison for Category 2 detectors is given in Table 4. With respect to our previous evaluations it should be noted that:

a) For $^{59}Co(n,\gamma)$ the evaluation by Simons and McElroy is not satisfactory at low energies;

b) For $^{24}Mg(n,p)$ the agreement is satisfactory with the data from NDCC-74

c) For $^{54}Fe(n,p)$ the 25% discrepancy which had already been noted remains also in the reflector;

d) For $^{93}Nb(n,2n)$ the agreement with ENDF/B-III data is satisfactory only in the core.

6. FUTURE PROGRAMME

The future programme involves a major revision of the calculations of the neutron spectra. A 35 group structure will be used (see Table 1) which allows a better resolution at high energies and therefore more accurate reaction rates for threshold detectors. Calculations will be carried out with P3 or P5 instead of P1-equivalent cross sections. Other possible causes of errors will be investigated.

REFERENCES

/1/ A.FABRY, J.C.SCHEPERS, EANDC(E)127 v (1970)

/2/ R.L.SIMONS, W.N.McELROY, BNWL 1312 (1970)

/3/ ENDF/B-III, Evaluated Nuclear Data Files, Version 3 (1972)

/4/ Compilation of Threshold Reaction Neutron Cross Sections, NDCC (1974)

/5/ Cross Section Library, CCC 1128 of SAND-II

/6/ ENDF/B-IV, Evaluated Nuclear Data Files, Version 4 (1975)

TABLE 1

27 AND 35 ENERGY GROUP STRUCTURE

Lower energy limit	Group N. in 35 gr. structure	Group N. in 27 gr. stucture	Lower energy limit	Group N. in 35 gr. structure	Group N. in 27 gr. structure
13.50 MeV	1		907. KeV	27	
12.21 "	2		821. "	28	5
11.05 "	3		498. "	29	6
10.00 "	4		320. "	30	7
9.05 "	5		183. "	31	8
8.19 "	6		111. "	32	9
7.41 "	7		67.4 "	33	10
6.70 "	8		40.9 "	34	11
6.06 "	9	1	24.8 "		12
5.48 "	10		15.0 "		13
4.97 "	11		9.12 "		14
4.50 "	12		5.53 "		15
4.07 "	13		3.36 "		16
3.68 "	14	2	2.04 "		17
3.33 "	15		1.23 "		18
3.01 "	16		748. eV		19
2.73 "	17		545. "		20
2.47 "	18		275. "		21
2.23 "	19	3	101. "		22
2.02 "	20		37.3 "		23
1.83 "	21		13.7 "		24
1.65 "	22		5.04 "		25
1.50 "	23		.683 "		26
1.35 "	24	4	Thermal	35	27
1.22 "	25				
1.00 "	26				

TABLE 2

Calculated neutron spectra at 5 KW power

Group	r=0	r=10	r=20	r=30
1	.1807E+11	.1143E+10	.6067E+8	.6321E+7
2	.7907E+11	.5253E+10	.2620E+9	.2450E+8
3	.1623E+12	.1363E+11	.8176E+9	.8263E+8
4	.2137E+12	.2752E+11	.2454E+10	.3106E+9
5	.2213E+12	.4430E+11	.5646E+10	.8792E+9
6	.2104E+12	.6645E+11	.1289E+11	.2661E+10
7	.1720E+12	.7025E+11	.1809E+11	.4475E+10
8	.1125E+12	.5807E+11	.1884E+11	.5392E+10
9	.6325E+11	.4288E+11	.1781E+11	.5941E+10
10	.3126E+11	.2487E+11	.1195E+11	.4374E+10
11	.1473E+11	.1629E+11	.9L89E+10	.3625E+10
12	.5923E+10	.8292E+10	.5022E+10	.2082E+10
13	.2578E+10	.6556E+10	.4526E+10	.1997E+10
14	.1022E+10	.4484E+10	.3477E+10	.1626E+10
15	.5364E+9	.3687E+10	.3163E+10	.1851E+10
16	.1389E+9	.1548E+10	.1475E+10	.9259E+9
17	.4023E+8	.6241E+9	.6378E+9	.4148E+9
18	.1610E+8	.8565E+9	.9527E+9	.6769E+9
19	.5497E+7	.4848E+9	.5793E+9	.4392E+9
20	.2628E+6	.2147E+9	.2686E+9	.2120E+9
21	.1003E+6	.1312E+9	.1737E+9	.1567E+9
22	.2044E+5	.1317E+9	.1873E+9	.2020E+9
23	.3603E+5	.8883E+8	.1370E+9	.1789E+9
24	.5104E+4	.5951E+8	.9973E+8	.1485E+9
25	.2244E+4	.3286E+8	.5914E+8	.9873E+8
26	.6220E+4	.6730E+7	.1292E+8	.3047E+8
27	.3812E+2	.5925E+5	.1105E+7	.2846E+8

TABLE 3

Comparison of calculated and experimental reaction rates for category 1 detectors in different irradiation positions

Reaction ° Rate	Position r=0 Exp.	Calc.	E-C / C %	Position r=10 Exp.	Calc.	E-C / C %	Position r=20 Exp.	Calc.	E-C / C %	Position r=30 Exp.	Calc.	E-C / C %
$^{235}U(n,f)$	$7.40\ 10^{9}$ ±.37	7.40 /3/		$2.29\ 10^{9}$ ±.11	2.62	-12.6	$1.08\ 10^{9}$ ±.05	1.02	5.9	$5.79\ 10^{8}$ ±.29	5.45	6.2
$^{238}U(n,f)$	$1.09\ 10^{9}$ ±.05	1.07 /3/	2.3	$1.68\ 10^{8}$ ±.03	1.05	60.0						
$^{55}Mn(n,\gamma)$	$.997\ 10^{8}$	1.39 /3/	-28.3	$.498\ 10^{8}$	1.64	-69.6	$.425\ 10^{8}$	1.03	-58.4	$2.80\ 10^{7}$	7.25	-61.4
	±.49	1.25 /6/	-20.3	±.25	1.48	-66.4	±.81	1.23	-65.4	±.14	9.09	-69.2
$^{197}Au(n,\gamma)$	$1.05\ 10^{9}$ ±.05	.984 /2/	6.7	$1.06\ 10^{9}$ ±.05	.785	35.0	$8.37\ 10^{8}$ ±.41	5.37	-55.9	$6.29\ 10^{8}$ ±.31	4.61	36.4
$^{115}In(n,n')$	$1.44\ 10^{9}$	1.53 /2/	-5.9	$1.42\ 10^{8}$	1.80	-21.1	$1.58\ 10^{7}$	1.71	-7.6	$2.84\ 10^{7}$	3.42	17.4
	±.07	1.45 /1/	-.7	±.07	1.68	-15.5	±.07	1.58	0.	±.14	2.22	27.9
$^{58}Ni(n,p)$	$1.38\ 10^{9}$	1.38 /2/	0.	$.938\ 10^{8}$	1.06	-11.5	$6.23\ 10^{6}$	6.32	-1.4	$7.50\ 10^{5}$	6.65	12.9
	±.07	1.54 /1/	-10.4	±.47	1.23	-23.7	±.31	7.79	-20.0	±.37	8.60	-12.8
$^{27}Al(n,\alpha)$	$2.60\ 10^{7}$	2.05 /3/	26.8	$1.34\ 10^{6}$	1.30	3.1	$8.70\ 10^{4}$	6.88	26.5	$1.16\ 10^{4}$	.716	62.0
	±.13	2.11 /2/	23.2	±.06	1.34	0.	±.41	7.08	22.9	±.06	.736	57.6

° Absolute activities at saturation per gr of the irradiation isotope at 5 KW power

TABLE 4

Comparison of calculated and experimental reaction rates for category two detectors in different irradiation positions

Reaction ° Rate	Position r=0 Exp.	Calc.	E-C / C %	Position r=10 Exp.	Calc.	E-C / C %	Position r=20 Exp.	Calc.	E-C / C %	Position r=30 Exp.	Calc.	E-C / C %
$^{59}Co(n,\gamma)$	$2.08\ 10^{8}$ ±.12	1.99 /2/	4.52	$1.46\ 10^{8}$ ±.08	2.89	-49.5	$1.31\ 10^{8}$ ±.08	2.84	-53.9	$.990\ 10^{8}$ ±.59	2.75	-64.0
$^{23}Na(n,2n)$	$1.47\ 10^{5}$ ±.12	1.33 /3/	10.5									
$^{24}Mg(n,p)$	$4.53\ 10^{7}$ ±32	4.70 /4/	-3.6	$.274\ 10^{7}$ ±019	.297	-7.7						
$^{27}Al(n,\alpha)$	$.942\ 10^{8}$ ±.66	1.09 /2/	-13.6	$6.71\ 10^{6}$ ±.47	7.26	-7.6	$4.47\ 10^{5}$ ±.29	3.80	17.6	$2.68\ 10^{4}$ ±.18	3.76	-28.7
$^{54}Fe(n,p)$	$1.12\ 10^{9}$ ±.05	1.51 /2/	-25.8	$.830\ 10^{8}$ ±.04	1.11	-25.2						
$^{59}Co(n,\alpha')$	$1.88\ 10^{6}$ ±.13	2.25 /2/	-16.4	$1.42\ 10^{5}$ ±.09	1.43	-.7						
$^{63}Cu(n,\alpha)$	$8.60\ 10^{6}$ ±.51	7.11 /1/	21.0									
$^{64}Zn(n,p)$	$4.63\ 10^{8}$ ±.32	5.97 /5/	-22.5	$.365\ 10^{9}$ ±.025	.439	-16.9						
$^{93}Nb(n,2n)$	$3.70\ 10^{6}$ ±.26	3.77 /3/	-1.9	$.261\ 10^{6}$ ±.018	.239	9.21						

° Absolute activities at saturation per gr of the irradiated isotope at 5 KW power.

II.11. Comparison of Integral Cross Section Values of Several Cross Section Libraries in the SAND-II Format.

Willem L. Zijp
Henk J. Nolthenius

Abstract:
A comparison of some integral cross section values for several cross section libraries in the SAND-II format is presented. The integral cross section values are calculated with aid of the spectrum functions for a Watt fission spectrum, a 1/E spectrum and a Maxwellian spectrum. The libraries which are considered here are CCC-112B, ENDF/B-IV, DETAN74, LAPENAS and CESNEF. These 5 cross section libraries used have all the SAND-II format.

Keywords:

cross sections	tables
integrals	Watt fission spectrum
comparative evaluations	Boltzmann statistics
data processing	spectral functions
data	resonance integrals

1. INTRODUCTION

In this report a comparison is given of the cross section libraries CCC-112B, ENDF/B-IV BNL, DETAN74, LAPENAS and CESNEF.
These libraries are written in the SAND-II groups format and can be used in neutron spectrum evaluations with the SAND-II program package |1|.
For the comparison use is made of integral cross section data obtained with a fission spectrum for the fast cross section part, a thermal Maxwellian for the thermal part and a 1/E for the intermediate part of the cross section distribution. The average value and the standard deviation of the integral cross section values were determined for each reaction of the different libraries.
Especially the standard deviation of this average value may show the agreement between the different cross sections for a particular reaction, but one has to be careful because a small standard deviation can also indicate that the original data for all evaluations were identical. In some cases where it was known that exactly the same cross section was present in two libraries only one of the integral values was applied in the calculation of the average and standard deviation (e.g. CCC-112B and DETAN74).

2. ORIGIN OF THE LIBRARIES

The cross section library coded CCC-112B is part of the code package SAND-II, which was received from the Reactor Shielding Information Centre (RSIC) in Oak Ridge. The library CCC-112B is a more recent version of the library described in |1|. The ENDF/B-IV dosimetry file has been described by Magurno |2|. This file includes also a few unmodified ENDF/B-III cross section data, e.g. for the reactions $^{32}S(n,p)$, $^{54}Fe(n,p)$, $^{56}Fe(n,p)$, $^{115}In(n,n')$ and $^{58}Ni(n,p)$. The cross section data in the 620 groups as used in the SAND-II program were kindly supplied by Dr. A. Fabry from the CEN/SCK at Mol in Belgium. These data have been coded here as ENDF/B-IV BNL. At present no description of the procedure for deriving these 620 groups cross section data is available.

The cross section library DETAN-74 and the accompanying documentation were also received from Dr. A. Fabry. This file contained the cross

section data also in the SAND-II energy structure. The DETAN-74 library is partly based on the data presented by Simons and McElroy |3|, and partly equal to data in the CCC-112B library. The DETAN-74 library contains 9 new cross section sets, obtained by adjustment of cross section sets, to achieve consistent results with integral measurements. The actual source of the adjusted cross section set and other details on the adjustment procedure are not available; it was explicitly stated that the DETAN-74 file does not contain recommended values.

The microscopic cross section data, on which our LAPENAS library in 620 groups structure is based, were received from Dr. M. Vlasov of the Nuclear Data Section of the IAEA in Vienna. The data were originally obtained in the form of a copy of the tables from the work of A.A. Lapenas |4| from the Physics Institute of the Letland Academy of Science at Riga. The library comprises 22 threshold reactions. The primary cross section values for each reaction were treated as point cross section values. They were available from threshold energy to about 17.5 MeV for energy steps of 0.1 MeV. For each evaluated point cross section value also the accompanying error is supplied. In our laboratory a conversion from point values to group values was performed. This conversion consisted of a linear interpolation between the successive cross section points and the determination of the (unweighted) average cross section value for each of the 620 energy groups.

The cross section library CESNEF is based on cross section data supplied by Dr. R. Dierckx (Joint Research Centre, Ispra) as part of the data set for an international intercomparison of neutron spectrum unfolding codes. The intercomparison was proposed in February 1974 by the subgroup on unfolding techniques of the EWGRD (Euratom Working Group on Reactor Dosimetry). The original data were supplied in the form of a lineprinter output. The library comprises 13 reactions. It was assumed that the values of the lineprinter output represented group cross section values. The group cross section values in the listing comprise the energy range from the threshold energy or from 0.5 eV up to 18 MeV, and are presented in the SAND-II group structure.
The origin of the non-fission threshold reactions is given by Dierckx |5|. The choice of these reactions is made on the indications of the Nuclear Data Group (CNEN, Bologna, Italy). The $^{103}Rh(n,n')^{103}Rh^{m}$ cross section is based on the work by Butler and Santry |6|.

The $^{115}In(n,n')^{115}In^{m}$, $^{47}Ti(n,p)^{47}Sc$, $^{54}Fe(n,p)^{54}Mn$ and $^{46}Ti(n,p)^{46}Sc$ reaction cross sections originate from Simons and McElroy |3|.
The $^{238}U(n,f)^{140}Ba$ cross section is obtained from the UKAEA file (DFN4010, 1970).
The cross section data for the reactions $^{58}Ni(n,p)^{58}Co$, $^{24}Mg(n,p)^{24}Na$ and $^{27}Al(n,\alpha)^{24}Na$ are based on the work by Bresesti et al. |7|.
The cross section values for the fission reactions were supplied by the Centro di Calcolo, CNEN, Bologna, Italy.

3. PLOTS AND TABLES

Tables with the 620 group cross section values and corresponding plots have been prepared for each reaction present in the libraries mentioned. These tables and plots are given in RCN reports with restricted distribution, which are available on request (ref. 8 to 12).

4. CALCULATION OF INTEGRAL CROSS SECTIONS

The integral cross sections were calculated for three theoretical neutron spectrum functions:

a) The Maxwellian spectrum function describing the distributions of thermal neutrons corresponding to a temperature of 293 K was applied to calculate the average cross section.
This spectrum function is given by the relation:

$$\chi_m(E) = 1.5918\times10^{15}E \exp(-3.987\times10^{7}E)$$

where E is the neutron energy expressed in MeV. No upper cut-off was used.

b) The 1/E spectrum function for the calculation of the resonance integral.
This function is applied as follows:

$\chi_{1/E}(E) = 1/E$ for 0.55 eV < E < 1 MeV

$\chi_{1/E}(E) = 0$ outside this range.

c) The Watt spectrum function with an average neutron energy of 2 MeV was used to calculate the average fission cross section.

The following relation holds here:

$$\chi_w(E) = 0.484 \sinh(\sqrt{2E}) \times e^{-E}$$

where E is the neutron energy in MeV, comprising the energy range between 10^{-10} MeV and 18 MeV.

The integral cross section values for each spectrum function and reaction of the different libraries was averaged. As measure of the spread in the values of the 2, 3 or 4 libraries considered the standard deviation was chosen. This measure does not imply a preference for one set or the other, as for instance may occur when the average deviation from one reference set, or the range between extreme values is considered. The chosen measure serves only as an indication of a disagreement between different sets.

5. RESULTS

Table 1 presents the results for the Maxwell spectrum function.
The results for the 1/E neutron spectrum are given in table 2.
The average cross section for the Watt fission spectrum function are listed in table 3.
The last 2 columns of these tables show the average value and the standard deviations in these values.
For the Maxwellian spectrum (table 1) a standard deviation higher than 5% is found for the reaction $^{238}U(n,\gamma)^{239}$.
Table 2 shows a standard deviation higher than 5% for the reactions $^{23}Na(n,\gamma)^{24}Na$, $^{58}Fe(n,\gamma)^{59}Fe$, $^{63}Cu(n,\gamma)^{64}Cu$ and $^{115}In(n,\gamma)^{116}In^m$.
From table 3 it follows that for most threshold reactions the standard deviation is smaller than 5%.
Exceptions are found for the reactions $^{46}Ti(n,p)^{46}Sc$, $^{47}Ti(n,p)^{47}Sc$, $^{48}Ti(n,p)^{48}Sc$, $^{55}Mn(n,2n)^{54}Mn$, $^{60}Ni(n,p)^{60}Co$, $^{63}Cu(n,2n)^{62}Cu$, $^{64}Zn(n,p)^{64}Cu$ and $^{127}I(n,2n)^{126}I$.
In figures 1...4 the cross section distributions for the reaction $^{58}Ni(n,p)^{58}Co$ are shown. Figures 5...8 show the corresponding data for the reaction $^{54}Fe(n,p)^{54}Mn$.
From these figures it is clear that important deviations between corresponding cross sections of different libraries are easily detectable. Specially in the region of the sharp increase near the threshold different shapes have been found, but also above about 13 MeV the shapes differ.

DISCUSSION

From the numerical results presented in the tables it follows that for a number of reactions the integral values show an important scatter reflecting the discrepancies in the cross section data.
This is especially the case for the 1/E and the fission neutron spectrum.
The absence of scatter and the agreement does not necessarily imply the correctness of the cross section data, but it only represents consistency of the data files considered.
The consistency may be due to the absence of new experimental data.
We did not yet try to trace the origin of important differences. Our main interest was to look for systematic differences in the data sets, which influence the integral values of importance to reactor neutron metrology.
Moreover, a tracing of discrepancies would have delayed this report since the considerations of the evaluators were not all readily available.

7. REFERENCES

|1| McElroy, W.N. et al.: "SAND-II. Neutron flux spectra determination by multiple foil activation iterative method"
RSIC Computer code collection CCC-112 (Oak Ridge National Laboratory, Radiation Shielding Information Center, May 1969).

|2| Magurno, B.A.: "ENDF/BIV dosimetry file"
BNL-NCS-50446 (ENDF-216); NEACRP-L-145; NEANDC(US)-193/L; INDC(US)-80/L
(National Neutron Cross Section Center, Brookhaven National Laboratory, Upton New York, April 1975).

|3| Simons, R.L.; McElroy, W.N.: "Evaluated reference cross section library"
BNWL-1312 (May 1970).

|4a| Лапенас А.А.;
"Измерение спектров нейтронов активационным методом".
Академия Наук Латвийской ССР, институт физики.
(Издательство "Зинатне", Рига 1975)

|4b| Lapenas, A.A.: "Izmerenie Spektrov Nejtronov Aktivacionym Metodom"
Publishing House "ZINATNE", Riga, USSR (1975)
(It contains an evaluation of 22 dosimetry reactions).

|5| Dierckx, R.; Guidetti, D.; Nimis, M.; Sangiust, V.; Terrani, M.: "Determination of the fast neutron spectrum at the 454 reactor core centre"
Energia Nucleare 20 (1973) 49.

|6| Butler, J.P.; Santry, D.C.: "The neutron inelastic cross section for the production of ^{103}Rh"
AECL-3043 (1968). Proc. Second Conf. on Neutron Cross Sections and Technology, Washington, March 4-7, 1968. NBS Special Publication 299, Vol. II, p. 803 (NBS, Washington D.C., September 1968).

|7| Bresesti, A.M.; Bresesti, M.; Rota, A.; Rydin, A.; "Threshold reaction excitation functions intercalibrated in a pure fission spectrum"
Nucl. Sci. Eng. 40 (1970) 331.

|8| Keller, J.M.; Voorbraak, W.P.:"Cross section library (CCC-112B) of SAND-II"
Internal Laboratory note 73/11 (Reactor Centrum Nederland, Petten, July 6, 1973).

|9| Rieffe, H.Ch.; Nolthenius, H.J.: "Cross section library ENDF/B-IV BNL (in the SAND-II format)"
RCN-75-157 (Reactor Centrum Nederland, Petten, December 1975).

|10| Rieffe, H.Ch.; Nolthenius, H.J.: "Cross section library DETAN74 (in the SAND-II format)"
RCN-75-139 (Reactor Centrum Nederland, Petten, October 1975).

|11| Kramer, L.G.A.; Nolthenius, H.J.: "Cross section library LAPENAS (presented in the SAND-II format)"
RCN-76-020 (Reactor Centrum Nederland, Petten, February 1976).

|12| Kramer, L.G.A.; Nolthenius, H.J.: "Cross section library CESNEF (presented in the SAND-II format)"
RCN-76-019 (Reactor Centrum Nederland, Petten, February 1976).

ACKNOWLEDGEMENT

The authors gratefully acknowledge the assistance of L.G.A. Kramer (student from the H.T.S. Dordrecht), who performed a large part of the data treatment necessary for this work.

Table 1: Maxwellian neutron spectrum

reaction	<σ> (in b)					average <σ>	standard deviation $s_{<\sigma>}$ (in %)
	CCC-112B	ENDF/B-IV BNL	DETAN74	LAPENAS	CESNEF		
$^{6}Li(n,\alpha)^{3}H$		8.373×10^{2}	8.376×10^{2}			8.375×10^{2}	0.03
$^{10}B\ (n,\alpha)^{7}Li$		3.417×10^{3}	3.417×10^{3}			3.417×10^{3}	0.00
$^{19}F\ (n,2n)^{18}F$							
$^{23}Na(n,\gamma)^{24}Na$	4.805×10^{-1}	4.757×10^{-1}	4.805×10^{-1} *			4.781×10^{-1}	0.71
$^{24}Mg(n,p)^{24}Na$							
$^{27}Al(n,\alpha)^{24}Na$							
$^{27}Al(n,p)^{27}Mg$							
$^{28}Si(n,p)^{28}Al$							
$^{31}P\ (n,p)^{31}Si$							
$^{32}S\ (n,p)^{32}P$							
$^{34}S\ (n,\alpha)^{31}Si$							
$^{35}Cl(n,\alpha)^{32}P$							
$^{45}Sc(n,\gamma)^{46}Sc$	2.244×10^{1}	2.349×10^{1}	2.244×10^{1} *			2.297×10^{1}	3.23
$^{46}Ti(n,p)^{46}Sc$							
$^{47}Ti(n,p)^{47}Sc$							
$^{47}Ti(n,np)^{46}Sc$							
$^{48}Ti(n,p)^{48}Sc$							
$^{48}Ti(n,np)^{47}Sc$							
$^{54}Fe(n,p)^{54}Mn$							
$^{55}Mn(n,\gamma)^{56}Mn$	1.185×10^{1}		1.185×10^{1} *				
$^{55}Mn(n,2n)^{54}Mn$							
$^{56}Fe(n,p)^{56}Mn$							
$^{58}Ni(n,2n)^{57}Ni$							
$^{58}Ni(n,p)^{58}Co$							
$^{59}Co(n,\alpha)^{56}Mn$							
$^{58}Fe(n,\gamma)^{59}Fe$		1.052×10^{0}	1.063×10^{0}			1.059×10^{0}	0.74
$^{59}Co(n,\gamma)^{60}Co$	3.288×10^{1}	3.318×10^{1}	3.288×10^{1} *			3.303×10^{1}	0.64
$^{59}Co(n,\alpha)^{56}Mn$							
$^{60}Ni(n,p)^{60}Co$							
$^{63}Cu(n,2n)^{62}Cu$							
$^{63}Cu(n,\alpha)^{60}Co$			4.371×10^{-6} **				
$^{63}Cu(n,\gamma)^{64}Cu$	4.019×10^{0}	4.005×10^{0}	4.019×10^{0} *			4.012×10^{0}	0.25

Table 1 (continued):

reaction	<σ> (in b) CCC-112B	ENDF/B-IV BNL	DETAN74	LAPENAS	CESNEF	average <σ>	standard deviation $s_{<\sigma>}$ (in %)
$^{64}Zn(n,p)^{64}Cu$							
$^{64}Zn(n,2n)^{63}Zn$							
$^{65}Cu(n,2n)^{64}Cu$							
$^{90}Zr(n,p)^{90}Y$							
$^{90}Zr(n,2n)^{89}Zr$							
$^{103}Rh(n,n')^{103}Rh^{m}$							
$^{109}Ag(n,\gamma)^{110}Ag^{m}$			3.681×10^{0}				
$^{115}In(n,n')^{115}In^{m}$							
$^{115}In(n,\gamma)^{116}In^{m}$	1.411×10^{2}	1.510×10^{2}	1.411×10^{2} *			1.461×10^{2}	4.79
$^{127}I\ (n,2n)^{126}I$							
$^{151}Eu(n,\gamma)^{152}Eu$	7.453×10^{3}						
$^{164}Dy(n,\gamma)^{165}Dy$	2.218×10^{3}						
$^{175}Lu(n,\gamma)^{176}Lu^{m}$	2.254×10^{1}						
$^{176}Lu(n,\gamma)^{177}Lu$	3.014×10^{3}						
$^{181}Ta(n,\gamma)^{181}Ta$			1.865×10^{1}				
$^{197}Au(n,\gamma)^{198}Au$	8.813×10^{2}	8.847×10^{2}	8.844×10^{2}			8.835×10^{2}	0.21
$^{232}Th(n,f)FP$							
$^{232}Th(n,\gamma)^{233}Th$	6.936×10^{0}	6.563×10^{0}	6.936×10^{0} *			6.750×10^{2}	3.91
$^{232}Th(n,2n)^{231}Th$							
$^{235}U\ (n,f)FP$	4.989×10^{2}	5.096×10^{2}	5.051×10^{2}		4.989×10^{2}	5.021×10^{2}	1.02
$^{237}Np(n,f)FP$	1.654×10^{-2}	1.429×10^{-2}	1.654×10^{-2}*		1.654×10^{-2}	1.579×10^{-2}	8.23
$^{238}U\ (n,f)FP$		4.104×10^{-9} ***					
$^{238}U\ (n,f)^{239}U$	2.661×10^{0}	2.411×10^{0}	2.661×10^{0} *			2.536×10^{0}	6.97
$^{239}Pu(n,f)FP$		6.969×10^{2}	6.959×10^{2}			6.855×10^{2}	2.76
$^{241}Am(n,f)FP$					2.022×10^{-7}		

*Cross section set DETAN74 = cross section set CCC-112B (only one value applied for the calculation of average value and the standard deviation).

**The DETAN-74 cross section data for the $^{63}Cu(n,\alpha)^{60}Co$ reaction show subthreshold activation, corresponding to a 1/v shape.

***This values is due to subthreshold fission with sharp peaks in the keV region superimposed on a small 1/v contribution.

Table 2: The 1/E neutron spectrum

reaction	σ (in b)					average σ	standard deviation s_σ (in %)
	CCC-112B	ENDF/B-IV BNL	DETAN74	LAPENAS	CESNEF		
$^{6}Li(n,\alpha)^{3}H$		4.002×10^{2}	4.001×10^{2}			4.002×10^{2}	0.01
$^{10}B\ (n,\alpha)^{7}Li$		1.622×10^{3}	1.622×10^{3}			1.622×10^{3}	0.00
$^{19}F\ (n,2n)^{18}F$							
$^{23}Na(n,\gamma)^{24}Na$	2.864×10^{-1}	3.315×10^{-1}	2.864×10^{-1} *			3.090×10^{-1}	10.3
$^{24}Mg(n,p)^{24}Na$							
$^{27}Al(n,\alpha)^{24}Na$							
$^{27}Al(n,p)^{27}Mg$							
$^{28}Si(n,p)^{28}Al$							
$^{31}P\ (n,p)^{31}Si$							
$^{32}S\ (n,p)^{32}P$		1.226×10^{-6}					
$^{34}S\ (n,\alpha)^{31}Si$							
$^{35}Cl(n,\alpha)^{32}P$							
$^{45}Sc(n,\gamma)^{46}Sc$	9.953×10^{1}	1.060×10^{1}	9.953×10^{0} *			1.028×10^{1}	4.45
$^{46}Ti(n,p)^{46}Sc$							
$^{47}Ti(n,p)^{47}Sc$		3.500×10^{-5}	3.669×10^{-5}		3.449×10^{-5}	3.539×10^{-5}	3.25
$^{47}Ti(n,np)^{46}Sc$							
$^{48}Ti(n,p)^{48}Sc$							
$^{48}Ti(n,np)^{47}Sc$							
$^{54}Fe(n,p)^{54}Mn$			2.039×10^{-5}	6.000×10^{-5}		4.020×10^{-5}	69.7
$^{55}Mn(n,\gamma)^{56}Mn$	1.560×10^{1}		1.560×10^{1} *				
$^{55}Mn(n,2n)^{54}Mn$							
$^{56}Fe(n,p)^{56}Mn$							
$^{58}Ni(n,2n)^{57}Ni$							
$^{58}Ni(n,p)^{58}Co$			1.163×10^{-5}	4.000×10^{-5}	4.375×10^{-5}	3.179×10^{-5}	55.3
$^{58}Fe(n,\gamma)^{59}Fe$		1.558×10^{0}	1.398×10^{0}			1.478×10^{0}	7.66
$^{59}Co(n,2n)^{58}Co$							
$^{59}Co(n,\gamma)^{60}Co$	7.254×10^{1}	7.576×10^{1}	7.254×10^{1} *			7.415×10^{1}	3.07
$^{59}Co(n,\alpha)^{56}Mn$							
$^{60}Ni(n,p)^{60}Co$							
$^{63}Cu(n,2n)^{62}Cu$							
$^{63}Cu(n,\alpha)^{60}Co$			6.169×10^{-6}				
$^{63}Cu(n,\gamma)^{64}Cu$	4.664×10^{0}	5.386×10^{0}	4.664×10^{0} *			5.025×10^{0}	10.2

Table 2 (continued):

reaction	σ (in b)					average σ	standard deviation s_σ (in %)
	CCC-112B	ENDF/B-IV BNL	DETAN74	LAPENAS	CESNEF		
$^{64}Zn(n,p)^{64}Cu$							
$^{64}Zn(n,2n)^{63}Zn$							
$^{65}Cu(n,2n)^{64}Cu$							
$^{90}Zr(n,p)^{90}Y$							
$^{90}Zr(n,2n)^{89}Zr$							
$^{103}Rh(n,n')^{103}Rh^m$				3.697×10^{-1}	4.005×10^{-1}	3.851×10^{-1}	5.66
$^{109}Ag(n,\gamma)^{110}Ag^m$			6.552×10^{1}				
$^{115}In(n,n')^{115}In^m$		1.800×10^{-2}	2.146×10^{-2}	2.022×10^{-2}	2.069×10^{-2}	2.009×10^{-2}	7.39
$^{115}In(n,\gamma)^{116}In^m$	2.842×10^{3}	3.230×10^{3}	2.842×10^{3} *			3.036×10^{3}	9.04
$^{127}I\ (n,2n)^{126}I$							
$^{151}Eu(n,\gamma)^{152}Eu$	2.365×10^{3}						
$^{164}Dy(n,\gamma)^{165}Dy$	4.192×10^{2}						
$^{175}Lu(n,\gamma)^{176}Lu^m$	1.189×10^{3}						
$^{176}Lu(n,\gamma)^{177}Lu$	1.461×10^{3}						
$^{181}Ta(n,\gamma)^{182}Ta$			7.634×10^{2}				
$^{197}Au(n,\gamma)^{198}Au$	1.616×10^{3}	1.564×10^{3}	1.600×10^{3}			1.597×10^{3}	1.95
$^{232}Th(n,f)FP$				1.827×10^{-4}	5.625×10^{-4}	3.726×10^{-4}	72.1
$^{232}Th(n,\gamma)^{233}Th$	8.021×10^{1}	8.512×10^{1}	8.021×10^{1} *			8.267×10^{1}	4.20
$^{232}Th(n,2n)^{231}Th$							
$^{235}U\ (n,f)FP$	2.870×10^{2}	2.702×10^{2}	2.702×10^{2}		2.870×10^{2}	2.786×10^{2}	3.48
$^{237}Np(n,f)FP$	9.825×10^{0}	1.214×10^{0}	9.825×10^{-1}*	9.426×10^{-1}	9.826×10^{-1}	1.030×10^{0}	12.0
$^{238}U\ (n,f)FP$		4.580×10^{-3}	3.925×10^{-3}	3.259×10^{-3}	3.358×10^{-3}	3.781×10^{-3}	16.1
$^{238}U\ (n,\gamma)^{239}U$	2.800×10^{2}	2.769×10^{2}	2.800×10^{2} *			2.785×10^{2}	0.79
$^{239}Pu(n,f)FP$		2.919×10^{2}	2.797×10^{2}			2.858×10^{2}	3.02
$^{241}Am(n,f)FP$					1.393×10^{1}		

*Cross section set DETAN74 = cross section set CCC-112B (only one value applied for the calculation of average value and the standard deviation).

Table 3: Watt fission neutron spectrum

reaction	<σ> (in b)					average <σ>	standard deviation $s_{<\sigma>}$ (in %)
	CCC-112B	ENDF/B-IV BNL	DETAN74	LAPENAS	CESNEF		
$^{6}Li(n,\alpha)^{3}H$		4.795×10^{-1}	4.672×10^{-1}			4.734×10^{-1}	1.84
$^{10}B\ (n,\alpha)^{7}Li$		5.038×10^{-1}	5.605×10^{-1}			5.322×10^{-1}	7.53
$^{19}F\ (n,2n)^{18}F$				6.633×10^{-6}			
$^{23}Na(n,\gamma)^{24}Na$	2.686×10^{-4}	2.849×10^{-4}	2.686×10^{-4}*			2.768×10^{-4}	4.17
$^{24}Mg(n,p)^{24}Na$	1.498×10^{-3}		1.498×10^{-3}*	1.515×10^{-3}	1.446×10^{-3}	1.486×10^{-3}	2.42
$^{27}Al(n,\alpha)^{24}Na$	6.631×10^{-4}	6.843×10^{-4}	6.630×10^{-4}*	6.872×10^{-4}	6.896×10^{-4}	6.810×10^{-4}	1.79
$^{27}Al(n,p)^{27}Mg$		4.100×10^{-3}	3.839×10^{-3}	3.901×10^{-3}		3.947×10^{-3}	3.45
$^{28}Si(n,p)^{28}Al$	9.709×10^{-3}						
$^{31}P\ (n,p)^{31}Si$	3.301×10^{-2}		3.301×10^{-2}*				
$^{32}S\ (n,p)^{32}P$	6.092×10^{-2}	6.505×10^{-2}	6.091×10^{-2}*	6.304×10^{-2}		6.300×10^{-2}	3.28
$^{34}S\ (n,\alpha)^{31}Si$	2.234×10^{-3}						
$^{35}Cl(n,\alpha)^{32}P$	1.326×10^{-2}						
$^{45}Sc(n,\gamma)^{46}Sc$	6.241×10^{-3}	5.715×10^{-3}	6.241×10^{-3}*			5.965×10^{-3}	5.92
$^{46}Ti(n,p)^{46}Sc$	1.128×10^{-2}	9.920×10^{-3}	1.128×10^{-2}*		1.130×10^{-2}	1.083×10^{-2}	7.30
$^{47}Ti(n,p)^{47}Sc$	1.719×10^{-2}	2.174×10^{-2}	1.719×10^{-2}*		1.719×10^{-2}	1.871×10^{-2}	14.0
$^{47}Ti(n,np)^{46}Sc$		3.171×10^{-6}					
$^{48}Ti(n,p)^{48}Sc$	2.364×10^{-4}	1.695×10^{-4}	2.364×10^{-4}*			2.030×10^{-4}	23.3
$^{48}Ti(n,np)^{47}Sc$		1.820×10^{-6}					
$^{54}Fe(n,p)^{54}Mn$	7.628×10^{-2}	7.846×10^{-2}	7.627×10^{-2}*	8.358×10^{-2}	7.634×10^{-2}	7.866×10^{-2}	4.30
$^{55}Mn(n,\gamma)^{56}Mn$	3.561×10^{-3}		3.560×10^{-3}*				
$^{55}Mn(n,2n)^{54}Mn$		2.320×10^{-4}		2.003×10^{-4}		2.162×10^{-4}	10.4
$^{56}Fe(n,p)^{56}Mn$	1.086×10^{-3}	1.035×10^{-3}	1.086×10^{-3}*	1.099×10^{-3}		1.073×10^{-3}	3.15
$^{58}Ni(n,2n)^{57}Ni$	2.393×10^{-6}	2.539×10^{-6}	2.393×10^{-6}*	2.438×10^{-6}		2.456×10^{-6}	3.10
$^{58}Ni(n,p)^{58}Co$	1.022×10^{-1}	1.028×10^{-1}	1.022×10^{-1}*	1.132×10^{-1}	1.043×10^{-2}	1.056×10^{-1}	4.85
$^{58}Fe(n,\gamma)^{59}Fe$	2.864×10^{-3}	1.675×10^{-3}	2.864×10^{-3}*			2.270×10^{-3}	37.0
$^{59}Co(n,2n)^{58}Co$		1.624×10^{-4}					
$^{59}Co(n,\gamma)^{60}Co$	5.316×10^{-3}	6.381×10^{-3}	5.315×10^{-3}*			5.849×10^{-3}	12.9
$^{59}Co(n,\alpha)^{56}Mn$		1.457×10^{-4}		1.561×10^{-4}		1.509×10^{-4}	4.87
$^{60}Ni(n,p)^{60}Co$	5.302×10^{-3}	2.443×10^{-3}				3.873×10^{-3}	52.2
$^{63}Cu(n,2n)^{62}Cu$	8.46×10^{-5}		8.463×10^{-5}*	7.816×10^{-5}		8.140×10^{-5}	5.62
$^{63}Cu(n,\alpha)^{60}Co$	3.562×10^{-4}	3.471×10^{-4}	4.728×10^{-4}			3.920×10^{-4}	17.9
$^{63}Cu(n,\gamma)^{64}Cu$	1.088×10^{-2}	1.082×10^{-2}	1.087×10^{-2}*			1.085×10^{-2}	0.39

Table 3 (continued):

reaction	<σ> (in b)					average <σ>	standard deviation $s_{<\sigma>}$ (in %)
	CCC-112B	ENDF/B-IV BNL	DETAN74	LAPENAS	CESNEF		
$^{64}Zn(n,p)^{64}Cu$	3.800×10^{-2}			4.293×10^{-2}		4.047×10^{-2}	8.62
$^{64}Zn(n,2n)^{63}Zn$				1.657×10^{-5}			
$^{65}Cu(n,2n)^{64}Cu$		2.976×10^{-4}		3.135×10^{-4}		3.056×10^{-4}	3.68
$^{90}Zr(n,p)^{90}Y$				3.566×10^{-4}			
$^{90}Zr(n,2n)^{89}Zr$	7.952×10^{-5}		7.952×10^{-5}*				
$^{103}Rh(n,n')^{103}Rh^{m}$				7.134×10^{-1}	7.221×10^{-1}	7.178×10^{-1}	0.86
$^{109}Ag(n,\gamma)^{110}Ag^{m}$			1.151×10^{-2}				
$^{115}In(n,n')^{115}In^{m}$	1.853×10^{-1}	1.704×10^{-1}	1.853×10^{-1}*	1.770×10^{-1}	1.846×10^{-1}	1.793×10^{-1}	3.93
$^{115}In(n,\gamma)^{116}In^{m}$	1.464×10^{-1}	1.350×10^{-1}	1.463×10^{-1}*			1.407×10^{-1}	5.73
$^{127}I\ (n,2n)^{126}I$	6.865×10^{-4}	1.149×10^{-3}	6.864×10^{-4}*			9.177×10^{-4}	35.6
$^{151}Eu(n,\gamma)^{152}Eu$	2.109×10^{-1}						
$^{164}Dy(n,\gamma)^{165}Dy$	9.893×10^{-2}						
$^{175}Lu(n,\gamma)^{176}Lu^{m}$	8.328×10^{-2}						
$^{176}Lu(n,\gamma)^{177}Lu$	1.305×10^{-1}						
$^{181}Ta(n,\gamma)^{182}Ta$			1.035×10^{-1}				
$^{197}Au(n,\gamma)^{198}Au$	8.283×10^{-2}	8.305×10^{-2}	8.555×10^{-2}			8.381×10^{-2}	1.80
$^{232}Th(n,f)FP$	7.132×10^{-2}	7.025×10^{-2}	7.131×10^{-2}*	7.156×10^{-1}	7.557×10^{-2}	7.218×10^{-2}	3.23
$^{232}Th(n,\gamma)^{233}Th$	1.018×10^{-1}	1.019×10^{-1}	1.018×10^{-1}			1.019×10^{-1}	0.07
$^{232}Th(n,2n)^{231}Th$				1.503×10^{-2}			
$^{235}U\ (n,f)FP$	1.230×10^{0}	1.241×10^{0}	1.241×10^{0}		1.230×10^{0}	1.233×10^{0}	0.52
$^{237}Np(n,f)FP$	1.293×10^{0}	1.337×10^{0}	1.292×10^{0} *	1.351×10^{0}	1.293×10^{0}	1.319×10^{0}	2.28
$^{238}U\ (n,f)FP$	2.869×10^{-1}	3.015×10^{-1}	3.004×10^{-1}	2.867×10^{-1}	3.083×10^{-1}	2.967×10^{-1}	3.25
$^{238}U\ (n,\gamma)^{239}U$	8.704×10^{-2}	7.429×10^{-2}	8.703×10^{-2}*			8.066×10^{-2}	11.2
$^{239}Pu(n,f)FP$	1.762×10^{0}	1.785×10^{0}	1.817×10^{0}			1.788×10^{0}	1.55
$^{241}Am(n,f)FP$					1.253×10^{0}		

*Cross section set DETAN74 = cross section set CCC-112B (only one value applied for the calculation of average value and the standard deviation).

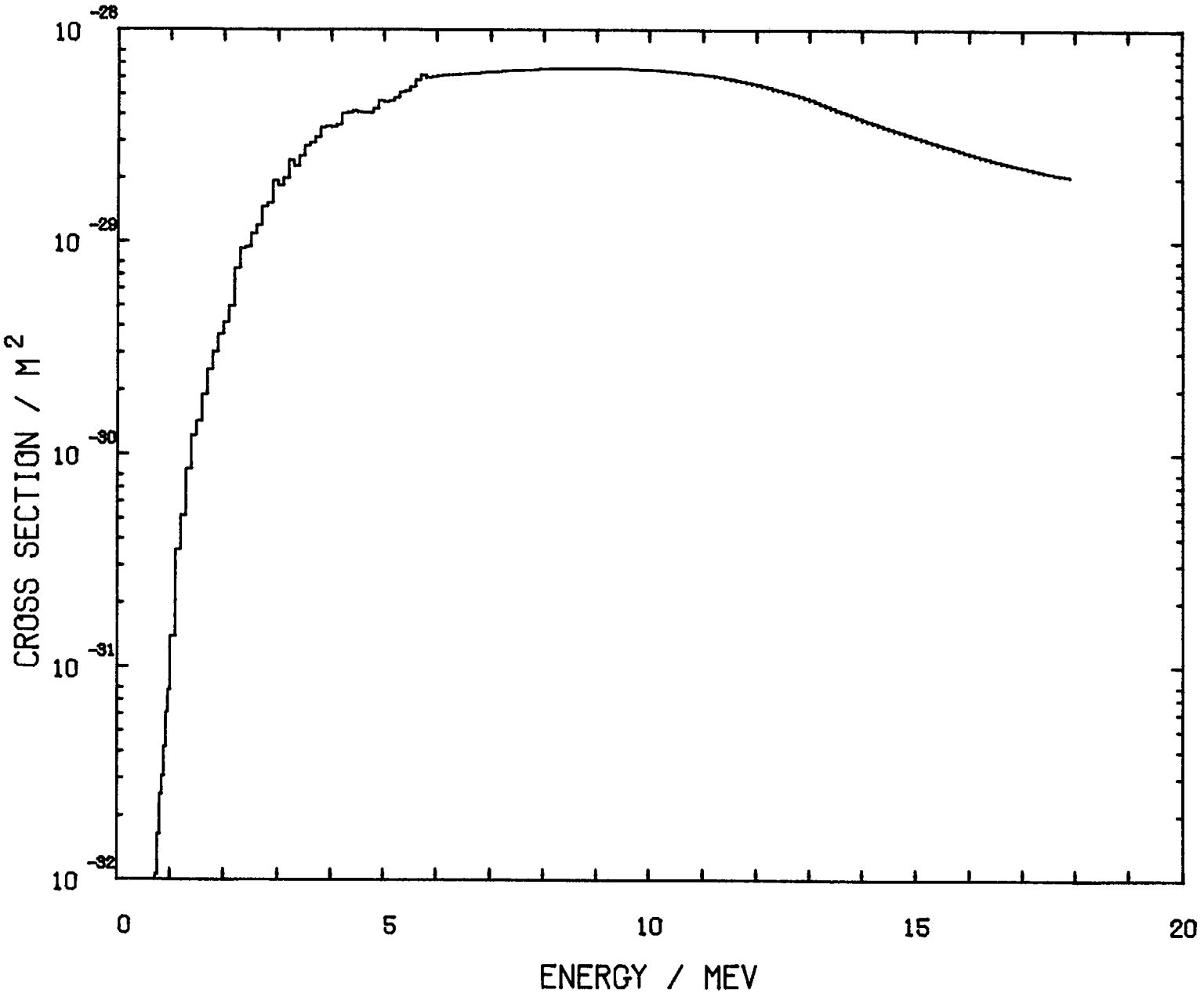

RMG 4515

Fig. 1 Cross section curve for the reaction ^{58}Ni (n,p) ^{58}Co (from ENDF/B–IV BNL).

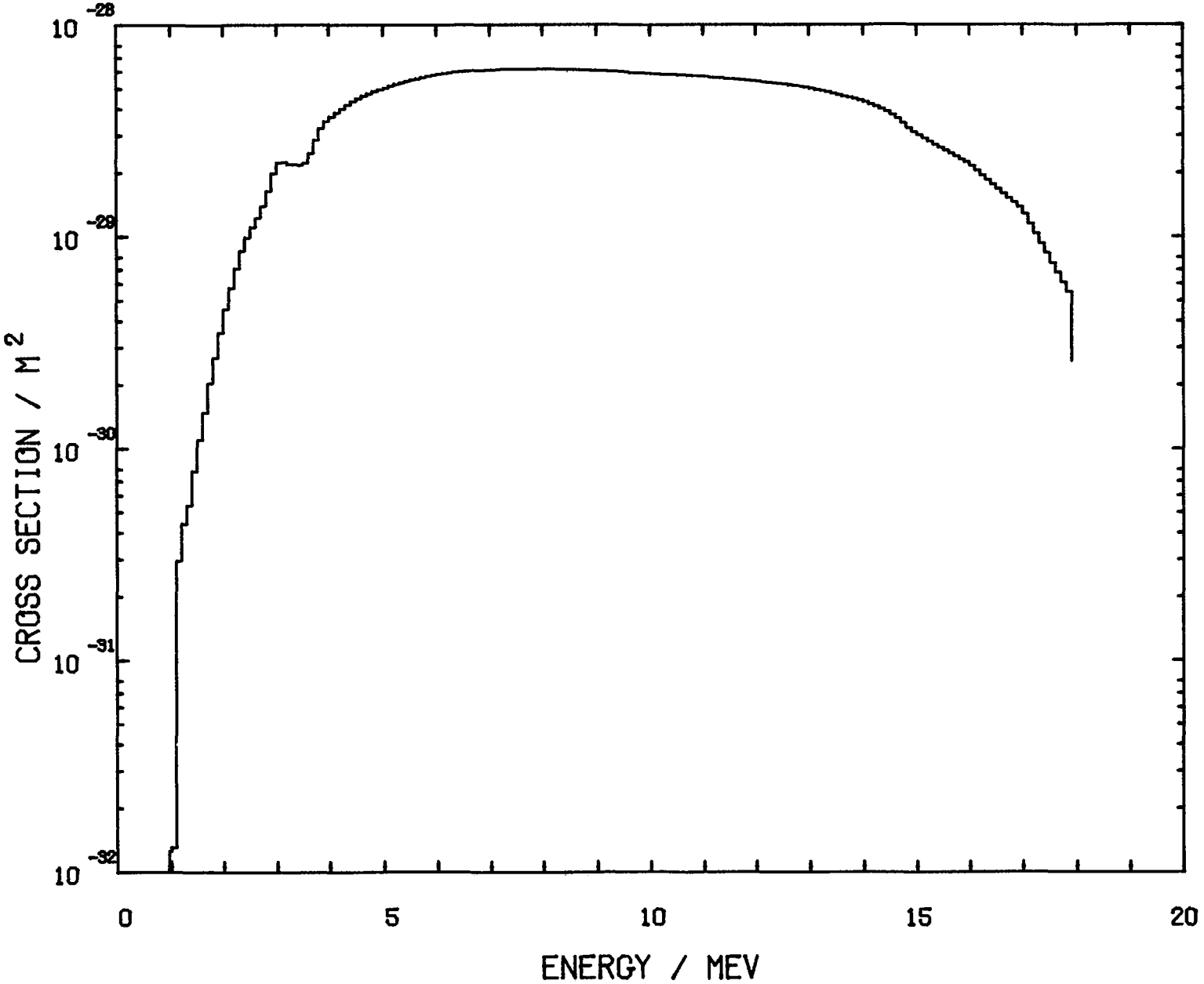

RMG 4516

Fig. 2 Cross section curve for the reaction $^{58}Ni\ (n,p)^{58}Co$ (from DETAN 74).

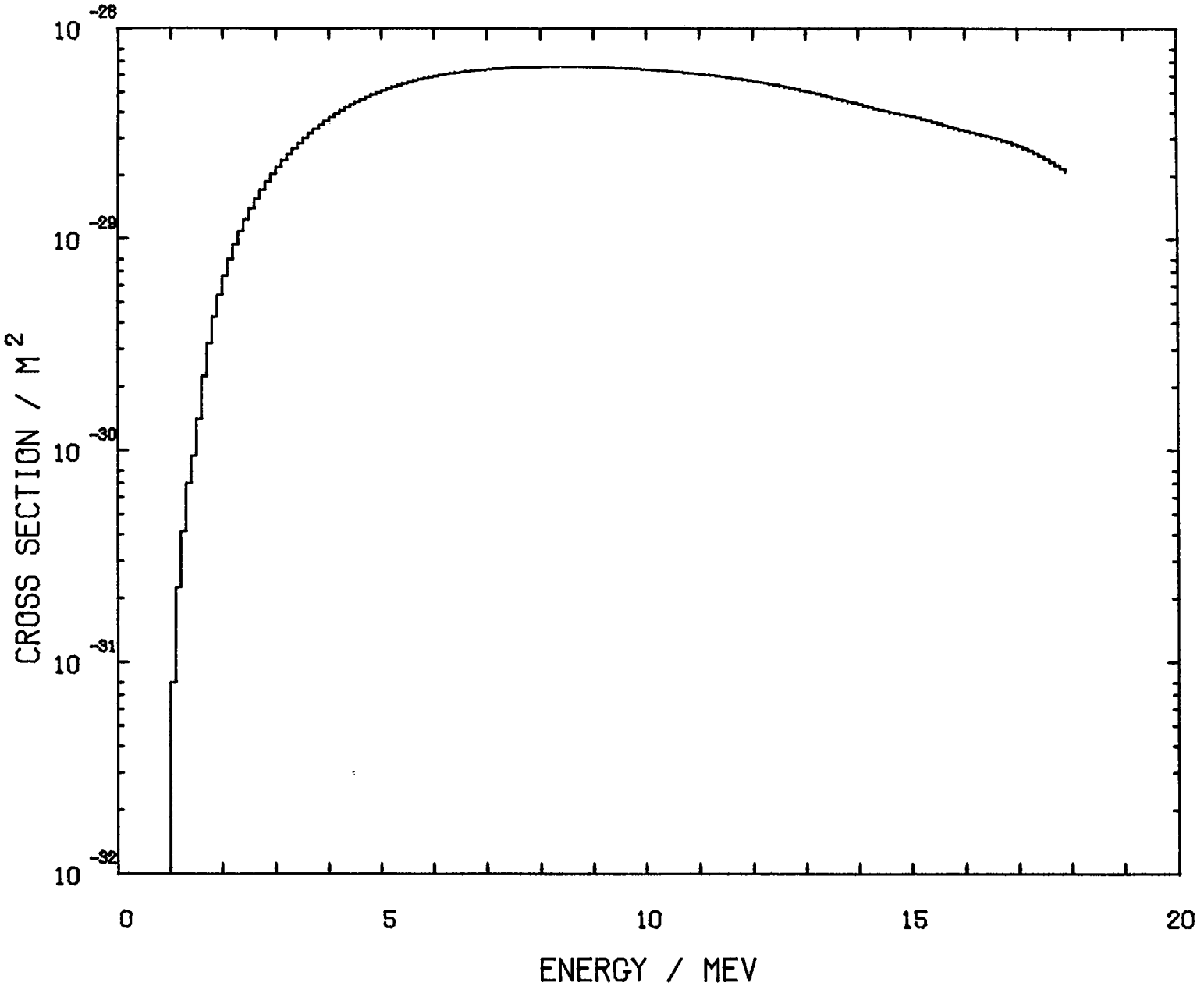

Fig. 3 Cross section curve for the reaction ^{58}Ni (n,p) ^{58}Co (from LAPENAS).

RMG 4517

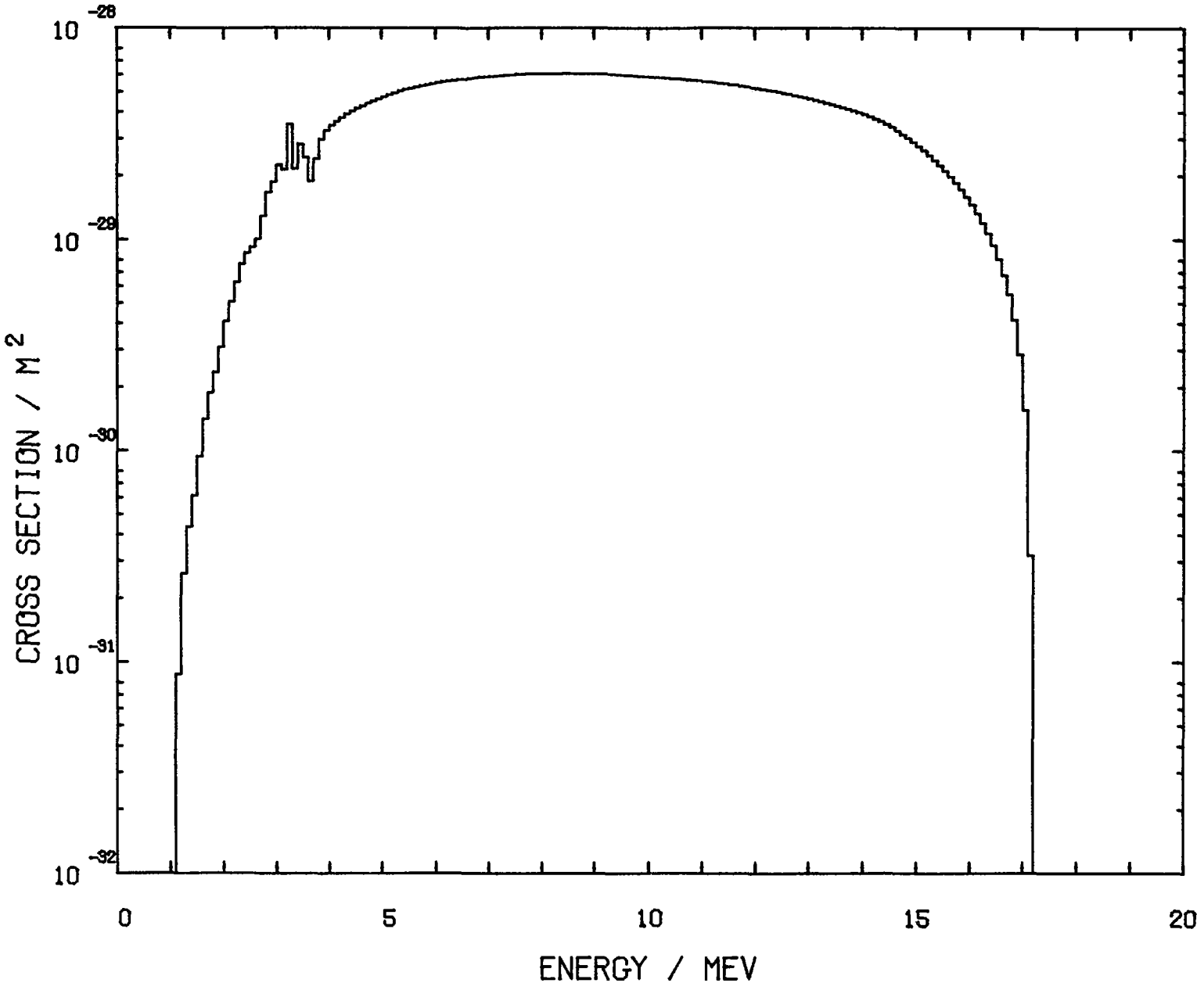

Fig. 4 Cross section curve for the reaction ^{58}Ni (n,p) ^{58}Co (from CESNEF).

RMG 4518

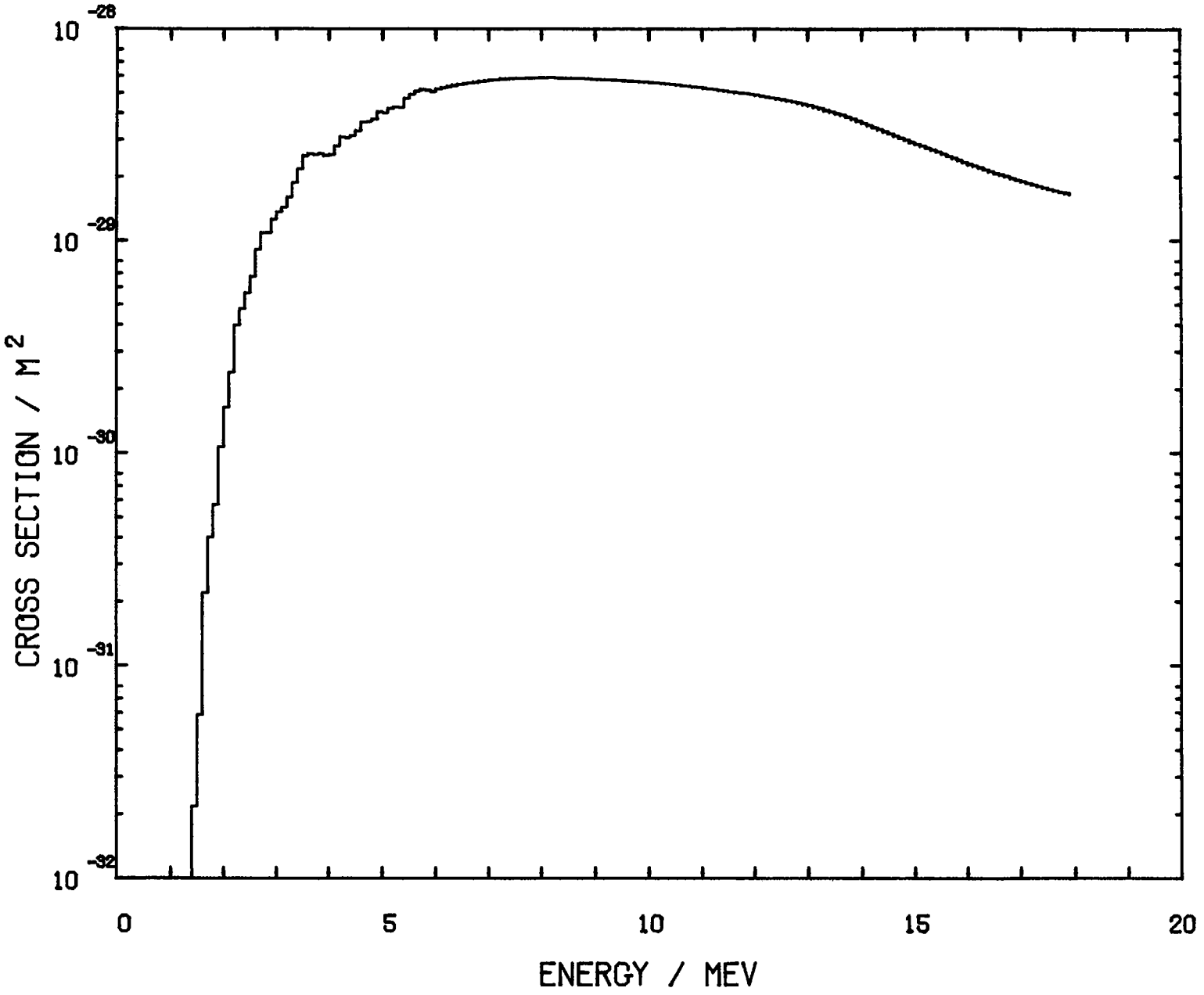

RMG 4519 Fig. 5 Cross section curve for the reaction $^{54}Fe(n,p)\ ^{54}Mn$ (from ENDF/B–IV BNL).

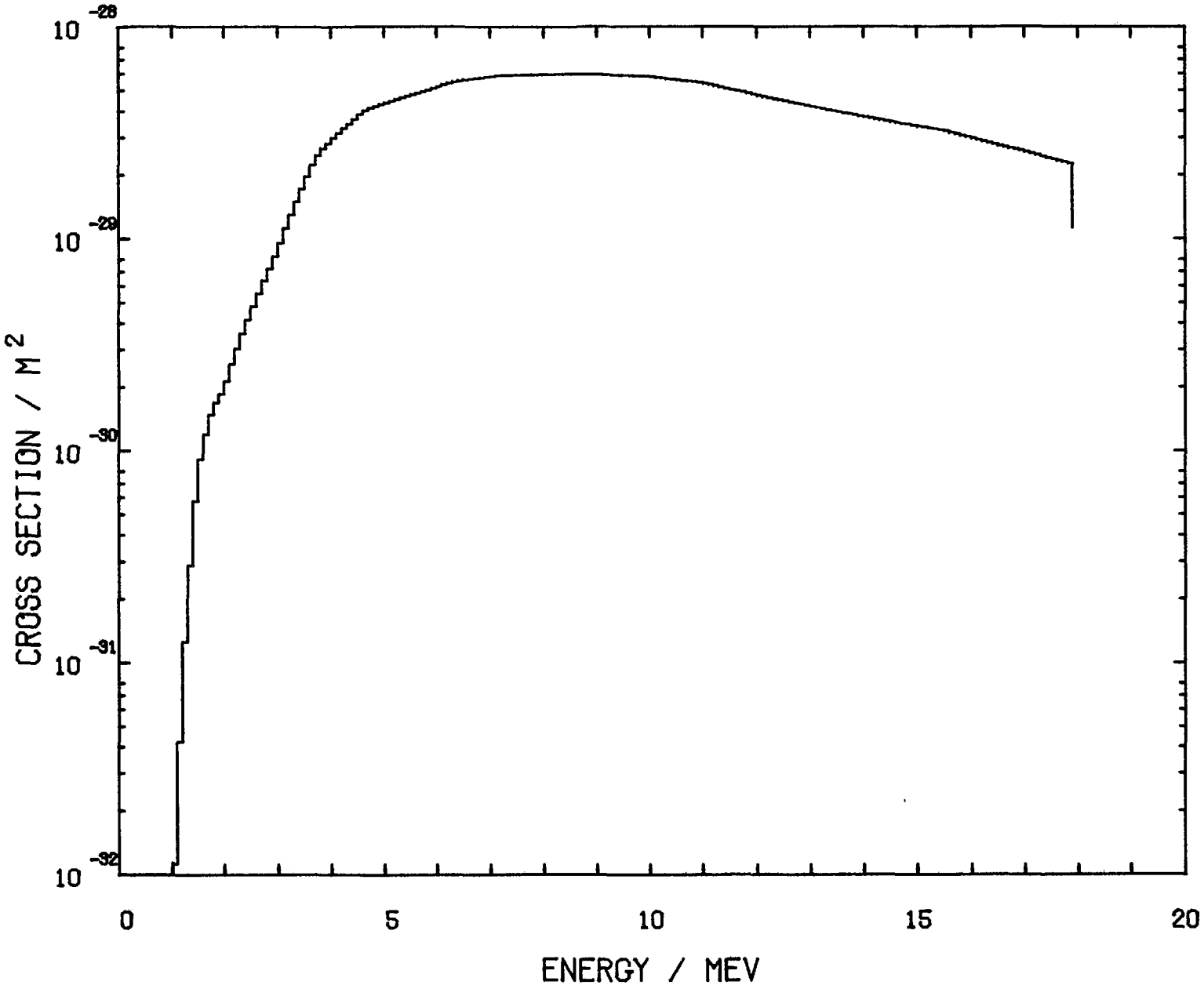

Fig. 6 Cross section curve for the reaction $^{54}Fe(n,p)\ ^{54}Mn$ (from DETAN 74).

RMG 4520

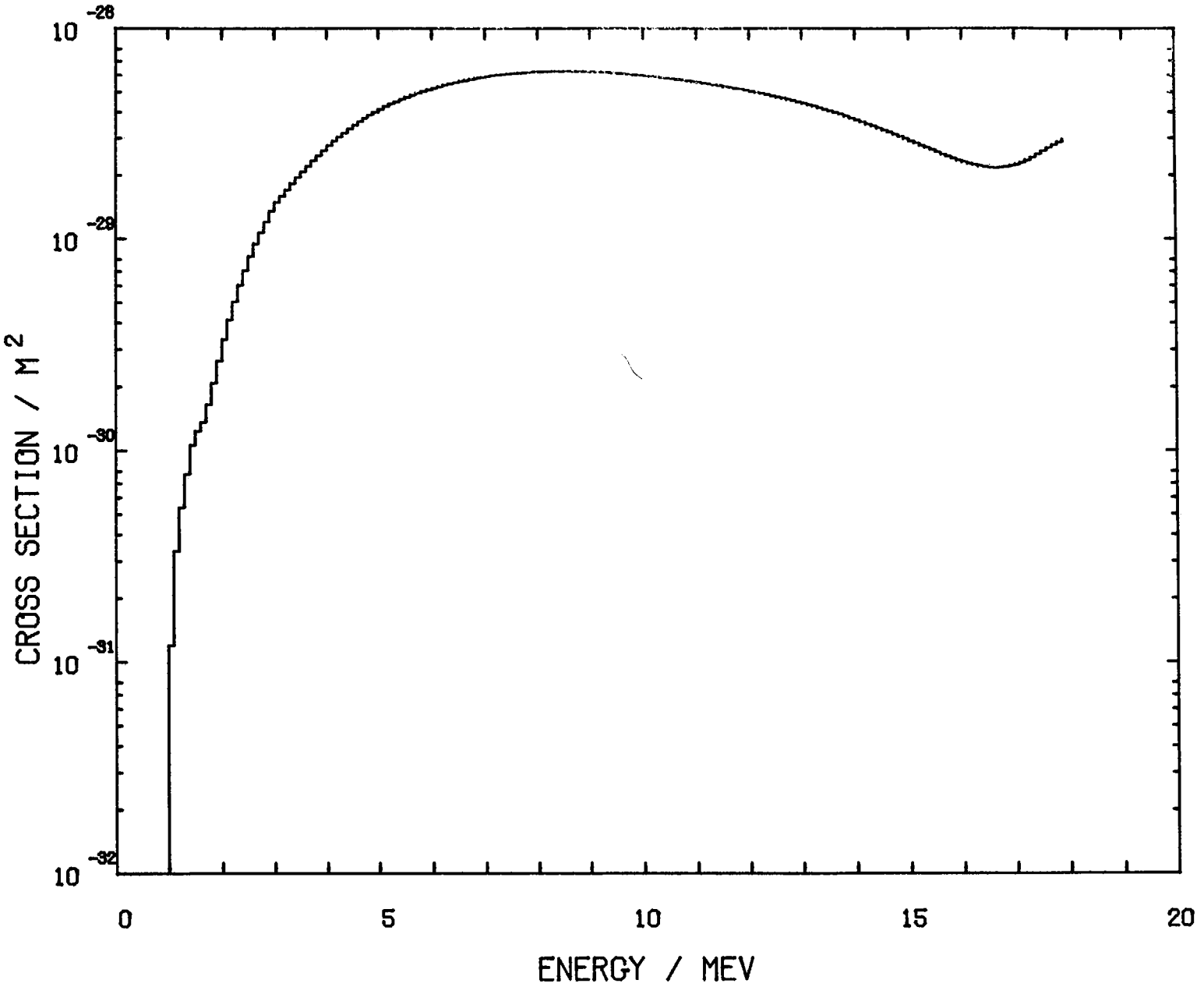

Fig. 7 Cross section curve for the reaction $^{54}Fe(n,p)\ ^{54}Mn$ (from LAPENAS).

RMG 4521

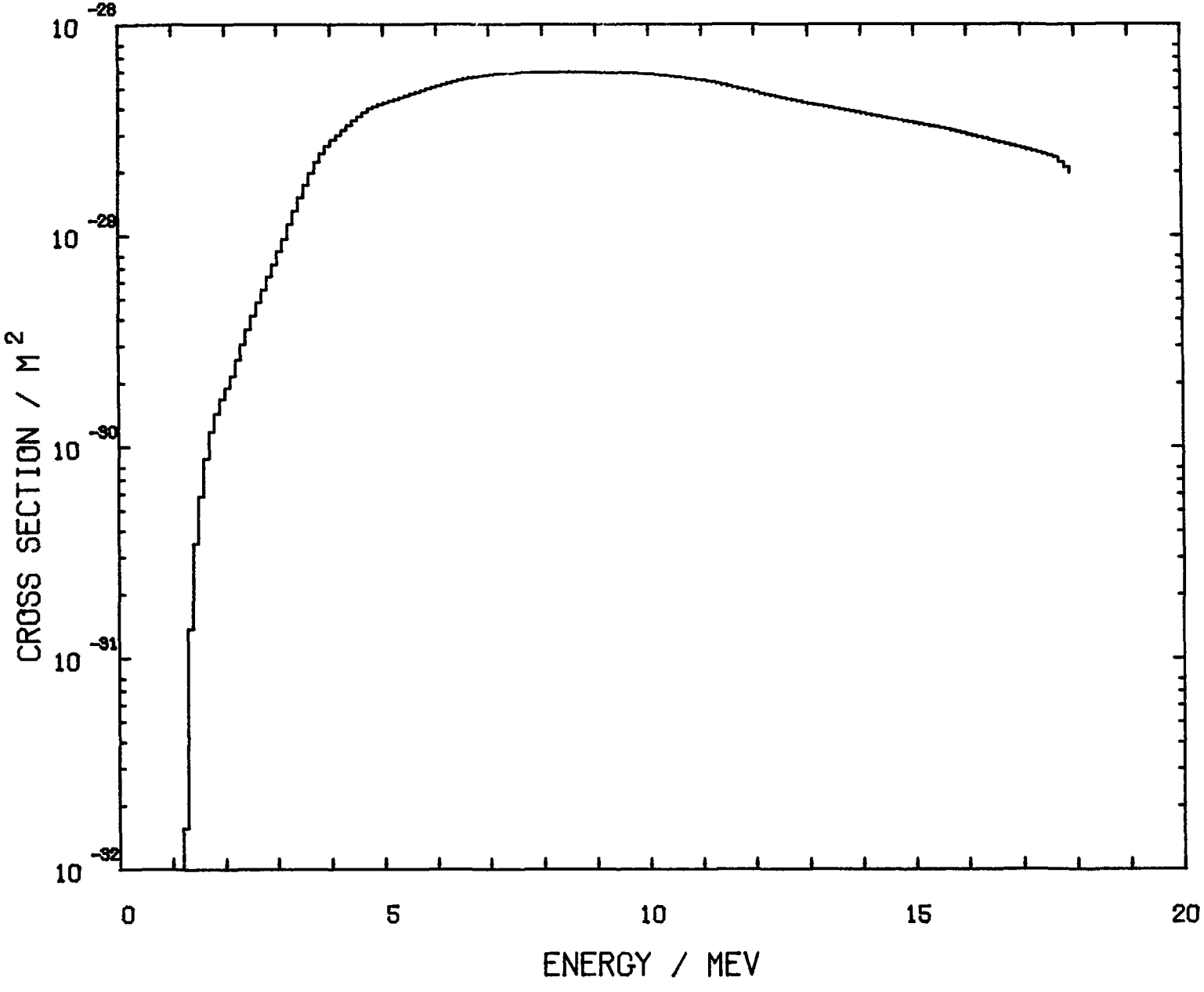

Fig. 8 Cross section curve for the reaction $^{54}Fe(n,p)\ ^{54}Mn$ (from CESNEF).

RMG 4522

II.12. Comparison of DETAN-74 and ENDF/B-IV Cross Section Data in 620 Groups

Willem L. Zijp,
Henk J. Nolthenius,
Henk Ch. Rieffe

Stichting Energieonderzoek Centrum Nederland

Abstract:

The report presents computer plots of the ratios of the energy dependent cross section values present in both the DETAN-74 and the ENDF/B-IV cross section library, using a 620 group structure.
The ENDF/B-IV cross sections show more detailed structure in the resonance region than the DETAN-74 data. Where the cross section ratio fluctuates strongly, a 155 group structure is used for the plots.
The cross section data are very much alike, for those cases where the DETAN-74 data were based on the ENDF/B-III evaluations.
For threshold reactions the two libraries show often larger deviations near the threshold energy.
Remarkable discrepancies were observed between the library data for the category I reactions $^{46}Ti(n,p)^{46}Sc$ and $^{237}Np(n,f)$.
The character of the report does not allow to make conclusions concerning the quality of the two libraries. Its main purpose is to visualize difference in energy dependent cross section data in the two libraries.

1. INTRODUCTION

For metrology purposes and especially for spectrum unfolding several group cross section libraries are available in the 620 group structure, which can be used in combination with spectrum unfolding programs (e.g. SAND-II, RFSP-JÜL, CRYSTAL BALL).
Two cross section libraries which are rather extended (e.g. cross section data for thermal, intermediate as well as fast neutrons) are available. These are the ENDF/B-IV dosimetry file and the DETAN-74 cross section library, both with 36 reactions.
The cross section data for the same 29 reactions are available on both libraries.
In this report an illustration is given of the deviations between the data for particular reactions present in these two libraries. Integral data obtained with a Maxwellian spectrum, a 1/E spectrum and a Watt fission neutron spectrum are presented in |1|. Those integral data do not show the magnitude of the deviations at specific energy values which can be important in spectrum unfolding.
For this reason the ratio of the cross section data present in the two libraries was plotted as function of the neutron energy. Sometimes this ratio fluctuates strongly from group to group. For this reason sometimes an averaging of cross section data over 4 neighbouring groups was performed before the cross section ratio was calculated.

2. CROSS SECTION LIBRARIES

The two cross section libraries of interest were obtained from Dr A. Fabry from the CEN/SCK laboratory at Mol in Belgium (June 2nd, 1975) |2|.
The history of the two libraries is different. The ENDF/B-IV dosimetry file |3| is a rather recent evaluation. The dosimetry file has been evaluated for dosimetry purposes in the interlaboratory LMFBR reaction rate program. The dosimetry file consists of reaction data already present in the ENDF/B file and a number of new evaluations.
The most recent data in this library are from 1974 while the oldest evaluation originates from 1966.
The history of the DETAN-74 is not so well documented.

A number of reaction data originate from the library accompanying the SAND-II program |4| and updating of this library is given in |5|.
Rather recently a few new reaction data sets were included.
Both libraries were available in a 620 group structure covering the energy range from 10^{-10} to 18 MeV.

3. SOFTWARE

A small program has been written to prepare computer plots of the cross section ratio of identical reactions of the two libraries as a function of the energy.
For all ratio determinations the ENDF/B-IV dosimetry data were in the denominator. The ratios were plotted if cross section data for the energy group of interest are present in both libraries. The latter may lead to undetected differences in some cases (e.g. for the reaction $^{238}U(n,\gamma)$ the resonances present in the ENDF/B-IV data are not present in the DETAN-74 values).
The energy scale is logarithmic for those reactions which have a non zero cross section at 10^{-10} MeV. The threshold reactions are plotted with a linear energy scale.
In a number of cases the ratio fluctuates strongly, due to the presence of resolved resonance data in one library and less resolved or unresolved ones in the other library.
To decrease the fluctuation to some extent the ratio was calculated for the average cross section data.
The average cross section is calculated by averaging the cross section data belonging to four successive energy groups.
The plots for which this procedure was applied can easily be recognized from the clear histogram structure.

4. PRESENTATION OF RESULTS

The cross section information is presented in the sequence which is used in |6|. This classification can be used in the interpretation of the results.

In all ratio determinations the ENDF/B-IV data were applied as a reference. For this reason these data were put in the denominator of the ratios.

4.1. Integral cross section ratios

The integral cross section data for the Maxwellian, the 1/E spectrum and the Watt fission neutron spectrum, were applied to calculate the ratios of these data for the DETAN-74 and the ENDF/B-IV |1| dosimetry cross section data libraries.
The results for these ratios are presented in table 1 and table 2 for category I and II respectively.

4.2. Energy dependent ratios

These data are presented in figure 1 to figure 29. In a number of cases rather strong fluctuations were found as function of the energy.
In these cases the averaging procedure was applied. The plots show in this case a rather course structure (e.g. the ratio for the reaction $^{197}Au(n,\gamma)$).

5. DISCUSSION

The results for category I reactions presented in table 1 show that the ratios for the following reactions of category I deviate less than 5%: $^{6}Li(n,\alpha)$, $^{27}Al(n,\alpha)$, $^{58}Ni(n,p)$, $^{197}Au(n,\gamma)$, $^{235}U(n,\gamma)$, $^{238}U(n,f)$ and $^{239}Pu(n,f)$.
Three reactions give higher deviations for one or more ratios.
The same procedure applied to category II reactions (see table 2) leads to deviation less than 5% for $^{54}Fe(n,p)$, $^{56}Fe(n,p)$ and $^{232}Th(n,\gamma)$. All other reactions of this table give ratios with deviations larger than 5%.
The results for the cross section ratios presented in the figures show in most cases clear differences. The differences are relatively small (<25%) for the following category I reactions: $^{6}Li(n,\alpha)$, $^{235}U(n,\gamma)$, $^{238}U(n,f)$ and $^{239}Pu(n,f)$.

The other reactions show important differences at one or more energy regions. The resonance region gives for most (n,γ) and (n,f) reactions large differences in the ratios as a function of energy.
The differences are situated at the resonance energies (e.g. $^{237}Np(n,f)$) but also different ratios are found in the valley between the first and the following resonances (e.g. $^{137}Au(n,\gamma)$).
For the fast neutron reactions in most cases clear differences can be detected in the energy region below and around the threshold (e.g. $^{27}Al(n,\alpha)$).
Other cross sections differ so much that the plot does not give enough information on the real ratios (e.g. $^{46}Ti(n,p)$, $^{237}Np(n,f)$).
From table 3 and 4 it will be clear that for all reactions which yield rather good ratios of the integral responses, the cross section data in the DETAN-74 file originate from the ENDF/B-III file.
The rather small deviations of the ratio from the value 1 are due to the difference of the ENDF/B-III and the updated ENDF/B-IV dosimetry file.

6. REFERENCES

|1| Zijp, W.L.; Nolthenius, H.J.: "Comparison of integral cross section values of several cross section libraries in the SAND-II format" ECN-2 (Netherlands Energy Research Foundation, Petten, September 1976)

|2| Private communication from Dr A. Fabry coded: Eisenhauer, C.; Fabry, A.: "DETAN-74, computer code for calculating detector responses in reactor neutron spectra" October 1974.

|3| Magurno, B.A.: "ENDF/B-IV dosimetry file" BNL-NCS-50446 (National neutron cross section center Brookhaven National Laboratory, April 1975).

|4| McElroy, W.N.; Berg, S.: "Reference cross section library for SAND-II. A computer-automated iterative method for neutron flux spectra determination by foil activation" AFWL-TR-67-41, vol. III (Air Force Weapons Laboratory, Kirtland AFB, New Mexico, July 1967).

|5| Simons, R.L.; McElroy, W.N.: "Evaluated reference cross section library"
BNWL-1312 (Battelle Memorial Institute, Richland, Washington, May, 1970).

|6| Proceedings of a Consultants Meeting on Nuclear Data for Reaction Neutron Dosimetry, Vienna 10-12 September 1973.
Report INDC(NDS)-56/U (IAEA, Vienna, 1974).

7. TABLES

Table 1: Ratios of integral cross section data category I reactions

reaction	spectrum			figure number
	Maxwellian	1/E	fission	
$^{6}Li(n,\alpha)^{3}H$	1.003	1.000	0.974	1
$^{10}B\ (n,\alpha)^{7}Li$	1.000	1.000	1.113	2
$^{27}Al(n,\alpha)^{24}Na$			0.969	3
$Ti(n,np)^{46}Sc$			1.137	4
$^{58}Ni(n,p)^{58}Co$			0.994	5
$^{197}Au(n,\gamma)^{198}$	1.000	1.023	1.030	6
$^{235}U(n,f)$	0.991	1.000	1.000	7
$^{238}U(n,f)$		1.011	0.996	8
$^{237}Np(n,f)$	1.157	0.809	0.966	9
$^{239}Pu(n,f)$	0.999	0.958	1.018	10

Table 2: Ratios of integral cross section data, category II reactions

reaction	spectrum			figure number
	Maxwellian	1/E	fission	
$^{23}Na(n,\gamma)^{24}Na$	1.010	0.864	0.943	11
$^{45}Sc(n,\gamma)^{46}Sc$	0.955	0.939	1.092	12
$^{58}Fe(n,\gamma)^{59}Fe$	1.010	0.897	1.710	13
$^{59}Co(n,\gamma)^{60}Co$	0.991	0.957	0.833	14
$^{63}Cu(n,\gamma)^{64}Cu$	1.004	0.866	1.005	15
$^{115}In(n,\gamma)^{116}In$	0.934	0.880	1.084	16
$^{232}Th(n,\gamma)^{233}Th$	1.057	0.942	0.999	17
$^{238}U(n,\gamma)^{239}U$	1.104	1.011	1.171	18
$^{27}Al(n,p)^{24}Mg$			0.936	19
$^{32}S(n,p)^{32}P$			0.936	20
$^{47}Ti(n,p)^{47}Sc$		1.048	0.791	21
$^{48}Ti(n,p)^{48}Sc$			1.299	22
$^{54}Fe(n,p)^{54}Mn$			0.972	23
$^{56}Fe(n,p)^{56}Mn$			1.049	24
$^{58}Ni(n,2n)^{57}Ni$			0.943	25
$^{63}Cu(n,\alpha)^{60}Co$			1.362	26
$^{115}In(n,n')^{115}In^{m}$		1.192	1.087	27
$^{127}I(n,2n)^{126}I$			0.597	28
$^{232}Th(n,f)$			1.015	29

Table 3: Source of cross section data and evaluation data; category I

reaction	DETAN-74	ENDF/B-IV
$^{6}Li(n,\alpha)^{3}H$	ENDF/B-III	1973
$^{10}B(n,\alpha)^{7}Li$	ENDF/B-III	1973
$^{27}Al(n,\alpha)^{24}Na$	CCC-112	1973
$Ti(n,np)^{46}Sc$	BNWL-1312	1972
$^{58}Ni(n,p)^{58}Co$	CCC-112	1973
$^{197}Au(n,\gamma)^{198}Au$	ENDF/B-III	1973
$^{235}U(n,f)$	ENDF/B-III	1974
$^{238}U(n,f)$	ENDF/B-III	1973
$^{237}Np(n,f)$	BNWL-1312	1973
$^{239}Pu(n,f)$	ENDF/B-III	1974

CCC-112B May 1969.
BNWL-1312 May 1970.

Table 4: Source of cross section and evaluation data; category II

reaction	DETAN-74	ENDF/B-IV
$^{23}Na(n,\gamma)^{24}Na$	BNWL-1312	1971
$^{45}Sc(n,\gamma)^{46}Sc$	BNWL-1312	1974
$^{58}Fe(n,\gamma)^{59}Fe$	BNWL-1312	1973
$^{59}Co(n,\gamma)^{60}Co$	BNWL-1312	1974
$^{63}Cu(n,\gamma)^{64}Cu$	BNWL-1312	1972
$^{115}In(n,\gamma)^{116}In$	CCC-112B	1973
$^{232}Th(n,\gamma)^{233}Th$	CCC-112B	1966
$^{238}U(n,\gamma)^{239}U$	CCC-112B	1973
$^{27}Al(n,p)^{24}Mg$	BNWL-1312	1973
$^{32}S(n,p)\ P$	CCC-112B	1972
$^{47}Ti(n,p)^{47}Sc$	BNWL-1312	1972
$^{48}Ti(n,p)^{48}Sc$	BNWL-1312	1972
$^{54}Fe(n,p)^{54}Mn$	BNWL-1312	1973
$^{56}Fe(n,p)^{56}Mn$	BNWL-1312	1972
$^{58}Ni(n,2n)^{57}Ni$	CCC-112B	1973
$^{63}Cu(n,\alpha)^{60}Co$	BNWL-1312	1972
$^{115}In(n,n')^{115}In^{m}$	BNWL-1312	1972
$^{127}I(n,2n)^{126}I$	CCC-112B	1972
$^{232}Th(n,f)$	CCC-112B	1966

BNWL-1312 May 1970.
CCC-112B May 1969.

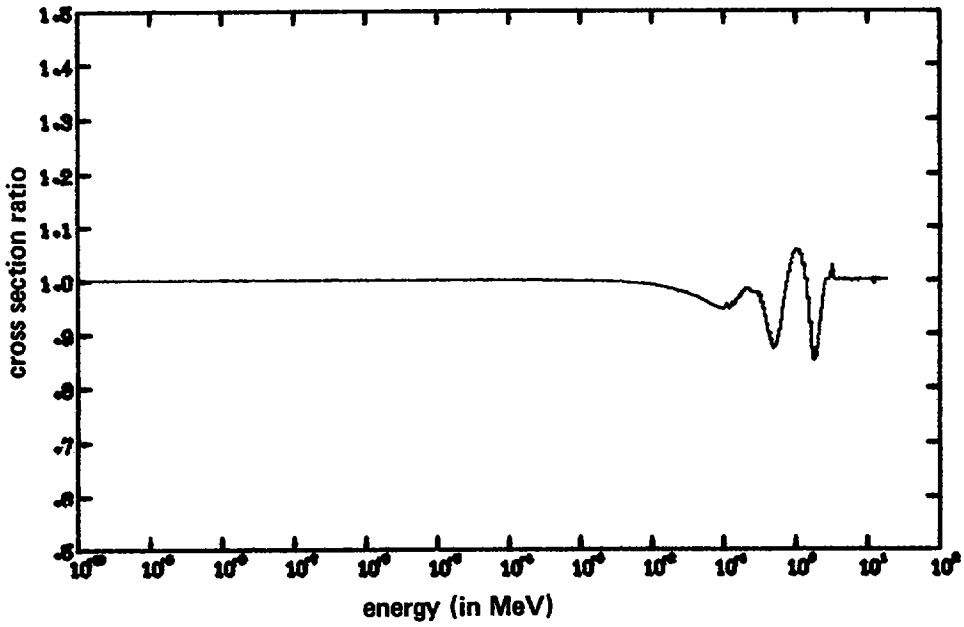

Fig. 1. CROSS SECTION RATIO FOR THE REACTION Li6(n,α)H3

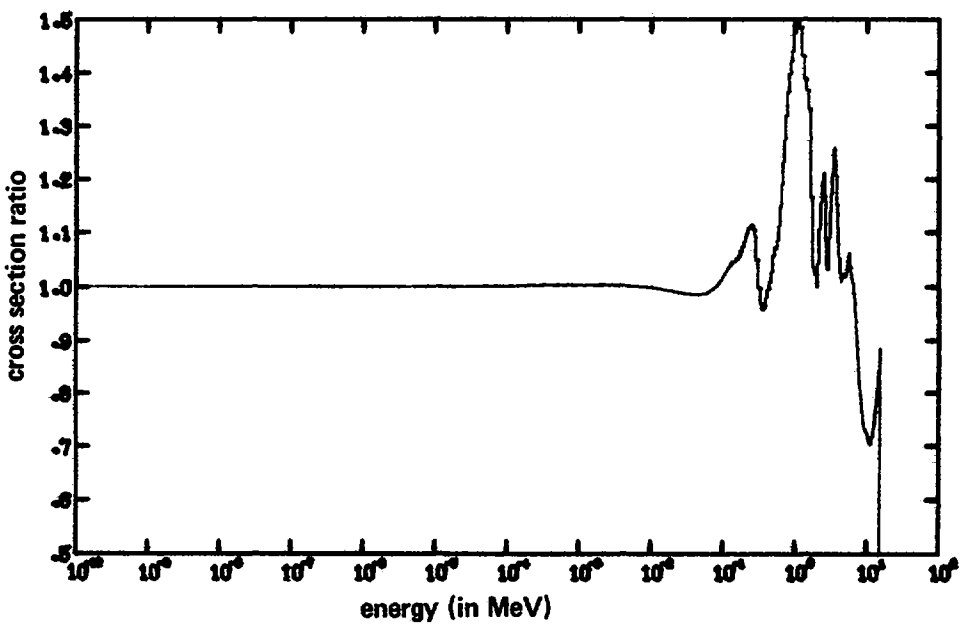

Fig. 2. CROSS SECTION RATIO FOR THE REACTION B10(n,α)Li 7

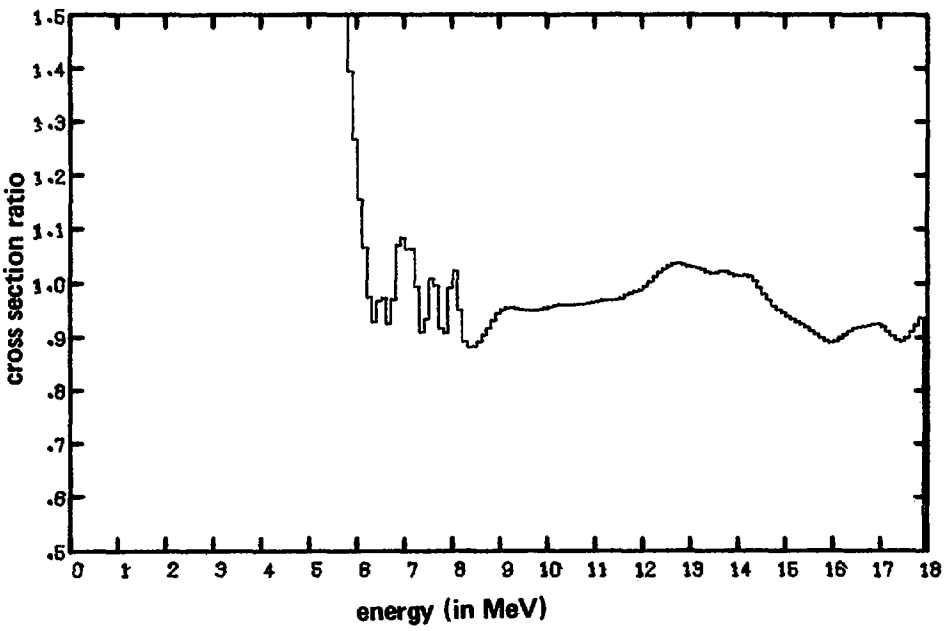

Fig. 3. CROSS SECTION RATIO FOR THE REACTION Al27(n,α)Na24

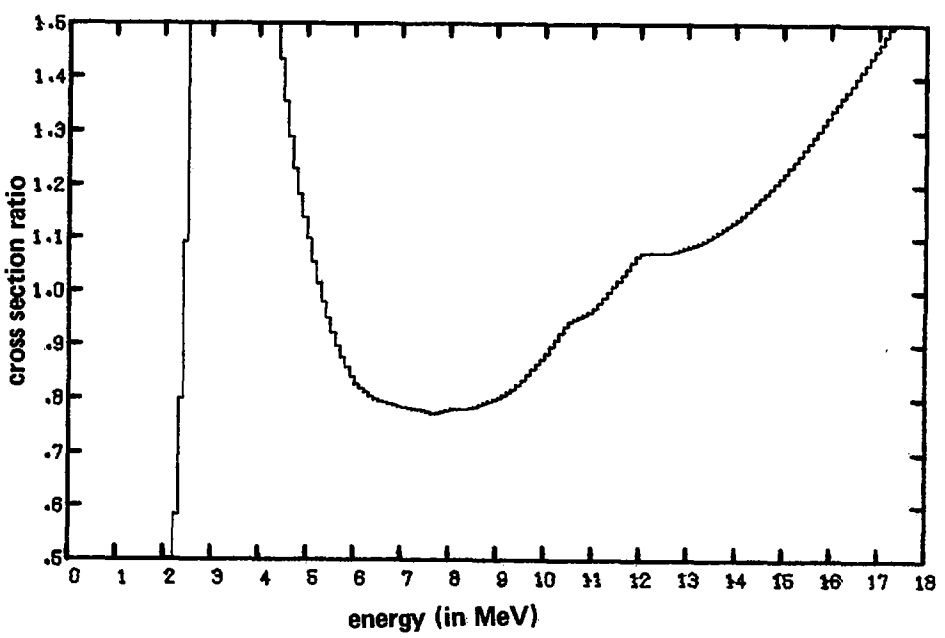

Fig. 4. CROSS SECTION RATIO FOR THE REACTION Ti46(n,p)Sc46

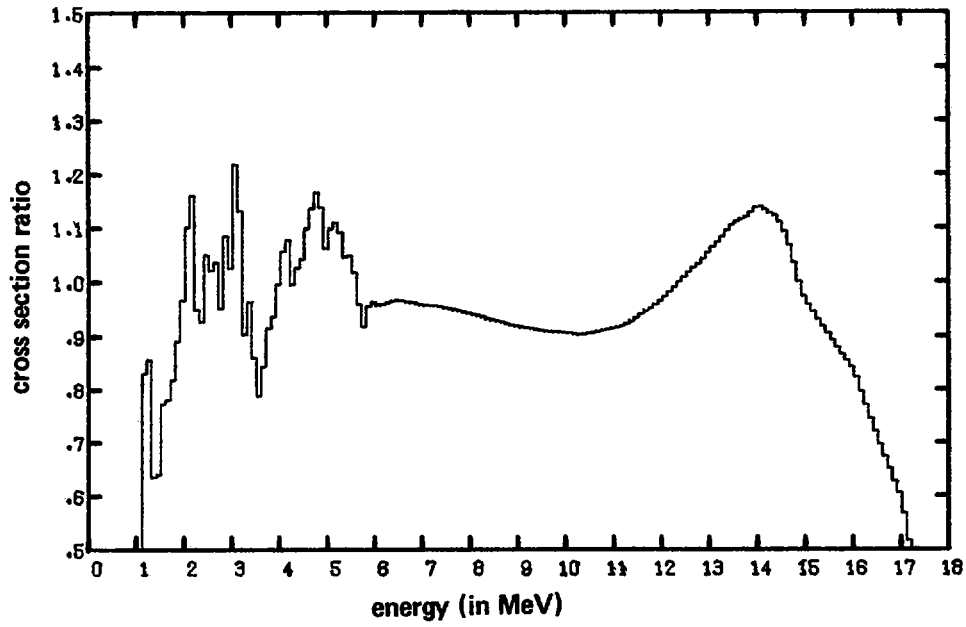

Fig. 5. CROSS SECTION RATIO FOR THE REACTION Ni58(n,p)Co58

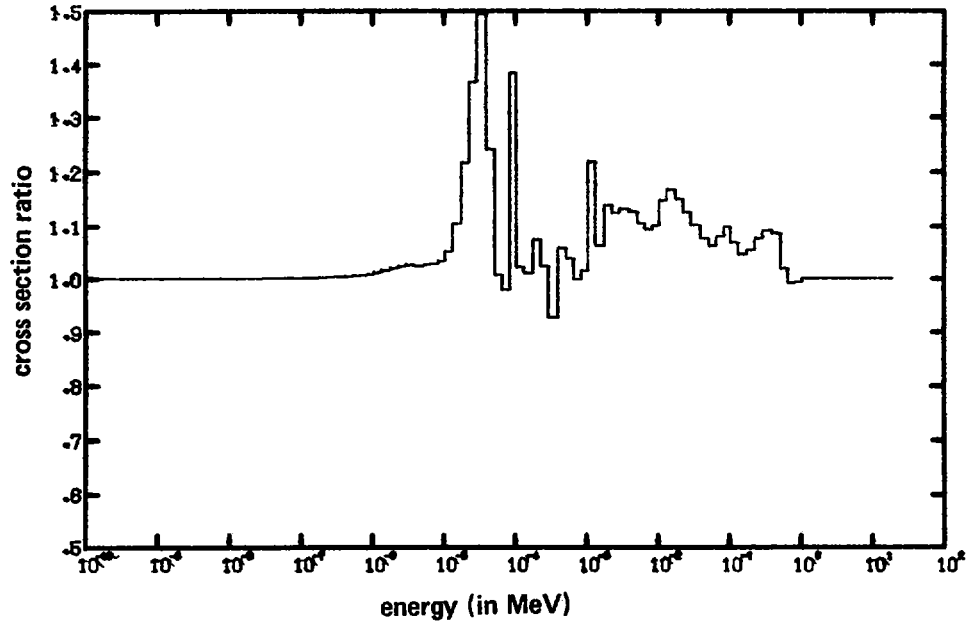

Fig. 6. CROSS SECTION RATIO FOR THE REACTION Au197(n,γ)Au198

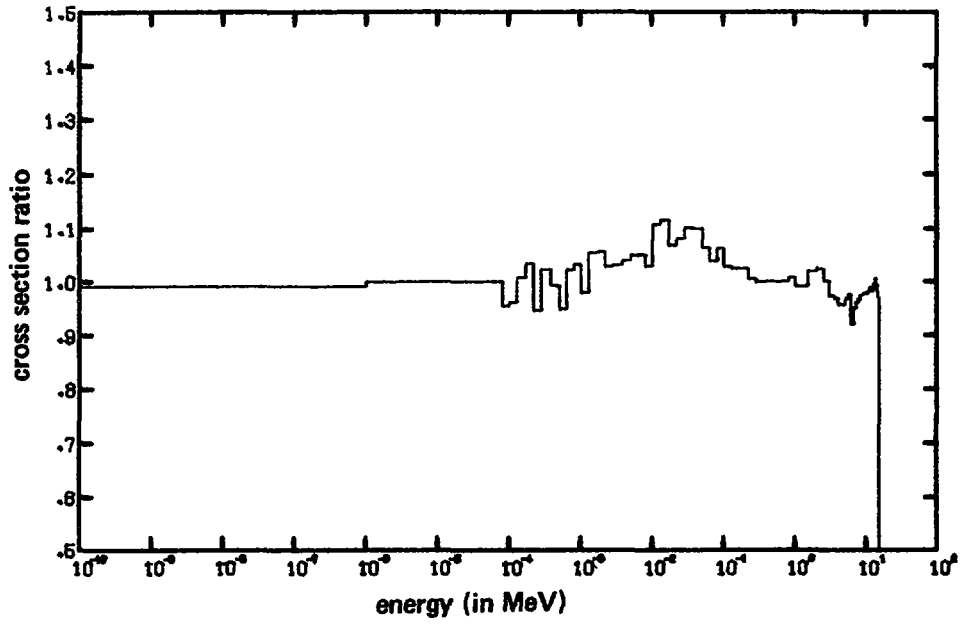

Fig. 7. CROSS SECTION RATIO FOR THE REACTION U235(n,f)FP

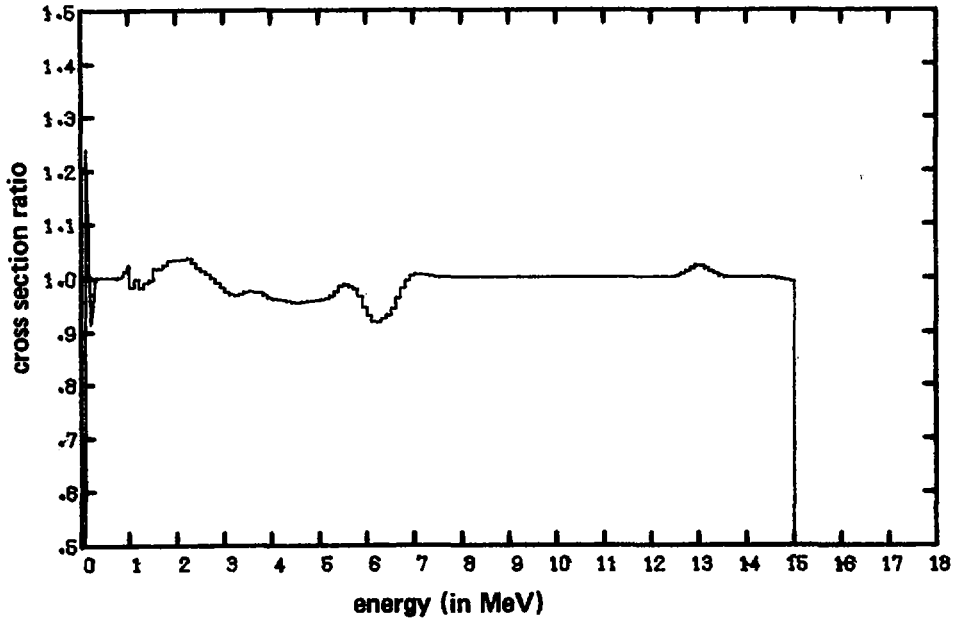

Fig. 8. CROSS SECTION RATIO FOR THE REACTION U238(n,f)FP

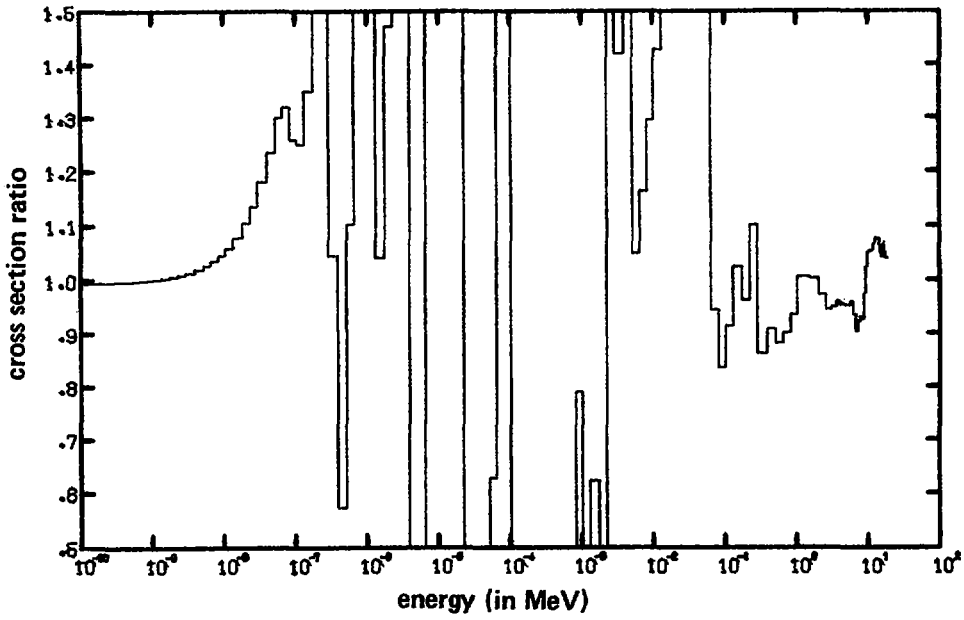

Fig. 9. CROSS SECTION RATIO FOR THE REACTION Np237(n,f)FP

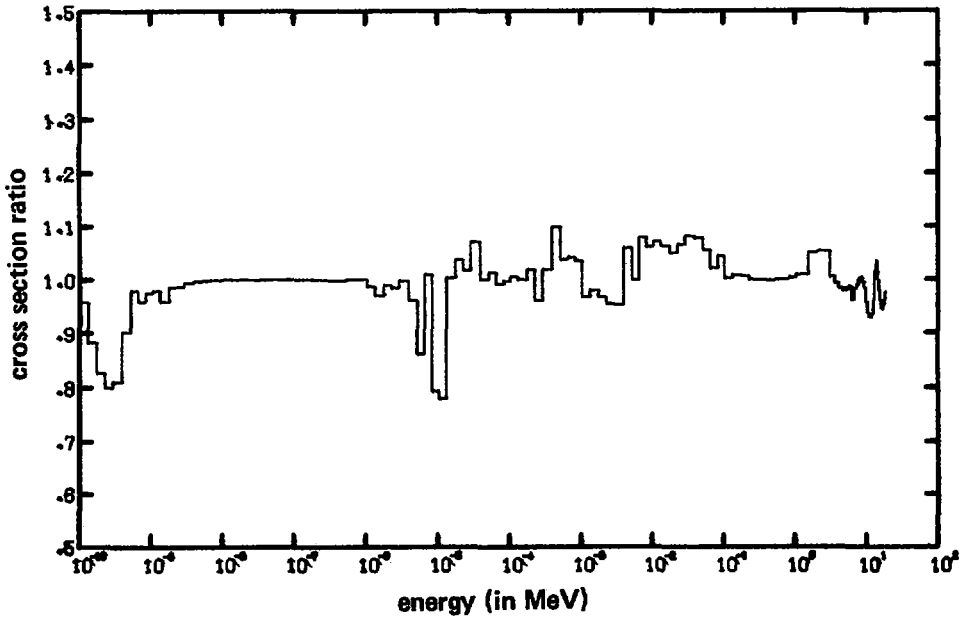

Fig. 10. CROSS SECTION RATIO FOR THE REACTION Pu239(n,f)FP

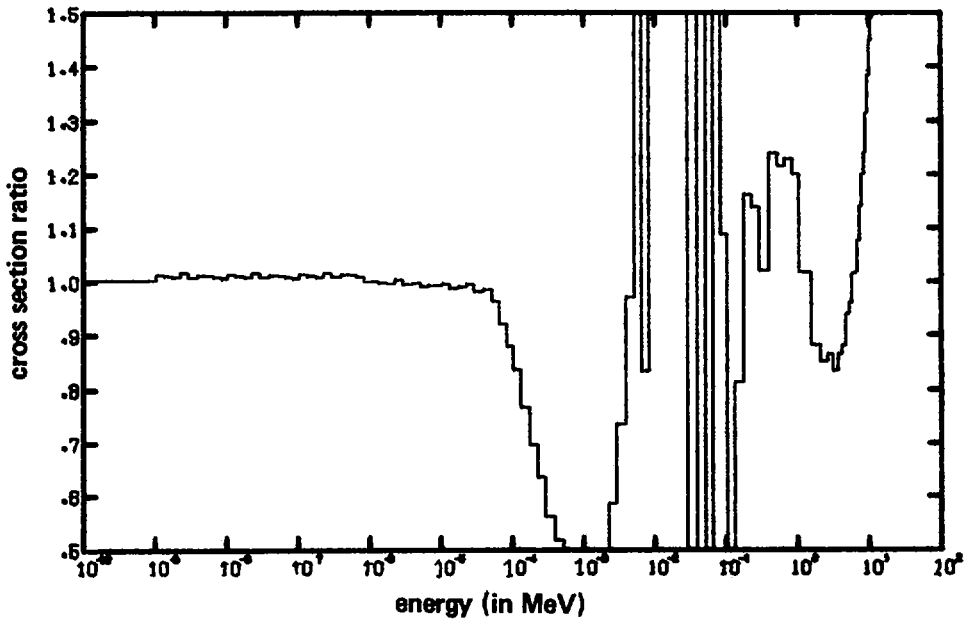

Fig. 11. CROSS SECTION RATIO FOR THE REACTION Na23(n,γ)Na24

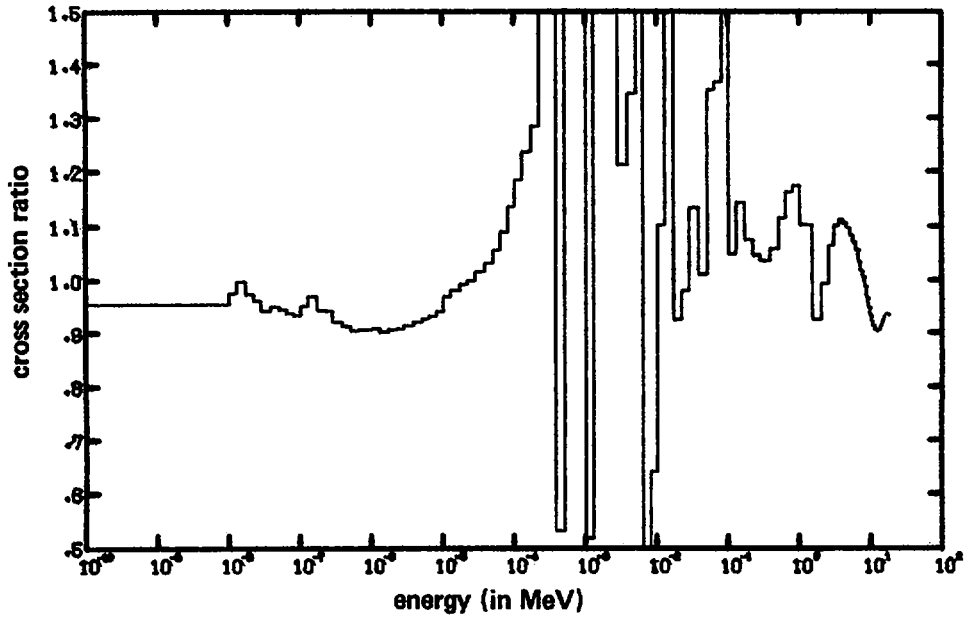

Fig. 12. CROSS SECTION RATIO FOR THE REACTION Sc45(n,γ)Sc46

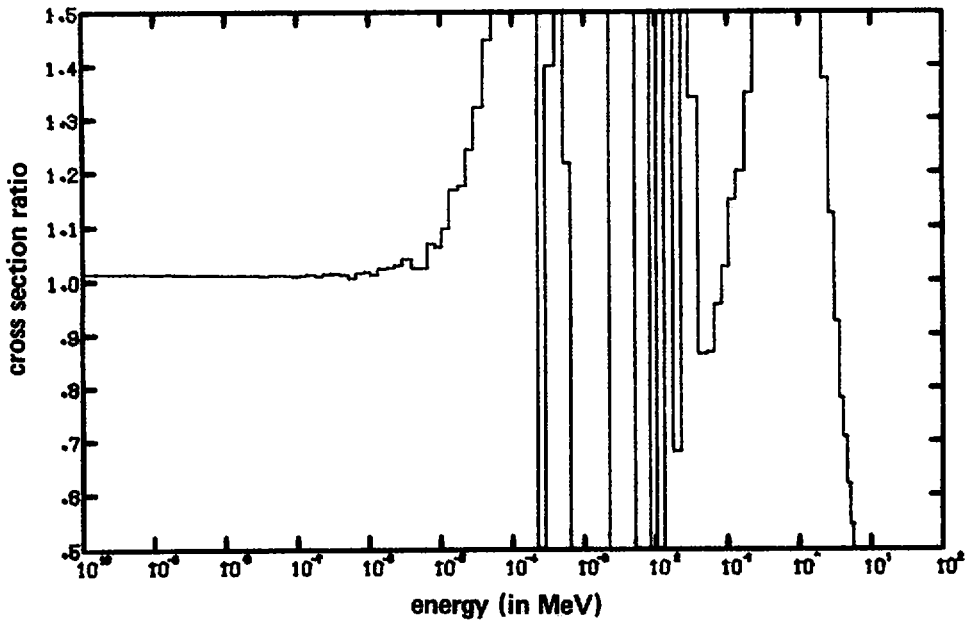

Fig. 13. CROSS SECTION RATIO FOR THE REACTION Fe58(n,γ)Fe59

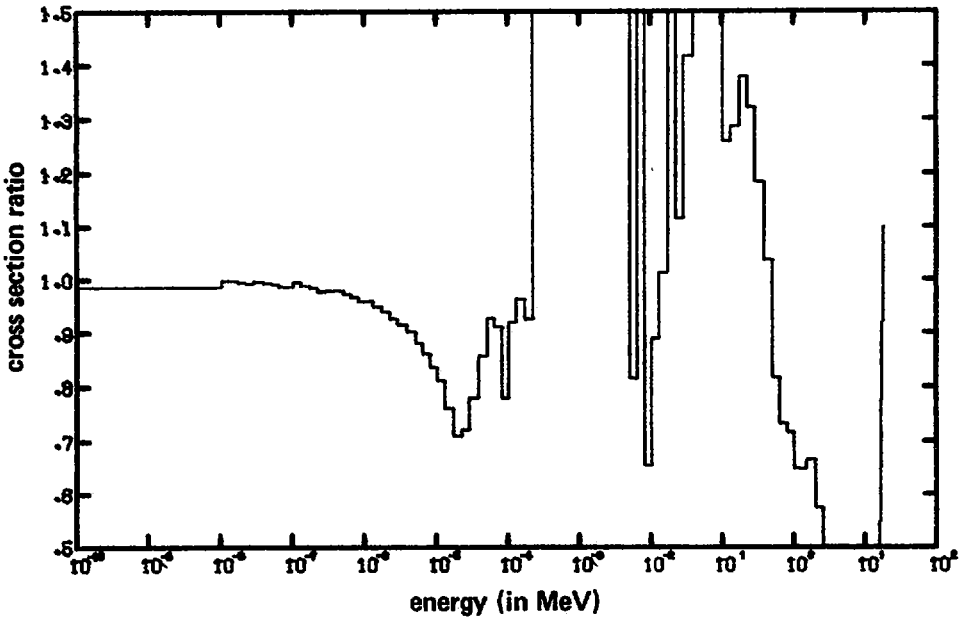

Fig. 14. CROSS SECTION RATIO FOR THE REACTION Co59(n,γ)Co60

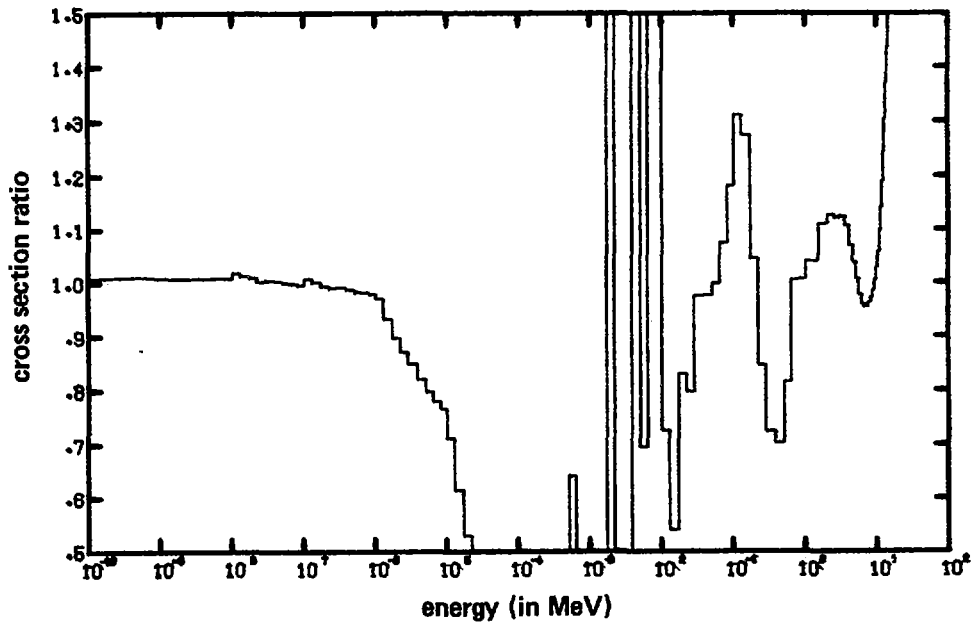

Fig. 15. CROSS SECTION RATIO FOR THE REACTION Cu63(n,γ)Cu64 .

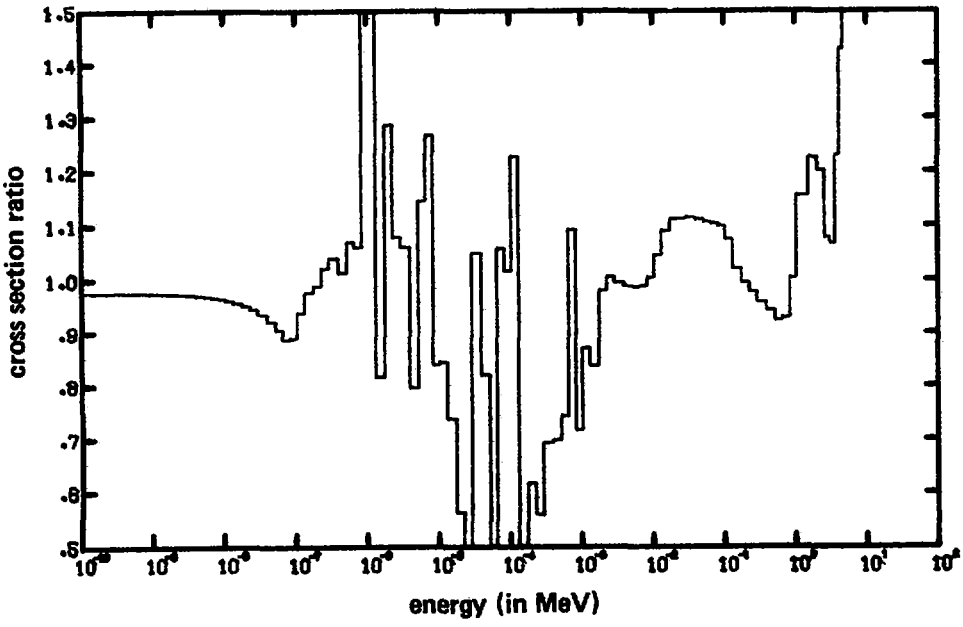

Fig. 16. CROSS SECTION RATIO FOR THE REACTION In115(n,γ)In116^{m}

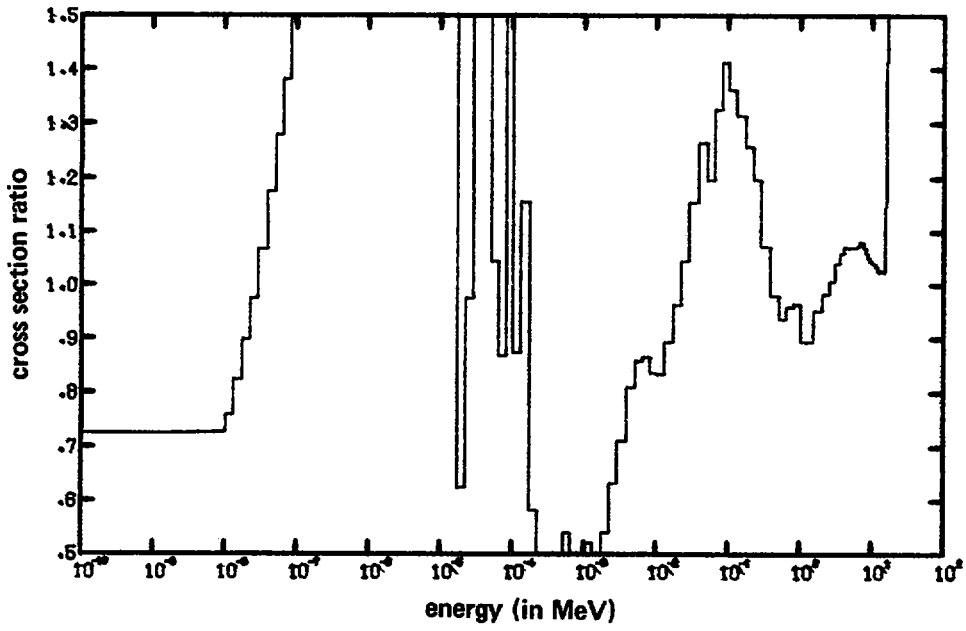

Fig. 17. CROSS SECTION RATIO FOR THE REACTION Th232(n,γ)Th233

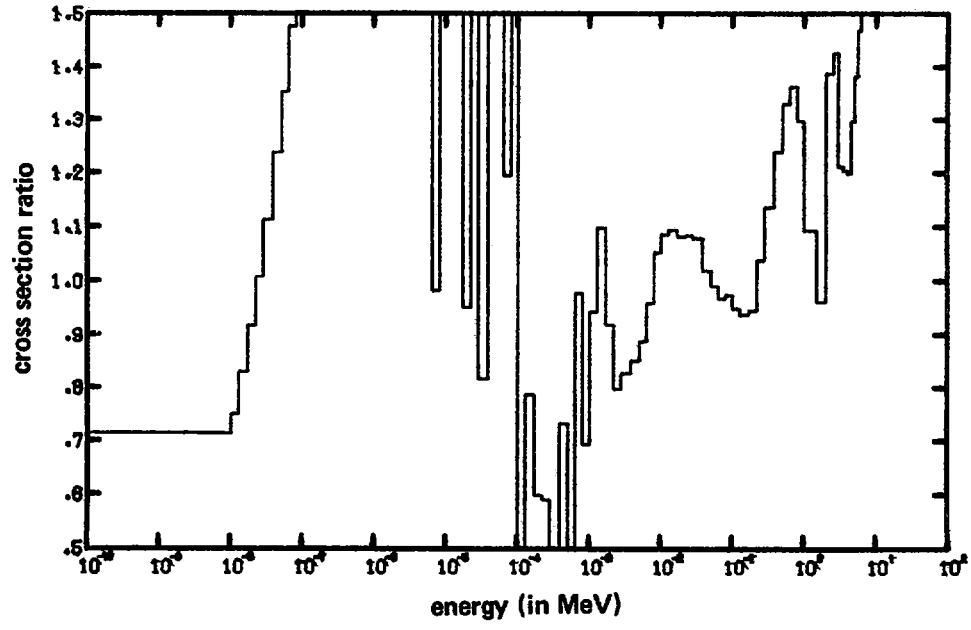

Fig. 18. CROSS SECTION RATIO FOR THE REACTION U238(n,γ)U239

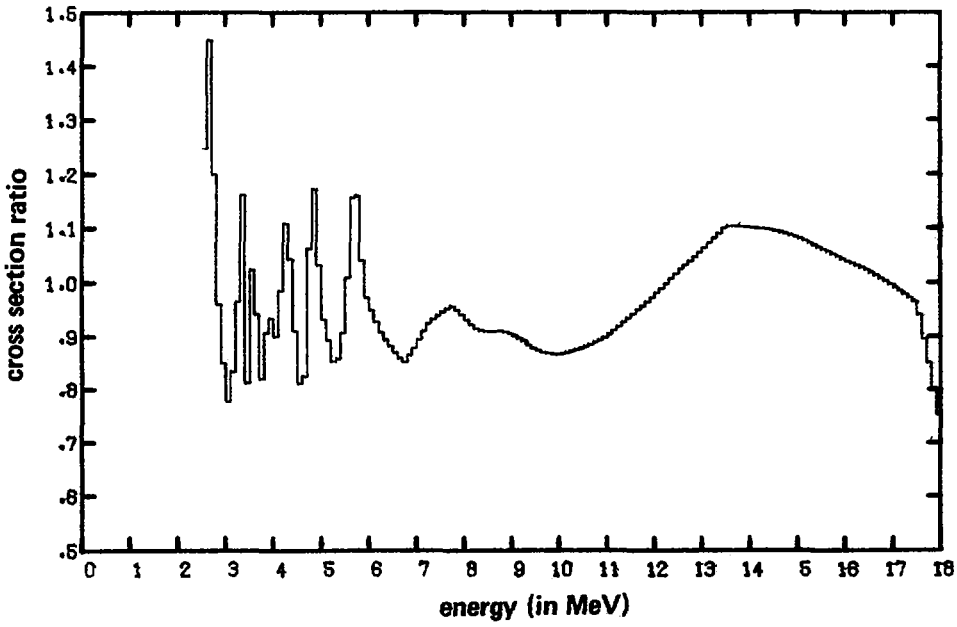

Fig. 19. CROSS SECTION RATIO FOR THE REACTION Al27(n,p)Mg27

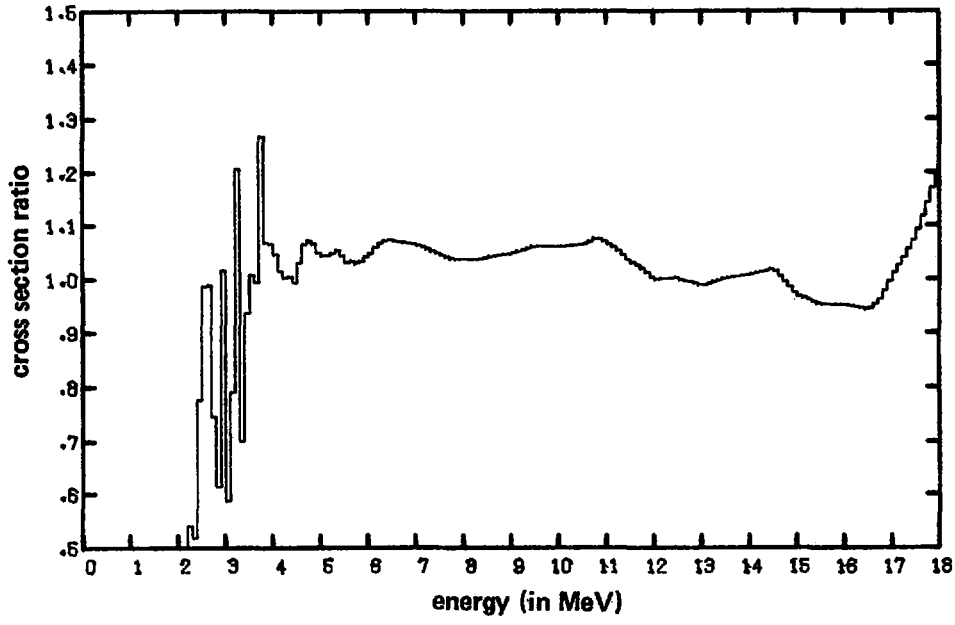

Fig. 20. CROSS SECTION RATIO FOR THE REACTION S32(n,p)P32

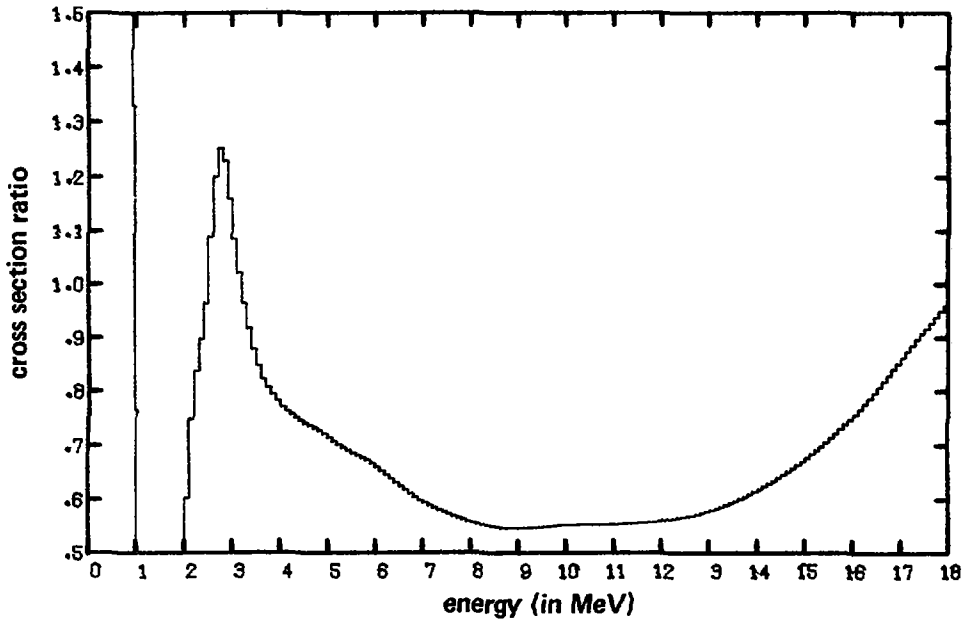

Fig. 21. CROSS SECTION RATIO FOR THE REACTION Ti47(n,p)Sc47

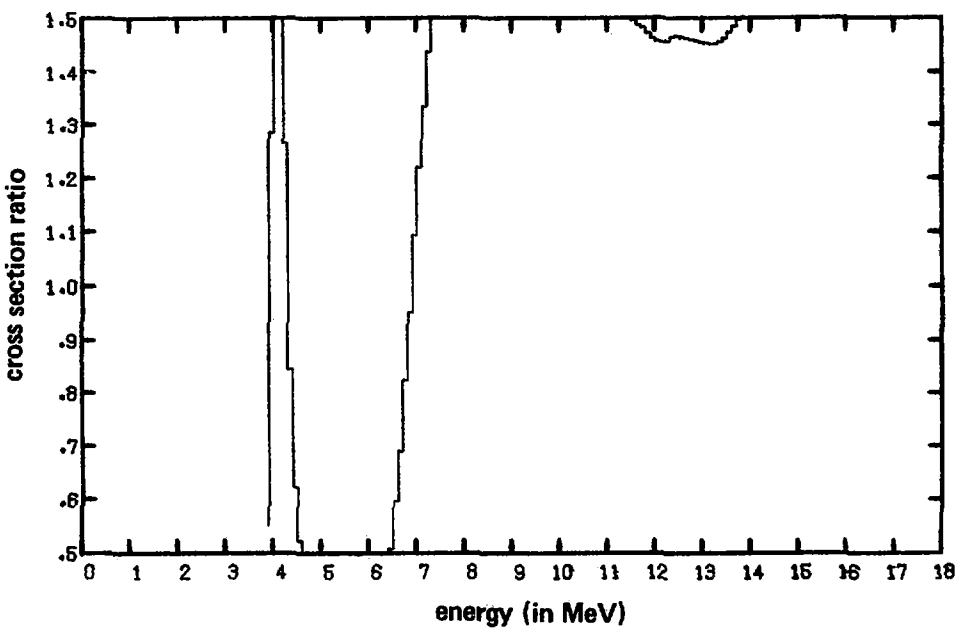

Fig. 22. CROSS SECTION RATIO FOR THE REACTION Ti48(n,p)Sc48

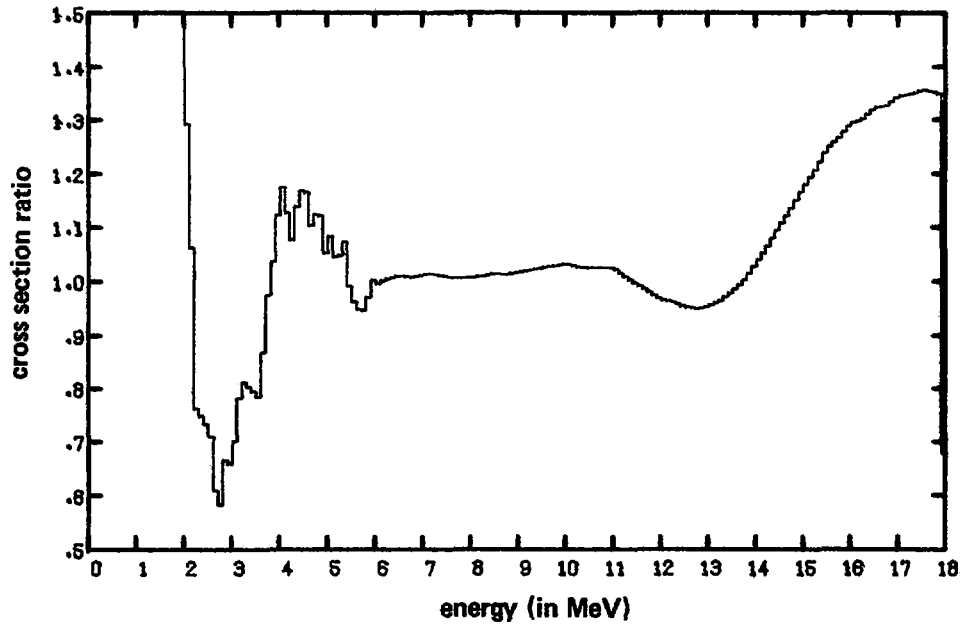

Fig. 23. CROSS SECTION RATIO FOR THE REACTION Fe54(n,p)Mn54

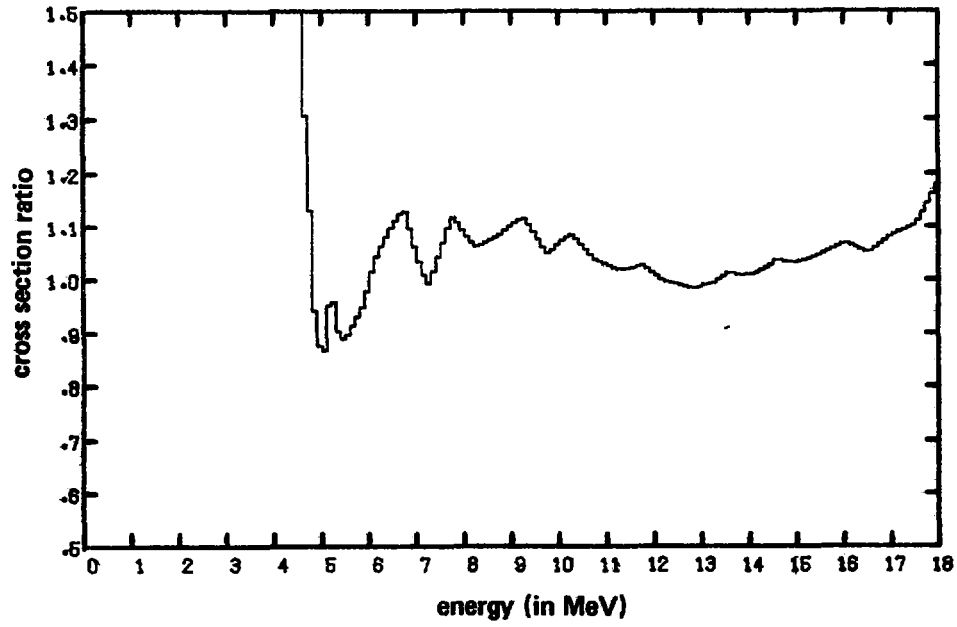

Fig. 24. CROSS SECTION RATIO FOR THE REACTION Fe56(n,p)Mn56

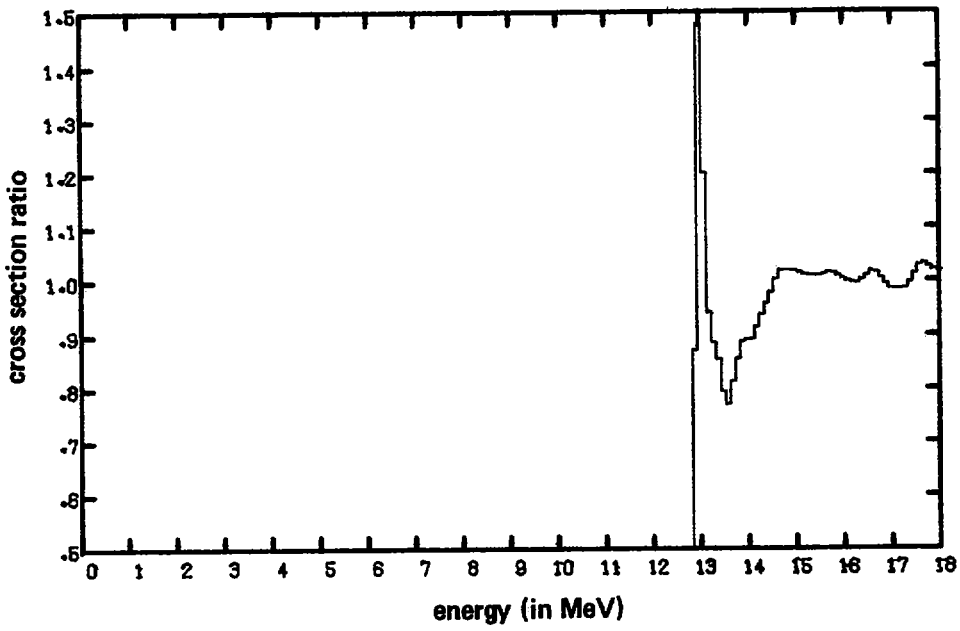

Fig. 25. CROSS SECTION RATIO FOR THE REACTION Ni58(n,p)Ni57

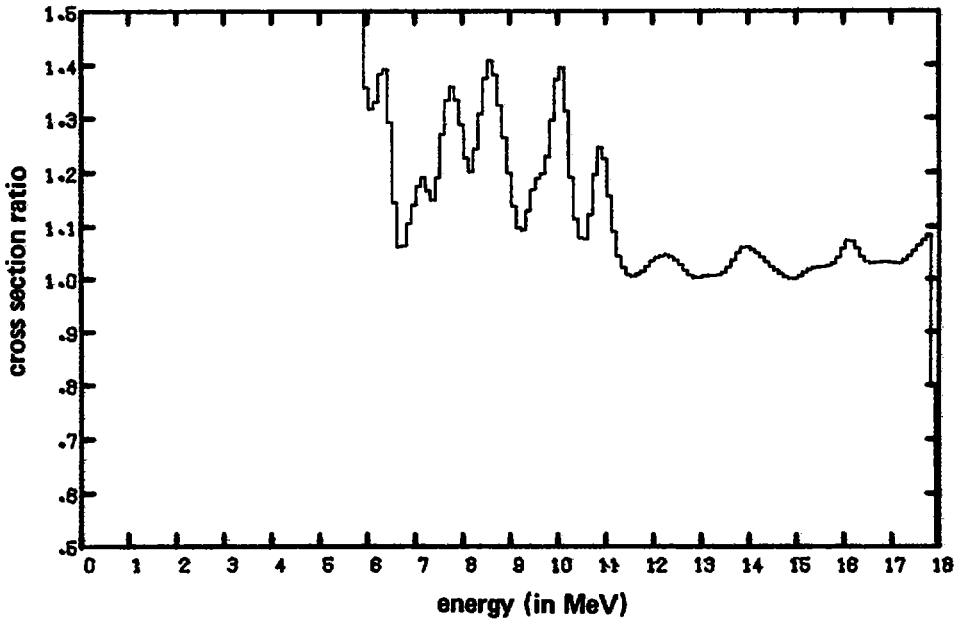

Fig. 26. CROSS SECTION RATIO FOR THE REACTION Cu63(n,α)Co60

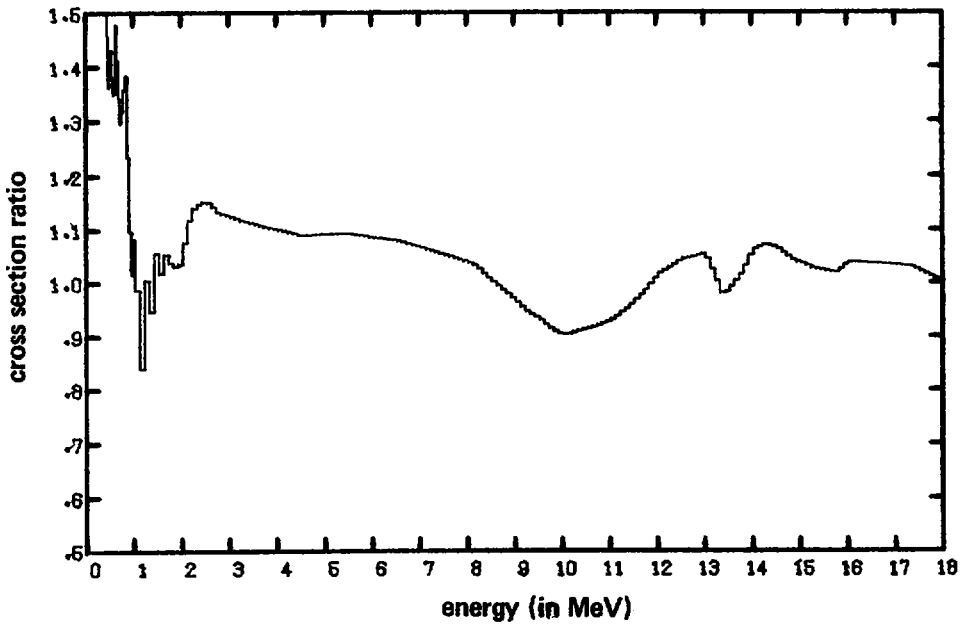

Fig. 27. CROSS SECTION RATIO FOR THE REACTION In115(n,n')In115^{m}

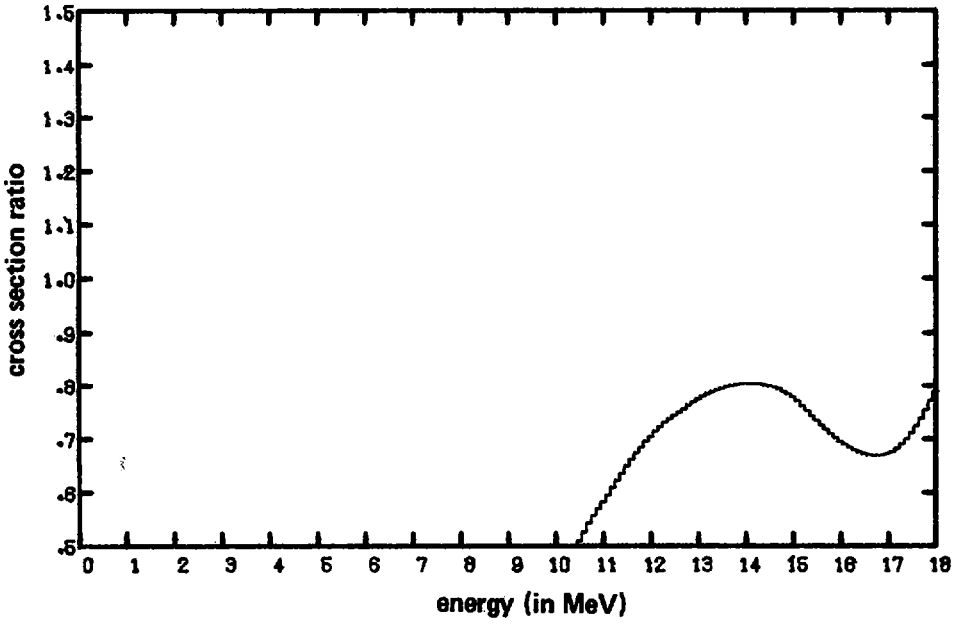

Fig. 28. CROSS SECTION RATIO FOR THE REACTION I127(n,2n)I126

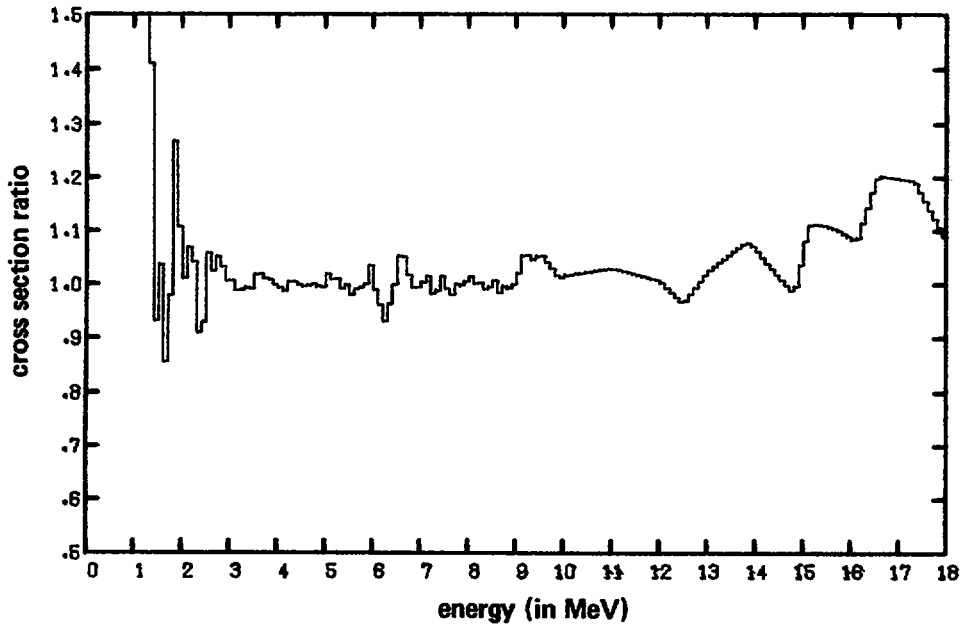

Fig.29. CROSS SECTION RATIO FOR THE REACTION Th232(n,f)FP

II. 13. One Material Experiments in the Frame of Power Reactor Pressure Vessel Benchmarks

G. De Leeuw-Gierts, S. de Leeuw
Reactor Physics Department
C.E.N.-S.C.K., Mol, Belgium

ABSTRACT

The one-material experiments in a one-dimensional geometry performed at present on Fe, have demonstrated the possibility of using certain configurations to study the neutronic irradiation characteristics of power reactor pressure vessels. These configurations, presenting the same geometrical and experimental advantages as MOL-ΣΣ, are described and the spectra compared to few pressure vessel calculated neutron spectra.

1. GENERALITIES

Uncertainties on nuclear data for structural materials play an important role in the prediction of the reactor core and environmental characteristics.
Critical and shielding mock-up experiments are generally unsatisfactory with respect to nuclear data improvement , because of the large number of parameters present in the analysis.

Experiments involving a small number of materials in a simple geometrical arrangement and under well controlled environmental conditions are expected to contribute to the cross section evaluation work. An experiment of this type is at present under way at C.E.N./S.C.K. The materials under concern up to now are U_{nat} and pure iron.

The study of the group cross sections and the neutron transport calculation methods, aimed with these experiments, are also expected to contribute to a better physical understanding of the penetration of fast neutrons through thick steel structures and the production of damage. Proper evaluation of steel embrittlement indeed requires the knowledge of the neutron spectrum variation at different penetrations; this variation is directly related to the neutron group cross sections of the materials, as used in the computation.

2. ONE MATERIAL EXPERIMENT

The experimental iron set-up, presently studied at C.E.N./S.C.K. is driven by a fast neutron source : a spherical shell of natural uranium placed in the centre of the 1 m cavity hollowed in the vertical graphite thermal column of the BR1 reactor (Fig. 1).
The mean energy of the driver spectrum can be changed by varying the thickness of the U_{nat} shell. In Fig. 2 the driver spectra, obtained with shell thicknesses of 1, 3 and 6 cm are compared.
In the largest U_{nat} shell, Fe-shells of 2 cm up to 14 cm thickness can be inserted.

The neutron spectra in the centre of the U_{nat} shells, with or without inner iron shells are measured by means of the (n,p) and $^{6}Li(n,\alpha)t$ neutron spectrometry techniques.
Fig. 3 displays the 208 gr DTF IV (Kedak library) calculated spectra for the 1 cm U_{nat} driver and 1 cm U_{nat} + respectively 7, 9 and 14 cm U inner Fe shells.
The comparison of the experimental results to the theoretical ones computed with different cross section libraries, leads to the selection of the most adequate, or to the improvement of, the group cross section set.

The adequacy of the set-up to simulate some neutronic irradiation conditions of a pressure vessel has been established on the basis of reactor vessel calculations found in literature [1] or performed at C.E.N./S.C.K. for BR3 and in the frame of an international comparison organized by the NEA, as a result of the Paris meeting on sensitivity studies and shielding benchmarks (October 1975) [2] .
Fig. 4 compares the interface spectrum of the 1 cm U_{nat}+ 9 cm Fe configuration to the theoretical incident spectra on the pressure vessel published in [1, 2, 3]. The relative fluxes ($n/cm^2sec^{-1} > 0.5$ MeV) from [1] are compared in Fig. 5 to those through the Fe Shells of the 1 cm U_{nat}+ 7 cm Fe and 1 cm U_{nat}+ 14 cm Fe configurations, respectively for $E_n > 0.1$, 0.4 and 1.4MeV.

At the Paris meeting, the high sensitivity of the reactor benchmark calculations to the Legendre expansion of the scattering cross section was put forward. Consequently accuracy is not only required on the differential cross sections but also on the angular distributions and this up to the third order.
It is expected that the neutron spectra and reaction rate transverse measurements performed in several configurations will lead to a better understanding of the fast neutron penetration in iron, and consequently in the pressure vessel. The same measurements performed in the inverted configuration could also largely contribute to an improved insight in the role of the angular cross section data.

REFERENCES

[1] SERPAN C.Z. and WATSON H.E.
Nucl. Eng. and Design 11 (1970) 393-415.

[2] MINSART G., VAN BOSSTRAETEN C.
Joint technical Meeting on "Differential and Integral Data Requirements for Shielding Calculations"
Vienna, October 12-15 (1976).

[3] VANDEPLAS P.
Private communication.

FIGURES

Fig. 1 Experimental one material set-up in the 1 m cavity of the BR1 thermal graphite column.

Fig. 2 Theoretical neutron spectra for the U_{nat} drivers of 1, 3 and 6 cm thickness.

Fig. 3 Theoretical neutron spectra for the 1 cm U_{nat} driver without and with inner iron shells of respectively 7, 9 and 14 cm.

Fig. 4 Comparison of the theoretical neutron spectrum at the U_{nat}- Fe interface of the 1 cm U_{nat}+ 7 cm Fe configuration to three theoretical spectra incident on the pressure vessel of a power reactor.

Fig. 5 Decrease in neutron flux intensity through the iron shells.

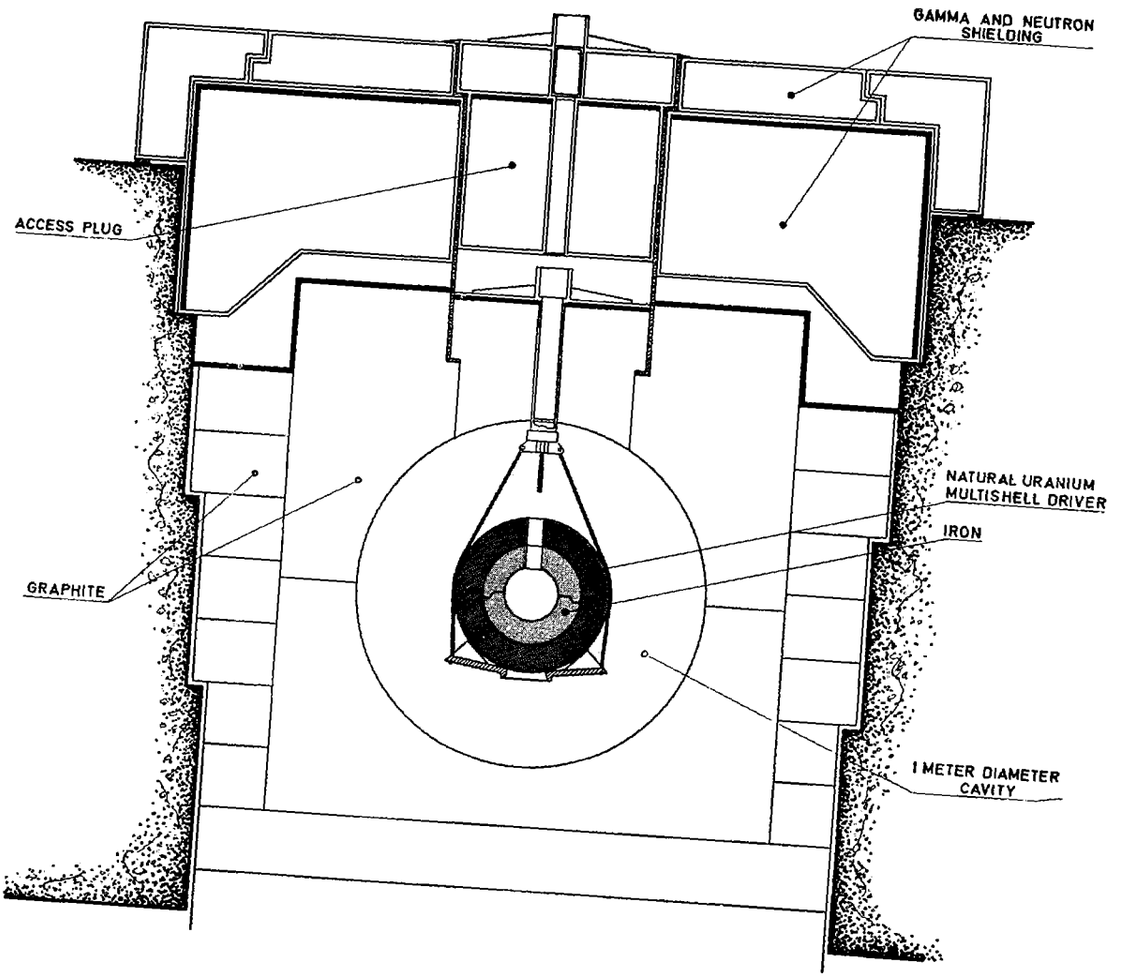
GAMMA AND NEUTRON SHIELDING
ACCESS PLUG
NATURAL URANIUM MULTISHELL DRIVER
IRON
GRAPHITE
1 METER DIAMETER CAVITY

Figure 1

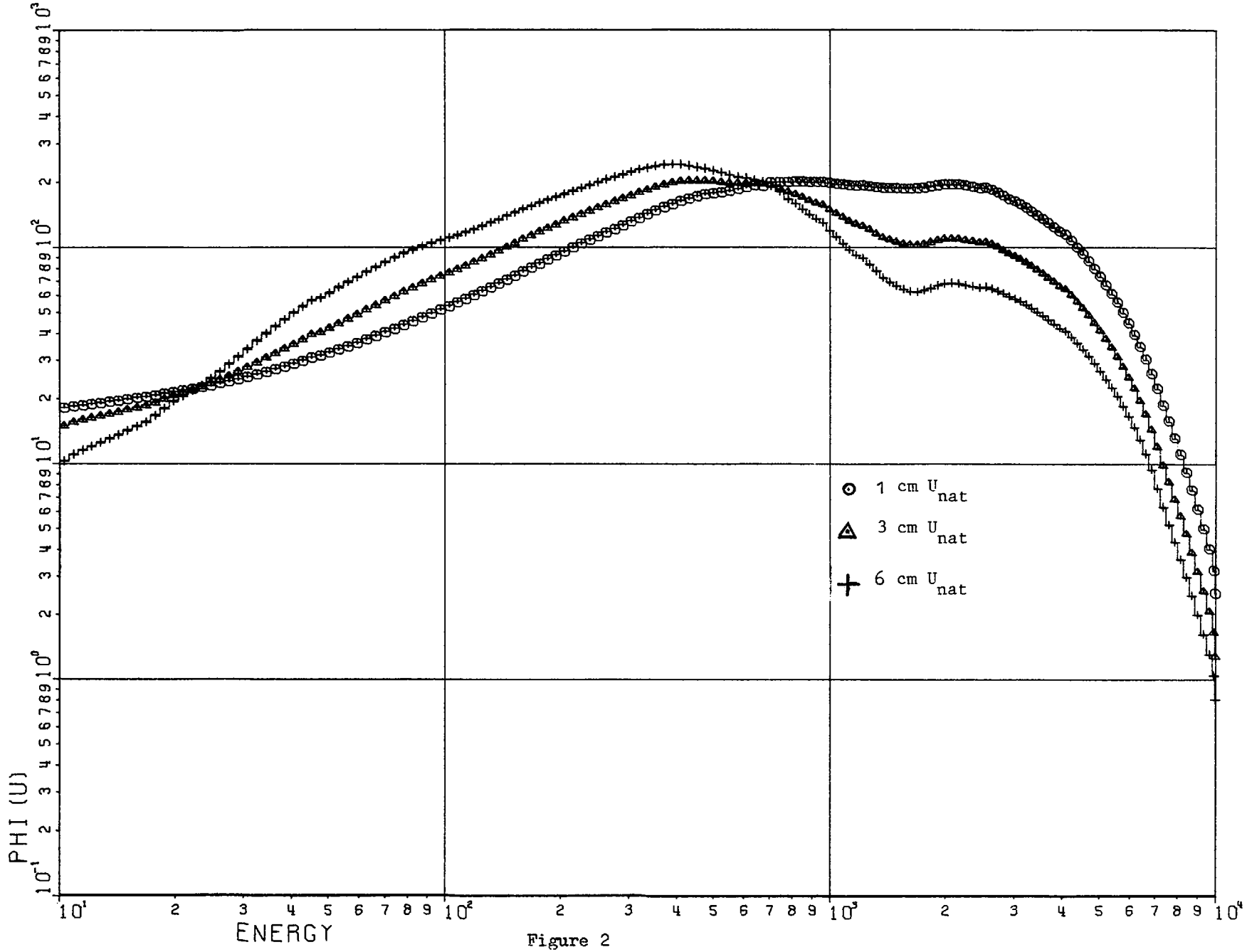

Figure 2

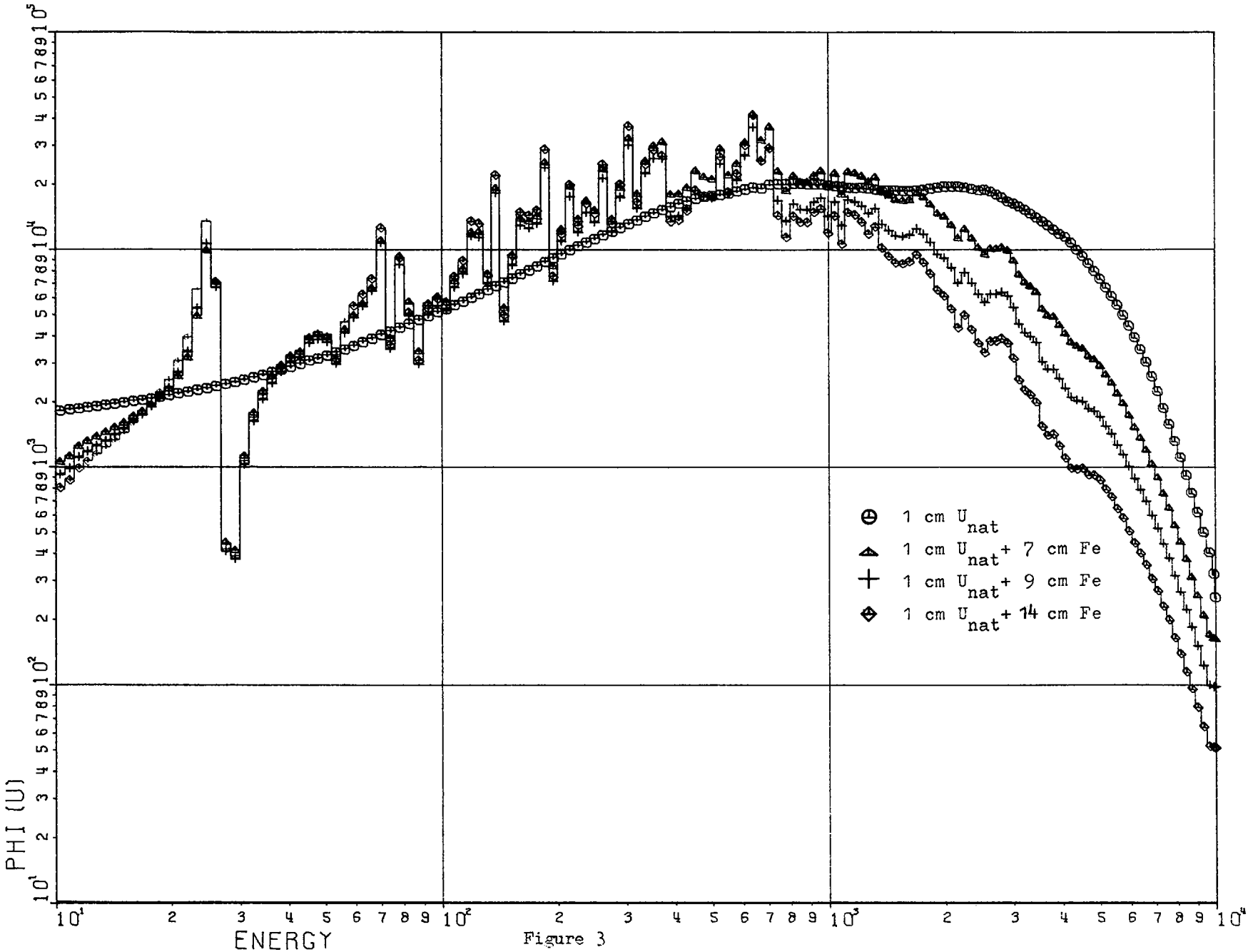
PHI (U)
ENERGY
1 cm U_{nat}
1 cm U_{nat} + 7 cm Fe
1 cm U_{nat} + 9 cm Fe
1 cm U_{nat} + 14 cm Fe

Figure 3

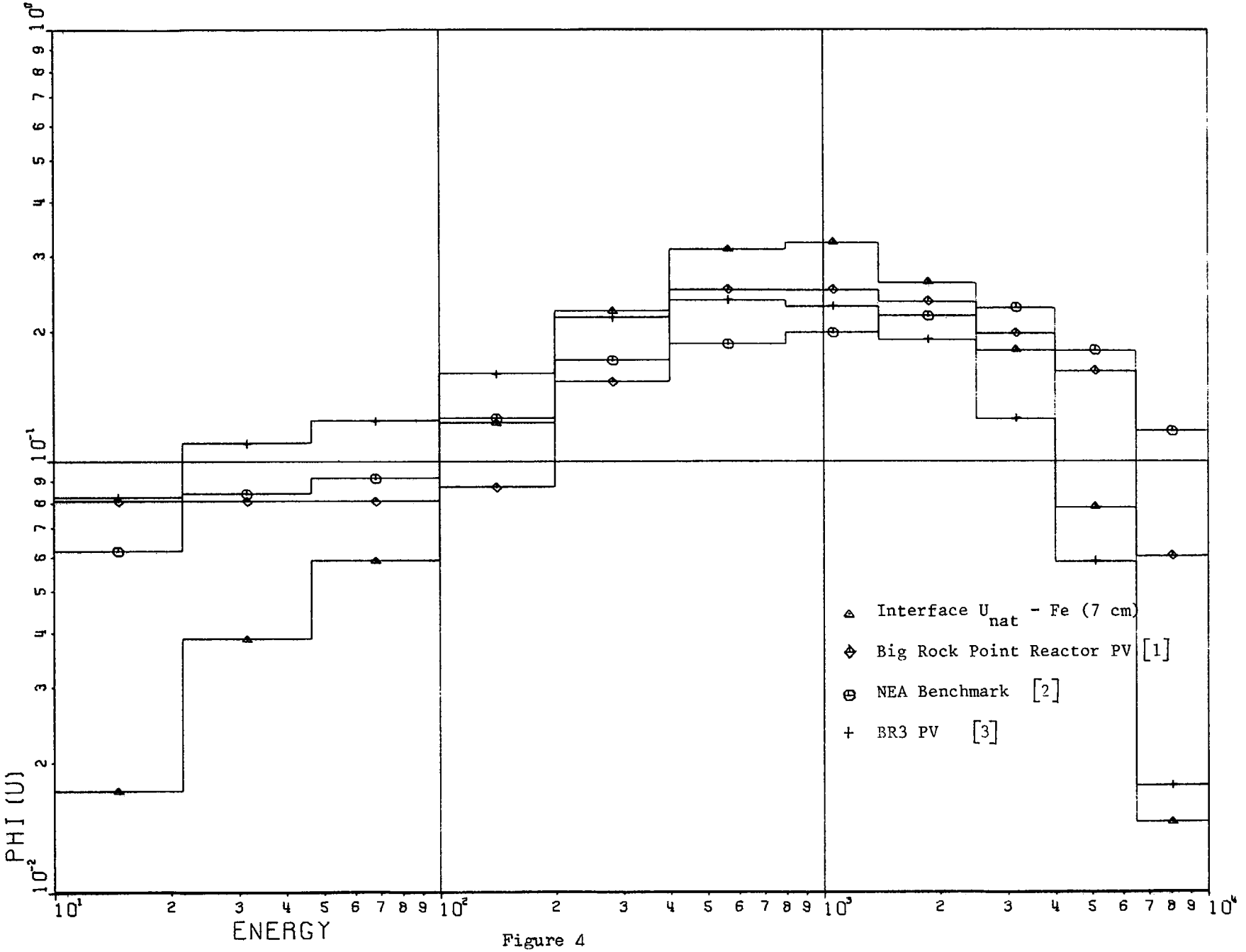
PHI (U)
ENERGY
Interface U_{nat} - Fe (7 cm)
Big Rock Point Reactor PV [1]
NEA Benchmark [2]
BR3 PV [3]

Figure 4

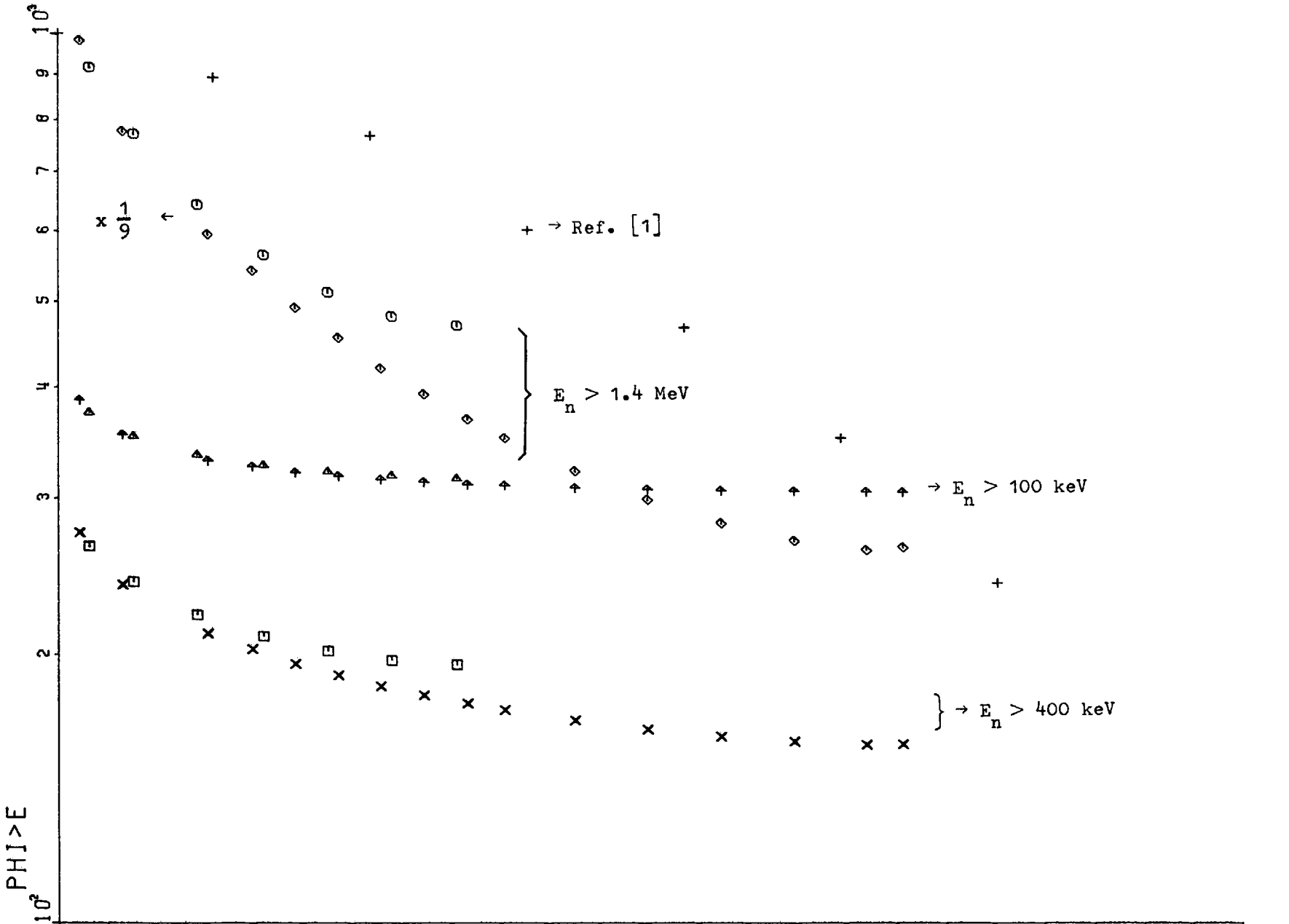
PHI>E
ABSTAND IN CM IN FE
0.00
1.60
3.20
4.80
6.40
8.00
9.60
11.20
12.80
14.40
16.00
17.60
19.20
+ → Ref. [1]
E_n > 1.4 MeV
→ E_n > 100 keV
→ E_n > 400 keV

Figure 5

III. DIFFERENTIAL CROSS-SECTION DATA FOR REACTOR DOSIMETRY

III.1. Point de vue de l'utilisateur sur les besoins en jeux de sections efficaces pour l'analyse des irradiations d'essai.

P. Mas and R. Lloret

C.E.A. - Centre 'Etudes Nucléaires de Grenoble, Service des Piles, Groupe Dosimetrie
85 X, 38041 Grenoble Cedex

RESUME :

La dosimétrie des irradiations d'essais de matériaux pose dans la pratique un certain nombre de problèmes : mesures des fluences, connaissance du spectre, choix du jeu de sections efficaces adapté à la mesure, détermination du taux de dommage, transposition du réacteur d'essai au réacteur de puissance.

Partant de ces problèmes, on considère qu'une recommandation provisoire concernant les sections efficaces différentielles de quelques détecteurs intégrateurs doit être faite, que disposer de plusieurs champs de neutrons standard accessibles pour corréler sections efficaces et codes de calculs est une nécessité.

ABSTRACT :

The dosimetry of testing materials irradiations involves in practice a lot of problemes : fluences measurements, knowledge of spectrum, choice of a convenient set of cross section, damage rate determination, transposition from testing reactor to power reactor.

From those problems, we consider that a temporary recommandation concerning the differential cross section of some fluence detectors is to be done, and that it is necessary to dispose of more accessible benchmarks in order to correlate cross section and computer codes.

Point de vue de l'utilisateur sur les besoins en jeux de sections efficaces pour l'analyse des irradiations en réacteur d'essai

P. MAS - R. LLORET

On ne traite dans ce rapport, que des problèmes concernant les irradiations de matériaux de structure, intéressées essentiellement par les neutrons rapides.

Dans l'analyse des irradiations effectuées en réacteur d'essais de matériaux, le premier besoin est de caractériser les rayonnements incidents, puis d'analyser les effets afin de transposer les observations faites aux réacteurs de puissance. En toute rigueur, le premier point n'apparaît que comme un intermédiaire, mais presque toujours obligatoire, pour atteindre le second, qui est en définitive la seule quantité intéressante. Cette remarque n'est pas sans importance, ainsi que nous le verrons plus loin, quant à la définition des besoins pratiques en jeux de sections efficaces. Une deuxième remarque préliminaire doit être faite : elle concerne la précision requise. En règle générale, les métallurgistes interrogés répondent "aussi bien que possible", ce qui peut être interprété par : "précision supérieure à laquelle j'effectue mes propres mesures". Pourtant, de plus en plus, des chiffres de précision requise sont cités [1]. En ce qui concerne par exemple les aciers de cuve de pression de réacteur, la précision demandée au dosimétreur pourrait atteindre quelques pourcents.

Voyons maintenant dans la pratique, comment et où les problèmes se posent pour essayer de déterminer en conséquence les besoins les plus urgents.

1. DETERMINATION DES FLUENCES DE NEUTRONS RAPIDES

Pour chaque irradiation, des détecteurs à seuil (ou un jeu de détecteurs) sont choisis en fonction des diverses contraintes : grandeur des fluences attendues, durée, intensité des flux, place disponible, environnement, etc... A l'heure actuelle, parmi les plus utilisés, on peut citer ^{58}Ni (n,p) , ^{54}Fe (n,p) , ^{46}Ti(n,p) ^{63}Cu (n,α). Leur activité absolue est mesurée, le plus souvent, avec une précision suffisante. Se pose alors le problème de la section efficace moyenne à utiliser :

$$\bar{\sigma} = \frac{\int_0^\infty \sigma(E) \cdot \varphi(E) \cdot dE}{\int_{1Mev}^\infty \varphi(E) \cdot dE}$$

afin d'obtenir la fluence des neutrons d'énergie supérieure à 1 Mev.

On voit qu'il est nécessaire de connaître à la fois σ (E) et φ (E). Nous parlerons des spectres plus loin.

A l'heure actuelle, la connaissance des sections efficaces différentielles n'est pas très bonne et même pour les sections les mieux connues, l'imprécision atteint 10 %. Ce n'est pas seulement par l'accumulation de nouvelles mesures de σ (E) que l'on pourra procéder à des recommandations, c'est à dire faire un choix. Des expériences en champs de neutrons standard (benchmarks) peuvent notablement faire avancer cette question du choix.

Faisons maintenant une remarque : plus le seuil des détecteurs est bas (voisin de 1 Mev) et plus l'erreur commise sur $\bar{\sigma}$ sera faible. A la limite, l'activité d'un détecteur à seuil échelon à partir de 1 Mev sera toujours proportionnelle à la fluence supérieure à 1 Mev. C'est pourquoi nous avons particulièrement développé l'utilisation de la réaction ^{93}Nb (n,n') [2], qui, de plus, présente l'avantage d'avoir une période assez longue (16,3 a).

Inversement, un détecteur à seuil élevé peut conduire, si le spectre n'est pas bien connu, à des erreurs importantes. Nous présentons dans le tableau suivant des indices de spectre (act In/act X) mesurés dans différents emplacements d'un réacteur à eau, choisi à titre d'exemple.

Réaction / Caractéristique du spectre	In^{115} (n,n') Nb^{93} (n,n')	Ni^{58} (n,p) Fe^{54} (n,p)	Ti^{46} (n,p) Cu^{63} (n,α)	Al^{27} (n,α)
Fission	1	1	1	1
Voisinage du coeur	1	0,98	0,89	0,88
Eau après quelques cm	1	0,96	0,84	0,82
Réflecteur	1	0,79	0,55	0,41
Coeur (environnement Alu)	1	1,07	1,11	1,12
Dispositif expérimental acier	1	1,23	1,34	1,32

Ces quantités sont les rapports normalisés à une position des activités absolues des détecteurs. Elles varient comme l'inverse du rapport des sections efficaces moyennes des détecteurs correspondants.

On constate que ces rapports varient beaucoup d'un emplacement à l'autre, c'est à dire d'un spectre à l'autre. On dépasse ainsi un rapport 2 pour l'indice In/Cu. Ce qui signifie qu'en l'absence de mesures d'indices, une incertitude de 10% sur la section efficace du cuivre conduira à une incertitude de 10 % sur la fluence- ce qui est vrai pour n'importe quel détecteur - mais aussi qu'une mauvaise connaissance du spectre conduira à une incertitude de même grandeur sur la fluence de neutrons d'énergie supérieure à 1 Mev.

Si on doit, pour des raisons pratiques, utiliser un détecteur à $\bar{\sigma}$ inconnu, un moyen de s'en tirer sera de faire une mesure d'étalonnage préalable du dé-

tecteur à utiliser par rapport à un détecteur de seuil 1 Mev (par exemple ^{115}In (n,n'). Lorsque cela n'est pas possible (compatibilité des détecteurs, niveaux de flux, environnement, ...) mais que par contre on connaisse le spectre de neutrons, on procèdera à un étalonnage par rapport à un détecteur de section efficace différentielle mieux connue (par exemple ^{58}Ni (n,p)).

Enfin, l'expérience montre qu'il est toujours préférable d'utiliser le détecteur le mieux adapté à telle mesure de fluence. Ainsi, ces détecteurs intégrateurs sont différents d'une expérience à l'autre ; il faudra néanmoins les corréler. D'où l'intérêt majeur d'avoir une bibliothèque de sections efficaces différentielles de détecteurs intégrateurs corrélés. Pour ceci, des expériences en spectres de neutrons standard et très différents peuvent donner des informations très précieuses.

2. - SPECTRE DES NEUTRONS

Nous avons vu dans le paragraphe précédent que sauf dans des cas très particuliers (détecteur à seuil de 1 Mev), ou moyennant des expériences préliminaires, la connaissance du spectre des neutrons est nécessaire pour obtenir une bonne évaluation des fluences de neutrons rapides.

Pour obtenir cette connaissance des spectres, on peut procéder par le calcul. A l'heure actuelle, il existe des outils de calcul satisfaisants, basés sur la théorie du transport à deux dimensions (comme par exemple le système ANISN-DOT 3), que nous utilisons. Mais, étant donné les précisions demandées, des vérifications expérimentales s'avèrent nécessaires (qui serviront éventuellement à ajuster les constantes du code de calcul). Elles peuvent être faites à partir d'un jeu de détecteurs et de méthodes de déconvolution [3] , [4] , [5] . Mais il est indispensable que les sections efficaces différentielles soient connues et bien corrélées entre elles et ceci pour des spectres très différents.

Cette vérification expérimentale à l'aide de détecteurs à seuil ne peut pas atteindre la région inférieure à 1 Mev. Les autres méthodes expérimentales - spectromètre à protons, à Li^6,... - ne sont pas toujours utilisables en pratique et sont très chères d'emploi. Or, les neutrons d'énergie inférieure a 1 Mev peuvent intervenir pour une part non négligeable -par exemple pour environ 25 % dans les variations de propriétés mécaniques des aciers ferritiques irradiés en réacteur à eau légère dans les phénomènes de dommage.

Donc, on devrait pouvoir qualifier les codes de calculs de spectres dans des spectres de neutrons standard et bien déterminés dans le domaine d'énergie inférieure à 1 Mev.

3. - ANALYSE DES IRRADIATIONS

Ce qui intéresse en définitive l'expérimentateur métallurgiste, c'est de pouvoir transposer les effets observés en réacteur d'essai à ceux devant advenir en réacteur de puissance. Il va s'intéresser à un taux de dommages et de plus, utiliser une bibliothèque de sections efficaces de chocs (élastiques, inélastiques, de capture, ...) convenable et si possible standardisée [6] .

Pour atteindre le but final, à savoir la comparaison de la capacité d'endommagement de différents spectres, une grande partie des imprécisions peut disparaître si les mêmes données de section efficaces -aussi bien pour les détecteurs que pour les calculs- sont utilisées, puisqu'on ne s'intéresse qu'à des valeurs relatives. Ceci est une indication importante qui pourrait nous conduire à faire une recommandation provisoire de sections efficaces différentielles pour un nombre très limité de détecteurs (les plus couramment utilisés et à seuils les plus bas possibles), ce qui aurait de plus l'avantage de nous faire parler le même langage même si celui-ci est arbitraire.

Remarques

1. La meilleure solution est, par ailleurs, d'irradier en spectres étalonnés et les plus proches possibles des spectres réels (de réacteurs expérimentaux et de réacteurs de puissance) des échantillons des matériaux étudiés.
2. Une autre solution est d'avoir un détecteur de dommage qui réponde comme les matériaux étudiés [7] comme par exemple pour le graphite le détecteur GAMIN [8].

4. DOSIMETRIE DE SURVEILLANCE

Avec la construction des réacteurs de puissance est mise en place une dosimétrie de surveillance. Elle fait appel à des détecteurs généralement de na-

ture différente de ceux utilisés en réacteur d'essai -par exemple ^{238}U (n,f) , ^{237}Np (n,f) ...- Il devient alors nécessaire de corréler soigneusement et dans des spectres assez proches des conditions expérimentales, les différentes sections efficaces utilisées.

5. CONCLUSIONS

Les besoins les plus urgents nous semblent être les suivants :

1. Faire une recommandation proviroire de sections efficaces différentielles pour quelques détecteurs intégrateurs parmi lesquels :

^{93}Nb (n,n') , ^{58}Ni (n,p) , ^{54}Fe (n,p) , ^{46}Ti (n,p) , ^{63}Cu (n,α) ,

^{238}U (n,f) , ^{237}Np (n,f).

2. L'utilisation des champs de neutrons standard (benchmarks) peut être un progrès majeur pour une meilleure précision en dosimétrie, en permettant :

a) la corrélation des données différentielles des détecteurs intégrateurs cités en 1°. Pour être possible et valable, il est nécessaire que ces champs de neutrons soient d'intensité suffisante, de spectres bien déterminés et suffisamment différents, tout en se rapprochant le plus possible des spectres réels (réacteurs d'essai et réacteurs de puissance).

b) La qualification d'un jeu de sections efficaces différentielles bien corrélées entre elles (réactions de catégorie I, par exemple), destiné à des mesures de spectre de neutrons par des méthodes de déconvolution.

c) La qualification de codes de calcul des spectres neutroniques. Ceci suppose que toutes les données neutroniques de benchmarks soient disponibles.

Enfin, il serait souhaitable que l'ensemble des benchmarks soit d'accès libre pour les expérimentateurs.

3. Un travail devrait être poursuivi concernant les sections efficaces utiles dans l'analyse des dommages d'irradiation : sections (n,α) et (n,p) , bibliothèque de sections de chocs neutroniques (n,n) , (n,n') , (n,γ) , (n,p) , (n,α), ... intéressant les matériaux de structure des réacteurs.

B I B L I O G R A P H I E

[1] W.N. Mc ELROY, R.A. BENNETT, D.L. JOHNSON and N.D. DUDEY.
Neutron environmental characterization requirements reactor fuels and materials development and surveillance programs.

1st ASTM. Euratom Symposium on Reactor Dosimetry - PETTEN - 22-26 september 1976.

[2] R. LLORET
Application de la réaction ^{93}Nb (n,n') à la dosimétrie des irradiations de matériaux.

1st ASTM. Euratom Symposium on Reactor Dosimetry - PETTEN- 22-26 september 1976.

[3] W.Mc ELROY , S. BERT , T. CROCKETT , R. HAWKINS.
A computer automated iterative method for neutron flux spectra determination by foil activation.
AFWL - TR - 67-41 , Vol. 1 (1967).

[4] F.B.K. KAM , F.W. STALLMANN
Crystal Ball. A computer program for determining neutron spectra from Activation Measurements.
ORNL - TM 4601 (1974).

[5] A. FISCHER , L. TURI
The RFST Programm for unfolding neutron spectra from activation data
INDC (HUN) - 8/V , may 1972.

[6] Recommandations du Comité Technique AIEA sur les unités de dommages radio-induits. HARWELL - 2-3 novembre 1976.

[7] P. MAS
Méthodes spéciales utilisées en dosimétrie des neutrons
1st Symposium ASTM - EURATOM on Reactor Dosimetry - PETTEN
22-26 septembre 1976.

[8] M. CANCE , J.P. GENTHON and al.
Le détecteur neutronique en graphite G.A.M.I.N.
CEA-N-1823 - 1975.

III.2. Evaluation of $^{27}Al(n,\alpha)^{24}Na$, $^{27}Al(n,p)^{27}Mg$ and $^{58}Ni(n,p)^{58}Co$ Cross Sections

Tetsuo ASAMI

Japan Atomic Energy Research Institute

Tokai-mura, Naka-gun, Ibaraki-ken, Japan

ABSTRACT

The evaluation of the $^{27}Al(n,\alpha)^{24}Na$, $^{27}Al(n,p)^{27}Mg$ and $^{58}Ni(n,p)^{58}Co$ cross sections were performed in the neutron energies up to 20 MeV. The original experimental data were examined with respect to the measuring procedures and the data analyses, and some data were modified by using the recent data of the standard cross sections and the decay data. The evaluation procedures are described, and the evaluated excitation curves for these three reactions are shown. The present values for the $^{27}Al(n,\alpha)^{24}Na$ cross section are close to the recent other data. The evaluated values for the $^{27}Al(n,p)^{27}Mg$ and $^{58}Ni(n,p)^{58}Co$ cross sections are somewhat lower than those of ENDF/B-IV around the maxima of the excitation curves. The ^{235}U fission-neutron average cross-sections calculated from the present evaluated values are compared with the corresponding values from the other evaluations and with the recent experimental data.

INTRODUCTION

The threshold reactions such as (n,p),(n,α), (n,n'), (n,2n), etc. have been used in neutron dosimetry, in particular in the measurements on reactor neutron spectrum and on neutron flux. For the threshold reactions which are frequently used in this field, there are some excellent sets of the evaluated cross-section data, for example the ENDF/B-IV dosimetry file[1], the set of Simons and McElroy[2], etc.. However, there still remain some discrepancies among these evaluated data, and the accurate cross-section values for these reactions are required.

In this work, an attempt has been made on the reevaluation of the cross-section data for the $^{27}Al(n,\alpha)^{24}Na$, $^{27}Al(n,p)^{27}Mg$ and $^{58}Ni(n,p)^{58}Co$ reactions which are important for neutron-dosimetry applications. The ^{235}U fission-spectrum average cross-sections calculated from the present evaluated data are compared with the calculated values from the other evaluations and with the recent experimental ones.

EVALUATION PROCEDURES

The evaluations were based entirely on the experimental data published before June 1976, the original data being searched mainly through CINDA 75. The data were examined with respect to the experimental method and the data derivation in detail.

The evaluation was made in the following procedures.

(1) Data modification: In order to deal with the data on the same standpoint, some data are modified when the data used in the analysis are unsuitable. The data measured relative to the standard are modified by using of the recent evaluated values of the standard cross sections. Also for the data from activation measurements, if the decay data used in the analysis such as the branching ratio, the half-life, etc. are unsuitable, the original data are modified using the recent decay data.

As the standards of the cross section, the $^{27}Al(n,\alpha)^{24}Na$, $^{56}Fe(n,p)^{56}Mn$, $^{65}Cu(n,2n)^{64}Cu$, $^{235}U(n,f)$ and $^{238}U(n,f)$ reactions were chosen. These cross-section values have been well established for the present purpose. The values for the $^{235}U(n,f)$ and $^{238}U(n,f)$ cross sections were taken from the ENDF/B-III file[4)]*, and for the other three standards the evaluated data of Kanda and Nakasima[3)] were used.

(2) Estimation of "14 MeV" cross-section value: A most probable value of the cross section around 14 MeV is estimated by use of the data from the one-point measurement at the "14 MeV", in particular the accurate data from the recent absolute measurements.

(3) Data renormalization: For each set of the measured data on excitation function the least-squares fittings are made with a quadratic or cubic function of energy, and original values are renormalized to the value obtained in (2) by using of the above best-fit function.

(4) Estimation of excitation curve: A most probable curve of the excitation function is estimated mainly by use of the fitted curves obtained in (3) and by an eye guide in part. In this process the data with large renormalization factor are treated as less weighted and the data set for which the energy dependence is largely different from the others is rejected.

---

* The recent data of Smith and Meadows[5)] on the $^{27}Al(n,p)^{27}Mg$ and $^{58}Ni(n,p)^{58}Co$ cross sections have weight with the present evaluations. They have measured the cross sections relative to the $^{235}U(n,f)$ and $^{238}U(n,f)$ data of ENDF/B-III. Therefore we used these values for the $^{235}U(n,f)$ and $^{238}U(n,f)$ cross sections tentatively.

RESULTS

The details on the evaluations of the cross section for these three reactions will be described elsewhere. Only a brief description on the evaluated data is given here.

$^{27}Al(n,\alpha)^{24}Na$: Although this reaction was selected as one of the standard in the present work as described above, the values of Kanda and Nakasima[3] are somewhat different from those of ENDF/B-IV[6] and of Simons and McElroy[2]. The deviations are about 4 % around the maximum of the excitation function (12~13 MeV). Therefore the reevaluation for this cross section was performed, apart from the use of the cross-section standard in the present work.

Figure 1(a) shows the original experimental data for the $^{27}Al(n,\alpha)^{24}Na$ cross section excluding the one-point data around 14 MeV. A value of 116 mb at 14.5 MeV was estimated from the one-point data measured around 14 MeV, in accordance with that of Kanda and Nakasima[3]. As shown in Fig. 1(b), some data were renormalized in this evaluation and a most probable curve of the excitation function was estimated. This curve is compared with both the curves of ENDF/B-IV[6] and of Kanda and Nakasima[3] in Fig. 1(b). The present curve is close to these two leaving small deviations near the threshold energy and at the energies of 12 to 14 MeV. These evaluated data would be used as the cross-section standard within the accuracies of a few percents.

$^{27}Al(n,p)^{27}Mg$: Figure 2(a) shows the whole original data for this reaction. A cross-section value of 75 mb at 14.2 MeV was estimated from the data for the one-point measurement around 14 MeV, some of which were modified on the standard cross section and/or the decay data. Using the data sets normalized to this value, a probable curve of the cross section was obtained and compared with that of ENDF/B-IV[6], as shown in Fig. 2(b).

The present values are fairely lower than those of ENDF/B-IV[6] in the whole energy range of the excitation curve.

$^{58}Ni(n,p)^{58}Co$: A value of 350 mb at 14.6 MeV was estimated from the one-point data around 14 MeV. Figures 3(a) and 3(b) show the original experimental data and the data modified or renormalized, respectively, together with the evaluated curves. The present values are lower than those of ENDF/B-IV[7] around the maximum of the excitation curve(6~12 MeV).

COMPARISON OF AVERAGE CROSS SECTIONS FOR FISSION SPECTRUM

As an over-all test of the evaluated data, the comparison was made for the cross section averaged over the neutron spectrum from the low-energy neutron-induced fission of ^{235}U. Since the ^{235}U fission spectrum has been generally interpreted in terms of the Watt-type and Maxwellian distributions, the calculations for the average cross section were made for these two forms of the fission neutron distributions. The parameters used in the calculations were taken from the recent measurements[8)-10)] as shown in the footnote of Table 1. The calculated values of the average cross sections for the present evaluations are listed in Table 1 and compared with the corresponding values calculated for the other evaluated data and with the recent experimental values.

The evaluated values of ENDF/B-IV[6] for the $^{27}Al(n,p)^{27}Mg$ cross section are higher than both the present values and those of Simons and McElroy[2] in the whole energy range. The average cross section obtained from the data of ENDF/B-IV seems also to be higher than the experimental data[13),14)].

The present values for the $^{58}Ni(n,p)^{58}Co$ cross section are somewhat different from those of ENDF/B-IV[7] and of Bresesti et al[11]. From the comparison of the average cross section, there is no definite evidence to make clear this discrepancies.

In the comparison of the average cross sections, there are some indications to be noticed: (1) The recommended value of Fabry[14] for the $^{58}Ni(n,p)^{58}Co$ average cross section seems to be evidently higher than both the values obtained from the present data and from the other evaluated data. (2) For all of these three reactions, the average cross sections obtained from the present data using the Watt-type spectrum are in good agreement with the experimental values of Kimura et al [13]

REFERENCES

1) MAGURNO, B.A. (edited) : "ENDF/B-IV Dosimetry File", BNL-NCS-50446 (1975)
2) SIMONS, R.L. and MCELROY, W.N. : BNWL-1312 (1970)
3) KANDA,Y. and NAKASIMA,R. : JAERI-1207 (1972)
4) OZER,O. and GARBER,D.(assembled) : BNL-17541 (1973)
5) SMITH,D.L. and MEADOWS, J.W. : ANL/NDM-10 (1975)
6) YOUNG, P.G. and FOSTER, Jr.D.G. : BNL-NCS-50446 (1975) p.21
7) SCHENTER, R.E. : ibid. p.114
8) JOHANSSON, P.I., HOLMQVIST, B., WIEDLING, T. and JEKI, L. : Proc. of a Conf. on Nuclear Cross Section and Technology, Washington, March 3-7, 1975 (National Bureau of Standard, 1975) p.572
9) JOHANSSON, P.I. and ADAMS, J.M. : ibid. p.631
10) GRUNDL, J.A. and EISENHAUER, G.M. : ibid. p.250
11) BRESESTI, A.M., BRESESTI, M., ROTA, A. and RYDIN,R.A. : Nucl. Sci. Eng. 40, 331 (1970)
12) SMITH, D.L. and MEADOWS, J.W. : ANL/NDM-13 (1975)
13) KIMURA, I., KOBAYASHI, K. and SHIBATA, T. : J. Nucl. Sci. Tech. 10, 574 (1973) ; ibid. 13, 531 (1976)
14) FABRY, A. : BLG-465 (1972)

TABLE 1

Comparison of Average Cross Sections for ^{235}U Fission Neutron Spectrum

(mb)

	$^{27}Al(n,\alpha)^{24}Na$ (Q = -3.13 MeV)		$^{27}Al(n,p)^{27}Mg$ (Q = -1.83 MeV)		$^{58}Ni(n,p)^{58}Co$ (Q = +0.395 MeV)	
	Maxwellian[a]	Watt[b]	Maxwellian[a]	Watt[b]	Maxwellian[a]	Watt[b]
Present	0.790	0.684	3.82	3.74	99.7	101
ENDF/B-IV[6),7)]	0.787	0.681	4.21	4.11	102	104
Kanda & Nakasima[3)]	0.798	0.693				
Simons & McElroy[2)]	0.762	0.660	3.94	3.85	101	103
Bresesti et al[11)]	0.794	0.686			103	105
Smith & Meadows[12)]			3.72		99.4	
Kimura et al[13)]	0.644 ± 0.036		3.64 ± 0.17		102 ± 6	
Fabry[14)]	0.725 ± 0.02		4.0 ± 0.4		113 ± 2.5	

a) Calculated using the Maxwellian spectrum ($E^{1/2}\exp(-E/T)$, T = 1.313 MeV)[10)].

b) Calculated using the Watt type spectrum ($\exp(-AE)\sinh(BE)^{1/2}$, A = 1.000 MeV^{-1} and B = 1.970 MeV^{-1})[8),9)].

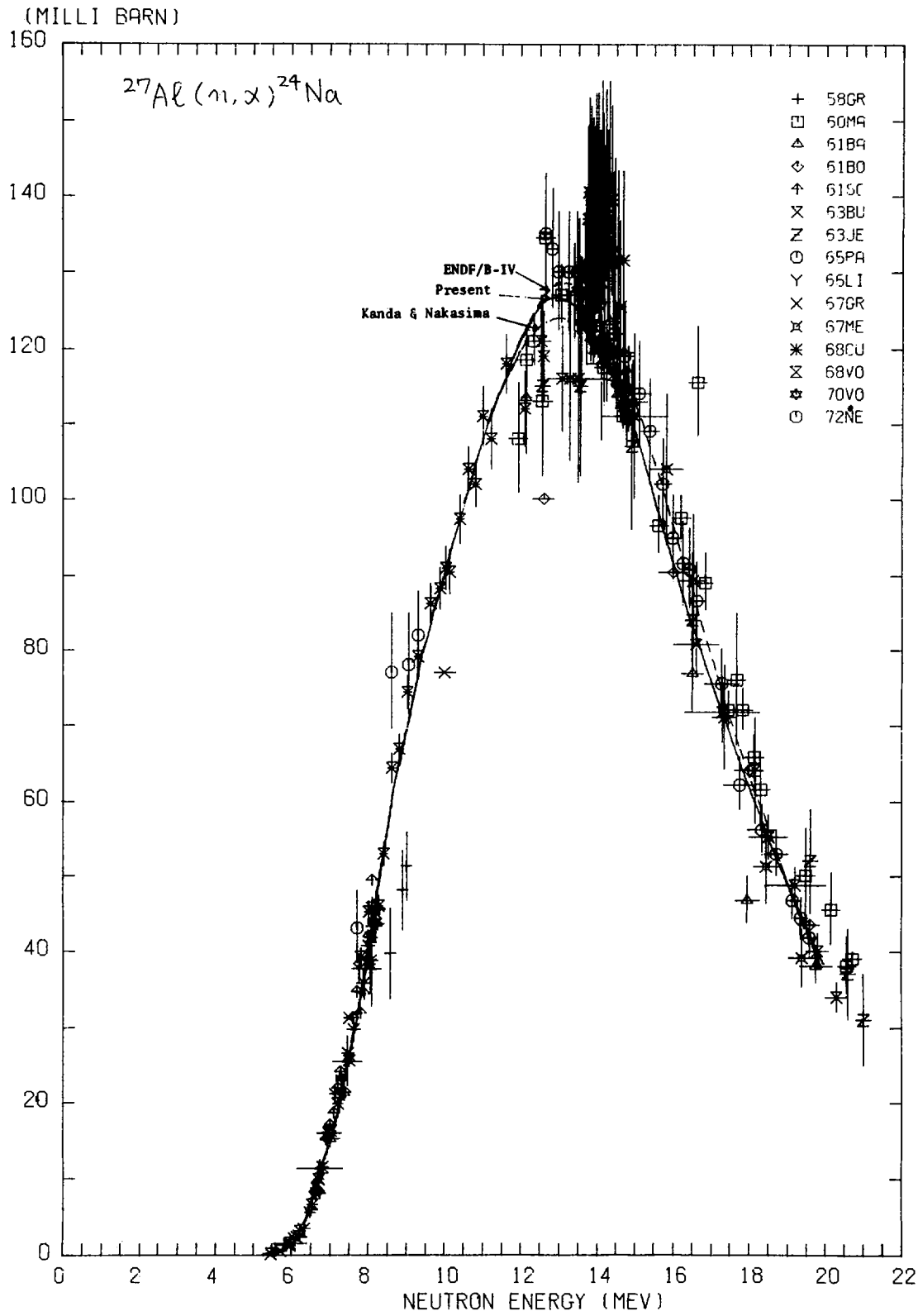

Fig. 1(a). Original experimental data for the $^{27}Al(n,\alpha)^{24}Na$ cross section, excluding the one-point data around 14 MeV.

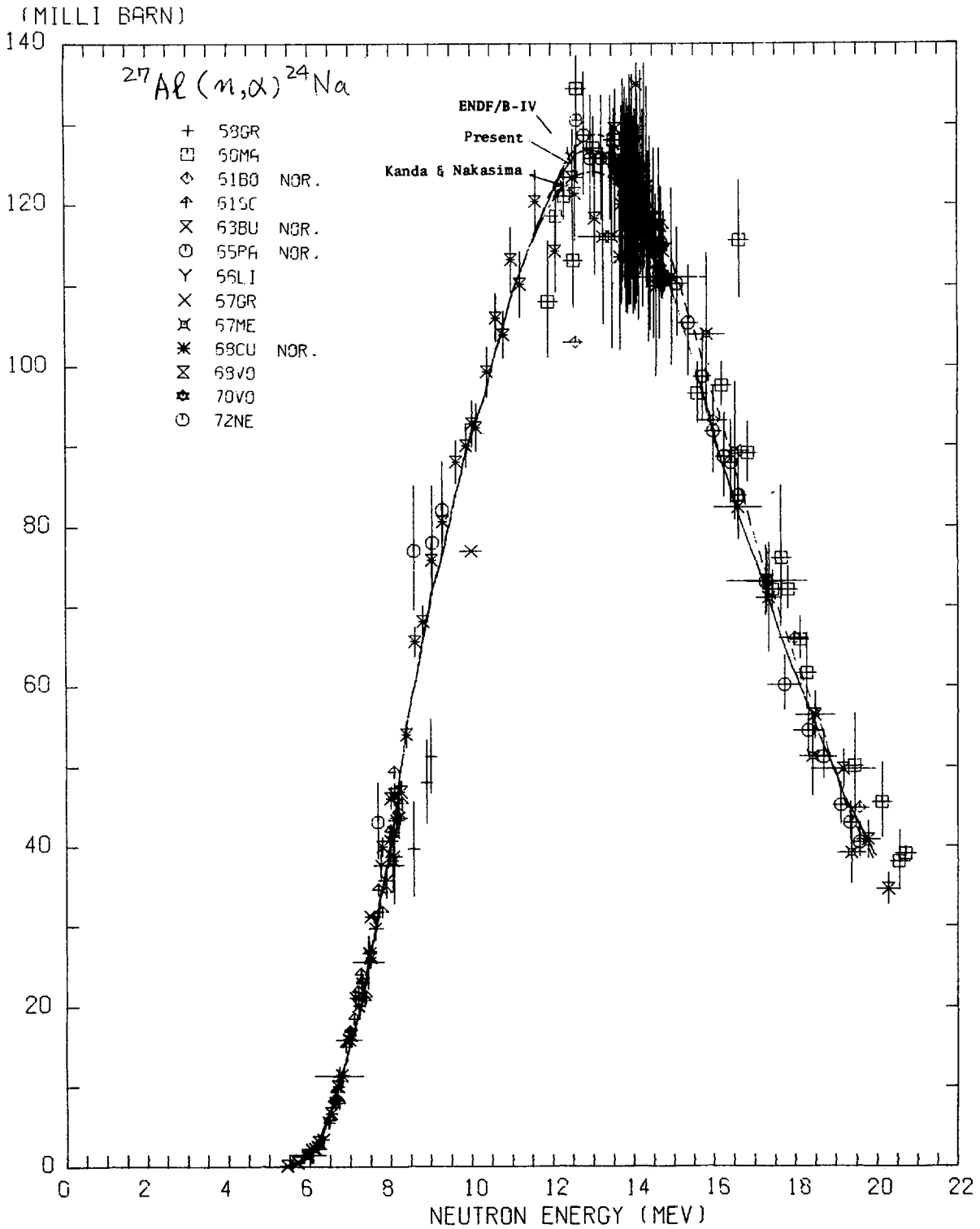

Fig. 1(b). $^{27}Al(n,\alpha)^{24}Na$ cross-section data used in the present evaluation. For the one-point data around 14 MeV, only an evaluated value of 116 mb at 14.5 MeV is shown. "NOR" denotes the data renormalized in the present work. A curve obtained in this work is compared with both the curves of ENDF/B-IV[6] and of Kanda and Nakasima[3].

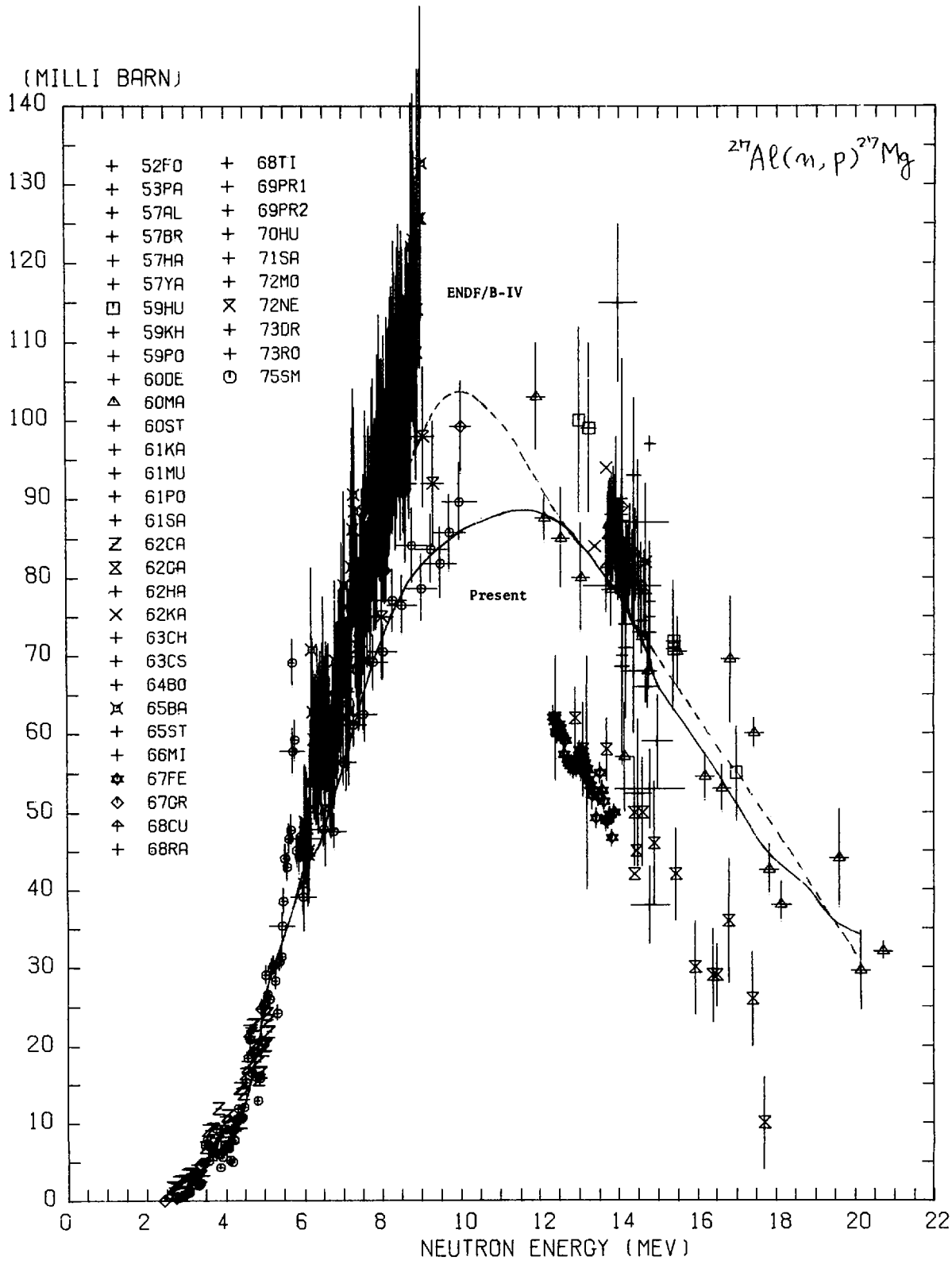

Fig. 2(a). Original experimental data for the $^{27}Al(n,p)^{27}Mg$ cross section.

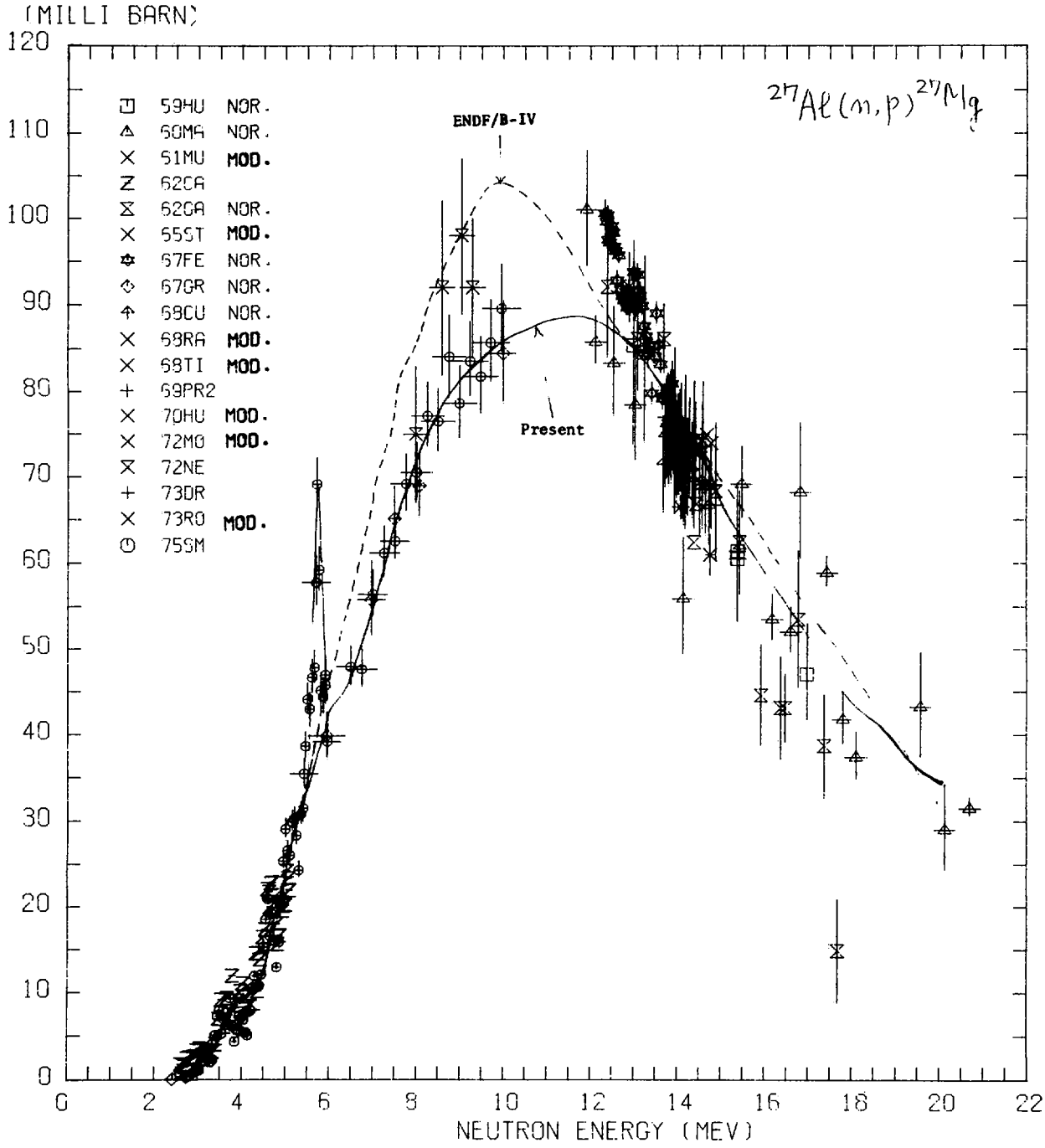

Fig. 2(b). $^{27}Al(n,p)^{27}Mg$ cross-section data used in the present evaluation. "MOD." and "NOR." denote the data modified and renormalized in the present work, respectively. A curve obtained in this work is compared with that of ENDF/B-IV[6].

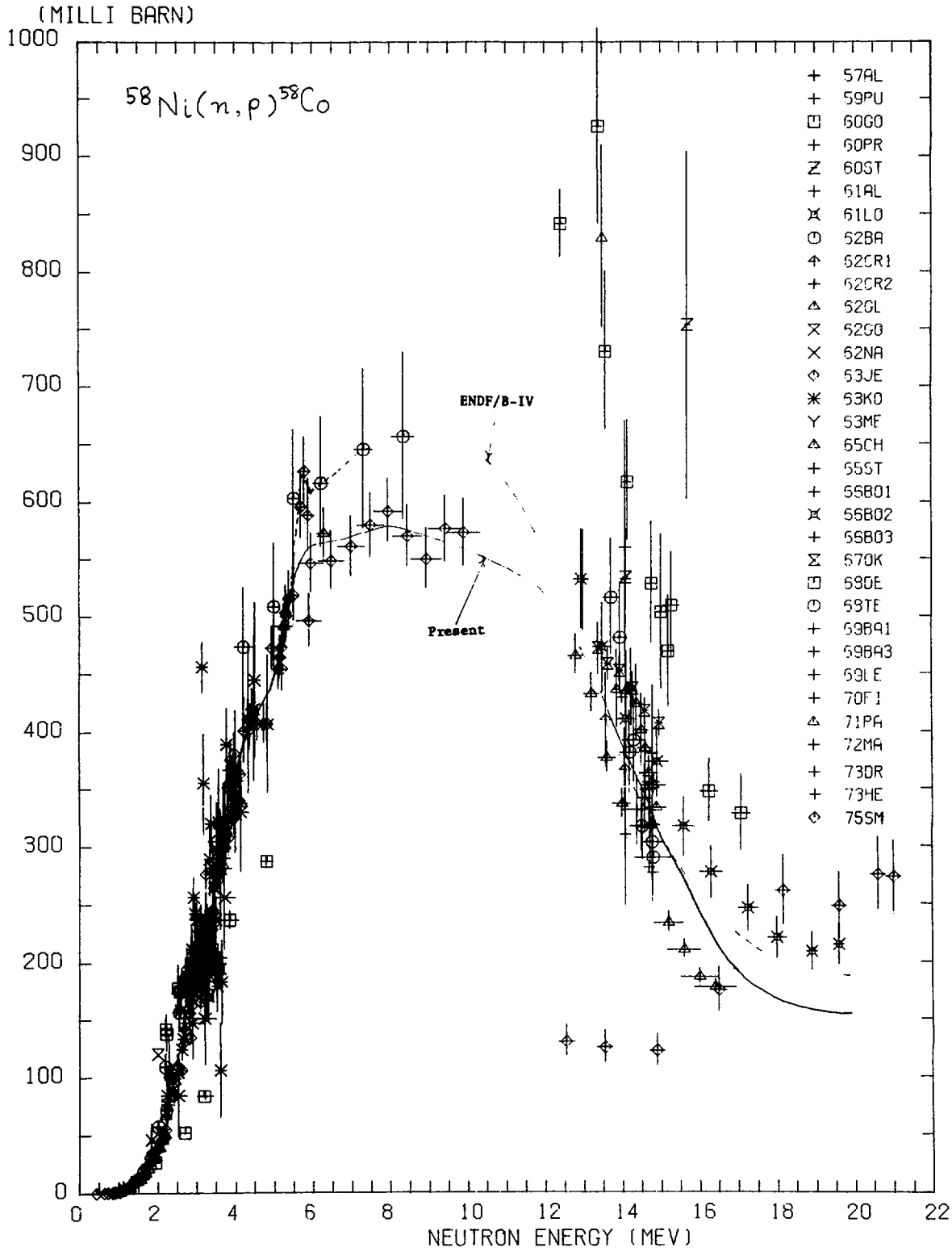

Fig. 3(a). Original experimental data for the $^{58}Ni(n,p)^{58}Co$ cross section.

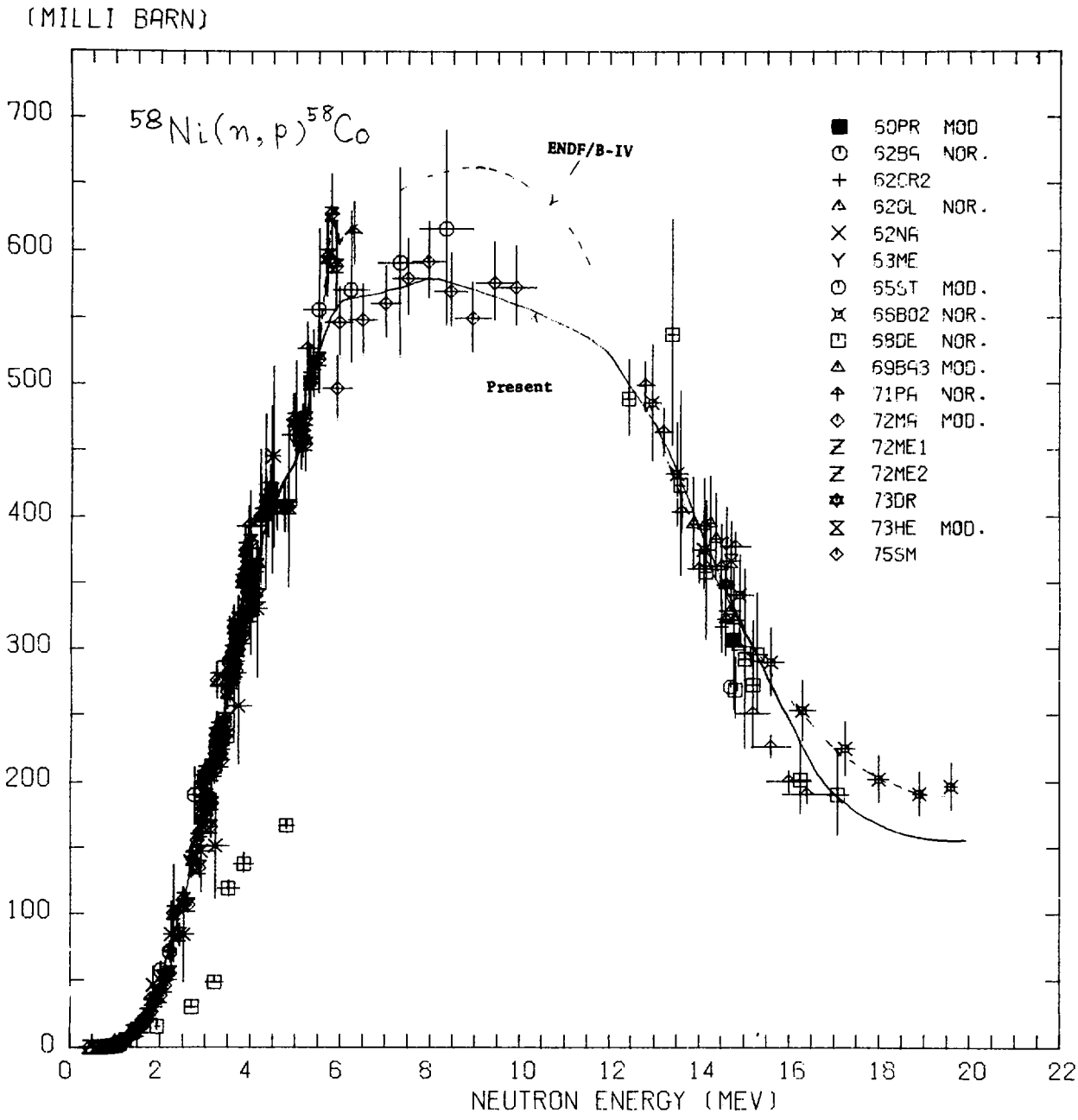

Fig. 3(b). $^{58}Ni(n,p)^{58}Co$ cross-section data used in the present evaluation. "MOD." and "NOR." denote the data modified and renormalized in the present work, respectively. A curve obtained in this work is compared with that of ENDF/B-IV[7].

IV. VALIDATION AND ADJUSTMENT OF DIFFERENTIAL CROSS SECTIONS ON THE BASIS OF INTEGRAL DATA

IV.1. On the Possibility of Unfolding Simultaneously Data from Multiple Foil, Proton Recoil and Other Neutron Spectrometers by the SAND II Type Unfolding Codes.

M. Najžer

University of Ljubljana
J. Stefan Institute

Abstract

General arguments are given showing that the SAND II type iterative codes could be used for the simultaneous unfolding of experimental data from different neutron spectrometers. Special attention is paid to the choice of the number of pulse height bins and their widths, to the determination of the neutron energy group structure and to the normalization of the experimental data to the same neutron flux intensity. Techniques are proposed to optimize the above mentioned quantities.

Introduction

Neutron energy spectra important for reactor dosimetry span a large energy interval from below thermal energy up to about 15 MeV. The most important neutron spectrometry methods are the multiple foil technique /1/ and a group of techniques sometimes called differential neutron spectrometry /3/. Among the latter the most widely used are proton recoil spectrometers (proportional counters /4/, organic scintillators /5/) and ^{6}Li sandwich spectrometers /6/. However, no single one of these methods has until now been capable of covering satisfactorily the whole energy range of interest. Therefore, different experimental techniques were used to determine the neutron spectrum when high precision was required, as for example in the case of standard and reference neutron fields, some shielding experiments, etc. The neutron spectrum is then calculated from experimental data using different unfolding codes. Recently, the unfolding code RADAK /7/ based on the maximum likelihood principle has been developed which is able to unfold all experimental data simultaneously. Until now, at least to the author's knowledge, it has found application only in Great Britain. On the other hand the most common method of combining different experimental data in a single spectrum /8/ can be summarized as follows. First the data from each single differential spectrometer are unfolded. A set of neutron spectra of limited energy range, defined by the spectrometer response, is obtained. Each spectrum is then rather arbitrarily normalized to the spectrum computed by a transport code. The accuracy of the computation and/or measurements is judged from the consistency of both computed and measured spectra. The spectrum evaluated in this way is used in the next step as the input spectrum for the unfolding of multiple foil data. The

code most widely used for the unfolding is SAND II /9/ followed by CRYSTAL BALL /10/ and SPECTRA /11/. The final result of the whole procedure is represented by the spectrum obtained from multiple foil data unfolding. A comparison is finally made again with transport theory calculation. It may be worth mentioning some possible weaknesses of this procedure: (i) The final spectrum is derived from the multiple foil measurements which are known to be inefficient in the neutron energy range from approximately 0,1 to 0,7 Mev. (ii) It is the inherent weakness of integral measurements to be prone to uncontrolled transfer of intensities from one energy region to the other, especially in regions not well covered by detector responses. (iii) High precision differential spectrometry influences the final spectrum only indirectly through the evaluated shape of the input spectrum. On the other hand, these data cover well just the energy region where multiple foil data are insufficient. (iv) The intercomparison of the transport calculation and experimental data is influenced by rather subjective normalization in the case of differential spectrometry, while in the case of the multiple foil technique the intercomparison is biased by the correlation between the unfolded spectrum and the input spectrum, which is usually the same transport calculation to be checked by the experiment.

Many of the above mentioned difficulties could be resolved by simultaneous unfolding of all available experimental data. The aim of this paper is to discuss the possibility of performing the task by an existing well established code such as SAND II.

2. Statement of multispectrometer unfolding

A typical problem solved by the SAND II code can be summarized as follows: for a set of activation detectors irradiated in an unknown neutron spectrum $\Phi(E)$, reaction rates N_i are given by:

$$N_i \pm \delta_i = \int R_i(E)\ \Phi(E)\ dE \qquad i = 1,2,\ldots,M_1 \qquad (1)$$

where M_1 is the number of detectors, δ_i is the variance of the i^{th} reaction rate, R_i is the response (in the above case equal to the energy dependent cross-section for the formation of the detected reaction product) of the i^{th} detector and E is the neutron energy. Given also the response functions, their variances and the input spectrum $\Phi^o(E)$, an estimate $\hat{\Phi}(E)$ of the unknown spectrum is required. The SAND II code solves the problem by the method of successive approximations.

Let us suppose now that the same spectrum is also measured by a differential spectrometer such as the proton recoil proportional counter. The output of this spectrometer is given in the form of the measured pulse height spectrum. The number of counts N_j in the j^{th} pulse height bin can be written in the form:

$$N_j \pm \delta_j = \int R_j(E)\ \Phi(E)\ dE \qquad j = 1,2,\ldots,M_2 \qquad (2)$$

where R_j is the response of the j^{th} bin and M_2 the number of bins in the pulse height spectrum. In analogy with (1) one can consider each pulse height bin as an integral detector. If there are more spectrometers the whole set of experimental data is given by:

$$N_i \pm \delta_i = \int R_i(E)\ \Phi(E)\ dE, \qquad (3)$$

$$i = 1,2,\ldots,M_1,\ M_1+1,\ldots,\ (M_1+M_2),\ldots,\ M$$

$$M = \sum_{j=1}^{n} M_j$$

where M is the total number of bins and activation detectors and n is the number of spectrometers. Though (1) and (3) are formally the same, they are different in the number of equations $M \gg M_1$ and in the shapes of the response functions involved. It is therefore not a priori evident if the SAND II code is able to produce a solution which is an acceptable estimate of the measured spectrum.

3. Discussion of the ability of SAND II in multispectrometer unfolding

No evidence was found that SAND II was used to solve problems other than multiple foil unfolding. However the ITER-2 code /12/, which is similar to SAND II and was also developed for multiple foil unfolding, has recently been shown /13/ to be able to unfold a Po-Be neutron spectrum measured by a proton recoil single crystal scintillation spectrometer. In this case the number of bins was 113 and the number of energy points 77. Taking into account the similarity of both codes, it seems that the SAND II can also perform such a job. It can be concluded that both the response of a single proton recoil spectrometer and the high number of equations can be handled by SAND II type iterative codes.

Further discussion can be based on the assumption that the shape of the response function is the main parameter determining the difficulties encountered in spectrum unfolding. With respect to this statement, it is interesting to compare responses of activation detectors and responses of differential spectrometers. A sketch of some typical response functions is shown in Figs. 1a, b and c. Looking at the proton recoil spectrometer response Fig. 1a, b, one can see that there is a close correspondence between the i^{th} bin in the pulse height spectrum and a definite neutron energy E_n, which is an analogue of the threshold energy of threshold detectors, Fig. 1c. Also the shape of the bin response, though much more regular, resembles to some extent the response of threshold detectors. So one can think of a proton recoil spectrometer as of a set of threshold detectors with regulary spaced thresholds and a regular response shape. Qualitatively, the same conclusion can be also applied to other differential spectrometers. On the contrary, comparing threshold and non-treshold activation detectors, one can see that their responses are basically much more different. So it seems probable that a code such as SAND II or ITER-2, which is able to unfold simultaneously such different detectors as nonthreshold and threshold foils, can also handle simultaneously the data from differential spectrometers. There are, however, parameters given little or no attention in multiple foil unfolding, which become important in multiple spectrometer unfolding. These are the choice of the number of bins and their widths, the determination of the energy group representation and the normalization of the experimental data to the same neutron flux intensity.

3.1. Determination of the number of bins and their widths

There are a few factors which must be compromised to determine the optimal bin width. One of them is how much new spectral information the $(i+1)^{th}$ bin contains relative to the i^{th} bin. This depends on the difference of their responses. For a differential spectrometer this difference is in the first approximation proportional to the bin width, at least as long as the responses are significantly overlaping. It is therefore useless to process too a large number of narrow bins which may only waste computer time without an equivalent improvement in the unfolding. On the other hand, a significant part of the information may be lost with a bin width that is too wide. A reasonable way to determine the bin width is that based on the natural resolution of the spectrometer. Possibly, the bin width can be made equal to a prescribed fraction of the FWHM. If, for example, a spectrometer covers an energy range from 0,1 MeV to 0,8 MeV, its FWHM is roughly 10 % over this range, and two bins are prescribed per FWHM, then supposing a linear neutron energy pulse height relationship, the bin width is 5 % and the total number of bins is 43. The total number of bins in a multispectrometer case is then equal to the sum of the bins for each differential spectrometer plus the number of activation detectors.

3.2. Energy group representation of the unfolded spectrum

Each group flux in the unfolded spectrum can be considered as a parameter calculated from the finite set of experimental data. There exist a maximum number of independent parameters which can be determined /14/, depending on the accuracy and the correlation between the data. If the solution is represented

by a larger number of parameters they are no longer independent, and the problem becomes more ill conditioned. The SAND II 620 group structure is far from being optimal in this respect. Though unfolding by a SAND II type code is not so seriously influenced by ill conditioning as in the case of methods leading to the solution of matrix equations, it is at least a waste of computing time to process so many energy groups. On the other hand, responses of some activation detectors cannot be properly represented by broader groups due to the resonance structure. One can then try a compromised procedure. It is suggested the unfolding be performed in two steps. In the first step only a fraction of the final number of iterations is performed, keeping all 620 groups. Due to the high convergence of these first successive approximations the resulting spectrum is already near to the final solution, with the exception of the fine structure which is smoothed out. Now 620 group responses can be collapsed to an appropriate smaller representation using the unfolding spectrum as the weighting function. In the second step the unfolding is carried on in this smaller representation until the final solution is obtained.

3.3. Normalization of experimental data

Normalization of the data from different spectrometers to the same neutron flux intensity is a difficult task because measurements are performed at greatly different flux levels. A certain error is therefore inherent in the normalization and it is sometimes even difficult to obtain a realistic estimate of this error. One can, however, check and possibly also correct for this error as follows. Data are multiplied by the normalization factors k_1, k_2,...,k_n which are equal for all bins of a spectrometer, but can be different for different spectrometers. At the beginning the normalization

factors are set to the initial values k_1^o, k_2^o,..., k_n^o which are calculated from a knowledge of the experimental conditions. Also estimated are the variances of these factors δ_{k1}, δ_{k2}, ..., δ_{kn}. Then a quantity S characterizing the quality of the fit is calculated. A suitable form of S can be defined by:

$$S^o = \frac{1}{M} \sum_{i=1}^{M} \frac{1}{\delta_i^2} \left(N_i - \hat{N}_i\right)^2$$

$$\hat{N}_i = \int R_i(E) \quad \hat{\Phi}(E) \, dE \tag{4}$$

Now, one of the normalization factors k_i is changed by a prescribed fraction of its variance:

$$k_i^1 = k_i^o + \alpha \, \delta_{ki} \tag{5}$$

where α is a constant depending on the expected accuracy. The unfolding is repeated keeping the number of iterations constant and a new value S^1 is calculated. The new value k_i^1 is retained or rejected depending on $S^1 < S^0$ or $S^1 > S^0$. The procedure is continued by this and the other normalization factors until a minimal value of S is found. At the end a new solution spectrum $\hat{\Phi}'$ and a set of corrected normalization factors is obtained. The interpretation of the results is not necessarily unique. Two facts should be taken into account: (i) the proposed procedure is meaningful only if there exists an appreciable overlapping of energy ranges covered by different spectrometers, and (ii), calculated normalization factors also reflect possible systematic errors in the spectrometer efficiency calibrations. In any case deviations of k's from the initial values and the difference between $\hat{\Phi}$ and $\hat{\Phi}'$ contribute to a better estimate of errors. Depending in addition on the konwledge of experimental conditions and personal feelings, one can trust $\hat{\Phi}$ more than $\hat{\Phi}'$, or vice-versa.

4. Conclusions

General arguments were given showing that the SAND II type unfolding codes could be used for multispectrometer unfolding. It would be interesting to compare the proposed procedure with the RADAK /7/ code, because basically different unfolding algorithms are used in bots methods. The SAND II method should be probably less sensitive to ill conditioning because it is based on the method of successive approximations, while RADAK solves matrix equations.

With respect to the usual way of evaluation of data from different spectrometers /8/, the proposed method presents some advantages:

(i) All experimental data are unfolded directly by a single unfolding method. In consequance, the whole neutron spectrum is obtained in one step.

(ii) An objective estimate of the normalization error as well as its effect on the solution can be obtained, if there is a significant overlapping between the energy ranges covered by single spectrometers.

(iii) Normally the whole energy interval of interest will be well covered by the responses of the spectrometers. Consequently, the influence of the input spectrum on the solution will be small or even negligible.

(iv) As a consequence of (iii), a selfconsistent experimental spectrum will be obtained. An unbiased comparison with the transport calculation is therefore made possible.

(v) Interesting sensitivity studies are possible by playing with the weights assigned to single detectors or even whole experimental methods.

References

/1/ W.N.McElroy et al., Nucl. Sci. Engng. 27 (1967) 533 and ibid. 36 (1969) 15.

/2/ W.N. McElroy et al., Nucl. Technol. 25 (1975) 180

/3/ G. De Leeuw-Gierts, In Pile Neutron Spectroscopy: Status, Contribution to this meeting

/4/ R. Gold, Neutron Spectrometry for Reactor Applications: Status, Limitations and Future Directions, First ASTM-EURATOM Symp. on Reactor Dosimetry, Petten, September 22-26.1975

/5/ L. Harris et. al., Reports GA 9882 (1970)

/6/ G. De Leeuw-Gierts et al., Lithium 6 Neutron Spectrometry In-Core, First ASTM-EURATOM Symp. on Reactor Dosimetry, Petten, Sept. 22-26, 1975

/7/ A.K. McCracken et al., The Experimental Data Processing Program, RADAK, First ASTM-EURATOM Symp. on Reactor Dosimetry, Petten, Sept. 22-26, 1976 and Foil Activation Detectors. Some Remarks on the Choice of Detectors, The Adjustment of Cross-Sections and the Unfolding of Flux Spectra, Contribution to this Meeting

/8/ W.N. McElroy et al., Spectral Characterization by Combining Neutron Spectroscopy, Analytical Calculations and Integral Measurements, this meeting.

/9/ W.N. McElroy et al., Report AFWL-TR-67-41 (1967), Vol. I-IV

/10/ F.B.K. Kam et al., Report ORNL-TM-4601 (1974)

/11/ C.R. Greer et al., Report SC-RR-67-746

/12/ M. Najžer et al., Proc. XIVth Yugoslav Conference ETAN, (1970) 417

/13/ M. Najžer et al., A New Method for the Unfolding of Pulse Height Distributions from Continuous Energy Spectra, First ASTM-EURATOM Symposium on Reactor Dosimetry, Petten, Sept. 22-26, 1975

/14/ P.G. Kirmser et al., Proceedings of Seminar Workshop on Radiation Energy Spectra Unfolding, ORNL/RS/C-40, (1976) 93.

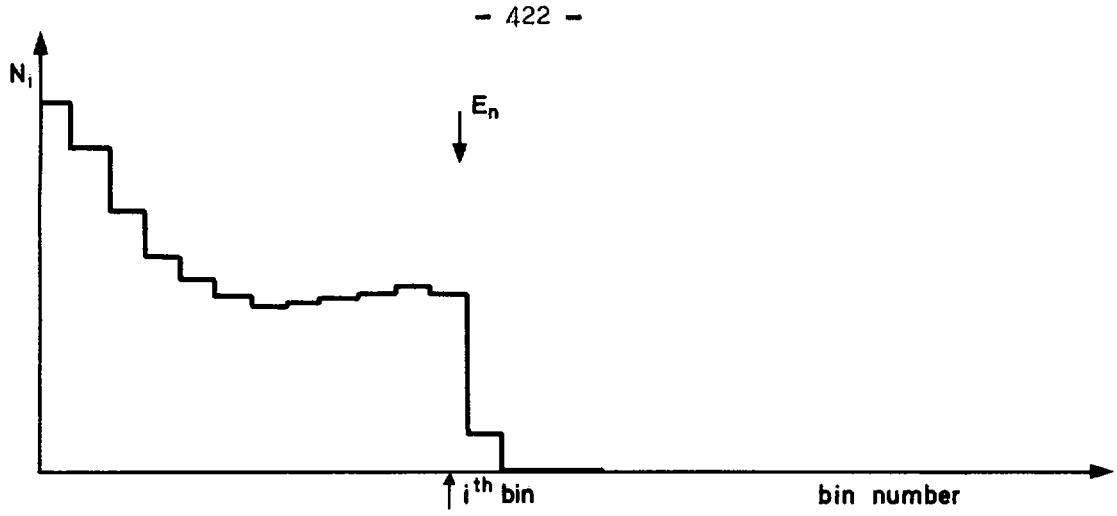

Fig. 1a Typical proton recoil spectrometer response to monochromatic neutrons of energy E_n

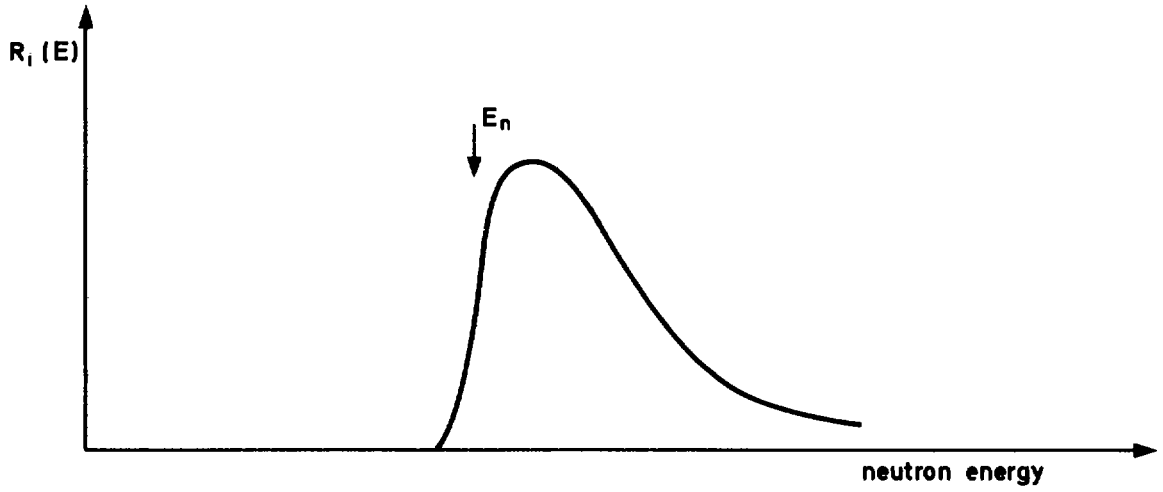

Fig. 1b Response of the i^{th} pulse height bin to neutrons of different energies

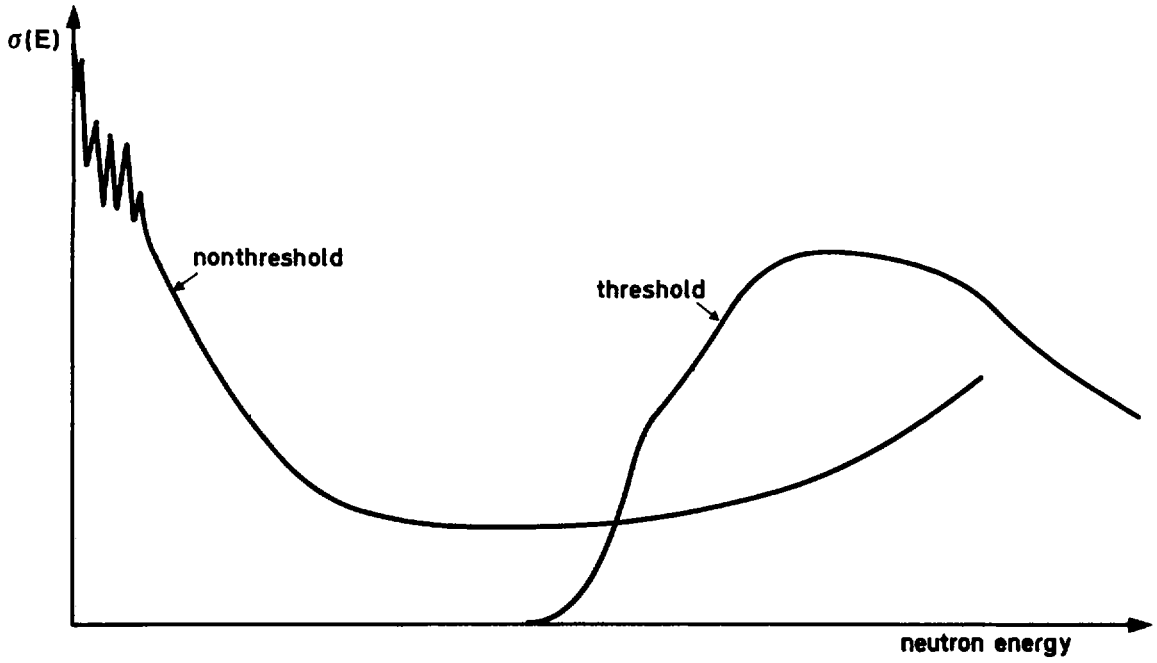

Fig. 1c Typical response of activation detectors